INSIGHTS IN PLANT NUTRITION: 2021

EDITED BY: Marta Wilton Vasconcelos

PUBLISHED IN: Frontiers in Plant Science

frontiers Research Topics

ISSN 1664-8714
ISBN 978-2-83250-314-0
DOI 10.3389/978-2-83250-314-0

About Frontiers

Frontiers is more than just an open-access publisher of scholarly articles: it is a pioneering approach to the world of academia, radically improving the way scholarly research is managed. The grand vision of Frontiers is a world where all people have an equal opportunity to seek, share and generate knowledge. Frontiers provides immediate and permanent online open access to all its publications, but this alone is not enough to realize our grand goals.

Frontiers Journal Series

The Frontiers Journal Series is a multi-tier and interdisciplinary set of open-access, online journals, promising a paradigm shift from the current review, selection and dissemination processes in academic publishing. All Frontiers journals are driven by researchers for researchers; therefore, they constitute a service to the scholarly community. At the same time, the Frontiers Journal Series operates on a revolutionary invention, the tiered publishing system, initially addressing specific communities of scholars, and gradually climbing up to broader public understanding, thus serving the interests of the lay society, too.

Dedication to Quality

Each Frontiers article is a landmark of the highest quality, thanks to genuinely collaborative interactions between authors and review editors, who include some of the world's best academicians. Research must be certified by peers before entering a stream of knowledge that may eventually reach the public - and shape society; therefore, Frontiers only applies the most rigorous and unbiased reviews.
Frontiers revolutionizes research publishing by freely delivering the most outstanding research, evaluated with no bias from both the academic and social point of view. By applying the most advanced information technologies, Frontiers is catapulting scholarly publishing into a new generation.

What are Frontiers Research Topics?

Frontiers Research Topics are very popular trademarks of the Frontiers Journals Series: they are collections of at least ten articles, all centered on a particular subject. With their unique mix of varied contributions from Original Research to Review Articles, Frontiers Research Topics unify the most influential researchers, the latest key findings and historical advances in a hot research area! Find out more on how to host your own Frontiers Research Topic or contribute to one as an author by contacting the Frontiers Editorial Office: frontiersin.org/about/contact

INSIGHTS IN PLANT NUTRITION: 2021

Topic Editor:
Marta Wilton Vasconcelos, Catholic University of Portugal, Portugal

Citation: Vasconcelos, M. W., ed. (2022). Insights in Plant Nutrition: 2021. Lausanne: Frontiers Media SA. doi: 10.3389/978-2-83250-314-0

Table of Contents

frontiers in Plant Science

ORIGINAL RESEARCH
published: 08 February 2022
doi: 10.3389/fpls.2022.835835

Cytosolic Glutamine Synthetase GS1;3 Is Involved in Rice Grain Ripening and Germination

*Takayuki Fujita[1‡], Marcel Pascal Beier[1,2‡], Mayumi Tabuchi-Kobayashi[1], Yoshitaka Hayatsu[1], Haruka Nakamura[1], Toshiko Umetsu-Ohashi[1], Kazuhiro Sasaki[3†], Keiki Ishiyama[1], Emiko Murozuka[1], Mikiko Kojima[4], Hitoshi Sakakibara[4,5], Yuki Sawa[1], Akio Miyao[6], Toshihiko Hayakawa[1], Tomoyuki Yamaya[1,7] and Soichi Kojima[1]**

[1]Graduate School of Agricultural Science, Tohoku University, Sendai, Japan, [2]Faculty of Science/Institute for the Advancement of Higher Education, Hokkaido University, Sapporo, Japan, [3]Graduate School of Agricultural and Life Sciences, The University of Tokyo, Tokyo, Japan, [4]Center for Sustainable Resource Science, RIKEN, Yokohama, Japan, [5]Graduate School of Bioagricultural Sciences, Nagoya University, Nagoya, Japan, [6]Institute of Crop Science, National Agriculture and Food Research Organization, Tsukuba, Japan, [7]Division for Interdisciplinary Advanced Research and Education, Tohoku University, Sendai, Japan

Ammonium is combined with glutamate to form glutamine. This reaction is catalyzed by glutamine synthetase (GS or GLN). Plants harbor several isoforms of cytosolic GS (GS1). Rice *GS1;3* is highly expressed in seeds during grain filling and germination, suggesting a unique role in these processes. This study aimed to investigate the role of GS1;3 for rice growth and yield. *Tos17* insertion lines for *GS1;3* were isolated, and the nitrogen (N), amino acid, and ammonium contents of *GS1;3* mutant grains were compared to wild-type grains. The spatiotemporal expression of *GS1;3* and the growth and yield of rice plants were evaluated in hydroponic culture and the paddy field. Additionally, the stable isotope of N was used to trace the foliar N flux during grain filling. Results showed that the loss of GS1;3 retarded seed germination. Seeds of *GS1;3* mutants accumulated glutamate but did not show a marked change in the level of phytohormones. The expression of *GS1;3* was detected at the beginning of germination, with limited promoter activity in seeds. *GS1;3* mutants showed a considerably decreased ripening ratio and decreased N efflux in the 12th leaf blade under N deficient conditions. The *β-glucuronidase* gene expression under control of the *GS1;3* promoter was detected in the vascular tissue and aleurone cell layer of developing grains. These data suggest unique physiological roles of GS1;3 in the early stage of seed germination and grain filling under N deficient conditions in rice.

Keywords: rice, GS1, yield, nitrogen translocation, germination, amino acids, grain filling

OPEN ACCESS

Edited by:
Marta Wilton Vasconcelos, Catholic University of Portugal, Portugal

Reviewed by:
Marco Betti, Sevilla University, Spain
Yuji Suzuki, Iwate University, Japan

****Correspondence:***
Soichi Kojima
soichi.kojima.a2@tohoku.ac.jp

†Present address:
Kazuhiro Sasaki, Japan International Research Center for Agricultural Sciences, Tsukuba, Japan

‡These authors have contributed equally to this work and share first authorship

Specialty section:
This article was submitted to Plant Nutrition, a section of the journal Frontiers in Plant Science

Received: *14 December 2021*
Accepted: *17 January 2022*
Published: *08 February 2022*

Citation:
Fujita T, Beier MP, Tabuchi-Kobayashi M, Hayatsu Y, Nakamura H, Umetsu-Ohashi T, Sasaki K, Ishiyama K, Murozuka E, Kojima M, Sakakibara H, Sawa Y, Miyao A, Hayakawa T, Yamaya T and Kojima S (2022) Cytosolic Glutamine Synthetase GS1;3 Is Involved in Rice Grain Ripening and Germination. Front. Plant Sci. 13:835835. doi: 10.3389/fpls.2022.835835

INTRODUCTION

Nitrogen (N) is one of the most important macronutrients required for plant growth (Marschner, 1995). Plants absorb inorganic N from the soil in the forms of free N ions, nitrate, and ammonium (Marschner, 1995). Glutamine synthetase (GS or GLN) combines ammonium with glutamate in an ATP-dependent manner to form glutamine (Lea and Azevedo, 2007; Thomsen et al., 2014). Two types of GS enzymes are present in plants: cytosolic GS (GS1) and chloroplastic

GS (GS2). Quantitative trait locus (QTL) analyses suggested the importance of GS1 for N use efficiency in crop plants (Obara et al., 2001; Gallais and Hirel, 2004; Habash et al., 2007; Gadaleta et al., 2014; Thomsen et al., 2014). Plants harbor several *GS1* genes (Orsel et al., 2014), for example, the rice (*Oryza sativa*) genome encodes three GS1 enzymes (Tabuchi et al., 2005). Variable spatiotemporal distribution of *GS1* expression and different enzymatic characteristics of GS1 isozymes suggests that each GS1 isozyme has a specific physiological function (Thomsen et al., 2014).

Some of the GS1 isoforms exhibit seed-specific expression. The contribution of these seed-specific GS1 isoforms toward the growth and productivity of crop plants remains unclear, although several lines of evidence indicate the importance of GS1 in cereal grains. For example, in rice, *GS1;1* is expressed in the vascular tissue of ripening grains (Yabuki et al., 2017) and GS1;3 is highly expressed in both maturing and germinating grains (Tabuchi et al., 2005, 2007). In barley (*Hordeum vulgare*), all GS1 isoforms are detected in barley grains during the early milk stage (Goodall et al., 2013).

In *Arabidopsis thaliana*, the involvement of GS1 isozymes, Gln1;1 and Gln1;2, in the germination and production of seeds has been demonstrated using reverse genetics (Guan et al., 2015) though both Gln1 isoforms are not seed-specific (Lothier et al., 2011; Guan et al., 2015, 2016; Guan and Schjoerring, 2016; Konishi et al., 2017, 2018). Microarray analysis has shown that Arabidopsis *GLN1;5* is highly expressed in ripening seeds (Schmid et al., 2005; Le et al., 2010). The expression of *GLN1;5* is also observed in germinating seeds (Bassel et al., 2008). These data reveal a unique expression profile of *GLN1;5* during the life cycle of Arabidopsis plants.

However, reverse genetics studies directly linking the seed-specific expression of *GS1* genes with crop productivity are limited because of the unavailability of knockout mutants. Rice GS1;1 is ubiquitously expressed in whole plants and is essential for normal growth, as the loss of GS1;1 leads to severe growth retardation (Tabuchi et al., 2005; Kusano et al., 2011). In maize (*Zea mays*), Gln1-3 and Gln1-4 are expressed in leaves and are involved in grain production, which suggests their importance during N translocation to source organs (Martin et al., 2006). Rice GS1;2 is expressed mainly in roots and is thought to be responsible for primary ammonium assimilation in roots, as GS1;2 knockout mutants accumulate free ammonium in xylem sap under high ammonium supply (Funayama et al., 2013).

In this study, we investigated the role of GS1;3, a seed-specific isoform, during seed germination and grain filling in rice. Real-time PCR and promoter analyses revealed the temporal and spatial distribution of *GS1;3* expression in rice. We also isolated and characterized *GS1;3* knockout rice mutants. We measured the concentrations of amino acids and plant hormones in germinating seeds, tissue dry weight, and N flux in leaves using a stable isotope tracer during reproductive growth of *GS1;3* knockout mutants. Our results suggest that rice GS1;3 functions in ammonium assimilation in the aleurone layer and the endosperm during storage protein biosynthesis and degradation, as well as it is likely involved in the energy provision for these processes. GS1;3 is therefore important for seed germination and spikelet filling, with a more pronounced function during nitrogen limitation.

MATERIALS AND METHODS

Seed Material

All seeds used in this study derived from rice plants cv. Nipponbare, harvested on the 19th October 2010 in the Kashimadai Field of the Tohoku University in Japan. Before experimental use, seed dormancy was broken by incubation at 30°C for 7 days. Seeds were selected by water density (1.13 g ml^{-1}), incubated at 60°C for 10 min, and sterilized by 70% ethanol for 30 s followed by 2% of sodium hypochlorite for 20 min and subsequent washing. The following steps were described in the respective protocols.

Definition of Seed and Plant Stages, Germination, and Yield Component Analysis

Filled spikelet, selected by saltwater with a density of 1.06 g ml^{-1}, is the term used for seeds in the yield component analysis, while mature seeds, selected by saltwater with a density of 1.13 g ml^{-1} were used for physiological analysis.

Developing seeds are harvested before they reach full maturity. During the rice ripening stage, 5 sub-stages can be defined as heading, milky, dough, yellow ripe, and maturity stage. The specific sub-stages were therefore either dough or yellow ripe (before the seeds turn brown on the surface).

A seed was regarded as germinating when the radicle emerged from the husk.

The general life cycle of rice plants after seedling establishment can be divided into vegetative (until tiller reaches maximal height), the reproductive stage (until heading), and finally the ripening stage (until harvest).

The yield component analysis was done to determine which of the main determinants of yield, the panicle number, the weight of brown rice (dehusked filled spikelets), the spikelet number, and the ratio of filled spikelets compared to unfilled spikelets at harvest (not sinking in saltwater with a density of 1.06 g ml^{-1}) is influenced in the mutants compared to the WT.

All definitions are based on Yoshida (1981).

Hydroponic Culture

Mature seeds of WT Nipponbare and *GS1;3* mutants were germinated on a moistened filter paper in Petri dishes at 30°C for 2 days. The seeds were placed on nets floating on 8 l of water with a pH adjusted to 5.8 by HCl. Twenty three days after sowing (DAS), single seedlings were rolled in moltopren and fixed to holes in a sieve placed on a Wagner pot (1:5000). Each Wagner pot contained 4 seedlings.

The nutrient solution used from this point on was based on a previous description (Mae and Ohira, 1981), with slight modifications: 0.5 mM NH_4Cl, 0.6 mM NaH_2PO_4, 0.3 mM K_2SO_4, 0.3 mM $CaCl_2$, 0.6 mM $MgCl_2$, 45 μM Fe-EDTA, 50 μM H_3BO_3, 9 μM $MnSO_4$, 0.3 μM $CuSO_4$, 0.7 μM $ZnSO_4$, and 0.1 μM Na_2MoO_4. The nutrient solution was buffered at pH 5.5.

The strength of the nutrient solution was changed over time, and the solution was renewed every 4–6 days. One-quarter strength solution was used for 13 days (until 35 DAS), followed by half-strength solution for 11 days (until 46 DAS) and full-strength solution for 61 days (until 107 DAS). With the start of heading 107 DAS, the media was changed to one-quarter strength solution for 20 days (until 127 DAS) and to one-eighth strength solution for 5 days (until 132 DAS), followed by water until harvest.

Field Experiment

Plants of WT Nipponbare and *Tos17* insertion mutant lines of GS1;3 (*gs1;3-1* and *gs1;3-2*) were grown in a paddy field in Kashimadai, Miyagi, Japan for measuring agronomical traits. Seeds were sown in cell trays, with one seed per cell, and grown in the greenhouse under natural light for 29 days. Seedlings were then transplanted in the paddy field. The paddy field was fertilized with 30 kg ha^{-1} of basal fertilizer containing 16% each of N (4.8 kg ha^{-1}of N), P, and K (Coop Chemical Co., Tokyo, Japan) and additionally with 27 kg ha^{-1}of N (5.7 kg ha^{-1}of N) fertilizer in the form of ammonium sulfate (Ube Material Industries, Ube, Japan), before transplanting, resulting in a total N supply of 10.5 kg ha^{-1}. At 153 days after germination, five plants were harvested at the soil surface and used for measuring the panicle number, shoot dry weight, and panicle dry weight. Grain and straw were dried in a greenhouse and then in a dry chamber.

Yield Analysis

Brown rice yield was determined by multiplication of (1) panicle number per individual plant, (2) spikelet number per panicle, (3) filled spikelet ratio, and (4) weight of brown rice. Panicle number was counted from five plants after harvest. The number of spikelets was determined by counting all spikelets after the separation from the panicle. Filled spikelets were determined as spikelets that sank in saltwater (density at 1.06 g ml^{-1}) and unfilled spikelets as floated. The ratio of filled and unfilled spikelets was defined as filled spikelets (%). Filled spikelets were washed in tap water and dried. The weight of brown rice was determined after the harvest of brown rice by husking of filled spikelets.

Primers

All primers used in this article are listed in **Supplementary Table S1**.

Isolation of *Tos17* Insertion Lines of GS1;3

Tos17 insertion lines of *GS1;3* (Os03g0712800) were identified through the mutant panel database.[1] For the selection of not-listed *Tos17* insertion lines, a nested PCR-based screening (Funayama et al., 2013) was carried out with pooled DNA samples provided by the National Institute of Agrobiological Sciences, NIAS, Tsukuba, Japan (Miyao et al., 2003). *Tos17* and *GS1;3* specific primers were used for the initial as well as the subsequent (nested) PCR. For the reactions, which were all conducted using the Gene Amp PCR System 9,700 (Thermo Fisher Scientific KK, Yokohama, Japan), the LA Taq DNA polymerase (Takara Bio Inc., Shiga, Japan) was used. Nested PCR products were purified and sequenced.

Seeds containing an identified *Tos17* insertion in *GS1;3* were obtained from NIAS.

Genotyping of the two candidate lines ND0163, and NE4721 with genomic DNA as template was conducted as previously described (Tabuchi et al., 2005). Homozygous lines of ND0163 were named *gs1;3-1*, and NE4721 were named *gs1;3-2*.

Quantitative Real-Time PCR

Total RNA from mature seeds and seedlings was extracted with benzyl chloride (Suzuki et al., 2004) or the RNeasy Plant Mini Kit (Qiagen, Hilden, Germany), respectively. The RNA quality was determined using the Agilent 2,100 Bioanalyzer (Agilent Technologies Japan Ltd., Tokyo, Japan). Reverse transcription was carried out using either the SuperScript First-Strand Synthesis System for RT-PCR (Invitrogen, Tokyo, Japan), with 1 μg of total RNA, or the PrimeScript RT reagent Kit with gDNA Eraser (Takara Bio Inc., Otsu, Shiga, Japan), with 0.5 μg of total RNA, according to the manufacturer's instructions. The resulting cDNA was used to analyze the expression of *OsGS1;1* (Ishiyama et al., 2004), *OsGS1;2*, *OsGS1;3* (Tabuchi et al., 2005), and *actin* (Sonoda et al., 2003) with qPCR.

The qPCR was conducted in Light Cycler Capillaries (Roche Diagnostics K.K., Tokyo, Japan) using an initial denaturation for 10 min at 95°C, followed by 40 cycles of 95°C for 10 s, 60°C for 10 s, and 72°C for 7 s. Each 20 μl reaction contained 1 μl cDNA, 1x LC FastStart DNA Master SYBR Green I (Roche), and 0.5 μM primers. A standard curve was generated from a serial dilution of cDNA. The expression of GS1 genes was normalized relative to actin. Results were shown as a mean value of three independent samples harvested from three individual plants.

Semi-quantitative RT-PCR

Total RNA from mature not imbibed seeds was extracted with Sepasol RNA I Super G (Nacalai Tesque, Kyoto, Japan) according to the manufacturer's instructions. The reverse transcription was carried out with the Prime Script RT reagent Kit with gDNA Eraser, as described for the qPCR. Gene-specific primers for *OsGS1;1* (Ishiyama et al., 2004), *OsGS1;2*, *OsGS1;3* (Tabuchi et al., 2005), and actin (Sonoda et al., 2003) were used for the semi-quantitative RT-PCR. The reactions were conducted in a Takara PCR thermal cycler with either 30 or 35 cycles of 98°C for 10 s, 60°C for 30 s, and 72°C for 30 s, and a final elongation for 1 min. Each reaction contained 0.5 U Takara Ex Taq, 1x Ex Taq Buffer, 4 nmol dNTPs, 5 ng cDNA, and 2 pmol primers. The semi-quantitative RT-PCR products were separated on a 1.5% agarose gel and stained with ethidium bromide.

Vector Construction and Plant Transformation

As a promoter, 1983 bp of the *GS1;3* upstream region were amplified from the genomic DNA of *Oryza sativa L. ssp.*

[1]http://tos.nias.affrc.go.jp/

Japonica cv. Nipponbare and flanked with *attB* sites in a subsequent PCR (Hartley et al., 2000). The promoter sequence was cloned into pDONR221 *via* BP clonase (Thermo Fisher Scientific KK, Yokohama, Japan). Following sequence confirmation and linearization with PvuII and XhoI, the promoter was transferred from pDONR221 to pGWB3 (Nakagawa et al., 2007) *via* LR clonase (Thermo Fisher Scientific KK), resulting in the final construct *proGS1;3::GUS*. The recombinant vector was used for Agrobacterium-mediated transformation of rice as described previously (Hiei et al., 1994), with slight modifications (Kojima et al., 2000). Genomic DNA isolated from transgenic lines was subjected to PCR analysis to confirm the transformation.

GUS Staining

Sterilized seeds were incubated in water at 4°C for 5 days in the dark for seed synchronization and then transferred to 30°C in the dark and incubated for either 0 h or 72 h. Seedlings were transferred to a 20 l container containing 14 kg of silt loam soil and 24 g of slow fertilizer containing 16% each of N, P, and K (Coop Chemical Co., Tokyo, Japan). Plants were cultured in a greenhouse with 26°C during a 14 h light period with supplementary artificial light, and 23°C during a 10 h dark period. Developing seeds were harvested at 35 days after flowering. For the GUS staining procedure seeds at both germination stage and ripening stage were cut in half and incubated in the GUS staining solution (100 mM sodium phosphate [pH 7.0], 10 mM EDTA, 0.5 mM $K_3Fe(CN)_4$, 0.5 mM $K_4Fe(CN)_6$-$3H_2O$, 0.1% Triton X, 1 g L^{-1} X-Gluc, and 20% methanol; Kojima et al., 2000). Images were taken with a stereomicroscope (MZ12.5, Leica Microsystems K. K., Tokyo, Japan).

Germination Ratio Measurement

The mature seed germination ratio for WT Nipponbare, *GS1;3* and *GS1;2* insertion lines (Funayama et al., 2013) was analyzed as previously described (Sasaki et al., 2015). Fully ripened seeds were germinated in 9 cm diameter Petri dishes containing 4.5 ml water. Petri dishes were kept in a dark incubator box at 30°C for 72 h. Four independent repetitions, each containing 50 seeds per line, were tested. The ratio of germinated seeds was determined 14 times during 72 h for each independent set-up.

Amino Acid Measurement

Mature seeds of WT Nipponbare were imbibed in water for 0, 12, 24, 48, or 72 h. Another set of WT, *gs1;3-1*, and *gs1;3-2* seeds were imbibed in water for 0, 30, or 66 h. After imbibition, seeds were frozen in liquid N and powdered with an MB601U Multi-Bead Shocker (Yasui Co. Ltd., Tokyo, Japan). A 10-fold volume of 10 mM HCl was added, and the samples were homogenized with the Multi-Bead Shocker. The samples were cleared from debris by a 21,900 · *g* centrifugation for 10 min, and the supernatant was filtered with an Amicon Ultra-0.5 Centrifugal Filter (Millipore, Tokyo, Japan). Samples were derivatized with the AccQ-Fluor Reagent Kit (Nihon Waters K. K., Tokyo, Japan), and amino acid concentrations were determined as previously described (Tabuchi et al., 2005). Three to five independent samples were used for each data point, the samples were harvested from individual plants.

Phytohormone Measurement

Mature seeds of WT Nipponbare, *gs1;3-1*, and *gs1;3-2* were imbibed in water for 24 h. After imbibition, seeds were frozen in liquid N and powdered with MB601U Multi-Bead Shocker (Yasui Co. Ltd., Tokyo, Japan). Concentrations of plant hormones were determined as previously described (Kojima et al., 2009). The plant hormone cytokinin was quantified *via* ultra-performance liquid chromatography (UPLC)-electrospray interface (ESI) tandem quadrupole mass spectrometry (qMS/MS; AQUITY UPLC™ System/Xevo-TQS; Waters) as described previously (Kojima et al., 2009). Auxins, gibberellins, abscisic acid, salicylic acid, and jasmonic acid were quantified with ultra-high-performance liquid chromatography (UHPLC)-ESI quadrupole-orbitrap mass spectrometer (UHPLC/Q-Exactive™; Thermo Scientific) as described previously (Kojima and Sakakibara, 2012; Shinozaki et al., 2015). Three to four independent samples were used for each data point.

^{15}N Tracing and N Content

When the 12th leaf was expanding, plants were supplied with ^{15}N-labeled 0.5 mM NH_4Cl (4.06 atom %) for 5 days. Leaves from the 8th leaf to the flag leaf, main stem panicles, and leaf blades, leaf sheaths, and panicles of tillers were harvested. Dry weights of the 8th, 9th, 10th, 11th, 12th, 13th, and 14th leaf blades and main stem panicles were measured. Four plants were used for the measurements per genotype. Yield components were determined as previously described (Tamura et al., 2010). The 12th leaf blades were powdered with Multi-Beads Shocker, and the $^{15}N/^{14}N$ ratio and N content were determined with an elemental analyzer (Flash 2000, Thermo Fisher Scientific, Tokyo, Japan) equipped with isotope ratio MS (Delta V Advantage, Thermo Fisher Scientific). Efflux and influx were calculated as previously described (Makino et al., 1984).

Statistical Analysis

Data were analyzed using Microsoft Excel add in software (Social Survey Research Information Co., Ltd., Tokyo, Japan). Correlation and partial correlation coefficients were determined between the root system architecture and biomass of plants. Correlations with a Value of $p < 0.05$ were considered statistically significant.

RESULTS

GS1;3 Is Highly Expressed in the Aleurone Layer and Endosperm During Seed Germination

To investigate the temporal expression of GS1 isoforms during rice seed germination, a quantitative PCR (qPCR) analysis was conducted on wild-type (WT) Nipponbare seeds in a 72 h time course after imbibition (**Figure 1A**). While the expression of *GS1;3* was the highest at imbibition and decreased over

time, *GS1;1* and *GS1;2* expression levels were low in the beginning of germination. From 48 h after imbibition onwards, *GS1;1* had the highest expression of all 3 isoforms, whereas *GS1;2* exceeded *GS1;3* expression at 72 h (**Figure 1A**).

Besides the temporal analysis by qPCR, the spatial expression of the GS1 isoforms was analyzed by β-glucuronidase (GUS) expression under the control of *GS1* isoform promoters.

At 24 h after imbibition, no GUS activity was detected in *proGS1;1::GUS* transgenic lines (**Figures 1B**,**C**), whereas *proGS1;2::GUS* was detected in the embryo (**Figures 1D**,**E**). The *proGS1;3::GUS* line showed an expression in the aleurone layer (**Figures 1F**,**G**). To visualize the expression pattern after the emergence of roots and shoots, the same transgenic lines were observed 72 h after imbibition (**Figures 1H–J**). The *GS1;1* promoter showed an expression in the shoots and roots (**Figure 1H**), while the *GS1;2* promoter showed mainly expression in the embryo with only a slight expression in the roots and shoots (**Figure 1I**). In contrast, the *GS1;3* promoter line showed an additional expression in the endosperm, compared to the aleurone-specific expression detected at 24 h after imbibition (**Figure 1J**).

These data suggest a physiological role of GS1;3 in the aleurone and endosperm during seed germination, a physiological role of GS1;2 in the embryo and a general function of GS1;1 in roots and shoots.

Loss of GS1;3 Delays Seed Germination

To investigate the physiological function of GS1;3 in seed germination and seedling growth, a reverse genetics approach was used. Two independent *Tos17* insertion lines of *GS1;3* were identified by a screen of pooled *Tos17* insertion line DNA samples. **Figure 2A** illustrates the *Tos17* insertion position in the *GS1;3* mutant lines. Semi-quantitative real-time PCR (RT-PCR) analysis 24 h after imbibition revealed that *GS1;3* was not expressed in the mutant lines, but in the WT (**Figure 2B**). By contrast, *GS1;1* and *GS1;2* expressions were detected neither in WT seeds nor in mutant seeds (**Figure 2B**). *Actin* was expressed in all samples tested (**Figure 2B**).

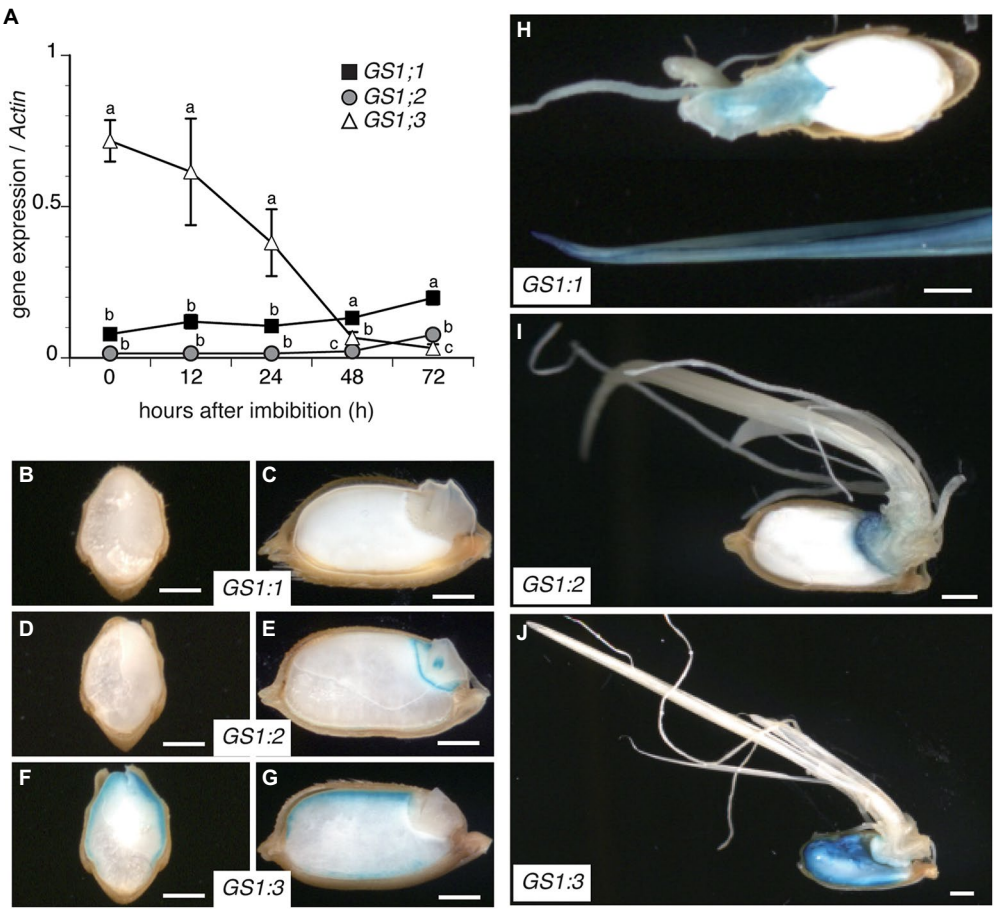

FIGURE 1 | Differential expression and localization of cytosolic glutamine synthetase (GS1) genes during rice seed germination. **(A)** Time course qPCR analysis of *GS1* isoforms in WT plants during rice seed germination after imbibition of mature seeds. Data represent mean ± SD ($n = 3$). **(B–J)** *GS1* promoter-driven GUS activity in germinating rice seeds. Transgenic rice seeds harboring *GS1;1pro::GUS*, *GS1;2pro::GUS*, or *GS1;3pro::GUS* construct were germinated and cultured under controlled conditions for 72 h. Transverse **(B,D,F)** and longitudinal **(C,E,G)** sections of seeds expressing *GS1;1* **(B,C,H)**, *GS1;2* **(D,E,I)**, and *GS1;3* **(F,G,J)**. Images of seeds and seedlings were captured using a stereomicroscope at 24 h **(B–G)** and 72 h **(H–J)** after imbibition. Bars indicate 1 mm.

Based on the aleurone layer and endosperm specific expression, the expected function of GS1;3 during seed germination and grain quality was analyzed in *GS1;3* mutant and WT seeds. Neither the loss of function of *GS1;3* nor the loss of function of GS1;2 in mutant seeds affected the weight of individual mature seeds, based on seeds selected against a salt water density selection (**Figure 2C**). The N concentration of mutant and WT seeds did not change significantly during the 72 h observation after imbibition (**Figure 2D**). Though the weight and N concentration of the *GS1;3* mutant seeds were not changed at 0 h, they took significantly longer to germinate compared to WT seeds (**Figure 2E**). It took 51 h until 50% of *GS1;3* mutant seeds germinated, whereas 50% of WT seeds germinated in 45 h. Thus, the germination of *GS1;3* mutant seeds was delayed by 6 h compared with WT seeds (**Figure 2E**).

By contrast, the loss of function of GS1;2 did not affect seed germination (**Supplementary Figure S1**). Together the data suggest that GS1;3 is involved in the germination process itself.

GS1:3 Mutant Lines Showed Altered Amino Acid Levels During Germination

For further analysis of the GS1;3 role in germination a time course measurement of ammonium and amino acids was conducted during seed germination. To get an overview of the time-dependent changes, mature WT seeds were analyzed first (**Figures 3A–C**). In WT seeds, the total concentration of free amino acids started to increase 24 h after imbibition and doubled at 72 h (**Figure 3A**). The time course did not show significant differences in the concentrations of aspartate (Asp), glutamine (Gln), asparagine (Asn), and glutamate (Glu) over time (**Figures 3B**,**C**). However, the concentration of free ammonium slightly decreased from 24 to 48 h after imbibition and increased at 72 h (**Figure 3A**).

To analyze the GS1;3 specific functions, WT and *GS1;3* mutant lines were analyzed at three time points (**Figures 3D–G**). The concentration of aspartate (Asp) in *GS1;3* mutant seeds was significantly higher than that in WT seeds at the start of imbibition but sharply decreased after 30 h, reaching a similar concentration level compared to WT seeds (**Figure 3D**). Initially, the concentration of glutamate (Glu) was comparable in WT and mutant seeds (**Figure 3E**). However, while the Glu concentration decreased in WT 30 and 66 h after imbibition, it increased temporally at 30 h and decreased again to the initial level at 66 h for *GS1;3* mutant lines (**Figure 3E**). Asparagine (Asn) showed only a temporal increase in the GS1;3 mutant lines at 30 h, compared to WT, while both WT and mutant plants showed a decrease in Asn at 66 h (**Figure 3F**). Glutamine (Gln) showed no marked changes in concentration during germination (**Figures 3D**,**G**). The data indicate on one hand that the storage components in mature grains of the *gs1;3* mutants might be different (higher Asp at 0 h), which leads to a possible role of GS1;3 in seed ripening. On the other hand, the higher levels of Glu at 30 and 66 h in the mutant seeds indicate involvement in the GS/GOGAT cycle during germination.

Interestingly, though the germination speed was altered in *gs1;3* knockout mutants, no significant differences between WT and *GS1;3* mutants were detected in the plant hormone level in germinating seeds at 24 h after imbibition (**Supplementary Figure S2**).

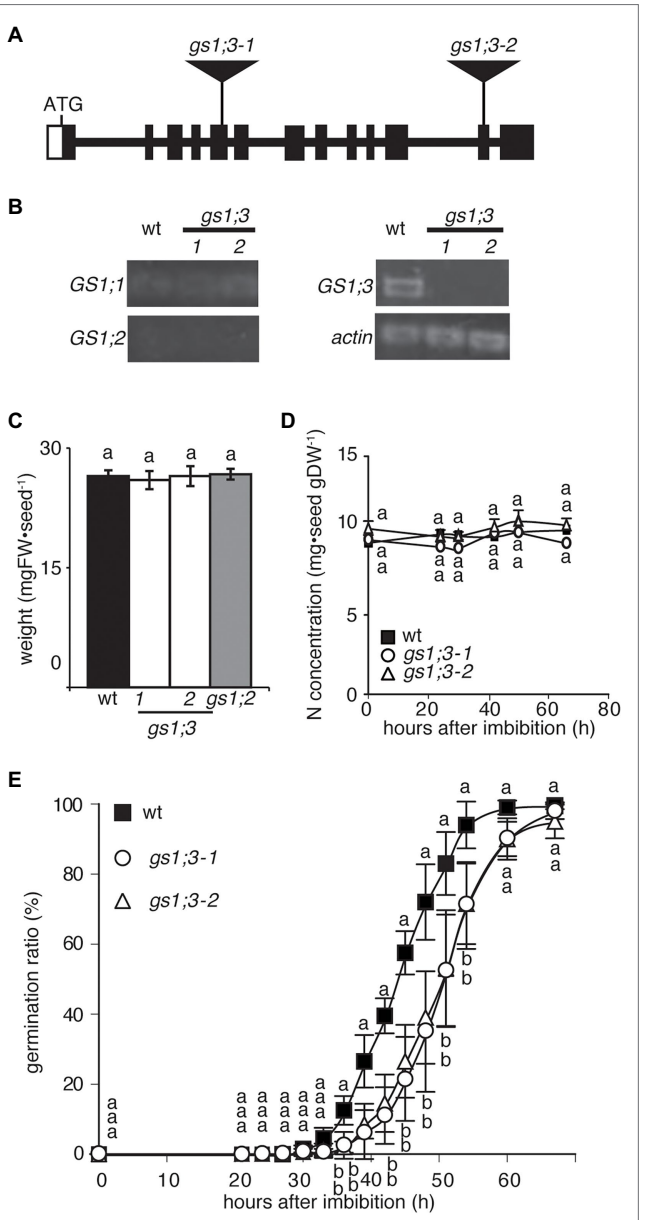

FIGURE 2 | Loss of function of GS1;3 retarded seed germination in rice. **(A)** Schematic representation of the positions of *Tos17* insertions in *gs1;3-1* and *gs1;3-2* mutants. Filled box indicates exon, and line indicates intron. Opened box indicates untranslated region. **(B)** Semi-quantitative RT-PCR analysis (30 cycles) of *GS1* isoforms and *actin* in mature WT and *GS1;3* mutant seeds. **(C)** Weight and **(D)** N concentration of mature WT, *GS1;2* and *GS1;3* mutant seeds. Each data point represents mean ± SD ($n = 5$–10 seeds). **(E)** Germination time course analysis of WT and GS1;3 mutants. During 20–72 h after imbibition, the ratio of germinated seeds was calculated every 3–6 h. Fifty seeds per line were analyzed during this period, and the experiment was repeated three times ($n = 3$ with 50 seeds each). The data represent the mean of 3 experiments ± SD. Significant differences within each group were determined using one-way analysis of variance (ANOVA) followed by Bonferroni tests and are indicated with different letters ($p < 0.05$).

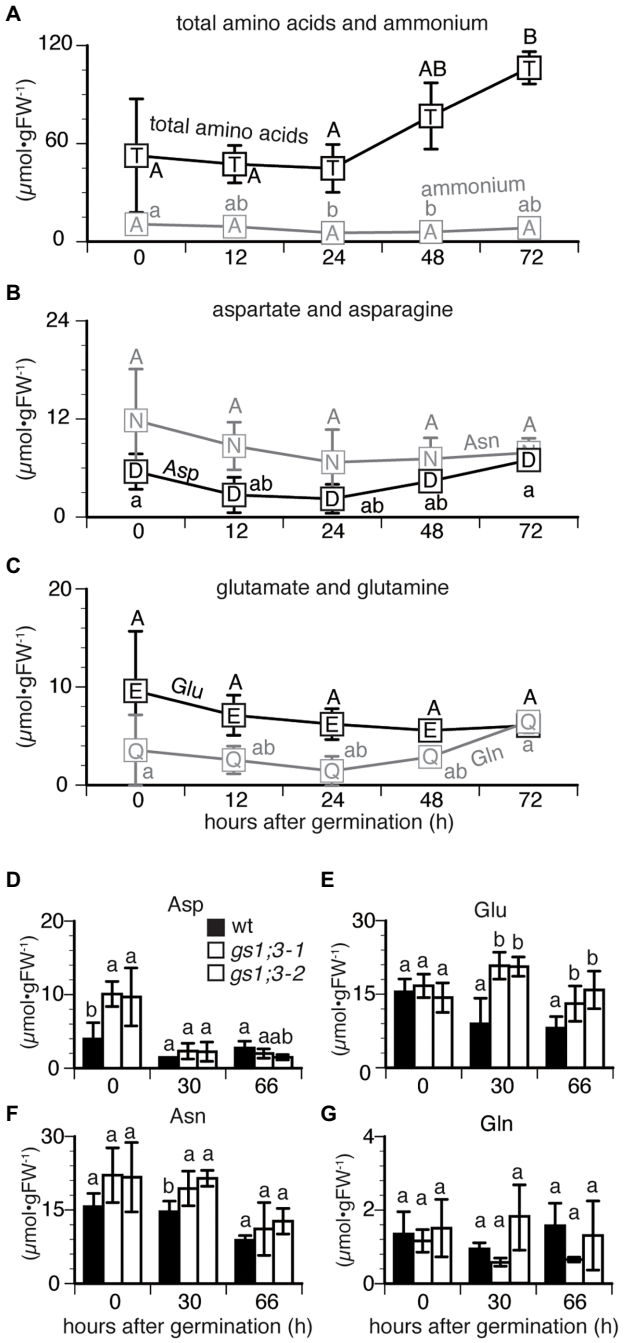

FIGURE 3 | Changes in the concentration of free amino acids and ammonium in germinating rice seeds. Concentrations of **(A)** total amino acids and ammonium and **(B,C)** four selected amino acids in Nipponbare (WT) seeds sampled at 0, 12, 24, 48, and 72 h after imbibition. Data represent mean ± SD ($n = 3$–5). Mature seeds of WT and *GS1;3* mutants harvested at 0, 30, and 66 h after imbibition **(D–G)**. Data represent mean ± SD ($n = 5$). Significant differences within each group **A–C**, changes of each compound in different time and **D–G**, changes of compound at certain time point in different genotypes) were determined using one-way analysis of variance (ANOVA) followed by Bonferroni tests and are indicated with different letters ($p < 0.05$).

Delayed Seed Storage Use and Slower Seedling Development of *GS1;3* Mutants

To evaluate the GS1;3 loss-of-function effects during germination, *GS1* expression was measured after 10 days of growth under different N regimes. Among the three *GS1* genes, *GS1;1* was expressed at high levels in roots and low levels in shoots, *GS1;2* was mainly expressed in roots, and *GS1;3* was barely expressed in seedlings in WT plants (**Supplementary Figure S3**). *Actin* was expressed under all conditions (**Supplementary Figure S3**). None of the genes of GS isoforms showed a differential expression under 5 or 1,000 μM ammonium supply, suggesting that transcriptional regulation by ammonium plays no role in the gene regulation of GS isoforms in the analyzed time-scale.

The loss of function of GS1;3 resulted in slight growth retardation in seedlings, when grown in water for 21 days (**Figures 4A**–**E**). The two *GS1;3* mutants showed a significant decrease in shoot length, but only one line showed an increased root length compared to WT (**Figure 4A**). Compared with WT, the root and shoot weight was in both *GS1;3* mutant lines not significantly different (**Figure 4B**). However, seeds of *gs1;3-1* and *gs1;3-2* were significantly heavier than those of WT 21 days after imbibition (**Figure 4C**), and the nitrogen amount in the seeds remained higher in the mutants (**Figure 4D**). Furthermore, the size of expanding 3rd leaf blades (**Figure 4E**) in GS1;3 mutants was significantly lower compared to WT plants.

This suggests a decreased use of N in the grains during the growth of mutant seedlings since the mature seed weight and N concentration were the same for WT and *GS1;3* mutants before imbibition (**Figures 2C**,**D**) while the seeds after 21 days of imbibition retained a higher weight and nitrogen content in *GS1;3* mutants compared to WT plants. Taken together, the lack of GS1;3 resulted in the delayed germination, which led to retardation of the seedling growth. This could be due to limited ability to use nitrogen source in the seed.

GS1;3 Did Not Influence the Yield of Rice Grown in a Paddy Field

While the involvement of GS1;3 was confirmed for the germination and the seedling growth under nitrogen-limited conditions, the question remained if the loss of GS1;3 also influences plant growth in a paddy field with normal nitrogen supply. We analyzed the growth and yield of *GS1;3* mutant and WT plants in a paddy field in Kashimadai, Osaki-shi, Miyagi, Japan. **Figure 5** illustrates the biomass and yield of mutant and WT rice at harvest. The shoot biomass of one *GS1;3* mutant plant was heavier, whereas that of the other mutant plant was lighter than the WT (**Figure 5A**). Neither panicle dry weight (**Figure 5B**) nor yield (**Figure 5C**) was the same in *GS1;3* mutant plants. The loss of GS1;3 functions significantly decreased the ratio of filled spikelets (%) by 6–8% compared to WT (**Figure 5G**). The panicle number was increased by 17–30% in both *GS1;3* mutant plants compared to WT (**Figure 5D**), whereas the weight of dehusked, filled spikelets (brown rice) and spikelet number per panicle were not the same in *GS1;3* mutant plants (**Figures 5E**,**F**). The different trend in several parameters like the shoot biomass and the weight of brown rice suggests that

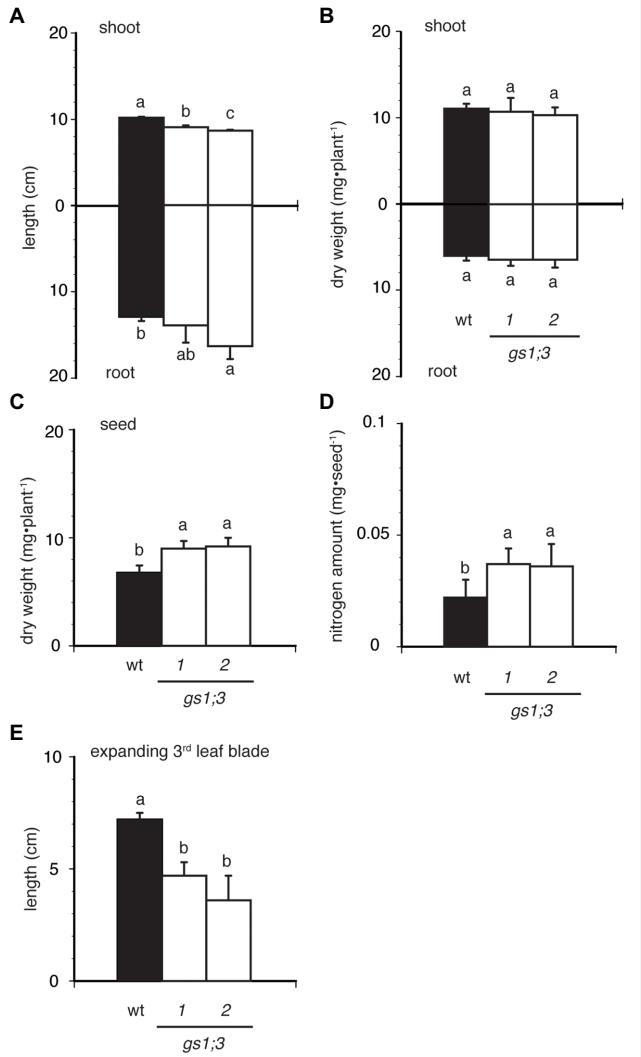

FIGURE 4 | Seedling growth of WT and GS1;3 mutants in water. Seedling growth of WT and GS1;3 mutant plants cultured for 21 days in water. **(A)** root and shoot length, **(B)** root and shoot dry weight, **(C)** seed dry weight, **(D)** seed nitrogen amount after 21 days, and **(E)** third leaf blade length. Data represent mean ± SD ($n = 5$). Significant differences within each group were determined using one-way analysis of variance (ANOVA) followed by Bonferroni tests and are indicated with different letters ($p < 0.05$).

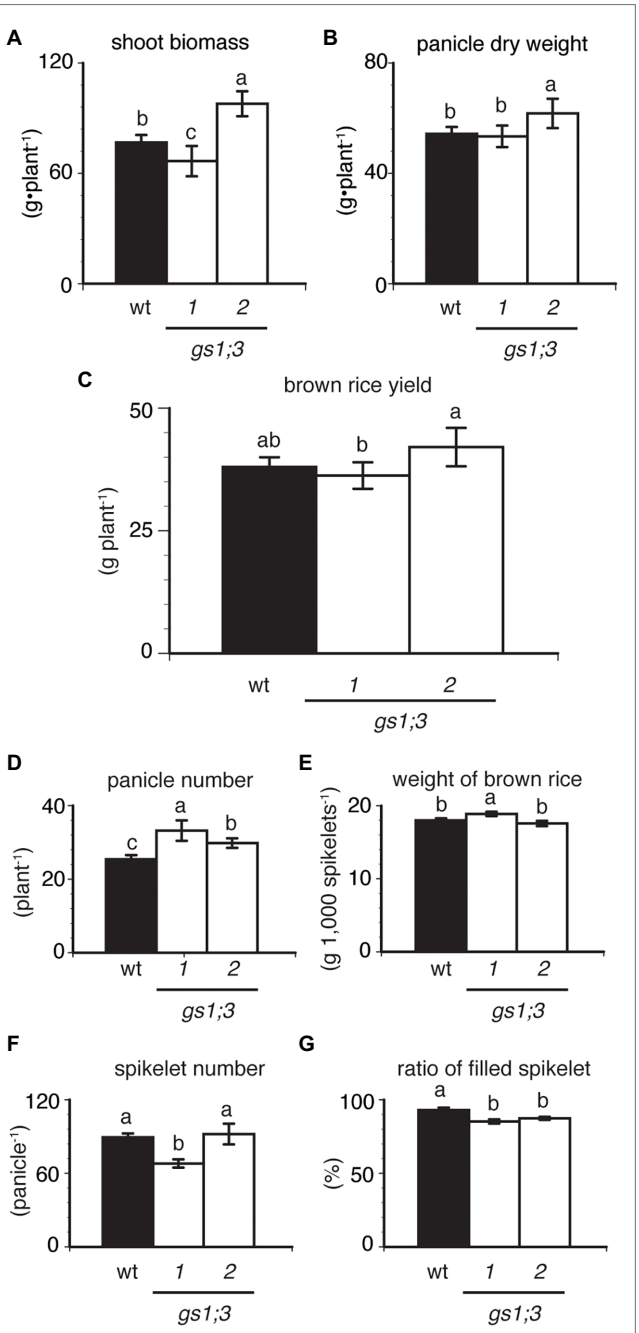

FIGURE 5 | Productivity of GS1;3 mutants grown in the paddy field. **(A)** Shoot biomass, **(B)** panicle dry weight, **(C)** brown rice yield (yield of dehusked, filled spikelets), **(D)** total panicle number, **(E)** weight of brown rice, **(F)** spikelet number per panicle, and **(G)** the ratio of filled spikelets of Nipponbare (WT; closed column) and *GS1;3* mutant (opened columns) plants harvested after 174 days at full maturity are shown. Data represent mean ± SD ($n = 5$). Significant differences within each group were determined using one-way analysis of variance (ANOVA) followed by Bonferroni tests and are indicated with different letters ($p < 0.05$).

either an unspecified *Tos17* insertion or low-level *GS1;3* transcripts might influence these factors. Only when both lines showed a trend in the same direction the phenotype was regarded as GS1;3 specific. Overall, the field analysis indicated no impact of the loss of function of GS1;3 on yield, but a significant difference in grain filling and panicle number.

GS1;3 Mutants Decreased Yield Under N Deficient Conditions

While the analysis of *GS1;3* mutants in paddy led to the identification of its involvement in grain filling, the nitrogen conditions in a paddy are hard to control. A reverse genetics study in maize demonstrated the impact of Gln1_3 and Gln1_4 on N translocation (Martin et al., 2006), and in order to investigate the physiological role of GS1;3 in N translocation, we analyzed the mutants grown with supply of the controlled N source in hydroponic culture. The growth and yield of *GS1;3*

mutants and WT plants were compared at harvest when grown with 0.5 mM NH_4Cl as the sole N source.

The panicle dry weight of individual *GS1;3* mutant plants was reduced by 26–64% at harvest (**Figure 6A**). The yield of *GS1;3* mutants was more than 60% lower than that of the WT (**Figure 6B**). To identify what led to the yield decrease, a yield component analysis was performed. As the cause of the mutant yield decrease, a 20% reduction in spikelet number per panicle (**Figure 6E**) and > 30% reduction in the ratio of filled spikelets (**Figure 6F**) was identified. However, the panicle number was not significantly different (**Figure 6C**), and the 1,000-spikelet weight (**Figure 6D**) showed only a decrease for one of the two *GS1;3* mutant lines compared to WT. This indicates that GS1;3 is mainly involved in grain filling during ripening.

GS1;3 Influences N Translocation and Panicle Development Under N Deficient Conditions

To further analyze the cause of the reduced yield, the panicle weight of the main stem was measured at heading and 21 days after heading. One of two *GS1;3* mutant lines showed a significant decrease in the dry weight of the main stem panicles at the heading date, and both lines showed a decrease to around 50% of WT main stem panicle weight 21 days after heading (**Figure 7A**). The much lower weight of the mutant main stem panicles 21 days after heading is based on the significant increase of the WT main stem panicle and the marginal increase of the mutant main stem panicles compared to the heading date (**Figure 7A**). To confirm that GS1;3 is involved in the N translocation, ^{15}N-labeled NH_4Cl was supplied to trace the N movement. Plants were labeled with ^{15}N at 19 days before heading when the 12th leaf was emerging. The 12th leaf blade was chosen as a proxy to determine the N translocation rate since the growth rate was minimal between the heading date and 21 days after (**Figure 7B**). The influx and efflux of N in the 12th leaf blade over the time course, ranging from 19 days before heading to 61 days after heading show that in WT, the N efflux was 5-fold higher than the N influx (**Figure 7C**). In *GS1;3* mutants, the N efflux showed a significant reduction (21–38%) in the 12th leaf over time compared to the WT; however, no significant difference was detected in the N influx between WT and *GS1;3* mutants (**Figure 7C**). In addition to the nitrogen translocation, the analysis of a *GS1;3* promoter-driven GUS activity in a ripening grain at 35 days after heading revealed the localization of the promoter activity in the dorsal vascular bundles and aleurone layer (**Figure 7D**). These data support a role of GS1;3 in N translocation to seeds during the grain filling stage.

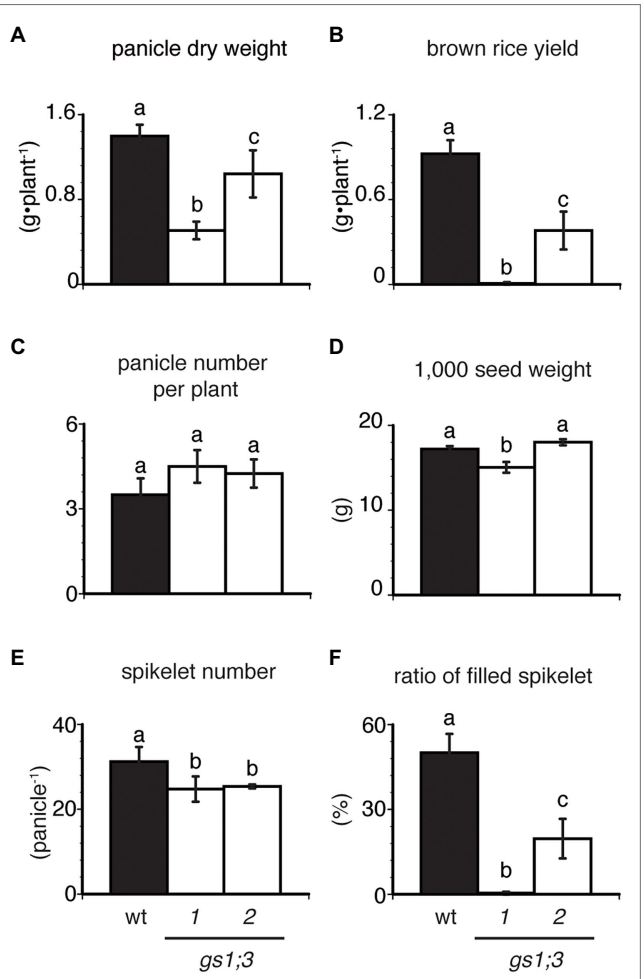

FIGURE 6 | Productivity and growth of GS1;3 mutants in hydroponic culture. **(A)** panicle dry weight, **(B)** brown rice yield, **(C)** panicle number per plant, **(D)** 1,000 seed weight, **(E)** spikelet number per panicle, and **(F)** ratio of filled spikelets of WT and *GS1;3* mutant plants grown in hydroponic culture with 0.5 mM NH_4^+ are shown. All samples were harvested 61 days after heading. Data represent mean ± SD ($n = 5$). Significant differences within each group were determined using one-way analysis of variance (ANOVA) followed by Bonferroni tests and are indicated with different letters ($p < 0.05$).

DISCUSSION

GS1;3 Function in the Aleurone Layer and Endosperm Promotes Seed Germination in Rice

After imbibition *GS1;3* showed a specific expression in the aleurone layer followed by a delayed expression in the endosperm, while *GS1;1* and *GS1;2* were expressed in the emerging plants, and lowly in the germinating seeds (**Figure 1**). The expression pattern of rice *GS1;3* is comparable to the barley *GS1;3* orthologue, *HvGS1_3*, which also showed an expression in the endosperm and was suggested to be important for seed maturation and germination, with a suggested role in the assimilation of ammonium from protein degradation in senescing leaves and/or seed reserves (Goodall et al., 2013). The localization of both, rice and barley GS1;3 isoforms are slightly different from wheat GS1;3, which showed an expression in the transfer cells, indicating a function in translocation similar to GS1;2 in barley and rice (Tabuchi et al., 2007; Goodall et al., 2013; Wei et al., 2021).

The delayed germination of the *gs1;3* mutants (**Figure 2**) is likely based on the involvement of GS1;3 in storage component mobilization, that is, the assimilation of free ammonium derived

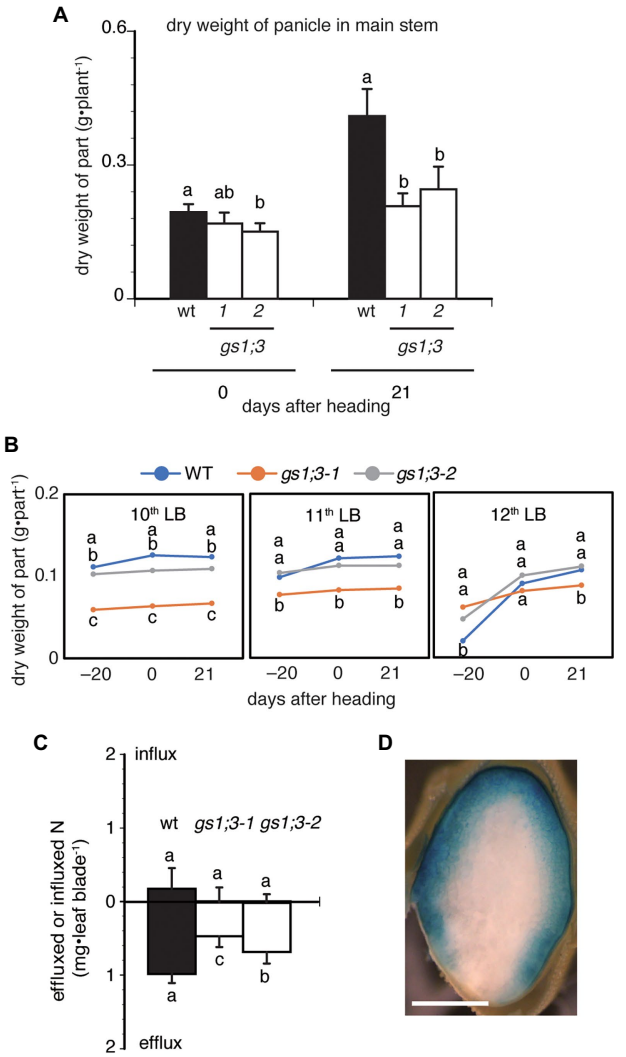

FIGURE 7 | Influx and efflux of nitrogen in the 12th leaf blade on the main stem and GS1;3 promoter activity in ripening grains. **(A)** Dry weight of main stem panicles, and **(B)** dry weights of the 10th to 12th leaf blades of WT and GS1;3 mutant plants grown in hydroponic culture with 0.5 mM NH_4^+ are shown. For **(A,B)**, plant organs were harvested 19 days before heading, at heading, 20 days after heading. **(C)** The influx and efflux of nitrogen in WT and *GS1;3* mutant plants in the 12th leaf blades at 61 days after heading. Plants were grown in hydroponic culture and were supplied with ^{15}N-labeled NH_4Cl for 5 days from 19 days before heading onwards. Significant differences within each group were determined using one-way ANOVA followed by Bonferroni tests and are indicated with different letters ($p < 0.05$). Data represent mean ± SD ($n = 8$, for wt, *gs1;3-1*, and *gs1;3-2*; **D**) *GS1;3* promoter-driven GUS activity in ripening rice grain. Transgenic plants expressing *GS1;3pro::GUS* were grown in the greenhouse on fully fertilized soil. Ripening grains were harvested at 35 days after heading and used for GUS staining. The transverse section is shown. Bar indicates 1 mm.

from proteolysis. The limited N assimilation over time due to lack of the GS1;3 function in *gs1;3* mutants resulted in the increase in the remaining nitrogen concentration in form of glutamate compared to WT (**Figure 3E**). The free ammonium level was unchanged in the GS1;3 mutants (data not shown) compared to WT, indicating that the conversion of storage protein to free ammonium is feedback regulated by the glutamate level. This supports the role of GS1;3 suggested by Goodall et al. (2013).

In addition to that function, it is likely that GS1;3 is important for the energy status in the germinating seed. The germinating seed is heterotroph, and the supply of oxygen is limited due to the dense seed structure as well as to waterlogged conditions in the case of rice seeds. Amino acids can serve as energy donors through their catabolism in the TCA cycle (Angelovici et al., 2011; Araújo et al., 2011; Kirma et al., 2012), and the aspartate family pathway plays a crucial role under energy shortage (Galili, 2011; Credali et al., 2013). When we analyze the amino acid data (**Figure 3**), we see an accumulation of Asn after 30 h, and an accumulation of Glu after 30 and 66 h in the *GS1;3* mutant seeds. The role of Asn as an energy donor starts from its conversion to aspartate, the precursor of the branched Asn family pathway (Mini-review by Galili et al., 2014). Considering that Asp can be converted by the Asp aminotransferase to Glu, a substrate of GS1;3, and that gln, a product of GS1;3, is an important precursor to produce Asn *via* the Asn synthetase (Gaufichon et al., 2016), we can assume a detrimental effect in the initial steps of the energy donor function of Asn in the GS1;3 mutant lines. Since no energy is needed for the action of the Asp aminotransferase, an equilibrium between the glutamate and aspartate concentration is likely. With the decreased function of GS1;3, we see the increased levels of glutamate after 30 and 66 h. The accumulation of Asn could be a result of the product accumulation (aspartate) which could decrease the asparaginase activity. Since this blocks the initial step in this pathway, the energy production is reduced. Though amino acids are precursors of phytohormones, the phytohormone level is unchanged in the *GS1;3* mutant plants (**Supplementary Figure S2**).

The role of rice GS1;3 in germinating seeds is therefore to assimilate ammonium derived from protein catabolism in the aleurone layer and the endosperm, which is linked to the energy status that is needed to maintain the storage protein proteolysis for seedling growth.

Nitrogen Limitation Enhances *GS1;3* Importance for Seed Ripening in Rice

Under normal field conditions, the only remarkable phenotype of the *GS1;3* mutants was a significant reduction in the ratio of filled spikelets (**Figure 5G**). This suggests that GS1;3 is not important for vegetative growth, besides the initial involvement in seed germination, which is consistent with former studies about major GS1 isoforms in rice (Tabuchi et al., 2005, 2007). However, the reduction in the ratio of filled spikelets suggested involvement in seed ripening in addition to germination.

Since N supply is one of the major factors, which influence grain filling and yield (Uribelarrea et al., 2004), and *GS1;3* is expressed in ripening spikelets (Tabuchi et al., 2005), the *GS1;3* mutants were analyzed under nitrogen-limited conditions.

The reduction of nitrogen supply markedly reduced the yield of *GS1;3* mutant plants, mainly based on the reduction of the

ratio of filled spikelets, leading to a decrease in panicle dry weight and brown rice, with a smaller but still significant decrease in the spikelet number (**Figure 6**).

The localization of rice GS1;3 in spikelets is in the endosperm and the aleurone layer (**Figure 7D**). While the effect of different GS1 isoforms on yield is well documented, most articles focus on isoforms that are important during vegetative growth, like Gln1_3 and Gln1_4, which exert their function due to their localization in the mesophyll and bundle sheath cells of maize leaves (Martin et al., 2006). The only known GS1 isoforms with predominant localization in seeds are GS1;3 in wheat (Wei et al., 2021), and GS1;3 in barley (Goodall et al., 2013), *GLN1;5* in Arabidopsis (Schmid et al., 2005; Winter et al., 2007; Bassel et al., 2008; Le et al., 2010), and GS1;3 in rice (this study).

Considering the specific localization in spikelets and seeds, likely explanations for the phenotype are similar to the germinating seeds, namely, the involvement in the GS/GOGAT cycle for the build-up of the storage proteins, as well as its involvement in the energy metabolism.

As reviewed by Galili et al., 2014, monocotyledonous plants do not generate energy through photosynthesis in seeds, leaving again the asparagine pathway as a possible root for energy supply. Indeed, the Asp concentration in *GS1;3* mutant line seeds was significantly higher compared to WT upon imbibition (**Figure 3**), suggesting that the production of energy is affected by the lack of GS1;3, due to the disturbance of the GS/GOGAT cycle in the endosperm/aleurone layer. Further support for this hypothesis is given in **Figure 7A**, which showed that the developing main stem panicle nearly doubled its weight in WT seeds 21 days after heading, while *GS1;3* mutant seeds just slightly increased. With the production of storage components during heading, the spikelets get thicker, making them more and more impenetrable to oxygen, which is increasing the need for alternative energy sources, which cannot be supplied anymore in the case of GS1;3 seeds.

Since the plant weight in the *GS1;3* mutant lines was not affected, they do not have a nitrogen limitation *per se*. When the 12th leave was used as a proxy for nitrogen translocation (**Figures 7B**,**C**), it was shown that the nitrogen efflux from the leave was reduced, which can be explained by a reduction in the sink strength (reduced ratio of filled spikelets) caused by the lack of GS1;3.

In conclusion, the GS1;3 involvement in seed germination and its influence on spikelet filling, which is more pronounced under nitrogen limitation, is based on its involvement in the assimilation of free ammonium in the aleurone layer and the endosperm during storage protein biosynthesis and degradation. It furthermore seems to be involved in the energy provision that fuels these processes. Future research will focus on the contribution of GS1;3 to the energy metabolism in non-photosynthetic tissues.

Outlook

The importance of GS1;3 under nitrogen limitation makes it a possible target for improving crop productivity. A possible approach might be an overexpression of GS1;3, which has the potential to improve yield specifically under nitrogen-limited conditions. Successful examples are the overexpression of GS1;1 and GS1;2, that led to an improved tolerance to abiotic stress in rice (James et al., 2018), and the overexpression of GS1-1, which improved the nitrogen utilization efficiency in barley (Gao et al., 2019). Considering the assumed role of GS1;3 in the energy metabolism a positive effect might occur also in developing seeds without nitrogen limitation.

DATA AVAILABILITY STATEMENT

The original contributions presented in the study are included in the article/**Supplementary Material**, further inquiries can be directed to the corresponding author.

AUTHOR CONTRIBUTIONS

MT-K, KI, TH, TY, and SK contributed to conception and design of the study. MT-K, TU-O, EM, and HN performed the promoter analysis. YH, KS, and TF performed the seed germination analysis. MT-K and YH performed the amino acid measurement. TF, MT-K, YH, HN, KS, YS, and SK performed the growth analysis. MK, HS, HN, and KI performed the hormone analysis. TF, MT-K, YS, and AM isolated the *Tos17* insertion lines. TF, MB, and SK performed the tracing analysis. MB and SK wrote the first draft of the manuscript. All authors contributed to the article and approved the submitted version.

FUNDING

Japan Advanced Plant Research Network supported by JSPS was also acknowledged for the use of Elemental Analyzer. JSPS KAKENHI Grant Numbers, 21688006 and 26450073 to SK and 22119003 to TY supported this work. TH was supported by a Grant-in-Aid for Scientific Research from the Ministry of Education, Culture, Sports, Science, and Technology of Japan (KIBAN B; 17H03780). This study was supported by the Network of Centers of Carbon Dioxide Resource Studies in Plants (NC-CARP).

ACKNOWLEDGMENTS

We are grateful to Ikumi Sakurada-Enomoto, Noriyuki Konishi, Wataru Tamura, Keiichi Kanno, Yosuke Nakayama, Fumi Imagawa, Masahide Saito, and Takanori Yasuda for technical assistance.

SUPPLEMENTARY MATERIAL

The Supplementary Material for this article can be found online at: https://www.frontiersin.org/articles/10.3389/fpls.2022.835835/full#supplementary-material

REFERENCES

Angelovici, R., Fait, A., Fernie, A. R., and Galili, G. (2011). A seed high-lysine trait is negatively associated with the TCA cycle and slows down Arabidopsis seed germination. *New Phytol.* 189, 148–159. doi: 10.1111/j.1469-8137.2010.03478.x

Araújo, W. L., Tohge, T., Ishizaki, K., Leaver, C. J., and Fernie, A. R. (2011). Protein degradation - an alternative respiratory substrate for stressed plants. *Trends Plant Sci.* 16, 489–498. doi: 10.1016/j.tplants.2011.05.008

Bassel, G. W., Fung, P., Chow, T. F. F., Foong, J. A., Provart, N. J., and Cutler, S. R. (2008). Elucidating the germination transcriptional program using small molecules. *Plant Physiol.* 147, 143–155. doi: 10.1104/pp.107.110841

Credali, A., García-Calderón, M., Dam, S., Perry, J., Díaz-Quintana, A., Parniske, M., et al. (2013). The K+-dependent asparaginase, NSE1, is crucial for plant growth and seed production in Lotus japonicus. *Plant Cell Physiol.* 54, 107–118. doi: 10.1093/pcp/pcs156

Funayama, K., Kojima, S., Tabuchi-Kobayashi, M., Sawa, Y., Nakayama, Y., Hayakawa, T., et al. (2013). Cytosolic glutamine synthetase1;2 is responsible for the primary assimilation of ammonium in rice roots. *Plant Cell Physiol.* 54, 934–943. doi: 10.1093/pcp/pct046

Gadaleta, A., Nigro, D., Marcotuli, I., Giancaspro, A., Giove, S. L., and Blanco, A. (2014). Isolation and characterisation of cytosolic glutamine synthetase (GSe) genes and association with grain protein content in durum wheat. *Crop Pasture Sci.* 65, 38–45. doi: 10.1071/CP13140

Galili, G. (2011). The aspartate-family pathway of plants: linking production of essential amino acids with energy and stress regulation. *Plant Signal. Behav.* 6, 192–195. doi: 10.4161/psb.6.2.14425

Galili, G., Avin-Wittenberg, T., Angelovici, R., and Fernie, A. (2014). The role of photosynthesis and amino acid metabolism in the energy status during seed development. *Front. Plant Sci.* 5:447. doi: 10.3389/fpls.2014.00447

Gallais, A., and Hirel, B. (2004). An approach to the genetics of nitrogen use efficiency in maize. *J. Exp. Bot.* 55, 295–306. doi: 10.1093/jxb/erh006

Gao, Y. J., de Bang, T. C., and Schjoerring, J. K. (2019). Cisgenic overexpression of cytosolic glutamine synthetase improves nitrogen utilization efficiency in barley and prevents grain protein decline under elevated CO_2. *Plant Biotechnol. J.* 17, 1209–1221. doi: 10.1111/pbi.13046

Gaufichon, L., Rothstein, S. J., and Suzuki, A. (2016). Asparagine metabolic pathways in Arabidopsis. *Plant Cell Physiol.* 57, 675–689. doi: 10.1093/pcp/pcv184

Goodall, A. J., Kumar, P., and Tobin, A. K. (2013). Identification and expression analyses of cytosolic glutamine synthetase genes in barley (*Hordeum vulgare* L.). *Plant Cell Physiol.* 54, 492–505. doi: 10.1093/pcp/pct006

Guan, M., de Bang, T. C., Pedersen, C., and Schjoerring, J. K. (2016). Cytosolic glutamine synthetase Gln1;2 is the main isozyme contributing to GS1 activity and can be up-regulated to relieve ammonium toxicity. *Plant Physiol.* 171, 1921–1933. doi: 10.1104/pp.16.01195

Guan, M., Møller, I. S., and Schjoerring, J. K. (2015). Two cytosolic glutamine synthetase isoforms play specific roles for seed germination and seed yield structure in Arabidopsis. *J. Exp. Bot.* 66, 203–212. doi: 10.1093/jxb/eru411

Guan, M., and Schjoerring, J. K. (2016). Peering into the separate roles of root and shoot cytosolic glutamine synthetase 1;2 by use of grafting experiments in Arabidopsis. *Plant Signal. Behav.* 11:e1245253. doi: 10.1080/15592324.2016.1245253

Habash, D., Bernard, S., Schondelmaier, J., Weyen, J., and Quarrie, S. (2007). The genetics of nitrogen use in hexaploid wheat: N utilisation, development and yield. *Theor. Appl. Genet.* 114, 403–419. doi: 10.1007/s00122-006-0429-5

Hartley, J. L., Temple, G. F., and Brasch, M. A. (2000). DNA cloning using in vitro site-specific recombination. *Genome Res.* 10, 1788–1795. doi: 10.1101/gr.143000

Hiei, Y., Ohta, S., Komari, T., and Kumashiro, T. (1994). Efficient transformation of rice (*Oryza-sativa* L) mediated by agrobacterium and sequence-analysis of the boundaries of the T-DNA. *Plant J.* 6, 271–282. doi: 10.1046/j.1365-313X.1994.6020271.x

Ishiyama, K., Inoue, E., Tabuchi, M., Yamaya, T., and Takahashi, H. (2004). Biochemical background and compartmentalized functions of cytosolic glutamine synthetase for active ammonium assimilation in rice roots. *Plant Cell Physiol.* 45, 1640–1647. doi: 10.1093/pcp/pch190

James, D., Borphukan, B., Fartyal, D., Ram, B., Singh, J., Manna, M., et al. (2018). Concurrent overexpression of OsGS1;1 and OsGS2 genes in transgenic Rice (*Oryza sativa* L.): impact on tolerance to abiotic stresses. *Front. Plant Sci.* 9:786. doi: 10.3389/fpls.2018.00786

Kirma, M., Araújo, W., Fernie, A., and Galili, G. (2012). The multifaceted role of aspartate-family amino acids in plant metabolism. *J. Exp. Bot.* 63, 4995–5001. doi: 10.1093/jxb/ers119

Kojima, M., Kamada-Nobusada, T., Komatsu, H., Takei, K., Kuroha, T., Mizutani, M., et al. (2009). Highly sensitive and high-throughput analysis of plant hormones using MS-probe modification and liquid chromatography tandem mass spectrometry: an application for hormone profiling in *Oryza sativa*. *Plant Cell Physiol.* 50, 1201–1214. doi: 10.1093/pcp/pcp057

Kojima, S., Kimura, M., Nozaki, Y., and Yamaya, T. (2000). Analysis of a promoter for the NADH-glutamate synthase gene in rice (*Oryza sativa*): cell type-specific expression in developing organs of transgenic rice plants. *Aust. J. Plant Physiol.* 27, 787–793. doi: 10.1071/PP99145

Kojima, M., and Sakakibara, H. (2012). "Highly sensitive high-throughput profiling of six phytohormones using MS-probe modification and liquid chromatography–tandem mass spectrometry," in *High-Throughput Phenotyping in Plants*. ed. J. Normanly (New York, USA: Humana Press), 151–164.

Konishi, N., Ishiyama, K., Beier, M. P., Inoue, E., Kanno, K., Yamaya, T., et al. (2017). Contribution of two glutamine synthetase isozymes to ammonium assimilation in Arabidopsis roots. *J. Exp. Bot.* 68, 613–625. doi: 10.1093/jxb/erw454

Konishi, N., Saito, M., Imagawa, F., Kanno, K., Yamaya, T., and Kojima, S. (2018). Cytosolic glutamine synthetase isozymes play redundant roles in ammonium assimilation under low-ammonium conditions in roots of *Arabidopsis thaliana*. *Plant Cell Physiol.* 59, 601–613. doi: 10.1093/pcp/pcy014

Kusano, M., Tabuchi, M., Fukushima, A., Funayama, K., Diaz, C., Kobayashi, M., et al. (2011). Metabolomics data reveal a crucial role of cytosolic glutamine synthetase 1;1 in coordinating metabolic balance in rice. *Plant J.* 66, 456–466. doi: 10.1111/j.1365-313X.2011.04506.x

Le, B. H., Cheng, C., Bui, A. Q., Wagmaister, J. A., Henry, K. F., Pelletier, J., et al. (2010). Global analysis of gene activity during Arabidopsis seed development and identification of seed-specific transcription factors. *Proc. Natl. Acad. Sci. U. S. A.* 107, 8063–8070. doi: 10.1073/pnas.1003530107

Lea, P. J., and Azevedo, R. A. (2007). Nitrogen use efficiency. 2. Amino acid metabolism. *Ann. Appl. Biol.* 151, 269–275. doi: 10.1111/j.1744-7348.2007.00200.x

Lothier, J., Gaufichon, L., Sormani, R., Lemaitre, T., Azzopardi, M., Morin, H., et al. (2011). The cytosolic glutamine synthetase GLN1;2 plays a role in the control of plant growth and ammonium homeostasis in Arabidopsis rosettes when nitrate supply is not limiting. *J. Exp. Bot.* 62, 1375–1390. doi: 10.1093/jxb/erq299

Mae, T., and Ohira, K. (1981). The remobilization of nitrogen related to leaf growth and senescence in rice plants (*Oryza-sativa*-L). *Plant Cell Physiol.* 22, 1067–1074.

Makino, A., Mae, T., and Ohira, K. (1984). Relation between nitrogen and ribulose-1,5-bisphosphate carboxylase in rice leaves from emergence through senescence. *Plant Cell Physiol.* 25, 429–437.

Marschner, H. (1995). *Mineral Nutrition of Higher Plants*. p. 889. Academic Press, London.

Martin, A., Lee, J., Kichey, T., Gerentes, D., Zivy, M., Tatout, C., et al. (2006). Two cytosolic glutamine synthetase isoforms of maize are specifically involved in the control of grain production. *Plant Cell* 18, 3252–3274. doi: 10.1105/tpc.106.042689

Miyao, A., Tanaka, K., Murata, K., Sawaki, H., Takeda, S., Abe, K., et al. (2003). Target site specificity of the *Tos17* retrotransposon shows a preference for insertion within genes and against insertion in retrotransposon-rich regions of the genome. *Plant Cell* 15, 1771–1780. doi: 10.1105/tpc.012559

Nakagawa, T., Kurose, T., Hino, T., Tanaka, K., Kawamukai, M., Niwa, Y., et al. (2007). Development of series of gateway binary vectors, pGWBs, for realizing efficient construction of fusion genes for plant transformation. *J. Biosci. Bioeng.* 104, 34–41. doi: 10.1263/jbb.104.34

Obara, M., Kajiura, M., Fukuta, Y., Yano, M., Hayashi, M., Yamaya, T., et al. (2001). Mapping of QTLs associated with cytosolic glutamine synthetase and NADH-glutamate synthase in rice (*Oryza sativa* L.). *J. Exp. Bot.* 52, 1209–1217. doi: 10.1093/jexbot/52.359.1209

Orsel, M., Moison, M., Clouet, V., Thomas, J., Leprince, F., Canoy, A. S., et al. (2014). Sixteen cytosolic glutamine synthetase genes identified in the *Brassica napus* L. genome are differentially regulated depending on nitrogen regimes and leaf senescence. *J. Exp. Bot.* 65, 3927–3947. doi: 10.1093/jxb/eru041

Sasaki, K., Takeuchi, Y., Miura, K., Yamaguchi, T., Ando, T., Ebitani, T., et al. (2015). Fine mapping of a major quantitative trait locus, qLG-9, that controls seed longevity in rice (*Oryza sativa* L.). *Theor. Appl. Genet.* 128, 769–778. doi: 10.1007/s00122-015-2471-7

Schmid, M., Davison, T. S., Henz, S. R., Pape, U. J., Demar, M., Vingron, M., et al. (2005). A gene expression map of *Arabidopsis thaliana* development. *Nat. Genet.* 37, 501–506. doi: 10.1038/ng1543

Shinozaki, Y., Hao, S. H., Kojima, M., Sakakibara, H., Ozeki-Iida, Y., Zheng, Y., et al. (2015). Ethylene suppresses tomato (*Solanum Lycopersicum*) fruit set through modification of gibberellin metabolism. *Plant J.* 83, 237–251. doi: 10.1111/tpj.12882

Sonoda, Y., Ikeda, A., Saiki, S., von Wiren, N., Yamaya, T., and Yamaguchi, J. (2003). Distinct expression and function of three ammonium transporter genes (*OsAMT1;1-1;3*) in rice. *Plant Cell Physiol.* 44, 726–734. doi: 10.1093/pcp/pcg083

Suzuki, Y., Kawazu, T., and Koyama, H. (2004). RNA isolation from siliques, dry seeds, and other tissues of *Arabidopsis thaliana*. *BioTechniques* 37, 542–544. doi: 10.2144/04374BM03

Tabuchi, M., Abiko, T., and Yamaya, T. (2007). Assimilation of ammonium ions and reutilization of nitrogen in rice (*Oryza sativa* L.). *J. Exp. Bot.* 58, 2319–2327. doi: 10.1093/jxb/erm016

Tabuchi, M., Sugiyama, K., Ishiyama, K., Inoue, E., Sato, T., Takahashi, H., et al. (2005). Severe reduction in growth rate and grain filling of rice mutants lacking *OsGS1;1*, a cytosolic glutamine synthetase1;1. *Plant J.* 42, 641–651. doi: 10.1111/j.1365-313X.2005.02406.x

Tamura, W., Hidaka, Y., Tabuchi, M., Kojima, S., Hayakawa, T., Sato, T., et al. (2010). Reverse genetics approach to characterize a function of NADH-glutamate synthase1 in rice plants. *Amino Acids* 39, 1003–1012. doi: 10.1007/s00726-010-0531-5

Thomsen, H. C., Eriksson, D., Moller, I. S., and Schjoerring, J. K. (2014). Cytosolic glutamine synthetase: a target for improvement of crop nitrogen use efficiency? *Trends Plant Sci.* 19, 656–663. doi: 10.1016/j.tplants.2014.06.002

Uribelarrea, M., Below, F. E., and Moose, S. P. (2004). Grain composition and productivity of maize hybrids derived from the Illinois protein strains in response to variable nitrogen supply. *Crop Sci.* 44, 1593–1600. doi: 10.2135/cropsci2004.1593

Wei, Y., Xiong, S., Zhang, Z., Meng, X., Wang, L., Zhang, X., et al. (2021). Localization, gene expression, and functions of glutamine synthetase isozymes in wheat grain (*Triticum aestivum* L.). *Front. Plant Sci.* 12:580405. doi: 10.3389/fpls.2021.580405

Winter, D., Vinegar, B., Nahal, H., Ammar, R., Wilson, G. V., and Provart, N. J. (2007). An "electronic fluorescent pictograph" browser for exploring and analyzing large-scale biological data sets. *PLoS One* 2:e718. doi: 10.1371/journal.pone.0000718

Yabuki, Y., Ohashi, M., Imagawa, F., Ishiyama, K., Beier, M. P., Konishi, N., et al. (2017). A temporal and spatial contribution of asparaginase to asparagine catabolism during the development of rice grains. *Rice* 10:3. doi: 10.1186/s12284-017-0143-8

Yoshida, S. (1981). *Fundamentals of Rice Crop Science*. International Rice Research Institute.

Conflict of Interest: The authors declare that the research was conducted in the absence of any commercial or financial relationships that could be construed as a potential conflict of interest.

Publisher's Note: All claims expressed in this article are solely those of the authors and do not necessarily represent those of their affiliated organizations, or those of the publisher, the editors and the reviewers. Any product that may be evaluated in this article, or claim that may be made by its manufacturer, is not guaranteed or endorsed by the publisher.

frontiers in Plant Science

REVIEW
published: 01 March 2022
doi: 10.3389/fpls.2022.840770

Priming With Silicon: A Review of a Promising Tool to Improve Micronutrient Deficiency Symptoms

*Lourdes Hernandez-Apaolaza**

Department of Agricultural Chemistry and Food Science, Universidad Autónoma de Madrid, Madrid, Spain

Priming consists of a short pretreatment or preconditioning of seeds or seedlings with different types of primers (biological, chemical, or physical), which activates various mechanisms that improve plant vigor. In addition, stress responses are also upregulated with priming, obtaining plant phenotypes more tolerant to stress. As priming is thought to create a memory in plants, it is impairing a better resilience against stress situations. In today's world and due to climatic change, almost all plants encounter stresses with different severity. Lots of these stresses are relevant to biotic phenomena, but lots of them are also relevant to abiotic ones. In both these two conditions, silicon application has strong and positive effects when used as a priming agent. Several Si seed priming experiments have been performed to cope with several abiotic stresses (drought, salinity, alkaline stress), and Si primers have been used in non-stress situations to increase seed or seedlings vigor, but few has been done in the field of plant recovery with Si after a stress situation, although promising results have been referenced in the scarce literature. This review pointed out that Si could be successfully used in seed priming under optimal conditions (increased seed vigor), to cope with several stresses and also to recover plants from stressful situations more rapidly, and open a promising research topic to investigate, as priming is not an expensive technique and is easy to introduce by growers.

Keywords: silicon, priming, stress memory, plant recovery, micronutrient deficiency

OPEN ACCESS

Edited by:
Marta Wilton Vasconcelos, Catholic University of Portugal, Portugal

Reviewed by:
Suprasanna Penna, Bhabha Atomic Research Centre (BARC), India
Jen-Tsung Chen, National University of Kaohsiung, Taiwan

***Correspondence:**
Lourdes Hernandez-Apaolaza
lourdes.hernandez@uam.es

Specialty section:
This article was submitted to Plant Nutrition, a section of the journal Frontiers in Plant Science

Received: *21 December 2021*
Accepted: *02 February 2022*
Published: *01 March 2022*

Citation:
Hernandez-Apaolaza L (2022) Priming With Silicon: A Review of a Promising Tool to Improve Micronutrient Deficiency Symptoms. Front. Plant Sci. 13:840770. doi: 10.3389/fpls.2022.840770

INTRODUCTION

According to the National Climate Assessment (NCA)-USDA, the highest losses in global crop production can be attributed to abiotic stresses (∼50%), followed by weeds, insects, and pathogens (Srivastava et al., 2021). To cope with biotic and abiotic stresses, and due to their sessile life, plants have developed a great variety of adaptation strategies to mitigate their stressor effects and to survive in such stress conditions. These strategies are especially relevant to fight against climate changes that crops should afford, which significantly affect biotic and abiotic stressors (pests, drought, salinity, etc.) or nutrient imbalances (deficiencies or toxicities).

What Priming Means? General Concepts

The plant stress responses should be first divided into two different approaches: acclimatation and priming. Acclimation is referred to plant strategies induced to cope with long periods of

stress duration, to which the metabolism of plants, with more or less success, will be adjusted (Wiszniewska, 2021), maintaining higher amounts of stress-protective compounds and therefore being prepared for future stress episodes. On the contrary, priming is defined as the stimulation of a specific physiological state that allows plants to give a stronger and rapid response against stress compared with plants without priming (Balmer et al., 2015), which is like a vaccine. Usually, priming is carried out by short pretreatment or preconditioning with different compounds (chemical, biological) or by altering physical factors for a determined period (Filippou et al., 2012; Leuendorf et al., 2020). Most of the primers are used to affect the synchronization of seed germination and give plants a better resistance against stressful conditions (Srivastava et al., 2021). Primer treatments in seeds activate various enzymes such as proteases, dehydrogenases, hydrolases, and α-amylase, and this weakens endosperm and mobilizes reserve substances, which finally improve seed vigor. In addition, DNA repair proteins, stress-responsive transcription factors, and metabolites such as antioxidants, osmolytes, and sugars are upregulated, which contributes to performing phenotypes more tolerant to stress in the primed plants (Farooq et al., 2019). It is also considered that priming promotes the development of stress memory in plants, which improves plant resilience against adverse conditions (Savvides et al., 2016). Priming effects can last for the complete growth cycle of the plant or several generations, although priming is given only during the initial seed germination or at the seedling stages and has a short duration (hours for seeds or a few weeks for seedlings).

There is increasing evidence that not only animals but also organisms without a specific nervous system (plants, fungi, or bacteria) can "remember" a past event (i.e., Thellier and Lüttge, 2013). This memory may shape or "prime" future responses to environmental conditions, which gives a stimulus-dependent and phenotypic plasticity of response traits. So, the environmental adaptation of an individual by adjusting its physiological or developmental phenotype is mediated by such plasticity (Sultan, 2000; West-Eberhard, 2003).

Induction of direct defenses can minimize the benefits of enhanced protection because this is usually correlated with high physiological expenses. By contrast, primed plants are almost equally protected but need considerably lower fitness costs (van Hulten et al., 2006; Wang et al., 2015). This makes priming-based approaches valuable to cope with several biotic and abiotic stresses. Due to its resource-saving character, priming is considered advantageous over acclimation (Leuendorf et al., 2020).

Pastor et al. (2014) and Balmer et al. (2015) defined different states in a priming process: (1) "Priming state" achieved after the application of the priming stimulus and lasts until plant exposure to stress. During this period, the levels of various primary and secondary metabolites, hormones, enzymes, and other molecules are slightly altered (tricarboxylic acid cycle metabolites; amino acids, sugars, reactive oxygen species (ROS), pathogenesis-related proteins (PRPs), salicylic acid), placing the plant in a standby state. (2) "Postchallenge primed state" appears when the plant becomes stressed, and the plants rapidly induced the corresponding reactions to fight the stressor. (3) "Transgenerational primed state" observed in plants that have a priming memory due to become from seeds obtained from primed parental plants.

It is generally assumed that priming acts on the phenotype of individuals, and its effects are attributed to epigenetic, hormonal, cellular, and other phenotypic changes (Hilker et al., 2016). A clear link between changes in protein synthesis or gene expression and alterations in phenotype is not usually observed (Balmer et al., 2015). For that reason, it is considered reversible, because the applied stimulus apparently keeps the DNA sequence unchanged. So, priming allows for reversion to the original state. During the poststress phases, the primed plant behavior is influenced by factors such as developmental stage or environmental conditions and strongly depends on the plant–stressor combination (Balmer et al., 2015). The readjustment of an organism from a primed to inexperienced state, that is, the "forgetting" of the priming event, may be dependent on the lifetime of the cellular marks left by priming that are called upon exposure to stress (Hilker et al., 2016).

For activating the priming process, the priming agent and the stressor could be of the same nature; for instance, Ding et al. (2012) described that multiple exposures to drought "train" Arabidopsis responses to coping with this abiotic stress. Many other examples for abiotic and biotic stresses of this type are referred to in Hilker et al. (2016), like pathogen infection primes plant resistance against future pathogen infection. On the other hand, the priming agent and the stressor could have a different nature. Several studies have demonstrated that exogenous applications of H_2O_2 induce tolerance to drought, high temperatures, chilling and salinity, and also heavy metal stresses (Hossain et al., 2015). This could be explained by the primer action through the activation of general antioxidant and signaling pathways.

Priming can be applied at various developmental stages of the plant life cycle and to various plant parts. The most used is seed priming because its simplicity allows a wide utilization of this technique. Seed priming is a presowing treatment that exposes seeds to ascertain a solution for a certain period that allows partial hydration, but germination does not occur, because the moisture of the seed is not enough to cause the seed to germinate. However, this level is enough to start many of the physiological processes associated with the early phase of germination (pregermination metabolism) (Ibrahim, 2016). After priming, seeds are redried to their initial moisture content to allow the storage of the primed seeds (Di Girolamo and Barbanti, 2012) or could be directly sown. The optimization of the priming process is necessary, due to lots of factors that can affect the seed response to primers, such as duration, temperature, seed vigor, plant species, and storage condition. There have been different reports about the positive effects of priming in plants. In general, primed seeds present improved vigor, reduction in germination time with changes in molecular, cellular, physiological, and biochemical aspects and result in higher seed vigor and a better crop establishment and yield of crops (Yacoubi et al., 2011; Di Girolamo and Barbanti, 2012; Finch-Savage and Bassel, 2016). These changes include cell division and elongation, plasma

membrane fluidity, the induction of stress-responsive proteins, changes in transcriptome and proteome, H^+-ATPase activity (Soeda et al., 2005; Zhuo et al., 2009; Kubala et al., 2015; Finch-Savage and Bassel, 2016), and changes in the antioxidant system activity (Chen and Arora, 2011; Kubala et al., 2015). Moreover, priming will facilitate the seeds to cope with environmental stresses during seedling establishment and show increased stress tolerance at the whole-plant level (Yacoubi et al., 2011; Srivastava et al., 2021), because, during the dehydration and soaking steps, it may generate moderate abiotic stress (Ashraf and Foolad, 2005) probably due to the radicle protrusion repression. Plants will remember such stress and their memory phase is long term, which ranges from weeks to months (Srivastava et al., 2021), and remember that seed priming is applied only once. Similarly, during soaking, seeds bind water and absorb protective and biologically active compounds (Wiszniewska, 2021). Beneficial effects are then expressed in developing seedlings and increased plant vigor and survivability under biotic or abiotic stresses.

Less often, priming is applied to seedlings or their parts, and also young plants in active growth phases. This approach is focused on remediation of plant stresses in specific plant regions or organs. For example, to cope with metal toxic levels using phytohormone priming treatments, which application to seedlings and developed plants are preferred than to seeds (Sytar et al., 2019). Moreover, priming can be applied *in vitro* culture to organs, or their fragments excised from donor plants (Wiszniewska, 2021). As a result of prolonged selection in the presence of stress agents, such as salinity, for example, the plant cells' behavior and the regenerated plantlets are modified when compared with plants without a priming treatment (Chun et al., 2019).

A well-nourished plant that is supplied with enough and complete essential nutrients diet will have sufficient and more energy and metabolic resources to invest in memory stress responses than a plant grown with not all the nutrients or with a low amount of them. The same for other environmental conditions influences plant development, such as light, humidity, oxygen, etc. Defense strategies impose a substantial demand for resources, which reduce growth (Huot et al., 2014) and could decrease photosynthesis, which means a reduction of energy reserves. So, a balance between nutrition, growth, and defense should be achieved to optimize plant wellness.

Moreover, how much an organism invests in priming depends on the age at which experiences this stimulus (Hilker et al., 2016). After priming, short and long-term stress memories could be activated. The first should work to cope with imminent stress and the second with future stressors. The different plant costs of these two strategies will be the key point of the process, and plant age plays an important role in it, as the plant that expends the costs of long-term memory also needs to maintain enough resources for growth and plant protection. Mechanistic differences between these types of memories and if they are different approaches or depend on plant species or age or even nutritional factors require further study. In general, young plants could benefit from a long-term stress memory, and adult plants are expected to invest in short-term memory, to have resources for its reproduction (Huot et al., 2014).

Stress Memory and Priming

Srivastava et al. (2021) considered that seed priming and stress memory are the two faces of the same coin. These authors proposed that primers generate a mild (sublethal) stress inside the seed that prepares the future seedlings to cope with stresses more efficiently than unprimed plants. This fact was based on the observation that the growth of seedlings from primed seeds is slower than that of non-primed seeds a few hours after postpriming. It could be said that seed priming forces plants to begin germination under stress, which will create a stress memory on the seeds. Several stress marks can be imprinted on the seed genome just as in stress-primed plants, which lead to improved stress tolerance. However, in the case of seedlings or plant priming, the stress memory was created specifically in the plant.

Plants have to cope with different stresses all along their crop cycle and retain "memories" of previously encountered stresses as an adaptive mechanism that helps them to encounter forthcoming stresses more rapidly and efficiently. These memories are called "acquired tolerance." They can produce a short-term effect (somatic memory), a memory that can be transmitted to succeeding generations (intergenerational memory), or, in some cases, a memory that can be inherited across generations (transgenerational memory). Such memories can be induced artificially through preexposure to a low-dose stressor or by the addition of beneficial compounds such as silicon, or by natural exposure to recurrent stress episodes (e.g., stational drought) (Srivastava et al., 2021). "Somatic memory" in plants has been explained through several mechanisms that include chromatin remodeling, alternative transcript splicing, metabolite accumulation, and autophagy. However, chromatin-dependent regulation is considered as a key mechanism for regulating stress memories (Bäurle, 2018; Friedrich et al., 2019; Bäurle and Trindade, 2020). Chromatin could be defined as a substance within a chromosome consisting of DNA and proteins, being histones the most common proteins in chromatin. Proteins help package the DNA in a compact form that fits in the cell nucleus. Moreover, DNA replication and gene expression are associated with changes in chromatin structure. At the chromatin level, stress memory is granted by different epigenetic modifications, which alter the overall accessibility of genes for transcription. The deposition of active histone marks (cellular marks) is known to be regulated by stress situations. As mentioned, other mechanisms, independent from changes in chromatin, also regulate stress-induced somatic memory in plants. The accumulation of cellular metabolites attributed to stressful situations can also modulate plant responses during the memory phase. Moreover, the adjustment of physical properties, such as building a thicker cell wall with higher lignin content by salt primed cells of *A. thaliana,* is important for regulating salt stress-induced memory (Chun et al., 2019). Finally, autophagy in plants plays an opposite role because it degrades stress-induced proteins and other biomolecules during the recovery phase (Su et al., 2020), so this process could act as a negative regulator of stress-induced memory.

Epigenetics studies changes in genes' work due to the environment. Epigenetic changes are reversible (unlike genetic

changes) and do not change the DNA sequence, but they can change how a plant reads a DNA sequence. These characteristics of epigenetic changes give a dynamic and persistent stress response mechanism by which a gene, or a network, is activated to cope with a stress situation. When the stressor stopped, two options are possible, and it reverses to the initial state or keeps a cellular stress mark to facilitate a more potent and quicker answer to future stresses. Epigenetics includes a heritable (mitotic or meiotic) component that allows preserving this mark between generations (Ding et al., 2012). Therefore, two types of cellular marks could be distinguished, the first associated with the stressor presence, but removed when the stress situation finish, called a chromatin mark and the second, which implies the persistence of the chromatin mark after the disappearance of the stressor, called an epigenetic mark (Ding et al., 2012). This second type of marks are related to the "transcriptional memory," which could be defined as a type of information that persists after the plant's recovery from the stress and which influences subsequent transcriptional responses (Ding et al., 2012). These authors described the transcriptional memory of *Arabidopsis* plants after applying successive dehydration–watered treatments in a relatively short time. They observed that *Arabidopsis* leaf cells' ability to retain water was altered during repetitive exposures to dehydration stress, and this observation was sustained by increased rates of transcription and elevated transcript levels from a subset of the stress–response genes (trainable genes). Two different marks were found only at the trainable genes during their recovery period, and therefore, transcriptional memory was associated with them. The marks were as follows: high levels of trimethylated histone H3 Lys4 (H3K4me3) nucleosomes and the presence of Ser5P polymerase II (serine 5 phosphorylated Polymerase II) (the transcription initiation form of RNA polymerase II). At the trainable genes, the persistence of H3K4me3 and Ser5P polymerase II marks was related to the transcriptional memory length. In contrast, in the non-trainable genes, these two marks increase during stress but were reduced to basal levels when the stress was eliminated, and the plants try to recover from this situation. In diverse plant species and tissue cultures, changes in histones, including H3K4me3, in trainable genes have been reported when studied several abiotic stresses such as salinity, low temperatures, hypoxia, and drought (Sokol et al., 2007; Kim et al., 2008). Likewise, stress-induced memory has been reported in various crops that include sugarcane (Marcos et al., 2018), rice (Li et al., 2019), maize (Virlouvet et al., 2018), and wheat (Wang et al., 2020), apart from model plant *A. thaliana*.

Moreover, there are some reports concerning crosstolerance, crossresistance, or crossprotection, which means that the stress response mechanism activated in a plant to cope with specific stress could have a beneficial effect on the plants when a different stress situation appears. This is a similar mechanism that the one observed in several pests against pesticides, and which severely minimized their efficacy. This has been observed, for instance, in the case of pepper (*Capsicum annuum* L.). When grown in an excess of Cu, severe stress was caused in the plants, and several responses were induced to mitigate it, but a decrease in the disease symptoms generated by the inoculation of *Verticillium dahlia* was obtained (Chmielowska et al., 2010).

Plant Stress Recovery

Dealing with recurrent stress situations is a key point in plant memory. In such situations, plants could reduce their response under recurrent stimulus or present a positive and reinforced response to the stressor (see **Table 1** for a summary of the different memory types). The most important thing to consider in a recovery situation is that the previously caused damage needs to be repaired. Then, the plant needs to continue its growth. As mentioned before, plants have the ability to remember previous stress by maintaining some cellular marks that prepare them for developing a better strategy to cope with future stresses. But these responses are frequently accompanied by a growth reduction (Huot et al., 2014). Therefore, after the stress, an efficient and quick recovery with a reversion of the stress changes is necessary to obtain the maximal growth and reproduction rates under the new conditions. In this situation, plants must balance the necessary recovery and maintenance of stress memory to cope with future stresses. For this purpose, autophagy plays an important role in regulating recovery from stress, by eliminating compounds and cellular marks not currently needed and resetting cellular memory (Thirumalaikumar et al., 2021).

In that way, plants submitted to several stressors are reported to maintain stress memory when the stress disappears, due to memory of trainable genes. Based on their transcriptional profile, Bäurle (2018) classified them into following types: type I genes that are upregulated upon first stress and show sustained expression during the recovery phase; and type II-genes that are induced upon first stress and hyperinduced upon recurrent stress separated by a few days or weeks of recovery under stress-free conditions, but without sustained expression during recovery. However, the mechanisms that control the regulation of these genes, and which characteristics distinguish them from

TABLE 1 | A comparative among seed priming, somatic stress memory, and effect on resupply or restoration of optimal conditions in plants.

	Seed priming	Stress memory	Resupply
Application	Before seed germination	Seedlings/Plants	Seedlings/Plants
Number of applications	One	Every sublethal stress situation	After stress
Memory phase	Long term (weeks-months)	Short-term (hours-days)	Under investigation
Primers	Not necessary to be the same as future stress	The same as future stress (exception cross-tolerance)	Elimination of the stressor
Mechanism	Under investigation	Chromatin modifications (trainable genes), metabolite accumulation, etc.	Under investigation (trainable genes with sustained expression during recovery?)
Stress response	Improved	Improved	No stress
Non-stress situation	Possible plant growth reduction	Possible plant growth reduction	Total/partial recovery

non-trainable genes, need further research. Marcos et al. (2018) observed that sugarcane plants that have suffered a water deficit improved their responses when submitted to a new drought event. Even more, when rewatered, they used water with more efficiency than those plants grown with an optimal irrigation pattern. This suggests that sugarcane plants present stress memory under varying water availability and is a clear example of trainable genes of type I. The same was previously observed by Ding et al. (2012). A rapid increase in a specific abscisic acid (ABA) transporter expression and distribution and an increase in the endogenous ABA content were obtained under drought and probably under other stresses. This hormone plays a key role in the plant stress resistance and changed the postresponse gene type into the memory gene type. This improved the tolerance to following stress episodes and also the recovery capacity of the plant. Qin et al. (2021) in Arabidopsis plants submitted to different drought–water periods observed that during a second recovery period, the ABA transporter expression level and ABA content were higher than at the first recovery.

After metal stress conditions, plant growth recovery depends on different factors such as the applied metal, stress intensity, and duration, and plant species. For example, soybean seedlings were able to restore their growth during 7 days of recovery, after 2 days under high Cd concentration (89 and 223 μM Cd). They showed the same levels of chlorophyll and photosynthetic parameters as the control. The only significant difference was the shortening of the roots in plants previously treated with Cd (Holubek et al., 2020). Although, in a similar study with tobacco suspension cells treated with 50 μM Cd, a fully restored growth was obtained when treated for 3 days but not when stress conditions were prolonged only 1 day more (Fojtova, 2002). Similarly, the recovery of Arabidopsis after 21 days of phosphate deficiency was studied, and after just 1 day of P resupply, the expression of 40% of induced genes was reversed and 80% after 3 days. This latter corresponded to the reestablishment of the adequate root phosphate concentration. However, after 31 days of resupply, 80 genes remained differentially regulated, and the reversion of chromatin states during recovery (Secco et al., 2015). Plant recovery from Fe deficiency was tested in strawberry (a very susceptible plant to this stress), in which plants were grown initially with two Fe concentrations (0 or 10 μM), and then, half of the plants growing without Fe were Fe-resupplied by adding 10 μM Fe (Gama et al., 2016). These authors concluded that Fe stress does not induce permanent damages in the photosynthetic apparatus, as they observed a complete regreening of Fe resupply plants. The rapid response to the resupply of iron (12 days) has been assigned to quick access of Fe *via* the xylem to young leaves (Pestana et al., 2012). This also leads to significant biomass recovery, although, as expected, resupply plants were smaller than plants with optimal Fe nutrition. After Fe resupply, there was a boost of Fe reduction (an increase of Fe chelate reductase). Thus, explaining the high Fe contents in flowers and similar content in the rest of the organs of the recovered plants is compared with well-fed plants. Also, the Fe distribution in plants was altered in resupply plants, whereas Fe-sufficient plants accumulated Fe mainly in mature leaves, but recovered plants mobilized Fe to flowers (future fruits). All these facts may be related to modifications in trainable genes that persist after stress suppression (type I genes) and are reflected in **Table 1**.

PRIMING WITH SILICON

Although Si's essentiality for plant metabolism has not been proved yet, the sustainability of the production of several crops, such as rice or sugarcane, depends on this element. Chemical speciation and amount of Si in the soil affect the absorption taken place by plants, being silicic acid (H_4SiO_4), the form of Si which is absorbed. Silicon dioxide constitutes 50–70% of the mass of the soil (Ma and Yamaji, 2006), and clay minerals and sand are the most important soil components with silicon on their structure. Weathering, as a natural phenomenon, causes the release of Si into the soil solution and provides Si to plants; however, intensive cropping contributes to a Si depletion in the soils. The knowledge on the Si effect on the mitigation of biotic and abiotic stresses and the Si reduction in soils make Si fertilizers application a relevant agricultural practice. Generally, two aspects of Si effects are considered: (1) The usefulness level of Si application varies in different plant species: beneficial effects are usually more obvious in plants that accumulate high levels of Si in their shoots (see an example in Gonzalo et al., 2013); and (2) The positive and multilateral effect of Si is more observable when the plant is under stress or in the recovering process from this stress (i.e., Bityutskii et al., 2014; Carrasco-Gil et al., 2018; Nikolic et al., 2019; Hernandez-Apaolaza et al., 2020; Thorne et al., 2020; Arafa et al., 2021; Martín-Esquinas and Hernández-Apaolaza, 2021).

In plants, the polymerization of Si in the intercellular spaces and beneath the leaf's cuticles due to its accumulation in shoot creates a physical barrier against pathogen attack and contributes to maintaining plant erectness, with the subsequent improvement of photosynthesis. Moreover, the Si in the root apoplast contributes to reducing some nutrient–contaminants translocation to shoot and activates various metabolic pathways. These physical and biochemical combination enhances plant defenses against abiotic (drought, salinity, nutrient imbalances, etc.) and biotic stresses (insects, fungus, and bacteria). In addition, soluble Si in the plant system attracts beneficial predators and parasitoids during pest attacks and consequently increases biological control (Bakhat et al., 2018). An example of the beneficial effect of priming with Si against an abiotic stress situation (see **Table 2**), such as drought, was given by Hameed et al. (2021), who observed the improvement in wheat yield when seeds were primed with Si, by inducing a priming memory in seeds that increased drought tolerance during seed germination, seedling growth, and plant developmental stages. In the same way, Si has been used as a primer to minimize metal toxicity (Abd_Allah et al., 2019) in mustard (*Brassica juncea*) seedlings under Ni toxic exposure. In this experiment, after 1 week of Ni treatment, plants (18-day-old seedlings) were primed with 10^{-5} M Si as Na_2SiO_3 added to the nutrient solution, for 1 week, and finally, they were collected after 2 weeks more. They observed that Si decreased root to shoot Ni translocation and upregulate enzymes associated with antioxidant defense, glyoxalase detoxification systems, and also a sufficient primary

TABLE 2 | Different Si sources use for priming and control abiotic stresses.

Priming agent	[Si]	Stress	Priming period (h)	Crop	References
		Seed priming			
Sodium silicate	0, 10, 20, 30, 40, 50 mM	Salinity	8	Wheat	Azeem et al., 2015
	1.5 mM	Alkaline	12	Maize	Abdel Latef and Tran, 2016
	20,40, 60 mM	Drought	8	Wheat	Hameed et al., 2021
Sodium silicate nano	0, 300, 600, 900, 1,200 mg/L	Cd toxicity	20	Wheat	Hussain et al., 2019
Nanosilicon ($nSiO_2$)	1.66, 6.65, 13.3, 19.97, 26.63 mM	None	4	Maize	Kumaraswamy et al., 2021
	0.2, 0.4, 0.6, 0.8, 1, 1.2 mM	None	8	Sunflower	Janmohammadi and Sabaghnia, 2015
	0, 100, 500 mg/L	None	24	Lemon balm	Hatami et al., 2021
SiO_2	0.01% w/v	None	4	Maize	Kumaraswamy et al., 2021
	0.5, 1.0, 1.5%	Drought	6	Wheat	Ahmed et al., 2016
	3% 3.5% w/v	Drought	8	Rice	Ali et al., 2021
Silicic acid	0.5, 1.0, 1.5%	Drought	6	Wheat	Ahmed et al., 2016
	0, 0.063, 0.125, 0.25, 0.5 mM	Drought	24	Tomato	Chakma et al., 2021
3-aminopropyl triethoxy silane (pH 5.95)	0, 5, 10, 15, 20, 25 g·L-1	None		Maize	Sun et al., 2021
3-glycidoxypropyl trimethoxy silane (pH 9.42)	0, 5, 10, 15, 20, 25 g·L-1	None		Maize	Sun et al., 2021
		Seedling priming			
	[Si] mM	**Stress**	**Priming period (weeks)**	**Crop**	**References**
Sodium silicate	0.0, 0.5, 1.0	Fe deficiency	2	Soybean	Gonzalo et al., 2013
	0.0, 0.5, 1.0	Fe deficiency	2	Cucumber	Gonzalo et al., 2013
	0.0, 0.5, 1.0	Zn deficiency	2	Soybean	Pascual et al., 2016
	0.0, 2.25	Alkaline	36 h	Alfalfa	Liu et al., 2018
	0.01	Ni toxicity	1	Mustard	Abd_Allah et al., 2019
		Plant recovery			
	[Si] mM	**Stress**	**Recovery time**	**Crop**	**References**
Silicic acid	0.0, 1.5	Fe deficiency	5 days	Cucumber	Hernandez-Apaolaza et al., 2020
	0.0, 1.5	Zn deficiency	11 days	Cucumber	Lozano-González et al., 2021
Potassium silicate	0.0, 1.8, 3.6	Hyperhydricity	2 weeks	Carnation	Soundararajan et al., 2017
Sodium silicate	0.0, 0.6	Cd toxicity	4 days	Rice	Farooq et al., 2016

and secondary osmoprotectant accumulation, which ameliorated Ni toxic symptoms in this crop. Another example of the beneficial effect of Si priming is given under alkaline stress conditions (Liu et al., 2018). In this research, 30-day-old alfalfa seedlings were primed with 0 or 2.25 mM $Na_2SiO_3 \cdot 9H_2O$ during 36 h, and then, plants were stressed for 48 h by adding 25 mM Na_2CO_3 to the nutrient solution. It has been obtained that Si priming significantly alleviated the damage symptoms and greatly increased the chlorophyll content of stressed plants. Although the Si treatment did not show appreciable benefits under unstressed conditions, which indicates that the Si priming effect was specific to alkaline-stressed plants. Moreover, it altered the root morphology of alfalfa seedlings, which enhanced the uptake ability of the roots to uptake nutrients and water, and significantly increased root dry weight, decreasing membrane injury and malondialdehyde content, and increasing antioxidant enzyme activities. Furthermore, Si priming significantly decreased Na accumulation and increased K accumulation in the leaves under alkaline stress. Meanwhile, Si priming decreased the accumulation of metal ions such as Mg, Fe, Mn, and Zn in the roots of alfalfa seedlings under alkaline stress.

Seed priming is a technique that has been in use for more than 100 years. Around 2,600 research articles have been published between 2010 and 2022, but only around 50 documents were related to Si priming (e.g., Azeem et al., 2015; Ahmed et al., 2016). Different Si sources used for priming have been summarized in **Table 2**. In general, for seed priming, the ratio of 1:5 (w/v) seed weight to solution volume was maintained and seeds were dried before being sown (Ali et al., 2021; Chakma et al., 2021). Most of the studies are performed with sodium or potassium silicate. But only at solution pH above 8.5, silicates are the main form of Si in solution, being the monosilicic acid the prevalent form

at pH below this (optimal pH for crop cultures). As silicates are highly used, the pH of the priming solution becomes very high, which could probably alter the seed performance, metabolism, and growth after desiccation or the seedlings–plant development. If the pH of the priming solution with silicate is reduced by adding some acid, as hydrochloric acid or others, silicon will precipitate as $SiO_2 \cdot nH_2O$, so the priming effect is clearly reduced by reducing the concentration of silicon in the priming solution. On the contrary, silicic acid solutions let to adjust different pHs of the priming solution without any precipitation of the priming agent at the optimal range for plant production. Its main problem is the polymerization of the monosilicic acid into polisilicic acid at high concentrations, but concentrations used in plant culture are low enough to avoid it.

SILICON PRIMING EFFECT ON PLANT GROWTH UNDER NON-STRESSED CONDITIONS

Although the Si effect is described in the literature to be more relevant under plant stress situations, also beneficial effects of seed priming with this element are described in well-fed plants. Kumaraswamy et al. (2021) tested SiO_2 (0.01% w/v) and SiO_2 encapsulated in a chitosan (a cationic amino-polysaccharide)-tripolyphosphate nanomatrix (0.01, 0.04, 0.08, 0.12, 0.16%, w/v) as a slow-release Si source in priming solutions for maize seeds. They have found that seeds primed with 0.04–0.12%, w/v of the nano-Si fertilizer exhibited up to 3.7-fold increased seedling vigor index as compared to SiO_2 and treatments without Si. The higher index was attributed to enhanced activities of α-amylase and protease to promote remobilization of reserved nutrients (glucose and amino acids) to the growing embryo (Kumaraswamy et al., 2021). Janmohammadi and Sabaghnia (2015) studied the effect of seed soaking in different concentrations of nanosilicon ($nSiO_2$) solutions (0.0, 0.2, 0.4, 0.6, 0.8, 1.0, and 1.2 mM) for 8 h on the germination of sunflower. Seed soaking in 0.2 and 0.4 mM solutions significantly reduced the germination days to 50% and improved root length, mean daily germination, seedling vigor index, and final germination percentage. Hameed et al. (2021) primed spring wheat seeds with 20, 40, and 60 mM sodium silicate solutions, for 8 h; after drying, seeds were cultivated for 98 days. In flag leaves of mature wheat plants, they have observed significant increases of the total soluble protein content and the reducing and total sugars with increasing Si concentrations. Moreover, the Si priming treatments significantly increased the CAT and POD activities, and also both hydrolytic (protease and a-amylase) enzymes. This suggested the facilitating role of Si in protein synthesis under optimal conditions. The role of sugars as osmoprotectants and membrane stability providers was also accentuated with Si addition to the media (O'Hara et al., 2013). The enhancement of proteins and sugar content could have assisted in the regulation of metabolic pathways and provided energy and nutrients for the induction of stress tolerance, if appears. Consequently improving yield, plant biomass, and grain weight of wheat plants grown under optimal conditions (Hameed et al., 2021).

Moreover, Sun et al. (2021) tested the effect of two water-soluble Si fertilizers (3-aminopropyl triethoxy silane (pH 5.95) and 3-glycidoxypropyl trimethoxy silane (pH 9.42) synthesized by high-temperature chemical reactions in maize at different concentrations in the soaking solution: 0, 5, 10, 15, 20, and 25 $g \cdot L^{-1}$. In this study, Si treatments significantly increased the seed germination, chlorophyll content, osmotic material accumulation, antioxidant activity, and per-plant dry weight of seedlings, and the optimal concentration was 15 $g \cdot L^{-1}$. Hatami et al. (2021) have studied the priming of lemon balm (*Melissa officinalis* L.) seeds with SiO_2 nanoparticles (100 and 500 $mg \cdot L^{-1}$). Seeds were soaked in dark at 20°C for 24 h (seed weight: solution ratio, 1.4 g: mL^{-1}) and then surface-dried for 2 h and stored at 4°C. They have concluded that Si priming increased plant biomass indices, leaf relative water content, photosynthetic pigments values, total soluble protein, phenolic contents, and essential oil yield. These results suggest that the incorporation of silicon in priming solution enhanced germination and invigoration of the seedling and provides fitted plants to cope with biotic and abiotic stresses and thus contributes to growth and crop yield. The mechanisms described to explain this effect have been related to the alteration of the surface texture of seed coat (testa) (Hatami et al., 2021). These authors using scanning electron microscopy (SEM) images confirmed the rupture of testa by Si priming, although no alteration was detected in control treatments with water. A high porosity degree and large pores, and also a partial disorganization of the surface testa structure, facilitate the entry of water, nutrients, and oxygen into the germinating seed and may explain the Si effect on the future plants. This may also enhance the plant biomass and growth in comparison with untreated plants. Moreover, it has been described that Si increase the relative water content found in plants raised from seeds primed with nSi (Hatami et al., 2021), which was attributed to the Si deposition in leaves, which diminish transpiration rate from leaf surface and significantly contribute to increase photosynthetic pigments content, due to plant erectness.

The most used primers are silicates and SiO_2, but Si concentrations tested ranged from 0.2 to 60 mM, so further research is required to adjust the most adequate Si source and the concentration to be used. Such parameters could be different depending on plant species, but it is worthwhile to dedicate time and effort to establish optimal conditions for priming with Si according to the benefits already described with this simple and affordable technique.

SILICON PRIMING EFFECT UNDER MICRONUTRIENT DEFICIENCY STRESS CONDITIONS

Silicon seed priming has been used to mitigate several stresses (**Table 2**); however, to our knowledge, it has not been used for micronutrient stress amelioration until now. Although less often, priming is applied also to seedlings or their parts in active growth phases (Sytar et al., 2019). Few papers tested the Si seedling priming effect under micronutrient shortage. In that way, to

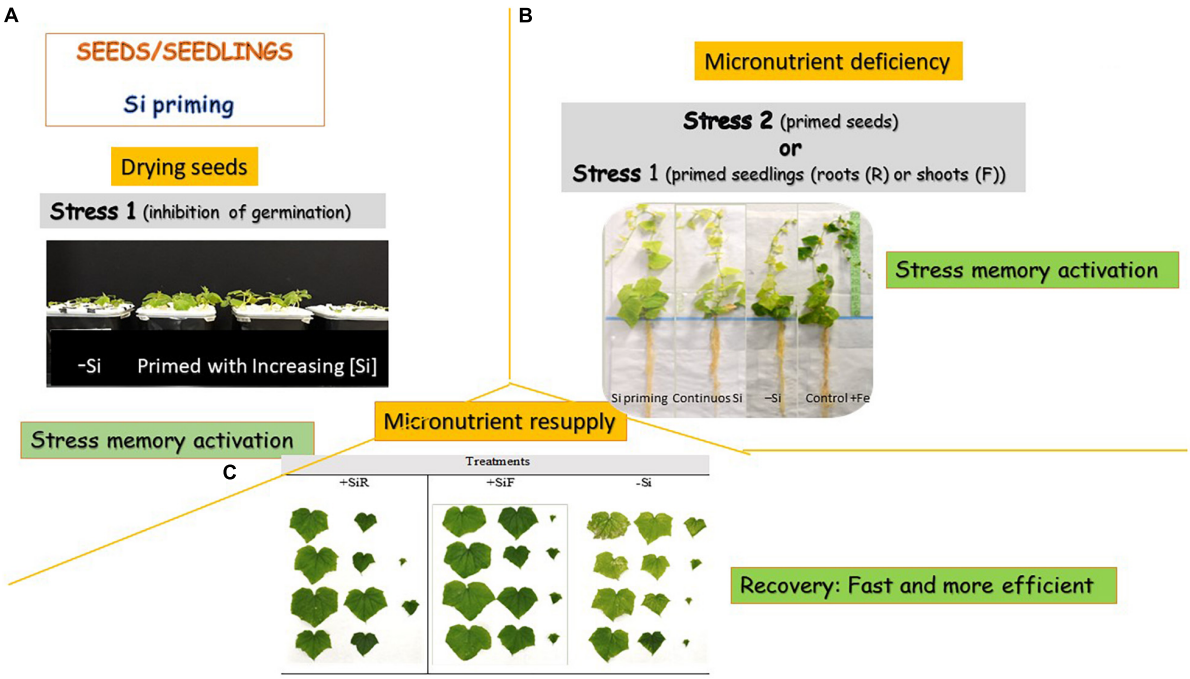

FIGURE 1 | Silicon priming could be done in **(A)** seeds or seedlings or even in plant parts, and in all cases, stress memory is activated by a stress caused by seeds desiccation. When another stress condition appears, such as a micronutrient deficiency **(B)**, plant stress memory is activated again, prevent plants from stress symptoms and accelerate plant recovery **(C)** when stress stops. In this case, the scheme and photos are referred to micronutrient deficiency (Fe) and its resupplying to cucumber plants.

mitigate Fe chlorosis symptoms, Gonzalo et al. (2013) compared soybean and cucumber seedlings primed with different doses of root Si (**Figure 1**), with unprimed plants, and with plants with a continuous Si supply. For that purpose, germinated seeds were grown for 2 weeks with a sufficient Fe supply and three Si doses as $Na_2SiO_3 \cdot 9H_2O$ (0.0, 0.5, and 1.0 mM). Then, Fe was removed from the nutrient solution, at the same time, half of the plants of each Si treatment continued with their Si supply for 3 weeks more, and for the other half, Si was eliminated from the nutrient solution (seedling priming). A control with Fe and without Si addition was also studied. For soybean, no differences were observed in SPAD index and leaves dry weight between plants treated with 0.5 mM Si either when this element was applied initially (seedling priming) or continuously during the experiment. Both presented intermediate SPAD values in between plants growing with Fe and without Si (positive control plants) and plants growing without both Fe and Si (negative control plants), and leaves dry weight were similar to plants with an optimal Fe supply. However, concerning the stem's dry weight and length, only the initial addition of 0.5 mM of Si showed similar data to plants treated with an optimal Fe supply. Plants primed with 1.0 mM Si showed an enhancement of Fe accumulation in the roots compared to the others, although the total Fe concentration in plants was similar for all the deficient treatments. This fact may explain the lowest efficacy of this treatment compared to the primed 0.5 mM Si one. These authors concluded that for soybean, a priming treatment of 2 weeks with 0.5 mM Si will contribute to better coping with Fe deficiency symptoms than a continuous Si supply or no Si addition. This could be attributed to that Si priming-induced physiological responses that allow the plant to give a more efficient and rapid answer to the imposed Fe deficiency stress. Becker et al. (2020) reported that the cause of this quick answer was the Fe uptake reduction caused by the Si-mediated apoplastic obstruction in the roots and the subsequent onset of Fe deficiency responses (the root Fe-homeostasis-related genes were upregulated), even when Fe was given to plants at an optimal level. Therefore, when plants were submitted to iron deficiency, primed plants, which have already activated the strategies to mitigate Fe chlorosis, are ready to fight against Fe shortage in the media. Data obtained by Carrasco-Gil et al. (2018) in rice support these findings. On the other hand, results obtained after priming cucumber plants with 0.5 and 1.0 mM Si to cope with Fe deficiency showed similar severe chlorosis symptoms to unprimed plants and plants grown with a continuous Si supply (Gonzalo et al., 2013). However, these authors observed that plants primed with 0.5 mM Si showed a relevant enhancement in growth parameters. So clearly, the effect of Si priming was related to plant species tested. The link between the Si transport system and its accumulation could give a plant classification into active, passive, and rejective. In the active uptake system of Si, Si absorption is mediated by both influx and efflux transporters of Si; Lsi1 and Lsi2, and both of them show polar localization (e.g., rice) (Mitani-Ueno and Ma, 2021). In the passive transport system (employed by plants having intermediate Si accumulation such as cucumber, in which CsLsi1 and CsLsi2 have been partially characterized), most of

the Si transporters do not show polar localization at the cortex cells except CsLsi1, and Lsi1 and Lsi2 in these plant species are not localized at the same cell, which results in low efficiency in Si uptake (Mitani-Ueno and Ma, 2021). The rejective uptake system is used by non-Si accumulators such as soybean, in which other transporters homolog of Lsi1 and Lsi2 have been described (GmNIP2-1 and GmNIP2-2) (Deshmukh et al., 2013), which seems to be less effective than the previously described. Beneficial effects of Si are usually obvious in plants that accumulate high levels of Si in their shoots, such as rice or sugarcane, so the beneficial effect of Si in cucumber should be more visible than in soybean. However, it is considered that Si promotes apoplastic obstruction, which limits Fe and other micronutrient absorption in the plant, so the more Si was absorbed the less Fe uptake. When this element is deficient in the media, soybean plants that are supposed to absorb less amount of Si showed the highest benefits from its addition; but in cucumber, the higher Si absorption, although benefit several growth parameters, may induce the Fe apoplastic obstruction, and activating the Fe deficiency strategy with the corresponding energy loss, which makes its benefit less clear. Gonzalo et al. (2013) indicated that in cucumber, the primed plants, either with 0.5 or 1.0 mM Si, significantly decreased the pH of the nutrient solution, from 7.5 until pH 4.5, after 14 days of -Fe culture, but after 21 days of Fe deficiency, only seedlings primed with 1.0 mM Si gave a pH value in the nutrient solution of 5.9 (the initial pH of the nutrient solution was 7.5). This showed the onset of the strategies to cope with Fe deficiency, as the release of acidic compounds to solubilize Fe in the rhizosphere, and the finite duration of them. Priming with Si seemed to maintain Fe deficiency strategy more time than a continuous Si supply or the absence of this element, but future research is required to confirm this fact. The soybean did not decrease the pH of the nutrient solution. Likewise, Pascual et al. (2016) tested the effect of initial or continuous Si supply in soybean Zn-deficient seedlings. Three Si doses were tested: 0.0, 0.5, and 1.0 mM under Zn limiting conditions. The initial addition of 0.5 mM of Si to the nutrient solution led to an enhancement of plant growth, Zn and Si content in leaves, and higher storage of Zn in the root apoplast. The results suggest that primed seedlings with 0.5 mM Si enhanced the mitigation of Zn deficiency symptoms. To the author's knowledge, no further Si seedling prime experiments have been done, but the ones presented here suggest a very promising tool in nurseries to get plants more prepared to cope with Fe or Zn deficiency situations.

RECOVERY EXPERIMENTS WITH SILICON ADDITION

Very few papers are related to plant recovery memory (plant memory after a stress situation) dealing with Si application. For example, Si-mediated recovery from hyperhydricity was studied in 4-week-old hyperhydric shoots of carnation (*D. caryophyllus* L.) plants in a growth media supplemented with 0.0, 1.8 mM, or 3.6 mM of potassium silicate (Soundararajan et al., 2017). Hyperhydricity (excess of water) causes severe problems during *in vitro* propagation, organogenesis, and acclimatization of carnation, which is one of the major floricultural crops, mainly used as a cut flower and potted plant worldwide. After 2 weeks of culture, 20, 44, and 36% of hyperhydric shoots were recovered in 0.0, 1.8, and 3.6 mM Si treatments, respectively. Shoots in control possessed higher lipid peroxidation rate and damaged stomata were detected in the control without Si. Furthermore, Si upregulated 17 protein spots at 1.8 mM Si treatment and 10 protein spots at 3.6 mM of Si when compared to Si untreated plants. The proteins that have been identified were involved in several processes such as oxide-reduction reactions, ribosomal binding, hormone–cell signaling, photosynthesis, and defense. These results showed that Si was directly involved in the acceleration of shoots recovery from hyperhydricity (Soundararajan et al., 2017). The influence of Si in metal toxicity recovery was also studied. At the age of 38 days, rice plants were stressed with 10 μM Cd added to the nutrient solution for 8 days, and then, the silicon treatments (0.0 or 0.6 mM Si) were introduced 4 days after Cd stress using a sodium silicate (Na_2SiO_3) solution which was maintained for 4 days more (Farooq et al., 2016). In this experiment, Si remarkably contributes to recovering plants from the Cd toxicity, as reflected in plant growth increase and the photosynthetic activity recovery within 48 h following Si supply and the partial reversion of the deregulation of nutrient homeostasis caused by Cd. The transcriptional response to Cd was mostly reversed following Si supply as several proteins–enzymes as phytochelatin synthase 1 and the transcription factor genes whose transcript levels were highly activated in the Cd stressed roots were downregulated in the presence of Si (Farooq et al., 2016).

Finally, the Si effect on plant recovery from micronutrient deficiencies has also been investigated (**Figure 1**). Silicon addition as silicic acid at a 1.5 mM Si concentration (applied to roots or shoot) was evaluated on cucumber plants recovery exposed to fluctuations in stress–recovery Fe regime (Fe sufficiency followed by Fe deficiency and, in turn, by Fe resupply) (Hernandez-Apaolaza et al., 2020). Si-treated plants, either when this element was added to the root or the leaves, showed a more effective and quick plant recovery after the Fe deficiency period compared to the untreated plants. However, the SPAD index increment after resupply was higher and the ROS concentration lower when Si was supplied to the roots than to the shoot, which indicates that these plants had recovered from the chlorosis faster than the others. It was suggested that the extra-activation of the strategies to cope with Fe deficiency promoted by Si in the roots, due to the apoplastic obstruction theory (Coskun et al., 2019), may cause this better recovery. However, there is another hypothesis that may explain this behavior. As mentioned above, several stress memories resulted in a rapid increase in endogenous ABA content. ABA plays a key role in plant stress resistance and changed the postresponse gene type into the memory gene type, which probably enhances plant recovery (Qin et al., 2021). The higher ABA concentration in the shoots of the cucumber plants treated with root Si was in accordance with this theory. Meanwhile, the foliar addition of Si did not show any differences in this hormone. Plant recovery was also correlated with an increase in the endoreplication cycle when Si was applied to the

roots; this mechanism prevents plants from damage and then facilitates their recovery from stress. It is known that ABA inhibits cell division, so cells are devoted to the endoreplication cycle. The higher ABA concentration that promotes the switch on of the endoreplication cycle may explain the quick recovery from Fe deficiency of root Si treated plants. Likewise, Lozano-González et al. (2021) studied the effect of Si supply (1.5 mM as silicic acid applied to roots or shoots) on cucumber plants' recovery from Zn deficiency. They concluded that the Si application reduced plant recovery time. In that case, foliar application of Si showed faster improvement in SPAD index, higher weight recovery, and a significant decrease in ROS quantity, but this effect was slightly lower when Si was applied through the root.

The state of the art today indicates that using Si to accelerate and improve plant recovery from different stresses such as hyper hydricity, metal toxicities or deficiencies are very promising tools. Silicon addition may not cause toxicity itself, but the Si source used and its concentration needs to be addressed for each specific recovery, and also the application form (roots of foliar sprays) and the consequences on fruit quality and shelf life.

PERSPECTIVES

The increasing amount of published papers dealing with plant memory may open a new research field to cope with plant stresses in a smart form that takes profit from very simple management practices, such as seed or seedling priming to ameliorate yield losses in various crops. It is especially interesting considering the global climate change in which plants have to cope with higher temperatures, drought, salinity, and other stresses as nutrient imbalances. Plant stress memory not only contributes to dealing with the stress itself but also makes plant recovery after it in a more fast and efficient way. Although several mechanisms have been studied to explain the effect of primming in stress memory and plant recovery, being the histone marks in chromatin the most studied, there is an increasing necessity of knowing how primers interact with the plants. Likewise, it is necessary to define the amount of them and the time needed to obtain the desired beneficial effect or a crosseffect for various biotic or abiotic stresses at the same time. Several priming agents are tested for different stresses, most of them with great success, but several questions are still open. For example, the beneficial effect of their application could be observed only in the stress plants or through different generations? It happens in all crops and for all types of stresses? In which crops it finishes when stress finishes? What happens with recurrent stresses (a normal situation in drought and high-temperature episodes)? May priming agents cause negative reactions? Is it better to use seed or seedling priming for specific stress? All these features and more need to be addressed to maximize the advantages of plant memory, which like vaccination in humans and animals may create a plant physiological state to prepare to fight against stresses but minimize the energy expenses.

There are four accepted and common ways of silicon addition to the plants which are silicon addition to the soil, silicon added through the nutrient solution in hydroponics, add as foliar–fruit sprays, and the less-studied Si seed–seedling priming. Silicon priming is an economical non-expensive and easy to handle way to promote plant growth, fight against different biotic and abiotic stresses in plants, and promote plant recovery after stress. In recent years, prospective research works have been done about Si application as a primer on alleviation of the effects of several environmental biotic and abiotic stresses. But it is expected that novel research works will be done regarding this issue.

AUTHOR CONTRIBUTIONS

LH-A conceived, designed the review, wrote the manuscript, and corrected the manuscript, read and approved the manuscript.

FUNDING

The author gratefully acknowledges the financial support by the FEDER/Spanish Ministry of Science, Innovation, and Universities Project: RTI2018-096268-B-I00. This work was partially supported by Comunidad de Madrid (Spain) and Structural Funds 2014-2020 (ERDF and ESF) (Project AGRISOST-CM S2018/BAA-4330).

ACKNOWLEDGMENTS

I acknowledge the contribution of Seyed Javad Azimzadeh to this review during his Ph.D. stage at our laboratory.

REFERENCES

Abd_Allah, E. F., Hashem, A., Alam, P., and Ahmad, P. (2019). Silicon alleviates nickel-induced oxidative stress by regulating antioxidant defense and glyoxalase systems in mustard plants. *J. Plant Growth Regul.* 38, 1260–1273. doi: 10.1007/s00344-019-09931-y

Abdel Latef, A. A., and Tran, L. S. (2016). Impacts of priming with silicon on the growth and tolerance of maize plants to alkaline stress. *Front. Plant Sci.* 7:243. doi: 10.3389/fpls.2016.00243

Ahmed, M., Qadeer, U., Ahmed, Z. I., and Hassan, F. (2016). Improvement of wheat (Triticum aestivum) drought tolerance by seed priming with silicon. *Arch. Agron. Soil Sci.* 62, 299–315. doi: 10.1080/03650340.2015.1048235

Ali, L. G., Nulit, R., Ibrahim, M. H., and Yien, C. Y. S. (2021). Efficacy of KNO3, SiO2 and SA priming for improving emergence, seedling growth and antioxidant enzymes of rice (Oryza sativa), under drought. *Sci. Rep.* 11:3864. doi: 10.1038/s41598-021-83434-3

Arafa, S. A., Attia, K. A., Niedbała, G., Piekutowska, M., Alamery, S., Abdelaal, K., et al. (2021). Seed priming boost adaptation in pea plants under drought stress. *Plants* 10:2201. doi: 10.3390/plants10102201

Ashraf, M., and Foolad, M. R. (2005). Pre-sowing seed treatment—a shotgun approach to improve germination, plant growth, and crop yield under saline and non-saline conditions. *Adv. Agron.* 88, 223–271. doi: 10.1016/S0065-2113(05)88006-X

Azeem, M., Iqbal, N., Kausar, S., Javed, M. T., Akram, M. S., and Sajid, M. A. (2015). Efficacy of silicon priming and fertigation to modulate seedling's vigor

and ion homeostasis of wheat (Triticum aestivum L.) under saline environment. *Environ. Sci. Pollut. Res.* 22, 14367–14371. doi: 10.1007/s11356-015-4983-8

Bakhat, H. F., Bibi, N., Zia, Z., Abbas, S., Hammad, H. M., Fahad, S., et al. (2018). Silicon mitigates biotic stresses in crop plants: a review. *Crop Prot.* 104, 21–34. doi: 10.1016/j.cropro.2017.10.008

Balmer, A., Pastor, V., Gamir, J., Flors, V., and Mauch-Mani, B. (2015). The 'prime-ome': towards a holistic approach to priming. *Trends Plant Sci.* 20, 443–452. doi: 10.1016/j.tplants.2015.04.002

Bäurle, I. (2018). Can't remember to forget you: chromatin-based priming of somatic stress responses. *Semin. Cell Dev. Biol.* 83, 133–139. doi: 10.1016/j.semcdb.2017.09.032

Bäurle, I., and Trindade, I. (2020). Chromatin regulation of somatic abiotic stress memory. *J. Exp. Bot.* 71, 5269–5279. doi: 10.1093/jxb/eraa098

Becker, M., Ngo, N. S., and Schenk, M. K. A. (2020). Silicon reduces the iron uptake in rice and induces iron homeostasis related genes. *Sci. Rep.* 10:5079. doi: 10.1038/s41598-020-61718-4

Bityutskii, N., Pavlovic, J., Yakkonen, K., Maksimoviæ, V., and Nikolic, M. (2014). Contrasting effect of silicon on iron, zinc and manganese status and accumulation of metal-mobilizing compounds in micronutrient-deficient cucumber. *Plant Physiol. Biochem.* 74, 205–211. doi: 10.1016/j.plaphy.2013.11.015

Carrasco-Gil, S., Rodríguez-Menéndez, S., Fernández, B., Pereiro, R., de la Fuente, V., and Hernandez-Apaolaza, L. (2018). Silicon induced Fe deficiency affects Fe, Mn, Cu and Zn distribution in rice (Oryza sativa L.) growth in calcareous conditions. *Plant Physiol. Biochem.* 125, 153–163. doi: 10.1016/j.plaphy.2018.01.033

Chakma, R., Saekong, P., Biswas, A., Ullah, H., and Datta, A. (2021). Growth, fruit yield, quality, and water productivity of grape tomato as affected by seed priming and soil application of silicon under drought stress. *Agric. Water Manage.* 256:107055. doi: 10.1016/j.agwat.2021.107055

Chen, K., and Arora, R. (2011). Dynamics of the antioxidant system during seed osmopriming, post-priming germination, and seedling establishment in Spinach (Spinacia oleracea). *Plant Sci.* 180, 212–220. doi: 10.1016/j.plantsci.2010.08.007

Chmielowska, J., Veloso, J., Gutiérrez, J., Silvar, C., and Díaz, J. (2010). Cross-protection of pepper plants stressed by copper against a vascular pathogen is accompanied by the induction of a defence response. *Plant Sci.* 178, 176–182. doi: 10.1016/j.plantsci.2009.11.007

Chun, H. J., Baek, D., Cho, H. M., Jung, H. S., Jeong, M. S., Jung, W.-H., et al. (2019). Metabolic adjustment of Arabidopsis root suspension cells during adaptation to salt stress and mitotic stress memory. *Plant Cell Physiol.* 60, 612–625. doi: 10.1093/pcp/pcy231

Coskun, D., Deshmukh, R., Sonah, H., Menzies, J. G., Reynolds, O., Ma, J. F., et al. (2019). The controversies of silicon's role in plant biology. *New Phytol.* 221, 67–85. doi: 10.1111/nph.15343

Deshmukh, R. K., Vivancos, J., Guérin, V., Sonah, H., Labbé, C., Belzile, F., et al. (2013). Identification and functional characterization of silicon transporters in soybean using comparative genomics of major intrinsic proteins in *Arabidopsis* and rice. *Plant Mol. Biol.* 83, 303–315. doi: 10.1007/s11103-013-0087-3

Di Girolamo, G., and Barbanti, L. (2012). Treatment conditions and biochemical processes influencing seed priming effectiveness. *Ital. J. Agron.* 7:25. doi: 10.4081/ija.2012.e25

Ding, Y., Fromm, M., and Avramova, Z. (2012). Multiple exposures to drought "train" transcriptional responses in Arabidopsis. *Nat. Commun.* 3:740. doi: 10.1038/ncomms1732

Farooq, M. A., Detterbeck, A., Clemens, S., and Dietz, K.-J. (2016). Silicon-induced reversibility of cadmium toxicity in rice. *J. Exp. Bot.* 67, 3573–3585. doi: 10.1093/jxb/erw175

Farooq, M., Usman, M., Nadeem, F., ur Rehman, H., Wahid, A., Basra, S. M. A., et al. (2019). Seed priming in field crops: potential benefits, adoption and challenges. *Crop Pasture Sci.* 70, 731–771. doi: 10.1071/CP18604

Filippou, P., Antoniou, C., Yelamanchili, S., and Fotopoulos, V. (2012). NO loading: efficiency assessment of five commonly used application methods of sodium nitroprusside in Medicago truncatula plants. *Plant Physiol. Biochem.* 60, 115–118. doi: 10.1016/j.plaphy.2012.07.026

Finch-Savage, W. E., and Bassel, G. W. (2016). Seed vigour and crop establishment: extending performance beyond adaptation. *J. Exp. Bot.*67, 567–591. doi: 10.1093/jxb/erv490

Fojtova, M. (2002). Recovery of tobacco cells from cadmium stress is accompanied by DNA repair and increased telomerase activity. *J. Exp. Bot.* 53, 2151–2158. doi: 10.1093/jxb/erf080

Friedrich, T., Faivre, L., Bäurle, I., and Schubert, D. (2019). Chromatin-based mechanisms of temperature memory in plants: chromatin-based temperature memory in plants. *Plant Cell Environ.* 42, 762–770. doi: 10.1111/pce.13373

Gama, F., Saavedra, T., da Silva, J. P., Miguel, M. G., de Varennes, A., Correia, P. J., et al. (2016). The memory of iron stress in strawberry plants. *Plant Physiol. Biochem.* 104, 36–44. doi: 10.1016/j.plaphy.2016.03.019

Gonzalo, M. J., Lucena, J. J., and Hernández-Apaolaza, L. (2013). Effect of silicon addition on soybean (Glycine max) and cucumber (Cucumis sativus) plants grown under iron deficiency. *Plant Physiol. Biochem.* 70, 455–461. doi: 10.1016/j.plaphy.2013.06.007

Hameed, A., Farooq, T., Hameed, A., and Sheikh, M. A. (2021). Silicon-mediated priming induces acclimation to mild water-deficit stress by altering physio-biochemical attributes in wheat plants. *Front. Plant Sci.* 12:625541. doi: 10.3389/fpls.2021.625541

Hatami, M., Khanizadeh, P., Bovand, F., and Aghaee, A. (2021). Silicon nanoparticle-mediated seed priming and *Pseudomonas* spp. inoculation augment growth, physiology and antioxidant metabolic status in Melissa officinalis L. plants. *Ind. Crops Prod.* 162:113238. doi: 10.1016/j.indcrop.2021.113238

Hernandez-Apaolaza, L., Escribano, L., Zamarreño, A. M., Garcia-Mina, J. M., Cano, C., and Carrasco-Gil, C. (2020). Root silicon addition induces Fe deficiency in cucumber plants, but facilitates their recovery after Fe resupply. A comparison with Si foliar sprays. *Front. Plant Sci.* 11:580552. doi: 10.3389/fpls.2020.580552

Hilker, M., Schwachtje, J., Baier, M., Balazadeh, S., Bäurle, I., Geiselhardt, S., et al. (2016). Priming and memory of stress responses in organisms lacking a nervous system: priming and memory of stress responses. *Biol. Rev.* 91, 1118–1133. doi: 10.1111/brv.12215

Holubek, R., Deckert, J., Zinicovscaia, I., Yushin, N., Vergel, K., Frontasyeva, M., et al. (2020). The recovery of soybean plants after short-term cadmium stress. *Plants* 9:782. doi: 10.3390/plants9060782

Hossain, M. A., Bhattacharjee, S., Armin, S.-M., Qian, P., Xin, W., Li, H.-Y., et al. (2015). Hydrogen peroxide priming modulates abiotic oxidative stress tolerance: insights from ROS detoxification and scavenging. *Front. Plant Sci.* 6:420. doi: 10.3389/fpls.2015.00420

Huot, B., Yao, J., Montgomery, B. L., and He, S. Y. (2014). Growth–defense tradeoffs in plants: a balancing act to optimize fitness. *Mol. Plant* 7, 1267–1287. doi: 10.1093/mp/ssu049

Hussain, A., Rizwan, M., Ali, Q., and Ali, S. (2019). Seed priming with silicon nanoparticles improved the biomass and yield while reduced the oxidative stress and cadmium concentration in wheat grains. *Environ. Sci. Pollut. Res.* 26, 7579–7588. doi: 10.1007/s11356-019-04210-5

Ibrahim, E. A. (2016). Seed priming to alleviate salinity stress in germinating seeds. *J. Plant Physiol.* 192, 38–46. doi: 10.1016/j.jplph.2015.12.011

Janmohammadi, M., and Sabaghnia, N. (2015). Effect of pre-sowing seed treatments with silicon nanoparticles on germinability of sunflower (Helianthus Annuus). *Bot. Lith.* 21, 13–21. doi: 10.1515/botlit-2015-0002

Kim, J.-M., To, T. K., Ishida, J., Morosawa, T., Kawashima, M., Matsui, A., et al. (2008). Alterations of lysine modifications on the histone H3 N-tail under drought stress conditions in *Arabidopsis thaliana*. *Plant Cell Physiol.* 49, 1580–1588. doi: 10.1093/pcp/pcn133

Kubala, S., Garnczarska, M., Wojtyla, Ł, Clippe, A., Kosmala, A., Żmieńko, A., et al. (2015). Deciphering priming-induced improvement of rapeseed (Brassica napus L.) germination through an integrated transcriptomic and proteomic approach. *Plant Sci.* 231, 94–113. doi: 10.1016/j.plantsci.2014.11.008

Kumaraswamy, R. V., Saharan, V., Kumari, S., Chandra Choudhary, R., Pal, A., Sharma, S. S., et al. (2021). Chitosan-silicon nanofertilizer to enhance plant growth and yield in maize (Zea mays L.). *Plant Physiol. Biochem.* 159, 53–66. doi: 10.1016/j.plaphy.2020.11.054

Leuendorf, J. E., Frank, M., and Schmülling, T. (2020). Acclimation, priming and memory in the response of *Arabidopsis thaliana* seedlings to cold stress. *Sci. Rep.* 10:689. doi: 10.1038/s41598-019-56797-x

Li, P., Yang, H., Wang, L., Liu, H., Huo, H., Zhang, C., et al. (2019). Physiological and transcriptome analyses reveal short-term responses and formation of memory under drought stress in rice. *Front. Genet.* 10:55. doi: 10.3389/fgene.2019.00055

Liu, D., Liu, M., Liu, X.-L., Cheng, X.-G., and Liang, Z.-W. (2018). Silicon priming created an enhanced tolerance in alfalfa (Medicago sativa L.) seedlings in response to high alkaline stress. *Front. Plant Sci.* 9:716. doi: 10.3389/fpls.2018.00716

Lozano-González, J. M., Valverde, C., Hernández, C. D., Martin-Esquinas, A., and Hernández-Apaolaza, L. (2021). Beneficial effect of root or foliar silicon applied to cucumber plants under different zinc nutritional statuses. *Plants* 10:2602. doi: 10.3390/plants10122602

Ma, J. F., and Yamaji, N. (2006). Silicon uptake and accumulation in higher plants. *Trends Plant Sci.* 11, 392–397. doi: 10.1016/j.tplants.2006.06.007

Marcos, F. C. C., Silveira, N. M., Mokochinski, J. B., Sawaya, A. C. H. F., Marchiori, P. E. R., Machado, E. C., et al. (2018). Drought tolerance of sugarcane is improved by previous exposure to water deficit. *J. Plant Physiol.* 223, 9–18. doi: 10.1016/j.jplph.2018.02.001

Martín-Esquinas, A., and Hernández-Apaolaza, L. (2021). Rice responses to silicon addition at different Fe status and growth pH. Evaluation of ploidy changes. *Plant Physiol. Biochem.* 163, 296–307. doi: 10.1016/j.plaphy.2021.04.012

Mitani-Ueno, N., and Ma, J. F. (2021). Linking transport system of silicon with its accumulation in different plant species. *Soil Sci. Plant Nutr.* 67, 10–17. doi: 10.1080/00380768.2020.1845972

Nikolic, D. B., Nesic, S., Bosnic, D., Kostic, L., Nikolic, M., and Samardzic, J. T. (2019). Silicon alleviates iron deficiency in barley by enhancing expression of strategy II genes and metal redistribution. *Front. Plant Sci.* 10:416. doi: 10.3389/fpls.2019.00416

O'Hara, L. E., Paul, M. J., and Wingler, A. (2013). How do sugars regulate plant growth and development? new insight into the role of trehalose-6-phosphate. *Mol. Plant* 6, 261–274. doi: 10.1093/mp/sss120

Pascual, M. B., Echevarria, V., Gonzalo, M. J., and Hernández-Apaolaza, L. (2016). Silicon addition to soybean (Glycine max L.) plants alleviate zinc deficiency. *Plant Physiol. Biochem.* 108, 132–138. doi: 10.1016/j.plaphy.2016.07.008

Pastor, V., Balmer, A., Gamir, J., Flors, V., and Mauch-Mani, B. (2014). Preparing to fight back: generation and storage of priming compounds. *Front. Plant Sci.* 5:295. doi: 10.3389/fpls.2014.00295

Pestana, M., Correia, P. J., Saavedra, T., Gama, F., Abadía, A., and de Varennes, A. (2012). Development and recovery of iron deficiency by iron resupply to roots or leaves of strawberry plants. *Plant Physiol. Biochem.* 53, 1–5. doi: 10.1016/j.plaphy.2012.01.001

Qin, M., Li, X., Tang, S., Huang, Y., Li, L., and Hu, B. (2021). Expression of AhATL1, an ABA transport factor gene from peanut, is affected by altered memory gene expression patterns and increased tolerance to drought stress in *Arabidopsis*. *Int. J. Mol. Sci.* 22:3398. doi: 10.3390/ijms22073398

Savvides, A., Ali, S., Tester, M., and Fotopoulos, V. (2016). Chemical priming of plants against multiple abiotic stresses: mission possible? *Trends Plant Sci.* 21, 329–340. doi: 10.1016/j.tplants.2015.11.003

Secco, D., Wang, C., Shou, H., Schultz, M. D., Chiarenza, S., Nussaume, L., et al. (2015). Stress induced gene expression drives transient DNA methylation changes at adjacent repetitive elements. *eLife* 4:e09343. doi: 10.7554/eLife.09343

Soeda, Y., Konings, M. C., Vorst, O., van Houwelingen, A. M., Stoopen, G. M., Maliepaard, C. A., et al. (2005). Gene expression programs during brassica oleracea seed maturation, osmopriming, and germination are indicators of progression of the germination process and the stress tolerance level. *Plant Physiol.* 137, 354–368. doi: 10.1104/pp.104.051664

Sokol, A., Kwiatkowska, A., Jerzmanowski, A., and Prymakowska-Bosak, M. (2007). Up-regulation of stress-inducible genes in tobacco and *Arabidopsis* cells in response to abiotic stresses and ABA treatment correlates with dynamic changes in histone H3 and H4 modifications. *Planta* 227, 245–254. doi: 10.1007/s00425-007-0612-1

Soundararajan, P., Manivannan, A., Cho, Y. S., and Jeong, B. R. (2017). Exogenous supplementation of silicon improved the recovery of hyperhydric shoots in Dianthus caryophyllus L. by stabilizing the physiology and protein expression. *Front. Plant Sci.* 8:738. doi: 10.3389/fpls.2017.00738

Srivastava, A. K., Suresh Kumar, J., and Suprasanna, P. (2021). Seed 'primeomics': plants memorize their germination under stress. *Biol. Rev.* 96, 1723–1743. doi: 10.1111/brv.12722

Su, T., Li, X., Yang, M., Shao, Q., Zhao, Y., Ma, C., et al. (2020). Autophagy: an intracellular degradation pathway regulating plant survival and stress response. *Front. Plant Sci.* 11:164. doi: 10.3389/fpls.2020.00164

Sultan, S. E. (2000). Phenotypic plasticity for plant development, function and life history. *Trends Plant Sci.* 5, 537–542. doi: 10.1016/S1360-1385(00)01797-0

Sun, Y., Xu, J., Miao, X., Lin, X., Liu, W., and Ren, H. (2021). Effects of exogenous silicon on maize seed germination and seedling growth. *Sci. Rep.* 11:1014. doi: 10.1038/s41598-020-79723-y

Sytar, O., Kumari, P., Yadav, S., Brestic, M., and Rastogi, A. (2019). Phytohormone priming: regulator for heavy metal stress in plants. *J. Plant Growth Regul.* 38, 739–752. doi: 10.1007/s00344-018-9886-8

Thellier, M., and Lüttge, U. (2013). Plant memory: a tentative model. *Plant Biol.* 15, 1–12. doi: 10.1111/j.1438-8677.2012.00674.x

Thorne, S. J., Hartley, S. E., and Maathuis, F. J. M. (2020). Is silicon a panacea for alleviating drought and salt stress in crops? *Front. Plant Sci.* 11:1221. doi: 10.3389/fpls.2020.01221

Thirumalaikumar, V. P., Gorka, M., Schulz, K., Masclaux-Daubresse, C., Sampathkumar, A., Skirycz, A., et al. (2021). Selective autophagy regulates heat stress memory in *Arabidopsis* by NBR1-mediated targeting of HSP90.1 and ROF1. *Autophagy* 17, 2184–2199. doi: 10.1080/15548627.2020.1820778

van Hulten, M., Pelser, M., van Loon, L. C., Pieterse, C. M. J., and Ton, J. (2006). Costs and benefits of priming for defense in Arabidopsis. *Proc. Natl. Acad. Sci. U. S. A.* 103, 5602–5607. doi: 10.1073/pnas.0510213103

Virlouvet, L., Avenson, T. J., Du, Q., Zhang, C., Liu, N., Fromm, M., et al. (2018). Dehydration stress memory: gene networks linked to physiological responses during repeated stresses of *Zea mays*. *Front. Plant Sci.* 9:1058. doi: 10.3389/fpls.2018.01058

Wang, K., Liao, Y., Kan, J., Han, L., and Zheng, Y. (2015). Response of direct or priming defense against Botrytis cinerea to methyl jasmonate treatment at different concentrations in grape berries. *Int. J. Food Microbiol.* 194, 32–39. doi: 10.1016/j.ijfoodmicro.2014.11.006

Wang, W., Wang, X., Zhang, J., Huang, M., Cai, J., Zhou, Q., et al. (2020). Salicylic acid and cold priming induce late-spring freezing tolerance by maintaining cellular redox homeostasis and protecting photosynthetic apparatus in wheat. *Plant Growth Regul.* 90, 109–121. doi: 10.1007/s10725-019-00553-8

West-Eberhard, M. J. (2003). *Developmental Plasticity and Evolution*. New York, NY: Oxford University Press.

Wiszniewska, A. (2021). Priming strategies for benefiting plant performance under toxic trace metal exposure. *Plants* 10:623. doi: 10.3390/plants10040623

Yacoubi, R., Job, C., Belghazi, M., Chaibi, W., and Job, D. (2011). Toward characterizing seed vigor in alfalfa through proteomic analysis of germination and priming. *J. Proteome Res.* 10, 3891–3903. doi: 10.1021/pr101274f

Zhuo, J., Wang, W., Lu, Y., Sen, W., and Wang, X. (2009). Osmopriming-regulated changes of plasma membrane composition and function were inhibited by phenylarsine oxide in soybean seeds. *J. Integr. Plant Biol.* 51, 858–867. doi: 10.1111/j.1744-7909.2009.00861.x

Conflict of Interest: The author declares that the research was conducted in the absence of any commercial or financial relationships that could be construed as a potential conflict of interest.

Publisher's Note: All claims expressed in this article are solely those of the authors and do not necessarily represent those of their affiliated organizations, or those of the publisher, the editors and the reviewers. Any product that may be evaluated in this article, or claim that may be made by its manufacturer, is not guaranteed or endorsed by the publisher.

frontiers in Plant Science

SYSTEMATIC REVIEW
published: 02 March 2022
doi: 10.3389/fpls.2022.858804

Uncovering New Insights and Misconceptions on the Effectiveness of Phosphate Solubilizing Rhizobacteria in Plants: A Meta-Analysis

Noémie De Zutter[1,2], Maarten Ameye[1], Boris Bekaert[1], Jan Verwaeren[3], Leen De Gelder[2] and Kris Audenaert[1]*

[1] Laboratory of Applied Mycology and Phenomics (LAMP), Department of Plants and Crops, Faculty of Bioscience Engineering, Ghent University, Ghent, Belgium, [2] Laboratory of Environmental Biotechnology, Department of Biotechnology, Faculty of Bioscience Engineering, Ghent University, Ghent, Belgium, [3] Research Unit Knowledge-based Systems (KERMIT), Department of Data Analysis and Mathematical Modelling, Ghent University, Ghent, Belgium

OPEN ACCESS

Edited by:
Nicola Tomasi, University of Udine, Italy

Reviewed by:
Marco Nuti, Sant'Anna School of Advanced Studies, Italy
Sumera Yasmin, National Institute for Biotechnology and Genetic Engineering, Pakistan
Olubukola Oluranti Babalola, North-West University, South Africa

***Correspondence:**
Noémie De Zutter
noemie.dezutter@ugent.be

Specialty section:
This article was submitted to Plant Nutrition, a section of the journal Frontiers in Plant Science

Received: *20 January 2022*
Accepted: *07 February 2022*
Published: *02 March 2022*

Citation:
De Zutter N, Ameye M, Bekaert B, Verwaeren J, De Gelder L and Audenaert K (2022) Uncovering New Insights and Misconceptions on the Effectiveness of Phosphate Solubilizing Rhizobacteria in Plants: A Meta-Analysis. Front. Plant Sci. 13:858804. doi: 10.3389/fpls.2022.858804

As the awareness on the ecological impact of chemical phosphate fertilizers grows, research turns to sustainable alternatives such as the implementation of phosphate solubilizing bacteria (PSB), which make largely immobile phosphorous reserves in soils available for uptake by plants. In this review, we introduce the mechanisms by which plants facilitate P-uptake and illustrate how PSB improve the bioavailability of this nutrient. Next, the effectiveness of PSB on increasing plant biomass and P-uptake is assessed using a meta-analysis approach. Our review demonstrates that improved P-uptake does not always translate in improved plant height and biomass. We show that the effect of PSB on plants does not provide an added benefit when using bacterial consortia compared to single strains. Moreover, the commonly reported species for P-solubilization, *Bacillus* spp. and *Pseudomonas* spp., are outperformed by the scarcely implemented *Burkholderia* spp. Despite the similar responses to PSB in monocots and eudicots, species responsiveness to PSB varies within both clades. Remarkably, the meta-analysis challenges the common belief that PSB are less effective under field conditions compared to greenhouse conditions. This review provides innovative insights and identifies key questions for future research on PSB to promote their implementation in agriculture.

Keywords: phosphorus deficiency, meta-analysis, plant-bacteria interactions, plant nutrition, phosphate solubilizing bacteria

INTRODUCTION

Phosphorus (P) is vital for plant growth and development as it is an essential component in biomolecules such as nucleic acids, phospholipids, and ATP (Schachtman et al., 1998; Tian et al., 2021). For P-uptake, adult plants depend entirely on their root system to retrieve the available P from the soil as orthophosphates (Shen et al., 2011). However, due to their highly reactive

nature, orthophosphates are prone to adsorption onto mineral surfaces (e.g., clay minerals), precipitation into various salts (e.g., Ca-, Fe-, Al-, and Mn-phosphates) or immobilization into organic phosphorus (Owen et al., 2015). Additionally, the processes making P inaccessible for plants are influenced by abiotic factors such as soil pH, soil texture and aeration, soil temperature, and soil composition (Amery and Vandecasteele, 2015).

Plant Responses to P-Deficiency

As sedentary organisms, plants have developed sophisticated ways to maintain their P homeostasis when P is scarcely available in soils (Rouached et al., 2010). Several physiological responses have been reported upon P-deprivation. For example, in the light reactions of photosynthesis, low levels of phosphate lead to reduced ATP synthesis (**Figure 1A**). In the Calvin cycle, these ATP-limitations cause a reduced net CO_2 assimilation and $NADP^+$ to remain in its reduced form (NADPH) (de Bang et al., 2021). Upon P-depletion, the accumulation of phosphorylated intermediates is bypassed by channeling triosephosphate molecules to starch biosynthesis and to the accumulation of non-phosphorylated products, hence releasing phosphate (Hernández and Munné-Bosch, 2015). Additionally, other adaptive responses comprise internal P-remobilization from source leaves to sinks within the plant (**Figure 1B**). At a subcellular level, P-remobilization occurs between storage pools in vacuoles and other organelles such as chloroplasts. At the level of membrane lipids, physiological changes take place and phospholipids are replaced by galactolipids (Härtel et al., 2000; Wang et al., 2021). A last typical metabolic hallmark of P-deficiency, especially in C4 plants, is the accumulation of anthocyanins. Anthocyanins are formed in epidermal cell layers through the flavonoid metabolism upon P-deficiency and act as protectant to alleviate the photooxidative stress (**Figure 1C**; Jiang et al., 2007; Hernández and Munné-Bosch, 2015).

Besides the internal adaptation of the plant's physiology and metabolism, plants invest in the external acquisition of P from soils by optimizing their rhizosphere environment. At a macromorphological scale, modifications of the root architecture in response to low P influence the P acquisition. These adaptations include reduced primary root growth, increased lateral root development, increased development of root hairs, and formation of cluster roots (Niu et al., 2013), in which plant hormones such as auxins, ethylene, abscisic acid, and cytokinins play an important role. An increased root-to-shoot ratio allows plants to access larger volumes of the soil solution, consequently improving P-uptake (**Figure 1D**; Lynch and Brown, 2008). Additionally, at a biochemical level, the excretion of root exudates can influence the P-availability in the rhizosphere. For example, increased extracellular enzymes activity, such as phytase and acid phosphatase activity, can release P from organic substrates (Dakora and Phillips, 2002). Finally, the excretion of organic acid anions as a response to P-deficiency induces acidification in the rhizosphere, solubilizing (calcium-)P and rendering it available to plants (Hinsinger, 2001).

Rhizodeposits and Microbial Crosstalk Shape the Rhizosphere Environment

Rhizodeposits comprise (dead) plant cells, border cells, mucilage, root exudates, and volatile compounds (Tian et al., 2020), however, the proportion and amounts are dependent on plant species, variety, age, lateral position on the root, and (a)biotic conditions (Sasse et al., 2018). Rhizodeposits do not only improve P-availability, e.g., through pH-modifications or enzyme secretion, but also serve as signaling molecules that allow the plant to actively recruit bacteria and fungi from the bulk soil to the rhizosphere. The rhizosphere is a complex, carbon rich zone on the interface between the plant root and bulk soil, in which the release of rhizodeposits influences the diversity, composition, and activity of the rhizobiome (**Figure 1E**; Sasse et al., 2018; Liu et al., 2021). Anticipating (a)biotic stresses, plants actively shape their rhizobiome by exuding chemo-attractants, enhancing the root colonizing ability of certain microorganisms (Berendsen et al., 2012; Feng et al., 2019). Specifically for plants grown under P-deficiency, the release of gamma-aminobutyric acid (GABA) and carbohydrates through root exudates is stimulated. GABA has been associated with signaling in several abiotic stress responses and may act as a signaling compound in P-deprived plants (Kinnersley and Turano, 2000; Bouche and Fromm, 2004), while carbohydrates induce bacterial genes involved in chemotaxis and motility (Carvalhais et al., 2013). Once the microorganisms have reached the rhizosphere, the rhizobiome composition is not only shaped by the plant, but is influenced by mutual interactions between the members of the microbial community (Kai et al., 2016; Sasse et al., 2018).

After recruiting microorganisms to counter P-deficiency, the plant depends on those microorganisms to alleviate P-starvation (**Figure 1F**). Phosphate solubilizing bacteria (PSB) and arbuscular mycorrhizal fungi (AMF) are types of, respectively, plant growth promoting rhizobacteria (PGPR) and fungi (PGPF) which are able to solubilize P through different mechanisms, rendering P available for plants. AMF engage in a mutualistic, symbiotic partnership with plants, where the heterotrophic fungi depend on the plant for organic carbon sources, while the plant depends on the fungi for its P-supply. AMF enhance plant P-uptake primarily by expanding the mycorrhizal hyphal network, serving as an extension of the root system, to reach beyond the rhizosphere (Begum et al., 2019; Etesami et al., 2021). Despite not being included in present meta-analysis, the dual role of AMF in P-solubilization is of paramount importance: besides solubilizing P, they might interact with PSB when co-occurring in and on roots. For example, AMF provide a niche for bacteria through their extraradical hyphal network (Zhang et al., 2016). Depending on the P-availability in soils, AMF might supply the required carbon through hyphal exudates to PSB, while PSB in its turn might help AMF by supplying P (Etesami et al., 2021). However, under low P-availability, PSB and AMF might compete with one another for this nutrient (Zhang et al., 2016). Comparable to plant roots, AMF hyphae produce exudates, which in turn might alter the soil microbial community composition (Scheublin et al., 2010). For example, Nuccio et al. (2013) described that the relative abundance of *Firmicutes* in soil

was positively influenced by AMF, while the relative abundance of *Actinobacteria* was negatively influenced.

Phosphate Solubilizing Bacteria: Modes of Action

Phosphate solubilizing bacteria can release P from both inorganic and organic sources through solubilization and biochemical- and biological mineralization, respectively (Sharma et al., 2013). The modes-of-action by which microorganisms solubilize P are well documented in literature and will be briefly summarized (**Figure 1G**; Zaidi et al., 2009; Sharma et al., 2013; Alori et al., 2017; Rawat et al., 2021). Inorganic P-solubilization is mediated by organic acid production, siderophore production, H_2S-production, and metal-binding exopolysaccharides (EPS). Biochemical mineralization of organic P is regulated by three enzyme groups: non-specific phosphatases, phytases, and C-P lyases. Finally, biological mineralization of organic P comprises the release of P during substrate degradation. By rapidly immobilizing bioavailable P, PSB may serve as P-sinks, whereas upon P-release from their cells, they become a source of P to plants (Sharma et al., 2013; Raymond et al., 2021).

Apart from their inherent phosphate solubilizing mechanisms, microorganisms can also mitigate P-deficiency by influencing the plant's metabolism and hormonal pathways, for example, through the production of, or interference with phytohormones (Friesen et al., 2011; Lapsansky et al., 2016). A well-known example hereof is the bacterial production of the auxin indole-acetic acid (IAA), which provokes changes in the plant root phenotype (Nacry et al., 2005). The combination of plant- and bacterial IAA activates the auxin response factors and subsequently regulates the P-response (Friesen et al., 2011; Lim and Kim, 2013).

Summarizing, the use of PSB can both directly and indirectly influence plant health, and its nutritional status. Taking the above into account, the application of PSB in agricultural systems provides a sustainable alternative for, or a complement to, chemical P-fertilizers and has spurred many research groups to explore highly promising PSB.

Phosphate Solubilizing Bacteria: From Isolation and Selection to Application

In search for these highly promising PSB strains, the most adopted isolation and selection pipeline is a top-down strategy which comprises large scale *in vitro* screenings on selective growth media, followed by preliminary *in planta* screenings of the best performing isolates under greenhouse conditions, which finally results in small-scaled field experiments with the "top-of-the-class" isolates. There are several factors affecting the success and failure of PSB in the field, amongst which their rhizosphere competence is a critical one.

Numerous research articles have been published describing the (variable) performance of PSB in association with a host plant. Consensus on the (in)effectiveness of PSB is lacking, and a recent article critically reviews the shortcomings of PSB (Raymond et al., 2021). However, insights in the reasons behind this potential (in)effectiveness constitutes a knowledge gap in literature, demonstrating the necessity of a comprehensive literature review by means of a meta-analysis. In this study, we evaluated the effect of several variables of PSB's effectiveness on crop biomass growth (root and shoot) and P-uptake. Variation caused by the following parameters was evaluated: (1) at plant level: plant group and plant species; (2) at inoculum level: inoculum composition, application, and species distribution; and (3) at experiment level: experiment type, fertilizer treatment, and soil acidity.

METHODS

Search Strategy and Data Collection

A thorough literature research was conducted in Web Of Science using the keywords "phosphate solubilizing bacteria" (*title*) AND "plant growth" (*topic*), resulting in 253 identified records published between April 1976 and May 2021. After filtering and extracting information from relevant studies, 104 articles were retained (**Figure 2** and **Supplementary Note 1**). The meta-analysis was conducted on 506 single treatments to evaluate the effect of PSB-inoculation on plant P-uptake and shoot- and root biomass. The effect size of each treatment was calculated by means of the Hedges' g (unless indicated otherwise), which represents the standardized difference of the means between the treatment and control (Hedges, 1981). A Hedges' g of zero indicates no treatment effect is present, while a Hedges' g of 1 indicates that two groups differ by 1 standard deviation.

After removing extreme values (as defined by Tukey, 1977), data robustness and publication bias were evaluated by means of the fail-safe number (FSN) and visual inspection of funnel plots using the R-packages "*meta*" and "*metafor*" (Viechtbauer, 2010; Balduzzi et al., 2019). Different factors that might introduce variation in plant response to PSB were evaluated and the data were statistically compared at the 5% significance level by means of ANOVA analysis, followed by *post-hoc* Dunnett T3 tests.

Fail-Safe Number to Evaluate Data Robustness

To verify the robustness of the observed treatment effects, the fail-safe number was calculated as reported by Rosenberg (2005). This number represents the amount of observations displaying a non-significant treatment effect that should be added to the meta-analysis to disprove the observed effects. The fail-safe number for each effect (P-uptake and shoot- and root biomass) was calculated in RStudio V4.0.2 using the package "*meta*" (**Table 1**; Balduzzi et al., 2019).

Funnel Plots to Evaluate Publication Bias

Funnel plots were generated in RStudio V4.0.2 using the package "*meta*" in order to verify the presence of potential publication bias (i.e., whether the conclusion of a study influences the decision to publish it; Sterne and Egger, 2001; Balduzzi et al., 2019). Duval and Tweedie's (2000) trim and fill method was used to help interpret the results. In the absence of publication bias, a symmetrical distribution of the studies around the mean treatment effect will be observed when both positive and negative

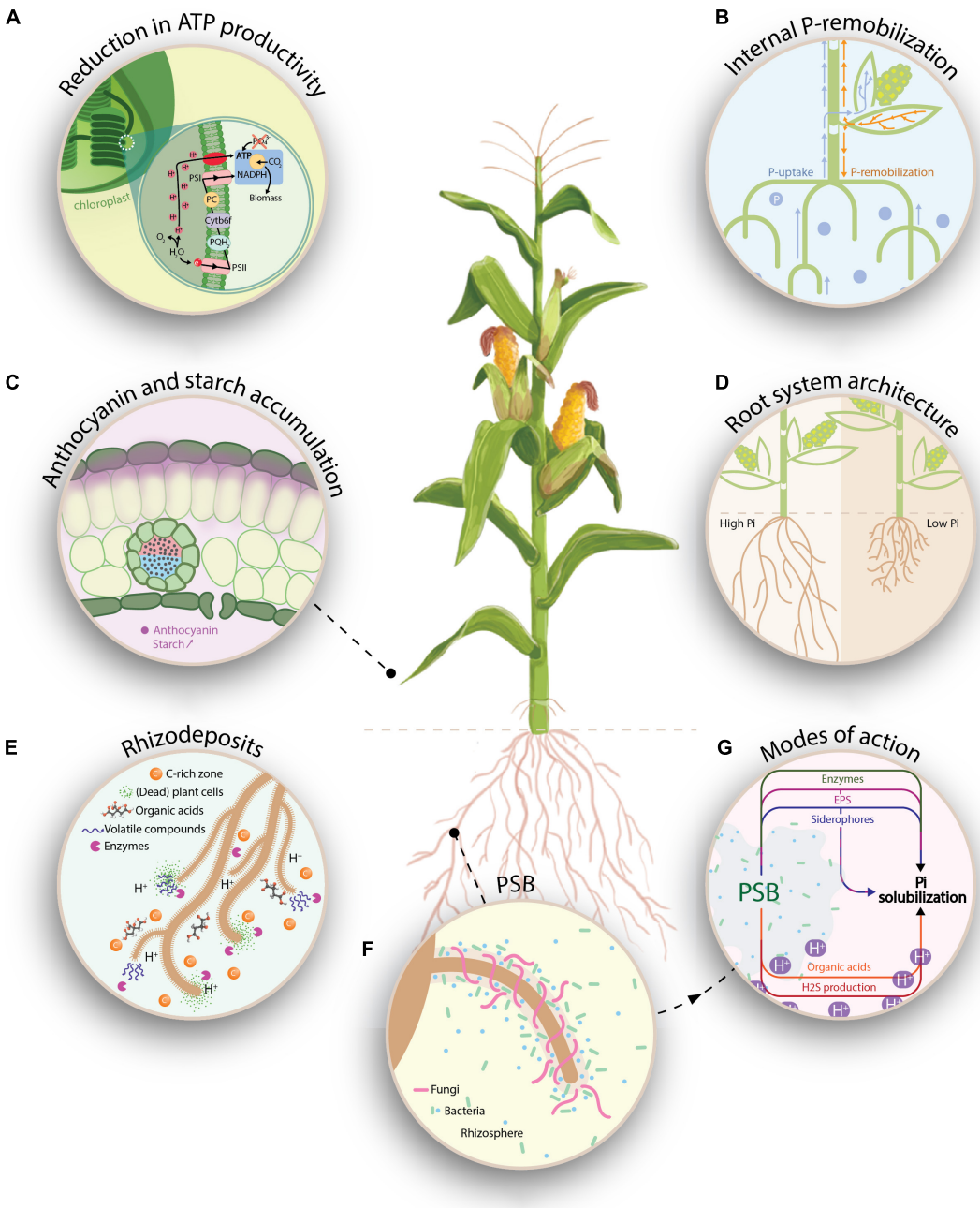

FIGURE 1 | Graphical representation on how P-deficiency affects plant physiology and morphology **(A–D)**, how it affects the rhizobiome **(E,F)** and how PSB can interfere with the bioavailable P-fraction **(G)**. **(A)** Low levels of P lead to reduced ATP synthesis, causing the accumulation of protons in the thylakoid, which results in a disruption of the linear electron flow. In the Calvin cycle, these ATP-limitations reduce the net CO_2 assimilation and cause $NADP^+$ to remain in its reduced form. **(B)** Plants can absorb P through the soil solution, which is subsequently transported through the xylem. Upon P-depletion, internal P-remobilization occurs, whereas P is translocated through the phloem from mature leaves to younger tissue. **(C)** In P-deprived plants, enhanced starch accumulation occurs in the chloroplasts as a result of redirecting triosephosphates to the starch biosynthesis in order to release P. In the epidermal layer, anthocyanins are formed through the flavonoid pathway and serve as a photo-protectants against photo-oxidative stress. **(D)** Adaptations in the plant root system under P-deficiency (e.g., reduced primary root growth and increased lateral root formation) allow plants to access a larger volume of the soil solution. **(E)** The release of rhizodeposits, which comprises of (dead) plant cells, border cells, root exudates (e.g., organic acids and enzymes) and volatile compounds causes the rhizosphere to be a nutrient (carbon) rich zone. Upon P-deficiency, specific root exudates such as GABA (gamma-aminobutyric acid) and carbohydrates are released, serving as chemo-attractants for (beneficial) PSB. **(F)** Recruitment of PSB and AMF in the rhizosphere to enhance bioavailable P, hence improving the plant's nutritional status. **(G)** Representation of potential modes of action (MOA) by which PSB can render P available for the plant. Amongst others, the production of organic acids and H2S cause an acidification of the rhizosphere environment, rendering inorganic P bioavailable. Additionally, inorganic P-solubilization can also by mediated by the release of siderophores and exopolysaccharides (EPS), which bind to metal ions (Fe^{3+} resp. Al^{3+}, Ca^{2+}, and Fe^{3+}). Finally, organic P-mineralization can be regulated by three groups of enzymes, namely, non-specific phosphatases, phytases and C-P-lyases. Inspired by de Bang et al. (2021).

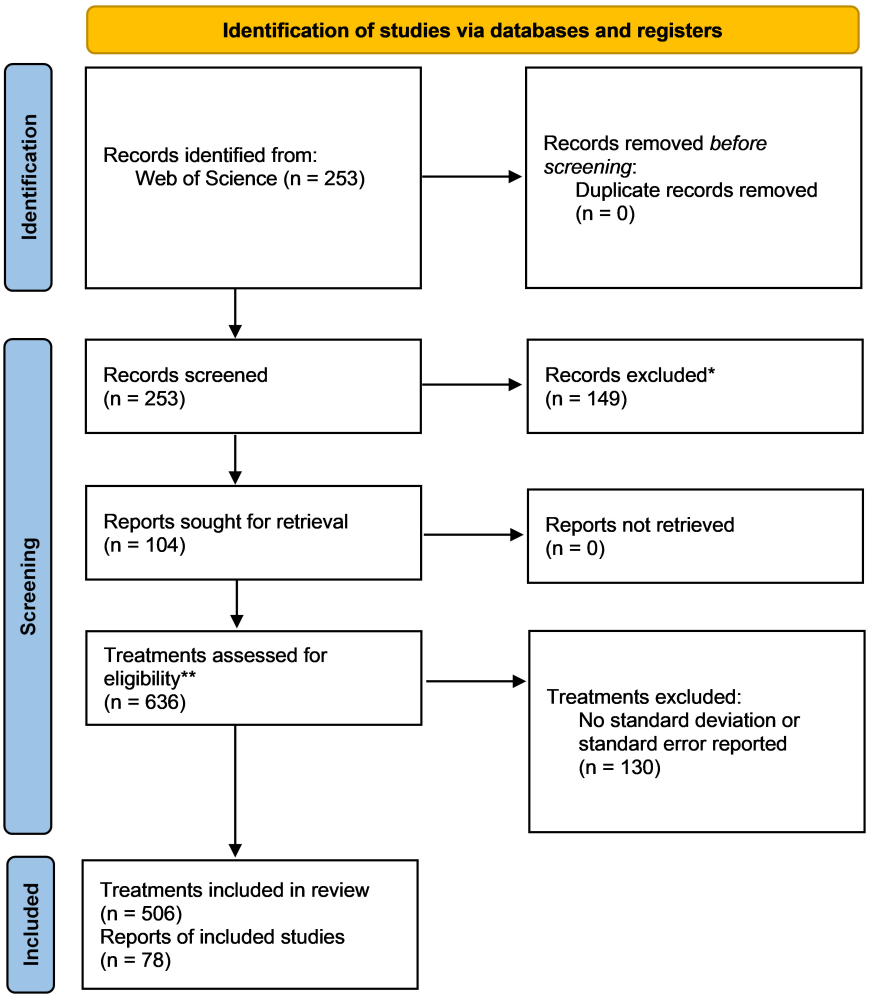

FIGURE 2 | PRISMA flow chart demonstrating the data acquisition, selection and processing pipeline used in this meta-analysis (Page et al., 2021).

effects compared to the control are expected. The funnel plots were asymmetrical for each effect (**Supplementary Figure 1**), however, in our opinion, this is by and large attributed to a lack of negative effect sizes when working with biostimulant traits. After trimming and filling the data, a rather small decrease in mean treatment effect is observed (**Supplementary Figure 2**). Combined with the high fail-safe number, we can state that the data are robust.

RESULTS

Plant Growth Promotion Is Not Always Related to Improved P-Uptake

In order to assess the *in planta* effect of highly promising PSB, plant height or biomass are often monitored. The representativeness of these parameters for the plant's P-uptake was evaluated in the present meta-analysis. To this end, the ratio of the means (P-uptake, biomass, and height) between the treatment and control plants were used (independent on the experiment size and variation). When comparing the effect of PSB on plant P-uptake versus biomass and height at full growth, many datapoints are distant from the first bisector, which refers to differences between the P-uptake and the effect on the plant's biomass or height (**Figure 3**). The PSB which caused the highest impact on shoot-biomass and height, showed little to no effect on plant P-uptake, and vice versa.

Additionally, the predictive power of the plant biomass and height is dependent on the crop type (**Supplementary Figure 3**). For example, in monocots, maize biomass is aberrant from the

TABLE 1 | Overview of the fail-safe number per effect type (P-uptake, shoot biomass, and root biomass) as determined by the Rosenberg's approach and the respective number of studies included in this meta-analysis.

Treatment	Fail-safe number	Number of studies
P-uptake	69,305	327
Shoot biomass	92,433	378
Root biomass	60,940	283

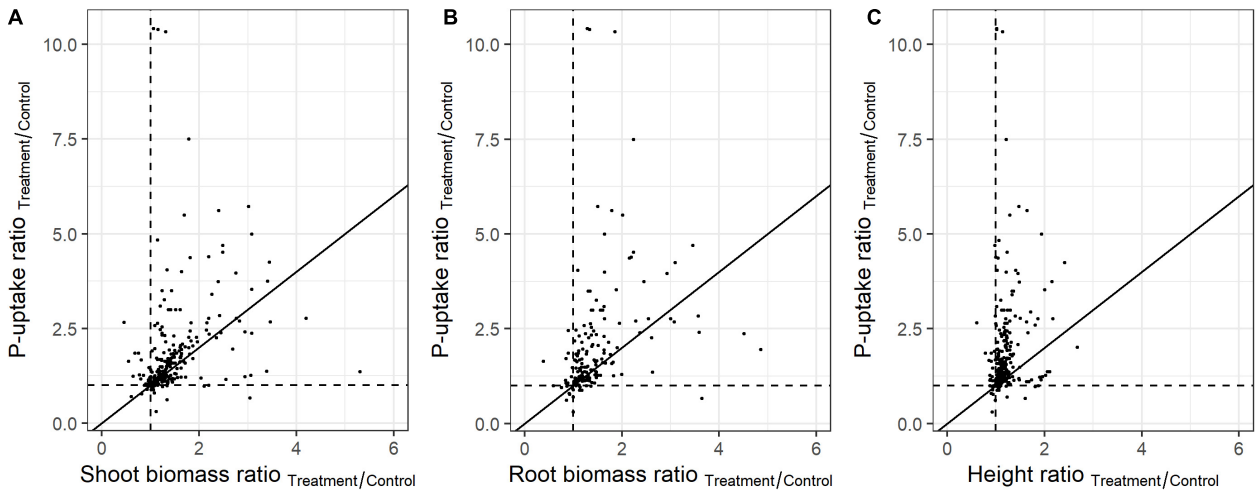

FIGURE 3 | Relationship between plant P-uptake and **(A)** shoot biomass ($n = 261$), **(B)** root biomass ($n = 190$), and **(C)** length ($n = 252$) upon bacterial inoculation. Values represent the ratio of the means (P-uptake, biomass, and length) between the treatment and control. Black lines represents the first bisector ($y = x$).

first bisector, while rice biomass is adversely affected, showing a reciprocal relationship with plant P-uptake (**Supplementary Figures 3A–C**). In eudicots, *Camellia oleifera* and Mung bean biomass are aberrant to the first bisector, while all other eudicots follow the first bisector (**Supplementary Figures 3D–F**). The predictive power of plant height proved to be limited in both monocots and eudicots (**Supplementary Figures 3C,F**).

The Application of Phosphate Solubilizing Bacteria Has Different Effects Within the Plant Families

Although P-deficiency in plants is a widespread problem, research on the use of PSB as an ecological alternative or complement to chemical fertilizers is mainly situated in (Southern-) America and Asia (**Supplementary Figure 4**). In these studies, monocotyledons are more often used as test plants than dicotyledons (311 resp. 195 studies), with maize (*Zea mays* L.) being prominently used in 25.9% of all studies (**Figure 4A**). As cereal crops account for the largest total cultivation and production area worldwide, with maize (*Zea mays* L.), rice (*Oryza sativa* L.), wheat (*Triticum aestivum* L.), and sugarcane (*Saccharum officinarum* L.) as leading crops (FAOSTAT, 2021), it is expected that they represent the majority amongst the test subjects.

The application of PSB to both monocotyledon (monocots) and dicotyledon plants (eudicots) resulted in an overall positive effect on plant P-uptake, root- and shoot biomass, albeit no significant difference was found between PSB's effectiveness on monocots and eudicots (**Figure 4B**). In addition, no differences in plant response between bacterial genera used as PSB were uncovered when comparing monocots and eudicots (data not shown). Moreover, in 92.7% of all studies, the bacterial species tested on the monocot (resp. eudicot) was also tested on an eudicot (resp. monocot) in another study. When focusing on the *Poaceae*, a clear differentiation between the plant species can be observed, with rice showing a tendency for superior P-uptake upon PSB inoculation (**Figure 4C**).

Multispecies Inocula Do Not Always Provide Added Value Over Single-Species Inocula

The primary selection of PSB is commonly done through *in vitro* screenings, in which bacteria are tested for their P-solubilizing capacity on selective growth media. Once potential PSB's are singled out, they can be applied to a host plant, either as a single-species inoculum or in combination with other (bacterial) isolates as a multispecies inoculum. Plant parameters are improved upon both single and multispecies inoculation, albeit P-uptake proved to be superior upon single species inoculation (**Figure 5A**). We identified 13 studies that tested both single isolates and combinations of those specific isolates in the same paper, or in a back-to-back paper. These records were selected, resulting in 87 single treatments (64 single-species inocula, 23 multispecies inocula). When comparing those specific cases, no significant differences in plant P-uptake were identified between single and multispecies inoculation ($p = 0.85$; **Supplementary Figure 5**).

Phosphate Solubilizing Bacteria's Effectiveness Is Influenced by the Application Method

The most adopted bacterial inoculation strategies were soil drench (41.7% of all studies), followed by seed coating (28.1%) and root dip (11.5%). Other inoculation methods (e.g., spray inoculation) accounted for less than 5% of all studies and were omitted from this particular analysis. Bacterial inoculation by means of root dip resulted in the largest increase in P-uptake and shoot biomass, followed by seed coating (**Figure 5B**). The combined application of bacteria by means of root dip and soil drench resulted in a lower P-effect compared to their individual applications.

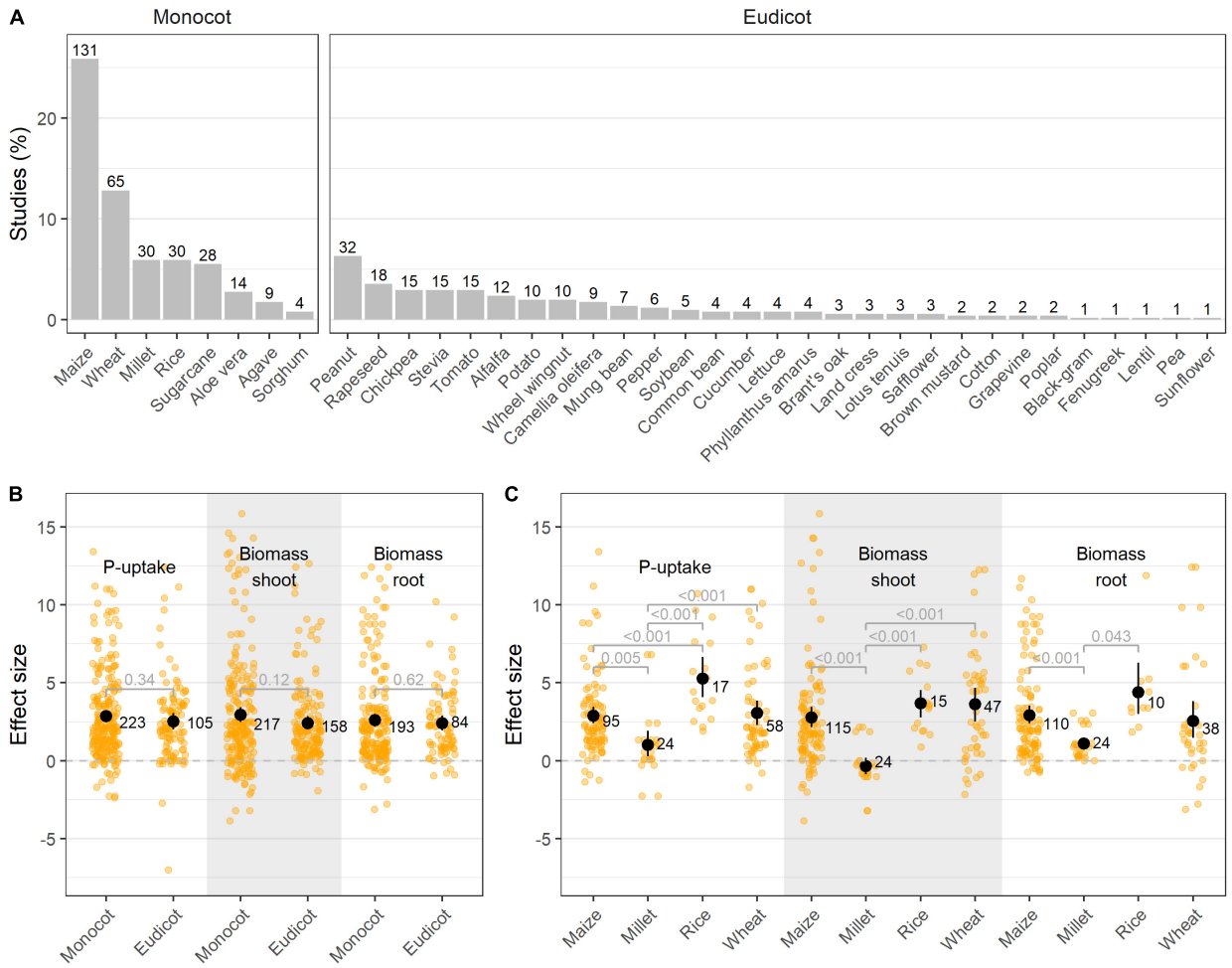

FIGURE 4 | (A) Visualization of the different crops included in this meta-analysis per group (monocotyledon vs. dicotyledon plants). Bars represent the relative frequency of the studies as opposed to the complete dataset (% studies), while absolute numbers represent the amount of observations; **(B)** Effect size on P-uptake, shoot- and root biomass upon PSB inoculation in monocot vs. dicot plants; and **(C)** Effect size on P-uptake, shoot- and root biomass upon PSB inoculation in the four most abundant monocot crops reported in this meta-analysis. Values represent the means ± 95% c.i. Statistical differences were calculated by means of ANOVA and *post-hoc* Dunnett T3 tests.

Burkholderia spp. Outperform *Bacillus* spp. and *Pseudomonas* spp. for Improved P-Uptake

Focusing on the studies using single species inocula, *Bacillus* spp. and *Pseudomonas* spp. have primarily been tested for their phosphate solubilizing capabilities (21.7% resp. 20.3%, **Figure 6A**). A pairwise comparison between the six most abundant bacterial species ($n > 10$ studies) shows that application of the scarcely implemented *Burkholderia* spp. outperforms the more commonly reported *Bacillus* spp. and *Pseudomonas* spp. for increased plant P-uptake, while the application of *Enterobacter* spp. resulted in the highest increased shoot- and root biomass (**Figure 6B**). Although the formulation and storage of *Bacillus* spp. is straightforward due to their sporulation abilities, their beneficial effect is considered ambiguous due to their poor root colonizing capacity (Gao et al., 2016). However, in this meta-analysis the beneficial effect of *Bacillus* spp. was confirmed, displaying positive effects on plant P-uptake, shoot- and root biomass in resp. 92, 88, and 89% of all studies using *Bacillus* spp.

Phosphate Solubilizing Bacteria Are Effective Under Field Conditions

The majority of the studies in this meta-analysis were conducted in pot trials under greenhouse conditions (90% of all studies). When comparing pot and field trials, our analysis of the data does not support the generally accepted notion that PSB are less effective when tested in the field (**Figure 7A**). To investigate this, a subset of papers were selected in which the same isolate(s) were tested in both pot- and field trials. Application of these isolates resulted in similar effect sizes in the field trials as in their respective pot trials (**Supplementary Figure 6**). However, care should be taken when interpreting the increased performance on the field versus in pots (**Figure 7A**), as a bias toward isolates which perform well in pot trials are selected for field trials.

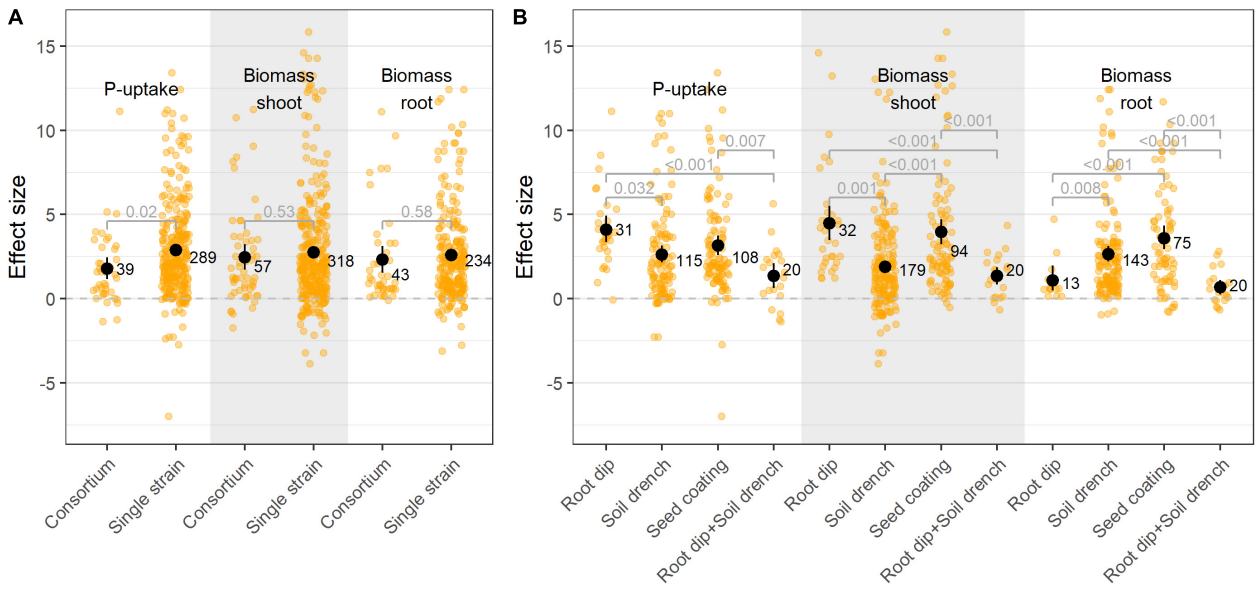

FIGURE 5 | (A) Effect size on P-uptake, shoot- and root biomass upon single and multiple species inoculation; and **(B)** Effect size on P-uptake, shoot- and root biomass upon bacterial inoculation by means of root dip, soil drench, seed coating, and combined root dip and soil drench. Values (black dots) represent the means ± 95% c.i. Orange jitter represent the distribution of all datapoints. Statistical differences were calculated by means of ANOVA and *post-hoc* Dunnett T3 tests.

Additionally, the effectiveness of bacterial isolates in greenhouse or field experiments was not influenced by the application of phosphate fertilizer (**Figure 7B**).

Soil pH Proves to Be an Important Factor for Phosphate Solubilizing Bacteria's Effectiveness

P-availability and P-type are influenced by soil pH. In acidic soils, the majority of P is precipitated into iron- and aluminum phosphates, while in alkaline soils P is primary fixed by calcium (Penn and Camberato, 2019). In present meta-analysis, research was mainly situated in low pH-zones (**Supplementary Figures 4, 7**), however, the majority of the trials were conducted under neutral to alkaline conditions (75% of all studies in which pH was indicated; $n_{all} = 369$). Additionally, when reported, the majority of the preliminary *in vitro* screenings were also conducted in neutral to alkaline medium, supplemented with tri-calcium phosphate (TCP, 65%). PSB's effectiveness proved to be dependent on the pH of the soil, with bacteria introduced in alkaline soils showing better treatment effects (**Figure 7C**). This effect proved to be independent on the crop type, bacterial species or P-fertilizer, as within resp. specific crop types, bacterial species and P-fertilizer groups, the same effects were observed.

DISCUSSION

Plant Growth Promotion Is Not Always Related to Improved P-Uptake

The relevance of plant height, shoot and root biomass as proxies for plant P-uptake was evaluated for all studies included in this meta-analysis. The use of these criteria should be handled with care, since their predictive power dependent on the crop type. Plant relative height proved to be an ineffective parameter for the assessment of a crop's P-status, both in monocots and eudicots. Shoot biomass proved to be a good proxy for most of the eudicots, but not for monocots such as maize and rice. This might be the result of so called "excess-uptake" or "luxury uptake," which means that plant P-uptake reached beyond the essential uptake necessary for immediate growth (Ågren, 2008; Sims et al., 2012; Gagnon et al., 2020). This is an important observation to take into account when selecting high potential PSB for pot or field trials, since biomass is recurrently chosen as the indicative parameter to evaluate a plant's P-status (36.8% of all studies in present meta-analysis). Recently, research has also turned to the non-destructive estimation of plant health and plant nutrient status. The use of multi- and hyperspectral imaging for the monitoring and estimation of a crop's P-status is an uprising technique and could be used as a tool to better non-destructively assess the claim of P solubilization instead of plant growth promotion (Gitelson et al., 2009; Rouphael et al., 2018; De Zutter et al., 2021).

Differential Responses Between Plant Families and Their Growth Conditions Complicate the Use of a Generalistic Inoculum

It is well described in literature that the P-status of plants is tightly regulated through plant hormone crosstalk, and although sharing several branches, these plant hormone regulatory networks differ considerably in monocots and eudicots (Ha and Tran, 2014; Nelissen et al., 2016; Chen et al., 2018). Despite the

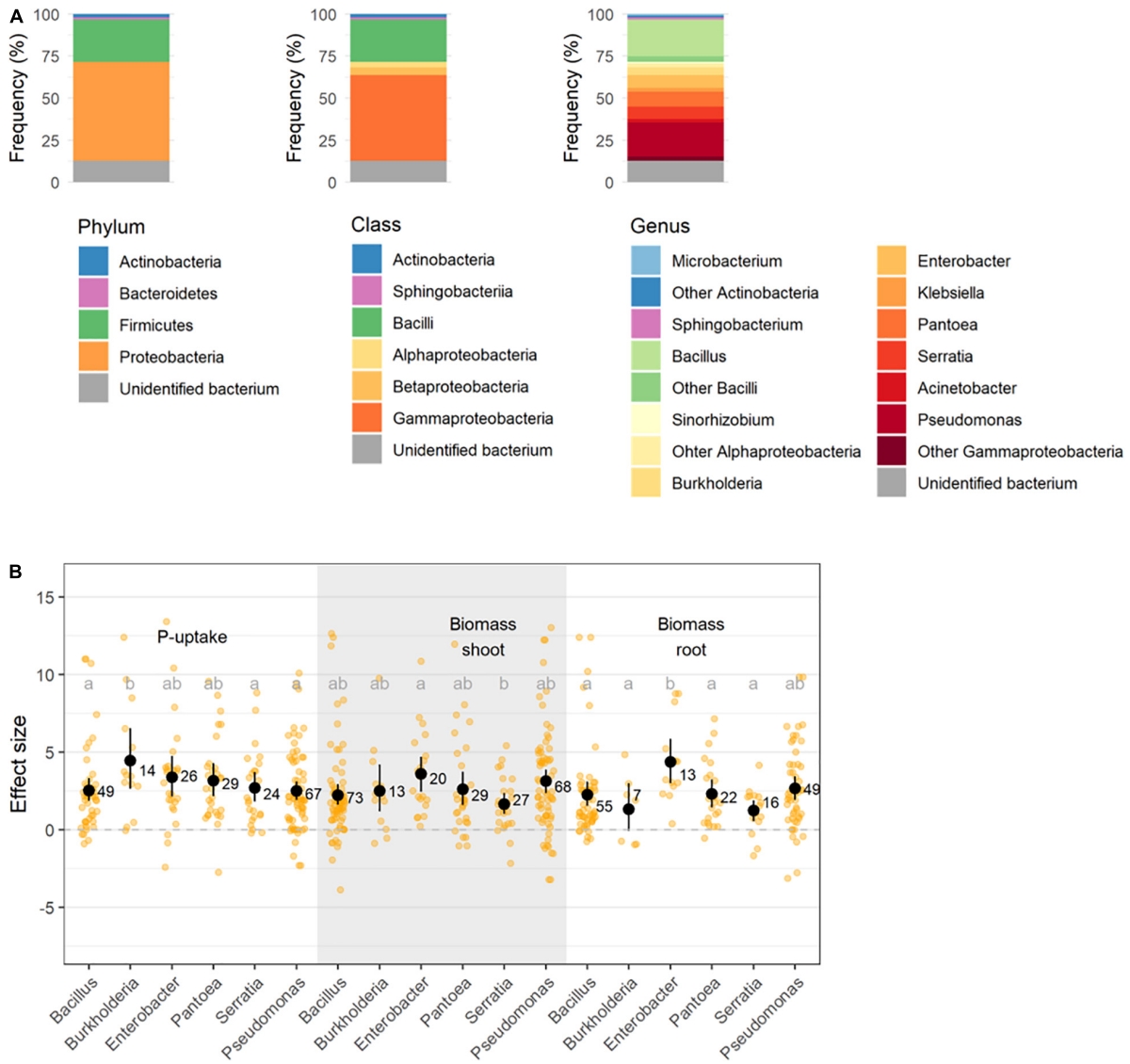

FIGURE 6 | (A) Representation of bacterial phyla, classes, and genera used in this meta-analysis; and **(B)** Effect size on P-uptake, shoot- and root biomass upon inoculation with the six most abundant bacterial genera. Values represent the means ± 95% c.i. Statistical differences were calculated by means of ANOVA and *post-hoc* Dunnett T3 tests.

regulatory differences regarding root development, the response to exogenously applied PSB is not significantly different between both plant clades.

The apparently well conserved trait of plants to react to PSB activity merges with the holobiont theorem, which states that plants as organisms from an evolutionary perspective have always been dependent on their interaction with microorganisms (Lyu et al., 2021a). A major constraint in the transition from aquatic to terrestrial plant life, was the inadequate water and nutrient supply. To meet these requirements and facilitate nutrient acquisition, plants engaged in symbiotic relationships with soil microorganisms such as PSB (Lyu et al., 2021b). The co-evolution between a plant and its microbiome has led to a highly structured rhizosphere characterized by an interactive rhizobiome, in which cross-kingdom communication results in improved performance for both partners (Wallenstein, 2017).

Within the monocots, rice plants experienced the largest increase in plant P-uptake upon bacterial inoculation. A possible explanation for this phenomenon lies within the cultivation method of rice. Rice is often grown in flooded wetlands called paddy soils, which provides a feasible environment for both aerobic and (facultative) anaerobic bacteria (Suzuki, 1967). Additionally, in these soils, P is generally adsorbed onto iron- and aluminum minerals or precipitated into iron- and aluminum phosphates (Yan et al., 2017). Under anaerobic conditions, bacteria capable of performing sulfur reduction (SO_4^{2-} to H_2S) might contribute to the release of P from iron phosphate present in the paddy soils (Sharma et al., 2013). When selecting PSB for

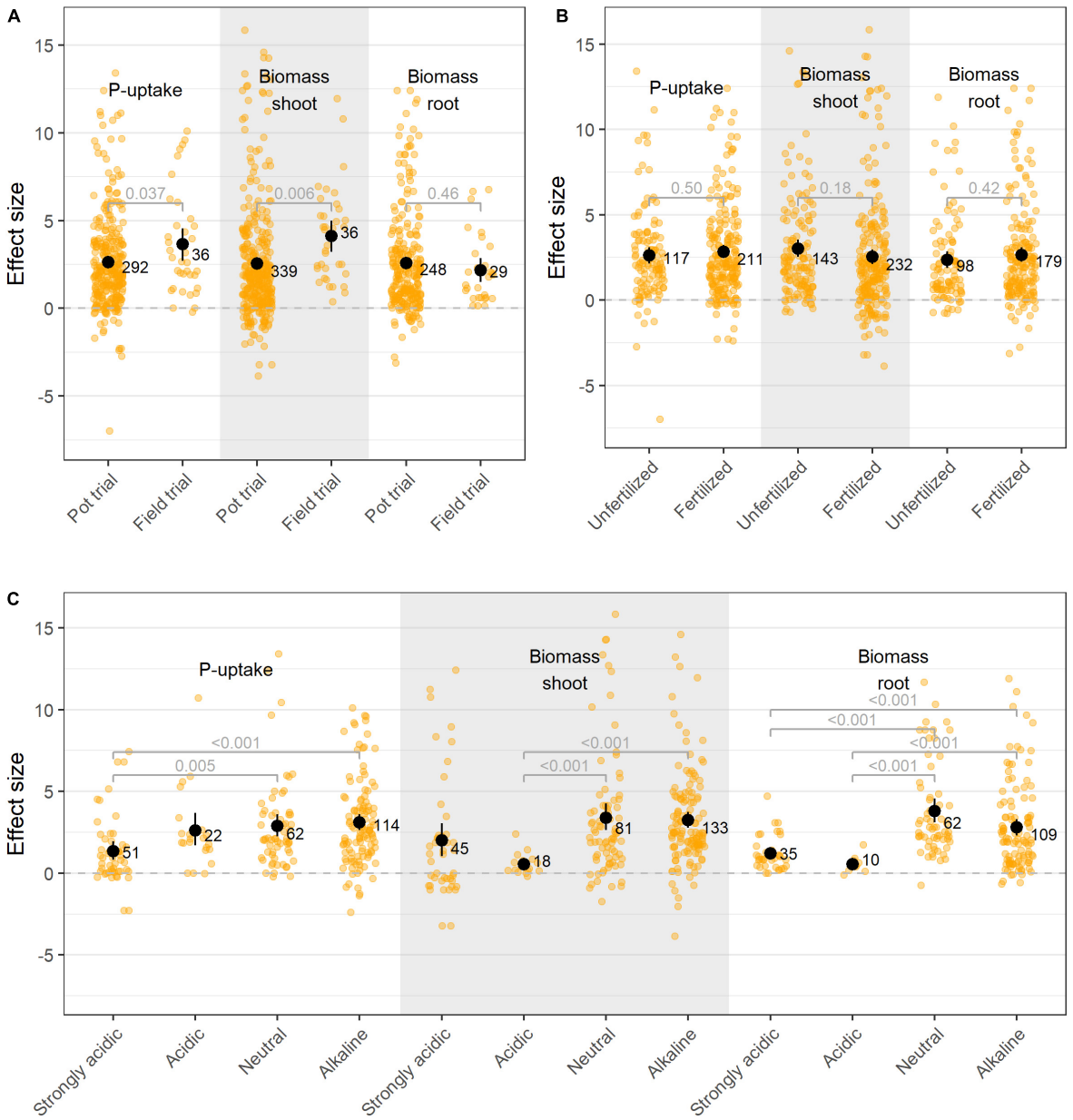

FIGURE 7 | (A) Effect size on P-uptake, shoot- and root biomass upon bacterial inoculation applied in pot- and field trials; **(B)** Effect size on P-uptake, shoot- and root biomass upon bacterial inoculation on plants grown in fertilized versus unfertilized soil; and **(C)** Effect size on P-uptake, shoot- and root biomass upon bacterial inoculation on plants under different soil acidities. Values represent the means ± 95% c.i. Statistical differences were calculated by means of ANOVA and *post-hoc* Dunnett T3 tests.

plant growth promoting trials, not only the bacteria and host plant, but also the intended environment should therefore be taken into account.

The Use of a Multi-Species Inoculum Should Be Well Considered and Designed

Multi-species microbial consortia are being increasingly used in agriculture with the aim of plant growth promotion. They are composed of a bacterial mixture, in which each bacterium might consist of a different mechanism to promote plant growth and health (Santos et al., 2019). However, in this meta-analysis, the effect of multi-species inoculation on plant P-uptake, shoot- and root biomass was not higher than that of single species inoculation. An important consideration is that the research included in this meta-analysis combined only two to four bacterial taxa, in which the rationale to pool these strains was limited to their individual positive effect. Notwithstanding the efforts of research to develop multispecies inocula, it is essential to

recognize the possible trade-offs (e.g., competition for nutrients) within these consortia. Therefore, the combination of several microorganisms should be designed with care.

Recent studies concerning synthetic microbial communities (SynComs) aim to expand the current application strategies of single and multispecies inocula (de Souza et al., 2020; Marín et al., 2021). SynComs are composed of PGPR species and strengthened with both accessory and keystone species to obtain a robust diversity and maintain the functional stability, respectively (Sánchez-Cañizares et al., 2017). These synthetic communities must form associations with the rest of the microbiome to mimic the interactive rhizobiome and function in the plant holobiont. We suggest that further research concerning PSB should explore the formulation of these types of SynComs anticipate competitive exclusion in the rhizosphere (Pandey et al., 2012; Rubin et al., 2017) and to establish long-term stable survival of the SynCom members in the soil.

Bearing in mind the added values of SynComs, the combined application of AMF and PSB should also be explored. It is known that AMF and (phosphate solubilizing) bacteria can engage in synergistic interactions to improve the plant's nutrient acquisition (Artursson et al., 2006). However, the functional mechanisms behind these interactions should be investigated before mixing AMF with specific microorganisms. Importantly, apart from abovementioned synergistic engagements, AMF can also negatively influence certain bacterial populations (i.e., *Actinobacteria*; Nuccio et al., 2013). Anticipating these interactions, it may be interesting to investigate the residing microbiome in the intended farmlands and adjust SynComs to be more compatible with this native microbiome. This topic was not covered in the present meta-analysis as the scope of our research lies with bacteria.

Bacterial Application Is More Efficient When Directly Introduced Into the Spermosphere

The direct introduction of PSB to the roots by means of seed coating and root dip resulted in the largest increase in plant P-uptake and shoot biomass. By applying microorganisms directly onto the roots, they gain the advantage for early root colonization (prior to exposure to indigenous soil microorganisms) and exploiting the rhizosphere niche. However, in practice, the formulation of a bacterial inoculant has to be cost efficient, and its application easy to handle to be widely adopted in agriculture, which is not the case for the root dip method. Additionally, inoculum formulations should be tailored toward the specific needs of the chosen microorganism(s) in the respective soil to optimize their survival. Although liquid formulations such as soil drench are easy to handle and apply, the lack of a carrier that provides protection and stabilization is a major limitation. The use of solid formulations, in which bacteria are mixed with a carrier, is more robust and bacteria are more likely to persist in the field (Herrmann and Lesueur, 2013). Microbial activity occurring in the spermosphere has long-lasting effects on plant health and development, making seed inoculation an attractive PBS-formulation method from an agricultural perspective (Berlanga-Clavero et al., 2020). Prior research confirms that PSB inoculation by means of seed coating results in larger increases in shoot biomass (Rubin et al., 2017), indicating the improved assimilation of PSB in the rhizobiome.

Implementation of High Potential Phosphate Solubilizing Bacteria Requires an Alternation in the European Legislation

In this research, the application of *Burkholderia* spp. had the largest effect on plant P-uptake, while *Enterobacter sp.* had the greatest effect on shoot biomass. The plant growth promoting and root colonizing capacity of *Burkholderia* spp. has been well documented in literature, however, the use of *Burkholderia* spp. is often restricted because of their potential hazardous nature as phytopathogens and opportunistic human pathogens (Compant et al., 2008; Eberl and Vandamme, 2016). The closely related genus *Paraburkholderia* might in this respect provide a valuable alternative for future research.

The majority of the studies focus on the application of *Bacillus* spp., which is an easy-to-use and store genus due to its sporulation. Our meta-analysis indicates that future studies should reach beyond these usual suspects. However, to this end there is a need for an altered legislation on the use of bacterial species in agriculture. According to the European Regulation (EU) 2019/1009 on biostimulants, the list of microorganisms that can currently be used as biostimulants is limited to only four species: *Azotobacter* spp., *Rhizobium* spp., *Azospirillum* spp., and mycorrhizal fungi. At a national level, other microbial species can be recognized as biostimulants once there is scientific evidence that the species ensure agronomic efficiency and do not provide a risk to the environment or to human, animal or plant health. However, the legislation hereon differs amongst the different Member States (Sundh et al., 2021). Some countries have specific authorization systems for microbial plant biostimulants, while others do not (Caradonia et al., 2019). This discrepancy has currently restricted the exploitation of a common market for (microbial) biostimulants in Europe.

Possible Pitfalls in the Current Phosphate Solubilizing Bacteria Selection Pipeline

The most adopted method for selecting high performance PSB consists of a large-scale *in vitro* screening followed by small scale greenhouse and field trials with the best performing isolates. Through this sequential selection pipeline, the majority of the selected isolates fail to deliver consistently under practical conditions, possibly due to their lack of rhizosphere competence (Chauhan et al., 2015). This strategy might also result in loss of slow growing and/or unculturable bacteria with high rhizosphere competence and high P-solubilizing capacity. In this regard, implementing the rhizosphere competence as a trait in selection and enrichment strategies has shown promising results (De Zutter et al., 2021).

The lack of performance under practical conditions is often not reported, resulting in a certain publication bias as observed in the funnel plots (**Supplementary Figures 1, 2**). This is also reflected in the P-uptake, height, shoot- and root biomass ratios (**Figure 3**), where a value of 1 represents no effect. Here, numerous datapoints are situated well above 1, which confirms that positive results are more likely to be reported than negative (no-effect) results.

A paramount concern in the first steps of the *in vitro* selection pipeline is the use of inappropriate P-sources during the isolate screenings. In the included studies in this meta-analysis, preliminary screenings were generally conducted in/on medium supplemented with tri-calcium phosphate. Given the pH dependency (and concomitant effectiveness) of PSB, this might be an important pitfall when tailoring the experiments to field trials. Therefore, the P-source used in both *in vitro* and *in planta* preliminary screenings should be a well-considered choice based on the soil physicochemical properties of the intended farmlands, rather than a choice by force of habit. In this meta-analysis, the effectiveness of PSB proved to be better in alkaline soils compared to acidic soils. Generally, in acidic soils the bio-available P-fraction is inherently higher than in alkaline soils, as the free protons in the acidic environment compete with cations for PO_4^{3-} binding positions (Barrow, 2017; Zheng et al., 2019). Since this process has similar effects as PSB's organic acid production, PSB's added value for P-solubilization is diminished. Upon increased soil pH, P is bound to Ca^{2+} or Mg^{2+}, whereas the phosphate solubilizing capacity of PSB by means of organic acid production increases.

As previously described by Bashan et al. (2013), a combination of several metal-P compounds (in tandem or together) might form an ecologically relevant alternative. Bearing in mind the pH-zones in which the research used in this meta-analysis was situated (**Supplementary Figures 4, 7**), the (combined) use of iron- and aluminum phosphate as P-sources poses a relevant representation of the field conditions. Finally, soil chemical characteristics, and particularly soil pH, are known to influence the residing microbial community composition and diversity. Although some phyla remain largely unaffected by soil pH (e.g., *Proteobacteria*), others are strongly influenced (e.g., *Actinobacteria*, *Acidobacteria,* and *Bacteroidetes*) (Lauber et al., 2008; Rousk et al., 2010).

CONCLUSION

Due to its highly reactive nature, phosphorus bio-availability is often limited and plants frequently suffer from P-deficiency. The use of PSB as a complement to phosphate fertilizers, or as an alternative of chemical fertilizers to cope with this P-deficiency is uprising. Despite the controversy on the effectiveness of PSB, this meta-analysis proves the added value of PSB in association with a host plant. Finally, future research and applications should take the soil physicochemical properties of the intended region into account, as the effectiveness of PSB is largely dependent on substrate acidity.

DATA AVAILABILITY STATEMENT

The original contributions presented in the study are included in the article/**Supplementary Material**, further inquiries can be directed to the corresponding author.

AUTHOR CONTRIBUTIONS

KA, MA, JV, LD, and ND provided the concept of the review article. ND performed the literature research, and data exploration and analyses. KA and ND prepared the manuscript. BB provided the concept and graphics of **Figure 1**. All authors revised the manuscript.

FUNDING

This project was supported by a research grant provided by the Research Foundation–Flanders (FWO), through a SB scholarship (1S01620N).

SUPPLEMENTARY MATERIAL

The Supplementary Material for this article can be found online at: https://www.frontiersin.org/articles/10.3389/fpls.2022.858804/full#supplementary-material

REFERENCES

Ågren, G. I. (2008). Stoichiometry and nutrition of plant growth in natural communities. *Annu. Rev. Ecol. Evol. Syst.* 39, 153–170.

Alori, E. T., Glick, B. R., and Babalola, O. O. (2017). Microbial phosphorus solubilization and its potential for use in sustainable agriculture. *Front. Microbiol.* 8:971. doi: 10.3389/fmicb.2017.00971

Amery, F., and Vandecasteele, B. (2015). Wat Weten We Over Fosfor En Landbouw? Deel 1 Beschikbaarheid Van Fosfor In Bodem En Bemesting. Flanders Institute for Agriculture, Fisheries and Food. ILVO Mededeling. Merelbeke: ILVO, 195.

Artursson, V., Finlay, R. D., and Jansson, J. K. (2006). Interactions between arbuscular mycorrhizal fungi and bacteria and their potential for stimulating plant growth. *Environ. Microbiol.* 8, 1–10. doi: 10.1111/j.1462-2920.2005.00942.x

Balduzzi, S., Rücker, G., and Schwarzer, G. (2019). How to perform a meta-analysis with R: a practical tutorial. *Evid. Based Ment. Health* 22, 153–160. doi: 10.1136/ebmental-2019-300117

Barrow, N. J. (2017). The effects of pH on phosphate uptake from the soil. *Plant Soil* 410, 401–410. doi: 10.1007/s11104-016-3008-9

Bashan, Y., Kamnev, A. A., and de-Bashan, L. E. (2013). Tricalcium phosphate is inappropriate as a universal selection factor for isolating and testing phosphate-solubilizing bacteria that enhance plant growth: a proposal for an alternative procedure. *Biol. Fertil. Soils* 49, 465–479. doi: 10.1007/s00374-012-0737-7

Begum, N., Qin, C., Ahanger, M. A., Raza, S., Khan, M. I., Ashraf, M., et al. (2019). Role of arbuscular mycorrhizal fungi in plant growth regulation: implications in abiotic stress tolerance. *Front. Plant Sci.* 10:1068. doi: 10.3389/fpls.2019.01068

Berendsen, R. L., Pieterse, C. M., and Bakker, P. A. (2012). The rhizosphere microbiome and plant health. *Trends Plant Sci.* 17, 478–486. doi: 10.1016/j.tplants.2012.04.001

Berlanga-Clavero, M. V., Molina-Santiago, C., de Vicente, A., and Romero, D. (2020). More than words: the chemistry behind the interactions in the plant holobiont. *Environ. Microbiol.* 22, 4532–4544. doi: 10.1111/1462-2920.15197

Bouche, N., and Fromm, H. (2004). GABA in plants: just a metabolite? *Trends Plant Sci.* 9, 110–115. doi: 10.1016/j.tplants.2004.01.006

Caradonia, F., Battaglia, V., Righi, L., Pascali, G., and La Torre, A. (2019). Plant biostimulant regulatory framework: prospects in Europe and current situation at international level. *J. Plant Growth Regul.* 38, 438–448. doi: 10.1007/s00344-018-9853-4

Carvalhais, L. C., Dennis, P. G., Fan, B., Fedoseyenko, D., Kierul, K., Becker, A., et al. (2013). Linking plant nutritional status to plant-microbe interactions. *PLoS One* 8:e68555. doi: 10.1371/journal.pone.0068555

Chauhan, H., Bagyaraj, D. J., Selvakumar, G., and Sundaram, S. P. (2015). Novel plant growth promoting rhizobacteria—Prospects and potential. *Appl. Soil Ecol.* 95, 38–53. doi: 10.1016/j.apsoil.2015.05.011

Chen, Y., Xie, Y., Song, C., Zheng, L., Rong, X., Jia, L., et al. (2018). A comparison of lateral root patterning among dicot and monocot plants. *Plant Sci.* 274, 201–211. doi: 10.1016/j.plantsci.2018.05.018

Compant, S., Nowak, J., Coenye, T., Clément, C., and Ait Barka, E. (2008). Diversity and occurrence of *Burkholderia* spp. in the natural environment. *FEMS Microbiol. Rev.* 32, 607–626. doi: 10.1111/j.1574-6976.2008.00113.x

Dakora, F. D., and Phillips, D. A. (2002). Root exudates as mediators of mineral acquisition in low-nutrient environments. *Plant Soil* 245, 35–47. doi: 10.1023/A:1020809400075

de Bang, T. C., Husted, S., Laursen, K. H., Persson, D. P., and Schjoerring, J. K. (2021). The molecular-physiological functions of mineral macronutrients and their consequences for deficiency symptoms in plants. *New Phytol.* 229, 2446–2469. doi: 10.1111/nph.17074

de Souza, R. S. C., Armanhi, J. S. L., and Arruda, P. (2020). From microbiome to traits: designing synthetic microbial communities for improved crop resiliency. *Front. Plant Sci.* 11:1179. doi: 10.3389/fpls.2020.01179

De Zutter, N., Ameye, M., Debode, J., De Tender, C., Ommeslag, S., Verwaeren, J., et al. (2021). Shifts in the rhizobiome during consecutive *in planta* enrichment for phosphate-solubilizing bacteria differentially affect maize P status. *Microb. Biotechnol.* 14, 1594–1612. doi: 10.1111/1751-7915.13824

Duval, S., and Tweedie, R. (2000). Trim and fill: a simple funnel-plot–based method of testing and adjusting for publication bias in meta-analysis. *Biometrics* 56, 455–463. doi: 10.1111/j.0006-341X.2000.00455.x

Eberl, L., and Vandamme, P. (2016). Members of the genus *Burkholderia*: good and bad guys. *F1000 Research* 5:1007. doi: 10.12688/f1000research.8221.1

Etesami, H., Jeong, B. R., and Glick, B. R. (2021). Contribution of arbuscular mycorrhizal fungi, phosphate–solubilizing bacteria, and silicon to p uptake by plant. *Front. Plant Sci.* 12:699618. doi: 10.3389/fpls.2021.699618

FAOSTAT (2021). *Food and Agriculture Organization of the United Nations. FAOSTAT Statistical Database*. Rome: FAO.

Feng, H., Zhang, N., Fu, R., Liu, Y., Krell, T., Du, W., et al. (2019). Recognition of dominant attractants by key chemoreceptors mediates recruitment of plant growth-promoting rhizobacteria. *Environ. Microbiol.* 21, 402–415. doi: 10.1111/1462-2920.14472

Friesen, M. L., Porter, S. S., Stark, S. C., von Wettberg, E. J., Sachs, J. L., and Martinez-Romero, E. (2011). Microbially mediated plant functional traits. *Annu. Rev. Ecol. Evol. Syst.* 42, 23–46. doi: 10.1146/annurev-ecolsys-102710-145039

Gagnon, B., Ziadi, N., Bélanger, G., and Parent, G. (2020). Validation and use of critical phosphorus concentration in maize. *Eur. J. Agron.* 120:126147. doi: 10.1016/j.eja.2020.126147

Gao, S., Wu, H., Yu, X., Qian, L., and Gao, X. (2016). Swarming motility plays the major role in migration during tomato root colonization by *Bacillus subtilis* SWR01. *Biol. Control* 98, 11–17. doi: 10.1016/j.biocontrol.2016.03.011

Gitelson, A. A., Chivkunova, O. B., and Merzlyak, M. N. (2009). Nondestructive estimation of anthocyanins and chlorophylls in anthocyanic leaves. *Am. J. Bot.* 96, 1861–1868. doi: 10.1016/j.jplph.2008.03.004

Ha, S., and Tran, L. S. (2014). Understanding plant responses to phosphorus starvation for improvement of plant tolerance to phosphorus deficiency by biotechnological approaches. *Crit. Rev. Biotechnol.* 34, 16–30. doi: 10.3109/07388551.2013.783549

Härtel, H., Dörmann, P., and Benning, C. (2000). DGD1-independent biosynthesis of extraplastidic galactolipids after phosphate deprivation in *Arabidopsis*. *Proc. Natll. Acad. Sci. U.S.A.* 97, 10649–10654. doi: 10.1073/pnas.180320497

Hedges, L. V. (1981). Distribution theory for Glass's estimator of effect size and related estimators. *J. Educ. Stat.* 6, 107–128. doi: 10.2307/1164588

Hernández, I., and Munné-Bosch, S. (2015). Linking phosphorus availability with photo-oxidative stress in plants. *J. Exp. Bot.* 66, 2889–2900. doi: 10.1093/jxb/erv056

Herrmann, L., and Lesueur, D. (2013). Challenges of formulation and quality of biofertilizers for successful inoculation. *Appl. Microbiol. Biotechnol.* 97, 8859–8873. doi: 10.1007/s00253-013-5228-8

Hinsinger, P. (2001). Bioavailability of soil inorganic P in the rhizosphere as affected by root-induced chemical changes: a review. *Plant Soil* 237, 173–195. doi: 10.1023/A:1013351617532

Jiang, C., Gao, X., Liao, L., Harberd, N. P., and Fu, X. (2007). Phosphate starvation root architecture and anthocyanin accumulation responses are modulated by the gibberellin-DELLA signaling pathway in *Arabidopsis*. *Plant Physiol.* 145, 1460–1470. doi: 10.1104/pp.107.103788

Kai, M., Effmert, U., and Piechulla, B. (2016). Bacterial-plant-interactions: approaches to unravel the biological function of bacterial volatiles in the rhizosphere. *Front. Microbiol.* 7:108. doi: 10.3389/fmicb.2016.00108

Kinnersley, A. M., and Turano, F. J. (2000). Gamma aminobutyric acid (GABA) and plant responses to stress. *Crit. Rev. Plant Sci.* 19, 479–509. doi: 10.1080/07352680091139277

Lapsansky, E. R., Milroy, A. M., Andales, M. J., and Vivanco, J. M. (2016). Soil memory as a potential mechanism for encouraging sustainable plant health and productivity. *Curr. Opin. Biotechnol.* 38, 137–142. doi: 10.1016/j.copbio.2016.01.014

Lauber, C. L., Strickland, M. S., Bradford, M. A., and Fierer, N. (2008). The influence of soil properties on the structure of bacterial and fungal communities across land-use types. *Soil Biol. Biochem.* 40, 2407–2415. doi: 10.1016/j.soilbio.2008.05.021

Lim, J. H., and Kim, S. D. (2013). Induction of drought stress resistance by multi-functional PGPR Bacillus licheniformis K11 in pepper. *Plant Pathol. J.* 29:201. doi: 10.5423/PPJ.SI.02.2013.0021

Liu, Y., Gao, J., Bai, Z., Wu, S., Li, X., Wang, N., et al. (2021). Unraveling mechanisms and impact of microbial recruitment on oilseed rape (*Brassica napus* L.) and the rhizosphere mediated by plant growth-promoting rhizobacteria. *Microorganisms* 9:161. doi: 10.3390/microorganisms9010161

Lynch, J. P., and Brown, K. M. (2008). "Root strategies for phosphorus acquisition," in *The Ecophysiology Of Plant-Phosphorus Interactions*, eds J. P. Hammond and P. J. White (Dordrecht: Springer), 83–116. doi: 10.1007/978-1-4020-8435-5_5

Lyu, D., Msimbira, L. A., Nazari, M., Antar, M., Pagé, A., Shah, A., et al. (2021b). The coevolution of plants and microbes underpins sustainable agriculture. *Microorganisms* 9:1036. doi: 10.3390/microorganisms9051036

Lyu, D., Zajonc, J., Pagé, A., Tanney, C. A., Shah, A., Monjezi, N., et al. (2021a). Plant holobiont theory: the phytomicrobiome plays a central role in evolution and success. *Microorganisms* 9:675. doi: 10.3390/microorganisms9040675

Marín, O., González, B., and Poupin, M. J. (2021). From microbial dynamics to functionality in the rhizosphere: A systematic review of the opportunities with synthetic microbial communities. *Front. Plant Sci.* 12:650609. doi: 10.3389/fpls.2021.650609

Nacry, P., Canivenc, G., Muller, B., Azmi, A., Van Onckelen, H., Rossignol, M., et al. (2005). A role for auxin redistribution in the responses of the root system architecture to phosphate starvation in *Arabidopsis*. *Plant Physiol.* 138, 2061–2074. doi: 10.1104/pp.105.060061

Nelissen, H., Gonzalez, N., and Inze, D. (2016). Leaf growth in dicots and monocots: so different yet so alike. *Curr. Opin. Plant Biol.* 33, 72–76. doi: 10.1016/j.pbi.2016.06.009

Niu, Y. F., Chai, R. S., Jin, G. L., Wang, H., Tang, C. X., and Zhang, Y. S. (2013). Responses of root architecture development to low phosphorus availability: a review. *Ann. Bot.* 112, 391–408. doi: 10.1093/aob/mcs285

Nuccio, E. E., Hodge, A., Pett-Ridge, J., Herman, D. J., Weber, P. K., and Firestone, M. K. (2013). An arbuscular mycorrhizal fungus significantly modifies the soil bacterial community and nitrogen cycling during litter decomposition. *Environ. Microbiol.* 15, 1870–1881. doi: 10.1111/1462-2920.12081

Owen, D., Williams, A. P., Griffith, G. W., and Withers, P. J. (2015). Use of commercial bio-inoculants to increase agricultural production through improved phosphrous acquisition. *Appl. Soil Ecol.* 86, 41–54. doi: 10.1016/j.apsoil.2014.09.012

Page, M. J., McKenzie, J. E., Bossuyt, P. M., Boutron, I., Hoffmann, T. C., Mulrow, C. D., et al. (2021). The PRISMA 2020 statement: an updated guideline for reporting systematic reviews. *Syst. Rev.* 10:89. doi: 10.1186/s13643-021-01626-4

Pandey, P., Bisht, S., Sood, A., Aeron, A., Sharma, G. D., and Maheshwari, D. K. (2012). "Consortium of plant-growth-promoting bacteria: future perspective in agriculture," in *Bacteria in Agrobiology: Plant Probiotics*, ed. D. Maheshwari (Berlin: Springer), doi: 10.1007/978-3-642-27515-9_10

Penn, C. J., and Camberato, J. J. (2019). A critical review on soil chemical processes that control how soil pH affects phosphorus availability to plants. *Agriculture* 9:120. doi: 10.3390/agriculture9060120

Rawat, P., Das, S., Shankhdhar, D., and Shankhdhar, S. C. (2021). Phosphate-solubilizing microorganisms: mechanism and their role in phosphate solubilization and uptake. *J. Soil Sci. Plant Nutr.* 21, 49–68. doi: 10.1007/s42729-020-00342-7

Raymond, N. S., Gómez-Muñoz, B., van der Bom, F. J., Nybroe, O., Jensen, L. S., Müller-Stöver, D. S., et al. (2021). Phosphate-solubilising microorganisms for improved crop productivity: a critical assessment. *New Phytol.* 229, 1268–1277. doi: 10.1111/nph.16924

Rosenberg, M. S. (2005). The file-drawer problem revisited: a general weighted method for calculating fail-safe numbers in meta-analysis. *Evolution* 59, 464–468. doi: 10.1111/j.0014-3820.2005.tb01004.x

Rouached, H., Arpat, A. B., and Poirier, Y. (2010). Regulation of phosphate starvation responses in plants: signaling players and cross-talks. *Mol. Plant* 3, 288–299. doi: 10.1093/mp/ssp120

Rouphael, Y., Spíchal, L., Panzarová, K., Casa, R., and Colla, G. (2018). High-throughput plant phenotyping for developing novel biostimulants: from lab to field or from field to lab? *Front. Plant Sci.* 9:1197. doi: 10.3389/fpls.2018.01197

Rousk, J., Bååth, E., Brookes, P. C., Lauber, C. L., Lozupone, C., Caporaso, J. G., et al. (2010). Soil bacterial and fungal communities across a pH gradient in an arable soil. *ISME J.* 4, 1340–1351. doi: 10.1038/ismej.2010.58

Rubin, R. L., van Groenigen, K. J., and Hungate, B. A. (2017). Plant growth promoting rhizobacteria are more effective under drought: a meta-analysis. *Plant Soil* 416, 309–323. doi: 10.1007/s11104-017-3199-8

Sánchez-Cañizares, C., Jorrín, B., Poole, P. S., and Tkacz, A. (2017). Understanding the holobiont: the interdependence of plants and their microbiome. *Curr. Opin. Microbiol.* 38, 188–196. doi: 10.1016/j.mib.2017.07.001

Santos, M. S., Nogueria, M. A., and Hungria, M. (2019). Microbial inoculants: reviewing the past, discussing the present and previewing an outstanding future for the use of beneficial bacteria in agriculture. *AMB Express* 9:205. doi: 10.1186/s13568-019-0932-0

Sasse, J., Martinoia, E., and Northen, T. (2018). Feed your friends: do plant exudates shape the root microbiome? *Trends Plant Sci.* 23, 25–41. doi: 10.1016/j.tplants.2017.09.003

Schachtman, D. P., Reid, R. J., and Ayling, S. M. (1998). Phosphorus uptake by plants: from soil to cell. *Plant Physiol.* 116, 447–453. doi: 10.1104/pp.116.2.447

Scheublin, T., Sanders, I., Keel, C., and van der Meer, J. R. (2010). Characterisation of microbial communities colonising the hyphal surfaces of arbuscular mycorrhizal fungi. *ISME J.* 4, 752–763. doi: 10.1038/ismej.2010.5

Sharma, S. B., Sayyed, R. Z., Trivedi, M. H., and Gobi, T. A. (2013). Phosphate solubilizing microbes: sustainable approach for managing phosphorus deficiency in agricultural soils. *SpringerPlus* 2:587. doi: 10.1186/2193-1801-2-587

Shen, J., Yuan, L., Zhang, J., Li, H., Bai, Z., Chen, X., et al. (2011). Phosphorus dynamics: from soil to plant. *Plant Physiol.* 156, 997–1005. doi: 10.1104/pp.111.175232

Sims, L., Pastor, J., Lee, T., and Dewey, B. (2012). Nitrogen, phosphorus and light effects on growth and allocation of biomass and nutrients in wild rice. *Oecologia* 170, 65–76. doi: 10.1007/s00442-012-2296-x

Sterne, J. A., and Egger, M. (2001). Funnel plots for detecting bias in meta-analysis: guidelines on choice of axis. *J. Clin. Epidemiol.* 54, 1046–1055. doi: 10.1016/S0895-4356(01)00377-8

Sundh, I., Del Giudice, T., and Cembalo, L. (2021). Reaping the benefits of microorganisms in cropping systems: is the regulatory policy adequate? *Microorganisms* 9:1437. doi: 10.3390/microorganisms9071437

Suzuki, T. (1967). Characteristics of microorganisms in paddyfield soils. *Actinomycetes* 2, 880–880.

Tian, J., Ge, F., Zhang, D., Deng, S., and Liu, X. (2021). Roles of phosphate solubilizing microorganisms from managing soil phosphorus deficiency to mediating biogeochemical p cycle. *Biology* 10:158. doi: 10.3390/biology10020158

Tian, T., Reverdy, A., She, Q., Sun, B., and Chai, Y. (2020). The role of rhizodeposits in shaping rhizomicrobiome. *Environ. Microbiol. Rep.* 12, 160–172. doi: 10.1111/1758-2229.12816

Tukey, J. W. (1977). *Exploratory Data Analysis*. Boston, MA: Addison-Wesley Pub. Co.

Viechtbauer, W. (2010). Conducting meta-analyses in R with the metafor package. *J. Stat. Softw.* 36, 1–48. doi: 10.18637/jss.v036.i03

Wallenstein, M. D. (2017). Managing and manipulating the rhizosphere microbiome for plant health: a systems approach. *Rhizosphere* 3, 230–232. doi: 10.1016/j.rhisph.2017.04.004

Wang, Y., Wang, F., Lu, H., Liu, Y., and Mao, C. (2021). Phosphate uptake and transport in plants: an elaborate regulatory system. *Plant Cell Physiol.* 62, 564–572. doi: 10.1093/pcp/pcab011

Yan, X., Wei, Z., Hong, Q., Lu, Z., and Wu, J. (2017). Phosphorus fractions and sorption characteristics in a subtropical paddy soil as influenced by fertilizer sources. *Geoderma* 295, 80–85. doi: 10.1016/j.geoderma.2017.02.012

Zaidi, A., Khan, M., Ahemad, M., and Oves, M. (2009). Plant growth promotion by phosphate solubilizing bacteria. *Acta Microbiol. Immunol. Hung.* 56, 263–284. doi: 10.1556/amicr.56.2009.3.6

Zhang, L., Xu, M., Liu, Y., Zhang, F., Hodge, A., and Feng, G. (2016). Carbon and phosphorus exchange may enable cooperation between an arbuscular mycorrhizal fungus and a phosphate-solubilizing bacterium. *New Phytol.* 210, 1022–1032. doi: 10.1111/nph.13838

Zheng, B. X., Zhang, D. P., Wang, Y., Hao, X. L., Wadaan, M. A., Hozzein, W. N., et al. (2019). Responses to soil pH gradients of inorganic phosphate solubilizing bacteria community. *Sci. Rep.* 9, 1–8. doi: 10.1038/s41598-018-37003-w

Conflict of Interest: The authors declare that the research was conducted in the absence of any commercial or financial relationships that could be construed as a potential conflict of interest.

frontiers in Plant Science

ORIGINAL RESEARCH
published: 10 March 2022
doi: 10.3389/fpls.2022.837517

Sulfur Stable Isotope Discrimination in Rice: A Sulfur Isotope Mass Balance Study

*Viviana Cavallaro[1], Moez Maghrebi[1,2], Mariachiara Caschetto[1,3], Gian Attilio Sacchi[1] and Fabio Francesco Nocito[1]**

[1] Dipartimento di Scienze Agrarie e Ambientali—Produzione, Territorio, Agroenergia, Università degli Studi di Milano, Milan, Italy, [2] Dipartimento di Scienze della Vita e Biologia dei Sistemi, Università degli Studi di Torino, Turin, Italy, [3] Dipartimento di Scienze dell'Ambiente e della Terra, Università degli Studi di Milano-Bicocca, Milan, Italy

The use of sulfur (S) stable isotopes to study S metabolism in plants is still limited by the relatively small number of studies. It is generally accepted that less S stable isotope discrimination occurs during sulfate (SO_4^{2-}) uptake. However, S metabolism and allocation are expected to produce separations of S stable isotopes among the different plant S pools and organs. In this study, we measured the S isotope composition of the main S pools of rice plants grown under different SO_4^{2-} availabilities in appropriate closed and open hydroponic-plant systems. The main results indicate that fractionation against ^{34}S occurred during SO_4^{2-} uptake. Fractionation was dependent on the amount of residual SO_4^{2-} in the solution, showing a biphasic behavior related to the relative expression of two SO_4^{2-} transporter genes (*OsSULTR1;1* and *OsSULTR1;2*) in the roots. S isotope separations among S pools and organs were also observed as the result of substantial S isotope fractionations and mixing effects occurring during SO_4^{2-} assimilation and plant S partitioning. Since the S stable isotope separations conserve the memory of the physiological and metabolic activities that determined them, we here underline the potential of the $^{32}S/^{34}S$ analysis for the detailed characterization of the metabolic and molecular processes involved in plant S nutrition and homeostasis.

Keywords: fractionation, *Oryza sativa* L., sulfate uptake, sulfur assimilation, sulfur stable isotopes

OPEN ACCESS

Edited by:
Marta Wilton Vasconcelos, Catholic University of Portugal, Portugal

Reviewed by:
Timothy O. Jobe, University of Cologne, Germany
Akiko Maruyama-Nakashita, Kyushu University, Japan

***Correspondence:**
Fabio Francesco Nocito
fabio.nocito@unimi.it

Specialty section:
This article was submitted to Plant Nutrition, a section of the journal Frontiers in Plant Science

Received: *16 December 2021*
Accepted: *11 February 2022*
Published: *10 March 2022*

Citation:
Cavallaro V, Maghrebi M, Caschetto M, Sacchi GA and Nocito FF (2022) Sulfur Stable Isotope Discrimination in Rice: A Sulfur Isotope Mass Balance Study. Front. Plant Sci. 13:837517. doi: 10.3389/fpls.2022.837517

INTRODUCTION

Since 1865, sulfur (S) has been recognized as an essential element for plant growth (Sachs, 1865; Epstein, 2000). In plants, S is found in the amino acid cysteine and methionine, short peptides, vitamins and cofactors, and secondary compounds (Takahashi et al., 2011).

Plants mainly utilize sulfate (SO_4^{2-}), an inorganic form of oxidized S present in the soil solution, to support their growth. SO_4^{2-} is taken up by roots and allocated to various sink tissues, where it is stored in the cell vacuoles or assimilated into S organic (S_{org}) compounds (Saito, 2004; Takahashi et al., 2011). To accomplish the assimilation of S into biomolecules, SO_4^{2-} is first activated by ATP sulfurylase to adenosine-5′-phosphosulfate (APS), which is then channeled toward reduction or sulfation (Leustek et al., 2000). Most of the APS enters the reductive pathway along which sulfite and, subsequently, sulfide are produced through two sequential reactions catalyzed by APS reductase and sulfite reductase, respectively. Sulfide is finally incorporated into *O*-acetylserine

(OAS) to form cysteine in a reaction catalyzed by OAS(thiol)lyase (Takahashi et al., 2011). In the sulfation pathway, the APS is first phosphorylated by APS kinase to form 3′-phosphoadenosine-5′-phosphosulfate, the donor of SO_4^{2-} groups for a variety of sulfation reactions catalyzed by sulfotransferases (Günal et al., 2019).

Sulfur has four stable isotopes, namely, ^{32}S, ^{33}S, ^{34}S, and ^{36}S; their relative abundances are 0.9499, 0.0075, 0.0425, and 0.0001 atom fraction, respectively (De Laeter et al., 2003). Mass differences between the S isotopes result in small but significant variations in their chemical and physical properties, which may produce considerable separation of the S isotopes during chemical reactions. The most abundant isotopes, i.e., ^{32}S and ^{34}S, are now commonly measured using elemental analyzers coupled with Isotope Ratio Mass Spectrometers (IRMS), and S isotope abundance is generally reported in δ notation ($\delta^{34}S$) as parts per thousand (‰) deviation relative to the Vienna-Cañon Diablo Troilite (VCDT; Coplen and Krouse, 1998) standard as follows:

$$\delta^{34}S\ (‰) = \frac{R_{sample} - R_{standard}}{R_{standard}} \cdot 1,000$$

where R_{sample} and $R_{standard}$ are the isotope ratios ($^{34}S/^{32}S$) of the sample and standard, respectively.

Unlike what has happened with carbon and nitrogen, the natural abundance S stable isotope analysis techniques have so far scarcely been employed to study S allocation and metabolism in plants (Trust and Fry, 1992; Tcherkez and Tea, 2013), mainly due to the lack of knowledge about the $^{32}S/^{34}S$ isotope effects occurring during S metabolism and partitioning among the different organs. Most of the irreversible reactions involving S discriminate between ^{32}S and ^{34}S by favoring the lighter ^{32}S isotope, thus enriching in ^{34}S the residual substrate molecules left behind. That is to say that irreversible reactions that do not consume all the substrate may likely produce a detectable separation of the S stable isotopes, i.e., a fractionation, at natural abundance, providing crucial insights into the understanding of S metabolic fluxes inside the plants, without the need for costly labeling experiments with radioactive (^{35}S) or stable (^{34}S) isotopes (Tcherkez and Tea, 2013).

Sulfate uptake and allocation in plants involve a family of SO_4^{2-} transporter proteins whose activities are tightly regulated and coordinated with those of the assimilation pathways to control plant S homeostasis (Buchner et al., 2004; Gigolashvili and Kopriva, 2014; Sacchi and Nocito, 2019; Takahashi, 2019). A few pioneering studies indicated that a less S isotope discrimination occurs during SO_4^{2-} uptake since the isotope composition measured for plant total S (S_{tot}) is typically depleted in ^{34}S by 1–2‰ with respect to that measured for the SO_4^{2-} source feeding the plants (Mekhtiyeva, 1971; Krouse et al., 1991). In contrast, less is known about the S isotope composition of the SO_4^{2-} ions in the plant tissues, which should reflect the metabolic activities in which SO_4^{2-} is involved as a substrate. Although the isotope effects linked to SO_4^{2-} metabolism largely remain to be investigated in plants, it is possible to suppose that reductive SO_4^{2-} assimilation fractionates against ^{34}S, since it involves changes in the covalent bonding of the S atoms (Rees, 1973). Significant isotope effects have been reported for bacterial SO_4^{2-} reduction, which enriches both the sulfide produced in the lighter ^{32}S isotope and the remaining SO_4^{2-} in the heavier ^{34}S isotope (Thode et al., 1949; Kemp and Thode, 1968).

This study presents a detailed study on the dynamics of S stable isotopes occurring in appropriate closed or steady-state hydroponic-plant systems to dissect the $^{32}S/^{34}S$ isotope effects associated with SO_4^{2-} uptake, allocation, and metabolism in rice plants. In this study, we also provided the first complete S isotope mass balance in rice which considers organic and inorganic S pools in roots and shoots.

MATERIALS AND METHODS

Plant Material and Pre-growing Conditions

Rice (*Oryza sativa* L. cv. Vialone Nano) caryopses were surface sterilized with 70% (v:v) ethanol for 1 min, washed three times with sterile deionized water, and finally sown on filter paper saturated with deionized water to be incubated in the dark at 26°C. After 7 days, seedlings selected for uniform growth were transferred into 3-L plastic tanks (18 seedlings per tank), containing the following complete nutrient solution: 1.5 mM KNO_3, 1 mM $Ca(NO_3)_2$, 100 μM $MgSO_4$, 250 μM $NH_4H_2PO_4$, 25 μM Fe-EDTA, 46 μM H_3BO_3, 9 μM $MnCl_2$, 1 μM $ZnCl_2$, 0.3 μM $CuCl_2$, 0.1 μM $(NH_4)_6Mo_7O_{24}$, and 30 μM Na_2O_3Si (pH 6.5). Seedlings were kept for a 14-days pre-growing period in a growth chamber maintained at 26°C and 80% relative humidity during the 16-h light period and at 22°C and 70% relative humidity during the 8-h dark period. The photosynthetic photon flux density was 400 μmol m^{-2} s^{-1}. Nutrient solutions were renewed two times a week to minimize nutrient depletion. At the end of the pre-growing period, roots were gently washed for 30 min in 3 L of deionized water (>18.2 MΩ cm). Plants were then transferred into fresh solutions and used in two distinct experimental setups (A and B). The parts of the plants were sampled, frozen in liquid N_2, and stored at −80°C for further analysis.

Experimental Setup and Tissue Sampling

In experimental setup A, pre-grown rice plants were transferred into fresh complete nutrient solutions and then grown further, under the same conditions described before, for 3–11 days, not renewing the growing media. Both plants and nutrient solutions were sampled at the beginning of the experiment and every day (starting from the third day).

In experimental setup B, pre-grown rice plants were transferred into fresh complete nutrient solutions ($+SO_4^{2-}$) or fresh minus sulfate nutrient solutions ($-SO_4^{2-}$), in which an equimolar amount of $MgCl_2$ replaced $MgSO_4$. Plants were grown under these conditions for 48 or 72 h by renewing the growing media every day.

In both the experimental setups, before sampling, plant roots were washed for 30 min in 3 L of deionized water to remove SO_4^{2-}, which was not absorbed, from the root apoplast. After

washing, plants were gently blotted with paper towels, shoots were separated from roots, and then, both were frozen in liquid N_2 and stored at −80°C for further analysis.

Xylem Sap Sampling

In each sampling period (experimental setup B in the presence of SO_4^{2-}), the shoots of four rice plants were cut at 1 cm above the roots with a microtome blade to collect, with a micropipette, the xylem sap exuded from the lower cut surface during a 90-min period (Maghrebi et al., 2021).

Preparation of Samples for Sulfur Isotope Analysis and Quantitative Determination of the Sulfur Pools

Frozen samples were ground to a fine powder using mortar and pestle in liquid N_2 and stored frozen in a cryogenic tank.

For S_{tot} analysis, powder samples of 5 g [fresh weight (FW)] were digested at 150°C in 10 ml 2:1 (v:v) nitric:perchloric acid mixture, in order to quantitatively convert all the S forms into SO_4^{2-} (Blair and Till, 2003). Samples were then added with 1 ml of concentrated HCl and finally evaporated to dryness at 200°C to release any HNO_3 still present. The mineralized material was dissolved in 50 ml of deionized water and then brought to pH 2.0 with a tiny volume of 6 N HCl.

Sulfate was extracted from roots and shoots by homogenizing powder samples of 5 g (FW) in 50 ml of deionized water. After heating at 80°C for 40 min, the extracts were filtered and then brought to pH 2.0 with a tiny volume of 6 N HCl.

Residual nutrient solutions were boiled to evaporate water until their volumes were reduced to 50 ml. Samples were then filtered and brought to pH 2.0 with 6 N HCl.

Xylem sap samples were diluted with deionized water to a final volume of 50 ml, filtered, and then brought to pH 2.0 with a tiny volume of 6 N HCl.

Aliquots of 2 ml were collected from each diluted sample for the quantitative determination of SO_4^{2-}, using the turbidimetric method described by Tabatabai and Bremner (1970). The SO_4^{2-} ions of each sample were precipitated overnight as $BaSO_4$ by adding 2.5 ml of a 0.5 M $BaCl_2$ solution. $BaSO_4$ was then collected by centrifugation, washed two times in 2 ml of deionized water, dried at 80°C, ground to a fine powder, and finally used for the S isotope analyses.

The amount of the S_{org} pool of both root and shoot extracts was estimated as follows:

$$S_{org} = S_{tot} - SO_4^{2-}$$

Sulfur Isotope Analysis

The $\delta^{34}S$ values of samples were measured using a Flash 2000 HT elemental analyzer coupled, *via* a ConFLo IV Interface, with a Delta V Advantage IRMS and interconnected to the software Isodat 3.0 (Thermo). The reaction tube, packed with tungstic oxide and copper wires separated by Quartz wool, was maintained at 1,020°C. The He carrier gas flow was 150 ml min^{-1}. The O_2 purge for flash combustion was 3 s at a flow rate of 250 ml min^{-1} per sample. The temperature of the gas chromatography separation column was 90°C. The SO_2 reference gas pulse was introduced three times (20 s each) at the beginning of each run.

Samples ($BaSO_4$ precipitates and reference materials) were weighed in tin capsules. Capsules were carefully closed by folding them with cleaned tweezers and then transferred to the autosampler. The run time of the analysis was approximately 500 s for a single run. The analysis of each sample was performed five times. Calibration was performed using three secondary reference materials provided by the International Atomic Energy Agency (IAEA): IAEA-S-1 ($\delta^{34}S = -0.30 \pm 0.03‰$); IAEA-S-2 ($\delta^{34}S = 22.62 \pm 0.08‰$); IAEA-S-3 ($\delta^{34}S = -32.49 \pm 0.08‰$). Two in-house standards were used for normalization and analytical quality assurance.

The data are reported in $\delta^{34}S$ notation, which is standardized to the VCDT international reference scale as follows:

$$\delta^{34}S\ (‰) = \frac{R_{sample} - R_{standard}}{R_{standard}} \cdot 1,000$$

The mass spectrometric uncertainty (1 σ) on the individual $\delta^{34}S$ measurements was better than 0.05‰.

The $\delta^{34}S$ values of the S_{org} pool were estimated by imposing the following mass balance:

$$\delta^{34}S\_S_{tot} \cdot S_{tot} = (\delta^{34}S\_SO_4^{2-} \cdot SO_4^{2-}) + (\delta^{34}S\_S_{org} \cdot S_{org})$$

where SO_4^{2-} and S_{tot} are the amount of SO_4^{2-} and S_{tot}, respectively, measured in the same sample.

Fractionation factors ($\Delta_{L/H}$), i.e., in positive per mil (‰) units, were calculated by fitting an approximation of the Rayleigh equation to the data obtained by measuring $\delta^{34}S$ values of the residual SO_4^{2-} in the hydroponic solution ($\delta^{34}S\_SO_4^{2-}{}_{res}$), according to Fry (2006). For these purposes, the following equation was used:

$$\delta^{34}S\_SO_{4\,res}^{2-} = \delta^{34}S\_SO_{4\,source}^{2-} - \Delta_{L/H} \cdot \ln(f)$$

where f is the fraction of SO_4^{2-} remaining in the hydroponic solution, and $\delta^{34}S\_SO_4^{2-}{}_{source}$ is the initial S isotope composition of the S source.

Finally, the trajectories of the $\delta^{34}S$ values of the instantaneous product (S_{ist}) that forms, inside the plants, instant by instant in time were calculated using the following equation:

$$\delta^{34}S\_S_{ist} = \delta^{34}S\_SO_{4\,source}^{2-} - \Delta_{(L/H)} \cdot [1 + \ln(f)]$$

RNA Extraction and Quantitative Real-Time PCR Analysis

Total RNA was extracted from rice roots using TRIzol Reagent (Life Technologies Corporation, Carlsbad, CA, United States) and then purified using PureLink® RNA Mini Kit (Life Technologies Corporation, Carlsbad, CA, United States), according to the manufacturer's instructions. Contaminant DNA was removed on-column using PureLink® DNase (Life Technologies Corporation, Carlsbad, CA, United States). The first-strand cDNA synthesis was carried out using the SuperScript™ III First-Strand Synthesis SuperMix for quantitative real-time PCR (qRT-PCR; Life Technologies

Corporation, Carlsbad, CA, United States), according to the manufacturer's instructions.

The qRT-PCR analysis of *OsSULTR1;1* (LOC_Os03g09970) and *OsSULTR1;2* was performed on the first-strand cDNA in a 20 μl reaction mixture containing GoTaq® qPCR Master Mix (Promega) and the specific primers, using an ABI 7300 Real-Time PCR system (Applied Biosystems). The relative transcript level of each gene was calculated by the $2^{-\Delta\Delta Ct}$ method using the expression of the *OsS16* (LOC_Os11g03400) gene as reference. Primers for qRT-PCR are listed in **Supplementary Table 1**.

Statistical Analysis

Quantitative values are presented as mean ± SEM of three independent experiments run in duplicate (n = 3). Two distinct 3-L tanks were used for each condition analyzed in each independent experiment. ANOVA was carried out using SigmaPlot for Windows version 11.0 (SYSTAT Software, Inc., San Jose, CA, United States). The significant values were adjusted for multiple comparisons using the Bonferroni correction. The Student's t-test was used to assess the significance of the observed differences between the values measured in root and shoot.

RESULTS

Sulfur Isotope Mass Balance in a Closed Hydroponic-Rice System (Experimental Setup A)

Potential $^{32}S/^{34}S$ isotope effects occurring during SO_4^{2-} uptake were investigated by setting up a closed hydroponic-rice system (**Figure 1A**) in which a finite amount of substrate (i.e., the SO_4^{2-} in the nutrient solution) was continuously removed from the solution, by the activity of the SO_4^{2-} transporters of the roots, and converted into a final product (i.e., S_{tot}). Using this system, we performed serial sacrifice experiments in which plant growth was terminated every 24 h (starting from the third day) for the S isotope analyses of both substrates and products.

During the experimental period (264 h), (i) plants continuosly grown (**Figure 1B**) and removed 98% of the SO_4^{2-} initially present in the nutrient solution (**Figure 1C**), (ii) SO_4^{2-} absorbed was quantitatively recovered in the plants as S_{tot} (**Figures 1D,E**), and (iii) no significant losses of S occurred during the growth (**Figure 1E**). The S_{tot} concentration of the plants ranged from 121.2 (at the beginning of the experiment) to 98.6 μmol g^{-1} dry weight (DW; at the end of the experiment), while the SO_4^{2-} concentration in the nutrient solution ranged from 100 to 6.5 μM, indicating that the regulation of plant S homeostasis occurred during SO_4^{2-} absorption (**Figure 1F**).

Figure 2A reports $\delta^{34}S$ data as a function of the fraction of SO_4^{2-} remaining in the hydroponic solution (f). The $\delta^{34}S$ of residual SO_4^{2-} in both the hydroponic solution and plant S_{tot} changed over time, tending toward higher values as f decreased. The $\delta^{34}S$ values of the residual SO_4^{2-} ($\delta^{34}S\_SO_4^{2-}$) increased from a minimum of −1.92‰ (at the beginning of the experiment) to a maximum of −0.21‰ (at the final sampling). In contrast, the $\delta^{34}S\_S_{tot}$ of the plants was always lower than the $\delta^{34}S\_SO_4^{2-}$ of the S source (−1.92 ± 0.02‰) and increased from −3.32‰ (the starting isotope composition of total plant biomass) to −2.30‰ at the final sampling, indicating that SO_4^{2-} uptake significantly enriches plant S_{tot} in the lighter ^{32}S isotope. It is worth noting that, due to mass balance in the closed system, the $\delta^{34}S\_S_{tot}$ of the rice plants tended to the $\delta^{34}S\_SO_4^{2-}$ of the initial S source as SO_4^{2-} concentration in the external medium approached zero, indicating that (i) SO_4^{2-} ions in the nutrient solution were the only S source used by plants and (ii) no significant loses/fractionations of S isotopes occurred during the experiments due to H_2S gaseous emission (Wilson et al., 1978; Winner et al., 1981).

The isotope effects that occurred in the closed system were analyzed using an approximation of the Rayleigh equation describing isotope partitioning between two reservoirs as one of them decreases in size (Fry, 2006). The S isotope profile of the residual SO_4^{2-} in the nutrient solution (**Figure 2A**) showed a marked deviation from a typical Rayleigh enrichment (R^2 = 0.79; black dashed line) due to an unexpected data point distribution at the final steps of the experiment ($f \leq 0.21$). Considering the Rayleigh fractionation model, it was possible to calculate a single fractionation factor, $\Delta_{L/H} = 0.48 \pm 0.09$‰, which describes an average of the net fractionation along the overall trajectory (profile). However, data distribution could be more appropriately described by assuming that a dual-phase Rayleigh fractionation occurred during SO_4^{2-} uptake. In the first phase ($1 \leq f \leq 0.31$), a significant isotope fractionation against $^{34}S\_SO_4^{2-}$ took place ($\Delta_{1(L/H)}$ = 1.09‰), while in the second phase ($f \leq 0.21$), a less pronounced isotope effect [$\Delta_{2(L/H)}$ = 0.16‰] was associated with SO_4^{2-} uptake. **Figure 2A** also reports the calculated trajectories of the $\delta^{34}S$ values of S_{ist} that forms, inside the plants, instant by instant in time from the external SO_4^{2-} due to SO_4^{2-} uptake; such a product is always offset in the isotope composition of the substrate ($\delta^{34}S\_SO_4^{2-}$) by the fractionation factor $\Delta_{L/H}$ (Fry, 2006). In each phase (I and II), S isotope fractionation ($\delta^{34}S\_SO_4^{2-}$–$\delta^{34}S\_S_{ist}$) was practically independent of f, as can be easily observed by comparing the isotope signatures of the substrate and cumulative product for each data point.

Aiming to decompose the two phases into their physiological and molecular components, we performed a transcriptional analysis of *OsSULTR1;1* and *OsSULTR1;2*, i.e., the main rice genes reasonably involved in SO_4^{2-} uptake (Godwin et al., 2003; Kumar et al., 2011; **Figure 2B**). Results revealed that the transition from the two phases was associated with significant changes in the ratio between the transcript levels of the two genes: the *OsSULTR1;2* transcript was always independent of f and was more abundant than the *OsSULTR1;1* transcript during the first phase ($1 \leq f \leq 0.31$), while the *OsSULTR1;1* transcript level rapidly increased in the second phase ($f \leq 0.21$), when the SO_4^{2-} concentration in the nutrient solution became limiting for plant growth [$(SO_4^{2-}) \leq 37$ μM; **Figure 2B**].

Sulfur Isotope Mass Balance in a Whole Plant: Steady-State vs. Sulfur Starvation (Experimental Setup B)

The possible $^{32}S/^{34}S$ isotope effects associated with both S partitioning among plant organs and cell metabolism were investigated by comparing plants pre-grown in complete nutrient

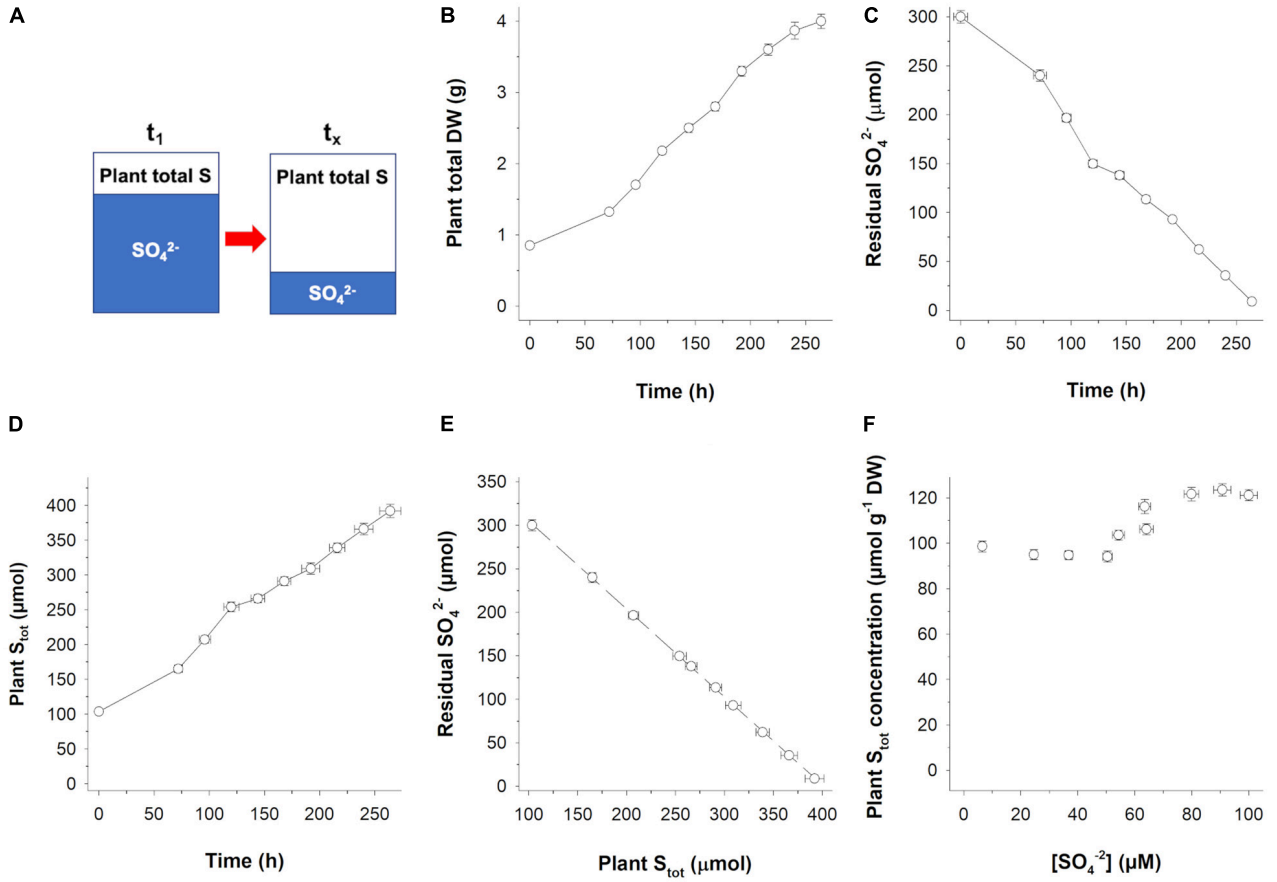

FIGURE 1 | Time course of S partitioning in a closed hydroponic-rice system. **(A)** Experimental setup: A finite amount of sulfate (SO_4^{2-}) is continuously removed from the hydroponic solution and converted into the total S of the plant (S_{tot}). **(B)** Plant total biomass accumulation. **(C)** Residual SO_4^{2-} in the hydroponic solution over time. **(D)** S_{tot} accumulation over time. **(E)** Residual SO_4^{2-} in the hydroponic solution vs. plant S_{tot} accumulation. **(F)** Plant S_{tot} concentration vs. SO_4^{2-} concentration in the hydroponic solution. Data are means ± SE of three independent experiments run in duplicate (n = 3).

solutions and then continuously maintained on media containing SO_4^{2-} or deprived of SO_4^{2-} for 72 h (experimental setup B). Nutrient solutions were changed every day to minimize the changes in the isotope signature of the S source (-1.92 ± 0.02‰) due to fractionation associated with SO_4^{2-} uptake.

Results showed that the S isotope composition of the whole plants did not significantly change over time since similar $\delta^{34}S\_S_{tot}$ values were measured at each time period (0, 48, and 72 h) in both of the growing conditions (**Figure 3**). At the beginning of the experiment (0 h), the S_{tot} of the whole plants was significantly depleted in ^{34}S by -1.40 ± 0.08‰ relative to the S source (**Figure 3**).

Plants maintained in hydroponic solutions containing SO_4^{2-} grew linearly in the observation period (**Figure 4A**). As expected, the concentrations of SO_4^{2-}, S_{tot}, and S_{org} did not significantly change in both root and shoot over time (**Figures 4B,C**). The invariance of each S pool was associated with the invariance of their isotope signatures, indicating that plants reached metabolic and isotope steady-states (**Figure 5**). The S_{tot} of root and shoot was significantly depleted in ^{34}S by -1.94 ± 0.08‰ and -1.09 ± 0.09‰, respectively, relative to the S source (**Figure 5A**); moreover, $\delta^{34}S\_S_{tot}$ values were significantly lower in the root than in the shoot in all the conditions analyzed (**Figure 5A**). In the root, the SO_4^{2-} pools were significantly ($P < 0.001$) ^{34}S-depleted relative to the S source, while in the shoot, they were significantly ($P < 0.001$) ^{34}S-enriched relative to the same S source (**Figure 5B**). The S_{org} pool of both root and shoot were significantly ^{34}S-depleted with respect to the S source; interestingly, both the S_{org} pools were also significantly ^{34}S-depleted with respect to their relative SO_4^{2-} pools of the cells (**Figure 5C**). Finally, no differences were found in comparing the $\delta^{34}S\_SO_4^{2-}$ values of the SO_4^{2-} pools in the xylem sap and in the whole root system (**Figure 5D**).

In contrast, SO_4^{2-}-deprived plants dynamically allocated S previously absorbed during the preliminary growth phase, preserving both the overall S isotope signature (**Figure 3**) and the total amount of S_{tot} over time (**Figure 4**). However, due to both continuous growth (**Figure 4D**) and S allocation processes, the S_{tot} concentration in rice organs changed over time, decreasing linearly in both root (R^2 = 0.993; **Figure 4E**) and shoot (R^2 = 0.999; **Figure 4F**). The SO_4^{2-} concentration sharply decreased over time in both root and shoot due to SO_4^{2-}

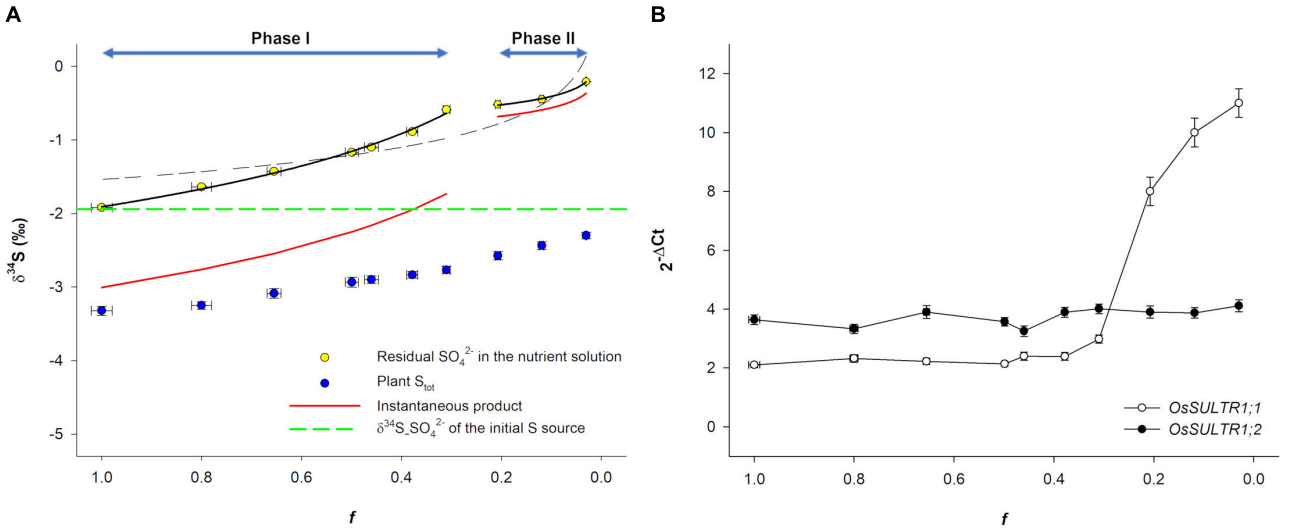

FIGURE 2 | Sulfur isotope dynamic in the closed system and transcriptional analysis of *OsSULTR1;1* and *OsSULTR1;2*. **(A)** S isotope dynamic as a function of the fraction (*f*) of SO_4^{2-} remaining in the hydroponic solution. Black dashed line is the Rayleigh curve calculated over the entire *f* interval, while the black continuous lines are the Rayleigh curves calculated over the two phases: Phase I ($1 \leq f \leq 0.31$) and Phase II ($f \leq 0.21$). Red continuous lines describe the trajectory of the calculated instantaneous product (S_{ist}) over the two phases. The dashed green line indicates the $\delta^{34}S\_SO_4^{2-}$ value of the initial S source. **(B)** Changes in the relative transcript levels of *OsSULTR1;1* and *OsSULTR1;2* in the roots. The numbers in brackets refer to the concentration of residual SO_4^{2-} (expressed as μM) in the hydroponic solution corresponding to each *f* value. Data are means ± SE of three independent experiments run in duplicate ($n = 3$).

assimilation (**Figures 4E,F**). In fact, the concentration of the S_{org} in the root slightly decreased over time from 7.26 ± 0.41 to 4.36 ± 0.14 μmol g^{-1} FW, while in the shoot, it remained relatively constant. The S_{tot} isotope composition of both root and shoot did not change over time (**Figure 6A**) and was significantly ^{34}S-depleted relative to the S source. As previously observed, the $\delta^{34}S\_S_{tot}$ values were significantly lower in the root than in the shoot (**Figure 6A**). Differently, the SO_4^{2-} pools of both root and shoot became progressively enriched in ^{34}S over time. It is worth noting that the most pronounced changes in the SO_4^{2-} isotope composition were observed in the shoot: the maximum variations observed at 72 h were 2.70 ± 0.05‰ and 6.71 ± 0.19‰ for root and shoot, respectively (**Figure 6B**). The S_{org} pools of both roots and shoot were significantly ^{34}S-depleted compared to the S source; their $\delta^{34}S\_S_{org}$ values changed differently over time since, in the root, they increased moving from 0 to 48 h and then remained constant at 72 h, while in the shoot, a significant increase was observed when moving from 48 to 72 h (**Figure 6C**).

DISCUSSION

It is generally assumed that terrestrial plants assimilate S from the soil (SO_4^{2-}) and from the atmosphere (SO_2) with less S isotope fractionation since the foliar $\delta^{34}S$ values are generally intermediate between those of the soil and the atmosphere or near to one extreme (Kennedy and Krouse, 1990; Krouse et al., 1991). However, the correct evaluation of the isotope effects due to S acquisition needs a direct comparison between the isotope compositions of the S_{tot} of a whole plant and the S source used by the same plant, since the $\delta^{34}S\_S_{tot}$ value of a single plant organ may result from fractionations and mixing effects occurring during SO_4^{2-} uptake, assimilation, and partitioning.

To address the S isotope effects during S acquisition, we performed an S isotope mass balance in a closed system, in which the accumulation of S_{tot} in the plants is considered as the result of the continuous consumption of a unique and finite S source (SO_4^{2-}) initially present in a hydroponic solution (**Figure 1A**). In such a model system, if fractionation occurs, the enrichment in a given isotope in one part of the system results in its depletion in the other, so that isotopic mass balance is always maintained (Fry, 2006).

Our data indicate that isotope discrimination against ^{34}S occurred during SO_4^{2-} uptake, which resulted in transient lighter S isotope compositions of the plants and concomitant ^{34}S enrichments of the residual SO_4^{2-} in the hydroponic solution (**Figure 2A**). Interestingly, fractionation exhibited two phases characterized by distinct fractionation factors [$\Delta_{1(L/H)}$ and $\Delta_{2(L/H)}$] that can be considered as "isotope phenotypes" reflecting plant physiological adaptation to the SO_4^{2-} concentrations in the nutrient solution, which changed during the experiment (**Figures 1F**, **2B**). The maximum fractionation observed was associated with *f* values ranging from 1 to 0.31 (corresponding to external SO_4^{2-} concentrations ranging from 100 to 50 μM), while the minimum isotope effect was associated with the smallest *f* values, when the concentration of SO_4^{2-} in the nutrient solution became critical (≤37 μM) and was potentially able to induce an array of S-deficiency physiological responses (Maruyama-Nakashita et al., 2003), including changes in the expression of the root high-affinity SO_4^{2-} transports, *OsSULTR1;1* and *OsSULTR1;2*, involved in SO_4^{2-} uptake (**Figure 2B**). Although a certain degree of

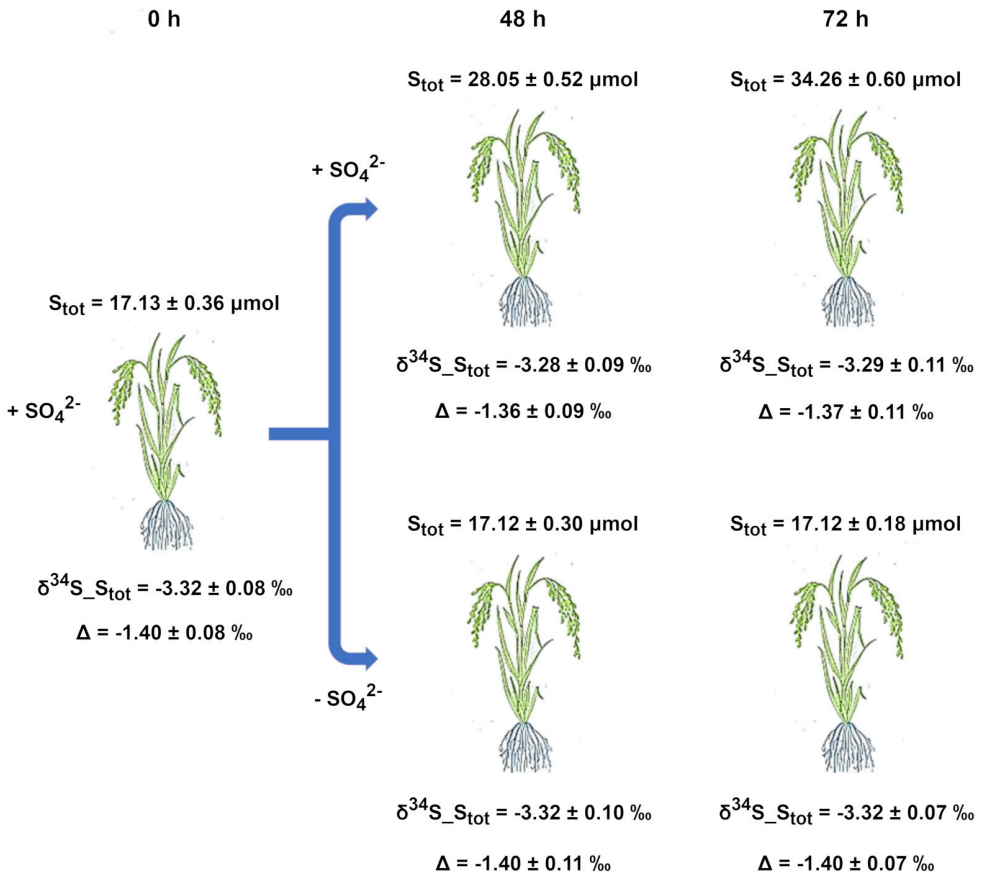

FIGURE 3 | Experimental setup and $^{32}S/^{34}S$ isotope effects associated with S partitioning and metabolism in rice plants. Plants were pre-grown in complete nutrient solutions and then continuously maintained on media containing SO_4^{2-} or deprived of SO_4^{2-} for 72 h (experimental setup B). S_{tot}, total S amount in a whole plant; $\delta^{34}S\_S_{tot}$, S isotope composition of the whole plant; Δ, ^{34}S depletion relative to the S source ($\delta^{34}S\_SO_4^{2-}{}_{source}$ = −1.92 ± 0.02‰). Data are means ± SE of three independent experiments run in duplicate (n = 3).

functional redundancy may exist, *OsSULTR1;2* is considered the major gene involved in SO_4^{2-} uptake under normal conditions, while *OsSULTR1;1* is a more specialized gene that is strongly induced under S limitation (Kumar et al., 2011). The prevalence of *OsSULTR1;1* or *OsSULTR1;2* under different environmental conditions could explain the two isotope phenotypes observed during plant SO_4^{2-} acquisition, assuming that the different isotope effects may be associated with the activity of the two SO_4^{2-} transporters. Thus, the plasticity of the isotope phenotype could reflect gene expression in response to changes in both environmental conditions and plant S-nutritional status.

Less information is currently available about the $^{32}S/^{34}S$ isotope effects occurring during S partitioning and metabolism in plants since the cycling of the S pools in a whole plant may attenuate the isotope differences between organs potentially caused by S reduction and assimilation. Most of the SO_4^{2-} ions that are taken up by root are translocated to the shoot, where they are assimilated into organic compounds (Takahashi et al., 2011). However, part of SO_4^{2-} is also assimilated into the root, and the continuous exchanges of SO_4^{2-} and S_{org} compounds occur in a shoot-to-root direction in order to ensure the S homeostasis of the root (Cooper and Clarkson, 1989; Bell et al., 1995; Yoshimoto et al., 2003; Larsson et al., 2006).

To analyze the isotope effects occurring during S partitioning and metabolism, we carried out experiments aimed at the following: (i) preventing possible perturbations due to the continuous changes of the $\delta^{34}S\_SO_4^{2-}$ values of the external solution and (ii) obtaining rice plants with the same overall S isotope composition (**Figure 3**). In these experiments, plants can be considered systems continuously supplied by an S source that does not change in concentration and isotope composition.

As previously described, plants continuously grown in the presence of SO_4^{2-} reached metabolic and S isotope steady-states characterized by the invariance of the concentration and the isotope signature of each S pool. It should be noted that the S isotope distribution between root and shoot observed in this study strongly differs from the pattern described by Tcherkez and Tea (2013), concerning the S natural isotope composition in different organs (roots, leaf, stem, glumes, and grains) of mature wheat. Such a discrepancy might depend on the growth conditions (closed hydroponic-plant system vs. field) or, more likely, on the different S nutritional status and/or growth stage

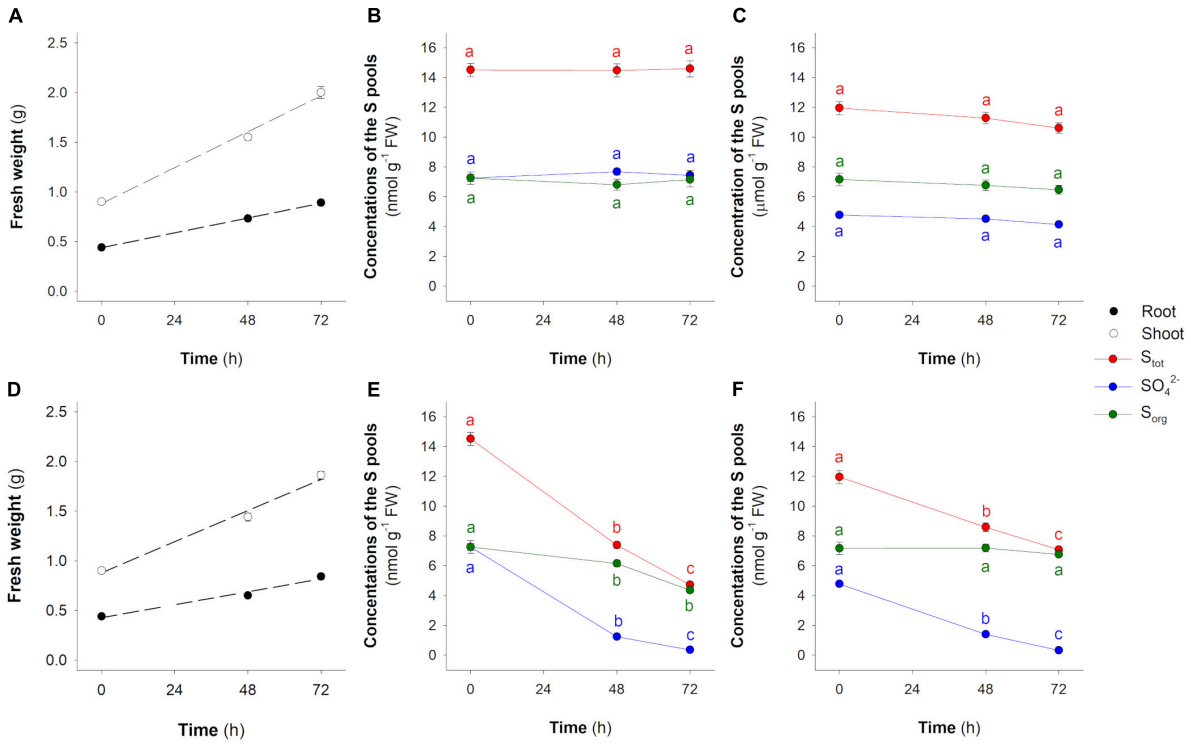

FIGURE 4 | Changes in the concentration of the S pools (S_{tot}, SO_4^{2-}, and S_{org}) in root and shoot of rice plants grown in the presence or in the absence of SO_4^{2-} in the hydroponic solution. **(A)** Root and shoot fresh weight (FW) in the presence of SO_4^{2-}. **(B)** S_{tot}, SO_4^{2-}, and S_{org} in the root of plants grown in the presence of SO_4^{2-}. **(C)** S_{tot}, SO_4^{2-}, and S_{org} in the shoot of plants grown in the presence of SO_4^{2-}. **(D)** Root and shoot FW in the absence of SO_4^{2-}. **(E)** S_{tot}, SO_4^{2-}, and S_{org} in the root of plants grown in the absence of SO_4^{2-}. **(F)** S_{tot}, SO_4^{2-}, and S_{org} in the shoot of plants grown in the absence of SO_4^{2-}. Data are means ± SE of three independent experiments run in duplicate ($n = 3$). Different letters indicate significant differences between the samples at different times ($P < 0.05$).

of the plants considered in the two studies since S stable isotope separations conserve the memory of the physiological and metabolic activities that determined them. Finally, differences may also originate from the different distribution of the S assimilation enzymes in the leaf, since rice assimilates SO_4^{2-} mainly in the bundle sheaths, while other species, also in the mesophyll (Hua et al., 2021).

The isotope composition of the SO_4^{2-} pools of the root was lighter relative to the S source but heavier with respect to the expected composition calculated according to the isotope discrimination occurring during SO_4^{2-} uptake at high external concentrations [i.e., $\delta^{34}S\_SO_4^{2-} > \delta^{34}S\_SO_4^{2-}{}_{source} - \Delta_{1(L/H)}$]. Interestingly, SO_4^{2-} translocation from root to shoot did not discriminate the S isotopes since no differences were found when comparing the isotope signatures of the SO_4^{2-} ions in root and xylem sap (**Figure 5**). However, the SO_4^{2-} pools of the shoot were significantly ^{34}S-enriched with respect to the SO_4^{2-} pools of both root and xylem sap. This was likely due to SO_4^{2-} assimilation that, favoring the lighter ^{32}S isotope, causes a ^{34}S enrichment of the residual SO_4^{2-} ions left behind. The occurrence of an S isotope separation during SO_4^{2-} assimilation is consistent with the observation that the S_{org} pools of the shoot were significantly depleted in ^{34}S relative to both the SO_4^{2-} pools of the shoot and the S source. Since the aerial portion of the plant is fed by the SO_4^{2-} ions continuously translocated from root to shoot and the S_{tot} of the shoot was lighter relative to the SO_4^{2-} coming from the root, we can reasonably suppose that a non-negligible portion of the ^{34}S-enriched SO_4^{2-} of the shoot is translocated to the root. Thus, the isotope signature of the SO_4^{2-} pool of the root could be the result of mixing effects due to the overall S isotope circulation, SO_4^{2-} uptake, and local S assimilation. Assuming that during the S isotope steady-state, (i) the $\delta^{34}S\_SO_4^{2-}$ values measured in the root are mainly influenced by root SO_4^{2-} uptake and SO_4^{2-} translocation from shoot to root, and (ii) the S isotope composition of the instantaneous SO_4^{2-} that continuously enters the root cells should theoretically differ from the S source by the fractionation factor $\Delta_{1(L/H)}$, so that

$$\delta^{34}S\_SO_{4\ ist}^{2-} = \delta^{34}S\_SO_{4\ source}^{2-} - \Delta_{1(L/H)}$$
$$= -1.92\ ‰ - 1.09‰ = -3.01‰$$

We can estimate the maximum amount of SO_4^{2-} that, coming from the shoot, is translocated and accumulated into the root (defined as $SO_4^{2-}{}_{StoR}$) by imposing the following mass balance:

$$\delta^{34}S\_SO_{4\ root}^{2-} \cdot SO_{4\ root}^{2-} = \delta^{34}S\_SO_{4\ shoot}^{2-} \cdot SO_{4\ StoR}^{2-} + \delta^{34}S\_SO_{4\ ist}^{2-} \cdot (SO_{4\ root}^{2-} - SO_{4\ StoR}^{2-})$$

where $\delta^{34}S\_SO_4^{2-}{}_{root}$ is the steady-state isotope composition of the SO_4^{2-} pool of the root, $SO_4^{2-}{}_{root}$ is the total amount of the

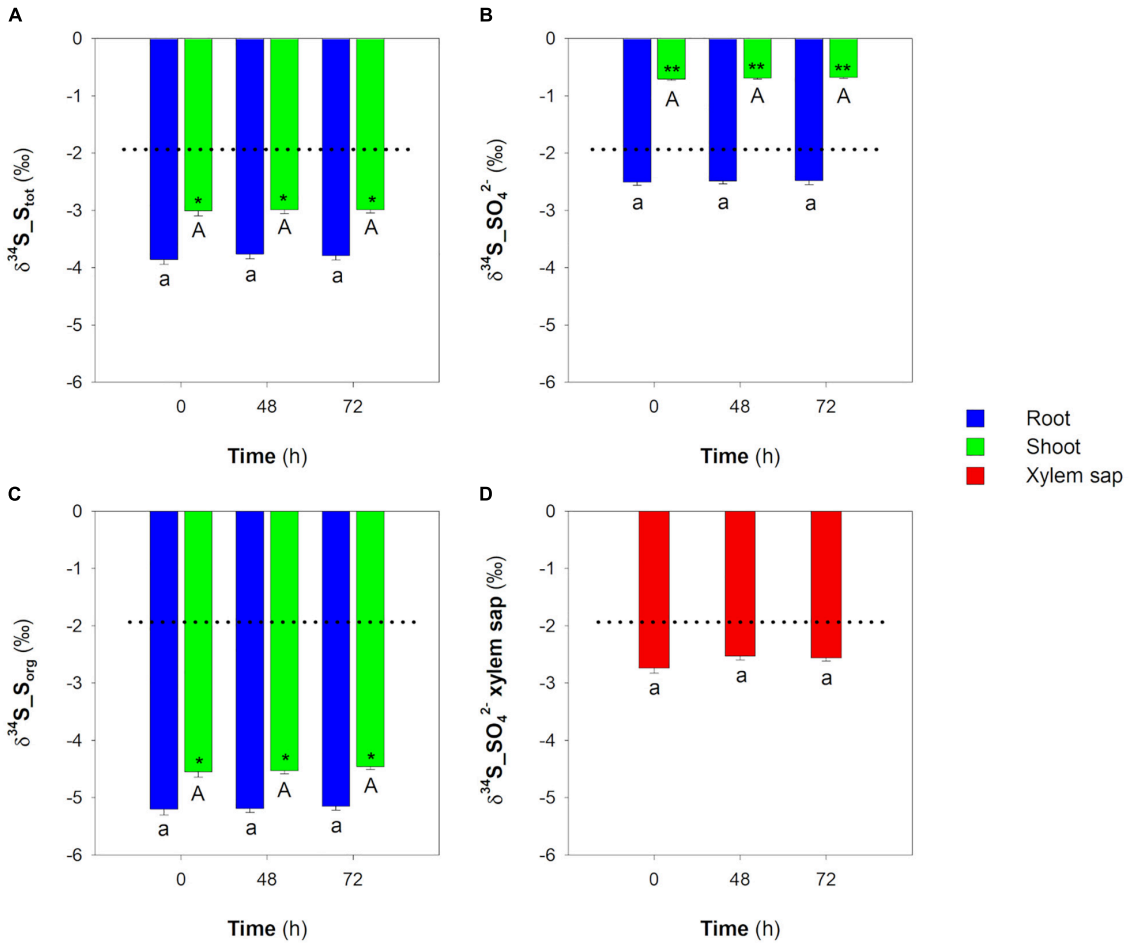

FIGURE 5 | Sulfur isotope composition of the main S pools in root and shoot and of SO_4^{2-} in the xylem sap of rice plants grown in the presence of SO_4^{2-} in the hydroponic solution. **(A)** S isotope composition of S_{tot} in root and shoot. **(B)** S isotope composition of SO_4^{2-} in root and shoot. **(C)** S isotope composition of S_{org} in root and shoot. **(D)** S isotope composition of SO_4^{2-} in xylem sap. Dotted lines indicate the $\delta^{34}S$ value of the S source used in the experiment ($\delta^{34}S\_SO_4^{2-}{}_{source} = -1.92 \pm 0.02‰$). Data are means ± SE of three independent experiments run in duplicate ($n = 3$). Asterisks indicate significant differences (Student's *t*-test; *$0.001 \leq P < 0.05$; **$P < 0.001$) between root and shoot of plants sampled at the same time. Different letters indicate significant differences between the samples (root, shoot, or xylem sap) at different times ($P < 0.05$).

SO_4^{2-} measured in the root, and $\delta^{34}S\_SO_4^{2-}{}_{shoot}$ is the isotope composition of the SO_4^{2-} ions coming from the shoot. Solving the equation for the unknown $SO_4^{2-}{}_{StoR}$ reveals that, in our conditions, 21.7% of the steady-state SO_4^{2-} pool of the rice root is inherited from the shoot.

Although less information is currently available on the long-distance transport of SO_4^{2-} from shoot to root, we can reasonably suppose that such an activity may involve the phloem and specific isoforms of SO_4^{2-} transporters mediating the loading of SO_4^{2-} into the sieve tubes (Takahashi, 2019). Feeding experiments with $^{35}SO_4^{2-}$ performed on *Arabidopsis* (Yoshimoto et al., 2003) support our finding, indicating the retranslocation of SO_4^{2-} as an important activity in controlling root SO_4^{2-} homeostasis and S isotope composition.

In contrast, during the growing period in the absence of SO_4^{2-}, rice plants can be considered closed systems assimilating the SO_4^{2-} ions previously absorbed during the preliminary growth phase and allocating the S_{org} pools to optimize the distribution of the limited S resources between root and shoot. It is worth noting that in these conditions, the invariance of the S_{tot} isotope composition of both root and shoot was associated with dramatic changes in the isotope composition of the relative SO_4^{2-} and S_{org} pools (**Figure 6**), mainly caused by the $^{32}S/^{34}S$ isotope effects occurring during SO_4^{2-} assimilation. During the observation period, plants rapidly consumed the available SO_4^{2-} pools: at the end of the experiment, the overall S_{org} pool was about 94% of the S_{tot}. The S isotope mass balance that was carried out considering the overall SO_4^{2-} and S_{org} pools of the plants (i.e., root + shoot; **Table 1**) revealed that continuous S assimilation progressively enriched both the overall S_{org} pool in the lighter ^{32}S isotope and the residual SO_4^{2-} in the heavier ^{34}S isotope, producing an apparent isotope separation that was closely dependent on the severity of the imposed S starvation, as indicated by calculated Δ values ($\Delta = \delta^{34}S\_S_{org} - \delta^{34}S\_SO_4^{2-}$)

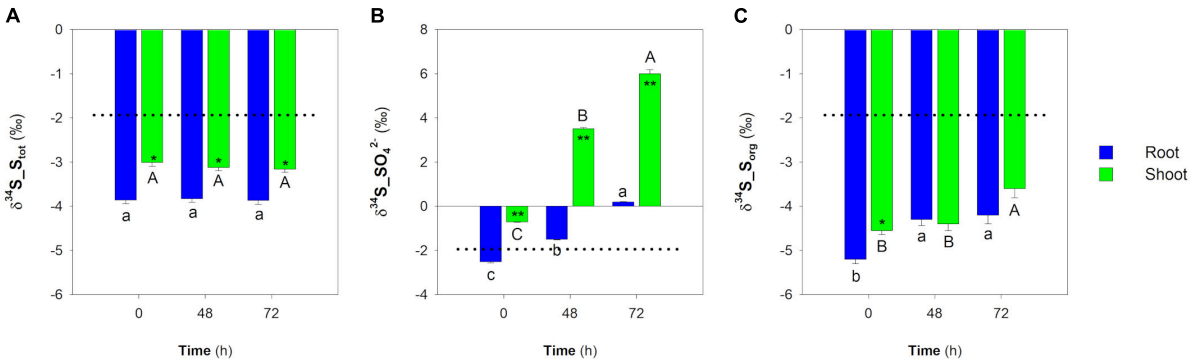

FIGURE 6 | Sulfur isotope composition of the main S pools in root and shoot of rice plants grown in the absence of SO_4^{2-} in the hydroponic solution. **(A)** S isotope composition of S_{tot} in root and shoot. **(B)** S isotope composition of SO_4^{2-} in root and shoot. **(C)** S isotope composition of S_{org} in root and shoot. Data are means ± SE of three independent experiments run in duplicate ($n = 3$). Asterisks indicate significant differences (Student's t-test; *$0.001 \leq P < 0.05$; ** $P < 0.001$) between root and shoot of plants sampled at the same time. Different letters indicate significant differences between the samples (root and shoot) at different times ($P < 0.05$).

TABLE 1 | Amount and sulfur (S) isotope composition of the overall SO_4^{2-} and S organic (Sorg) pools of rice plants grown in the absence of SO_4^{2-} in the hydroponic solution.

	Time (h)					
	0		48		72	
	Amount (μmol)	$\delta^{34}S$ (‰)	Amount (μmol)	$\delta^{34}S$ (‰)	Amount (μmol)	$\delta^{34}S$ (‰)
SO_4^{2-}	7.48 ± 0.13^{a}	-1.47 ± 0.05^{c}	2.80 ± 0.05^{b}	2.07 ± 0.08^{b}	0.90 ± 0.02^{c}	4.06 ± 0.18^{a}
S_{org}	9.65 ± 0.38^{c}	-4.76 ± 0.28^{a}	14.32 ± 0.31^{b}	-4.73 ± 0.17^{a}	16.22 ± 0.18^{a}	-3.73 ± 0.17^{b}

Data are means ± SE of three independent experiments run in duplicate (n = 3). Different letters indicate significant differences between the samples at different times ($P < 0.05$).

that ranged from -3.29 ± 0.40 (at the beginning of the experiment) to -7.80 ± 0.18‰ (at 72 h). As expected, the most pronounced isotope separations were observed in the shoot, confirming the prominent role of the rice aerial portion in SO_4^{2-} assimilation and S allocation (Takahashi et al., 2011).

CONCLUSION AND PERSPECTIVES

Our results provide an overview of the $^{32}S/^{34}S$ isotope effects occurring during SO_4^{2-} uptake, partitioning, and metabolism in rice. The main results clearly show that SO_4^{2-} uptake discriminates against ^{34}S, enriching plant total biomass in the lighter ^{32}S isotope relative to the S source. The S isotope discrimination observed during SO_4^{2-} acquisition closely depends on the amount of SO_4^{2-} in the growing medium, as well as on the plants' molecular and physiological responses aimed at optimizing S nutrition under different environmental conditions. Although further experiments will be necessary to directly measure the isotope effect associated with the activity of a single SO_4^{2-} transporter, we can reasonably conclude that *OsSULTR1;1* and *OsSULTR1;2* differently discriminate against ^{34}S, producing S isotope phenotypes closely dependent on their relative expression.

Results also indicate that the steady-state S isotope composition of the different S pools of both root and shoot mainly results from the substantial S isotope fractionations occurring during SO_4^{2-} assimilation and mixing effects due to the overall isotope circulation inside the whole plant. Finally, the extreme variability of the S isotope phenotypes observed under various S conditions underlines the potential of the $\delta^{34}S$ analysis to provide information for further detailed characterization of the metabolic and molecular processes involved in plant S homeostasis, as well as of the plant S systemic fluxes occurring in different nutritional and environmental conditions, since the S stable isotope separations conserve the memory of the activities that determined them.

DATA AVAILABILITY STATEMENT

The raw data supporting the conclusions of this article will be made available by the authors, without undue reservation.

AUTHOR CONTRIBUTIONS

VC, MC, GS, and FN designed the experiments. VC, MM, and MC performed the experiments. FN analyzed the data and wrote the manuscript. All authors revised the manuscript draft and approved the final version.

ACKNOWLEDGMENTS

The music of Gustav Mahler's IX Symphony inspired this study. We thank Clarissa Lancilli for her precious support during the revision of the manuscript.

SUPPLEMENTARY MATERIAL

The Supplementary Material for this article can be found online at: https://www.frontiersin.org/articles/10.3389/fpls.2022.837517/full#supplementary-material

REFERENCES

Bell, C. I., Clarkson, D. T., and Cram, W. J. (1995). Partitioning and redistribution of sulphur during S-stress in Macroptilium atropurpureum cv. Siratro. *J. Exp. Bot.* 46, 73–81.

Blair, G. J., and Till, A. R. (2003). *Guidelines for the Use of Isotopes of Sulfur in Soil-plant Studies*. Vienna: International Atomic Energy Agency (IAEA).

Buchner, P., Takahashi, H., and Hawkesford, M. J. (2004). Plant sulphate transporters: co-ordination of uptake, intracellular and long-distance transport. *J. Exp. Bot.* 55, 1765–1773. doi: 10.1093/jxb/erh206

Cooper, H. D., and Clarkson, D. T. (1989). Cycling of amino-nitrogen and other nutrients between shoots and roots in cereals – a possible mechanism integrating shoot and root in the regulation of nutrient uptake. *J. Exp. Bot.* 40, 753–762. doi: 10.1093/jxb/40.7.753

Coplen, T. B., and Krouse, H. R. (1998). Sulphur isotope data consistency improved. *Nature* 392:32.

De Laeter, J. R., Böhlke, J. K., De Bièvre, P., Hidaka, H., Peiser, H. S., Rosman, K. J. R., et al. (2003). Atomic weights of the elements: review 2000 (IUPAC technical report). *Pure Appl. Chem.* 75, 683–800.

Epstein, E. (2000). "The discovery of the essential elements" in *Discoveries in Plant Biology*. eds S.-D. Kung and S.-F. Yang (Singapore: World Scientific Publishing). 1–16. doi: 10.1142/9789812813503_0001

Fry, B. (2006). *Stable Isotope Ecology*. New York: Springer.

Gigolashvili, T., and Kopriva, S. (2014). Transporters in plant sulfur metabolism. *Front. Plant Sci.* 5:442. doi: 10.3389/fpls.2014.00442

Godwin, R. M., Rae, A. L., Carrol, B. J., and Smith, F. W. (2003). Cloning and characterization of two genes encoding sulfate transporters from rice (Oryza sativa L.). *Plant Soil* 257, 113–123. doi: 10.1023/a:1026202709134

Günal, S., Hardman, R., Kopriva, S., and Mueller, J. W. (2019). Sulfation pathways from red to green. *J. Biol. Chem.* 294, 12293–12312. doi: 10.1074/jbc.REV119.007422

Hua, L., Stevenson, S. R., Reyna-Llorens, I., Xiong, H., Kopriva, S., and Hibberd, J. M. (2021). The bundle sheath of rice is conditioned to play an active role in water transport as well as sulfur assimilation and jasmonic acid synthesis. *Plant Cell* 107, 268–286. doi: 10.1111/tpj.15292

Kemp, A. L. W., and Thode, H. G. (1968). The mechanism of the bacterial reduction of sulphate and of sulphite from isotope fractionation studies. *Geochim. Cosmochim. Acta* 32, 71–91.

Kennedy, B. V., and Krouse, H. R. (1990). Isotope fractionation by plants and animals: implications for nutrition research. *Can. J. Physiol. Pharmacol.* 68, 960–972. doi: 10.1139/y90-146

Krouse, H. R., Stewart, J. W. B., and Grinenko, V. A. (1991). "Pedosphere and biosphere" in *Stable Isotopes: Natural and Anthropogenic Sulfur in the Environment, SCOPE 43*. eds H. R. Krouse and V. A. Grinenko (New York: John Wiley & Sons). 267–306.

Kumar, S., Asif, M. A., Chakrabarty, D., Tripathi, R. D., and Trivedi, P. K. (2011). Differential expression and alternative splicing of rice sulphate transporter family members regulate sulphur status during plant growth, development and stress conditions. *Funct. Integr. Genomics* 11, 259–273. doi: 10.1007/s10142-010-0207-y

Larsson, C. M., Larsson, M., Purves, J. V., and Clarkson, D. T. (2006). Translocation and cycling through roots of recently absorbed nitrogen and sulfur in wheat (Triticum aestivum) during vegetative and generative growth. *Physiol. Plant.* 82, 345–352.

Leustek, T., Martin, M. N., Bick, J. A., and Davies, J. P. (2000). Pathways and regulation of sulfur metabolism revealed through molecular and genetic studies. *Annu. Rev. Plant. Physiol. Plant. Mol. Biol.* 51, 141–165. doi: 10.1146/annurev.arplant.51.1.141

Maghrebi, M., Baldoni, E., Lucchini, G., Vigani, G., Valè, G., Sacchi, G. A., et al. (2021). Analyisis of cadmium root retention for two contrasting rice accessions suggests an important role for OsHMA2. *Plants* 10:806. doi: 10.3390/plants10040806

Maruyama-Nakashita, A., Inoue, E., Watanabe-Takahashi, A., Yamaya, T., and Takahashi, H. (2003). Transcriptome profiling of sulfur-responsive genes in Arabidopsis reveals global effects of sulfur nutrition on multiple metabolic pathways. *Plant Physiol.* 132, 597–605. doi: 10.1104/pp.102.019802

Mekhtiyeva, V. L. (1971). Isotopic composition of sulfur of plants and animals from reservoirs of various salinity. *Geokhimiya* 6, 725–730.

Rees, C. E. (1973). A steady-state model for sulphur isotope fractionation in bacterial reduction processes. *Geochim. Cosmochim. Acta* 37, 1141–1162. doi: 10.1016/0016-7037(73)90052-5

Sacchi, G. A., and Nocito, F. F. (2019). Plant sulfate transporters in the low phytic acid network: some educated guesses. *Plants* 8:616. doi: 10.3390/plants8120616

Sachs, J. (1865). *Handbuch der Experimental-Physiologie der Pflanzen*. Leipzig: Wilhelm Engelmann.

Saito, K. (2004). Sulfur assimilatory metabolism. The long and smelling road. *Plant Physiol.* 136, 2443–2450. doi: 10.1104/pp.104.046755

Tabatabai, M. A., and Bremner, J. M. (1970). A simple turbidimetric method of determining total sulfur in plant material. *Agron. J.* 62, 805–806.

Takahashi, H. (2019). Sulfate transport systems in plants: functional diversity and molecular mechanisms underlying regulatory coordination. *J. Exp. Bot.* 70, 4075–4087. doi: 10.1093/jxb/erz132

Takahashi, H., Kopriva, S., Giordano, M., Saito, K., and Hell, R. (2011). Sulfur assimilation in photosynthetic organisms: molecular functions and regulations of transporters and assimilatory enzymes. *Annu. Rev. Plant Biol.* 62, 157–184. doi: 10.1146/annurev-arplant-042110-103921

Tcherkez, G., and Tea, I. (2013). 32S/34S isotope fractionation in plant sulphur metabolism. *New Phytol.* 200, 44–53. doi: 10.1111/nph.12314

Thode, H. G., Macnamara, J., and Collins, C. B. (1949). Natural variations in the isotopic content of sulphur and their significance. *Can. J. Res.* 27, 361–373. doi: 10.1139/cjr49b-038

Trust, B. A., and Fry, B. (1992). Stable sulphur isotopes in plants: a review. *Plant Cell Environ.* 15, 1105–1110. doi: 10.1111/j.1365-3040.1992.tb01661.x

Wilson, L. G., Bressan, R. A., and Filner, P. (1978). Light-dependent emission of hydrogen sulfide from plants. *Plant Physiol.* 61, 184–189. doi: 10.1104/pp.61.2.184

Winner, W. E., Smith, C. L., Koch, G. W., Mooney, H. A., Bewley, J. D., and Krouse, H. R. (1981). Rates of emission of H2S from plants and patterns of stable sulphur isotope fractionation. *Nature* 289, 672–673.

Yoshimoto, N., Inoue, E., Saito, K., Yamaya, T., and Takahashi, H. (2003). Phloem-localizing sulfate transporter, Sultr1;3, mediates re-distribution of sulfur from source to sink organs in Arabidopsis. *Plant Physiol.* 131, 1511–1517. doi: 10.1104/pp.014712

Conflict of Interest: The authors declare that the research was conducted in the absence of any commercial or financial relationships that could be construed as a potential conflict of interest.

Publisher's Note: All claims expressed in this article are solely those of the authors and do not necessarily represent those of their affiliated organizations, or those of the publisher, the editors and the reviewers. Any product that may be evaluated in this article, or claim that may be made by its manufacturer, is not guaranteed or endorsed by the publisher.

frontiers in Plant Science

OPINION
published: 22 March 2022
doi: 10.3389/fpls.2022.836835

On the Role of Iodine in Plants: A Commentary on Benefits of This Element

Vitor L. Nascimento[1], Beatriz C. O. Q. Souza[1], Guilherme Lopes[2] and Luiz R. G. Guilherme[2]*

[1] Biology Department, Universidade Federal de Lavras, Lavras, Brazil, [2] Soil Science Department, Universidade Federal de Lavras, Lavras, Brazil

Keywords: biofortification, essential element, metabolism, nutrition, transporters

OPEN ACCESS

Edited by:
Marta Wilton Vasconcelos, Catholic University of Portugal, Portugal

Reviewed by:
Leo Sabatino, University of Palermo, Italy
Boris Bokor, Comenius University, Slovakia

****Correspondence:***
Vitor L. Nascimento
vitor.nascimento@ufla.br

Specialty section:
This article was submitted to Plant Nutrition, a section of the journal Frontiers in Plant Science

Received: *16 December 2021*
Accepted: *11 February 2022*
Published: *22 March 2022*

Citation:
Nascimento VL, Souza BCOQ, Lopes G and Guilherme LRG (2022) On the Role of Iodine in Plants: A Commentary on Benefits of This Element. Front. Plant Sci. 13:836835. doi: 10.3389/fpls.2022.836835

Iodine (I) is one of the least abundant elements on Earth's surface; soils have only about 3 mg kg^{-1} of total I (Mohiuddin et al., 2019). However, this value can be higher in places close to the coast and lower in areas with slight marine influence (Fuge and Johnson, 2015). The marine environment is rich in this element, having about 60 $\mu g\ L^{-1}$ and being the largest I reservoir on the planet (Wong, 1991). Regarding availability of I in soils, a small amount of it is present in the soil solution, with the major fraction being associated with the solid phase, i.e., organic matter and clay minerals, as well as iron (Fe) and aluminum (Al) oxides (Fuge and Johnson, 1986). Some substrate characteristics, such as mineral/organic composition, pH, texture, and redox conditions, limit I mobility and, thus, its absorption by plants (Gonzali et al., 2017). Consequently, knowing the distribution of I worldwide is key for a better understanding of its importance in living beings, from microorganisms to humans, and in plants.

Iodine is an essential element for animals, being involved in regulation of growth, development, and metabolism (Blasco et al., 2008), as it is required for the synthesis of thyroid hormones (thyroxine and triiodothyronine) (Landini et al., 2012). According to Dai et al. (2004), I deficiency in humans can cause a series of diseases and health problems, such as goiter, cretinism, reduced intellectual capacity, spontaneous abortions in pregnant women, congenital defects in fetuses, and deaths in babies at birth. Iodine's bioavailability in food is considered high (∼99%) (Weng et al., 2013). However, some factors, such as food preparation and storage, among others, can affect the bioavailability of I in the human body, causing its deficiency (Gonzali et al., 2017). In the marine environment, algae (especially brown algae) and phytoplankton are I hyperaccumulators, helping to convert iodate (IO_3^-) into iodide (I^-), the most absorbable form for terrestrial plants (Chance et al., 2007). The importance of I in plants has not yet been fully explained, but application of I^- in plant species has provided greater accumulation of the element in edible parts of lettuce (*Lactuca sativa*), spinach (*Spinacia oleracea*), and curly endive (*Cichorium endivia* L. var. *crispum* Hegi) (Zhu et al., 2003; Weng et al., 2008a; Blasco et al., 2013; Smoleń et al., 2016; Sabatino et al., 2021), as well as rice (*Oryza sativa*), wheat (*Triticum aestivum*), and maize (*Zea mays*) (Cakmak et al., 2017), because this process of biofortification is an affordable way to avoid I deficiency in human populations (Blasco et al., 2008, 2013; Prom-u-thai et al., 2020), especially when I is applied as potassium iodate (KIO_3) (Cakmak et al., 2017). Plants, algae, and phytoplankton are also capable of volatilizing I in the form of iodomethane (also known as methyl iodide, CH_3I), and this reaction is catalyzed by enzymes with methyltransferase activity dependent on S-adenosyl-L-methionine (Itoh et al., 2009). Volatilization is possibly associated with defense function while also serving to aid in global I cycle (Fuge and Johnson, 2015; Gonzali et al., 2017). However, emissions, both terrestrial and marine,

can contribute to the damage in the ozone layer, with impacts on the stratosphere still uncertain (Koening et al., 2020). Thus, it is seen that I plays a substantial role in metabolism in animals and especially in humans, while its importance in plants has not yet been fully unveiled. However, what is known so far about the relationship of I with plants?

Iodine can be absorbed by plants from the soil solution *via* roots and through the air, by rain, or dissolved in saline solutions (Kiferle et al., 2021), entering across the stomata and cuticular layer of leaves (Whitehead, 1984). Absorption of I is more efficient through hydroponic systems than *via* soil applications (Smoleń et al., 2016), and both are apparently more efficient ways to supply I to plants than foliar sprays. However, the use of surfactants can increase the absorption of element through this technique (Lawson et al., 2015; Gonzali et al., 2017). Anyhow, more studies are needed to define the best methods for delivering I more efficiently to different crops. Through soil, I is transported into plants by H^+/anion symporters in cells of roots, following the same pathway as chloride (Cl^-) (White and Broadley, 2009). However, the molecular identity of these specific transporters has not yet been unveiled. Despite this, it is suspected that homologs of band 3 anion transporter (also known as anion exchanger 1—AE1) also carry I^- (Bruce et al., 2004), as well as specific Cl^- channels that are immediately permeable to these anions (Roberts, 2006). These channels are encoded by chloride channel (CLCs) transporter genes, which have family members that are I-permeable H^+/anion antiporters (White and Broadley, 2001; Nakamura et al., 2006). These same antiporters, together with anion channels in the tonoplast (i.e., lipoprotein membrane that limits the vacuoles), are likely to transport I^- into and out of the vacuoles in plant cells (De Angeli et al., 2006). Furthermore, halide (i.e., chemical compounds of the same family as I) fluxes can be facilitated by organic acid transporters (White and Broadley, 2001). Thus, it is only a matter of time for specific I^- transporters to be identified and their forms of action to be described. Moreover, in plant tissues, I accumulate in the vacuoles, and in a systemic view of plants, the accumulation process goes from roots to leaves, and then to stems (Weng et al., 2008a). Inside plant tissues, the inorganic form of I, mainly I^-, is predominant (Weng et al., 2008c), but it can also be absorbed as IO_3^- (Fuge and Johnson, 1986). However, plants can absorb organic molecules in the form of iodosalicylates, iodobenzoates, monoiodotyrosine, diiodotyrosine, and triiodothyronine (Smoleń et al., 2020). This element has a predominantly xylem movement in plants, but a phloem route has been identified in tomato (*Solanum lycopersicum*) and lettuce (Landini et al., 2012; Smoleń et al., 2014). Therefore, knowing the role of I in plants at the level of absorption and internal movement is key for establishing effects that this element has on plant nutrition, metabolism, and, consequently, on growth.

Iodine shows evidence of having a role in the metabolic process of plants, as demonstrated by Kiferle et al. (2021), where it increased biomass production and anticipated the flowering of Arabidopsis (*Arabdopsis thaliana*); it was also present in root and shoot proteins, and helped to modulate the expression of genes involved in defense responses. Some authors, such as Lehr et al. (1958) and Borst Pauwels (1961), six decades ago, considered I as a micronutrient for plants because when applied in small amounts it is related to positive effects on some plant species, such as those previously mentioned, in addition to the fact that I increase production of components of the antioxidant system in lettuce plants, as reported by Blasco et al. (2008). Nevertheless, when applied in high amounts, I can cause symptoms of toxicity, such as leaf lesions, stunted plant growth, and, ultimately, plant death (Lehr et al., 1958; Weng et al., 2008b). These factors make I comparable to other plant micronutrients, such as boron (B), chlorine (Cl), copper (Cu), Fe, manganese (Mn), molybdenum (Mo), nickel (Ni), and zinc (Zn). However, to what extent is this comparison applicable? Although several studies are being carried out to unravel the effects of I on plants, there is still lack of evidence that I can be considered a (micro)nutrient for plants instead of being just a beneficial element.

Brown et al. (2021), in a review addressing the concept of plant nutrients and their evolving definitions, provided a historical perspective on the conceptualization of essential elements for plants. One of the most important concepts was established by Arnon and Stout (1939), who considered that an element would only be essential if: "(*i*) its deficiency makes it impossible for the plant to complete the vegetative or reproductive phase of its life cycle; (*ii*) its deficiency is specific to the element in question, and can be prevented or corrected with its supplementation; and (*iii*) the element is directly involved in plant nutrition, regardless of its possible effects in the correction of any unfavorable microbiological or chemical condition of the soil or other culture medium." Over time, these definitions have changed slightly, and one of the most recent concepts is in the first chapter of the book "Mineral Nutrition of Higher Plants" (Kirkby, 2012), where for an element to be considered essential it must meet the following three requirements "(*i*) a plant should be unable to complete its life cycle in the absence of the element; (*ii*) the element's function must not be replaced by another element; and (*iii*) the element must be directly involved in plant metabolism, as a component of an essential plant constituent, such as an enzyme, or it must be required by a distinct metabolic step, such as an enzymatic reaction." According to Broadley et al. (2012), differentiation between beneficial and essential elements is difficult, especially in the case of trace elements, such as I. Whitehead (1984) considers I as a non-essential element, while more recent studies by Sahin (2020) and Medrano Macías et al. (2021) address I as a non-essential but beneficial element. With passage of time and occurrence of a greater number of studies on this subject, it is natural that more elements are added to the list of essentials (or beneficial) elements established by the previously mentioned authors. The fact that I is currently included in the list of beneficial elements shows an evolution of pre-established definitions and standards. These concepts are increasingly being adjusted to the realities of modern agriculture and to the needs of tackling micronutrient deficiencies in human populations (hidden hunger).

Thus, in this scenario of constant change, an ongoing debate on features and definitions of elements' essentiality becomes necessary, as science is done every day, and new research data

are always being published. For now, attentiveness is needed, as there is still a lot to be known about the effects, in the short and long terms, of I on plants, and its exogenous application not only in plants but also in the environment. In conclusion, it is fascinating that in 2022 we are still discovering the functionality of a chemical element in plant nutrition and metabolism. Here, we do not discard the possible essentiality of this element; however, we highlight that the findings in Arabidopsis need to be demonstrated in a greater number of plant (crop) species. Iodine is perhaps not an essential element, but it is beneficial as silicon (Si), selenium (Se), sodium (Na), and others. Finally, our position is in support of efforts to promote crop biofortification with this element to tackle hidden hunger.

AUTHOR CONTRIBUTIONS

All authors conceived the idea, collected the data, and contributed to writing the article.

FUNDING

This study was possible because of the support provided by the National Council for Scientific and Technological Development (CNPq), Coordination for the Improvement of Higher Education Personnel (CAPES), and Research Support Foundation of the State of Minas Gerais (FAPEMIG).

REFERENCES

Arnon, D. I., and Stout, P. R. (1939). The essentiality of certain elements in minute quantity for plants with special reference to copper. *Plant Physiol.* 14, 371–375. doi: 10.1104/pp.14.2.371

Blasco, B., Leyva, R., Romero, L., and Ruiz, J. M. (2013). Iodine effects on phenolic metabolism in lettuce plants under salt stress. *J. Agric. Food Chem.* 61, 2591–2596. doi: 10.1021/jf303917n

Blasco, B., Rios, J., Cervilla, L., Sánchez-Rodrigez, E., Ruiz, J., and Romero, L. (2008). Iodine biofortification and antioxidant capacity of lettuce: potential benefits for cultivation and human health. *Ann. Appl. Biol.* 152, 289–299. doi: 10.1111/j.1744-7348.2008.00217.x

Borst Pauwels, G. W. F. H. (1961). Iodine as a micronutrient for plants. *Plant Soil* 14, 377–392. doi: 10.1007/BF01666295

Broadley, M. R., Brown, P. H., Cakmak, I., Ma, J. F., Rengel, Z., and Zhao, F. J. (2012). "Chapter 8 Beneficial elements," in *Marschner's Mineral Nutrition of Higher Plants*, 3rd Edn, ed. P. Marschner (Amsterdam: AcademicPress), 249–269.

Brown, P. H., Zhao, F. J., and Dobermann, A. (2021). What is a plant nutrient? Changing definitions to advance science and innovation in plant nutrition. *X-MOL* [preprint] doi: 10.1007/s11104-021-05171-w

Bruce, L. J., Pan, R. J., Cope, D. L., Uchikawa, M., Gunn, R. B., Cherry, R. J., et al. (2004). Altered structure and anion transport properties of band 3 (AE1, SLC4A1) in human red cells lacking glycophorin. *A. J. Bio. Chem.* 279, 2414–2420. doi: 10.1074/jbc.M309826200

Cakmak, I., Prom-u-thai, C., Guilherme, L. R. G., Rashid, A., Hora, K. H., Yazici, A., et al. (2017). Iodine biofortification of wheat, rice and maize through fertilizer strategy. *Plant Soil* 418, 319–335. doi: 10.1007/s11104-017-3295-9

Chance, R., Malin, G., Jickells, T., and Baker, A. R. (2007). Reduction of iodate to iodide by cold water diatom cultures. *Mar. Chem.* 105, 169–180.

Dai, J. L., Zhu, Y. G., Zhang, M., and Huang, Y. Z. (2004). Selecting iodine-enriched vegetables and the residual effect of iodate application to soil. *Biol. Trace Elem. Res.* 101, 265–276. doi: 10.1385/BTER:101:3:265

De Angeli, A., Monachello, D., Ephritikhine, G., Frachisse, J. M., Thomine, S., Gambale, F., et al. (2006). The nitrate/proton antiporter AtCLCa mediates nitrate accumulation in plant vacuoles. *Nature* 442, 939–942. doi: 10.1038/nature05013

Fuge, R., and Johnson, C. C. (1986). The geochemistry of iodine – a review. *Env. Geochem. Health* 8, 31–54.

Fuge, R., and Johnson, C. C. (2015). Iodine and human health, the role of environmental geochemistry and diet, a review. *Appl. Geochem.* 63, 282–302. doi: 10.1016/j.apgeochem.2015.09.013

Gonzali, S., Claudia Kiferle, C., and Perata, P. (2017). Iodine biofortification of crops: agronomic biofortification, metabolic engineering and iodine bioavailability. *Curr. Opin. Biotech.* 44, 16–26. doi: 10.1016/j.copbio.2016.10.004

Itoh, N., Toda, H., Matsuda, M., Negishi, T., Taniguchi, T., and Ohsawa, N. (2009). Involvement of S-adenosylmethionine-dependent halide/thiol methyltransferase (HTMT) in methyl halide emissions from agricultural plants: isolation and characterization of an HTMT-coding gene from *Raphanus sativus* (daikon radish). *BMC Plant. Biol.* 9:116. doi: 10.1186/1471-2229-9-116

Kiferle, C., Martinelli, M., Salzano, A. M., Gonzali, S., Beltrami, S., Salvadori, P. A., et al. (2021). Evidences for a Nutritional Role of Iodine in Plants. *Front. Plant Sci.* 12:616868. doi: 10.3389/fpls.2021.616868

Kirkby, E. A. (2012). "Chapter 1: Introduction, definition and classification of nutrients," in *Marschner's Mineral Nutrition of Higher Plants*, 3rd Edn, ed. P. Marschner (Amsterdam: Academic Press), 3–5.

Koening, T. K., Baidar, S., Campuzano-Jost, P., Cuevas, C. A., Dix, B., Fernandez, R. P., et al. (2020). Quantitative detection of iodine in the stratosphere. *Proc. Natl. Acad. Sci. U.S.A.* 117, 1860–1866. doi: 10.1073/pnas.1916828117

Landini, M., Gonzali, S., Kiferle, C., Tonacchera, M., Agretti, P., Dimida, A., et al. (2012). Metabolic engineering of the iodine content in Arabidopsis. *Sci. Rep.* 2:338. doi: 10.1038/srep00338

Lawson, P. G., Daum, D., Czauderna, R., Meuser, H., and Härtling, J. W. (2015). Soil versus foliar iodine fertilization as a biofortification strategy for field-grown vegetables. *Front. Plant Sci.* 6:450. doi: 10.3389/fpls.2015.00450

Lehr, J. J., Wybenga, J. M., and Rosanow, M. (1958). Iodine as a micronutrient for tomatoes. *Plant Physiol.* 33, 421–427. doi: 10.1104/pp.33.6.421

Medrano Macías, J., López Caltzontzit, M. G., Rivas Martínez, E. N., Narváez Ortiz, W. A., Benavides Mendoza, A., and Martínez Lagunes, P. (2021). Enhancement to Salt Stress Tolerance in Strawberry Plants by Iodine Products Application. *Agronomy* 11:602. doi: 10.3390/agronomy11030602

Mohiuddin, M., Irshad, M., Ping, A., Hussain, Z., and Shahzad, M. (2019). Bioavailability of iodine to mint from soil applied with selected amendment. *Env. Poll. Bioaval.* 31, 138–144. doi: 10.1080/26395940.2019.1588077

Nakamura, A., Fukuda, A., Sakai, S., and Tanaka, Y. (2006). Molecular cloning, functional expression and subcellular localization of two putative vacuolar voltage-gated chloride channels in rice (*Oryza sativa* L.). *Plant Cell Physiol.* 47, 32–42. doi: 10.1093/pcp/pci220

Prom-u-thai, C., Rashid, A., Ram, H., Zou, C., Guilherme, L. R. G., Corguinha, A. P. B., et al. (2020). Simultaneous biofortification of rice with zinc, iodine, iron and selenium through foliar treatment of a micronutrient cocktail in five countries. *Front. Plant Sci.* 11:589835.

Roberts, S. K. (2006). Plasma membrane anion channels in higher plants and their putative functions in roots. *New Phyt.* 169, 647–666. doi: 10.1111/j.1469-8137.2006.01639.x

Sabatino, L., Di Gaudio, F., Consentino, B. B., Rouphael, Y., El-Nakhel, C., La Bella, S., et al. (2021). Iodine Biofortification Counters Micronutrient Deficiency and Improve Functional Quality of Open Field Grown Curly Endive. *Horticulturae* 7:58. doi: 10.3390/horticulturae7030058

Sahin, O. (2020). Combined biofortification of soilless grown lettuce with iodine, selenium and zinc and its effect on essential and non-essential elemental composition. *J. Plant Nutr.* 44, 673–678. doi: 10.1080/01904167.2020.1849300

Smoleń, S., Kowalska, I., Halka, M., Ledwozyw-Smoleń, I., Grzanka, M., Skoczylas, Ł, et al. (2020). Selected aspects of iodate and iodosalicylate metabolism in lettuce including the activity of vanadium dependent haloperoxidases as affected by exogenous vanadium. *Agronomy* 10:1. doi: 10.3390/agronomy10010001

Smoleń, S., Kowalska, I., and Sady, W. (2014). Assessment of biofortification with iodine and selenium of lettuce cultivated in the NFT hydroponic system. *Sci. Hort.* 166, 9–16. doi: 10.1016/j.scienta.2013.11.011

Smoleń, S., Ledwozyw-Smoleń, I., and Sady, W. (2016). The role of exogenous humic and fulvic acids in iodine biofortification in spinach (*Spinacia oleracea* L.). *Plant Soil* 402, 129–143. doi: 10.1007/s11104-015-2785-x

Weng, H. X., Hong, C. L., Xia, T. H., Bao, L. T., Liu, H. P., and Li, D. W. (2013). Iodine biofortification of vegetable plants—an innovative method for iodine supplementation. *Chin. Sci. Bull.* 58, 2066–2072. doi: 10.1007/s11434-013-5709-2

Weng, H. X., Hong, C. L., Yan, A. L., Pan, L. H., Qin, Y. C., Bao, L. T., et al. (2008a). Mechanism of iodine uptake by cabbage: effects of iodine species and where it is stored. *Biol. Trace Elem. Res.* 125, 59–71. doi: 10.1007/s12011-008-8155-2

Weng, H. X., Weng, J. K., Yan, A. L., Hong, C. L., Yong, W. B., and Qin, Y. C. (2008b). Increment of Iodine Content in Vegetable Plants by Applying Iodized Fertilizer and the Residual Characteristics of Iodine in Soil. *Biol. Trace Elem. Res.* 123, 218–228. doi: 10.1007/s12011-008-8094-y

Weng, H. X., Yan, A. L., Hong, C. L., Xie, L. L., Qin, Y. C., and Cheng, C. Q. (2008c). Uptake of different species of iodine by water spinach and its effect to growth. *Biol. Trace Elem. Res.* 124, 184–194. doi: 10.1007/s12011-008-8137-4

White, P. J., and Broadley, M. R. (2001). Chloride in soils and its uptake and movement within the plant: a review. *Ann. Bot.* 88, 967–988. doi: 10.1006/anbo.2001.1540

White, P. J., and Broadley, M. R. (2009). Biofortification of crops with seven mineral elements often lacking in human diets – iron, zinc, copper, calcium, magnesium, selenium and iodine. *New Phytol.* 182, 49–84. doi: 10.1111/j.1469-8137.2008.02738.x

Whitehead, D. C. (1984). The distribution and transformations of iodine in the environment. *Environ. Intern.* 10, 321–339. doi: 10.1016/0160-4120(84)90139-9

Wong, G. T. F. (1991). The marine geochemistry of iodine. *Rev. Aquat. Sci.* 4, 45–73.

Zhu, Y. G., Huang, Y. Z., Hu, Y., and Liu, Y. X. (2003). Iodine uptake by spinach (*Spinacia oleracea* L.) plants grown in solution culture: effects of iodine species and solution concentrations. *Environ. Int.* 29, 33–37. doi: 10.1016/S0160-4120(02)00129-0

Conflict of Interest: The authors declare that the research was conducted in the absence of any commercial or financial relationships that could be construed as a potential conflict of interest.

Publisher's Note: All claims expressed in this article are solely those of the authors and do not necessarily represent those of their affiliated organizations, or those of the publisher, the editors and the reviewers. Any product that may be evaluated in this article, or claim that may be made by its manufacturer, is not guaranteed or endorsed by the publisher.

frontiers | Frontiers in Plant Science

ORIGINAL RESEARCH
published: 25 April 2022
doi: 10.3389/fpls.2022.866855

MeNPF4.5 Improves Cassava Nitrogen Use Efficiency and Yield by Regulating Nitrogen Uptake and Allocation

Qiongyue Liang[1,2], Mengmeng Dong[1], Minghua Gu[1], Peng Zhang[3], Qiuxiang Ma[3] and Bing He[1]**

[1] State Key Laboratory for Conservation and Utilization of Subtropical Agro-Bioresources, College of Agriculture, Guangxi University, Nanning, China, [2] National Demonstration Center for Experimental Plant Science Education, College of Agriculture, Guangxi University, Nanning, China, [3] National Key Laboratory of Plant Molecular Genetics, CAS Center for Excellence in Molecular Plant Sciences, Chinese Academy of Sciences, Shanghai, China

OPEN ACCESS

Edited by:
Gianpiero Vigani, University of Turin, Italy

Reviewed by:
Zhenhua Zhang, Hunan Agricultural University, China
Erwan Le Deunff, Université de Caen Normandie, France

***Correspondence:**
Qiuxiang Ma
qxma@cemps.ac.cn
Bing He
hebing@gxu.edu.cn

Specialty section:
This article was submitted to Plant Nutrition, a section of the journal Frontiers in Plant Science

Received: *31 January 2022*
Accepted: *24 March 2022*
Published: *25 April 2022*

Citation:
Liang Q, Dong M, Gu M, Zhang P, Ma Q and He B (2022) MeNPF4.5 Improves Cassava Nitrogen Use Efficiency and Yield by Regulating Nitrogen Uptake and Allocation. Front. Plant Sci. 13:866855. doi: 10.3389/fpls.2022.866855

Improving nitrogen use efficiency (NUE) is a very important goal of crop breeding throughout the world. Cassava is an important food and energy crop in tropical and subtropical regions, and it mainly use nitrate as an N source. To evaluate the effect of the nitrate transporter gene *MeNPF4.5* on the uptake and utilization of N in cassava, two *MeNPF4.5* overexpression lines (*MeNPF4.5* OE-22 and *MeNPF4.5* OE-34) and one *MeNPF4.5* RNA interference (RNAi) line (*MeNPF4.5* Ri-1) were used for a tissue culture experiment, combining with a field trial. The results indicated that MeNPF4.5 is a plasma membrane transporter mainly expressed in roots. The gene is induced by NO_3^-. Compared with the wild type, *MeNPF4.5* OE-22 exhibited improved growth, yield, and NUE under both low N and normal N levels, especially in the normal N treatment. However, the growth and N uptake of RNAi plants were significantly reduced, indicating poor N uptake and utilization capacity. In addition, photosynthesis and the activities of N metabolism-related enzymes (glutamine synthetase, glutamine oxoglutarate aminotransferase, and glutamate dehydrogenase) of leaves in overexpression lines were significantly higher than those in wild type. Interestingly, the RNAi line increased enzymatic activity but decreased photosynthesis. IAA content of roots in overexpressed lines were lower than that in wild type under low N level, but higher than that of wild type under normal N level. The RNAi line increased IAA content of roots under both N levels. The IAA content of leaves in the overexpression lines was significantly higher than that of the wild type, but showed negative effects on that of the RNAi lines. Thus, our results demonstrated that the MeNPF4.5 nitrate transporter is involved in regulating the uptake and utilization of N in cassava, which leads to the increase of N metabolizing enzyme activity and photosynthesis, along with the change of endogenous hormones, thereby improving the NUE and yield of cassava. These findings shed light that MeNPF4.5 is involved in N use efficiency use in cassava.

Keywords: cassava, nitrate transport, nitrogen efficiency, growth, *MeNRT1.1/MeNPF4.5*

INTRODUCTION

Cassava (*Manihot esculenta* Crantz) is one of the three major root and tuber crops in the world, and it is the sixth largest food crop globally. It is known as the "underground granary" and "king of starch" because of its importance as a source of food, feed, and industrial processing material, and it is also an important energy crop (Zhuang et al., 2011). Nitrogen (N) is the major limiting factor for cassava yield. Fertilizers are necessary for increasing storage root yields, and thus excessive amounts of N fertilizer may be applied to obtain high yields. However, the N use efficiency (NUE) has decreased from 68 to 47% over the past 50 years (Lassaletta et al., 2014), and more than half of the N applied is lost to the environment. Excessive application of N fertilizer results in leaching of N from farmlands through surface runoff and water pollution (Li et al., 2017; Kyriacou et al., 2018). Because of this, reducing the amount of N fertilizer and improving the NUE of crops have become increasingly important goals for breeders. This is also the case for cassava, where improving the efficiency of N uptake and use is of important theoretical and practical significance for improving the ecological environment, ensuring food safety, and addressing food shortages due to population growth.

Most plants use nitrate (NO_3^-) as the main source of N (Wang W. et al., 2018). NO_3^- is a nutrient that regulates plant growth and development (Fenchel et al., 2012), and it also acts as a signaling substance regulating gene transcription, thus affecting seed germination, plant root growth, and leaf stomatal activity (Wang et al., 2012). The uptake and transport of NO_3^- in the roots and its redistribution among cells are realized through NO_3^- transporters (NRTs). By using isotopic tracers ^{13}N and ^{15}N, two NO_3^- transport systems have been found in higher plants: the high-affinity transport system, which mainly functions under low external NO_3^- concentrations (<0.50 mM), and the low-affinity transport system, which mainly functions under high external NO_3^- concentrations (≥0.50 mM) (Miller et al., 2007; Wang Y. Y. et al., 2018; Gao et al., 2019). High- and low-affinity NRTs are encoded by the *NRT2* and *NRT1* gene families, respectively. The Nitrate Transporter 1 (NRT1) gene family got its name because it was originally found to have the function of transporting NO_3^-, the function of transporting dipeptides was found later and then was further classified as the PEPTIDE TRANSPORTER (PTR) family. However, several studies in the past few years confirmed that an even wider range of molecules are transported by some family members (Zhou et al., 1998; Jeong et al., 2004). Léran et al. (2014) renamed it as NPF (NRT1/PTRFAMILY) family according to its systematic evolutionary characteristics. Currently, 53 *NRT1*/*PTR* family members and seven *NRT2* family members have been found in *Arabidopsis thaliana* (Okamoto et al., 2003). AtNRT1.1 also known as CHL1 and AtNPF6.3, was the first member identified as a low-affinity transporter, but it also functions as a high-affinity transporter at low external NO_3^- concentrations depending upon its phosphorylation state (Liu et al., 1999; Ho et al., 2009; Guo et al., 2014). It plays a key role in sensing and triggering many adaptive changes in response to external NO_3^-, such as stimulating lateral root elongation in NO_3^- rich patches (Remans et al., 2006). NRT1.1 can activate these responses through many independent mechanisms, which can be uncoupled by introducing point mutations in different regions of the protein (Bouguyon et al., 2015). In addition to NO_3^- uptake, NRT1.1 regulates the expression of many NO_3^- responsive genes (Undurraga et al., 2017). Furthermore, NRT1.1 is a master player in the NO_3^- mediated regulation of root system architecture because it stimulates the growth of lateral roots and tap roots of *Arabidopsis* (Remans et al., 2006; Fan et al., 2017; Maghiaoui et al., 2021). Some NRT1 family proteins transport NO_3^- and other diverse compounds, such as nitrite (Sugiura et al., 2007), amino acids (Zhou et al., 1998), peptides (Komarova et al., 2008), and phytohormones including auxin (Krouk et al., 2010), gibberellin (Tal et al., 2016), and abscisic acid (Kanno et al., 2012), which indicates that they have versatile functions.

At present, *NRT/NPF* genes have mainly been identified in *A. thaliana* and rice, and their functions and regulatory mechanisms have been studied in detail (Liu et al., 2015; Sakuraba et al., 2021). For example, studies have shown that rice NRT1.1B is located in the cell membrane and plays an important role in the transport of NO_3^- from the adventitious roots to the leaves (Hu et al., 2015; Zhao et al., 2017). Cassava is an allodiploid species ($2n$ = 36) with a highly heterozygous genome, therefore, the function and expression of NRT genes in cassava deserve our attention. *MeNRT2.1* of cassava was found to be mainly expressed in the root system, and transient expression experiments in protoplasts revealed that the MeNRT2.1 protein is localized on the cell membrane (Zou et al., 2019). Ren et al. (2019) discovered that the *MeNRT2.5* gene was expressed in the roots, stems, leaves, flowers, and other organs, with relatively high expression in the roots of mature cassava plants and the leaves of tissue-cultured seedlings; and the expression of this gene was found to be inhibited by high concentrations of NO_3^-. Despite the progress in characterizing members of the *NRT2* gene family, there has been no report on the *NRT1* gene family in cassava. In this study, the *MeNPF4.5* (*MeNRT1.1*) gene was identified and found to be mainly expressed in cassava roots. Overexpression of this gene in cassava improved the yield of storage roots by increasing the activities of enzymes related to N metabolism and enhancing photosynthesis. In contrast, RNA interference (RNAi) significantly decreased yield, which indicated that MeNPF4.5 plays a vital role in cassava growth by regulating the metabolism and distribution of N.

MATERIALS AND METHODS

Phylogenetic Analysis of NRT1.1

For phylogenetic analysis of NRT1.1, amino acid sequences of NRT1 from different species were obtained from GeneBank and sequence alignment was carried out using DNAMAN software (version 9.0). A phylogenetic tree based on entire amino acid sequences was constructed using the neighbor-joining method with 1000 bootstrap replicates in MEGA 7.0 (Li et al., 2018).

Plasmid Construction and Cassava Transformation

Cassava *MeNPF4.5* (GeneBank accession No. KU361329.1) was cloned from the root cDNA of TMS60444 seedlings, which was cultured in normal condition without NO_3^- induction. *MeNPF4.5* was controlled by the CaMV35S promoter. The expression cassettes was inserted into the binary vector pCAMBIA1301 containing the hygromycin phosphotransferase under the control of the CaMV 35S promoter to generate pC-35S:MeNPF4.5. And a binary expression vector p35S:MeNPF4.5 was constructed according to previous report (Vanderschuren et al., 2009). The plasmids were mobilized into *Agrobacterium tumefaciens* LBA4404, and cassava TMS60444 was used as donor plant to produce transgenic plants. Transgenic plants were produced by reported methods (Zhang et al., 2000).

Subcellular Localization of MeNPF4.5 Protein

The open reading frame of *MeNPF4.5* without a stop codon was amplified using *MeNPF4.5* gene-specific primers (F: cagtGGTCTCacaacatgcttttcactggacttta; R: cagtG GTCTCatacaaacttgtatcaattcga cct) The PCR amplification product was cloned into the pBWA(V)HS-ccdb-GLosgfp vector to generate the MeNPF4.5-enhanced green fluorescent protein (EGFP) C-terminal fusion construct, and 35S-EGFP was used as a negative control. The recombinant plasmids were transferred into *Agrobacterium tumefaciens* strain GV3101 by electroporation and then transformed into *Nicotiana benthamiana* leaves. Two days later, EGFP fluorescence was observed at 488 nm and chloroplast fluorescence was observed at 640 nm under a confocal laser scanning microscope (C2-ER, Nikon, Japan).

Southern Blot and qRT-PCR Analysis

Southern- blot analysis was carried out as described by Xu et al. (2012). Genomic DNA was extracted and digested with *Hind* III, separated by electrophoresis on a 0.8% (w/v) agarose gel, and then transferred to a nylon membrane with a positive charge (Roche, Shanghai, China). The *hygromycin phosphotransferase* (*HPT*) (1 kb) and *MeNPF4.5* (1.5 kb) probes were labeled with digoxigenin. Hybridization and detection were performed with the DIG-High Prime DNA Labeling and Detection Starter Kit II (Roche), according to the manufacturer's instructions.

Total RNA was extracted from different cassava tissues (100 mg each) using RNA Plant Plus Reagent (Tiangen Biotech, Co., Beijing, China), according to the manufacturer's instructions. cDNA was synthesized using the Prime Script^{TM} RT Reagent Kit with gDNA Eraser (Perfect Real Time) (Takara Bio Inc., Kyoto, Japan). The specificity of the gene specific primers was verified by melting curve analysis. The cassava *Actin* gene was used as an internal control, and the $2^{-\Delta\Delta Ct}$ method was used to calculate relative gene expression. The primer sequences were as follows: *MeNPF4.5* (F: 5′-CCT CAA TTC CAG TGA TAC CTC TGC TTT-3′; R: 5′-GGA TTC CTG TGA TCT TCC GAA CCA AT-3′) and *MeActin* (F: 5′-CTC GTG TCA AGG TGT CGT GA-3′; R: 5′-GCC CTC TCA TTT GCT GCA AT-3′).

Cassava Tissue Culture Experiment

The tested materials were the wild-type cassava (*Manihot esculenta* Crantz) cultivar TMS60444 (WT), overexpression lines *MeNPF4.5* OE-22 and *MeNPF4.5* OE-34, and RNAi line *MeNPF4.5* Ri-1. The stems of WT and *MeNPF4.5* transgenic cassava (with one sprout) were subcultured in 1/2 Murashige-Skoog (MS) (Murashige and Skoog, 1962) medium (Hope Bio-Technology, Qingdao, China) in a tissue culture room for 10 days. Germinated seedlings were then transferred in MS medium without $N–NH_4^+$, and the medium was supplemented with KNO_3 as a sole N source at the concentrations as indicated in each individual experiment. Three NO_3^- treatments as follows, N-free: 0 mM, low-N: 0.5 mM, and full-N: 20 mM. For N-free and low-N conditions, ion equilibrium of the medium was ensured by replacing KNO_3 by K_2SO_4. The pH of the medium was adjusted to 6.0 by using NaOH. The cassava seedlings were then incubated at 26°C and 50% relative humidity with a 14 h light/10 h dark cycle. Light intensity during the day period was 250 μmol m^{-2} s^{-1}. The medium contained 25 g L^{-1} sucrose and 1 g L^{-1} Gelrite. The roots were cut at the distance of 1.5 cm from root tip, stems were cut at the distance of 1.5 cm from tip, and the second expanded leaves samples were harvested 25 days after treatment with NO_3^-, frozen in liquid nitrogen, and stored at −80°C until further use.

Wild-type seedlings were grown in MS medium for 25 days and then transferred to hydroponic solution with 10 mM NO_3^-. After cultivation for 1 week, seedlings were transferred to 0.1 mM $CaSO_4$ for 2 days and then to a complete nutrient solution containing 20 mM NO_3^-. Roots were harvested at 1, 2, 4, 6, 8, 12, and 24 h after treatment in 20 mM NO_3^-, frozen in liquid nitrogen, and stored at −80°C for qRT-PCR analysis.

Root NO_3^- Uptake

Wild-type and *MeNPF4.5* transgenic cassava seedlings were grown in MS medium for 25 days and then transferred to hydroponic solution with 10 mM NO_3^-. After cultivation for 1 week, seedlings were transferred to 0.1 mM $CaSO_4$ for 2 days and then exposed to various NO_3^- concentrations for 6 h. Roots were separated from shoots and measure the fresh root weight. Root NO_3^- uptake were determined by disappearance of NO_3^- from the nutrient solution. Their NO_3^- concentration was determined by using Flow Injection Analyzer (FIASTAR 5000, Foss Analytical, Höganäs, Sweden).

$$NO_3^- \text{ uptake} = [(V1 \times C1) - (V2 \times C2)]/(W \times T)$$

where V1 and C1 are the volume of the system and the NO_3^- concentration before experiment, and V2 and C2 are the volume of the system and the NO_3^- concentration after experiment. W is fresh weight of root. T = 6 h.

Field Experiment

Plant Growth Condition

Field experiment was performed in 2016 at Jiatapo, Dingxi Village, Pumiao Town, Nanning City (22°81'N, 108°63'E).

The test soil was evenly flat and had uniform fertility. The chemical compositions of the cultivated soil layers before the experiment are listed in **Supplementary Table 1**. According to the NY/T1749-2009 Soil Fertility Diagnosis and Evaluation Method of Farmland in Southern China standards for total N (1.0 g kg^{-1}) and available N (105 mg kg^{-1}), the soil layers of the test plot were low in N.

A double factor split-plot design was used for field trial; the main and sub-plots were N treatment and cassava lines, respectively. There were two N treatments, low (0 kg ha^{-1}, N0) and normal N (125 kg ha^{-1}, N1), and the N fertilizer was urea (containing 46.7% N). A random block design was adopted with three replications. The same amounts of phosphorus (P) and potassium (K) fertilizers were used for all plots (P_2O_5 48 kg ha^{-1}; K_2O 162 kg ha^{-1}). Super phosphate was used as a P fertilizer, and potassium chloride was used as a K fertilizer. The P fertilizer was applied once at sowing, while the N and K fertilizers were applied thrice: 50% as a base fertilizer, 25% at 40 days after sowing, and 25% at 90 days after sowing.

For the basal fertilizer application, a 10 cm deep groove was dug at a distance of 15 cm away from the cassava stem; all the basal fertilizers were applied evenly in this groove and covered with soil. For the top dressing, the fertilizer was dissolved in water and then applied quantitatively to each plant. The size of the subplot was 10 m^2 (1 m × 10 m), and the distance between cassava plants was 1 m × 1 m. To prevent leaching of the fertilizer from the N1 plot to the N0 plot, the two N treatment plots were separated by 1 m. The cassava plants were planted on May 10, 2016, and conventional field management methods were used during the entire growth period. Plants were harvested for agronomic trait evaluation and subsequent experiments on January 10, 2017.

Nitrogen Use Efficiency and Metabolism Enzyme Assays

During the harvesting of cassava, the fresh weights of leaves, stems, and storage roots of individual plants were measured. A fixed amount of each component was collected and dried at 105°C for 30 min and then further dried at 65°C to a constant weight. Tissue N concentration was determined by the micro-Kjeldahl method (Mishra et al., 2016) after digestion by concentrated H_2SO_4–H_2O_2.

The methods for calculating each indicator were as follows:

$$\text{Dry matter mass of the whole plant } \left(\text{t ha}^{-1}\right) = \text{dry storage root weight} + \text{dry stem weight} + \text{dry leaf weight}$$

(Kang et al., 2020).

$$\text{N accumulation } \left(\text{g plant}^{-1}\right) = \text{N content of the organ} \times \text{dry matter mass of the organ}$$

(Kang et al., 2020).

$$\text{Transport index (\%)} = \text{Shoot N content} / (\text{Root N content} + \text{Shoot N content}) \times 100$$

(Léran et al., 2013).

$$\text{Nutilization efficiency } \left(\text{kg kg}^{-1}\right) = \text{Plant dry weight} / \text{N accumulation}$$

(Kang et al., 2020).

$$\text{N recovery efficiency } \left(\text{kg kg}^{-1}\right) = (\text{N uptake withfertilizer} - \text{N uptake with nofertilizer}) / \text{N application rate}$$

(Peng et al., 2006).

$$\text{Partial factor productivity of N fertilizer } \left(\text{kg kg}^{-1}\right) = \text{Storage root yield} / \text{N application rate}$$

(Peng et al., 2006).

The fifth expanded leaves from plants grown for 3 months were collected with three replications. The midrib was removed, and the sample was cut and mixed evenly to determine the activity of key enzymes involved in nitrogen metabolism. Nitrate reductase (NR) activity was measured using a kit from the Nanjing Jian Cheng Bioengineering Institute (Nanjing, China), according to the manufacturer's instructions. The activities of glutamine synthetase (GS), glutamine oxoglutarate aminotransferase (GOGAT), and glutamate dehydrogenase (GDH) were determined using the method described by Huang et al. (2015).

Leaf Photosynthesis and Chlorophyll Fluorescence Parameters Analysis

The photosynthetic activity of the fifth expanded leaves from plants grown for 3 months was measured with a 6400XT (LI-COR, Lincoln, Nebraska, United States) photosynthesis system on a sunny day from 9:00 to 11:00 in the morning. The net photosynthetic rate (Pn), intercellular CO_2 concentration (Ci), stomatal conductance (Gs), and transpiration rate (Tr) were determined. The photosynthetic photon flux density was 1,200 $\mu mol\ m^{-2}\ s^{-1}$.

The following chlorophyll fluorescence parameters were recorded from leaves at the same position as those used for photosynthetic parameter measurements using an imaging chlorophyll fluorimeter (Walz Imaging PAM, Walz GmbH, Effeltrich, Germany): Fv/Fm (PS II maximum quantum yield of photosynthesis), Y(II) (PS II actual quantum yield of photosynthesis), qP (photochemical quenching coefficient), and qN (non-photochemical quenching coefficient). The measurements were conducted at room temperature (25°C) using the standard saturated light mode. The actinic light intensity was 10 $\mu mol\ m^{-2}\ s^{-1}$. Prior to detection, leaves were adapted to darkness for 30 min.

Endogenous Hormone Analysis

Cassava seedlings were cultivated in tissue culture under different N conditions (0.5 and 20 mM NO_3^-) for 25 days, and then the endogenous hormone content in the roots (excised from 1.5 cm of primary root tips) and leaves (the second expanded leaves) of WT and transgenic plants were analyzed. The extraction, purification and determination of endogenous hormones levels were assayed by an indirect enzyme-linked immunosorbent assay (ELISA) technique, which performed with a kit from the Beijing Benongda Tianyi Biotechnology Co. (Beijing, China) according to the manufacturer's instructions.

Statistical Analysis

Data from at least three biological replicates are presented as the mean ± SE. Analysis of variance (ANOVA) followed by

independent sample Student's *t*-test was performed using SPSS software version 22.0 (IBM Corp., Armonk, NY, United States). $P < 0.05$ was considered statistically significant.

RESULTS

Phylogenetic Analysis of NRT1.1 and MeNPF4.5 Is a Plasma Membrane Localized Protein

Phylogenetic analysis showed that MeNPF4.5 is closely related to CsNRT1.2 of *Camellia sinensis* and HaNRT1.2 of *Helianthus annuus*. These results showed that MeNPF4.5 is a member of the NRT1/NPF subfamily (**Figure 1**).

A 35S-MeNPF4.5-EGFP fusion protein construct was used to determine the subcellular localization of MeNPF4.5, and 35S-EGFP served as control. The constructs were transiently transformed into leaf cells of *Nicotiana* using agroinfiltration. MeNPF4.5-EGFP was expressed in the plasma membrane, whereas EGFP was detected not only in the plasma membrane, but also in the cytoplasm and nucleus (**Figure 2D**). These results indicated that MeNPF4.5 is a transmembrane transport protein.

Expression of MeNPF4.5 Is Tissue Specific

To analyze the expression of *MeNPF4.5* in response to different N levels, young cassava seedlings were grown in N-free (0 mM NO_3^-), low-N (0.5 mM NO_3^-), and full-N (20 mM NO_3^-) media. We found that the expression level of *MeNPF4.5* in roots significantly decreased under N-free conditions. Compared with the N-free control where *MeNPF4.5* was expressed at the lowest levels, *MeNPF4.5* expression in roots was increased by 15.1-fold under low-N and 27.0-fold under full-N, which indicated that *MeNPF4.5* expression was induced by NO_3^- (**Figure 2A**).

MeNPF4.5 expression in roots was also analyzed with a time-course experiment. After NO_3^- induction, the expression

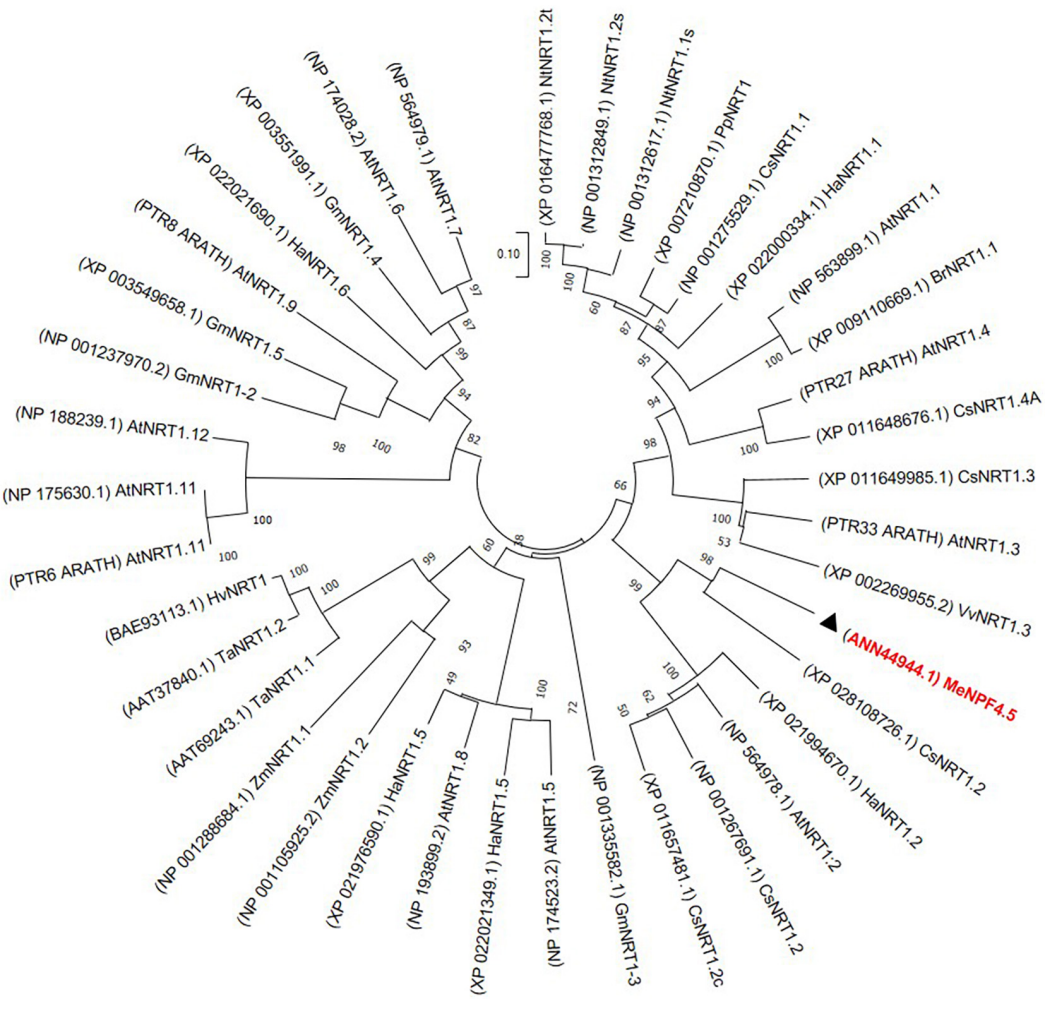

FIGURE 1 | Phylogenetic analysis of the MeNPF4.5 protein and other NO_3^- transporters (NRTs). The amino acid sequences were aligned using ClustalW software and the phylogeny was constructed using the neighbor-joining method with 1000 bootstrap replicates in MEGA7.

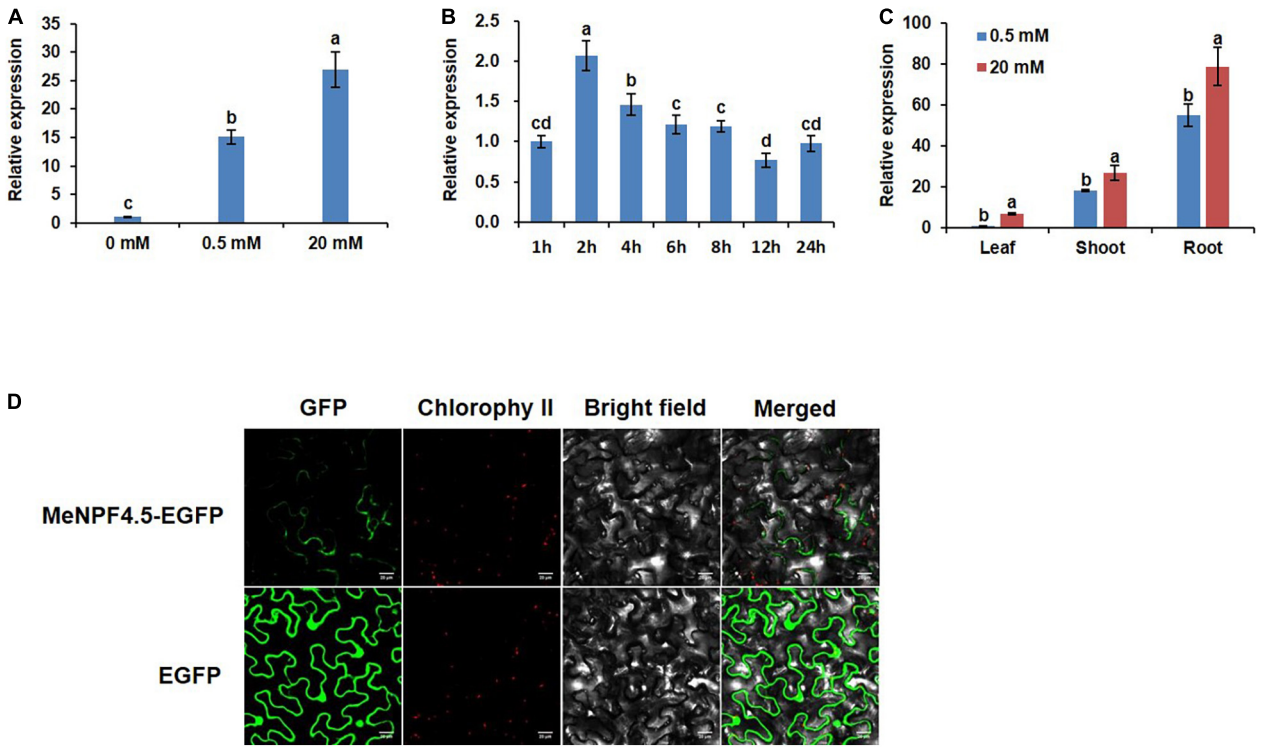

FIGURE 2 | Tissue-specific expression pattern and subcellular localization of the MeNPF4.5. **(A)** Relative expression of *MeNPF4.5* in the roots of plants grown under different N conditions for 25 days. **(B)** Expression levels of *MeNPF4.5* in N-starved roots at different times after N induction. Wild-type (WT) seedlings were grown in 10 mM NO_3^- for 20 days and under N starvation for 2 days, then were transferred to 20 mM NO_3^-. **(C)** Expression of *MeNPF4.5* in various tissues of cassava. Cassava seedlings were cultivated under different N conditions (0.5 and 20 mM NO_3^-) in tissue culture for 25 days. Values are the means of three biological replicates ± SE. Lowercase letters above the bars (a–d) represent significant differences between treatments as determined by Student's *t*-test ($P < 0.05$). **(D)** Subcellular localization of the MeNPF4.5-EGFP fusion protein in tobacco leaf epidermal cells. From left to right, GFP fluorescence, chlorophyll fluorescence, bright field, and merged images are shown. Bars = 20 μm.

of *MeNPF4.5* increased rapidly and reached a peak at 2 h. Expression then decreased gradually and stabilized at 6 h, but then decreased again, reaching the lowest level at 12 h before increasing again at 24 h (**Figure 2B**). Analysis of expression in different tissues showed that *MeNPF4.5* was expressed in stems and leaves in addition to roots; and the expression level was highest in roots under both 0.5 and 20 mM NO_3^-, with expression levels 54.9- and 11.4-times higher than those in leaves, respectively (**Figure 2C**).

Identification of MeNPF4.5 Transgenic Cassava Plants

To investigate the function of *MeNPF4.5*, the 3 transgenic lines (overexpression lines *MeNPF4.5* OE-22 and *MeNPF4.5* OE-34, and RNAi line *MeNPF4.5* Ri-1) were constructed. Southern blot analysis verified that the exogenous *MeNPF4.5* gene had been integrated into the genomes of *MeNPF4.5* OE-22 and *MeNPF4.5* OE-34 (**Supplementary Figure 1**), which confirmed that the overexpression lines *MeNPF4.5* OE-22 with a single copy of the transgenic construct and *MeNPF4.5* OE-34 with two copies. Quantitative RT-PCR was used to assess the levels of *MeNPF4.5* RNA in these lines. As shown in **Figure 3A**, the expression levels of *MeNPF4.5* in *MeNPF4.5* OE-22 and *MeNPF4.5* OE-34 were significantly higher than those in the WT under both N conditions, and the expression level in the Ri-1 line was decreased by 39.7 and 70.4% under low and normal N conditions, respectively. Therefore, these three lines were used for further analysis.

MeNPF4.5 Overexpression Enhances the Yield of Storage Roots

Lush foliage is the basis for healthy and high-yielding crops. Field evaluation of *MeNPF4.5* transgenic cassava showed that the two transgenic overexpression lines *MeNPF4.5* OE-22 and *MeNPF4.5* OE-34 and the RNAi line *MeNPF4.5* Ri-1 exhibited significant differences from WT in both the aerial and underground parts (**Figure 3**). Three of the four agronomic traits examined, namely leaf dry weight, storage root yield, and biomass accumulation, were significantly higher in *MeNPF4.5* OE-22 than in WT under both low and normal N conditions, whereas these trait values were lower in *MeNPF4.5* Ri-1. There was no significant difference in plant height between *MeNPF4.5* OE-22 and WT, but both lines were significantly taller than *MeNPF4.5* OE-34 and *MeNPF4.5* Ri-1 under both low and normal N conditions. These results demonstrated that *NRT1.1* overexpression can improve plant growth under low or normal N conditions. However, no

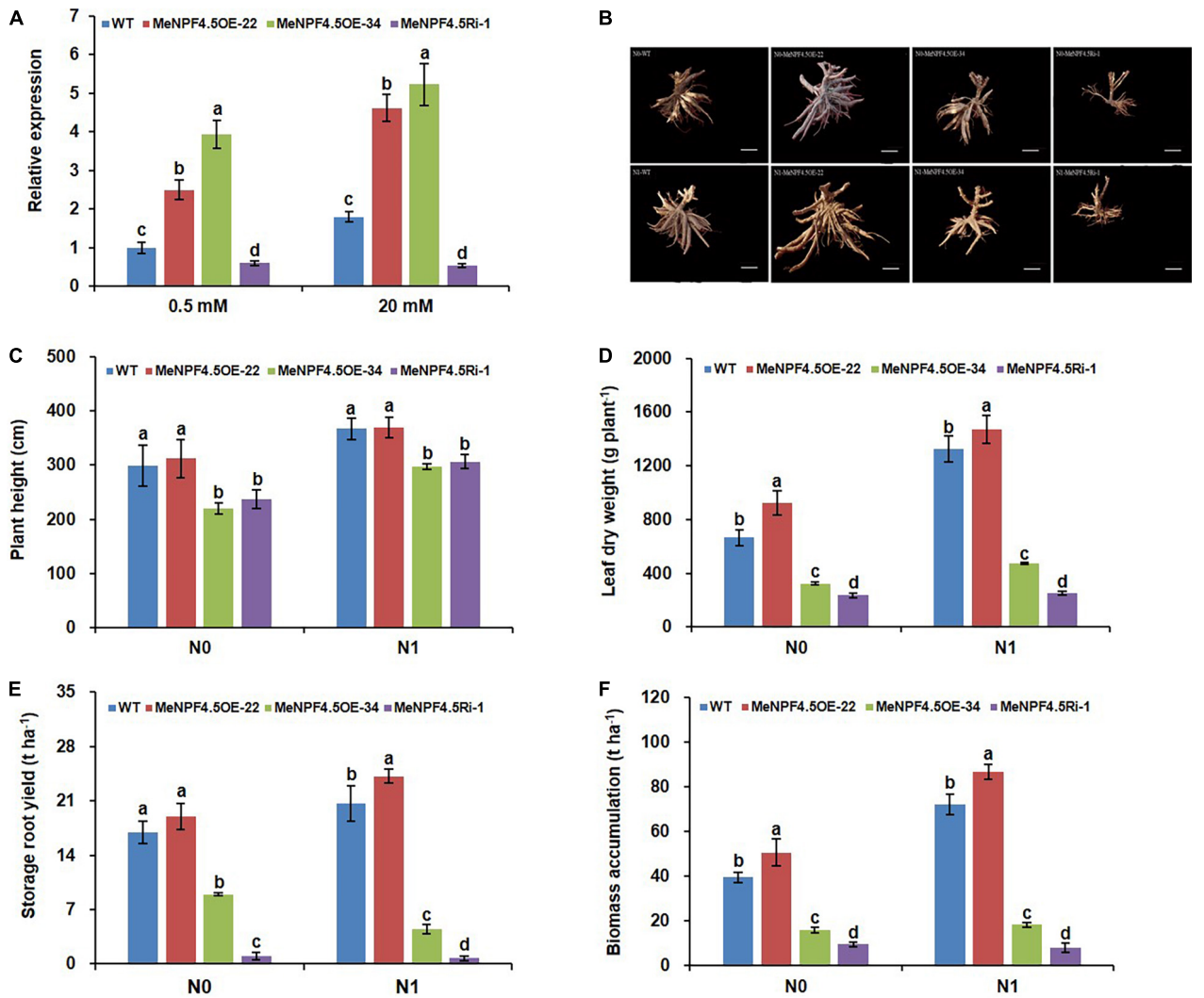

FIGURE 3 | Molecular identification and analysis of agronomic traits of WT and transgenic plants. **(A)** Real-time RT-PCR analysis of *MeNPF4.5* gene expression in the roots of WT and transgenic plants under 0.5 and 20 mM NO_3^-. *MeNPF4.5* OE, *MeNPF4.5* overexpression; *MeNPF4.5* Ri, *MeNPF4.5* RNA interference. The *Actin* gene was used as an internal control. **(B–F)** Agronomic traits of WT and transgenic plants grown in the field for 8 months under different N0 (0 kg ha^{-1}) and N1 (125 kg ha^{-1}) conditions. **(B)** Storage roots of cassava plants grown in the field. N0 treatment (upper panel), N1 treatment (lower panel); from left to right, WT, *MeNPF4.5* OE-22, *MeNPF4.5* OE-34, and *MeNPF4.5* Ri-1 images are shown. Bars = 10 cm. **(C)** Plant height (n = 10). **(D)** Leaf dry weight (n = 5). **(E)** Storage root yield (n = 5). **(F)** Biomass accumulation (n = 5). Values are means ± SE. Lowercase letters above the bars (a–d) represent significant differences between treatments as determined by Student's t-test ($P < 0.05$). N0, low-N treatment, 0 kg ha^{-1}; N1, normal N treatment, 125 kg ha^{-1}.

improvement in agronomic traits was observed for the *MeNPF4.5* OE-34 line; all four traits examined were lower than those in WT and *MeNPF4.5* OE-22, but higher than those in *MeNPF4.5* Ri-1.

MeNPF4.5 Improves N Uptake, N Translocation, N Accumulation, and Nitrogen Use Efficiency

To determine the MeNPF4.5 function in NO_3^- uptake by roots, we measured the NO_3^- uptake of cassava roots. The results showed that the NO_3^- uptake of WT and transgenic cassava roots increased gradually with increasing of NO_3^- concentration. The NO_3^- uptake was significantly higher in overexpression lines (*MeNPF4.5* OE-22 and *MeNPF4.5* OE-34) than those in the WT at relatively higher (1–20 mM) NO_3^- concentration. However, no significant difference was found at relatively lower (0.25 mM) NO_3^- concentrations. By contrast, the NO_3^- uptake was significantly lower in *MeNPF4.5* Ri-1 line than that in the WT at all tested NO_3^- concentrations (**Figure 4A**). Therefore, it seems that MeNPF4.5 is involved in the function of NO_3^- uptake.

Transport index was used as an indicator of NO_3^- translocation from roots to shoots (**Figure 4B**). Translocation of NO_3^- from roots to shoots between WT and transgenic lines, showing that the *MeNPF4.5* Ri-1 plants have lower N enrichment in the shoots compared to those of WT and OE transgenic plants under both N conditions. However, N

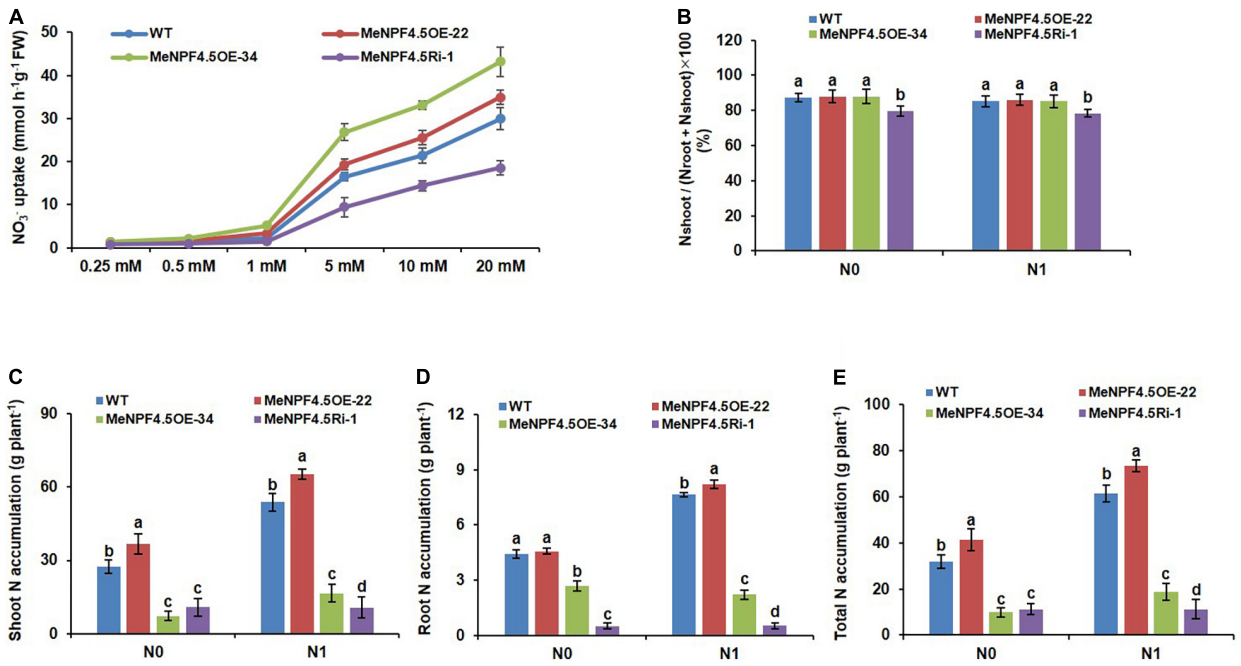

FIGURE 4 | Nitrogen uptake, tanslocation and accumulation in WT and *MeNPF4.5* transgenic cassava plants. **(A)** Root NO_3^- uptake in WT and *MeNPF4.5* transgenic cassava plants. WT and *MeNPF4.5* transgenic cassava plants grown in 20 mM KNO_3 for 25 days and then deprived of N for 3 days. N-starved plant roots were then exposed to various NO_3^- concentrations for 6 h, uptake of NO_3^- were measured by disappearance of NO_3^- from the nutrient solution. **(B)** Nitrate translocation in WT and *MeNPF4.5* transgenic cassava plants. **(C–E)** N accumulation in wild-type (WT) and *MeNPF4.5* transgenic cassava plants harvested from the field. **(C)** Shoot N accumulation. **(D)** Root N accumulation. **(E)** Total N accumulation. Values are the means of three biological replicates ± SE. Lowercase letters above the bars (a–d) represent significant differences between treatments as determined by Student's *t*-test ($P < 0.05$). N0, low-N treatment, 0 kg ha^{-1}; N1, normal N treatment, 125 kg ha^{-1}.

enrichment had no remarkable between OE transgenic plants (*MeNPF4.5* OE-22 and *MeNPF4.5* OE-34) and WT under the N0 and N1 conditions, indicating that the translocation of NO_3^- to shoots is slower when *MeNPF4.5* gene expression is suppressed, thus it can be seen that the MeNPF4.5 activity affects the NO_3^- translocation from roots to shoots.

As *NRT1.1* is one of the NRT genes involved in NO_3^- uptake in roots, we analyzed the N accumulation of transgenic lines and WT plants. N accumulation is equal to the N content in each part of the plant multiplied by the biomass. As shown in **Figures 4C–E**, the amounts of shoot and whole-plant N accumulation in *MeNPF4.5* OE-22 under low-N and normal N treatments were significantly higher than those in the WT, by 33.7% (N0) and 36.5% (N1) for shoots and by 29.5% (N0), 19.5% (N1) for the whole plant, but N accumulation was significantly lower in the *MeNPF4.5* Ri-1 line than in the WT. The amounts of N accumulation in storage roots of *MeNPF4.5*OE-22 were similar to those in WT under low-N conditions, but higher than those in WT under normal N conditions, which verified that *NRT1.1* was induced by high NO_3^- (≥0.50 mM). All these results show that *NRT1.1* enhances NO_3^- uptake and accumulation in cassava.

The NUE of crops is related to the N uptake efficiency and N utilization efficiency, but their contributions to N efficiency remain controversial (Bogard et al., 2013). Our results indicated that there were significant differences in N utilization efficiency (NUtE), N recovery efficiency (NRE), and the partial factor productivity of N (PFPN) of the different transgenic cassava lines. As shown in **Table 1**, there were no significant differences in NUtE (under N0) and NRE between *MeNPF4.5* OE-22 and WT, but NUtE (under N1) and PFPN of *MeNPF4.5* OE-22 were significantly higher than those of the WT (by 7.6 and 16.8%, respectively). The NUtE under both N levels, NRE, and PFPN of *MeNPF4.5* Ri-1 were significantly lower than those of the WT (reduced by 36.4, 130.1, and 94.7%, respectively). *MeNPF4.5* OE-34 had a lower NUtE (under N1), NRE, and PFPN than WT, but NUtE under N0 conditions was significantly higher than that in the WT. These results indicated that the *MeNPF4.5* gene expression level could severely affect the activity of NPF4.5 transporter in uptake and utilization of N under different N levels.

MeNPF4.5 Increases the Activities of Enzymes Related to N Metabolism in Cassava Leaves

The N absorbed by crop roots must be assimilated into organic matter through N metabolism enzymes before it can be used by the plant. The activity of key N metabolism enzymes can directly reflect the strength of N metabolism in crops (Andrews et al., 2004). The activities of enzymes involved in N metabolism, namely NR, GS, GOGAT, and GDH, were higher in WT and all the transgenic plants under the N1 treatment than under the N0

TABLE 1 | Differences in nitrogen uptake and utilization of wild-type and *MeNPF4.5* transgenic cassava.

Lines	N utilization efficiency (kg kg^{-1})		N recovery efficiency (kg kg^{-1})	Partial factor productivity of applied N (kg kg^{-1})
	N0	N1		
WT	124.73 ± 5.93b	109.72 ± 4.71b	2.78 ± 0.15a	166.34 ± 3.06b
MeNPF4.5 OE-22	127.15 ± 1.77b	118.08 ± 1.58a	2.68 ± 0.13a	194.28 ± 1.24a
MeNPF4.5 OE-34	179.57 ± 9.42a	99.29 ± 1.09c	0.79 ± 0.04b	36.31 ± 2.62c
MeNPF4.5 Ri-1	91.64 ± 3.27c	75.30 ± 1.8d	0.02 ± 0.00c	6.12 ± 0.83d

N0, low-N treatment, 0 kg ha^{-1}; N1, normal N treatment, 125 kg ha^{-1}. Values are the means of three biological replicates ± SE. Values labeled with different letters represent significant differences between respective treatments by Student's t-test ($P < 0.05$).

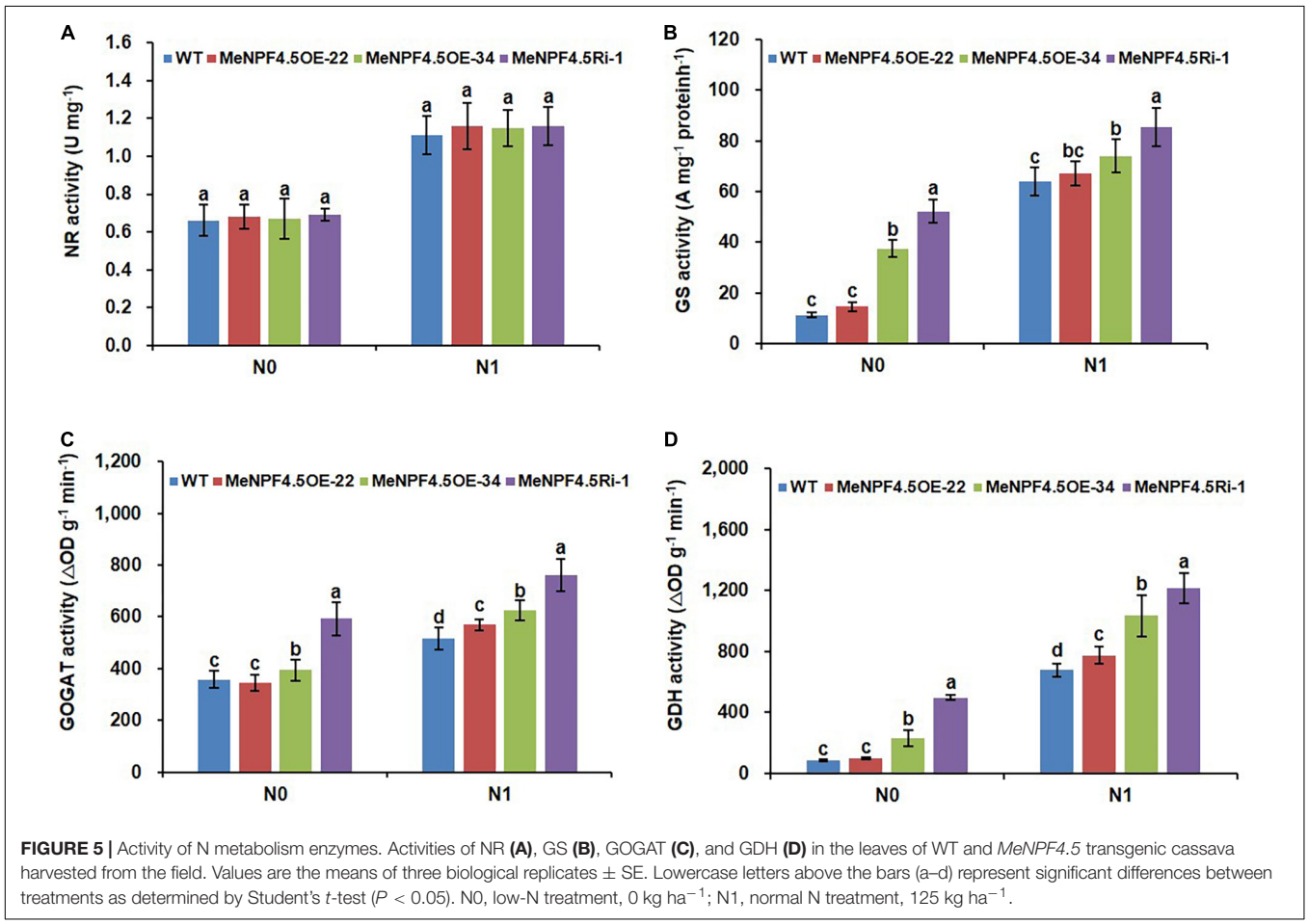

FIGURE 5 | Activity of N metabolism enzymes. Activities of NR **(A)**, GS **(B)**, GOGAT **(C)**, and GDH **(D)** in the leaves of WT and *MeNPF4.5* transgenic cassava harvested from the field. Values are the means of three biological replicates ± SE. Lowercase letters above the bars (a–d) represent significant differences between treatments as determined by Student's *t*-test ($P < 0.05$). N0, low-N treatment, 0 kg ha^{-1}; N1, normal N treatment, 125 kg ha^{-1}.

treatment, which showed that high N promoted the activities of these enzymes (**Figure 5**). The activities of all enzymes except for NR were higher in *MeNPF4.5* OE-34 and *MeNPF4.5* Ri-1 than in *MeNPF4.5* OE-22 and the WT under both the N0 and N1 conditions; at the same time, the activities of these enzyme were significantly higher in *MeNPF4.5* OE-22 than in WT under the N1 conditions.

MeNPF4.5 Increases Photosynthesis

Photosynthesis is the physiological basis of crop growth and yield formation, and 90–95% of crop dry matter accumulation originates from photosynthetic products. As shown in **Figures 6A–D**, there was no significant difference in photosynthetic parameters, namely Gs, Ci, and Tr, between *MeNPF4.5* OE-22, *MeNPF4.5* OE-34, and WT under both N levels. The Pn of *MeNPF4.5* OE-22 was 8.4% higher compared with that of WT under the N1 conditions. The Pn and Gs of *MeNPF4.5* Ri-1 were significantly lower than those of WT under both N levels.

Chlorophyll fluorescence is a direct indicator of plant physiology and reflects the photochemical process and its efficiency. As photosynthesis was altered by the *MeNPF4.5*

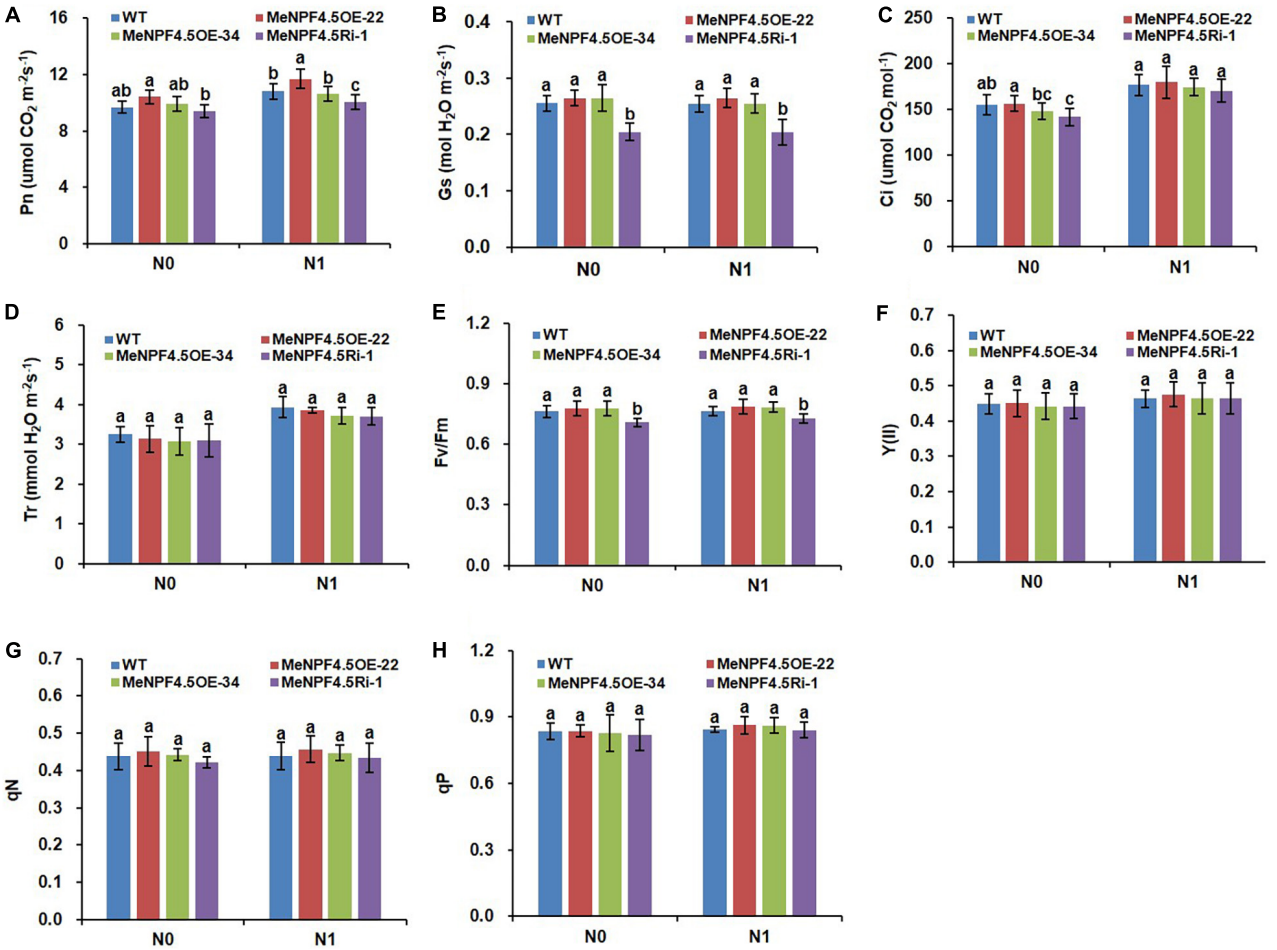

FIGURE 6 | Photosynthetic and chlorophyll fluorescence parameters of WT and *MeNPF4.5* transgenic cassava plants. **(A)** Photosynthetic rate (Pn). **(B)** Stomatal conductance (Gs). **(C)** Intercellular CO_2 concentration (Ci). **(D)** Transpiration rate (Tr). **(E)** Fv/Fm. **(F)** Y(II). **(G)** qN. **(H)** qP. Values are the means of five biological replicates ± SE. Lowercase letters above the bars (a-d) represent significant differences between treatments as determined by Student's *t*-test ($P < 0.05$). N0, low-N treatment, 0 kg ha^{-1}; N1, normal N treatment, 125 kg ha^{-1}.

gene (**Figures 6A–D**), we wanted to evaluate the differences in chlorophyll fluorescence parameters between the transgenic lines and WT. The Fv/Fm values of the leaves of *MeNPF4.5* Ri-1 plants were significantly lower compared with those of WT and OE transgenic plants under the N0 and N1 conditions (**Figures 6E–H**), but other chlorophyll fluorescence parameters did not significantly differ between the transgenic plants and WT.

MeNPF4.5 Regulates Endogenous Hormone Levels in Cassava

Significant changes were also detected in endogenous hormones, namely indoleacetic acid (IAA), zeatin-riboside (ZR), gibberellic acid (GA_3), abscisic acid (ABA), and brassinosteroid (BR), in the roots and leaves of transgenic cassava (**Figures 7**, **8**). In roots, compared with WT, the levels of IAA were 11.8 and 25.8% lower in *MeNPF4.5* OE-22 and OE-34, respectively, and 39.9% higher in *MeNPF4.5* Ri-1 under low-N conditions (**Figure 7**). In contrast, under the full-N conditions the levels of IAA in transgenic plants (*MeNPF4.5* OE-22, *MeNPF4.5* OE-34, and *MeNPF4.5* Ri-1) were 46.7, 65.2, and 38.2% higher than those in WT, respectively. For ZR and GA_3, very similar patterns were observed in transgenic plants under both N levels. All the transgenic lines had a significantly higher ZR and GA_3 contents than WT under both N conditions. Analysis of ABA revealed decreases of 20.5% in *MeNPF4.5* OE-22 and 31.0% in *MeNPF4.5* OE-34 compared with WT. ABA levels in *MeNPF4.5* Ri-1 plants did not significantly differ from those in WT under low-N conditions. Under full-N conditions, the ABA content was higher compared with that in WT in all transgenic plants. Compared with WT plants, there was a 21.5% decrease of BR in *MeNPF4.5* OE-22 and no significant difference between WT and the *MeNPF4.5* OE-34 and *MeNPF4.5* Ri-1 lines under low-N conditions. However, BR levels were higher in the three transgenic lines under full-N conditions. These results suggest that the *MeNPF4.5* gene alters plant endogenous hormone levels in transgenic plants.

Analysis results on content of endogenous hormone in leaves showed that IAA in *MeNPF4.5* OE-22 and MeNPF4.5 OE-34

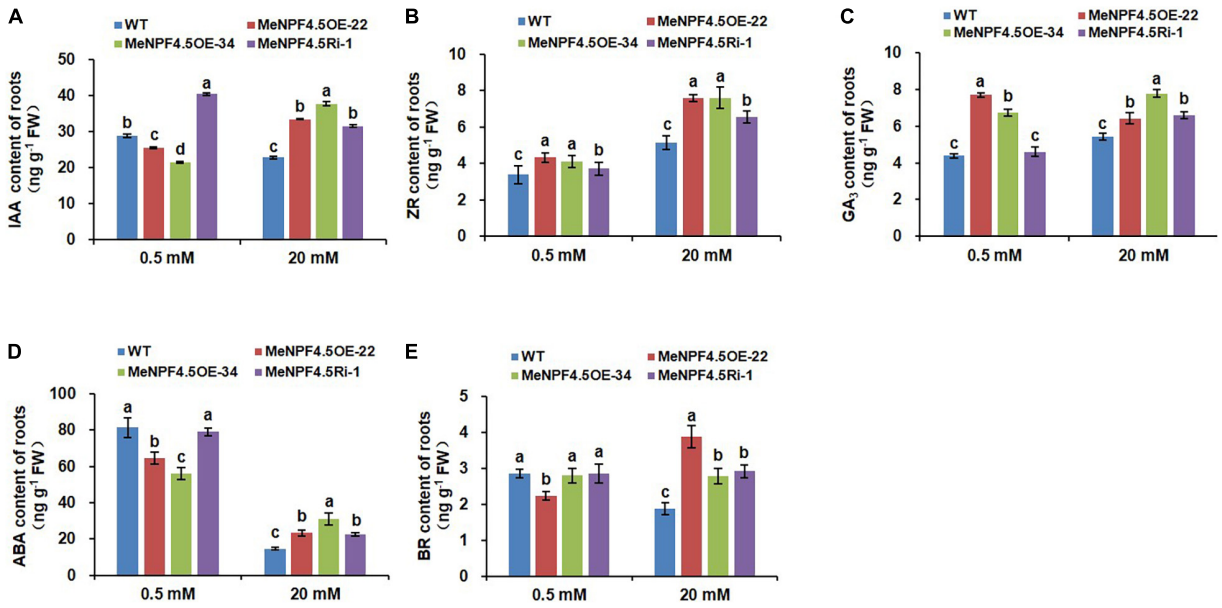

FIGURE 7 | Endogenous hormone levels in roots of WT and *MeNPF4.5* transgenic cassava plants cultivated in tissue culture for 25 days. **(A–E)** contents of indoleacetic acid (IAA) **(A)**, zeatin-riboside (ZR) **(B)**, gibberellic acid (GA_3) **(C)**, abscisic acid (ABA) **(D)**, and brassinolide (BR) **(E)**. Values are the means of three biological replicates ± SE. Lowercase letters above the bars (a–d) represent significant differences between treatments as determined by Student's *t*-test ($P < 0.05$).

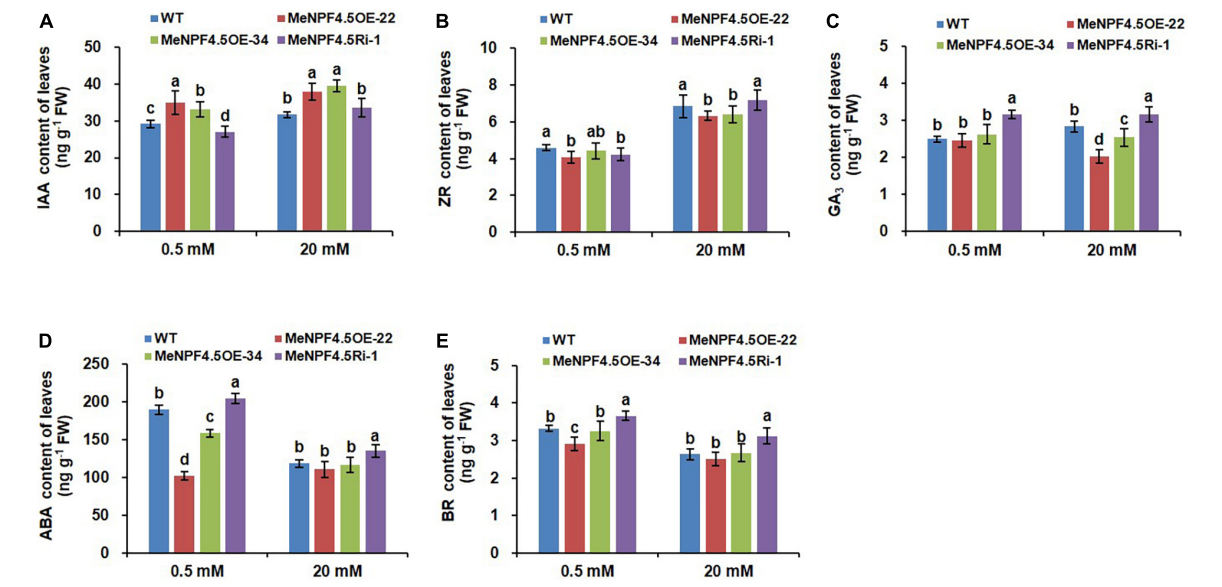

FIGURE 8 | Endogenous hormone levels in leaves of WT and *MeNPF4.5* transgenic cassava plants cultivated in tissue culture for 25 days. **(A–E)** Contents of indoleacetic acid (IAA) **(A)**, zeatin-riboside (ZR) **(B)**, gibberellic acid (GA_3) **(C)**, abscisic acid (ABA) **(D)**, and brassinolide (BR) **(E)**. Values are the means of three biological replicates ± SE. Lowercase letters above the bars (a–d) represent significant differences between treatments as determined by Student's *t*-test ($P < 0.05$).

were higher than those in WT under both N conditions, and IAA levels in *MeNPF*4.5 Ri-1 plants did not significantly differ from those in WT under full-N conditions but significantly lower than those in WT under low-N conditions (**Figure 8**). Compared with WT plants, there were significantly lower ZR contents in *MeNPF4.5* OE-22 and *MeNPF4.5* Ri-1 lines under low-N conditions. ZR levels in *MeNPF4.5* OE-34 plants did not significantly differ from that in WT under low-N conditions. Under full-N conditions, the ZR content was lower compared with that in WT in the overexpression lines. Meanwhile, the overexpression lines *MeNPF4.5* OE-22 and *MeNPF4.5* OE-34 had a significantly lower GA_3 contents than WT under full-N conditions. And the *MeNPF4.5* Ri-1 lines had a significantly higher GA_3 contents than those in WT under both N conditions.

For ABA and BR, similar patterns were observed in transgenic plants under both N levels. ABA and BR levels in *MeNPF4.5* Ri-1 plants was higher compared with those in WT and in the overexpression lines under both conditions. And the overexpression lines *MeNPF4.5* OE-22 and *MeNPF4.5* OE-34 had a significantly lower ABA and BR contents than those in WT under both N conditions. These results also suggest that the modulation of *MeNPF4.5* gene expression alters plant endogenous hormone levels in transgenic plants.

DISCUSSION

NRT1.1/*NPF6.3* (*CHL1*) was the first NRT gene discovered in plants, and it also was found to function not only in NO_3^- uptake (Tsay, 1993) but also in NO_3^- translocation from roots to shoots (Léran et al., 2014). At present, research on *NRT1.1* has mainly focused on the model plant *Arabidopsis* and the food crops rice (Hu et al., 2015; Fan et al., 2017; Wang Y. Y. et al., 2018) and wheat (Guo et al., 2014). Little information regarding this family is available in cassava, an important crop in much of the world. In this study, we investigated the spatiotemporal expression pattern and the function of the *MeNPF4.5* gene in cassava. Our data clearly showed that *MeNPF4.5* was barely detectable under N deficiency conditions, but its expression was maintained a high level under N sufficient conditions. This suggests that *MeNPF4.5* expression could be induced by NO_3^- just as *AtNRT1.1* is in *Arabidopsis* (Lejay et al., 1999; Liu et al., 1999). Once N-starved cassava plants were exposed to NO_3^-, *MeNPF4.5* expression first increased and then decreased (**Figure 2A**). It can be seen that *MeNPF4.5* responds to NO_3^- in the short term like many other plants *NRT1.1* (Cárdenas Navarro et al., 1998; Okamoto et al., 2003; Wang et al., 2007). In addition to being expressed in roots, *AtNRT1.1* is also expressed in shoots, young leaves, and developing flower buds of *Arabidopsis*, but it is more strongly expressed in roots (Miller et al., 2007; Sakuraba et al., 2021). Consistent with the expression pattern of *NRT1.1* in *Arabidopsis*, *MeNPF4.5* is expressed in roots, stems, and leaves of cassava plants, and it is predominantly expressed in roots. We also conducted subcellular localization studies on the MeNPF4.5 protein and found that it was located on the plasma membrane, which was consistent with the findings of previous studies on NRT1.1 (Hu et al., 2015; Zhao et al., 2017).

Nitrate affects all aspects of plant physiology including metabolism, resource allocation, growth, and development, and its accumulation and translocation are critical to dry matter production. NRTs are not only involved in the uptake and transport of NO_3^- in roots, but also in the redistribution of NO_3^- among cells. The influence of the expression of NRTs on the N uptake and NUE of crops are important topics in breeding research. For example, Hu et al. (2015) demonstrated that overexpression of indica-type *OsNRT1.1B* can potentially improve the NUE of the japonica variety Zhonghua. Furthermore, a recent study showed that 35S promoter- driven expression of *OsNRT1.1A* improves the grain yield of transgenic rice plants (Wang W. et al., 2018). Overexpression of the OsNRT1.2 in the rice cultivar 'Wuyunjing 7' resulted in a biomass increase under a high concentration of NO_3^- (Ma et al., 2011). These results suggest an intimate relationship between the function of *NRT1* and plant growth. To evaluate the effect of the *MeNPF4.5* gene on cassava growth, we analyzed the yield and biomass of transgenic lines under two different N levels in a field test. Our results revealed differences between the overexpression lines and RNAi line; the yield and biomass of the overexpression lines were higher than those of the RNAi line. Compared with the WT, the growth of cassava was promoted in the overexpression line *MeNPF4.5* OE-22 under both low and normal N conditions, while growth of the RNAi line *MeNPF4.5*Ri-1 was inhibited (**Figure 3**). This finding is consistent with the results of previous studies and shows that enhanced *MeNPF4.5* expression could improve growth in cassava under both low and normal N conditions. However, another *MeNPF4.5* overexpression line, *MeNPF4.5* OE-34, exhibited inhibited growth compared with WT and *MeNPF4.5* OE-22, although its growth was superior to that of *MeNPF4.5*Ri-1. This might be related to the high expression of *MeNPF4.5* in this line, which may affect the balance between N uptake and utilization; or maybe *MeNPF4.5* OE-34 has two copy of the transgenic construct, which might lead to the silence of target gene and thus affect plant growth (Vaucheret et al., 1998; Tenea et al., 2008; Ahlawat et al., 2014).

Nitrogen use efficiency can be simply defined as the yield of grain per unit of N available in the soil. NUE depends on N uptake efficiency and internal utilization efficiency, and N uptake-and-utilization efficiency reflects the capacity of crops to absorb N and transport it to the organs (Moll et al., 1982; Chen and Ma, 2015). Therefore, here we examined the association between N uptake, translocation, NUtE, and growth. *OsNRT1.1B* was reported to increase the NUtE of rice by 30% (Duan and Zhang, 2015; Hu et al., 2015), and Chen and Ma (2015) reported that *OsNRT1.1B* improves NUE in rice by enhancing root NO_3^- uptake. Here we found that *MeNPF4.5* enhanced N uptake, translocation, and accumulation in cassava; NUtE, NRE, and PFPN were improved in *MeNPF4.5* overexpressing plants but were significantly lower in the *MeNPF4.5* Ri-1 line compared with WT (**Table 1**). It is inferred that the higher yields of the overexpression lines *MeNPF4.5* OE-22 and *MeNPF4.5* OE-34 may be due to their high N uptake and transport capabilities, while the yield of *MeNPF4.5* Ri-1 decreased because of its reduced N uptake and allocation.

N is absorbed by cassava in the form of NO_3^-, and then it needs to be assimilated mainly in shoot part into organic N through the catalytic action of several enzymes. Studies have found that when NO_3^- addition to N-starved seedlings, all genes known to be directly required for NO_3^- assimilation were strongly induced, including N metabolism enzyme gene (Gowri et al., 1992; Wang et al., 2003; Scheible et al., 2004). Hu et al. (2009) also confirmed that NO_3^- assimilation genes are regulated by NO_3^-, and these genes are expressed at low levels in the absence of NO_3^- and are rapidly induced in its presence (priming effect). Much evidence suggests that NR and GS are the key enzymes for N assimilation (Thomsen et al., 2014). For most plants, there is a positive correlation between the amount of NO_3^- absorbed by the roots from the soil and NR activity (Andrews et al., 2004). Meanwhile, GS enzyme

activity and stability are positively correlated with substrate abundance (Andrews et al., 2004). Other enzymes responsible for N assimilation in addition to NR and GS, such as GOGAT, GDH, and asparagine synthetase, have also been reported to play important roles in N metabolism and improvement of NUE in plants (Ameziane et al., 2000; Wong et al., 2004; Yamaya and Kusano, 2014). In this study, we found that the activity of nitrogen metabolism enzymes in the same line under N1 level was higher than that under N0 level, indicating that N metabolism enzyme were induced by NO_3^-. The GS, GOGAT, and GDH activities in *MeNPF4.5* OE-34 and *MeNPF4.5* Ri-1 were higher than those in *MeNPF4.5* OE-22 and the WT under both the N0 and N1 conditions, but there was no significant difference in NR activity. Although the activities of these enzymes were higher in *MeNPF4.5* OE-34 and *MeNPF4.5* Ri-1 than in the WT, the growth of these plants was inhibited and N accumulation was lower. Studies have shown that compared with the WT, transgenic rice that overexpress GS1 (Tabuchi et al., 2007) show no difference in growth phenotype and have lower yields. Transgenic tobacco plants that overexpress GS2 show limited growth and leaf yellowing (Thomsen et al., 2014). Some studies suggest that these phenomena may be the result of feedback inhibition of nitrogen metabolites (Vincentz and Caboche, 1991). The results of this study may also related to this phenomenon.

Previous studies found that there is a significant positive correlation between photosynthesis and crop yield and NUE (Zhang et al., 2017). However, some studies have pointed out that the substantial increase in crop yield achieved in the past few decades has not been accompanied by a significant increase in leaf Pn. The yield gain is mainly attributed to an increase in leaf area index and biological yield (Sharma-Natu and Ghildiyal, 2005). In this study, the leaf dry weight and Pn in *MeNPF4.5* OE-22 were significantly higher compared with those in WT, while these two traits were significantly lower in the RNAi line. The Fv/Fm values in the RNAi line were also lower. Therefore, it is speculated that the difference in leaf area index and photosynthetic parameters may underlie the difference in NUE and yield between *MeNPF4.5* OE-22 plants and *MeNPF4.5* Ri-1 and WT plants.

Hormones play an important role in regulating various metabolic, growth, and development processes, and maintaining a dynamic balance under normal physiological conditions. Lots of plant hormones are transported by some NRT proteins and conversely regulate NRT gene expression (Zhao et al., 2021). NRT1.1 in roots can transport NO_3^- and auxin, but preferentially transports NO_3^- (Krouk et al., 2010; Bouguyon et al., 2015). Hormone metabolism appears transcriptional reprogramming and sensing as one of the early response to NO_3^- addition (Scheible et al., 2004), while higher supply of NO_3^- decreased IAA concentrations in phloem exudates, which affected root growth (Bhalerao et al., 2002; Tian et al., 2008; Liu et al., 2010). Krouk et al. (2010) propose that NRT1.1 represses lateral root growth at low NO_3^- availability by promoting basipetal auxin transport out of these roots. In this study, we had the similar results, the IAA content in roots of the two overexpression lines was significantly lower compared with that of WT under low-N conditions, was higher in roots of RNAi line, which might be resulted from MeNPF4.5 promoting basipetal auxin transport and lowering auxin accumulation in the roots in OE plants, while the transport ability was inhibited in RNAi lines. Under full-N conditions, it was speculated that MeNPF4.5 performed the NO_3^- transport function, which could lead to higher IAA content in roots of the transgenic lines than in that of WT. In addition, our results showed that the content of IAA in leaves of overexpressed lines remained at a high level under both N levels, which may be related with a higher translocation of N toward the aerial parts associated with more production of IAA. Previous studies found that the change of IAA levels in the root was closely related to NO_3^- mediated root growth, however, the latter process could not be explained exclusively by the former, due to NO_3^- has a comprehensive effect on other phytohormones, such as cytokinin (Beck, 1996; Takei et al., 2001) and ethylene (Singh et al., 2000), which also exert significant effects on root development. The changes of other hormones contents (ZR, GA_3, ABA, and BR) were also detected in roots and leaves of transgenic plants and WT under two N levels, in previous report, Tian et al. (2005) also discovered that cytokinin concentrations in roots enhanced with increasing NO_3^- supply. Therefore, it is supposed that IAA might synergistically interact with ZR, GA_3, ABA, and BR to affect the growth of cassava plants. And further study is required to elucidate the interaction among these hormones on NO_3^- mediated cassava growth.

In summary, *MeNPF4.5* is mainly expressed in cassava roots, and its expression is induced by NO_3^-. Overexpressing *MeNPF4.5* in cassava promoted growth and improved the NUE and yield. The main reasons for these effects may be increased photosynthesis and N metabolism enzyme activity. Down-regulation of *MeNPF4.5* expression resulted in inhibition of cassava growth and reduction of NUE, causing a decrease in biomass and yield. Overall, our study reveals the role of MeNPF4.5 in N uptake and utilization, which has not been previously reported, and shows that this NRT may have potential breeding value.

DATA AVAILABILITY STATEMENT

The original contributions presented in the study are included in the article/**Supplementary Material**, further inquiries can be directed to the corresponding authors.

AUTHOR CONTRIBUTIONS

QL and QM prepared the manuscript. MD and QL conducted the experiments and analyzed the data. BH designed the experiments. MG and PZ supervised the study. All authors have read and agreed to the published version of the manuscript.

FUNDING

This research was financially supported by the Natural Science Foundation of Guangxi (2018GXNSFDA281056

and 2016GXNSFBA380220) and China Agriculture Research System.

ACKNOWLEDGMENTS

We highly appreciate technical support from Xiaoguang Duan, who is a research scientist in the Center for Excellence in Molecular Plant Sciences, Chinese Academy of Sciences.

SUPPLEMENTARY MATERIAL

The Supplementary Material for this article can be found online at: https://www.frontiersin.org/articles/10.3389/fpls.2022.866855/full#supplementary-material

Supplementary Figure 1 | Southern blotting analysis of *MeNPF4.5* transgenic plants. WT, wild type; M, marker; OE22-OE34: *MeNPF4.5* overexpress transgenic plants. The probes were *HPT* in left three samples and *MeNPF4.5* in right three samples, and the restriction endinuclease was *Hind* III.

REFERENCES

Ahlawat, S., Saxena, P., Alam, P., Wajid, S., and Abdin, M. Z. (2014). Modulation of artemisinin biosynthesis by elicitors, inhibitor, and precursor in hairy root cultures of *Artemisia Annua* L. *J. Plant Interact.* 9, 811–824. doi: 10.1080/17429145.2014.949885

Ameziane, R., Bernhard, K., and Lightfoot, D. (2000). Expression of the bacterial gdhA gene encoding a NADPH glutamate dehydrogenase in tobacco affects plant growth and development. *Plant Soil* 221, 47–57. doi: 10.1023/A:1004794000267

Andrews, M., Lea, P. J., Raven, J. A., and Lindsey, K. (2004). Can genetic manipulation of plant nitrogen assimilation enzymes result in increased crop yield and greater N-use efficiency? An assessment. *Ann. Appl. Biol.* 145, 25–40. doi: 10.1111/j.1744-7348.2004.tb00356.x

Beck, E. H. (1996). Regulation of shoot/root ratio by cytokinins from roots in *Urtica dioica*: opinion. *Plant Soil* 185, 3–12. doi: 10.1007/bf02257560

Bhalerao, R. P., Eklof, J., Ljung, K., Marchant, A., Bennett, M., and Sandberg, È (2002). Shoot-derived auxin is essential for early lateral root emergence in *Arabidopsi*s seedlings. *Plant J* 29, 325–332. doi: 10.1046/j.0960-7412.2001.01217.x

Bogard, M., Allard, V., Martre, P., Heumez, E., Snape, J. W., Orford, S., et al. (2013). Identifying wheat genomic regions for improving grain protein concentration independently of grain yield using multiple inter-related populations. *Mol. Breed.* 31, 587–599. doi: 10.1007/s11032-012-9817-5

Bouguyon, E., Brun, F., Meynard, D., Kubeš, M., Pervent, M., Leran, S., et al. (2015). Multiple mechanisms of nitrate sensing by *Arabidopsis* nitrate transceptor NRT1.1. *Nat. Plants* 1, 2–9. doi: 10.1038/nplants.2015.15

Cárdenas Navarro, R., Adamowicz, S., and Robin, P. (1998). Modelling diurnal nitrate uptake in young tomato (Lycopersicon esculentum Mill.) plants using a homoeostatic model. *Acta Hortic.* 456, 247–253. doi: 10.17660/actahortic.1998.456.28

Chen, Z. C., and Ma, J. F. (2015). Improving nitrogen use efficiency in rice through enhancing root nitrate uptake mediated by a nitrate transporter. NRT1.1B. *J. Genet. Genomics* 42, 463–465. doi: 10.1016/j.jgg.2015.08.003

Duan, D. D., and Zhang, H. M. (2015). A single SNP in NRT1.1B has a major impact on nitrogen use efficiency in rice. *Sci. China Life Sci.* 58, 827–828. doi: 10.1007/s11427-015-4907-3

Fan, X., Naz, M., Fan, X., Xuan, W., Miller, A. J., and Xu, G. (2017). Plant nitrate transporters: from gene function to application. *J. Exp. Bot.* 68, 2463–2475. doi: 10.1093/jxb/erx011

Fenchel, T., King, G. M., and Blackburn, T. H. (2012). Transport mechanisms. *Bact. Biogeochem.* 3, 35–47. doi: 10.1016/b978-0-12-415836-8.00002-5

Gao, Z., Wang, Y., Chen, G., Zhang, A., Yang, S., Shang, L., et al. (2019). The indica nitrate reductase gene OsNR2 allele enhances rice yield potential and nitrogen use efficiency. *Nat. Commun* 10:5207. doi: 10.1038/s41467-019-13110-8

Gowri, G., Kenis, J. D., Ingemarsson, B., Redinbaugh, M. G., and Campbell, W. H. (1992). Nitrate reductase transcript is expressed in the primary response of maize to environmental nitrate. *Plant Mol. Biol.* 18, 55–64. doi: 10.1007/BF00018456

Guo, T., Xuan, H., Yang, Y., Wang, L., Wei, L., Wang, Y., et al. (2014). Transcription analysis of genes encoding the wheat root transporter NRT1 and NRT2 families during nitrogen starvation. *J. Plant Growth Regul.* 33, 837–848. doi: 10.1007/s00344-014-9435-z

Ho, C. H., Lin, S. H., Hu, H. C., and Tsay, Y. F. (2009). CHL1 Functions as a Nitrate Sensor in Plants. *Cell* 138, 1184–1194. doi: 10.1016/j.cell.2009.07.004

Hu, B., Wang, W., Ou, S., Tang, J., Li, H., Che, R., et al. (2015). Variation in NRT1.1B contributes to nitrate-use divergence between rice subspecies. *Nat. Genet.* 47, 834–838. doi: 10.1038/ng.3337

Hu, H. C., Wang, Y. Y., and Tsay, Y. F. (2009). AtCIPK8, a CBL-interacting protein kinase, regulates the low-affinity phase of the primary nitrate response. *Plant J.* 57, 264–278. doi: 10.1111/j.1365-313X.2008.03685.x

Huang, J., Wang, X., and Wang, G. (2015). Synthesis and characterization of copolymers with the same proportions of polystyrene and poly(ethylene oxide) compositions but different connection sequence by the efficient Williamson reaction. *Polym. Int.* 64, 1202–1208. doi: 10.1002/pi.4891

Jeong, J., Suh, S. J., Guan, C., Tsay, Y. F., Moran, N., Oh, C. J., et al. (2004). A nodule-specific dicarboxylate transporter from alder is a member of the peptide transporter family. *Plant Physiol.* 134, 969–978. doi: 10.1104/pp.103.032102

Kang, L., Liang, Q., Jiang, Q., Yao, Y., Dong, M., He, B., et al. (2020). Screening of diverse cassava genotypes based on nitrogen uptake efficiency and yield. *J. Integr. Agric.* 19, 965–974. doi: 10.1016/S2095-3119(19)62746-2

Kanno, Y., Hanada, A., Chiba, Y., Ichikawa, T., Nakazawa, M., Matsui, M., et al. (2012). Identification of an abscisic acid transporter by functional screening using the receptor complex as a sensor. *Proc. Natl. Acad. Sci. U.S.A.* 109, 9653–9658. doi: 10.1073/pnas.1203567109

Komarova, N. Y., Thor, K., Gubler, A., Meier, S., Dietrich, D., Weichert, A., et al. (2008). AtPTR1 and AtPTR5 transport dipeptides in planta. *Plant Physiol.* 148, 856–869. doi: 10.1104/pp.108.123844

Krouk, G., Lacombe, B., Bielach, A., Perrine-Walker, F., Malinska, K., Mounier, E., et al. (2010). Nitrate-regulated auxin transport by NRT1.1 defines a mechanism for nutrient sensing in plants. *Dev. Cell* 18, 927–937. doi: 10.1016/j.devcel.2010.05.008

Kyriacou, M. C., Leskovar, D. I., Colla, G., and Rouphael, Y. (2018). Watermelon and melon fruit quality: the genotypic and agro-environmental factors implicated. *Sci. Hortic. (Amsterdam).* 234, 393–408. doi: 10.1016/j.scienta.2018.01.032

Lassaletta, L., Billen, G., Grizzetti, B., Anglade, J., and Garnier, J. (2014). 50 year trends in nitrogen use efficiency of world cropping systems: the relationship between yield and nitrogen input to cropland. *Environ. Res. Lett* 9:105011. doi: 10.1088/1748-9326/9/10/105011

Lejay, L., Tillard, P., Lepetit, M., Olive, F. D., Filleur, S., and Plantes, Â (1999). Molecular and functional regulation of two NO 3 ± uptake systems by N- and C-status of arabidopsis plants. *Plant J* 18, 509–519. doi: 10.1046/j.1365-313x.1999.00480.x

Léran, S., Muños, S., Brachet, C., Tillard, P., Gojon, A., and Lacombe, B. (2013). *Arabidopsis* NRT1.1 is a bidirectional transporter involved in root-to-shoot nitrate translocation. *Mol. Plant* 6, 1984–1987. doi: 10.1093/mp/sst068

Léran, S., Varala, K., Boyer, J. C., Chiurazzi, M., Crawford, N., Daniel-Vedele, F., et al. (2014). A unified nomenclature of nitrate transporter 1/peptide transporter family members in plants. *Trends Plant Sci.* 19, 5–9. doi: 10.1016/j.tplants.2013.08.008

Li, H., Hu, B., and Chu, C. (2017). Nitrogen use efficiency in crops: lessons from *Arabidopsis* and rice. *J. Exp. Bot.* 68, 2477–2488. doi: 10.1093/jxb/erx101

Li, Y., Li, J., Yan, Y., Liu, W., Zhang, W., Gao, L., et al. (2018). Knock-down of CsNRT2.1, a cucumber nitrate transporter, reduces nitrate uptake, root length, and lateral root number at low external nitrate concentration. *Front. Plant Sci.* 9:722. doi: 10.3389/fpls.2018.00722

Liu, K. H., Huang, C. Y., and Tsay, Y. F. (1999). CHL1 is a dual-affinity nitrate transporter of *Arabidopsis* involved in multiple phases of nitrate uptake. *Plant Cell* 11, 865–874. doi: 10.1105/tpc.11.5.865

Liu, J., An, X., Cheng, L., Chen, F., Bao, J., Yuan, L., et al. (2010). Auxin transport in maize roots in response to localized nitrate supply. *Ann. Bot* 106, 1019–1026. doi: 10.1093/aob/mcq202

Liu, X., Feng, H., Huang, D., Song, M., Fan, X., and Xu, G. (2015). Two short sequences in OsNAR2.1 promoter are necessary for fully activating the nitrate induced gene expression in rice roots. *Sci. Rep.* 5, 1–10. doi: 10.1038/srep11950

Ma, C., Fan, X., and Xu, G. (2011). Responses of rice plant of wuyuanjing 7 to nitrate as affected by over-expression of OsNRT1.2. *Chinese J. Rice Sci.* 4, 349–356.

Maghiaoui, A., Gojon, A., and Bach, L. (2021). NRT1.1-centered nitrate signaling in plants. *J. Exp. Bot.* 71, 6226–6237. doi: 10.1093/JXB/ERAA361

Miller, A. J., Fan, X., Orsel, M., Smith, S. J., and Wells, D. M. (2007). Nitrate transport and signalling. *J. Exp. Bot.* 58, 2297–2306. doi: 10.1093/jxb/erm066

Mishra, B. K., Srivastava, J. P., Lal, J. P., and Sheshshayee, M. S. (2016). Physiological and biochemical adaptations in lentil genotypes under drought stress. *Russ. J. Plant Physiol.* 63, 695–708. doi: 10.1134/S1021443716040117

Moll, R. H., Kamprath, E. J., and Jackson, W. A. (1982). Analysis and interpretation of factors which contribute to efficiency of nitrogen utilization 1. *Agron. J.* 74, 562–564. doi: 10.2134/agronj1982.00021962007400030037x

Murashige, T., and Skoog, F. (1962). A revised medium for rapid growth and bio assays with tobacco tissue cultures. *Physiol. Plant.* 15, 473–497. doi: 10.1111/j.1399-3054.1962.tb08052.x

Okamoto, M., Vidmar, J. J., and Glass, A. D. M. (2003). Regulation of NRT1 and NRT2 gene families of *Arabidopsis thaliana*: Responses to nitrate provision. *Plant Cell Physiol.* 44, 304–317. doi: 10.1093/pcp/pcg036

Peng, S., Buresh, R. J., Huang, J., Yang, J., Zou, Y., Zhong, X., et al. (2006). Strategies for overcoming low agronomic nitrogen use efficiency in irrigated rice systems in China. *F. Crop. Res.* 96, 37–47. doi: 10.1016/j.fcr.2005.05.004

Remans, T., Nacry, P., Pervent, M., Filleur, S., Diatloff, E., Mounier, E., et al. (2006). The *Arabidopsis* NRT1.1 transporter participates in the signaling pathway triggering root colonization of nitrate-rich patches. *Proc. Natl. Acad. Sci. U.S.A.* 103, 19206–19211. doi: 10.1073/pnas.0605275103

Ren, N., Chen, X., Xia, Y., Bai, X., Jiang, X., and Zhou, Y. (2019). Cloning and expression analysis of MeNRT2.5 gene in cassava. *Tropical. biol.* 10, 111–118.

Sakuraba, Y., Chaganzhana, Mabuchi, A., Iba, K., and Yanagisawa, S. (2021). Enhanced NRT1.1/NPF6.3 expression in shoots improves growth under nitrogen deficiency stress in Arabidopsis. *Commun. Biol.* 4, 1–14. doi: 10.1038/s42003-021-01775-1

Sharma-Natu, P., and Ghildiyal, M. C. (2005). Potential targets for improving photosynthesis and crop yield. *Cur. Sci. India.* 88, 1918–1928.

Scheible, W. R., Morcuende, R., Czechowski, T., Fritz, C., Osuna, D., Palacios-Rojas, N., et al. (2004). Genome-wide reprogramming of primary and secondary metabolism, protein synthesis, cellular growth processes, and the regulatory infrastructure of *Arabidopsis* in response to nitrogen. *Plant Physiol.* 136, 2483–2499. doi: 10.1104/pp.104.047019

Singh, A., Maan, A., Singh, B., Sheokand, S., Vrat, D., and Sheoran, A. (2000). Ethylene evolution and antioxidant defence mechanism in *Cicer arietinum* roots in the presence of nitrate and aminoethoxyvinylglycine. *Plant Physiol. Biochem.* 38, 709–715. doi: 10.1016/s0981-9428(00)01174-8

Sugiura, M., Georgescu, M. N., and Takahashi, M. (2007). A nitrite transporter associated with nitrite uptake by higher plant chloroplasts. *Plant Cell Physiol.* 48, 1022–1035. doi: 10.1093/pcp/pcm073

Tabuchi, M., Abiko, T., and Yamaya, T. (2007). Assimilation of ammonium ions and reutilization of nitrogen in rice (*Oryza sativa* L.). *J. Exp. Bot.* 58, 2319–2327. doi: 10.1093/jxb/erm016

Takei, K., Sakakibara, H., Taniguchi, M., and Sugiyama, T. (2001). Nitrogen-dependent accumulation of cytokinins in root and the translocation to leaf: Implication of cytokinin species that induces gene expression of maize response regulator. *Plant Cell Physiol.* 42, 85–93. doi: 10.1093/pcp/pce009

Tal, I., Zhang, Y., Jørgensen, M. E., Pisanty, O., Barbosa, I. C. R., Zourelidou, M., et al. (2016). The *Arabidopsis* NPF3 protein is a GA transporter. *Nat. Commun* 7:11486. doi: 10.1038/ncomms11486

Tenea, G. N., Calin, A., Gavrila, L., and Cucu, N. (2008). Manipulation of root biomass and biosynthetic potential of Glycyrrhiza glabra L. plants by Agrobacterium rhizogenes mediated transformation. *Rom. Biotechnol. Lett.* 13, 3922–3932.

Thomsen, H. C., Eriksson, D., Møller, I. S., and Schjoerring, J. K. (2014). Cytosolic glutamine synthetase: a target for improvement of crop nitrogen use efficiency? *Trends Plant Sci.* 19, 656–663. doi: 10.1016/j.tplants.2014.06.002

Tian, Q., Chen, F., Zhang, F., and Mi, G. (2005). Possible involvement of cytokinin in nitrate-mediated root growth in maize. *Plant and Soil* 277, 185–196. doi: 10.1007/s11104-005-6837-5

Tian, Q., Chen, F., Liu, J., Zhang, F., and Mi, G. (2008). Inhibition of maize root growth by high nitrate supply is correlated with reduced IAA levels in roots. *J Plant Physiol* 165, 942–951. doi: 10.1016/j.jplph.2007.02.011

Tsay, Y. F. (1993). The herbicide sensitivity gene chl1 of arabidopsis encodes a nitrate-inducible nitrate transporter. *Cell* 72, 705–713. doi: 10.1016/0092-8674(93)90399-B

Undurraga, S. F., Ibarra-Henríquez, C., Fredes, I., Álvarez, J. M., and Gutiérrez, R. A. (2017). Nitrate signaling and early responses in *Arabidopsis* roots. *J. Exp. Bot.* 68, 2541–2551. doi: 10.1093/jxb/erx041

Vaucheret, H., Béclin, C., Elmayan, T., Feuerbach, F., Godon, C., Morel, J. B., et al. (1998). Transgene-induced gene silencing in plants. *Plant J.* 16, 651–659. doi: 10.1046/j.1365-313X.1998.00337.x

Vanderschuren, H., Alder, A., Zhang, P., and Gruissem, W. (2009). Dose-dependent RNAi-mediated geminivirus resistance in the tropical root crop cassava. *Plant Mol. Biol.* 70, 265–272. doi: 10.1007/s11103-009-9472-3

Vincentz, M., and Caboche, M. (1991). Constitutive expression of nitrate reductase allows normal growth and development of *Nicotiana plumbaginifolia* plants. *EMBO J.* 10, 1027–1035. doi: 10.1002/j.1460-2075.1991.tb08041.x

Wang, R., Okamoto, M., Xing, X., and Crawford, N. M. (2003). Microarray analysis of the nitrate response in Arabidopsis roots and shoots reveals over 1,000 rapidly responding genes and new linkages to glucose, trehalose-6-phosphate, iron, and sulfate metabolism. *Plant Physiol.* 132, 556–567. doi: 10.1104/pp.103.021253

Wang, R., Xing, X., and Crawford, N. (2007). Nitrite acts as a transcriptome signal at micromolar concentrations in *Arabidopsis* roots. *Plant Physiol.* 145, 1735–1745. doi: 10.1104/pp.107.108944

Wang, W., Hu, B., Yuan, D., Liu, Y., Che, R., Hu, Y., et al. (2018). Expression of the nitrate transporter gene OsNRT1.1A/ OsNPF6.3 confers high yield and early maturation in rice. *Plant Cell* 30, 638–651. doi: 10.1105/tpc.17.00809

Wang, Y. Y., Cheng, Y. H., Chen, K. E., and Tsay, Y. F. (2018). Nitrate transport, signaling, and use efficiency. *Annu. Rev. Plant Biol.* 69, 85–122. doi: 10.1146/annurev-arplant-042817-040056

Wang, Y. Y., Hsu, P. K., and Tsay, Y. F. (2012). Erratum to: " Uptake, allocation and signaling of nitrate". *Trends Plant Sci.* 17:624. doi: 10.1016/j.tplants.2012.08.007

Wong, H. K., Chan, H. K., Coruzzi, G. M., and Lam, H. M. (2004). Correlation of ASN2 gene expression with ammonium metabolism in *Arabidopsis*. *Plant Physiol.* 134, 332–338. doi: 10.1104/pp.103.033126

Xu, G. H., Fan, X. R., and Miller, A. J. (2012). Plant nitrogen assimilation and use efficiency. *Annu. Rev. Plant Biol.* 63, 153–182. doi: 10.1146/annurev-arplant-042811-105532

Yamaya, T., and Kusano, M. (2014). Evidence supporting distinct functions of three cytosolic glutamine synthetases and two NADH-glutamate synthases in rice. *J. Exp. Bot.* 65, 5519–5525. doi: 10.1093/jxb/eru103

Zhang, P., Potrykus, I., and Puonti-Kaerlas, J. (2000). Efficient production of transgenic cassava using negative and positive selection. *Transgenic Res.* 9, 405–415. doi: 10.1023/A:1026509017142

Zhang, Y., Wang, J., Gong, S., Xu, D., and Sui, J. (2017). Nitrogen fertigation effect on photosynthesis, grain yield and water use efficiency of winter wheat. *Agric. Water Manag.* 179, 277–287. doi: 10.1016/j.agwat.2016.08.007

Zhao, L., Chen, P., Liu, P., Song, Y., and Zhang, D. (2021). Genetic effects and expression patterns of the nitrate transporter (NRT) gene family in

populus tomentosa. *Front. Plant Sci.* 12:661635. doi: 10.3389/fpls.2021.661635

Zhao, M., Geng, X., Bi, W., Xu, Q., Sun, J., Huang, Y., et al. (2017). Recombination between dep1 and NRT1.1B under japonica and indica genetic backgrounds to improve grain yield in rice. *Euphytica* 213, 1–9. doi: 10.1007/s10681-017-2038-6

Zhou, J. J., Theodoulou, F. L., Muldin, I., Ingemarsson, B., and Miller, A. J. (1998). Cloning and functional characterization of a Brassica napus transporter that is able to transport nitrate and histidine. *J. Biol. Chem.* 273, 12017–12023. doi: 10.1074/jbc.273.20.12017

Zhuang, D., Jiang, D., Liu, L., and Huang, Y. (2011). Assessment of bioenergy potential on marginal land in China. *Renew. Sustain. Energy Rev.* 15, 1050–1056. doi: 10.1016/j.rser.2010.11.041

Zou, L., Qi, D., Sun, J., Zheng, X., and Peng, M. (2019). Expression of the cassava nitrate transporter NRT2.1 enables Arabidopsis low nitrate tolerance. *J. Genet.* 98:74. doi: 10.1007/s12041-019-1127-9

Conflict of Interest: The authors declare that the research was conducted in the absence of any commercial or financial relationships that could be construed as a potential conflict of interest.

frontiers | Frontiers in Plant Science

ORIGINAL RESEARCH
published: 28 April 2022
doi: 10.3389/fpls.2022.870681

Improved Utilization of Nitrate Nitrogen Through Within-Leaf Nitrogen Allocation Trade-Offs in *Leymus chinensis*

Xiaowei Wei[1,2], Yuheng Yang[1], Jialiang Yao[1], Jiayu Han[1], Ming Yan[1], Jinwei Zhang[1], Yujie Shi[1], Junfeng Wang[1] and Chunsheng Mu[1]**

[1] Key Laboratory of Vegetation Ecology of the Ministry of Education, Jilin Songnen Grassland Ecosystem National Observation and Research Station, Institute of Grassland Science, Northeast Normal University, Changchun, China, [2] Key Laboratory for Plant Resources Science and Green Production, Jilin Normal University, Siping, China

OPEN ACCESS

Edited by:
Honghai Luo,
Shihezi University, China

Reviewed by:
Shunfeng Ge,
Shandong Agricultural University, China
Qiangqiang Xiong,
Yangzhou University, China

***Correspondence:**
Chunsheng Mu
mucs821@nenu.edu.cn
Junfeng Wang
wangjf150@nenu.edu.cn

Specialty section:
This article was submitted to Plant Nutrition, a section of the journal Frontiers in Plant Science

Received: 07 February 2022
Accepted: 21 March 2022
Published: 28 April 2022

Citation:
Wei X, Yang Y, Yao J, Han J, Yan M, Zhang J, Shi Y, Wang J and Mu C (2022) Improved Utilization of Nitrate Nitrogen Through Within-Leaf Nitrogen Allocation Trade-Offs in Leymus chinensis. Front. Plant Sci. 13:870681. doi: 10.3389/fpls.2022.870681

The Sharply increasing atmospheric nitrogen (N) deposition may substantially impact the N availability and photosynthetic capacity of terrestrial plants. Determining the trade-off relationship between within-leaf N sources and allocation is therefore critical for understanding the photosynthetic response to nitrogen deposition in grassland ecosystems. We conducted field experiments to examine the effects of inorganic nitrogen addition (sole NH_4^+, sole NO_3^- and mixed NH_4^+/NO_3^-: 50%/50%) on N assimilation and allocation by *Leymus chinensis*. The leaf N allocated to the photosynthetic apparatus (N_{PSN}) and chlorophyll content per unit area (Chl_{area}) were significantly positively correlated with the photosynthetic N-use efficiency (PNUE). The sole NO_3^- treatment significantly increased the plant leaf PNUE and biomass by increasing the photosynthetic N allocation and Chl_{area}. Under the NO_3 treatment, *L. chinensis* plants devoted more N to their bioenergetics and light-harvesting systems to increase electron transfer. Plants reduced the cell wall N allocation or increased their soluble protein concentrations to balance growth and defense under the NO_3 treatment. In the sole NH_4^+ treatment, however, plants decreased their N allocation to photosynthetic components, but increased their N allocation to the cell wall and elsewhere. Our findings demonstrated that within-leaf N allocation optimization is a key adaptive mechanism by which plants maximize their PNUE and biomass under predicted future global changes.

Keywords: leaf N allocation, nitrate, ammonium, photosynthetic nitrogen-use efficiency, cell wall, *Leymus chinensis*

INTRODUCTION

Nitrogen (N) plays a vital role in ecosystems. This mineral element is required for plant growth and is typically absorbed as ammonium (NH_4^+) or nitrate (NO_3^-). Ammonium N (NH_4^+), and nitrate (NO_3^-) are also the main forms of N loading associated with atmospheric deposition (Galloway et al., 2008; Stevens, 2019; Liang et al., 2020). The N-use strategies of plant species of different

functional types vary, and different plants thus respond differently to N additions (Xia and Wan, 2008) as the grasses acquire N from the soil and adopt more flexible strategies for different soil N sources to meet their high N demand (Callow, 1999). Generally, larger plant growth responses to NH_4^+-N than NO_3^--N addition have been found in terrestrial plants, but not in shrubs or grasses (Yan et al., 2019; Liang et al., 2020). However, the differences in the N form uptaken by different species (Marschner and Marschner, 2012; Grassein et al., 2015) are likely to reflect differences in the N uptake and N use efficiency of the species (Lu et al., 2021). The availability of co-provisional NO_3^- affects the accumulation and assimilation of NH_4^+ in roots and leaves (Prinsi and Espen, 2018). Uptake of NH_4^+ and NO_3^- is mediated by low and high affinity systems in higher plants (Haynes and Goh, 1978; Forde, 2000; Howitt and Udvardi, 2000). The uptake and utilization of NH_4^+-N and NO_3^--N by plants is critical for agricultural production and ecosystem stability (Tho et al., 2017; Luo et al., 2021).

The metabolism of carbon and N are interactively coupled across scales, from the leaf scale to the whole plant scale. Thus, changes in the availability of N at one of these scales are likely to affect the metabolic system at other scales (Liang et al., 2020). The assimilation NH_4^+ and NO_3^- affects several biochemical and molecular mechanisms, thus altering various specific physiological processes throughout the plant development process (Liu and von Wirén, 2017). The majority of species are sensitive to excess NH_4^+ because less energy is required to uptake this form, but at high concentrations, this molecule might trigger numerous metabolic disorders (Britto and Kronzucker, 2002; Hessini et al., 2013). Generally, plants exposed to excess NH_4^+ and NO_3^- display reduced growth, increased N metabolism-related enzymes, and modified photosynthetic physiological characteristics (Guo et al., 2008; Mu and Chen, 2021). Nitrate reductase (NR), nitrite reductase (NiR), Glutamine synthetase (GS) I, and GSII activities and the transcriptional levels of the corresponding genes in wheat seedlings are significantly reduced by N deficiency (Balotf et al., 2016). In general, the activity of N metabolism enzymes is significantly related to the synthesis of photosynthesis (Marschner and Marschner, 2012). The results of a meta-analysis showed that the effects of N deposition on 14 photosynthesis-related traits and affecting moderators and the associated plant trait responses depended on biological, experimental, and environmental moderators (Liang et al., 2020). Moderators that affect the responses of photosynthetic N metabolism have less been simultaneously considered in previous studies.

N is absorbed by plants and distributed in plant leaves in different forms, such as soluble components (e.g., nitrates, amino acids, and proteins) and insoluble components (e.g., cell walls, membranes, and other structures; Feng et al., 2009; Liu et al., 2018). Approximately half of the total leaf N is used for photosynthesis and is allocated to three main systems: the carboxylation, bioenergetics, and light harvesting systems (Hikosaka and Terashima, 1995; Takashima et al., 2004). Small changes in photosynthetic N can affect the carboxylation efficiency and photosynthetic N use efficiency (PNUE) of plants (Feng et al., 2009; Onoda et al., 2017). Cell walls are a major N sink in leaves and are used for plant defense (Evans and Poorter, 2001; Feng et al., 2009). Mass and thickness of cell wall changed in response to sink–source perturbation, which caused decreases in gm and photosynthesis in soybean and French bean (Sugiura et al., 2020). Many studies have focused on the leaf N allocation trade-offs among different leaf components (Takashima et al., 2004; Feng et al., 2009; Onoda et al., 2017). For example, invasive species allocate more leaf N to their carboxylation and bioenergetics systems than native species, leading to invasive plants having higher A_n, PNUE, and respiration efficiencies (Feng, 2008; Feng et al., 2009). The invasive species generally had lower LMA than natives, allocate more N to soluble protein, amino acids, and nucleic acids and less N to cell wall protein, aligning them closer to the "high-return" end of the leaf economics spectrum (Funk et al., 2013). Maize plants tend to invest relatively more N into bioenergetics to sustain electron transport under low-N-stress conditions (Mu et al., 2016). This suggests that plants were able to optimally allocate their nutrients to achieve an adaptive "functional balance." Storage N is used for coordinating leaf expansion and photosynthetic capacity in winter oilseed rape (*Brassica napus* L.) from emergence to senescence, thereby promoting leaf growth and biomass (Liu et al., 2018). The mechanisms by which NH_4^+-N and NO_3^--N are allocated and utilized in the photosynthetic carbon assimilation process have rarely been studied.

Grasslands play an important role in coping with global change (Liu et al., 2019; Shi et al., 2021). *Leymus chinensis* is a perennial rhizomatous grass that is often considered the foundational and dominant species in the eastern Eurasian steppe regions (Zhu, 2004). Additionally, in these regions, the N availability in the soils is often limited. Although N preferences have been studied in relatively few grassland species, these responses of grassland plants to N availability and relative preferences for NH_4^+ and NO_3^- are important in structuring natural grassland communities (Cui et al., 2017), but have also become of recent interest in managed grasslands. Adding a small amount of NH_4^+-N to NO_3^--N can significantly affect the photosynthesis, growth, and biomass accumulation of *L. chinensis* (Zhang et al., 2018). In addition, other studies have shown that NH_4^+-N is more suitable for *L. chinensis* growth than NO_3^--N or glycine (Li et al., 2018). The results of previous studies on the effects of NH_4^+-N to NO_3^--N on the growth and biomass accumulation of *L. chinensis* have extensively varied.

This study aimed to clarify the trade-offs of within-leaf N allocation to the upregulation of photosynthesis responding to the varying N supply conditions. To date, studies on the effects of N forms have mainly focused on plant preference and root growth (Gansel et al., 2001; Leghari et al., 2016; Cui et al., 2017; Kumar et al., 2020), whereas few have reported its effects on N assimilation and absorption and within-leaf N allocation. In the present study, the effects of different N forms (sole NH_4^+, sole NO_3^- and mixed NH_4^+/NO_3^-: 50%/50%) supply on leaf N assimilation and within-leaf N allocation were examined under field conditions to elucidate the physiological mechanism of NO_3^--N assimilation and leaf N allocation in

L. chinensis leaves, and to enrich the theory of N absorption in *L. chinensis* leaves.

MATERIALS AND METHODS

Plant Materials and Growth Conditions

The field experiment was carried out at the Jilin Songnen Grassland Ecosystem National Observation and Research Station in Jilin Province, Northeast Normal University, China (44°34'N, 123°31'E). The experimental site was located in the semi-arid, semi-humid, and temperate continental monsoonal climate zone. The study area was characterized by hot and rainy summers and cold and dry winters. The soil properties in 0–20 cm soil layer were as follows: pH 8.75; EC, 79.16 μs cm^{-1}; total N, 1.04 g kg^{-1}; total phosphorous (P); 68 g kg^{-1}; organic Carbon (C), 6.43 g kg^{-1}; NH_4^+-N 1.24 mg kg^{-1}; NO_3^--N 1.91 mg kg^{-1}. The mean temperature ranges from 4.6 to 6.5°C. The annual mean precipitation ranges from 280 to 620 mm, with the majority of rainfall falling between June and September, and the mean annual rainfall ranging from 1,200 to 1,300 mm (Guo et al., 2020; Shi et al., 2021). The pot experiment was conducted according to a complete randomized block design with six replicates, with the plastic pots (15 cm in diameter and 25 cm in depth) filled with chestnut soil (3.5 kg soil pot $^{-1}$).

Leymus chinensis (Trin.) Tzvel. (C_3 perennial rhizomatous grass) was widely distributed in northern China, eastern Mongolia, Transbaikalia, and Russia. It has good ecological adaptability and tolerance to drought, saline-alkali, and low temperature environment. Thus, it often forms *L. chinensis* steppes and meadows as a dominant species (Liu et al., 2019). On April 20, shoots of *L. chinensis* were transplanted into plastic pots, while shoots were collected from the eastern of Eurasia meadow steppe. Based on the investigation of the population density of natural *L. chinensis* grassland in the field experimental site during the green period (April 10- May 10), all species were planted with four individuals per pot in monoculture, and the plots were harvested on August 20. Additional N was applied at four different treatment levels: unfertilized treatment (N0), sole NH_4^+-N [as $(NH_4)_2SO_4$] (NH_4), sole NO_3^--N [as $Ca(NO_3)_2$] (NO_3), and mixture of both NH_4^+-N and NO_3^--N in ratio of 1:1 (NH_4NO_3) for a total of 10 g N m^{-2}. Two equal portions of each mixture was added into each pot (May 10 and June 6). In the previous research conducted in the north grassland, N deposition at 10 g N m^{-2} y^{-1} was the maximum amount (Zhang et al., 2017). The medium containing NH_4^+ as the only N source was buffered with $CaCl_2$ (39.7 g m^{-2}). In addition, the nitrification inhibitor dicyandiamide (DCD, 98.0%) was added to the NH_4^+ (10 mg m^{-2} y^{-1}) and NH_4NO_3 treatment (5 mg m^{-2} y^{-1}) to inhibit nitrification of NH_4^+. Other fertilizers (P, K, S) and micronutrients (Zn, B, Mn, Mo, Cu, and Fe) were applied for all treatments to ensure that plant growth was not limited by nutrients other than N. The plots were kept free of weeds, insects, and diseases during the growth season, and all mesocosms were exposed to natural precipitation events and less irrigation to ensure normal plant growth. The plots were harvested on August 20 during the post fruiting vegetation growth stage.

Gas Exchange Measurements and Chlorophyll Fluorescence

From 24 to 30 July 2019, the leaf assimilation rate (A_n, μmol m^{-2} s^{-1}), stomatal conductance (g_s, mmol m^{-2} s^{-1}), and internal CO_2 (C_i, μmol mol^{-1}) were measured using a CIRAS-3 portable photosynthesis system (PP Systems, United States) equipped with a CO_2 concentration at 400 μmol mol^{-1} in the leaf chamber, at 500 μmol s^{-1} flow rate, and at 25°C. The photosynthetic photon flux density (PPFD) of the leaf chamber was set to 1,600 μmol m^{-2} s^{-1} (with 90% red light, 5% blue light, and 5% white light) and 65% relative humidity. For the rapid A/C_i response curve (Stinziano et al., 2017), the CO_2 partial pressure was changed from 50 to 1,200 μmol mol^{-1}. In each pot, the 2nd and 3rd leaf from the tip of the shoot were used for leaf gas exchange measurements and conducted between 8:00 a.m. and 16:00 a.m. (six replicates).

The maximum rate of Rubisco carboxylation (V_{cmax}, μmol m^{-2} s^{-1}) and maximum rate of electron transport (J_{max}, μmol m^{-2} s^{-1}) were calculated by the A/C_i curves data and fitted by using the models of von Caemmerer (2000) and Long and Bernacchi (2003). The details were calculated as follows:

$$V_{cmax} = \frac{(R_d + A_n)\left[C_i + K_C\left(1 + \frac{O}{K_0}\right)\right]}{(C_i - \Gamma^*)}$$

$$J_{max} = \frac{4(R_d + A_n)(C_i + 2\Gamma^*)}{(C_i - \Gamma^*)}$$

where R_d is the mitochondrial respiration rate in the light (μmol m^{-2} s^{-1}), K_c and K_o are Michaelis constants for carboxylation and oxygenation, O is the intercellular oxygen concentration close to 210 mmol mol^{-1}, and Γ* is the CO_2 compensation point in the absence of respiration (μmol mol^{-1}), Additionally, K_c, K_o, and Γ* calculated by the temperature dependence function from Bernacchi et al. (2001, 2003).

The chlorophyll fluorescence was obtained in order to analyze PSII quantum efficiency of plants by using an IMAGING PAM M-series (Walz, Effeltrich, Germany), and dark period of the samples was dark for 30 min before measurements. The maximum quantum yield of PSII (Fv/Fm), the effective quantum yield of PSII (φPSII), non-photochemical quenching coefficient (NPQ), and electron transport rate (ETR, μmol e^{-1} s^{-1} m^{-2}) were calculated according to Zhou et al. (2021).

Biochemical Measurements

After the determination of the chlorophyll fluorescence parameters, the leaf area was determined with a portable leaf area meter (AM350, ADC Bio Scientific Ltd., Herts, United Kingdom). Two leaves per plant were collected, immediately frozen in liquid N, and stored at -80°C for biochemical analysis. Two additional leaves were halted enzyme activity at 105°C for 30 min of leaves and dried to a constant weight at 65°C. Then biomass was measured and analyzed for total N content (N_m, mg g^{-1}) with an Elementar Vario EL Cube (Elementar, Langenselbold, Germany). A leaf mass per unit leaf area (LMA, g m^{-2}) and a leaf N content per unit leaf area (N_{area}, g m^{-2}) were calculated as $N_{area} = N_m \times LMA$. Chlorophyll per leaf mass (Chl_m, mg g^{-1})

was quantified by 0.1 g leaf in the ethanol extract, and measured using a spectrophotometer (UVmini-1240, Shimadzu, Japan) at 645 nm and 663 nm (Wellburn, 1994). The chlorophyll content was calculated as follows:

$$Chl_a = 12.43 \times A663 - 2.62 \times A645$$

$$Chl_b = 22.62 \times A645 - 4.36 \times A663$$

$$Chl_m = Chl_a + Chl_b$$

Chlorophyll per leaf area (Chl_{area}) was calculated as $Chl_{area} = Chl_m \times LMA$.

To quantify nitrate N and ammonium N contents in leaves, 2.0 g of lyophilized samples were incubated with 10 ml distilled water, boiled for 1 h, and filtered to obtain the crude extract. Subsequently, the NO_3^- concentration was measured by the salicylic acid chromogenic method of Cataldo et al. (1975), while NH_4^+ concentration was determined by the phenol-hypochlorite method of Felker (1977). Free amino acid was measured by ninhydrin colorimetric method (Hwang and Ederer, 1975).

Different forms of N were measured according to Takashima et al. (2004) and Onoda et al. (2017) with some modifications. The leaves were powdered with liquid N and homogenized in 2 ml of Na-phosphate buffer (pH 7.5, 100 mmol L^{-1}), then washed in a centrifuge tube. This procedure was repeated three times. The homogenates were centrifuged at 12,000 g at 4°C for 10 min, and the supernatant was regarded as soluble protein. The pellet was washed with 1 ml of phosphate buffer containing 3% sodium dodecyl sulfate (SDS), followed by centrifugation (12,000 g, 5 min) after heating in 90°C water for 5 min. This procedure was repeated six times while the supernatants regarded as SDS-soluble protein were collected. The residue, regarded as cell wall protein, was washed with ethanol into the quantitative filter paper. The supernatant was precipitated with 10% trichloroacetic acid (TCA) by heating at 85°C for 5 min. The precipitate was filtered with quantitative filter paper and washed with ethanol. The three types of components of N on the quantitative filter paper were dried at 85°C, and then analyzed by the Elementar Vario EL Cube.

Nitrate reductase, NiR, GSI, and GSII of frozen leaves was determined by plant NR, NiR, GSI, and GSII activity *ELISA* kit (Shanghai Enzyme Biotechnology Co., Ltd., China) according to the manufacturer's instructions.

Calculation of N Allocation in the Photosynthetic Apparatus and Photosynthetic N-Use Efficiency

According to the LUNA model developed by Niinemets and Tenhunen (1997), Niinemets et al. (2011), leaf photosynthetic N is divided into three major parts: the fractions of the total leaf N allocated to carboxylation system (PN_C, g g^{-1}), electron transport components (PN_B, g g^{-1}), and light harvesting components (PN_L, g g^{-1}). The photosynthetic apparatus were calculated as follows:

$$PN_C = \frac{V_{c\,max}}{6.25 \times V_{cr} \times N_{area}}$$

$$PN_B = \frac{J_{max}}{8.06 \times J_{mc} \times N_{area}}$$

$$PN_L = \frac{C_C}{N_{area} \times C_B}$$

where 6.25 (g Rubisco g^{-1} N) was the coefficient of Rubisco conversion into N at 25°C (Douglas et al., 1984), V_{cr} was 20.78 (μmol CO_2 g^{-1} Rubisco s^{-1}) at 25°C (Niinemets and Tenhunen, 1997), 8.06 was the N conversion coefficient of cytochrome (Nolan and Smillie, 1977), J_{mc} was the maximum electron transport rate per unit cytochrome f s^{-1} (155.65 μmol e^{-1} μmol cytochrome f s^{-1}) at 25°C (Niinemets and Tenhunen, 1997; Niinemets et al., 2011), Cc was leaf chlorophyll content (mmol g^{-1}), and C_B was chlorophyll binding to light harvesting components (2.15 mmol g^{-1} N; Hikosaka and Terashima, 1995). The fractions of leaf N allocated to the thylakoid (PN_{B+L}, g g^{-1}) and the photosynthetic apparatus (PN_{PSN}, g g^{-1}) were the sum of PN_B and PN_L, and the sum of PN_C, PN_B, and PN_L, respectively. N content in carboxylation (N_C, g m^{-2}), bioenergetics (N_B, g m^{-2}), light-harvesting system (N_L, g m^{-2}), and all components of the photosynthetic apparatus (N_{PSN}, g m^{-2}) were calculated as the products of PN_C, PN_B, PN_L, and PN_{PSN} with N_{area}, respectively. The remaining leaf N was defined as other N. Photosynthetic N use efficiency (PNUE, μmol g N^{-2} s^{-1}) was calculated by A_n/N_{area} (Poorter and Evans, 1998).

Statistical Analysis

All data were examined for a normal distribution (Kolmogorov-Smirnov test) and homogeneity of variance (Levene' s test) and conducted using R version 4.0.4 (R Core Team, 2020). Analyses were performed using the "Tukey' s HSD" function from "agricolae" package and differences were considered significant at $p < 0.05$. A linear correlation was performed using "perason" function from the "ggpmisc" package. The biplot were plotted using the package "ggplot2."

RESULTS

Leaf Physiological and Morphological Traits

The effects of N0, NH_4, NO_3, and NH_4NO_3 on V_{cmax}, J_{max}, and g_s were significant ($p < 0.05$) (**Figure 1**). The V_{cmax}, J_{max}, and g_s values of the NO_3 treatment were significantly higher than those of the N0, NH_4, and NH4NO3 treatments ($p < 0.05$) (**Figures 1A–C**). The leaf mass per area (LMA) measured under the NH_4 treatment was significantly higher than under the N0 treatment, but no significant difference was found between NO_3 and NH_4NO_3 (**Figure 1D**). The N0, NH_4, NO_3, and NH_4NO_3 treatments had significant effects ($p < 0.05$) on N_{area}, Chl_{area}, A_n, and PNUE (**Figures 1E–H**). The N_{area} measured under the NO_3 treatment was significantly higher than that under the N0 and NH_4 treatments ($p < 0.05$), but no significant difference was found between the NO_3 and NH_4NO_3 treatments (**Figure 1E**). The Chl_{area}, A_n, PNUE, and total leaf biomass measured under the NO_3 treatment were significantly higher than those under the N0, NH_4, and NH_4NO_3 treatments ($p < 0.05$) (**Figures 1F–I**).

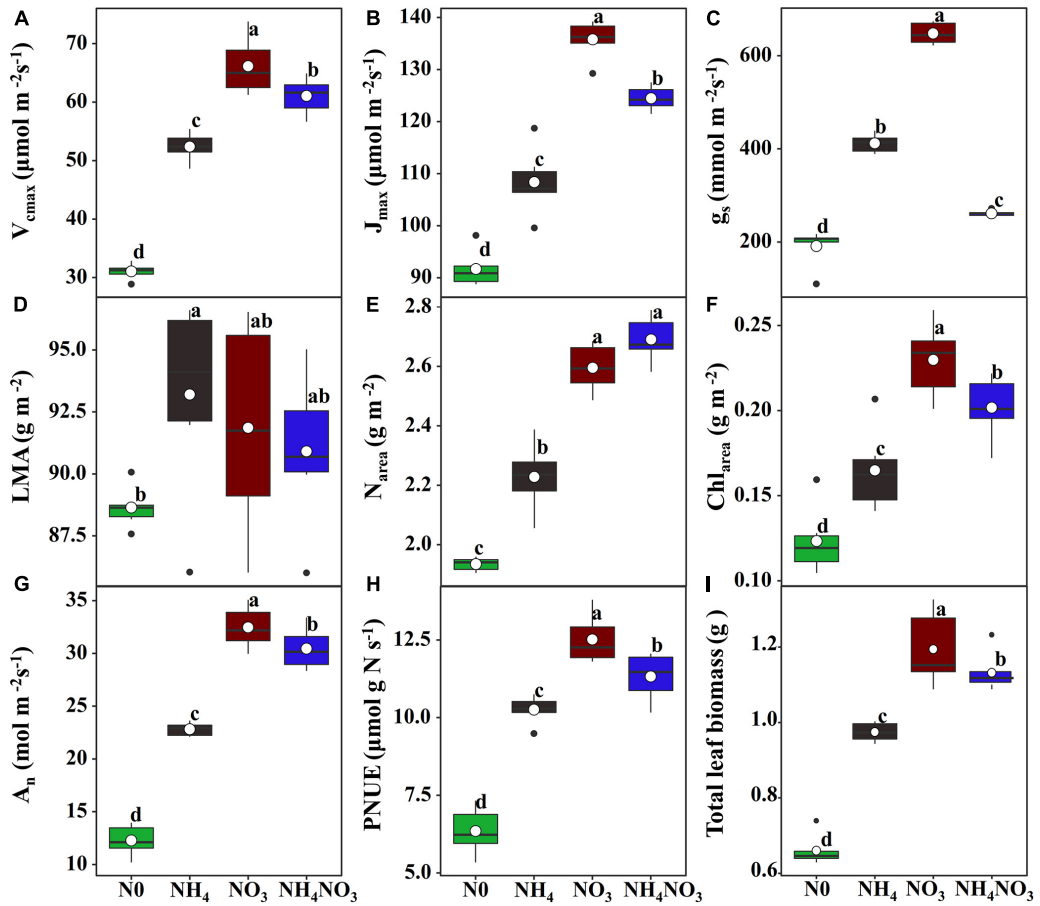

FIGURE 1 | Effect of N (N) forms treatments on maximum carboxylation rate (V_{cmax}) **(A)**, maximum photoelectron transfer rate (J_{max}) **(B)**, stomatal conductance (g_s) **(C)**, leaf mass area (LMA) **(D)**, area-based N content (N_{area}) **(E)**, area-based chlorophyll content (Chl_{area}) **(F)**, net CO_2 assimilation rate (A_n) **(G)**, photosynthetic N use efficiency (PNUE) **(H)**, and total leaf biomass **(I)** in *L. chinensis*. White dot is "Mean"; black dot is "Outlier"; horizontal is "Median"; the top of vertical line is "Max" and the bottom of vertical line is "Min." Different lower-case letters indicate significant differences between the measuring dates under the unfertilized (N0) treatment and the fertilized (NH_4, NO_3, NH_4NO_3) treatment, respectively ($p < 0.05$) ($n = 6$).

Leaf N Assimilation Enzyme Activity

To evaluate whether the induction of PNUE in the NH_4^+ and NO_3^- supply treatments was related to nitrate and ammonium accumulation or to the induction of NR, NiR, and GS activity, NR and NiR activities were stimulated in the NO_3 treatment. Conversely, they were inhibited in the NH_4 treatment (**Figures 2A,B**). In contrast, neither the GSI nor the GSII isoform activity was changed due to the effects of different N forms despite presenting higher values compared to the N0 treatment (**Figures 2C,D**).

Leaf N Allocation to Other Soluble-N Components

The nitrate contents in the NO_3- and NH_4NO_3-treated plants were higher than those measured in plants under the N0 and NH_4 treatments ($p < 0.05$) (**Table 1**). However, in the NO_3 treatment, the leaf nitrate content was very low, accounting for approximately 0.87% of the total leaf N (**Figure 3C**). The ammonium content measured under the NH_4 treatment was higher than those measured under the treatments with other N forms ($p < 0.05$) (**Table 1**), accounting for approximately 1.36% of the total leaf N (**Figure 3B**). Compared with the NH_4 treatment, the content of free amino acids was 21.07 and 31.44% higher under the NO_3 treatment and NH_4NO_3 treatment. The amount of N measured in other soluble protein was 10.88 and 19.62% higher under the NO_3 and NH_4NO_3 treatments than under the NH_4 treatment ($p < 0.05$) (**Table 1**).

Leaf N Allocation to Structure-N Components

The N_C (carboxylation) and N_B (bioenergetics) values expressed per unit leaf area were significantly higher under the NO_3 treatments than under the N0, NH_4, or NH_4NO_3 treatments ($p < 0.05$) (**Table 1** and **Figure 3**). No significant difference was found in N_L (light-harvesting system) between the NO_3 and NH_4NO_3 treatments, but N_L was significantly higher in these treatments than in the N0 and NH_4 treatments ($p < 0.05$) (**Table 1**). Compared to the N0, NH_4, and NH_4NO_3 treatments,

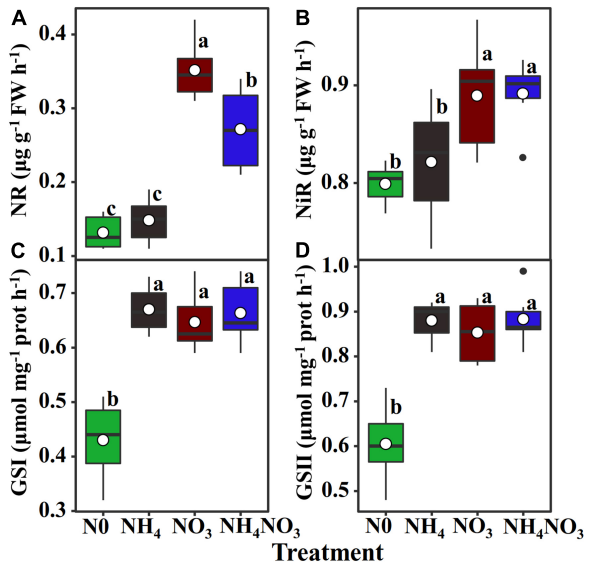

FIGURE 2 | Effect of N forms treatments on the changes in activities of nitrate reductase, nitrite reductase, and glutamine synthetase isoforms of leaves in *L. chinensis*. **(A)** Nitrate reductase (NR; EC. 1.6.6.1/2), **(B)** nitrite reductiase (NiR; EC. 1.7.2.1), **(C)** glutamine synthetase (GS) I, and **(D)** GS II. White dot is "Mean"; black dot is "Outlier"; horizontal is "Median"; the top of vertical line is "Max" and the bottom of vertical line is "Min." The changes in activities of enzyme under N0, NH_4, NO_3, and NH_4NO_3 treatments. Different lower-case letters indicate significant differences ($p < 0.05$) ($n = 6$).

N_B/N_{B+L} decreased under the NO_3 and NH_4NO_3 treatments, while N_L/N_{B+L} increased ($p < 0.05$) (**Figure 4B**). The leaf cell wall N content (N_{cw}) was 7.91% lower in the NO_3 treatment than in the NH_4 treatment (**Table 1**), while the cell wall per area was higher in the NH_4 treatment ($p < 0.05$) (**Figure 5**).

Within-Leaf N Allocation Estimate

The effects of different available N forms on the allocation of leaf N to different N components are shown in **Figure 3**. Relative to the NH_4 and NH_4NO_3 treatments, the NO_3 treatment significantly increased the percentages of N allocated to carboxylation (1.31 and 1.75%, respectively), bioenergetics (0.24 and 0.36%), and light-harvesting system (3.7 and 1.5%) proteins. Unexpectedly, the amounts of N allocated to the nitrate and other soluble protein N components were elevated under NO_3 treatment. The percentage of N in free amino acid was 1.06 and 0.08% higher under NO_3 treatment than NH_4 and NH_4NO_3 treatments. Assessing the other N proportions, under the NO_3 treatment, the N proportions were 5.45, 1.54, and 1.38% lower than those measured under the N0, NH_4, and NH_4NO_3 treatments, respectively. The percentage of N allocated to cell walls exhibited a similar trend as the cell wall biomass under the different N forms. In summary, the correlation analyses revealed highly active relationships between N_{area} and PNUE and between N_{PSN} and PNUE (**Figures 6A,B**).

PSII Quantum Efficiencies

Since *L. chinensis* plants exhibited an advantage characterized by allocating N to photosynthetic components in leaves under the NO_3 treatment, we investigated whether nitrate and ammonium affect the PSII quantum efficiencies. Positive and highly significant linear relationships between PNUE and Chl_{area} were observed in *L. chinensis* (**Figure 6C**). The Fv/Fm, φPSII, non-photochemical quenching (NPQ), and electron transfer rate (ETR) were significantly higher under the NO_3 and NH_4NO_3 treatments than under the NH_4 and N0 treatments ($p < 0.05$) (**Figure 7**).

DISCUSSION

In this study, a set of experimental observations was conducted on the photosynthetic responses of *L. chinensis* (a C_3 plant) to varying N nutrient sources to capture leaf economics spectrum response mechanism. For a better understanding of absorption and utilization of nitrate N, observations ranged from plants' morphological features, trough overall photosynthesis, and

TABLE 1 | Effect of nitrotgen (N) forms treatments on the content of N compounds in *L. chinensis*.

Parameters (mg m^{-2})	N forms treatment			
	N0	NH_4	NO_3	NH_4NO_3
Nitrate	23.38 ± 0.33 c	25.53 ± 0.49 b	27.63 ± 0.38 a	27.72 ± 0.34 a
Ammonium	27.87 ± 0.66 c	36.27 ± 0.25 a	31.42 ± 0.81 b	33.30 ± 0.78 b
Free amino acids	45.40 ± 2.04 d	75.31 ± 2.24 c	91.18 ± 1.70 b	98.99 ± 1.43 a
Other soluble protein	473.66 ± 6.61 b	502.66 ± 17.76 b	557.35 ± 15.47 a	601.33 ± 27.29 a
Cell wall	168.04 ± 1.71 ab	175.96 ± 0.90 a	162.05 ± 3.93 b	167.56 ± 4.17 ab
Carboxylation	249.86 ± 4.21 d	418.06 ± 7.71 c	527.81 ± 15.87 a	484.15 ± 8.57 b
Bioenergetics	72.75 ± 1.01 d	86.37 ± 2.06 c	108.23 ± 1.18 a	99.22 ± 0.74 b
Light-harvesting system	318.74 ± 18.21 c	412.23 ± 25.64 b	582.08 ± 21.91a	544.80 ± 31.87a
Other N	428.26 ± 8.38b	427.35 ± 18.53 b	466.18 ± 14.57 ab	502.34 ± 26.67 a
Total N (g kg^{-1})	21.82 ± 0.05 d	23.90 ± 0.23 c	28.28 ± 0.29 b	29.60 ± 0.11 a

Data were reported as the arithmetic mean ± 1 standard error (n = 6). Numbers followed by different lower-case letters indicate significant differences, according to Tukey's test (p < 0.05).

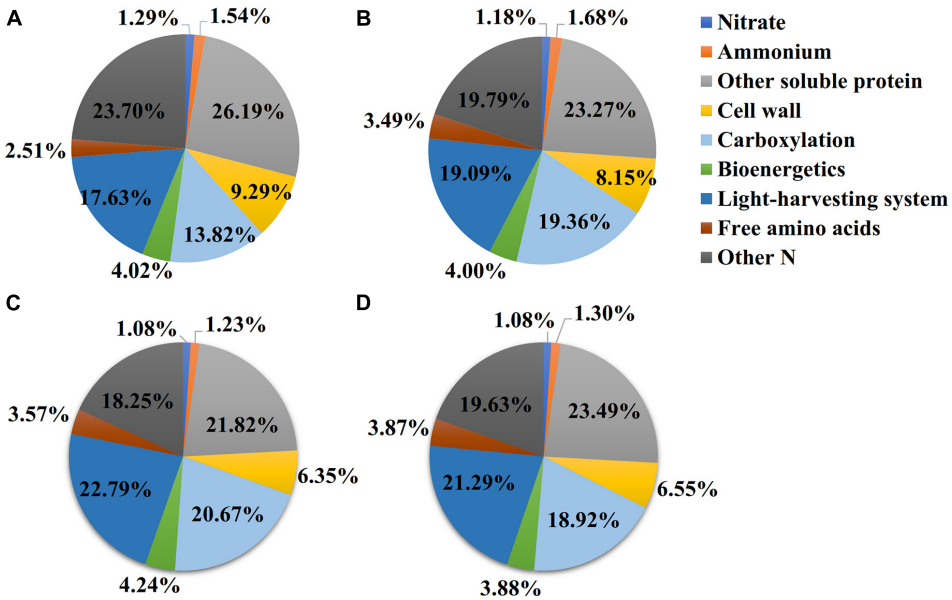

FIGURE 3 | Effect of N forms treatments on the N allocation in leaves. The data of percentages are the content of N in the corresponding components accounting for total leaf N content in *L. chinensis*. N0-treated **(A)**, NH_4-treated **(B)**, NO_3-treated **(C)**, and NH_4NO_3-treated **(D)**. The size of pie chart indicates N content ($p < 0.05$) ($n = 6$).

within-leaf N allocation, up to photosynthetic component N and nutrient concentration in plants tissues. During the growing season, NH_4^+ and NO_3^- strongly affected each of investigated aspects of plant functioning and development.

As is well documented, N is an essential nutrient in plant growth and development, and its form can affect leaf growth (Cui et al., 2017). Leaf morphological adjustments are generally recognized to be more striking than leaf biochemical characteristics in determining leaf photosynthesis adaptations to the environment (Niinemets et al., 2011; Onoda et al., 2017). N promotes leaf area growth and helps leaves absorb light energy, thereby contributing to the maintenance of A_n and PNUE (Poorter and Evans, 1998; Onoda et al., 2017). The NO_3-treated plants showed higher g_s values than the plants exposed to other treatments. As expected, the increased g_s affected CO_2 assimilation and the higher V_{cmax} values suggest that biochemical restrictions should have also been reduced. According to Guo et al. (2003), nitrate is a well-known anionic transporter involved in the stomatal opening mechanism. This result also illustrates that the NO_3-treated plants had higher g_s values than the NH_4-treated plants. In the present study, *L. chinensis,* as a group, had no significant LMA with higher A_n, Chl_{area}, and N_{area} under NO_3 treatment compared to the N0, NH_4, and NH_4NO_3 treatments, resulting in the PNUE improving by 22.02 and 10.51%, respectively. In support of this idea, in *L. chinensis*, PNUE was positively correlated with N_{area}, N_{PSN}, and Chl_{area}. V_{cmax} is a proxy for the enzymatic activity of Rubisco during the photosynthetic carbon-fixation reactions (Farquhar et al., 1980; Sharkey, 2016; Zhuang et al., 2021). The inorganic N sources significantly increased the V_{cmax} and J_{max} of *L. chinensis*. Variations in V_{cmax} can be explained by changes in LMA, N_{area}, or the proportion of N allocated to the carboxylation system (Yin et al., 2019; Zhuang et al., 2021). These findings indicated that the NO3- supply is closely related to the normal growth of *L. chinensis* leaves.

Nitrate reductase and NiR participate in the process of reducing NO_3^- to NH_4^+ in coupled regulation (Kovács et al., 2015). In our study, the NO_3 treatment strongly stimulated the NR and NiR activities. This finding is consistent with previous studies reporting that NR activity is mainly affected by the concentration of NO_3^- (Balotf et al., 2016; Wen et al., 2019). When NO_3^- is converted to other forms of N, the availability of NO_3^- decreases, but the N in the soil was continuously transferred to the leaves, which led to an increase in the NO_3^- content and NR and NiR activities (Britto and Kronzucker, 2002; Marschner and Marschner, 2012). In higher plants, GSI and GSII assimilate NH_4^+ into amino acids for plant absorption and utilization in leaves (Bloom, 2015). Interestingly, although the concentration of NH_4^+ is closely related to GSI and GSII enzyme activities (Forde and Clarkson, 1999), GSI and GSII enzyme activities have no significant difference under N supply treatments, as has been previously reported for rice plants (Alencar et al., 2019; Sugiura et al., 2020). The results of this study reveal the relationships between the NO_3^- and NH_4^+ supply with assimilation enzyme activity. According to our results, the enzyme activity of N isozyme significantly increased under NO_3^- treatment.

Intra-leaf N allocation should reflect trade-offs in the economic spectrum of leaves, with faster-growing species allocating more N to metabolism at the expense of structure (Funk et al., 2013). Thus, we hypothesized that *L. chinensis* under NO_3- treatment, which are generally located on the

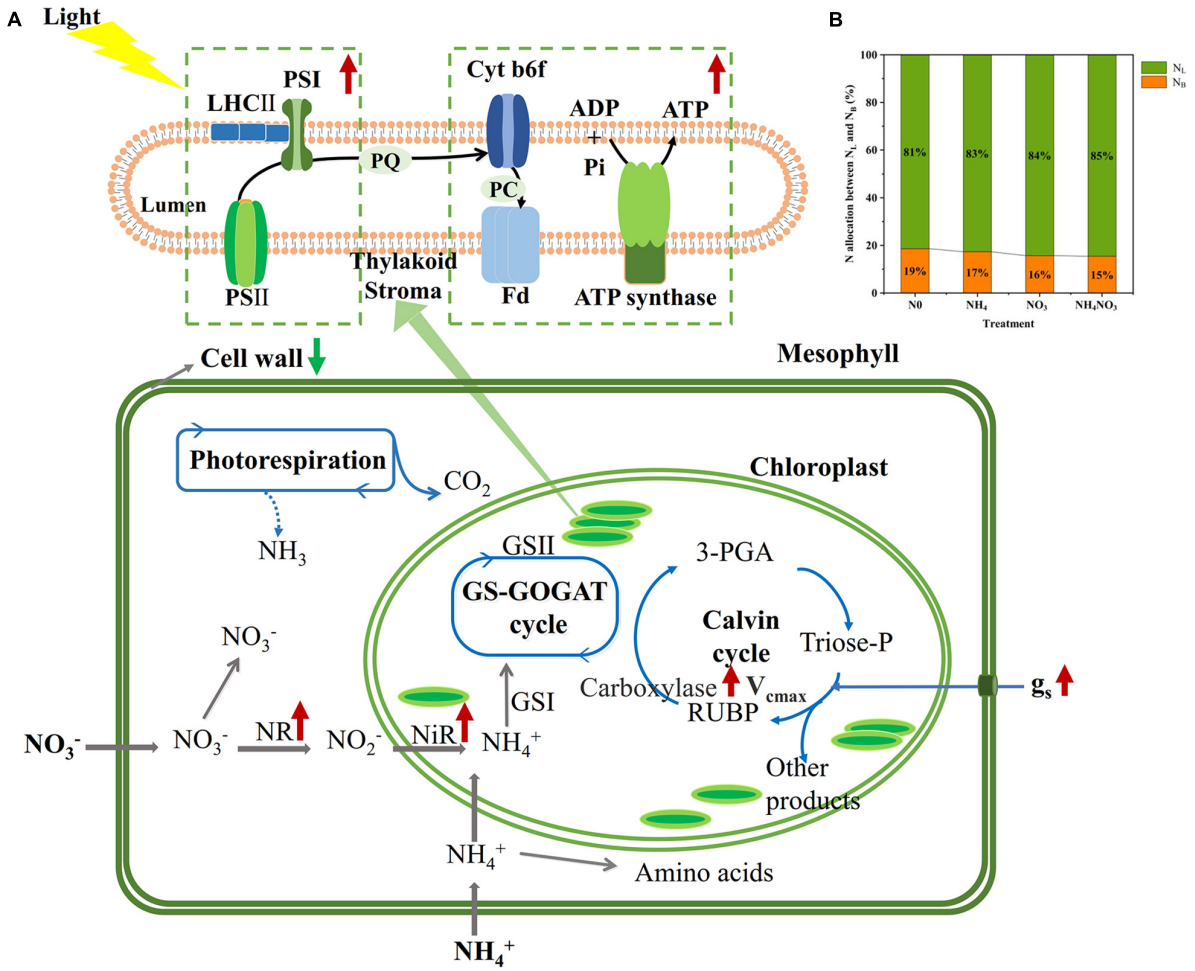

FIGURE 4 | Effect of N forms treatments on the change of N contents in photosynthetic apparatus of leaves in *L. chinensis*. **(A)** The percentage together with indicate the increase (red arrows) and the reduction (green arrows) of N in different photosynthetic apparatus under NO_3 compared to N0, NH_4, and NH_4NO_3 treatments. **(B)** The allocation of N between PN_B and PN_L within the thylakoid lumen under N0, NH_4, NO_3, and NH_4NO_3 treatments.

"high-return" of the leaf economics spectrum, would have higher A_n, N_{area}, and PNUE relative to other treatments. Therefore, it has greater allocation to leaf N pools associated with photosynthesis and growth. Species with greater N investments in photosynthetic proteins generally show higher PNUE in many natural ecosystems (Feng, 2008; Feng et al., 2009; Shi et al., 2019). Based on our original assumption of "high-return," we must assess the changes in the leaf N allocation process. In ecological models, N investments in the photosynthetic apparatus remain an important PNUE determinant (Feng et al., 2009; Liu et al., 2018). Photosynthesis is closely related to the leaf N content, which can be directly reflected by Calvin cycle proteins. Approximately three-quarters of leaf N is distributed to the photosynthetic apparatus (Dubreuil et al., 2017; Bahar et al., 2018; Zhang et al., 2020). In this study, *L. chinensis* allocated 47.7% of leaf N to the photosynthetic apparatus, and this was in accordance with previously reported results for rice plants (Zhong et al., 2019) and invade plants (Feng, 2008). Furthermore, we found that the amount of leaf N allocated to the photosynthetic apparatus was significantly positively correlated with PNUE ($R^2 = 0.83$, $p < 0.001$). *L. chinensis* leaves have lower cell wall protein with higher amino acid content under NO_3-treated plants, consistent with allocation to growth at the expense of structure. However, our hypothesis that *L. chinensis* leaves would allocate more resources to carbon assimilation and growth at the expense of structure was only partially supported under NO_3-treated plants. *L. chinensis* also had higher amounts of total N and membrane-bound protein.

Nitrate treatment caused a relative increase in content of other soluble protein N and carboxylation N and the percentage (42.49%) of total soluble protein-N in total leaf N, similar to the result of Makino et al. (2003), who reported that 25–45% of leaf N was allocated to soluble proteins. Soluble proteins and free amino acids are two of the most abundant N sources, and they store N in leaves (Liu et al., 2018). Among soluble proteins, Rubisco is a key enzyme involved in C_3 photosynthesis (composing up to 50% of the leaf soluble protein and 25% of the leaf N; Lin et al., 2014). In the present study, the high photosynthetic N (N_{PSN}) and low

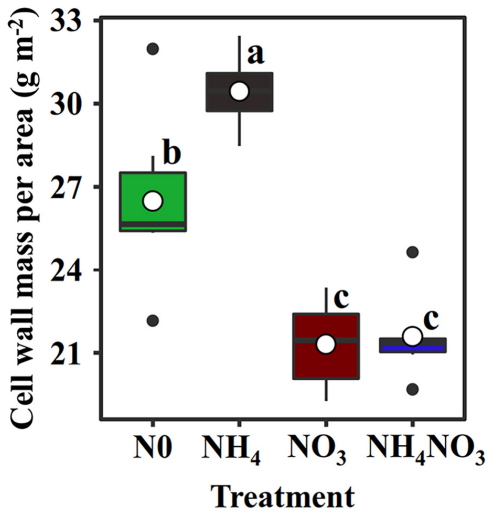

FIGURE 5 | Effect of N forms treatments on cell wall mass per area in *L. chinensis*. White dot is "Mean"; black dot is "Outlier"; horizontal is "Median"; the top of vertical line is "Max" and the bottom of vertical line is "Min." Different lower-case letters indicate significant differences under N0, NH_4, NO_3, and NH_4NO_3 treatments ($p < 0.05$) ($n = 6$).

cell wall N (N_{CW}) measured under the NO_3 treatment were presumably associated with a decrease in the cell wall biomass fraction (**Table 1** and **Figure 5**). Our finding that NO_3- treatment and other treatments have significant differences in the allocation of N to soluble protein, consistent with previously published results that faster grow species allocated more N to soluble protein at the expense of cell-wall protein (Feng et al., 2009; Landi and Esposito, 2017). Previous studies have highlighted that cell walls are a part of the plant apoplast, which is also an important N sink that can defend plants against stress (Feng et al., 2009; Shang et al., 2019). These results suggest that the allocation of N to cell walls was decreased under NO_3 conditions, thus possibly contributing to the increased absorption and utilization of N and the maintenance of photosynthesis in mesophyll cells to the greatest extent possible. The N investment strategy regarding these N components was changed under NO_3 conditions, suggesting that these components are essential for ensuring adaptations of normal growth and physiological activities to inorganic N.

The NO_3^--N used in our field experiment resulted in relatively even allocation of N to photosynthetic apparatus (e.g., carboxylation, bioenergetics, and light-harvesting components) and carbon assimilation (e.g., soluble protein, free amino acids) functions. Our data matched the theoretical estimates modeled from photosynthetic data, indicating that C_3 plants invest about 24% leaf N to thylakoids and allocate 75% of thylakoids N to light harvesting proteins and 25% in bioenergetics (Poorter and Evans, 1998; Makino et al., 2003; Zhong et al., 2019; Mu and Chen, 2021). There are two types of thylakoid N, namely, one related to the bioenergetics system, such as the electron transport chain and photosynthetic phosphorylation, and another involved in the light-harvesting component (Mu et al., 2016). The absolute N content was devoted to biogenetics and light harvesting under the NO_3 treatment. Relatively more N from the thylakoid was allocated to bioenergetics under the different N treatments. *L. chinensis* leaves had higher A_n and V_{max} compared under NO_3-treated with other treatments. This suggests that Rubisco content or activity may have been higher in *L. chinensis* leaves. Our carboxylation fraction includes Rubisco, but Rubisco was not directly measured in this study. This proved that a leaf prioritization process occurred for the stabilization of the light harvesting and electron transfer systems under the NO_3 treatment and thus the maximization of the PSII quantum yield (Antal et al., 2010; Wang F. et al., 2019; Wang P. et al., 2019). This conclusion is supported by the finding that the Fv/Fm, φPSII, and ETR values were significantly different under the NO_3 treatment. Similarly, the higher NPQ measured under the NO_3 treatment should have helped dissipate excess electrons. The NO_3 treatment coincided with a higher leaf N concentration,

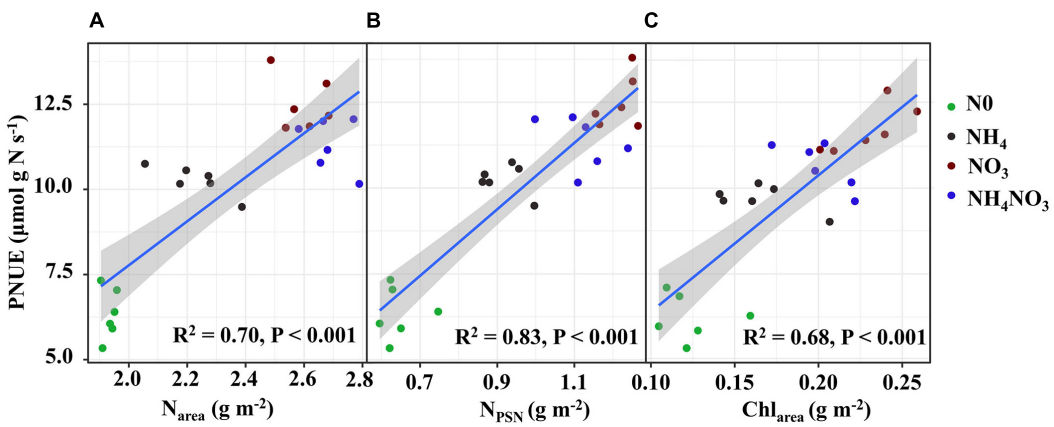

FIGURE 6 | Relationships of photosynthetic N use efficiency (PNUE) with area-based N content (N_{area}) **(A)**, photosynthetic N (N_{PSN}) **(B)** and area-based chlorophyll content (Chl_{area}) **(C)** in *L. chinensis*. The color of green, black, red, and blue correspond to the N0, NH_4, NO_3, and NH_4NO_3 treatments. Relationships between variables were assessed using linear regression analysis.

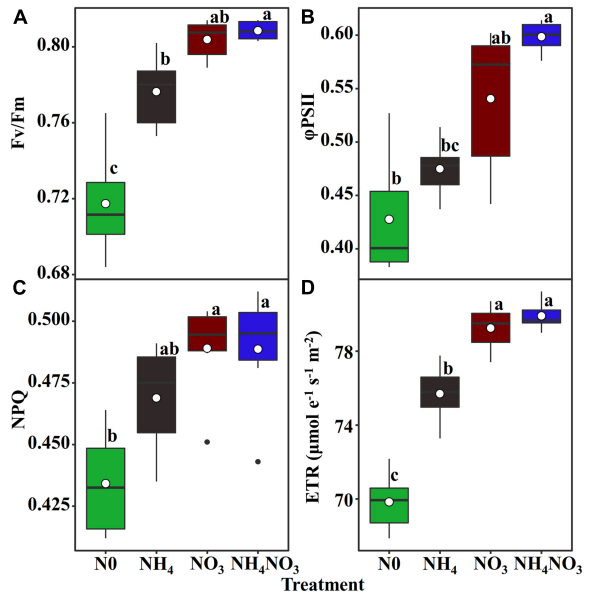

FIGURE 7 | Effect of N forms treatments on the maximum quantum yield of PSII (Fv/Fm) **(A)**, the effective quantum yield of PSII (φPSII) **(B)**, non-photochemical quenching coefficient (NPQ) **(C)**, and electron transport rate (ETR, μmol e^{-1} s^{-1} m^{-2}) **(D)** in *L. chinensis*. White dot is "Mean"; black dot is "Outlier"; horizontal is "Median"; the top of vertical line is "Max" and the bottom of vertical line is "Min." Different lower-case letters indicate significant differences under N0, NH_4, NO_3, and NH_4NO_3 treatments ($p < 0.05$) ($n = 6$).

and more N allocated to carboxylation compared to the other N treatments. It is likely that the relatively higher N in the bioenergetics and light-harvesting systems were well matched with the higher carboxylation capacity, promoting an increase in the photosynthetic rate and PNUE.

Our study examined within-leaf N partitioning in *L. chinensis* of the grassland dominant species in inorganic N absorption. *L. chinensis* leaves may succeed by allocating N to growth at the expense of higher leaf level carbon assimilation under NO_3^- treatment. Furthermore, the leaf N assimilate enzyme activity and within-leaf N allocation were observed to exhibit different trends in response to the NO_3 treatment compared to the other treatments (**Figure 4**), suggesting that the trade-off between N assimilation and N allocation was specific and dependent on the prioritization of N forms for absorption in the plants. The proportion of the cell wall N allocation and other N to growth decreased under the NO_3 treatment. Under the NO_3 treatment, the proportions of N allocated to soluble proteins and the photosynthetic system increased, whereas the amount of N allocated to the cell wall was reduced, characterizing a trade-off between growth and defense in *L. chinensis*. In this vein, we analyzed whether NO_3^- supply was able to induce PNUE improvement in leaves to establish if these changes could have contributed to promoted plant growth. The enzyme activity of N isozyme was significantly increased under NO_3^- treatment. However, further accurate studies employing additional and more systematic approach are needed to definite the different NO_3^- concentrations effected the leaf N allocation.

CONCLUSION

Our results evidence that NO_3^- supply causes changes in some important photosynthetic processes in *L. chinensis* leaves. NO_3^- induced increased in the NR and NiR enzyme activity which could have improved the process of reducing NO_3^- to NH_4^+. N allocation was optimized within *L. chinensis* leaves, thus exhibiting an evolutional adaptation mechanism regarding the utilization of N for photosynthesis, thus increasing the PNUE and biomass during the growing season under NO_3 environment. Under the NO_3 treatment, *L. chinensis* plants tended to devote relatively more N to bioenergetics and the light-harvesting system to increase their ETR. Moreover, Chl_{area} and NPQ were increased to reduce the damage caused by excess electron production. Within-leaf N allocation should reflect trade-offs in *L. chinensis* on the leaf economics spectrum with allocating more N to metabolic processes at the expense of structure. Taken together, the results of our study provide a comprehensive picture of the effects of nitrate N on within-leaf N assimilation and allocation and can help researchers obtain a better understanding of the mechanisms by which *L. chinensis* in meadow grasslands absorb and utilize NO_3^--N under the context of increasing N deposition.

DATA AVAILABILITY STATEMENT

The original contributions presented in the study are included in the article/supplementary material, further inquiries can be directed to the corresponding author/s.

AUTHOR CONTRIBUTIONS

CM, JW, and XW designed the study. XW, MY, JH, and JY conducted the study. XW, YY, and JZ collected the data. XW and YS analyzed the data and wrote the manuscript. All authors read and approved the manuscript.

FUNDING

This work was supported by the Fundamental Research Funds for the Science and Technology Project of the Jilin Provincial Education Department (JJKH20221169KJ), the China Postdoctoral Science Foundation (2021M690030), the Youth Talent Support Project of Jilin Province (QT202007), and the Fundamental Research Funds for the Central Universities (2412020QD022).

ACKNOWLEDGMENTS

We want to thank Jingtian Chen, Chao Li, Shicheng Jiang, and Yanan Li for their help during laboratory analyses. We would like to acknowledge the editor and reviewers for their helpful comments on the manuscript.

REFERENCES

Alencar, V. T. C. B., Lobo, A. K. M., Carvalho, F. E. L., and Silveira, J. A. G. (2019). High ammonium supply impairs photosynthetic efficiency in rice exposed to excess light. *Photosynth. Res.* 140, 321–335. doi: 10.1007/s11120-019-00614-z

Antal, T., Mattila, H., Hakala-Yatkin, M., Tyystjärvi, T., and Tyystjärvi, E. (2010). Acclimation of photosynthesis to nitrogen deficiency in Phaseolus vulgaris. *Planta* 232, 887–898. doi: 10.1007/s00425-010-1227-5

Bahar, N. H. A., Hayes, L., Scafaro, A. P., Atkin, O. K., and Evans, J. R. (2018). Mesophyll conductance does not contribute to greater photosynthetic rate per unit nitrogen in temperate compared with tropical evergreen wet-forest tree leaves. *New Phytol.* 218, 492–505. doi: 10.1111/nph.15031

Balotf, S., Kavoosi, G., and Kholdebarin, B. (2016). Nitrate reductase, nitrite reductase, glutamine synthetase, and glutamate synthase expression and activity in response to different nitrogen sources in nitrogen-starved wheat seedlings. *Biotechnol. Appl. Biochem.* 63, 220–229. doi: 10.1002/bab.1362

Bernacchi, C. J., Pimentel, C., and Long, S. P. (2003). In vivo temperature response functions of parameters required to model RuBP-limited photosynthesis. *Plant Cell Environ.* 26, 1419–1430. doi: 10.1046/j.0016-8025.2003.01050.x

Bernacchi, C. J., Singsaas, E. L., Pimentel, C., Portis, A. R., and Long, S. P. (2001). Improved temperature response functions for models of Rubisco-limited photosynthesis. *Plant Cell Environ.* 24, 253–259. doi: 10.1111/j.1365-3040.2001.00668.x

Bloom, A. J. (2015). Photorespiration and nitrate assimilation: a major intersection between plant carbon and nitrogen. *Photosynth. Res.* 123, 117–128. doi: 10.1007/s11120-014-0056-y

Britto, D. T., and Kronzucker, H. J. (2002). NH_4^+ toxicity in higher plants: a critical review. *J. Plant Physiol.* 159, 567–584. doi: 10.1078/0176-1617-0774

Callow, J. A. (1999). *Advances in Botanical Research*. Cambridge: Academic Press.

Cataldo, D. A., Maroon, M., Schrader, L. E., and Youngs, V. L. (1975). Rapid colorimetric determination of nitrate in plant tissue by nitration of salicylic acid. *Commun. Soil Sci. Plant Anal.* 6, 71–80. doi: 10.1080/00103627509366547

Cui, J., Yu, C., Qiao, N., Xu, X., Tian, Y., and Ouyang, H. (2017). Plant preference for NH_4^+ versus NO_3^- at different growth stages in an alpine agroecosystem. *Field Crops Res.* 201, 192–199. doi: 10.1016/j.fcr.2016.11.009

Douglas, B., Jordan William, L., and Ogren. (1984). The CO_2 /O_2 specificity of ribulose 1,5-bisphosphate carboxylase/oxygenase. *Planta* 161, 308–313. doi: 10.1007/BF00398720

Dubreuil, C., Jin, X., Barajas-Lopez, J. D., Hewitt, T. C., Tanz, S. K., Dobrenel, T., et al. (2017). Establishment of photosynthesis through chloroplast development is controlled by two distinct regulatory phases1. *Plant Physiol.* 176, 1199–1214. doi: 10.1104/pp.17.00435

Evans, J. R., and Poorter, H. (2001). Photosynthetic acclimation of plants to growth irradiance: the relative importance of specific leaf area and nitrogen partitioning in maximizing carbon gain. *Plant Cell Environ.* 24, 755–767. doi: 10.1046/j.1365-3040.2001.00724.x

Farquhar, G. D., Caemmerer, S., and von Berry, J. A. (1980). A biochemical model of photosynthetic CO_2 assimilation in leaves of C_3 species. *Planta* 149, 78–90. doi: 10.1007/BF00386231

Felker, P. (1977). Microdetermination of nitrogen in seed protein extracts with the salicylate-dichloroisocyanurate color reaction. *Anal. Chem.* 49:1080.

Feng, Y.-L. (2008). Nitrogen allocation and partitioning in invasive and native Eupatorium species. *Physiol. Plant* 132, 350–358. doi: 10.1111/j.1399-3054.2007.01019.x

Feng, Y.-L., Lei, Y.-B., Wang, R.-F., Callaway, R. M., Valiente-Banuet, A., Inderjit, et al. (2009). Evolutionary tradeoffs for nitrogen allocation to photosynthesis versus cell walls in an invasive plant. *Proc. Natl. Acad. Sci. USA* 106, 1853–1856. doi: 10.1073/pnas.0808434106

Forde, B. G. (2000). Nitrate transporters in plants: structure, function and regulation. *Biochim. Biophys. Acta* 1465, 219–235.

Forde, B. G., and Clarkson, D. T. (1999). "Nitrate and Ammonium Nutrition of Plants: Physiological and Molecular Perspectives," in *Advances in Botanical Research*, ed. J. A. Callow (Cambridge: Academic Press), 1–90. doi: 10.1016/j.plaphy.2020.06.051

Funk, J. L., Glenwinkel, L. A., and Sack, L. (2013). Differential allocation to photosynthetic and non-photosynthetic nitrogen fractions among native and invasive species. *PLoS One* 8:e64502. doi: 10.1371/journal.pone.0064502

Galloway, J. N., Townsend, A. R., Erisman, J. W., Bekunda, M., Cai, Z., Freney, J. R., et al. (2008). Transformation of the nitrogen cycle: recent trends, questions, and potential solutions. *Science* 320, 889–892. doi: 10.1126/science.1136674

Gansel, X., Muños, S., Tillard, P., and Gojon, A. (2001). Differential regulation of the NO_3^- and NH_4^+ transporter genes AtNrt2.1 and AtAmt1.1 in Arabidopsis: relation with long-distance and local controls by N status of the plant. *Plant J.* 26, 143–155. doi: 10.1046/j.1365-313x.2001.01016.x

Grassein, F., Lemauviel-Lavenant, S., Lavorel, S., Bahn, M., Bardgett, R. D., Desclos-Theveniau, M., et al. (2015). Relationships between functional traits and inorganic nitrogen acquisition among eight contrasting European grass species. *Ann. Bot.* 115, 107–115. doi: 10.1093/aob/mcu233

Guo, F.-Q., Young, J., and Crawford, N. M. (2003). The nitrate transporter AtNRT1.1 (CHL1) functions in stomatal opening and contributes to drought susceptibility in Arabidopsis. *Plant Cell* 15, 107–117. doi: 10.1105/tpc.006312

Guo, J., Li, H., Zhou, C., and Yang, Y. (2020). Effects of Flag Leaf and Number of Vegetative Ramets on Sexual Reproductive Performance in the Clonal Grass Leymus chinensis. *Front Plant Sci* 11:534278. doi: 10.3389/fpls.2020.534278

Guo, S., Zhou, Y., Li, Y., Gao, Y., and Shen, Q. (2008). Effects of different Nitrogen forms and osmotic stress on water use efficiency of rice (*Oryza sativa*). *Ann. Appl. Biol,* 153, 127–134. doi: 10.1111/j.1744-7348.2008.00244.x

Haynes, R. J., and Goh, K. M. (1978). Ammonium and nitrate nutrition of plants. *Biol. Rev.* 53, 465–510. doi: 10.1111/j.1469-185X.1978.tb00862.x

Hessini, K., Hamed, K. B., Gandour, M., Mejri, M., Abdelly, C., and Cruz, C. (2013). Ammonium nutrition in the halophyte Spartina alterniflora under salt stress: evidence for a priming effect of ammonium? *Plant Soil* 370, 163–173. doi: 10.1007/s11104-013-1616-1

Hikosaka, K., and Terashima, I. (1995). A model of the acclimation of photosynthesis in the leaves of C3 plants to sun and shade with respect to nitrogen use. *Plant Cell Environ.* 18, 605–618. doi: 10.1111/j.1365-3040.1995

Howitt, S. M., and Udvardi, M. K. (2000). Structure, function and regulation of ammonium transporters in plants. *Biochim. Biophys. Acta* 1465, 152–170. doi: 10.1016/S0005-2736(00)00136-X

Hwang, M. N., and Ederer, G. M. (1975). Rapid hippurate hydrolysis method for presumptive identification of group B streptococci. *J. Clin. Microbiol.* 1, 114–115. doi: 10.1128/jcm.1.1.114-115.1975

Kovács, B., Puskás-Preszner, A., Huzsvai, L., Lévai, L., and Bódi, E. (2015). Effect of molybdenum treatment on molybdenum concentration and nitrate reduction in maize seedlings. *Plant Physiol. Biochem.* 96, 38–44. doi: 10.1016/j.plaphy.2015.07.013

Kumar, V., Kim, S. H., Priatama, R. A., Jeong, J. H., Adnan, M. R., Saputra, B. A., et al. (2020). NH_4^+ suppresses NO_3^--dependent lateral root growth and alters gene expression and gravity response in OsAMT1 RNAi mutants of rice (*Oryza sativa*). *J. Plant Biol.* 63, 391–407. doi: 10.1007/s12374-020-09263-5

Landi, S., and Esposito, S. (2017). Nitrate uptake affects cell wall synthesis and modeling. *Front. Plant Sci.* 8:1376. doi: 10.3389/fpls.2017.01376

Leghari, S. J., Wahocho, N. A., Laghari, G. M., HafeezLaghari, A., MustafaBhabhan, G., HussainTalpur, K., et al. (2016). Role of nitrogen for plant growth and development: a review. *Adv. Environ. Biol.* 10, 209–219.

Li, S., Jiang, F., Han, Y., Gao, P., Zhao, H., Wang, Y., et al. (2018). Comparison of nitrogen uptake in the roots and rhizomes of Leymus chinensis. *Biol. Plant.* 62, 149–156. doi: 10.1007/s10535-017-0748-1

Liang, X., Zhang, T., Lu, X., Ellsworth, D. S., BassiriRad, H., You, C., et al. (2020). Global response patterns of plant photosynthesis to nitrogen addition: a meta-analysis. *Glob. Chang. Biol.* 26, 3585–3600. doi: 10.1111/gcb.15071

Lin, M. T., Occhialini, A., Andralojc, P. J., Parry, M. A. J., and Hanson, M. R. (2014). A faster Rubisco with potential to increase photosynthesis in crops. *Nature* 513, 547–550. doi: 10.1038/nature13776

Liu, G., Li, X., and Zhang, Q. (2019). *Sheepgrass (Leymus chinensis): An Environmentally Friendly Native Grass for Animals*. Singapore: Springer.

Liu, T., Ren, T., White, P. J., Cong, R., and Lu, J. (2018). Storage nitrogen co-ordinates leaf expansion and photosynthetic capacity in winter oilseed rape. *J. Exp. Bot.* 69, 2995–3007. doi: 10.1093/jxb/ery134

Liu, Y., and von Wirén, N. (2017). Ammonium as a signal for physiological and morphological responses in plants. *J. Exp. Bot.* 68, 2581–2592.

Long, S. P., and Bernacchi, C. J. (2003). Gas exchange measurements, what can they tell us about the underlying limitations to photosynthesis? Procedures and sources of error. *J. Exp. Bot.* 54, 2393–2401. doi: 10.1093/jxb/erg262

Lu, P., Hao, T., Li, X., Wang, H., Zhai, X., Tian, Q., et al. (2021). Ambient nitrogen deposition drives plant-diversity decline by nitrogen accumulation in a closed grassland ecosystem. *J. Appl. Ecol.* 58, 1888–1898. doi: 10.1111/1365-2664.13858

Luo, X., Keenan, T. F., Chen, J. M., Croft, H., Colin Prentice, I., Smith, N. G., et al. (2021). Global variation in the fraction of leaf nitrogen allocated to photosynthesis. *Nat. Commun.* 12:4866. doi: 10.1038/s41467-021-25163-9

Makino, A., Sakuma, H., Sudo, E., and Mae, T. (2003). Differences between maize and rice in N-use efficiency for photosynthesis and protein allocation. *Plant Cell Physiol.* 44, 952–956. doi: 10.1093/pcp/pcg113

Marschner, H., and Marschner, P. (2012). *Marschner's mineral nutrition of higher plants*. London: Elsevier/Academic Press.

Mu, X., and Chen, Y. (2021). The physiological response of photosynthesis to nitrogen deficiency. *Plant Physiol. Biochem.* 158, 76–82. doi: 10.1016/j.plaphy.2020.11.019

Mu, X., Chen, Q., Chen, F., Yuan, L., and Mi, G. (2016). Within-leaf nitrogen allocation in adaptation to low nitrogen supply in maize during grain-filling stage. *Front. Plant Sci.* 7:699. doi: 10.3389/fpls.2016.00699

Niinemets, U., and Tenhunen, J. D. (1997). A model separating leaf structural and physiological effects on carbon gain along light gradients for the shade-tolerant species Acer saccharum. *Plant Cell Environ.* 20, 845–866. doi: 10.1046/j.1365-3040.1997.d01-133.x

Niinemets, U., Flexas, J., and Peñuelas, J. (2011). Evergreens favored by higher responsiveness to increased CO2. *Trends Ecol. Evol.* 26, 136–142.

Nolan, W. G., and Smillie, R. M. (1977). Temperature-induced changes in hill activity of chloroplasts isolated from chilling-sensitive and chilling-resistant plants. *Plant Physiol.* 59, 1141–1145. doi: 10.1104/pp.59.6.1141

Onoda, Y., Wright, I. J., Evans, J. R., Hikosaka, K., Kitajima, K., Niinemets, U., et al. (2017). Physiological and structural tradeoffs underlying the leaf economics spectrum. *New Phytol.* 214, 1447–1463. doi: 10.1111/nph.14496

Poorter, H., and Evans, J. R. (1998). Photosynthetic nitrogen-use efficiency of species that differ inherently in specific leaf area. *Oecologia* 116, 26–37. doi: 10.1007/s004420050560

Prinsi, B., and Espen, L. (2018). Time-course of metabolic and proteomic responses to different nitrate/ammonium availabilities in roots and leaves of maize. *Int. J. Mol. Sci.* 19:2202. doi: 10.3390/ijms19082202

R Core Team (2020). *R: A Language and Environment for Statistical Computing*. Vienna: R Foundation for Statistical Computing. Available online at: https://www.R-project.org/

Shang, B., Xu, Y., Dai, L., Yuan, X., and Feng, Z. (2019). Elevated ozone reduced leaf nitrogen allocation to photosynthesis in poplar. *Sci. Total Environ.* 657, 169–178. doi: 10.1016/j.scitotenv.2018.11.471

Sharkey, T. D. (2016). What gas exchange data can tell us about photosynthesis. *Plant Cell Environ.* 39, 1161–1163. doi: 10.1111/pce.12641

Shi, Y., Wang, J., Ao, Y., Han, J., Guo, Z., Liu, X., et al. (2021). Responses of soil N2O emissions and their abiotic and biotic drivers to altered rainfall regimes and co-occurring wet N deposition in a semi-arid grassland. *Glob. Chang. Biol.* 27, 4894–4908. doi: 10.1111/gcb.15792

Shi, Y., Wang, J., Le Roux, X., Mu, C., Ao, Y., Gao, S., et al. (2019). Trade-offs and synergies between seed yield, forage yield, and N-related disservices for a semi-arid perennial grassland under different nitrogen fertilization strategies. *Biol. Fertil. Soils* 55, 497–509. doi: 10.1007/s00374-019-01367-6

Stevens, C. J. (2019). Nitrogen in the environment. *Science* 363, 578–580. doi: 10.1126/science.aav8215

Stinziano, J. R., Morgan, P. B., Lynch, D. J., Saathoff, A. J., McDermitt, D. K., and Hanson, D. T. (2017). The rapid A-Ci response: photosynthesis in the phenomic era. *Plant Cell Environ.* 40, 1256–1262. doi: 10.1111/pce.12911

Sugiura, D., Terashima, I., and Evans, J. R. (2020). A decrease in mesophyll conductance by cell-wall thickening contributes to photosynthetic downregulation. *Plant Physiol.* 183, 1600–1611. doi: 10.1104/pp.20.00328

Takashima, T., Hikosaka, K., and Hirose, T. (2004). Photosynthesis or persistence: nitrogen allocation in leaves of evergreen and deciduous Quercus species. *Plant Cell Environ.* 27, 1047–1054. doi: 10.1111/j.1365-3040.2004.01209.x

Tho, B. T., Lambertini, C., Eller, F., Brix, H., and Sorrell, B. K. (2017). Ammonium and nitrate are both suitable inorganic nitrogen forms for the highly productive wetland grass *Arundo donax*, a candidate species for wetland paludiculture. *Ecol. Eng.* 105, 379–386. doi: 10.1016/j.ecoleng.2017.04.054

von Caemmerer, S. (2000). *Biochemical Models of Leaf Photosynthesis*. Clayton: CSIRO Publishing.

Wang, F., Gao, J., Shi, S., He, X., and Dai, T. (2019). Impaired electron transfer accounts for the photosynthesis inhibition in wheat seedlings (Triticum aestivum L.) subjected to ammonium stress. *Physiol. Plant* 167, 159–172. doi: 10.1111/ppl.12878

Wang, P., Wang, Z., Sun, X., Mu, X., Chen, H., Chen, F., et al. (2019). Interaction effect of nitrogen form and planting density on plant growth and nutrient uptake in maize seedlings. *J. Integrat. Agricult.* 18, 1120–1129. doi: 10.1016/S2095-3119(18)61977-X

Wellburn, A. R. (1994). The spectral determination of chlorophylls a and b, as well as total carotenoids, using various solvents with spectrophotometers of different resolution. *J. Plant Physiol.* 144, 307–313. doi: 10.1016/S0176-1617(11)81192-2

Wen, B., Li, C., Fu, X., Li, D., Li, L., Chen, X., et al. (2019). Effects of nitrate deficiency on nitrate assimilation and chlorophyll synthesis of detached apple leaves. *Plant Physiol. Biochem.* 142, 363–371. doi: 10.1016/j.plaphy.2019.07.007

Xia, J., and Wan, S. (2008). Global response patterns of terrestrial plant species to nitrogen addition. *New Phytol.* 179, 428–439. doi: 10.1111/j.1469-8137.2008.02488.x

Yan, L., Xu, X., and Xia, J. (2019). Different impacts of external ammonium and nitrate addition on plant growth in terrestrial ecosystems: a meta-analysis. *Sci. Total Environ.* 686, 1010–1018. doi: 10.1016/j.scitotenv.2019.05.448

Yin, L., Xu, H., Dong, S., Chu, J., Dai, X., and He, M. (2019). Optimised nitrogen allocation favours improvement in canopy photosynthetic nitrogen-use efficiency: Evidence from late-sown winter wheat. *Environ. Exp. Bot.* 159, 75–86. doi: 10.1016/j.envexpbot.2018.12.013

Zhang, J., Cun, Z., and Chen, J. (2020). Photosynthetic performance and photosynthesis-related gene expression coordinated in a shade-tolerant species Panax notoginseng under nitrogen regimes. *BMC Plant Biol.* 20:273. doi: 10.1186/s12870-020-02434-z

Zhang, L., Sun, Z., Xie, J., Wu, J., and Cheng, S. (2018). Nutrient removal, biomass accumulation and nitrogen-transformation functional gene response to different nitrogen forms in enhanced floating treatment wetlands. *Ecol. Eng.* 112, 21–25. doi: 10.1016/j.ecoleng.2017.12.021

Zhang, Y., Xu, W., Wen, Z., Wang, D., Hao, T., Tang, A., et al. (2017). Atmospheric deposition of inorganic nitrogen in a semi-arid grassland of Inner Mongolia, China. *J. Arid. Land* 9, 810–822. doi: 10.1007/s40333-017-0071-x

Zhong, C., Jian, S.-F., Huang, J., Jin, Q., and Cao, X. (2019). Trade-off of within-leaf nitrogen allocation between photosynthetic nitrogen-use efficiency and water deficit stress acclimation in rice (Oryza sativa L.). *Plant Physiol. Biochem.* 135, 41–50. doi: 10.1016/j.plaphy.2018.11.021

Zhou, X., Lyu, J., Sun, L., Dong, J., and Xu, H. (2021). Metabolic programming of Rhododendron chrysanthum leaves following exposure to UVB irradiation. *Funct. Plant Biol.* 48, 1175–1185. doi: 10.1071/FP20386

Zhu, T. C. (2004). *Biological and Ecological Study of Leymus Chinensis*. Changchun: Jilin Science and Technology Press.

Zhuang, J., Zhou, L., Wang, Y., and Chi, Y. (2021). Nitrogen allocation regulates the relationship between maximum carboxylation rate and chlorophyll content along the vertical gradient of subtropical forest canopy. *Agricult. Forest Meteorol.* 307:108512. doi: 10.1016/j.agrformet.2021.108512

Conflict of Interest: The authors declare that the research was conducted in the absence of any commercial or financial relationships that could be construed as a potential conflict of interest.

Publisher's Note: All claims expressed in this article are solely those of the authors and do not necessarily represent those of their affiliated organizations, or those of the publisher, the editors and the reviewers. Any product that may be evaluated in this article, or claim that may be made by its manufacturer, is not guaranteed or endorsed by the publisher.

frontiers | Frontiers in Plant Science

ORIGINAL RESEARCH
published: 31 May 2022
doi: 10.3389/fpls.2022.867967

Regulation and Function of Metal Uptake Transporter NtNRAMP3 in Tobacco

*Katarzyna Kozak, Anna Papierniak-Wygladala†, Małgorzata Palusińska, Anna Barabasz and Danuta Maria Antosiewicz**

Faculty of Biology, Institute of Experimental Plant Biology and Biotechnology, University of Warsaw, Warsaw, Poland

Natural resistance-associated macrophage protein (*NRAMP*) genes encode proteins with low substrate specificity, important for maintaining metal cross homeostasis in the cell. The role of these proteins in tobacco, an important crop plant with wide application in the tobacco industry as well as in phytoremediation of metal-contaminated soils, remains unknown. Here, we identified NtNRAMP3, the closest homologue to NRAMP3 proteins from other plant species, and functionally characterized it. A NtNRAMP3-GFP fusion protein was localized to the plasma membrane in tobacco epidermal cells. Expression of *NtNRAMP3* in yeast was able to rescue the growth of Fe and Mn uptake defective Δ*fet3fet4* and Δ*smf1* mutant yeast strains, respectively. Furthermore, *NtNRAMP3* expression in wild-type *Saccharomyces cerevisiae* DY1457 yeast strain increased sensitivity to elevated concentrations of iron (Fe), manganese (Mn), copper (Cu), cobalt (Co), nickel (Ni), and cadmium (Cd). Taken together, these results point to a possible role in the uptake of metals. NtNRAMP3 was expressed in the leaves and to a lesser extent in the roots of tobacco plants. Its expression occurred mainly under control conditions and decreased very sharply in deficiency and excess of the tested metals. GUS-based analysis of the site-specific activity of the *NtNRAMP3* promoter showed that it was primarily expressed in the xylem of leaf blades. Overall, our data indicate that the main function of NtNRAMP3 is to maintain cross homeostasis of Fe, Mn, Co, Cu, and Ni (also Cd) in leaves under control conditions by controlling xylem unloading.

Keywords: NtNRAMP3, tobacco, metal uptake, iron, zinc, manganese, cobalt, nickel

OPEN ACCESS

Edited by:
Anja Schneider, Ludwig Maximilian University of Munich, Germany

Reviewed by:
Gian Attilio Sacchi, University of Milan, Italy
Antoni Garcia-Molina, Spanish National Research Council (CSIC), Spain

***Correspondence:**
Danuta Maria Antosiewicz
dma@biol.uw.edu.pl

†Present address:
Anna Papierniak-Wygladala, Laboratory of Transport Through Biomembranes, Nencki Institute of Experimental Biology, Warsaw, Poland

Specialty section:
This article was submitted to Plant Nutrition, a section of the journal Frontiers in Plant Science

Received: *01 February 2022*
Accepted: *29 March 2022*
Published: *31 May 2022*

Citation:
Kozak K, Papierniak-Wygladala A, Palusińska M, Barabasz A and Antosiewicz DM (2022) Regulation and Function of Metal Uptake Transporter NtNRAMP3 in Tobacco. Front. Plant Sci. 13:867967. doi: 10.3389/fpls.2022.867967

INTRODUCTION

Excess metals taken up from the soil are accumulated by most plants in their leaves, however, the efficiency of accumulation in these organs differs among them. Those capable of storing very large amounts are frequently used in the phytoremediation of metal-contaminated soil. Tobacco is one such species. It is a high biomass plant effective in translocating metal from the root to the shoot, especially zinc (Zn) and cadmium (Cd), which is an important determinant of accumulation in leaves (Wagner and Yeargan, 1986; Angelova et al., 2004; Doroszewska and Berbeć, 2004; Lugon-Moulin et al., 2004). Furthermore, many attempts have been made to increase its usefulness in phytoremediation through genetic modification (Wojas et al., 2009; Grispen et al., 2011; Das et al., 2016; Rehman et al., 2019). Nevertheless, little is known about the mechanisms of metal tolerance and the accumulation of high concentrations of metals in tobacco leaves. Knowledge of these

processes is not only epistemic but also application-related for the use of tobacco in cleaning up contaminated soil.

One of the key factors in a plant's tolerance to Zn is the ability to store metal in leaves without detrimental effects. A commonly accepted symptom of Zn-sensitivity is the development of necrotic regions over the leaf blades, therefore, monitoring their appearance upon exposure to high Zn became a tool to assess sensitivity to excess Zn (Marschner, 1995). Our recent study demonstrated that in leaves of plants exposed to high Zn, necrotic regions develop from groups of mesophyll cells ("Zn accumulating cells") that contain very high Zn concentrations. They develop necrosis when the Zn concentration exceeds a certain threshold, and programmed cell death (PCD) is involved in this process (Siemianowski et al., 2013; Weremczuk et al., 2017, 2020). The neighboring, non-accumulating cells, do not experience high internal Zn. Such functional diversification of the ability to accumulate Zn at the cellular level in the leaf mesophyll was suggested to be crucial in maintaining the function of the whole leaf at high Zn exposure. This is achieved by mechanisms staving off toxic levels of Zn incertain cells (non-accumulating ones), thereby allowing them to continue with their basic functions. Thus, contrary to the general view, our data indicate that the development of necrosis resulting from the differentiation of mesophyll cells in terms of Zn accumulation can be considered a defense mechanism rather than merely a manifestation of Zn toxicity (Siemianowski et al., 2013).

In our previous research aimed at elucidating the molecular basis of the differential ability of mesophyll cells to accumulate Zn, several candidate genes were identified, including *NtZIP1-like*, *NtZIP11*, and *NtNRAMP3-like* (Papierniak et al., 2018). Subsequently, a detailed study of two of them, *NtZIP1-like* and *NtZIP11* (Zrt-Irt-like Proteins), showed that they likely participate in the cell-specific accumulation of Zn in the palisade parenchyma of tobacco leaves (Kozak et al., 2019; Papierniak-Wygladala et al., 2020). The third identified gene, *NtNRAMP3-like*, was shown to be highly upregulated shortly after administration of an elevated Zn concentration (200 μM), similarly to *NtZIP1-like* and *NtZIP11* (Papierniak et al., 2018), was considered a candidate that may also play a role in the distinct capacity of mesophyll cells to accumulate Zn. It is known that the accumulation of metals involves a range of gene encoding proteins responsible for their uptake and removal outside of the cell, loading into the vacuole, or exporting to the cytoplasm.

The NRAMP family includes proton-coupled metal ion transporters that mediate the transport of a broad range of metal ions, such as manganese (Mn^{2+}), Zn^{2+}, copper (Cu^{2+}), iron (Fe^{2+}), Cd^{2+}, nickel (Ni^{2+}), and cobalt (Co^{2+}), into the cytoplasm (Colangelo and Guerinot, 2006; Nevo and Nelson, 2006). The physiological role of NRAMPs in plants is not well-understood. Current research indicates diverse functions, depending on the gene, its regulation, the subcellular localization of the encoded protein, and its substrates (Legay et al., 2012; Qin et al., 2017; Tian et al., 2021). The NRAMPs were shown to participate in the uptake of essential metals, e.g., Fe, Mn, and Zn (Thomine et al., 2000; Cailliatte et al., 2010; Sasaki et al., 2012; Xiong et al., 2012; Yamaji et al., 2013; Tiwari et al., 2014; Zhang et al., 2020). They also affect subcellular redistribution localized in the tonoplast or the intracellular vesicles (Bereczky et al., 2003; Thomine et al., 2003; Languar et al., 2005; Li et al., 2019; Pottier et al., 2022). Several NRAMPs were also shown to be involved in the uptake of toxic Cd (Cailliatte et al., 2010; Takahashi et al., 2011) or its redistribution (Thomine et al., 2003; Languar et al., 2004).

Although the expression of most *NRAMP* genes was induced under mineral deficiency conditions, some showed an increase in transcript levels under stress generated by the presence of metal excess. For example, elevated expression at 100 μM Zn was detected in the shoots of *Thlaspi caerulescens* for *TcNRAMP3* and *TcNRAMP4* (Oomen et al., 2009), and for *TcNRAMP4* in the presence of 1,000 μM ferrozine or 600 μM Ni (Wei et al., 2009). Several soybean *NRAMPs* were also shown to be upregulated by toxic 200 μM Cu (*GmNRAMP1a*; *3a* and *5a*), 100 μM Cd (GmNRAMP1a, 1b, 3a, 5a), 1,000 μM Fe/EDTA (*GmNRAMP6a*), or 200 μM Mn (*GmNRAMP5a*) (Qin et al., 2017). Upregulation by unessential toxic Cd was also noted for *MhNRAMP1* (Zhang et al., 2020), *TcNRAMP3* (Wei et al., 2009), or *StNRAMP3* (Tian et al., 2021). Furthermore, the expression level of *NRAMP3* was also higher in Zn/Cd hyperaccumulator *A. halleri* than in *A. thaliana* (Weber et al., 2004). Therefore, participation of NRAMPs in regulating the response to high concentrations of metals seems certain, but it is not known what this role is.

Based on the results of preliminary studies on the *NtNRAMP3-like* sequence (increased expression in the presence of 200 Zn in leaves; Papierniak et al., 2018), and literature data, it was hypothesized that *NtNRAMP3-like*, in addition to *NtZIP1-like* and *NtZIP11*, may be another component of a network of processes regulating metal homeostasis in tobacco leaves exposed to excess Zn, including cell-specific accumulation of this metal in the leaf blades. In this work, we cloned *NtNRAMP3* and determined its metal transport activity and biological role in tobacco.

MATERIALS AND METHODS

Plant Material, Growth Conditions, and Experimental Design

Wild-type (WT) tobacco *Nicotiana tabacum* var. Xanthi and generated tobacco transgenic plants expressing *pMDC163::promNtNRAMP3::GUS* were used in the study. Seeds of the WT tobacco were obtained from the stock of the Institute of Biochemistry and Biophysics PAS (Warsaw, Poland; in 2002) and then propagated in the greenhouse of the University of Warsaw.

Plants were cultivated in a growth chamber at 23/16°C day/night, 40–50% humidity, 16 h photoperiod, and quantum flux density [photosynthetically active radiation (PAR)] 250 μMol m^{-2} s^{-1}, fluorescent Flora tubes (Siemianowski et al., 2011).

Seeds were surface sterilized in 8% sodium hypochlorite (w/v) for 2 min, washed with distilled water, then germinated and grown on vertically positioned Petri dishes containing quarter-strength Knop's medium, 2% sucrose (w/v), and 1% agar (w/v). After 3 weeks seedlings were transferred to

hydroponic conditions (five plants per 2.5 L pot) and further grown according to experiment-specific schemes presented below. In all experiments, the quarter-strength Knop's medium was applied as a reference control medium (Barabasz et al., 2010). All experiments were conducted in three independent biological replicates. The nutrient solution was renewed every third day.

To determine developmental regulation of *NtNRAMP3*, 3-week-old WT seedlings were transferred from the Petri dishes into the hydroponic control medium for up to 5.5 weeks. Plant material was collected at three developmental stages: (1) 4-week-old seedlings (3 weeks on plates and 1 week on hydroponics): whole roots and all leaves were collected separately; (2) 6-week-old plants (3 weeks on plates and 3 weeks on hydroponics): whole roots and all leaves were collected separately; (3) 9-week-old plants (3 weeks on plates and 6 weeks on hydroponics); the following plant parts were collected: (a) apical part of the root (3–4 cm from the tip), (b) basal part of the root (3–4 cm from the base), (c) stem (3 cm of the middle part), (d) young leaves (two leaves of minimum 0.5 cm length counting from the top), and (e) old leaves (two leaves counting from the base). Lateral roots were not included in the analysis. The material was pooled from a total of 30 (stage 1), 15 (stage 2), or 10 (stage 3) plants, frozen in the liquid nitrogen and stored at −80°C.

For assessment of metal status-dependent expression of *NtNRAMP3*, 3-week-old WT plants were further hydroponically grown on a control medium for 2 weeks. Then, they were exposed to different regimes: (i) metal excess (200 μM Fe or 100 μM Mn or 20 μM Co or 20 μM Cu or 30 μM Ni or 50 μM Zn or 4 μM Cd); (ii) metal deficiency (Fe or Mn or Co or Cu or Zn; metal was not added to the medium); (iii) control conditions. Metal was added to the control medium as $ZnSO_4$; Fe-EDTA; $MnSO_4$; $CoCl_2$; $CuSO_4$; $NiCl_2$ or $CdCl_2$. After 3 days, the following organs were collected: (i) 3–4 cm fragment of the apical part of the root; (ii) 3–4 cm fragment of the basal part of the root; (iii) leaves (2nd and 3rd leaf counting from the base of the stem) without petioles and major midribs. The material was pooled from a total of 10 plants, frozen in the liquid nitrogen, and stored at −80°C.

To compare the *NtNRAMP3* expression between leaves of tobacco exposed to a long-term treatment of elevated Zn, 3-week-old tobacco WT seedlings were grown on a liquid control medium for 18 days, then for 3 weeks at 10, 50, and 200 μM Zn. Next, all leaves (without petioles and midvein) were removed from the stem and collected in groups of two (e.g., 1st and 2nd leaves counting from the base of the stem were the 1st pair; 3rd and 4th−2nd pair, etc.), frozen in the liquid nitrogen and stored in −80°C. The material was pooled from a total of 8 plants.

To examine the tissue-specific *NtNRAMP3* expression patterns, transgenic plants expressing *pMDC163::promNtNRAMP3::GUS* were subjected to two different treatments. In the first experiment, three-week-old plants were transferred from agar plates to hydroponics and grown under control conditions for 7 days. Whole seedlings were used to determine GUS activity. In the second experiment, 5-week-old plants grown at control conditions (3 weeks on agar plates and 2 weeks on hydroponics) were exposed to 200 μM Zn for 3 days. In the end, the second leaf (counting from the base of the stem) was collected for GUS assay. Wild-type tobacco plants were used as a negative control.

Cloning and Generation of Constructs

A partial genomic sequence of *NtNRAMP3* (previously annotated as *NtNRAMP3-like*) was identified, and *NtNRAMP3* was reported as a candidate gene encoding metal transporter potentially involved in zinc transport in tobacco leaves (Papierniak et al., 2018). In brief, known nucleotide *NRAMP* sequences from *A. thaliana* were blasted against the *N. tabacum* genome (Sierro et al., 2013, 2014), which is deposited in GenBank, using NCBI (National Center for Biotechnology Information) BLASTn program (http://www.ncbi.nlm.nih.gov/blast). After screening with the FGENESH+ tool (SoftBerry, Mount Kisco, NY, United States), the full-length *NtNRAMP3* putative sequence was identified within the scaffold AWOK01S026429.

The full-length open reading frame (ORF) of *NtNRAMP3* (containing STOP codon or not) was amplified from cDNA transcribed from total RNA using appropriate primers (**Table 1**) by PCR with Phusion HF polymerase (Thermo Scientific). Then, the full-length *NtNRAMP3* sequence was cloned into the pENTR/D-TOPO vector using the pENTR Directional TOPO Cloning Kit (Invitrogen). Finally, two constructs were obtained—*pENTR/D-TOPO::NtNRAMP3* and *pENTR/D-TOPO::NtNRAMP3-STOP* (STOP codon was included).

To prepare the construct for subcellular localization, *pENTR/D-TOPO::NtNRAMP3* was recombined with the pMDC43 vector (purchased from Arabidopsis Biological Resource Center, https://abrc.osu.edu/) using LR reaction (Gateway Technology, Invitrogen). The resulting plasmid *pMDC43::GFP::NtNRAMP3* contained GFP linked at the N-terminus of NtNRAMP3. The fusion protein was expressed under 35S promoter control.

For yeast growth assay the vectors *pAG426GAL::NtNRAMP3* were generated by LR recombination between *pENTR/D-TOPO::NtNRAMP3* and pAG426GAL-ccdB-EGFP plasmid.

For a generation of the construct for GUS analysis, a 1,684 bp promoter region located upstream from the translation initiation codon of *NtNRAMP3* was amplified from genomic DNA using appropriate primers (**Table 1**) by PCR with Phusion HF polymerase (Thermo Scientific) and inserted into the pENTR/D-TOPO vector using pENTR Directional TOPO Cloning Kit (Invitrogen). Then, the LR reaction was used to obtain the *pMDC163::promNtNRAMP3::GUS* construct.

Bioinformatic Analysis

The nucleotide sequence of *NtNRAMP3* was translated to a protein sequence with the ExPASy translate tool (https://web.expasy.org/translate/). Then, to view predicted transmembrane domains of NtNRAMP3, the web-based software Protter (http://wlab.ethz.ch/protter/start/) that gathers protein features from various annotation sources, such as Uniprot, was used.

The NtNRAMP3 amino acid sequence was aligned to several chosen NRAMP amino acid sequences from other plant species (*Arabidopsis thaliana*, *Solanum lycopersicum*, *Zea mays*, *Theobroma caccoa,* and *Nicotiana*) identified in ARAMEMNON,

TABLE 1 | Sequences of primers used in the study.

Primer name	Primer sequence	Product length
Primers for expression analysis		
6429_1F	5' AGTTCATATCATCGGAGTCG 3'	222 bp
6429_2R	5' TGAACAAGTAGCCCAATAGCC 3'	
NtPP2A_F	5' GCACATTCATTCAGTTTGAACC 3'	142 bp
NtPP2A_R	5' GTAGCATATAAAGCAGTCAGC 3'	
Primers for the full-length *NtNRAMP3* cDNA amplification		
pENTR_NtNRAMP3_START	5' CACCATGCCTCCACACGATGAC 3'	1539 or 1542 bp
pENTR_NtNRAMP3_STOP	5' TCAATTCTCTATGCTGGTGATACT 3'	(including STOP codon)
pENTR_NtNRAMP3_END	5' ATTCTCTATGCTGGTGATACTCTT 3'	
Primers for promoter *NtNRAMP3* amplification		
promNtNRAMP3_for	5' AGAATCTGCGAGCATCTCAAAGGAATCT 3'	1684 bp
promNtNRAMP3_rev	5' TTAGAAGAGAAATCTGTAAAGAGGATATTAGCG 3'	

Solgenomics, MaizeSequence, Phytozome, and NCBI, using Clustal Omega (https://www.ebi.ac.uk/Tools/msa/clustalo/). The phylogenetic analyses were conducted with the MEGA X program (https://www.megasoftware.net) (Kumar et al., 2018) using the maximum likelihood method with 1000 bootstrap replicates. The prediction of membrane-spanning regions was performed with Phobius software (https://phobius.sbc.su.se/) (Käll et al., 2004).

All primers used in this study were designed with the OligoAnalyzer tool (https://www.idtdna.com/pages/tools/oligoanalyzer) based on the sequences of *NtNRAMP3* (primers for expression analysis and *NtNRAMP3* ORF amplification) and scaffold AWOK01S026429 (primers for *NtNRAMP3* promoter amplification). Primers sequences are listed in **Table 1**.

Regulatory elements within the *NtNRAMP3* promoter region were identified with the program PlantCARE (http://bioinformatics.psb.ugent.be/webtools/plantcare/html/).

Generation of Transgenic Plants

The construct *pMDC163::promNtNRAMP3::GUS* was stably transformed into tobacco plants using GV3101 *A. tumefaciens*-mediated transformation protocol for tobacco leaf disks (described in Siemianowski et al., 2011). Transgenic plants were selected in the presence of hygromycin B (100 $\mu g \cdot ml^{-1}$). The T1 heterozygous lines with a segregation ratio of 3:1 ($hygromycin^{toler}$: $hygromycin^{sensit}$) were self-pollinated to obtain the homozygous generation (T2). Developed independent homozygous lines were tested in a preliminary histochemical GUS assay in young 4-week-old seedlings, subsequently three lines were selected for more detailed analysis.

Quantitative RT-PCR Analysis

Total RNA extraction and quantitative real-time RT-PCR (qPCR) analysis were performed according to procedures described in Papierniak et al. (2018). In brief, Plant RNA Mini Kit (Syngen, Wrocław, Poland) was used for RNA isolation, then samples were digested with DNase I (Invitrogen, Waltham, MA, United States). The relative quantities of each transcript were calculated based on the comparative ΔCt (threshold cycle) method (Livak and Schmittgen, 2001). The *NtPP2A* (*Nicotiana tabacum Protein Phosphatase 2 A*) gene was used as an internal control, and its stability was measured in all plant tissue samples in the range of applied metal concentrations. At least three independent biological replicates were analyzed for each experiment. A minimum 2-fold change in relative gene expression level was considered significant.

Functional Analysis of NtNRAMP3 in Yeast

In the study, two wild-type (DY1457 and BY4742) and three mutants (Δ*smf1*, Δ*zrt1*, Δ*fet3fet4*) *Saccharomyces cerevisiae* strains (**Supplementary File S1**) were transformed with the empty vector *pAG426GAL* or with *pAG426GAL::NtNRAMP3* construct, according to lithium acetate method protocol (Gietz and Schiestl, 2007). Complementation and sensitivity tests were performed as described previously (Papierniak-Wygladala et al., 2020). Briefly, yeast cultures grown on liquid synthetic medium (SC-URA+GLU; yeast nitrogen base, amino acids without uracil, 2% glucose, pH 5.3), after setting the optical density (OD_{600}) to 0.2, were serially diluted (1.0; 0.1; 0.01 and 0.001), and then spotted on Petri dishes containing SC-URA+GAL solidified with 2% (w/v) agar and supplemented with required components (details below). Yeast growth was monitored for the next up to 10 days.

In complementation tests, for the Δ*fet3fet4* mutant, the restrictive medium was supplemented with (i) 10 or 30 μM $FeCl_3$, (ii) 30 or 100 μM ferric citrate, and/or (iii) 30 or 80 μM BPDS (bathophenanthrolinedisulfonic acid). For Δ*smf1* to the medium 2.5 mM EGTA (Ethylene glycol-bis(β-aminoethyl ether)-*N*, *N*, *N*′, *N*′-tetraacetic acid) alone or with 0.1 mM $MnCl_2$ (pH was adjusted to 6.0 with 50 mM MES or SC-URA+GAL medium of pH 5.3 was applied) were added. The Δ*zrt1* mutant was assayed for growth on medium containing (i) 1.0 mM EDTA (Ethylenediaminetetraacetic acid), and/or (ii) 100, 500, 600, or 700 μM $ZnCl_2$. Wild-type strains transformed with the empty *pAG426GAL* vector were included as a reference control in all assays (DY1457 in experiments including Δ*fet3fet4* and BY4742 in experiments including Δ*smf1* and Δ*zrt1*). Mutant strains transformed with the empty

pAG426GAL vector were included as a negative control in all experiments.

In sensitivity tests, the growth of DY1457 yeast transformed with *pAG426GAL::NtNRAMP3* construct was monitored on plates containing SC-URA+GAL supplemented with (i) 5, 10, 20, 50, or 75 μM $CdCl_2$, (ii) 50, 100, 250, 500, or 750 μM $CoCl_2$, (iii) 1.0, 1.4, 2.0, 2.2, or 2.4 mM $CuSO_4$, (iv) 0.2, 3.0, 4.0, 4.5, or 5.0 mM $FeCl_3$, (v) 0.2, 2.5, 5, 7.5, or 10.0 mM $MnCl_2$, (vi) 0.2, 0.3, 0.4, 0.5, or 0.6 mM $NiCl_2$, (vii) 0.2, 1.0, 2.5, 5.0, or 7.5 mM $ZnSO_4$, and (viii) 4.0, 4.5, 5.0, 5.5, or 6.0 mM $ZnSO_4$ (pH was adjusted to 4.0, 5.0, or 6.0 with 50 mM MES). DY1457 transformed with the empty *pAG426GAL* vector was included as a control in all assays.

Subcellular Localization of NtNRAMP3

The subcellular localization of NtNRAMP3 was determined by monitoring the transient expression of GFP-NtNRAMP3 translational fusion product in tobacco leaf epidermal cells accordingly to the previously described protocol (Siemianowski et al., 2013; Papierniak et al., 2018). The GV3101 *A. tumefaciens* (C58C1, Rif^R; pMP90, Gm^R) transformed with *pMDC43::GFP::NtNRAMP3* were used for infiltration of 7-week-old WT tobacco leaves. To visualize the cell wall, after 24–72 h from the infiltration leaf fragments were stained with 50 μM water solution of propidium iodide (PI) for 20 min. Then, GFP (excitation: 488 nm line of argon laser; emission: 500–560 nm) and PI (excitation: 543 nm; emission: 617 nm) signals were detected in Nikon A1 confocal laser scanning microscope (Melville, NY, USA).

Histochemical GUS Analysis

The GUS assay in young seedlings (4-week-old whole plants) was performed according to Weremczuk et al. (2020). In brief, 4-week-old whole seedlings were fixed in 90% ice-cold acetone and washed in the 50 mM phosphate buffer pH 7.0 with 0.2 % Triton X-100 with infiltration. Then, the plant material was incubated in a reaction buffer (50 mM phosphate buffer pH 7.0 with 0.2 % Triton X-100 and 2 mM X-Gluc), at 37°C in the darkness for 2.5 h. Next, they were fixed in FAA (formalin-acetic acid-alcohol) for 30 min, dehydrated in increasing ethanol concentrations, and stored in 70% ethanol. To visualize expression sites of *NtNRAMP3* within leaves of 5.5-week-old tobacco, we used the method described in Weremczuk et al. (2020). In brief, the determination of GUS activity in the leaves of 5.5-week-old tobacco was carried out on cross-sections of 130 μm thickness cut on a Vibratome (Leica VT1000S, Heidelberg, Germany). They were used for histochemical GUS staining, subsequently fixed in FAA for 30 min, dehydrated in increasing ethanol concentrations, and stored in 70% ethanol. Observations were performed with an OPTA-TECH microscope.

RESULTS

Characterization of NtNRAMP3 and Phylogenetic Analysis of Plant NRAMP Proteins

Earlier studies showed that the partial sequence of *NtNRAMP3-like* first identified in tobacco within the scaffold AWOK01S026429 was upregulated in the leaves by 200 μM Zn (Papierniak et al., 2018). Here, this sequence has been cloned. The full-length cDNA is comprised of 1,542 bp and encodes a protein of 514 amino acids (**Figure 2**; FGENESH+). Analyses of the nucleotide and amino acid sequences provided evidence that the identified sequence is *NtNRAMP3*.

First, phylogenetic analysis that included 32 NRAMP proteins from *A. thaliana*, *S. lycopersicum*, *T. cacao*, *Z. mays,* and *Nicotiana* species (*N. attenuata*, *N. sylvestris*, *N. tomentosiformis*, *N. tabacum*) showed that the newly identified protein was located on the same branch as other NRAMP3 proteins, with the closest relationship between NtomNRAMP3 and AtNRAMP3 (**Figure 1**). In general, the examined proteins were classified into four groups. Among them, NtNRAMP3 formed a separate clade with NaNRAMP3, NsNRAMP3, NtomNRAMP3, TheccNRAMP3, LeNRAMP3, AtNRAMP3, and AtNRAMP4, which was distinct from other NRAMPs (**Figure 1**, marked with bracket). Furthermore, among all NRAMP proteins included in the study, NtNRAMP3 was the most similar to NtomNRAMP3 (99.81%), and the highest identity of the amino acid sequences was observed within *Nicotiana* (98.82% and 98.23% between NtNRAMP3 and NaNRAMP3 and NsNRAMP3, respectively, **Table 2**). On the other hand, the lowest identity within this group was observed between NtNRAMP3 and AtNRAMP4 (73.81%).

Like many other NRAMP proteins, NtNRAMP3 consists of 12 transmembrane domains (TMDs) and has both N- and C-termini located intracellularly (Phobius, Käll et al., 2004; Protter, Omasits et al., 2014) (**Figure 2**; **Supplementary File S2**). *In silico* analysis based on Phobius and Protter suggested also that NtNRAMP3 has one N-glycosylation motif of amino acid position 505 located in the C-terminus.

Second, multiple amino acid sequence alignment showed high conservation between the NtNRAMP3 and examined NRAMP proteins (**Supplementary File S2**). NtNRAMP3 contains key sequences considered typical for NRAMP proteins. The consensus transport motif (CTM) [GQSSTIT(/A)G(/D)TYAGQY(/F)V(/I)MQ(/G/E)GFLD(/H/N)], which is the signature sequence of NRAMP family, was present in all examined proteins. Moreover, three highly conserved histidine residues (one within the region between II and III TMD and two within VI TMD) were identified.

Histidine residues occur at different locations in the NRAMP protein sequences. The location of some is highly conserved for all examined NRAMP proteins (as between II and III TMD and within VI TMD). Others are distributed in various locations within the sequence, however, the same for certain groups of plants. Thus, in the structure of NtNRAMP3 together with NtomNRAMP3, NaNRAMP3, NsNRAMP3, and LeNRAMP3, an additional histidine was present within CTM. Furthermore, additional histidine residues, H4 and H40, were present in the N-terminus of NtNRAMP3, and also within NtomNRAMP3, NaNRAMP3, and NsNRAMP3 (**Supplementary File S2**).

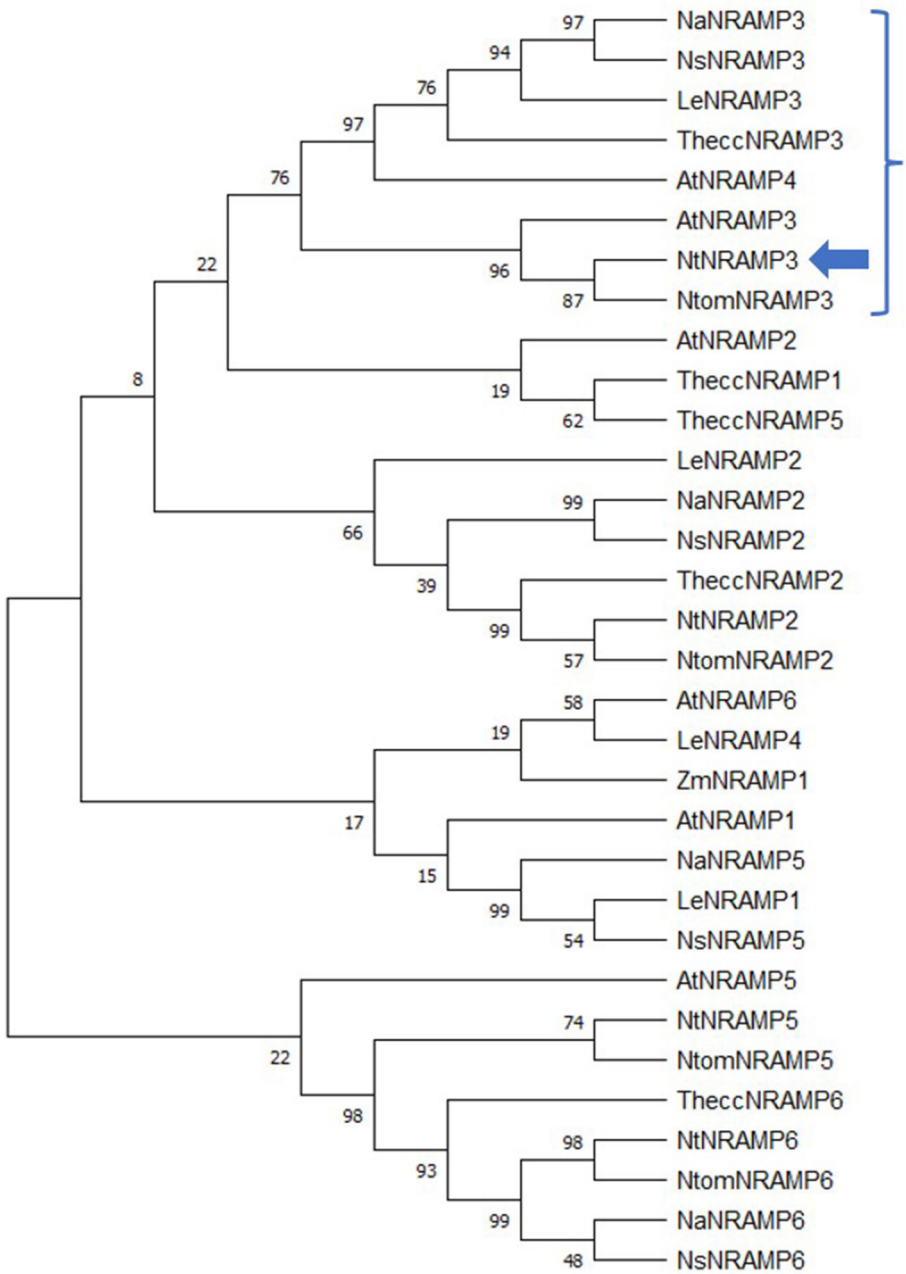

FIGURE 1 | A phylogenetic tree of the natural resistance-associated macrophage protein (NRAMP) transporters from *Arabidopsis thaliana*, *Solanum lycopersicum*, *Zea mays*, *Theobroma cacao*, and *Nicotiana*. Amino acid sequences of the 32 NRAMP proteins were identified in the ARAMEMNON (*A.thaliana*), Solgenomics (*S. lycopersicum*), MaizeSequence (*Z. mays*), Phytozome (*T. cacao*), and NCBI (*Nicotiana*) databases. The phylogenetic tree was constructed with the MEGA X software using Neighbor-Joining method. The length of branches corresponds to the degree of divergence. Numbers in the figure represent bootstrap values (1,000 replicates). Accession numbers for all proteins applied in the analysis: (i) *A. thaliana*: AtNRAMP1, AT1G80830; AtNRAMP2, AT1G47240; AtNRAMP3, AT2G23150; AtNRAMP4, AT5G67330; AtNRAMP5, AT4G18790; AtNRAMP6, AT1G15960; (ii) *S. lycopersicum*: LeNRAMP1, Solyc11g018530; LeNRAMP2, Solyc04g078250; LeNRAMP3, Solyc02g092800; LeNRAMP4, Solyc03g116900; (iii) *Z. mays*: ZmNRAMP1, GRMZM2G178190; (iv) *T. cacao*: TheccNRAMP1, Thecc1EG035168; TheccNRAMP2, Thecc1EG034751; TheccNRAMP3, Thecc1EG000729; TheccNRAMP5, Thecc1EG035174; TheccNRAMP6, Thecc1EG027424; (v) *Nicotiana attenuata*: NaNRAMP2, XP_019262545; NaNRAMP3, XP_019228309; NaNRAMP5, XP_019245559; NaNRAMP6, XP_019243869; (vi) *Nicotiana sylvestris*: NsNRAMP2, XP_009760309; NsNRAMP3, XP_009796782; NsNRAMP5, XP_009783885; NsNRAMP6, XP_009774026; (vii) *Nicotiana tabacum*: NtNRAMP2, XP_016477061; NtNRAMP3, NP_001312209 (marked with blue arrow); NtNRAMP5, XP_016434268; NtNRAMP6, XP_016480878; (viii) *Nicotiana tomentosiformis*: NtomNRAMP2, XP_009620156; NtomNRAMP3, XP_009616361; NtomNRAMP5, XP_009620069; NtomNRAMP6, XP_009594426. A bracket-marked branch of the phylogenetic tree indicates NRAMP proteins which are the most closely related to NtNRAMP3.

TABLE 2 | Amino acids sequence identity between selected NRAMP proteins.

	NtomNRAMP3	NaNRAMP3	NsNRAMP3	LeNRAMP3	TheccNRAMP3	AtNRAMP3	AtNRAMP2	AtNRAMP4	AtNRAMP1
NtNRAMP3	99.81	98.82	98.23	91.14	78.94	77.18	73.90	73.81	38.78
NtomNRAMP3		98.62	98.04	91.14	78.94	77.18	73.90	73.81	38.78
NaNRAMP3			98.23	90.93	79.56	77.00	74.70	74.05	39.51
NsNRAMP3				90.14	79.17	77.00	74.30	74.05	39.09
LeNRAMP3					76.98	75.60	73.90	72.46	39.14
TheccNRAMP3						80.20	76.00	74.60	40.12
AtNRAMP3							75.15	76.74	38.37
AtNRAMP2								70.32	37.80
AtNRAMP4									38.46

Abbreviations: At, Arabidopsis thaliana; Le, Solanum lycopersicum; Na, Nicotiana attenuata; Ns, Nicotiana sylvestris; Nt, Nicotiana tabacum; Ntom, Nicotiana tomentosiformis; Thecc, Theobroma cacao. All data is shown in percent [%]. Gray cells indicate repeated data.

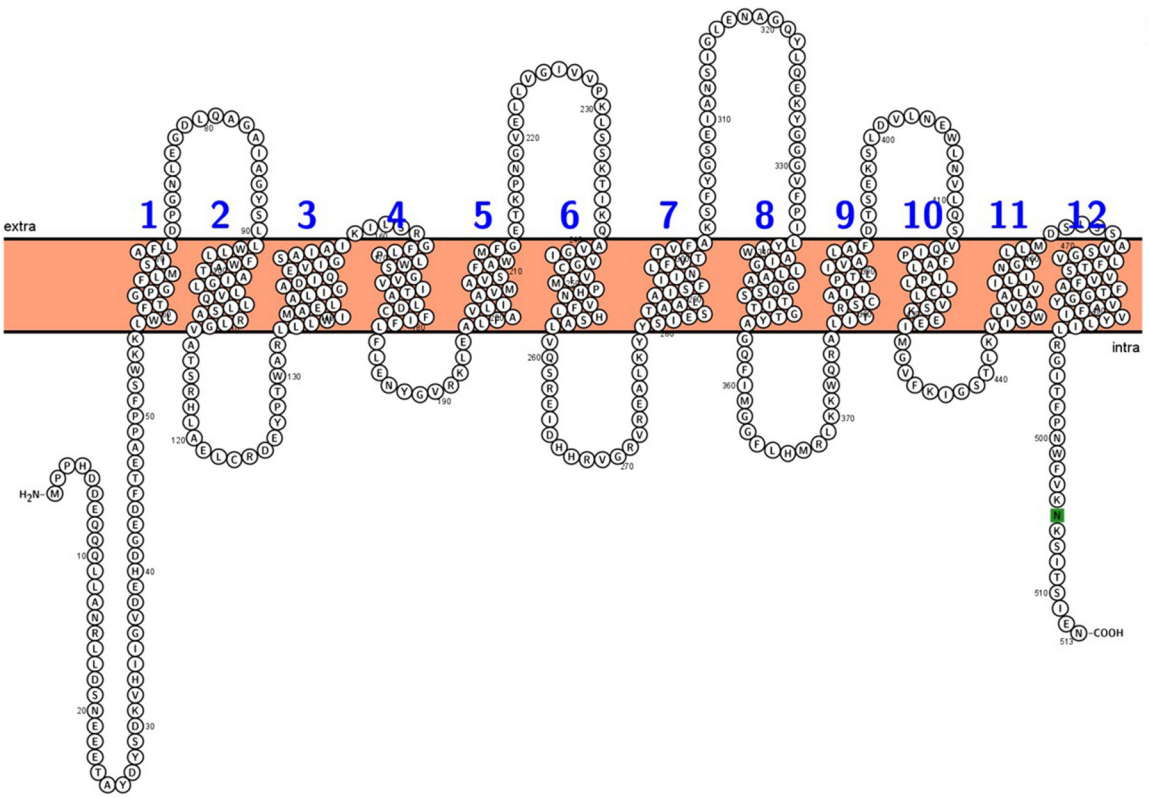

FIGURE 2 | Predicted transmembrane topology map of NtNRAMP3. The topology map was generated using the web-based Protter software (Omasits et al., 2014). NtNRAMP3 protein structure is comprised of 12 transmembrane regions and one N-glycosylation motif at amino acid position 505 (in green). N- and C- ends of NtNRAMP3 protein are located intracellularly.

NtNRAMP3 Encodes a Plasma Membrane Protein

To determine the subcellular localization of NtNRAMP3 protein, the *pMDC43::GFP::NtNRAMP3* construct was transiently expressed in tobacco leaf epidermal cells (**Figure 3**). The green fluorescence was present along the contours of the strongly folded cell walls of the lower epidermal cells (**Figure 3A1**) and overlapped with the red signal coming from the cell walls stained with propidium iodide (**Figures 3B1,D1**). Since the plasma membrane sticks to the primary cell wall, it is not distinguished by confocal light microscopy. Thus, the detected colocalization of both green and red signals indicates that NtNRAMP3 is localized in the plasma membrane. It is also known that the central vacuole does not enter the narrow projections of the epidermal cell, so

the lack of a green signal at their bases additionally confirms the location of the tested protein in the plasma membrane (Siemianowski et al., 2013; Pighin et al., 2014; Barabasz et al., 2019). Autofluorescence was extremely low (**Figures 3A3,D3**). The green fluorescence of GFP alone was observed only in small circular structures within the cells (**Figures 3A2,D2**).

Substrate Specificity of NtNRAMP3

Natural resistance-associated macrophage proteins are typically involved in the transport of several metals, including Fe, Mn, Ni, Co, Cu, Zn, and Cd (Gunshin et al., 1997; Thomine et al., 2000; Mizuno et al., 2005; Wang et al., 2019). Here, to identify substrates for NtNRAMP3, we applied two types of yeast growth assay—sensitivity tests (comparison of the growth of WT yeast transformed with either empty *pAG426GAL* vector or the construct *pAG426GAL::NtNRAMP3*) and complementation tests (comparison of the growth of mutant yeast transformed with either empty *pAG426GAL* vector or the construct *pAG426GAL::NtNRAMP3*; as the reference WT yeast transformed with the empty vector was used). Accordingly, *NtNRAMP3* expression was tested in the selected mutants (Δ*fet3fet4*, Δ*smf1,* or Δ*zrt1*) and WT (DY1457 or BY4742) yeast strains.

First, the sensitivity of strain DY1457 (WT) expressing *pAG426GAL* or *pAG426GAL::NtNRAMP3* to various concentrations of Fe, Mn, Co, Cu, Ni, Cd, and Zn was compared. Expression of *NtNRAMP3* led to inhibition of yeast growth in the presence of high concentrations of Fe (**Figure 4A**), Mn (**Figure 4C**), Co (**Figure 4E**), Cu (**Figure 4F**), Ni (**Figure 4G**), or Cd (**Figure 4H**). However, expression of *NtNRAMP3* in strain DY1457 increased yeast sensitivity to Zn only in the presence of a strictly defined concentration—around 5.0 mM (**Figure 4I**). To learn more, the experiments were extended by the use of three pH values (4.0, 5.0, and 6.0 adjusted with 50 mM MES; the pH of the SC-URA+GAL medium was 5.3) and five concentrations of Zn (4.0; 4.5; 5.0; 5.5; 6.0 mM). Likewise, *NtNRAMP3*-expressing yeast grew slower with the smallest difference to the control at 4.0 mM Zn applied at all tested pH values (**Figures 4J–L**).

Next, yeast mutants defective in Fe and Mn uptake were used. The expression of *NtNRAMP3* restored the growth of Δ*fet3fet4* (**Figure 4B**) and Δ*smf1* (**Figure 4D**) under Fe- or Mn-limited conditions, respectively. In contrast, expression of *NtNRAMP3* did not restore the growth of the Δ*zrt1* mutant under Zn-limited conditions induced with a strong chelator EDTA (**Figure 4M**), and the growth of Δ*zrt1* yeast carrying either the empty *pAG426GAL* vector or the construct (*pAG426GAL::NtNRAMP3*) was severely restricted.

These results indicate that NtNRAMP3 is an influx transporter for Fe, Mn, Co, Cu, Ni, and also toxic Cd. It also seems to transport Zn, but probably only under very specific environmental conditions/medium composition.

Developmental Regulation of *NtNRAMP3* Expression

To determine the role of *NtNRAMP3* in tobacco, the level of its expression in organs during vegetative development under control conditions was analyzed (**Figure 5**). In young 4-week-old and also in 6-week-old plants *NtNRAMP3* was preferentially expressed in the developing leaves, and its expression level was 2- to 3-fold higher in leaves compared with roots. The pattern changed in older, 9-week-old plants. Studies carried out on the apical and basal parts of the root, the stem, and young and older leaves did not show any significant differences. In general, however, the level was moderately lower compared with high expression in the leaves of younger plants.

Metal Status-Dependent Expression of *NtNRAMP3*

Knowing that NtNRAMP3 mediates the transport of Fe, Mn, Co, Ni, Cu, and Cd, subsequent experiments were performed to define how *NtNRAMP3* is regulated by the status of these metals. The main question was whether it is actively involved in the plant's response to excess metals or the supply of metals upon their deficiency. The appearance of plants after exposure to the tested metals is illustrated in **Supplementary File S3**. Organs, such as apical and basal parts of the roots and leaves, were included in the study. The stability of the reference *NtPP2A* gene is shown in **Supplementary File S4**.

With some exceptions, the highest level of expression of *NtNRAMP3* was detected under control conditions. In experiments with the deficiency of Fe, Mn, Co, or Cu, *NtNRAMP3* expression decreased significantly in all tested organs compared with control conditions (**Figures 6B,D,F,H**). Considering Zn deficiency, *NtNRAMP3* was lower only in the leaves (**Figure 6J**). Importantly, the transcript level also decreased after plants were exposed to high concentrations of metals (200 μM Fe or 100 μM Mn or 20 μM Co or 20 μM Cu or 30 μM Ni), excluding leaves and apical root parts after exposure to Co and Cu, respectively (**Figures 6A,C,E,G,I**). Also, no changes in the expression level were found after exposure to 50 μM Zn (**Figure 6K**), as well as in the presence of 4 μM Cd (**Figure 6L**).

A previous study showed that the expression of *NtNRAMP3* in tobacco leaves went up in response to up to 4-day exposure to very high (200 μM) Zn, suggesting *NtNRAMP3* involvement in plants' response to toxic zinc levels (Papierniak et al., 2018). To initially verify this possible function, a more detailed examination of the transcript level in consecutive pairs of leaves of long-term exposed tobacco plants to elevated concentrations of Zn was performed. Two key pieces of information were obtained in this experiment. The expression of *NtNRAMP3* was strongly induced by high Zn concentration, however, in a manner dependent on the age/position on the stem, but it was not regulated in the youngest leaves (5th pair) (**Figure 7**). The highest upregulation resulted from exposure to 200 μM Zn in the 2nd and 3rd pair of leaves. The 21-day exposure to 50 μM Zn also resulted in enhanced expression, however, to a much lesser extent.

Taken together, our results indicate a general role of *NtNRAMP3* in the regulation of the balance of several metals in plants grown under control conditions,

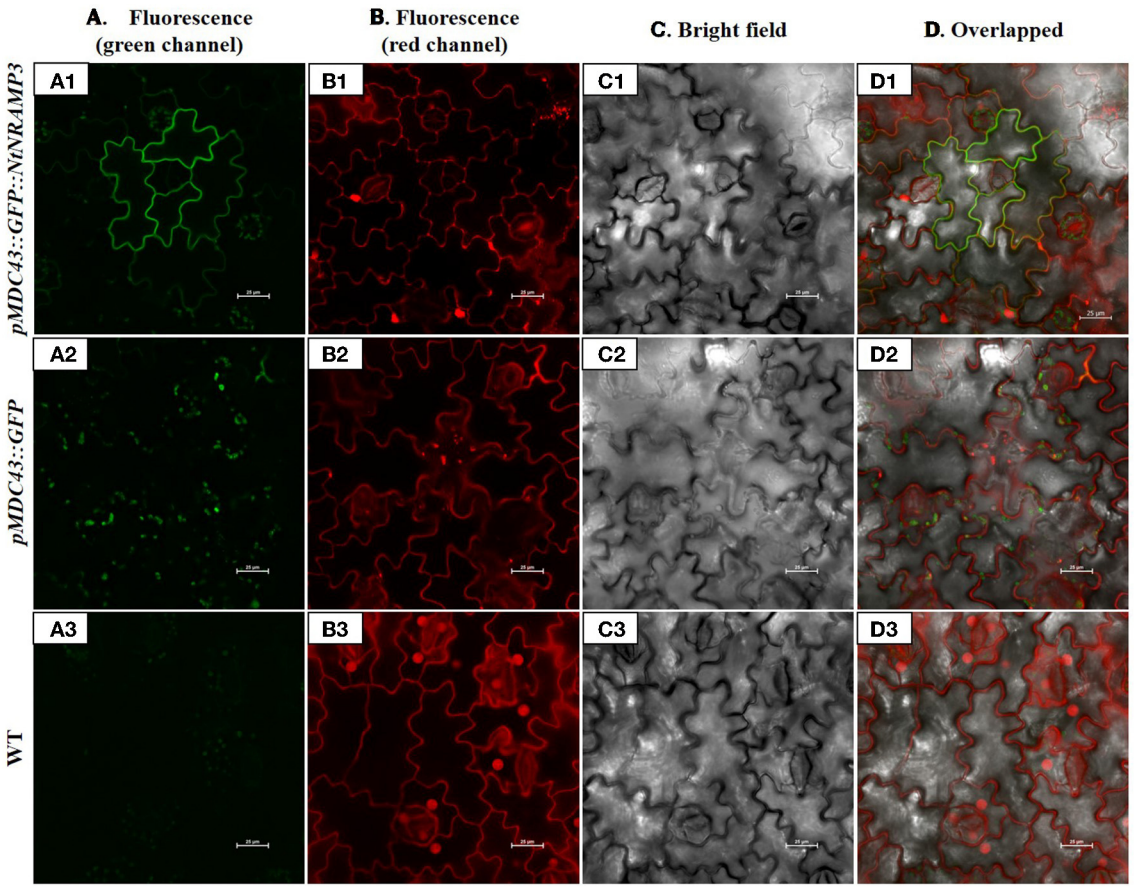

FIGURE 3 | Subcellular localization of NtNRAMP3 in the epidermal cells of tobacco leaves. *A. tumefaciens* GV3101 strains containing the *pMDC43::GFP* [control empty vector **(A2,B2,C2,D2)**] or *pMDC43::GFP::NtNRAMP3* **(A1,B1,C1,D1)** were used for transient expression in *N. tabacum* leaves. After 1–4 days from infiltration leaves were observed under a confocal microscope. **(A)** GFP fluorescence (green channel); **(B)** PI (propidium iodide) signal in the cell wall (red channel); **(C)** bright-field images; **(D)** merged images. WT tobacco plants **(A3,B3,C3,D3)** were used as a negative control for the GFP signal. The white bar represents 25 μm.

with a possible specific role at exposure to extreme Zn-imposed stresses.

The Activity of the *NtNRAMP3* Promoter Is Limited to Specific Tissues

Regulatory Sequences Identified Within the NtNRAMP3 Promoter Sequence

The sequence of the *NtNRAMP3* promoter region (−1,684 bp upstream to ATG) is shown in **Supplementary File S5**. Within its sequence, two *cis*-regulatory elements potentially involved in a plant's metal stress response, MRE1 (metal-responsive element 1, Li et al., 2013) and IDE2 (iron deficiency response element 2, Ogo et al., 2008), were identified. However, the MRE1 sequence in the *NtNRAMP3* promoter was incomplete. The presence of the TGCACC sequence was determined, thus compared with the original sequence, TGC(A/G)C(T/G/C/A)C (Li et al., 2013), it was lacking the last nucleotide. The *NtNRAMP3* promoter also contained *cis*-regulatory elements known to determine the plant's response to phytohormones (ABRE, CGTCA-motif), light (BOX4, G-box, GATA-motif, TCCC-motif, chs-CMA1a) and abiotic stresses (ARE) (Fink et al., 1988; Lafyatis et al., 1991; Paul and Ferl, 1991; Weisshaar et al., 1991; Shen and Ho, 1995; Hiratsuka and Chua, 1997; Sibéril et al., 2001; Basehoar et al., 2004; Chawla and DeMason, 2004; Frangeul et al., 2004; Zhu et al., 2014).

The Expression of NtNRAMP3 in Tobacco Is Limited to Specific Tissues

To investigate the tissue-specific expression, tobacco was stably transformed with the *pMDC163::promNtNRAMP3::GUS* construct containing a 1,684 bp promoter region. Out of 30 T1 heterozygous lines with the 3:1 segregation ratio of the transgene, nine homozygous T2 lines were derived and used for experiments (L004, L008, L009, L012, L013, L014, L015, L016, L022).

It was shown that the expression of *NtNRAMP3* was the highest under control conditions (**Figure 6**). Therefore, the tissue-specific promoter activity was examined in transgenic plants stably expressing the *promNtNRAMP3::GUS* construct in tobacco grown in the control medium.

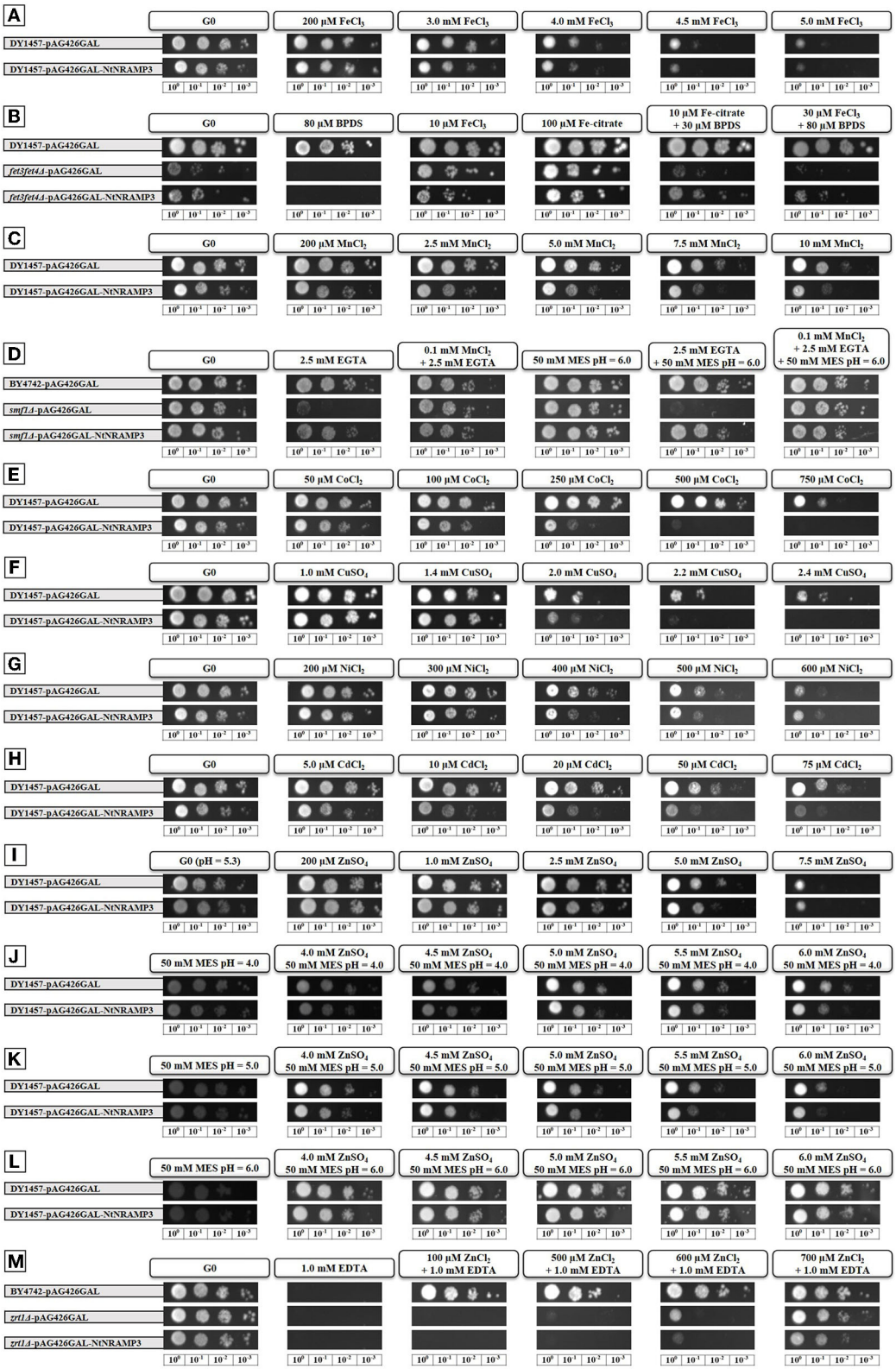

FIGURE 4 | *NtNRAMP3* expression in selected yeast strains. *Saccharomyces cerevisiae* strains (i) wild-type (WT; DY1457 or BY4742) and (ii) deletion mutants Δ*fet3fet4* (defective in Fe transport into the cell), Δ*smf1* (defective in Mn transport into the cell) or Δ*zrt1* (defective in Zn transport into the cell) were transformed with the empty vector *pAG426GAL* or with the construct *pAG426GAL::NtNRAMP3*. The transformed cells were adjusted to OD_{600} = 0.2, then a series of dilutions (1, 0.1,

(Continued)

FIGURE 4 | 0.01, and 0.001) were prepared. Yeast cultures were spotted (5 μl aliquotes) on SC-URA+GAL plates supplemented with required components and incubated at 30°C for up to 10 days. *Sensitivity tests*: Transformed DY1457 cells on SC-URA+GAL plates supplemented with: **(A)** 200 μM, 3.0, 4.0, 4.5, or 5.0 mM $FeCl_3$; **(C)** 200 μM, 2.5, 5.0, 7.5, or 10.0 mM $MnCl_2$; **(E)** 50, 100, 250, 500, or 750 μM $CoCl_2$; **(F)** 1.0, 1.4, 2.0, 2.2, or 2.4 mM $CuSO_4$; **(G)** 200, 300, 400, 500, or 600 μM $NiCl_2$; **(H)** 5, 10, 20, 50, or 75 μM $CdCl_2$; **(I)** 200 μM, 1.0, 2.5, 5.0, or 7.5 mM $ZnSO_4$; **(J)** 4.0, 4.5, 5.0, 5.5, or 6.0 mM $ZnSO_4$ (pH was adjusted to 4.0 with 50 mM MES); **(K)** 4.0, 4.5, 5.0, 5.5, or 6.0 mM $ZnSO_4$ (pH was adjusted to 5.0 with 50 mM MES) or **(L)** 4.0, 4.5, 5.0, 5.5, or 6.0 mM $ZnSO_4$ (pH was adjusted to 6.0 with 50 mM MES). DY1457 transformed with the empty vector *pAG426GAL* was used as a control. The same control plate is depicted in **(A,E,F,G)**—the experiments were done simultaneously. **(A,E,G)** Depict data from day 3, **(F)**—data from day 5. The same control plate is depicted in **(C,H)**—the experiments were done simultaneously (data from day 3). *Complementation tests*: **(B)** Transformed *fet3fet4*Δ cells on SC-URA+GAL plates supplemented with 80 μM BPDS; 10 μM $FeCl_3$; 100 μM Fe-citrate; 10 μM Fe-citrate + 30 μM BPDS; 30 μM $FeCl_3$ + 80 μM BPDS. **(D)** Transformed *smf1*Δ cells on SC-URA+GAL plates supplemented with 2.5 mM EGTA; 0.1 mM $MnCl_2$ + 2.5 mM EGTA; 50 mM MES pH = 6.0; 2.5 mM EGTA + 50 mM MES pH = 6.0; 0.1 mM $MnCl_2$ + 2.5 mM EGTA + 50 mM MES pH = 6.0. **(M)** Transformed *zrt1*Δ cells on SC-URA+GAL plates supplemented with 1 mM EDTA; 100 μM $ZnCl_2$ + 1 mM EDTA; 500 μM $ZnCl_2$ + 1 mM EDTA; 600 μM $ZnCl_2$ + 1 mM EDTA; 700 μM $ZnCl_2$ + 1 mM EDTA. DY1457 (for *fet3fet4*Δ) or BY4742 (for *smf1*Δ and *zrt1*Δ) transformed with the empty vector *pAG426GAL* was used as a control.

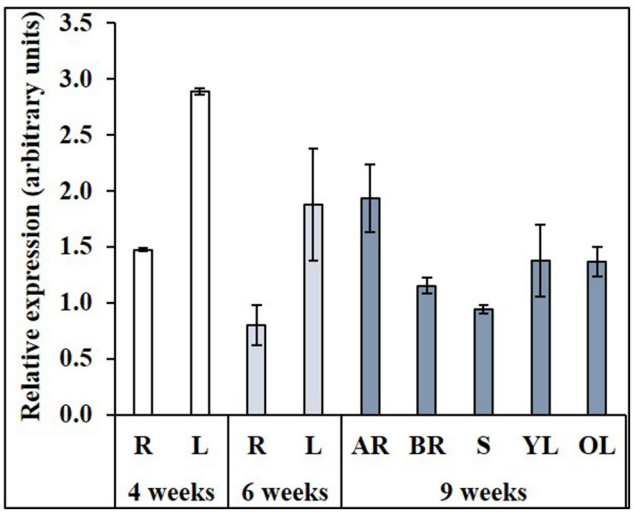

FIGURE 5 | Expression of *NtNRAMP3* during development. WT tobacco plants were grown at the control conditions (¼ Knop's medium) for up to 9 weeks. At three selected developmental stages *NtNRAMP3* transcript level was monitored by RT-qPCR and normalized to the *NtPP2A* expression level. Expression of *NtNRAMP3* was determined in (i) roots (R) and leaves (L) of 4-week-old plants; (ii) roots (R) and leaves (L) of 6-week-old plants; (iii) apical (AR) and basal fragments of roots, stem (S), young (YL) and old (OL) leaves of 9-week-old plants. Values correspond to mean ± *SD* ($n \geq 3$); those with a ratio greater than 2 are considered significantly different (Jain et al., 2013).

In the leaves of young seedlings, GUS activity was detected primarily in the veins (**Figure 8A**). However, *NtNRAMP3* expression was also present in the lower epidermis just below the main vein (**Figures 8A1,A2**), and in the trichomes (**Figure 8A3**).

In the roots, blue staining was not found (**Figures 8B1–B3,B5**), except in the apical meristem of the main and lateral roots (**Figure 8B4**), specifically in the procambium (**Figures 8B7–B9**), gradually disappearing distally (**Figure 8B10**). It was also seen in the early stages of differentiation of the vascular bundles (**Figure 8B6**). In wild-type tobacco, no GUS staining was detected (data not shown).

GUS activity was also examined in cross-sections through 5-week-old leaves from plants exposed for 3 days to 200 μM Zn. No differences were observed between control plants and those exposed to high Zn (**Figures 8C1,C2, D1,D2**). Blue staining was present only in the vascular bundles.

The promoter activity of the *NtNRAMP3* gene (encoding metal influx transporter) detected mainly in the xylem of leaves indicates that NtNRAMP3 may play an important role in the unloading of minerals carried by vessels from the roots to the leaves, thus supplying the leaf cells with essential micronutrients.

DISCUSSION

Natural resistance-associated macrophage protein genes are one of the key components of the plant metal homeostasis regulation network. However, they remain largely unknown in such an economically important plant species as tobacco (*Nicotiana tabacum*), also frequently used for phytoremediation of metal-contaminated soil. So far, only *NtNRAMP1* has been cloned from tobacco and preliminary characterization showed that the protein was targeted to the plasma membrane and contributed to Fe uptake (Sano et al., 2012). The present work fills this gap through the functional characterization of the newly cloned *NtNRAMP3* gene. Here, we report that plasma membrane-localized NtNRAMP3 is a broad range metal transporter mediating uptake of Fe, Mn, Co, Cu, Ni, Cd, and also Zn. Its role is likely to primarily maintain cross-homeostasis under control conditions in the leaves.

NtNRAMP3 Is a Broad Range Metal Uptake Transporter

The new sequence was assigned to the NRAMP family based on the degree of homology to nucleotide and amino acid sequences characteristic of this family, and also on the structure of the protein. The new sequence was named NtNRAMP3 based on its highest homology to NRAMP3 sequences from other plant species (**Figure 1**; **Table 2**). Dendrogram analysis showed the closest relationship between NRAMP3 from all eight plant species used for the study, which formed a separate branch (**Figure 1**). The highest degree of homology was found between NtNRAMP3 and NRAMP3 proteins from other tobacco species (99.81–98.04%), as well as for NRAMP3 from other plants, such as *S. lycopersicum* or *A. thaliana* (91.14 and 77.18%, respectively) (**Table 2**).

Homology-based analysis revealed that the overall structure of NtNRAMP3 is conserved, except for the N-terminal and C-terminal regions. These include the presence of 12 TMDs, a glycosylation signal at the C-terminus, and the consensus transport motif (CTM) between VIII and IX TMD (**Figure 2**;

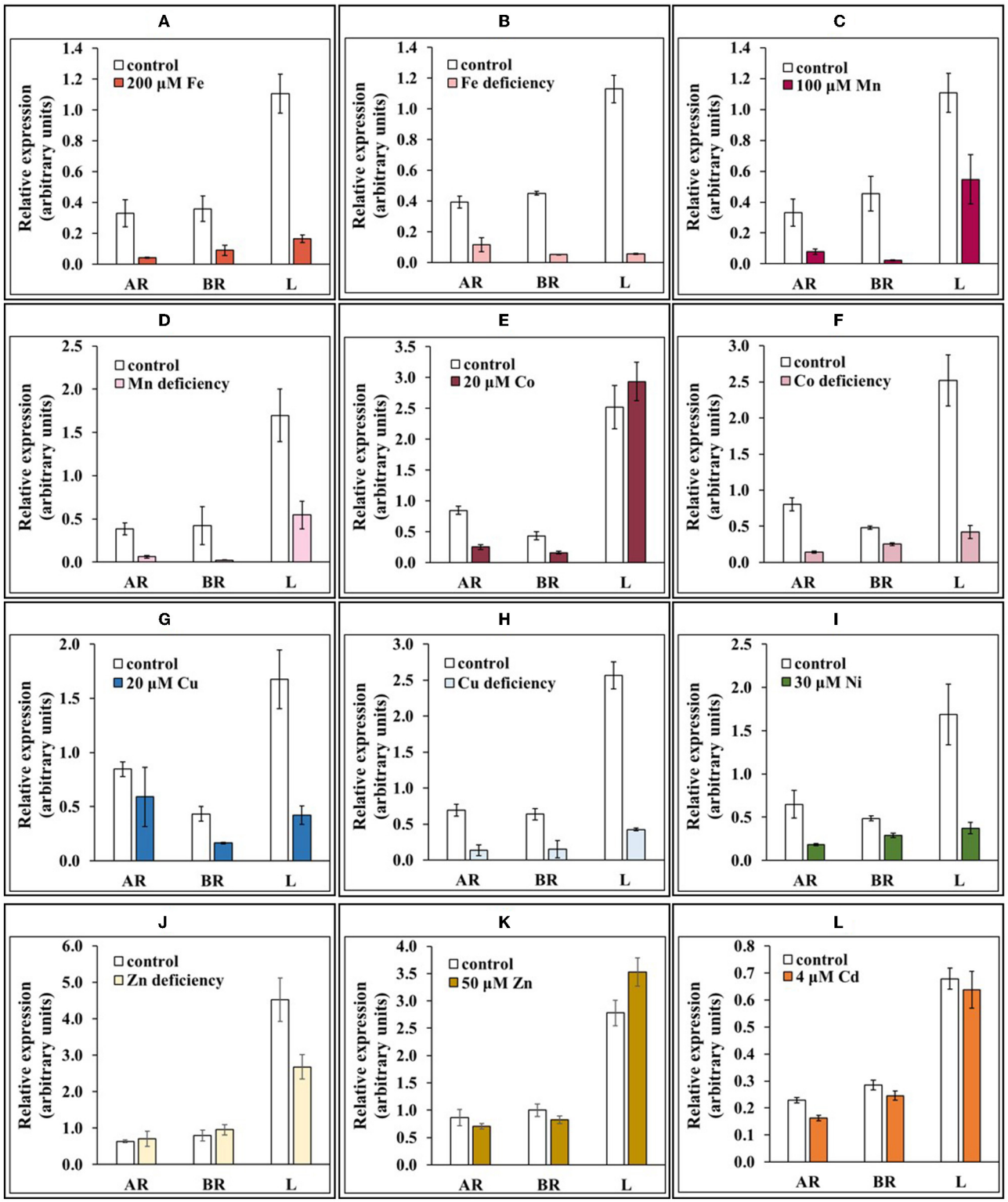

FIGURE 6 | Expression of *NtNRAMP3* under different metal regimes. **(A–I,L)** Wild-type (WT) tobacco plants were grown at control conditions (¼ Knop's medium) for 5 weeks and then were subjected to the different metal regimes for the next 4 days: **(A)** 200 µM Fe; **(B)** Fe deficiency; **(C)** 100 µM Mn; **(D)** Mn deficiency; **(E)** 20 µM Co; **(F)** Co deficiency; **(G)** 20 µM Cu; **(H)** Cu deficiency; **(I)** 30 µM Ni; **(J)** Zn deficiency; **(K)** 50 µM Zn; **(L)** 4 µM Cd. In parallel, WT tobacco plants were grown at control conditions. The expression of *NtNRAMP3* was determined in apical (AR) and basal (BR) segments of the roots, and in leaves **(L)**. *NtNRAMP3* transcript level was monitored by RT-qPCR and normalized to the *NtPP2A* expression level. Values correspond to mean ± *SD* ($n \geq 3$); those with a ratio >2 are considered significantly different (Jain et al., 2013).

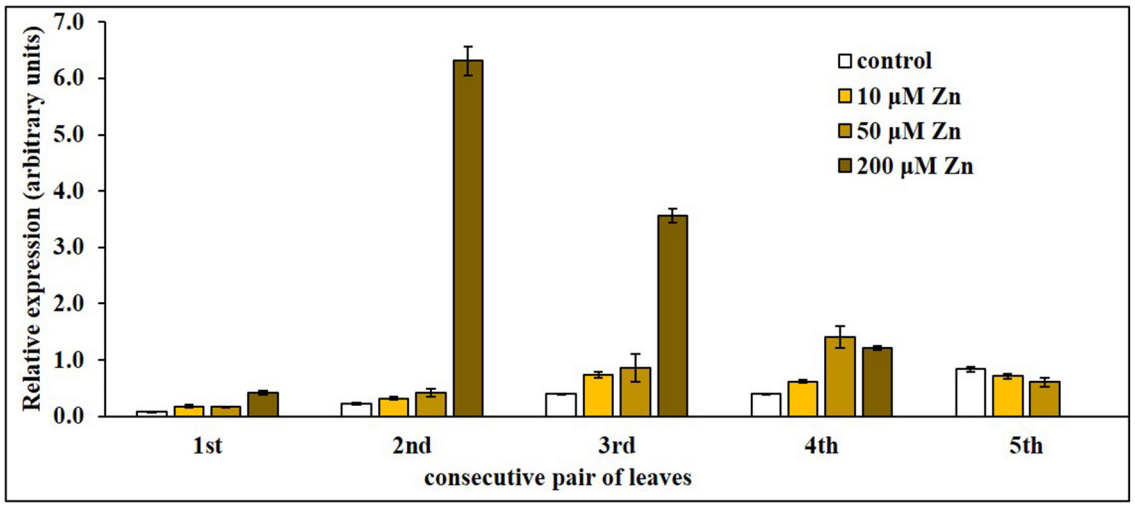

FIGURE 7 | *NtNRAMP3* in consecutive pairs of leaves of plants grown under different zinc regimes. 5.5-week-old wild-type (WT) tobacco plants were transferred for the next 3 weeks to control medium (¼ Knop's) supplemented with: (i) 10 μM Zn; (ii) 50 μM Zn; (iii) 200 μM Zn. In parallel, WT tobacco plants were grown at control conditions. Expression of *NtNRAMP3* was determined in consecutive pairs of leaves (numbered from 1 to 5; 1st and 2nd leaves counting from the base of the stem were the 1st pair, etc.). *NtNRAMP3* transcript level was monitored by RT-qPCR and normalized to the *NtPP2A* expression level. Values correspond to mean ± *SD* ($n \geq 3$); those with a ratio >2 are considered significantly different (Jain et al., 2013).

Supplementary File S2), which are indicative of the NRAMP family (Nevo and Nelson, 2006).

Furthermore, the NtNRAMP3 sequence contains essential amino acid residues important for the transport function. These include histidines, which are also believed to contribute to the functional divergence of the NRAMP family (Chaloupka et al., 2005; Ihnatowicz et al., 2014). First, NtNRAMP3 possesses conserved His residues, one within the loop between the II and III TMD and two within VI TMD, including the Met-Pro-His motif (**Supplementary File S2**). Secondly, in most NRAMP proteins, there are also His residues in a variable arrangement throughout a sequence. Three histidines (H4, H33, and H40) were found in the NtNRAMP3 sequence in the N- terminus, and interestingly, was also present in NRAMP3 from five plant species with the highest homology to NtNRAMP3 (NtomNRAMP3, NaNRAMP3 and NsNRAMP3 proteins, and also in LeNRAMP3 and AtNRAMP3). Two His residues were identified within the loop between VI and VII TMD, in NtNRAMP3 and NtomNRAMP3, NaNRAMP3, and NsNRAMP3 (**Supplementary File S2**).

The NRAMP proteins carry ions toward the cytoplasm (Nevo and Nelson, 2006). Thus, if a protein is targeted to the plasma membrane it mediates metal uptake, and localization to the tonoplast or the membranes or the Trans-Golgi Network (TGN) indicates involvement in redistribution. Thus, the detected localization of the NtNRAMP3-GFP fusion protein in the plasma membrane (**Figure 3**) provided indirect evidence for the contribution of the NtNRAMP3 to the uptake of metals. Further pieces of evidence come from yeast experiments. We showed that the NtNRAMP3 protein functions as a Fe, Mn, Co, Cu, Ni, and Cd uptake transporter, as revealed by the functional complementation of the *fet3fet4* and *smf1* yeast mutants, and by the sensitivity tests demonstrating growth inhibition of WT yeast DY1457 expressing the *NtNRAMP3* cDNA (relative to the WT expressing the empty vector), in the presence of elevated concentrations of all tested metals (**Figure 4**). However, when drawing conclusions, one must remember that sometimes the results of yeast complementation tests are not consistent with the subcellular localization of examined proteins. For example, AtZIP1 is localized to the vacuole of *Arabidopsis* protoplasts, but an expression of *AtZIP1* complemented a yeast mutant defective in plasma membrane Zn uptake. Two possible explanations for this phenomenon have been proposed. First, Zn deficiency-inducible *AtZIP1* might efflux Zn to the cytoplasm of transformed yeast cells which promotes growth on low Zn. Secondly, the plant transporter could be mislocalized to the yeast plasma membrane (Milner et al., 2013). Likewise, AtNRAMP3 and AtNRAMP4 were found to complement the *fet3fet4* Fe uptake mutant although, as being targeted to the tonoplast in plant cells, they participate in metal redistribution (Thomine et al., 2000, 2003; Languar et al., 2005). In our studies, however, the result of the subcellular localization of NtNRAMP3 (plasma membrane, **Figure 3**) was consistent with the direction of transport resulting from yeast tests (uptake, **Figure 4**). This supports the conclusion that NtNRAMP3, as a protein with low substrate specificity, is capable of carrying several metals.

For comparison, similar to tobacco, the presence of NRAMP3 in rice was found in the plasma membrane, but AtNRAMP3, TcNRAMP3, and LeNRAMP3 from three other plant species (*A. thaliana, T. caerulescens*, and tomato) were localized in the tonoplast (Bereczky et al., 2003; Thomine et al., 2003; Oomen et al., 2009). The NRAMP proteins with predominant localization in the plasma membrane include NRAMP1 and NRAMP5. This was shown for most of the NRAMP1 proteins known to date (from *A. thaliana, M. truncatula, N. tabacum*, *O. sativa,* and *Sedum alfredii*) (Thomine et al., 2000; Takahashi et al., 2011; Sano et al., 2012; Tejada-Jiménez et al., 2015; Zhang et al., 2020),

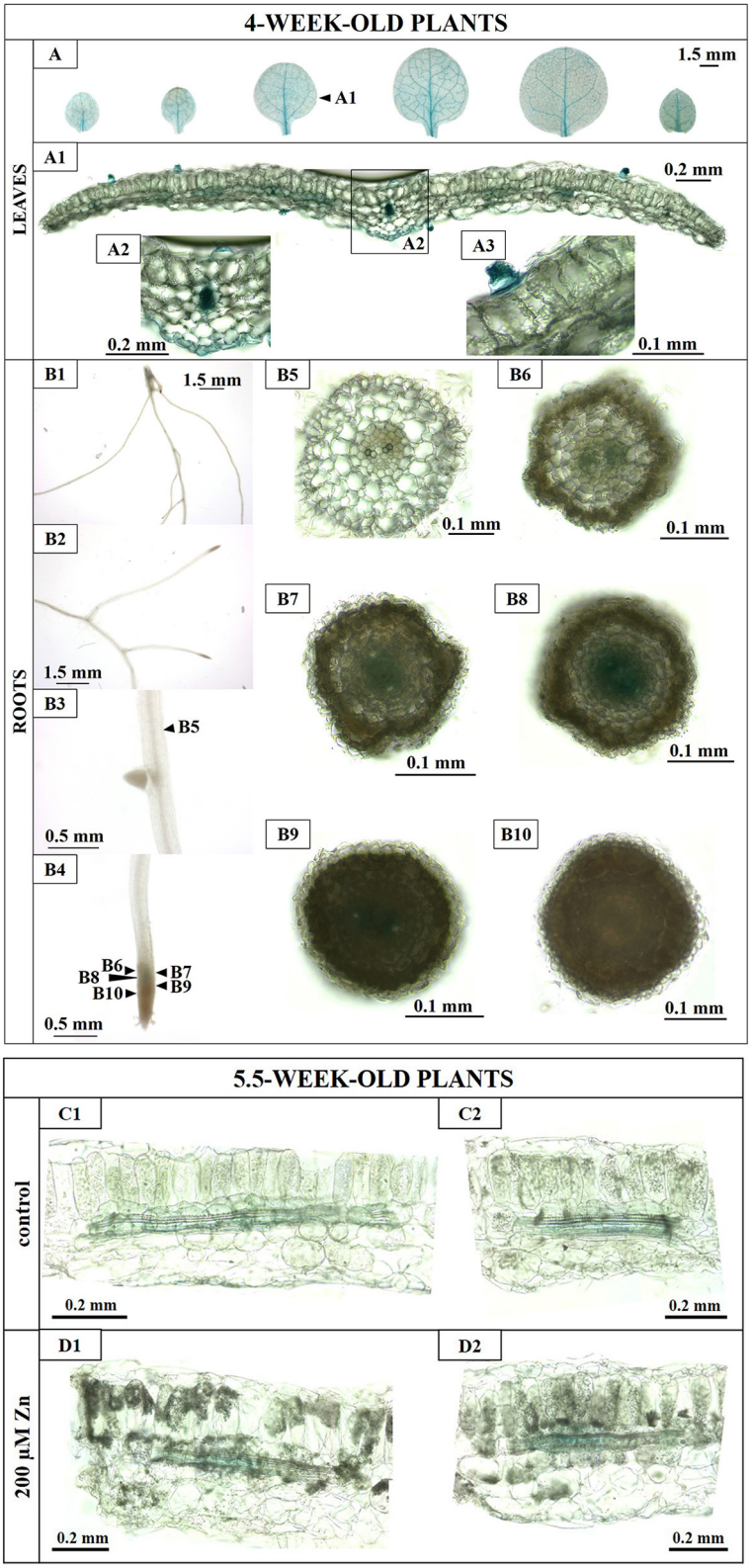

FIGURE 8 | Histochemical GUS assay in transgenic *promNtNRAMP3::GUS* tobacco. **(A–B4)**: *4-week-old plants:* Transgenic *promNtNRAMP3::GUS* tobacco plants were grown for 4 weeks at the control medium (¼ Knop's). **(A)** depicts leaves. **(A1)** Cross-section through the blade of the 3rd leaf (counting from the base). **(A2)** Magnifications of the main vein and surrounding tissues. **(A3)** Fragment of a cross-section of a leaf blade with a trichome. **(B)** Depicts roots. **(B1)** Basal part of the root; *(Continued)*

FIGURE 8 | (B2) middle part of the main root with lateral roots; **(B3)** the middle part of the main root (magnification); **(B4)** apical part of the main root; **(B5)** cross-section through the middle part of the main root; **(B6–B10)** cross-sections through the apical part of the main root. **(C1–D2)**: *5.5-week-old plants:* GUS activity in cross-sections through leaf blades of transgenic *promNtNRAMP3::GUS* tobacco plants. Transgenic *promNtNRAMP3::GUS* tobacco plants were grown for 5 weeks in the control medium and then subjected for 3 days to (i) control conditions **(C1,C2)** or 200 μM Zn **(D1,D2)**. Cross-sections through the 2nd leaf (counting from the bottom).

except for NRAMP1 from *G. max* or tomato, which was found in intracellular membranes (Bereczky et al., 2003; Qin et al., 2017). Similarly, known NRAMP5 proteins (from *O. sativa, G. max*, and *H. vulgare*) were also targeted in the plasma membrane (Sasaki et al., 2012; Qin et al., 2017).

Although NRAMPs are known as transporters mediating translocation of a broad range of metals (Nevo and Nelson, 2006), the ability of NtNRAMP3 to carry six possible substrates identified in this study (**Figure 4**) seems to be unique among plants for this class of the proteins. However, the identification of six substrates for NtNRAMP3 resulted from the large scope of yeast-based analyses performed. Until now, usually up to four metals have been tested as possible substrates for an examined protein. For comparison, it has been shown that within the NRAMP3 proteins, the substrate for OsNRAMP3 was Mn, but not Fe or Cd (Yamaji et al., 2013), for AtNRAMP3 or TcNRAMP3 Mn, Fe, Cd, but not Zn (Thomine et al., 2000; Languar et al., 2004; Oomen et al., 2009). Similarly, the number of metals transferred by NRAMP proteins from the other classes (NRAMP1-2, NRAMP4-6) is usually a maximum of 2 to 4 (Thomine et al., 2000; Bereczky et al., 2003; Languar et al., 2004, 2010; Yamaji et al., 2013; Zhang et al., 2020). TjNRAMP4 is an opposite example of an NRAMP protein with high substrate specificity, for which only Ni (but not Fe, Zn, Mn, or Cd) was identified as a substrate (Mizuno et al., 2005).

Considering these data, it seems that NtNRAMP3, capable of carrying up to six different metals, can play a unique role in tobacco. For the proper growth and development of a plant, it is necessary to maintain the correct concentration of many metals (both micro- and macro-elements) (Baxter, 2009; Sperotto et al., 2014; Che et al., 2018). This is due to the interconnected network of regulation of the metal-related genes, for which tissue-specific expression depends on the status of metals in the cells. Underlying mechanisms are poorly understood, especially when we take into account the simultaneous regulation of the level of various metals in a given cell, tissue, or organ. In general, these include the presence of a range of *cis*-acting elements present in the promoter region, as well as the specificity of the transcription factors. Important components of such regulation may also be genes encoding multi-metal transport proteins, such as NtNRAMP3.

Hypothetical Physiological Role of NtNRAMP3 in Tobacco

NtNRAMP3 Might Play a Specific Role in the Regulation of the Balance of Nutrients (Fe, Mn, Co, Cu, and Ni) Under Control Conditions

The uniqueness of the features determining the physiological role of NtNRAMP3 is not only its large number of substrates. The second characteristic important for the protein's function is the expression pattern in leaves and roots. Its highest level was found under control conditions, while reduction took place both at a mineral deficit (Fe, Mn, Co, and Cu) and upon the excess of metals (Fe, Mn, Co, Cu, Ni, and Cd) (**Figure 6**). Both of these features in association with the *NtNRAMP3* tissue-specific expression found primarily in the vascular bundles of leaves (detected by analysis of prom*NtNRAMP3*-GUS fusion activity; **Figure 8**) suggest that the encoded metal import protein localized in the plasma membrane (**Figure 3**) plays a specific role in the regulation of unloading a range of metals (Fe, Mn, Co, Cu, Ni, and Cd identified as NtNRAMP3 substrates) transported through the xylem from the roots to the leaves, primarily under control conditions. Thus, the tissue-specific expression of *NtNRAMP3* in leaves (**Figure 8**) may contribute to a proper supply of several micronutrients to leaf blades. Downregulation at mineral deficiency and moderate metal excess (**Figure 6**) support this conclusion. Similarly, OsNRAMP3 is an Mn uptake transporter expressed in the parenchyma cells of the vascular bundles. Experiments with knockout mutants showed that OsNRAMP3 is necessary for the unloading of metal ions from the xylem (Yamaji et al., 2013). Further research is needed to elucidate the molecular mechanisms behind the reduction in *NtNRAMP3* expression under both metal deficit and excess conditions (**Figure 6**). It cannot be excluded that *NtNRAMP3* is regulated through common or converging regulatory elements in response to such differing metal supply conditions. Similarly, the same direction of changes in expression (increase) in the presence of both excess and deficiency of Fe was demonstrated for *AhNRAMP3* in *Arabidopsis halleri* (Weber et al., 2004). It was hypothesized that *CsMTP6* proteins might participate in the protection of mitochondria from excess Fe and/or in the remobilization from mitochondria under deficiency conditions, however, the molecular background has not been studied.

Bioinformatic analysis showed the presence of various regulatory elements in the *NtNRAMP3* promoter sequence (**Supplementary File S5**). These include elements responding to metals (MRE1 and IDE2), phytohormones (ABRE and CGTCA-motif regulating responses to abscisic acid and jasmonic acid, respectively), and five light-response elements, pointing to the possible involvement of NtNRAMP3 in a network coordinating responses of tobacco to different factors, which ultimately might regulate several processes. In this study, we only identified the contribution of NtNRAMP3 in the supply of metals to tissues. Future research may indicate a broader function of this protein, for example in linking mineral nutrition with the role of other stimuli in growth and development. For instance, in rice, protein OsNRAMP6 has been assigned a role in regulating the tissue Fe level in connection to tolerance to a fungal pathogen. Such a relationship was given the term "nutritional immunity" (Peris-Peris et al., 2017).

Our results indicate that *NtNRAMP3* plays a role mainly in the leaves. However, Real-Time analysis showed that it

was also expressed in the roots, although at a much lower level (**Figure 5**). Furthermore, the *NtNRAMP3* promoter-derived GUS staining assay revealed that in the roots, *NtNRAMP3* was mainly expressed in the procambium of the apical meristems (**Figure 8B4**) pointing to its specific contribution to supplying a range of micronutrients to cells that differentiate into the vasculature of the root. In the upper root parts, GUS activity was histochemically undetectable. As a method of lower sensitivity compared with Real-Time, it was probably due to the low expression level of *NtNRAMP3*.

Contribution of NtNRAMP3 to Maintain Metal Cross-Homeostasis Specifically at Exposure to 200 μM Zn

The working hypothesis of the conducted research was the assumption that *NtNRAMP3* was involved in the processes determining the cell-specific accumulation of Zn in the mesophyll of tobacco leaves from plants exposed to a high concentration of this metal. It was assumed that *NtNRAMP3* might be an important component of multi-gene regulation of Zn loading into the mesophyll "Zn accumulating cells." Earlier research led to the identification of two genes important in this process—*NtZIP1-like* and *NtZIP11* (Weremczuk et al., 2020). Both genes encode Zn uptake transporters (Papierniak et al., 2018; Kozak et al., 2019), and their expression occurs specifically in the "Zn accumulating mesophyll cells" of tobacco leaves of plants exposed to high Zn concentrations (Weremczuk et al., 2020). *NtNRAMP3* was the third candidate gene, identified together with *NtZIP1-like* and *NtZIP11* during preliminary studies, which showed increased expression in tobacco leaves 1 to 4 days after exposure to 200 μM Zn (Papierniak et al., 2018).

In this study, however, we showed that at exposure to 200 μM Zn, *NtNRAMP3* unlike *NtZIP1-like* and *NtZIP11*, was not specifically expressed in the groups of "Zn accumulating mesophyll cells" (**Figures 8D1,D2**). Although, in the presence of 200 μM Zn a substantial increase in the *NtNRAMP3* transcript level was also noted (**Figure 7**), after administration of moderately enhanced Zn levels (10 or 50 μM) there was little or no increase in expression (**Figures 6**, **7**). Moreover, *NtNRAMP3* expression decreased in response to elevated concentrations of metals, such as Fe, Mn, Co, Cu, and Ni, which are NtNRAMP3 substrates (**Figure 6**), indicating fine-tuned metal-status-dependent regulation. It is known that exposure of a plant to a high concentration of Zn disrupts the homeostasis of other metals. In response, a range of metabolic pathways is induced to compensate for the generated changes (Sperotto et al., 2014; Ricachenevsky et al., 2015). *NtNRAMP3* may be one of the components of this regulatory response. It seems likely that due to the expression of *NtNRAMP3* in the conducting tissues, an encoded protein that is involved in the influx of metals might contribute to the regulation of the level of Fe, Mn, Co, Cu, and Ni (and also Cd) in leaves from plants exposed to high Zn. It should be noted, however, that the yeast growth assay does not exclude the possibility of transporting Zn *via* NtNRAMP3. As shown in **Figure 4M**, *NtNRAMP3* did not restore the ability of the high-affinity Zn uptake mutant *zrt1* to grow on a low Zn medium. However, the growth of transformants was impaired on a medium supplemented with high Zn (**Figures 4I–L**).

Interestingly, a strong increase in *NtNRAMP3* expression was observed only in the 2nd and 3rd pairs of leaves exposed to high Zn (**Figure 7**), which suggests a specific role of these leaves in Zn accumulation. Transcript levels might have increased due to a direct response to high zinc, or a manifestation of secondary changes to the disturbed balance of other metals within cells.

In conclusion, plants respond to a specific combination of environmental conditions, which should be taken into account in the functional analysis of a metal transporter. It seems that the main function of NtNRAMP3 is to maintain cross homeostasis of Fe, Mn, Co, Cu, Ni (also Cd) under control conditions, by controlling xylem unloading and transfer of metals to neighboring leaf cells. It seems, however, that it may perform the same function when tobacco is exposed to 200 μM Zn, primarily in the 2nd and 3rd pairs of leaves. Further research is necessary to show the underlying mechanisms of metal status-dependent regulation of *NtNRAMP3* expression in tobacco, and also why the response to high Zn is specific to the 2nd and 3rd pairs of leaves only.

DATA AVAILABILITY STATEMENT

The original contributions presented in the study are included in the article/**Supplementary Material**, further inquiries can be directed to the corresponding author/s.

AUTHOR CONTRIBUTIONS

KK carried out all experiments, performed data analysis, and contributed to writing the manuscript. AP-W contributed to cloning, hydroponic experiments, and expression analysis. MP and AB were involved in the hydroponic experiments and GUS assays. DMA designed the study concept, coordinated the research and supervised experiments, performed data analysis, and wrote the manuscript. All authors read and approved the final version of the manuscript.

FUNDING

This work was financially supported by National Science Center, Poland (grant HARMONIA no. NZ3/00527 to DMA).

ACKNOWLEDGMENTS

We would like to thank Dr. Bohdan Paterczyk (Imaging Laboratory, Faculty of Biology, University of Warsaw, Poland) for the technical and substantive service of the confocal microscope and for taking photographs.

SUPPLEMENTARY MATERIAL

The Supplementary Material for this article can be found online at: https://www.frontiersin.org/articles/10.3389/fpls.2022.867967/full#supplementary-material

REFERENCES

Angelova, V., Ivanov, K., and Ivanova, R. (2004). Effect of chemical forms of lead, cadmium, and zinc in polluted soils on their uptake by tobacco. *J. Plant Nutrit.* 27, 757–773. doi: 10.1081/PLN-120030609

Barabasz, A., Mills, R. F., Trojanowska, E., Williams, L. E., and Antosiewicz, D. M. (2010). Expression of *AtECA3* in tobacco modifies its responses to manganese, zinc and calcium. *Envir. Exp. Bot.* 72, 202–209. doi: 10.1016/j.envexpbot.2011.03.006

Barabasz, A., Palusińska, M., Papierniak, A., Kendziorek, M., Kozak, K., Williams, L. E., et al. (2019). Functional analysis of NtZIP4B and Zn status-dependent expression pattern of tobacco *ZIP* genes. *Front. Plant Sci.* 9, 1984. doi: 10.3389/fpls.2018.01984

Basehoar, A. D., Zanton, S., and Pugh, B. (2004). Identification and distinct regulation of yeast TATA box-containing genes. *Cell* 116, 699–709. doi: 10.1016/S0092-8674(04)00205-3

Baxter, I. (2009). Ionomics: studying the social network of mineral nutrients. *Curr. Opin. Plant Biol.* 12, 381–386. doi: 10.1016/j.pbi.2009.05.002

Bereczky, Z., Wang, H.-Y., Schubert, V., Ganal, M., and Bauer, P. (2003). Differential regulation of *nramp* and *irt1* metal transporter genes in wild type and iron uptake mutants of tomato. *J. Biol. Chem.* 278, 24697–24704. doi: 10.1074/jbc.M301365200

Cailliatte, R., Schikora, A., Briat, J.-F., Mari, S., and Curie, C. (2010). High-affinity manganese uptake by the metal transporter NRAMP1 is essential for *Arabidopsis* growth in low manganese conditions. *Plant Cell* 22, 904–917. doi: 10.1105/tpc.109.073023

Chaloupka, R., Courville, P., Veyrier, F., Knudsen, B., Tompkins, T. A., and Cellier, M. F. (2005). Identification of functional amino acids in the Nramp family by a combination of evolutionary analysis and biophysical studies of metal and proton cotransport *in vivo*. *Biochemistry* 44, 726–733. doi: 10.1021/bi048014v

Chawla, R., and DeMason, D. A. (2004). Molecular expression of PsPIN1, a putative auxin efflux carrier gene from pea (*Pisum sativum* L.). *Plant Growth Regul.* 44, 1–14. doi: 10.1007/s10725-004-2139-9

Che, J., Yamaji, N., and Ma, J. F. (2018). Efficient and flexible uptake system for mineral elements in plants. *New Phytol.* 2019, 1–5. doi: 10.1111/nph.15140

Colangelo, E. P., and Guerinot, M. L. (2006). Put the metal to the petal: metal uptake and transport throughout plants. *Curr. Opin. Plant Sci.* 9, 322–330. doi: 10.1016/j.pbi.2006.03.015

Das, N., Bhattacharya, S., and Maiti, M. K. (2016). Enhanced cadmium accumulation and tolerance in transgenic tobacco overexpressing rice metal tolerance protein gene *OsMTP1* is promising for phytoremediation. *Plant Physiol. Biochem.* 105, 297–309. doi: 10.1016/j.plaphy.2016.04.049

Doroszewska, T., and Berbeć, A. (2004). Variation for cadmium uptake among *Nicotiana* species. *Genet. Res Crop. Evol.* 51, 323–333. doi: 10.1023/B:GRES.0000024018.73632.69

Fink, J. S., Verhave, M., Kasper, S., Tsukada, T., Mandel, G., and Goodman, R. H. (1988). The CGTCA sequence motif is essential for biological activity of the vasoactive intestinal peptide gene cAMP-regulated enhancer. *Proc. Natl. Aacd. Sci. U. S. A.* 85, 6662–6666. doi: 10.1073/pnas.85.18.6662

Frangeul, L., Glaser, P., Rusniok, C., Buchrieser, C., Duchaud, E., Dehoux, P., et al. (2004). CAAT-box, contigs-assembly and annotation tool-box for genome sequencing projects. *Bioinformatics* 20:790–797. doi: 10.1093/bioinformatics/btg490

Gietz, D. R., and Schiestl, R. H. (2007). High-efficiency yeast transformation using the LiAc/SS carrier DNA/PEG method. *Nat. Protoc.* 3, 31–34. doi: 10.1038/nprot.2007.13

Grispen,. V. M. J., Hakvoort, H. W. J., Bliek, M., Verkleij, J. A. C., and Schat, H. (2011). Combined expression of the *Arabidopsis* metallothionein MT2b and the heavy metal transporting ATPase HMA4 enhances cadmium tolerance and the root to shoot translocation of cadmium and zinc in tobacco. *Environ. Exp. Bot.* 72, 71–76. doi: 10.1016/j.envexpbot.2010.01.005

Gunshin, H., Mackenzie, B., Berger, U. V., Gunshin, Y., Romero, M. F., Boron, W. F., et al. (1997). Cloning and characterization of a mammalian proton-coupled metal-ion transporter. *Nature* 388, 482–488. doi: 10.1038/41343

Hiratsuka, K., and Chua, N. H. (1997). Light regulated transcription in higher plants. *J. Plant. Res.* 110, 131–139. doi: 10.1007/BF02506852

Ihnatowicz, A., Siwinska, J., Meharg, A. A., Carey, M., Koornneef, M., Reymond, M. (2014). Conserved histidine of metal transporter AtNRAMP1 is crucial for optimal growth under manganese deficiency at chilling temperatures. *New Phytol.* 202, 1173–1183. doi: 10.1111/nph.12737

Jain, A., Sinilal, B., Dhandapani, G., Meagher, R. B., and Sahi, S. V. (2013). Effects of deficiency and excess of zinc on morphophysiological traits and spatiotemporal regulation of zinc-responsive genes reveal incidence of cross talk between micro- and macronutrients. *Environ. Sci. Technol.* 47, 5327–5335. doi: 10.1021/es400113y

Käll, L., Krogh, A., and Sonnhammer, E. L. L. (2004). A combined transmembrane topology and signal peptide prediction method. *J. Mol. Biol.* 338, 1027–1036. doi: 10.1016/j.jmb.2004.03.016

Kozak, K., Papierniak, A., Barabasz, A., Kendziorek, M., Palusińska, M., Williams, L. E., et al. (2019). NtZIP11, a new Zn transporter specifically upregulated in tobacco leaves by toxic Zn level. *Environ. Exp. Bot.* 157:69–78. doi: 10.1016/j.envexpbot.2018.09.020

Kumar, S., Stecher, G., Li, M., Knyaz, C., and Tamura, K. (2018). MEGA X: molecular evolutionary genetics analysis across computing platforms. *Mol. Biol. Evol.* 35, 1547. doi: 10.1093/molbev/msy096

Lafyatis, R., Denhez, F., Williams, T., Sporn, M., and Roberts, A. (1991). Sequence repeated TCCC motif. *Nucleic Acids Res.* 19, 6419–6425. doi: 10.1093/nar/19.23.6419

Languar, V., Lelièvre, F., Barbier-Brygoo, H., and Thomine, S. (2004). Regulation and function of AtNRAMP4 metal transporter protein. *Soil Sci. Plant Nutrit.* 50, 1141–1150. doi: 10.1080/00380768.2004.10408587

Languar, V., Lelièvre, F., Bolte, S., Hamès, C., Alcon, C., Neumann, D., et al. (2005). Mobilization of vacuolar iron by AtNRAMP3 and AtNRAMP4 is essential for seed germination on low iron. *EMBO J.* 24, 4041–4051. doi: 10.1038/sj.emboj.7600864

Languar, V., Ramos, M. S., Lelièvre, F., Barbier-Brygoo, H., Krieger-Liszkay, A., Krämer, U., et al. (2010). Export of vacuolar manganese by AtNRAMP3 and AtNRAMP4 is required for optimal photosynthesis and growth under manganese deficiency. *Plant Physiol.* 152, 1986–1999. doi: 10.1104/pp.109.150946

Legay, S., Guignard, C., Ziebel, J., and Evers, D. (2012). Iron uptake and homeostasis related genes in potato cultivated *in vitro* under iron deficiency and overload. *Plant Physiol. Biochem.* 60, 180–189. doi: 10.1016/j.plaphy.2012.08.003

Li, J., Wang, Y., Zheng, L., Li, Y., Zhou, X., Li, J., et al. (2019). The intracellular transporter AtNRAMP6 is involved in Fe homeostasis in *Arabidopsis*. *Front. Plant Sci.* 10, 1124. doi: 10.3389/fpls.2019.01124

Li, Y., Zhang, Y., Shi, D., Liu, X., Qin, J., Ge, Q., et al. (2013). Spatial-temporal analysis of zinc homeostasis reveals the response mechanisms to acute zinc deficiency in *Sorghum bicolor*. *New Phytol.* 200, 1102–1115. doi: 10.1111/nph.12434

Livak, K. J., and Schmittgen, T. D. (2001). Analysis of relative gene expression data using real-time quantitative PCR and the $2^{-\Delta\Delta CT}$ method. *Methods* 25, 402–408. doi: 10.1006/meth.2001.1262

Lugon-Moulin, N., Zhang, M., Gadani, F., Rossi, L., Krauss, D., and Wanger, G. J. (2004). Critical review of the science and options for reducing cadmium in tobacco (*Nicotiana tabacum* L.) and other plants. *Adv. Agron.* 83, 111–180. doi: 10.1016/S0065-2113(04)83003-7

Marschner, H. (1995). *Mineral Nutrition of Higher Plants, 2nd Edn*. London: Academic Press.

Milner, K. J., Seamon, J., Craft, E., and Kochian, L. V. (2013). Transport properties of members of the ZIP family in plants and their role in Zn and Mn homeostasis. *J. Exp. Bot.* 64, 369–381. doi: 10.1093/jxb/ers315

Mizuno, T., Usui, K., Horie, K., Nosaka, S., Mizuno, N., Obata, H. (2005). Cloning of three *ZIP/Nramp* transporter genes from a Ni hyperaccumulator plant *Thlaspi japonicum* and their Ni^{2+} transport abilities. *Plant Physiol. Biochem.* 43, 793–801. doi: 10.1016/j.plaphy.2005.07.006

Nevo, Y., and Nelson, N. (2006). The NRAMP family of metal-ion transporters. *Biochim. Biophys. Acta.* 1763, 609–620. doi: 10.1016/j.bbamcr.2006.05.007

Ogo, Y., Kobavashi, T., Itai, R. N., Nakanishi, H., Kakei, Y., Takahashi, M., et al. (2008). A novel NAC transcription factor, IDEF2, that recognizes the iron deficiency-responsive element 2 regulates the genes involved in iron homeostasis in plants. *J. Biol. Chem.* 283, 13407–13417. doi: 10.1074/jbc.M708732200

Omasits, U., Ahrens, C. H., Müller, S., and Wollscheid, B. (2014). Protter: interactive protein feature visualization and integration with experimental proteomic data. *Bioinformatics* 30, 884–886. doi: 10.1093/bioinformatics/btt607

Oomen, R. J. F. J., Wu, J., Lelièvre, F., Blanchet, S., Richaud, P., Barbier-Brygoo, H., et al. (2009). Functional characterization of NRAMP3 and NRAMP4 from the metal hyperaccumulator *Thlaspi caerulescens*. *New Phytol*. 181, 637–650. doi: 10.1111/j.1469-8137.2008.02694.x

Papierniak, A., Kozak, K., Kendziorek, M., Barabasz, A., Palusińska, M., Tiuryn, J., et al. (2018). Contribution of NtZIP1-like to the regulation of Zn homeostasis. *Front. Plant. Sci*. 9, 185. doi: 10.3389/fpls.2018.00185

Papierniak-Wygladala, A., Kozak, K., Barabasz, A., Palusińska, M., Całka, M., Maślińska, K., et al. (2020). Identification and characterization of a tobacco metal tolerance protein, NtMTP2. *Metallomics* 12, 2049–2064. doi: 10.1039/d0mt00210k

Paul, A.-L., and Ferl, R. J. (1991). *In vivo* footprinting reveals unique cis-elements and different modes of hypoxic induction in maize Adh1 and Adh2. *Plant Cell* 3, 159–168. doi: 10.1105/tpc.3.2.159

Peris-Peris, C., Serra-Cardona, A., Sánchez-Sanuy, F., Campo, S., Ariño, J., Segundo, B. S. (2017). Two NRAMP6 isoforms function as iron and manganese transporters and contribute to disease resistance in rice. *MPMI* 30, 385–398. doi: 10.1094/MPMI-01-17-0005-R

Pighin, J. A., Zheng, H., Balakshin, I. J., Goodman, I. P., Western, T. I., Jetter, R., et al. (2014). Plant cuticular lipid export requires an ABC transporter. *Science* 306, 702–704. doi: 10.1126/science.1102331

Pottier, M., Thi, V. A. L., Primard-Brisset, C., Marion, J., Bianchi, M., Victor, C., et al. (2022). Duplication of NRAMP3 gene in poplars generated two homologous transporters with distinct functions. *BioRxiv* doi: 10.1101/2021.12.04.471152

Qin, L., Han, P., Chen, L., Walk, T. C., Li, Y., Hu, X., et al. (2017). Genome-wide identification and expression analysis of NRAMP family genes in soybean (*Glycine max* L.). *Front. Plant Sci*. 8, 1436. doi: 10.3389/fpls.2017.01436

Rehman, M. Z., Rizwan, M., Sohail, M. I., Ali, S., Waris, A. A., Khalid, H., et al. (2019). Opportunities and challenges in the remediation of metal-contaminated soils by using tobacco (*Nicotiana tabacum* L.): a critical review. *Environ. Sci. Pollut. Res*. 26, 18053–18070. doi: 10.1007/s11356-019-05391-9

Ricachenevsky, F. K., Menguer, P. K., Sperotto, R. A., and Fett, J. P. (2015). Got to hide your Zn away: molecular control of Zn accumulation and biotechnological applications. *Plant Sci*. 236, 1–17. doi: 10.1016/j.plantsci.2015.03.009

Sano, T., Yoshihara, T., Handa, K., Sato, M. H., Nagata, T., and Hasezawa, S. (2012). "Metal ion homeostasis mediated by Nramp transporters in plant cells – focused on increased resistance to iron and cadmium ion," in *Crosstalk and Integration of Membrane Trafficking Pathways*, ed R. Weigert (Rijeka: INTECH), 214–228 doi: 10.5772/30905

Sasaki, A., Yamaji, N., Yokosho, K., and Ma, J. F. (2012). Nramp5 is a major transporter responsible for manganese and cadmium uptake in rice. *Plant Cell* 24, 2155–2167. doi: 10.1105/tpc.112.096925

Shen, Q., and Ho, T. H. (1995). Functional dissection of an abscisic acid (ABA)-inducible gene reveals two independent ABA-responsive complexes each containing a G-box and a novel cis-acting element. *Plant Cell* 7, 295–307. doi: 10.1105/tpc.7.3.295

Sibéril, Y., Doireau, P., and Gantet, P. (2001). Plant bZIP G-box binding factors. *Modular structure and activation mechanisms. Eur. J. Biochem*. 268, 5655–5666. doi: 10.1046/j.0014-2956.2001.02552.x

Siemianowski, O., Barabasz, A., Weremczuk, A., Ruszczyńska, A., Bulska, E., Williams, L. E., et al. (2013). Development of Zn-related necrosis in tobacco is enhanced by expressing *AtHMA4* and depends on the apoplastic Zn levels. *Plant Cell Environ*. 36, 1093–1104. doi: 10.1111/pce.12041

Siemianowski, O., Mills, R. F., Williams, L. E., and Antosiewicz, D. M. (2011). Expression of the P1B-type ATPase AtHMA4 in tobacco modifies Zn and Cd root to shoot partitioning and metal tolerance. *Plant Biotechnol. J*. 9, 64–74. doi: 10.1111/j.1467-7652.2010.00531.x

Sierro, N., Battey, J. N. D., Ouadi, S., Bakaher, N., Bovet, L., Willig, A., et al. (2014). The tobacco genome sequence and its comparison with those of tomato and potato. *Nat. Commun*. 5, 3833. doi: 10.1038/ncomms4833

Sierro, N., Battey, J. N. D., Ouadi, S., Bovet, L., Goepfert, S., Bakaher, N., et al. (2013). Reference genomes and transcriptomes of *Nicotiana sylvestris* and *Nicotiana tomentosiformis*. *Genome Biol*. 14, R60. doi: 10.1186/gb-2013-14-6-r60

Sperotto, R. A., Ricachenevsky, F. K., Williams, L. E., Vasconcelos, M. W., and Menguer, P. K. (2014). From soil to seed: micronutrient movement into and within the plant. *Front. Plant Sci*. 5, 438. doi: 10.3389/fpls.2014.00438

Takahashi, R., Ishimaru, Y., Senoura, T., Shimo, H., Ishikawa, S., Arao, T., et al. (2011). The OsNRAMP1 iron transporter is involved in Cd accumulation in rice. *J. Exp. Bot*. 62, 4843–4850. doi: 10.1093/jxb/err136

Tejada-Jiménez, M., Castro-Rodríguez, R., Kryvoruchko, I., Lucas, M. M., Udvardi, M., Imperial, J., et al. (2015). *Medicago truncatula* natural resistance-associated macrophage protein1 is required for iron uptake by rhizobia-infected nodule cells. *Plant Physiol*. 168, 258–272. doi: 10.1104/pp.114.254672

Thomine, S., Lelièvre, F., Debarbieux, E., Schroeder, J. I., and Barbier-Brygoo, H. (2003). AtNRAMP3, a multispecific vacuolar metal transporter involved in plant responses to iron deficiency. *Plant J*. 34, 685–695. doi: 10.1046/j.1365-313X.2003.01760.x

Thomine, S., Wang, R., Ward, J. M., Crawford, N. M., and Schroeder, J. I. (2000). Cadmium and iron transport by members of a plant metal transporter family in *Arabidopsis* with homology to *Nramp* genes. *Proc. Natl. Acad. Sci. U. S. A*. 97, 4991–4996. doi: 10.1073/pnas.97.9.4991

Tian, W., He, G., Qin, L., Li, D., Meng, L., Huang, Y., et al. (2021). Genome-wide analysis of the NRAMP gene family in potato (*Solanum tuberosum*): identification, expression analysis and response to five heavy metal stress. *Ecotoxicol. Environ. Safety*. 208, 111661. doi: 10.1016/j.ecoenv.2020.111661

Tiwari, M., Sharma, D., Dwivedi, S., Singh, M., Tripathi, R. D., Trivedi, P. K. (2014). Expression in *Arabidopsis* and cellular localization reveal involvement of rice NRAMP, OsNRAMP1, in arsenic transport and tolerance. *Plant Cell Environ*. 37, 140–152. doi: 10.1111/pce.12138

Wagner, G. J., and Yeargan, R. (1986). Variation in cadmium accumulation potential and tissue distribution of cadmium in tobacco. *Plant Physiol*. 82:274–279. doi: 10.1104/pp.82.1.274

Wang, N., Qiu, W., Dai, J., Guo, X., Lu, Q., Wang, T., et al. (2019). AhNRAMP1 enhances manganese and zinc uptake in plants. *Front. Plant Sci*. 10, 415. doi: 10.3389/fpls.2019.00415

Weber, M., Harada, E., Vess, C., Roepenack-Lahaye, E., and Clemens, S. (2004). Comparative microarray analysis of *Arabidopsis thaliana* and *Arabidopsis halleri* roots identifies nicotianamine synthase, a ZIP transporter and other genes as potential metal hyperaccumulation factors. *Plant J*. 37, 269–281. doi: 10.1046/j.1365-313X.2003.01960.x

Wei, W., Chai, T., Zhang, Y., Han, L., and Guan, Z. (2009). The *Thlaspi caerulescens* NRAMP homologue TcNRAMP3 is capable of divalent cation transport. *Mol. Biotechnol*. 41, 15–21. doi: 10.1007/s12033-008-9088-x

Weisshaar, B., Block, A., Armstrong, G. A., Herrmann, A., Schulze-Lefert, P., and Hahlbrock, K. (1991). Regulatory elements required for light-mediated expression of the *Petroselinum crispum* chalcone synthase gene. *Symp. Soc. Exp. Biol*. 45, 191–210.

Weremczuk, A., Papierniak, A., Kozak, K., Willats, W. G., and Antosiewicz, D. M. (2020). Contribution of NtZIP1-like, NtZIP11 and a WAK-pectin based mechanism to the formation of Zn-related lesions in tobacco leaves. *Environ. Exp. Bot*. 176, 104074. doi: 10.1016/j.envexpbot.2020.104074

Weremczuk, A., Ruszczyńska, A., Bulska, E., and Antosiewicz, D. M. (2017). NO-dependent programmed cell death is involved in the formation of Zn-related lesions in tobacco leaves. *Metallomics* 9, 924–935. doi: 10.1039/C7MT00076F

Wojas, S., Hennig, J., Plaza, S., Geisler, M., Siemianowski, O., et al. (2009). Ectopic expression of *Arabidopsis* ABC transporter MRP7 modifies cadmium root-to-shoot transport and accumulation. *Environ. Pollut*. 157, 2781–2789. doi: 10.1016/j.envpol.2009.04.024

Xiong, H., Kobayashi, T., Kakei, Y., Senoura, T., Nakazono, M., Nakanishi, H., et al. (2012). *AhNRAMP1* iron transporter is involved in iron acquisition in peanut. *J. Exp. Bot*. 63, 4437–4446. doi: 10.1093/jxb/ers117

Yamaji, N., Sasaki, A., Xia, J. X., Yokosho, K., and Ma, J. F. (2013). A node-based switch for preferential distribution of manganese in rice. *Nat. Commun*. 4, 2442. doi: 10.1038/ncomms3442

Zhang, J., Zhang, M., Song, H., Zhao, J., Shabala, S., Tian, S., et al. (2020). A novel plasma membrane-based NRAMP transporter contributes to Cd and Zn hyperaccumulation in *Sedum alfredii* Hance. *Environ. Exp. Bot.* 176, 104121. doi: 10.1016/j.envexpbot.2020.104121

Zhu, M., Zhang, F., Lv, Z., Shen, Q., Zhang, L., Lu, X., et al. (2014). Characterization of the promoter of *Artemisia annua* amorpha-4, 11-diene synthase (ADS) gene using homologous and heterologous expression as well as deletion analysis. *Plant Mol. Biol. Rep.* 32, 406–418. doi: 10.1007/s11105-013-0656-2

Conflict of Interest: The authors declare that the research was conducted in the absence of any commercial or financial relationships that could be construed as a potential conflict of interest.

Publisher's Note: All claims expressed in this article are solely those of the authors and do not necessarily represent those of their affiliated organizations, or those of the publisher, the editors and the reviewers. Any product that may be evaluated in this article, or claim that may be made by its manufacturer, is not guaranteed or endorsed by the publisher.

frontiers | Frontiers in Plant Science

ORIGINAL RESEARCH
published: 09 June 2022
doi: 10.3389/fpls.2022.878418

Crosstalk Between Iron and Sulfur Homeostasis Networks in *Arabidopsis*

Muhammad Sayyar Khan[1,2†], Qiao Lu[1,3†], Man Cui[1], Hala Rajab[2], Huilan Wu[1], Tuanyao Chai[3] and Hong-Qing Ling[1]**

[1]*The State Key Laboratory of Plant Cell and Chromosome Engineering, National Center for Plant Gene Research (Beijing), Institute of Genetics and Developmental Biology, Chinese Academy of Sciences, Beijing, China,* [2]*Institute of Biotechnology and Genetic Engineering, The University of Agriculture Peshawar, Peshawar, Pakistan,* [3]*College of Life Sciences, University of Chinese Academy of Sciences, Beijing, China*

OPEN ACCESS

Edited by:
Hatem Rouached, Institut National de la Recherche Agronomique (INRA), France

Reviewed by:
David G. Mendoza-Cozatl, University of Missouri, United States
María C. Romero-Puertas, Experimental Station of Zaidín (CSIC), Spain

***Correspondence:**
Tuanyao Chai
tychai@ucas.edu.cn
Hong-Qing Ling
hqling@genetics.ac.cn

†These authors have contributed equally to this work

Specialty section:
This article was submitted to Plant Nutrition, a section of the journal Frontiers in Plant Science

Received: *18 February 2022*
Accepted: *09 May 2022*
Published: *09 June 2022*

Citation:
Khan MS, Lu Q, Cui M, Rajab H, Wu H, Chai T and Ling H-Q (2022) Crosstalk Between Iron and Sulfur Homeostasis Networks in Arabidopsis. Front. Plant Sci. 13:878418. doi: 10.3389/fpls.2022.878418

The widespread deficiency of iron (Fe) and sulfur (S) is becoming a global concern. The underlying mechanisms regulating Fe and S sensing and signaling have not been well understood. We investigated the crosstalk between Fe and S using mutants impaired in Fe homeostasis, sulfate assimilation, and glutathione (GSH) biosynthesis. We showed that chlorosis symptoms induced by Fe deficiency were not directly related to the endogenous GSH levels. We found dynamic crosstalk between Fe and S networks and more interestingly observed that the upregulated expression of *IRT1* and *FRO2* under S deficiency in Col-0 was missing in the *cad2-1* mutant background, which suggests that under S deficiency, the expression of *IRT1* and *FRO2* was directly or indirectly dependent on GSH. Interestingly, the bottleneck in sulfite reduction led to a constitutively higher *IRT1* expression in the *sir1-1* mutant. While the high-affinity sulfate transporter (*Sultr1;2*) was upregulated under Fe deficiency in the roots, the low-affinity sulfate transporters (*Sultr2;1,* and *Sultr2;2*) were down-regulated in the shoots of Col-0 seedlings. Moreover, the expression analysis of some of the key players in the Fe–S cluster assembly revealed that the expression of the so-called Fe donor in mitochondria (*AtFH*) and S mobilizer of group II cysteine desulfurase in plastids (*AtNFS2*) were upregulated under Fe deficiency in Col-0. Our qPCR data and ChIP-qPCR experiments suggested that the expression of *AtFH* is likely under the transcriptional regulation of the central transcription factor *FIT.*

Keywords: iron, sulfur, crosstalk, homeostasis, *Arabidopsis*

INTRODUCTION

Iron (Fe) and sulfur (S) are essential nutrients for plants. Plant responses to the limited supply of S or Fe have been extensively investigated with different experimental approaches (Lewandowska and Sirko, 2008; Watanabe et al., 2010). Since both of them are closely linked, the deficiency of one nutrient is supposed to regulate the uptake and availability of the other (Forieri et al., 2013; Zuchi et al., 2015). Therefore, the crosstalk between Fe and S has sparked interest. S deficiency has become a major concern in plant nutrition in recent years, especially due to decreased emission of SO_2 and lower S supply through mineral fertilization (McGrath et al.,

2003). The responses of the plants to the S deficiency have been well documented in numerous studies (Hirai et al., 2003; Nikiforova et al., 2005; Watanabe et al., 2010). However, the mechanisms governing Fe and S sensing/signaling are far from being well understood. In contrast to soils that are depleted in S, Fe is abundant in soil, but its availability is very poor due to its insolubility in the soil matrix. Most of the studies aiming to elucidate Fe or S deficiency responses in plants were mainly focused on a single nutrient deficiency in *Arabidopsis* with few exceptions (Zuchi et al., 2009, 2015; Pii et al., 2015). However, in an agroecosystem, plants are likely subjected to the simultaneous deficiency of both nutrients, and it is reasonable to assume that the simultaneous limitation of the two nutrients may trigger responses quite distinct from those triggered by the individual limitations of the two nutrients. For example, earlier reports have shown that Fe deficiency induced more ethylene production in tomato roots, but this did not take place under dual starvation of Fe and S (Zuchi et al., 2009), suggesting that S deficiency alters the typical Fe deficiency responses in tomato (Zuchi et al., 2015). Other reports have demonstrated that the availability of S influences Fe uptake and that Fe deficiency results in modulation of S uptake and assimilation (Zuchi et al., 2009, 2015; Forieri et al., 2013). Since most of the metabolically active Fe is mainly conjugated with S to form Fe–S clusters, the provision of substrates (i.e., chelated Fe and reduced S in the form of cysteine) must be tightly regulated to meet the changing demands of plants for the assembly of Fe–S clusters and to avoid potentially toxic free Fe and sulfide (Forieri et al., 2013).

Recently, the correlation of an essential S-containing compound named glutathione (GSH) with tolerance to Fe has been demonstrated in *Arabidopsis* (Shanmugam et al., 2015). The GSH-deficient mutant *zir1* showed sensitivity to Fe limitation, whereas overexpression of *GSH* increased tolerance to Fe deficiency. These findings suggest that GSH plays an essential role in Fe-limited conditions. Moreover, this study further demonstrated that GSH-deficient mutants accumulated lower levels of Fe under Fe-limited conditions compared to wild-type plants. Interestingly, significantly higher Fe translocation from roots to shoots has been reported in GSH-overproduced *Brassica napus* lines. This study implied that GSH overproduction *via* the overexpression of the key primary S metabolism-related genes may be a biotechnological means to increase Fe in plants (Rajab et al., 2020).

There is accumulating evidence to support that Fe and S do interact with each other and that the deficiency of one nutrient may affect the uptake and availability of the other. Moreover, plants exposed to the simultaneous deficiency of S and Fe in different agroecosystems may trigger more complex responses. It is, therefore, imperative not only to understand the impact of deficiency of one nutrient over the other but also to understand how plants react to dual Fe and S deficiency. The present work aimed to study the crosstalk between Fe and S in terms of individual and dual nutrient deficiencies *via* various molecular and experimental approaches using *Arabidopsis* mutants impaired in Fe homeostasis, sulfite reduction, and GSH biosynthesis.

MATERIALS AND METHODS

Plant Material

The seeds of *Arabidopsis* mutant impaired in Fe homeostasis (*fit1-2*), sulfite reduction (*sir1-1*), and GSH biosynthesis (*cad2-1,* and *sir1-1X cad2-1*) were surface sterilized with 10% commercial bleach solution containing 0.1% Triton-X 100 for 15 min and then washed with sterile water 3–4 times. After 3 days of cold stratification at 4°C, the seeds were plated on solidified half-strength Murashige and Skoog (MS) medium plates consisting of 2.165 g/l MS basal salt mixture (PhytoTech United States), 0.5 g/l MES, 2% sucrose, 1% agar, pH 5.8. The seedlings were grown at 22°C under long-day conditions (16 h light and 8 h dark) for 7 days. 7-day-old seedlings were then used for further analysis.

Treatments of Fe and S Deficiency Stress

One-week old seedlings were transferred to half-strength MS medium with Fe and S (1/2MS + Fe + S), without Fe supply (1/2MS-Fe + S), without S supply (1/2MS + Fe-S), and without Fe and S supply (1/2MS-Fe-S) and cultivated for 4 days at 22°C under long-day conditions (16 h light and 8 h dark). The performance of the wild type (Col-0) and mutant lines under deficient conditions of nutrients were judged by documenting their phenotypes with the help of a digital camera.

Chlorophyll Measurement

One-week-old seedlings of Col-0, *fit1-2*, *sir1-1*, *cad2-1*, and *s1c2* grown on 1/2 MS were transferred to treatment plates for another 4 days. All shoots were collected, and fresh weights were determined. Chlorophyll was extracted in 10 ml of 90% acetone in the dark at room temperature. The supernatant was subjected to spectrophotometry at 647 and 664 nm. The total chlorophyll content was calculated as described previously (Jeffrey and Humphrey, 1975).

Root Length Measurement

One-week-old seedlings of Col-0, *fit1-2*, *sir1-1*, *cad2-1*, and *s1c2* grown on 1/2 MS were transferred to treatment plates for another 4 days and photographs were taken. Root length of seedlings was measured by Image J. For each experiment, at least 10 seedlings were measured for each repeat. Mean values of the three independent experiments were given.

RNA Extraction and Quantitative Real-Time PCR

Total RNA was extracted using TRIzol Reagent (Invitrogen, United States) and treated with DNase I (Ambion, United States) to eliminate genomic DNA contamination. Revert Aid First Strand cDNA Synthesis kit (Thermo Scientific, United States) was used to synthesize first-strand cDNA from total RNA. Gene expression analysis was performed on the roots and shoots of the seedlings exposed to individual and dual Fe and S stress for 4 days. Quantitative real-time PCR was performed on a LightCycler480 machine (Roche Diagnostics, Switzerland) with the gene-specific primers (**Supplementary Table S1**) and

SYBR Premix Ex Taq polymerase (Takara, Japan). The relative expression levels of genes were calculated by the $2^{-\Delta(\Delta Ct)}$ method using AtGADPH expression as a standard.

Chromatin Immunoprecipitation Assay

For quantitative Chromatin Immunoprecipitation (ChIP)-PCR assays, the roots of 35S:FIT-GFP (expressing the fusion protein FIT-GFP in wild type Col-0) were harvested after growing on half-strength MS agar plates without iron supply for 7 d. ChIP was performed as described by Bowler et al. (2004). The antibody against GFP was used to immunoprecipitate DNA/protein complexes from the chromatin preparation. DNA precipitated from the complexes was recovered, purified, and analyzed using the multiple-quantitative ChIP-PCR method, as described by Fan et al. (2014). The primers were designed to amplify fragments of 140–390 bp within the promoter region of genes and are provided in **Supplementary Table S1**.

Statistical Analysis

The statistics for the experimental data was performed using GraphPad Prism 8.0.1. The data were analyzed by two Way Repeated Measures Analysis of Variance (Two-Way ANOVA) followed by the Dunnett's test for the comparisons of all groups with the Col-0 control group.

RESULTS

Effect of Fe and S Deficiency Stress on the Phenotype of Seedlings

The physiological responses of GSH-deficient mutants *zir1*, *cad2-1*, and *pad2-1* under Fe-deficient conditions have been previously reported (Shanmugam et al., 2015). These findings suggested that *zir1*, *cad2-1*, and *pad2-1* mutants were more sensitive to Fe deficiency, and the endogenous levels of GSH in these mutants were associated with the Fe-sensitive phenotypes under Fe deficiency. To further investigate the association of steady-state levels of GSH with sensitivity to Fe limitation and its possible crosstalk with S metabolism, we used Fe-homeostasis related mutant *fit1-2* and mutant impaired in sulfite reduction *sir1-1* (Khan et al., 2010) along with *cad2-1* (Cobbett et al., 1998), and the double mutant *sir1-1Xcad2-1* (Speiser et al., 2018) in our study. The double mutant *sir1-1Xcad2-1* will be hereafter referred to as *s1c2*. It should be noted that despite severe sulfite reduction, the steady-state levels of GSH in the *sir1-1* mutants were still similar to Col-0 (Khan et al., 2010). After 4 days of exposure to Fe-deficient conditions, *sir1-1* and *s1c2* showed more chlorosis compared with Col-0 (**Figures 1B,D**). The *cad2-1* mutant, which has 39% of the wild-type level of GSH, also looked paler than that of Col-0, but the extent of chlorosis was lower compared to *s1c2*. Similarly, exposure of the seedlings to S-deficient conditions for 4 days led to a significant reduction in the overall growth of all the lines, including Col-0 (**Figures 1C,E**). However, the seedlings of all the mutants including Col-0 looked greener, compared to the seedlings growing on the Fe-deficient media.

Direct germination of seeds on Fe-deficient media for 2 weeks revealed an obvious Fe-sensitive phenotype for *sir1-1* and *s1c2* compared to Col-0 (**Supplementary Figure S1**). The *cad2-1* mutant did not exhibit such Fe-sensitive phenotype. The *s1c2* mutant was more chlorotic compared to *sir1-1*. The chlorosis became more and more pronounced over time under Fe-deficient conditions.

Expression Analysis of the Fe-Homeostasis Related Genes in the Roots of *Arabidopsis*

In strategy-I plants like *Arabidopsis,* the Fe-regulated metal transporter (*IRT1*) and ferric chelate reductase (*FRO2*) are induced in the root epidermal cells in response to Fe deficiency (Connolly and Guerinot, 2002; Connolly et al., 2003; Schmidt, 2003), partly under the transcriptional regulation of the basic helix–loop–helix transcription factor FER-LIKE IRON DEFICIENCY-INDUCED FACTOR (FIT; Bauer et al., 2007). FIT is a central transcription factor and is itself upregulated by Fe deficiency (Colangelo and Guerinot, 2004; Yuan et al., 2005). In addition to Fe limitation, we analyzed the expression of the genes related to Fe uptake under dual (Fe and S) and individual (S) nutrient limitations. Apart from Fe deficiency, S deficiency also upregulated the expression of *IRT1* in Col-0 (**Figure 2A**). Quite remarkably, the limitation of sulfate assimilation due to the lack of sulfite reduction in *sir1-1* mutant (Khan et al., 2010) constantly activated *IRT1* expression. Interestingly, the upregulated expression of *IRT1* under S deficiency was directly or indirectly dependent on GSH because the upregulated expression of *IRT1* disappeared in the *cad2-1* mutant.

Just like *IRT1*, the expression of *FRO2* was induced under S deficiency in addition to Fe limitation in Col-0 (**Figure 2B**). However, unlike *IRT1*, the lack of sulfite reduction in *sir1-1* mutant did not constantly activate *FRO2* expression. Moreover, the disappearance of upregulated *FRO2* expression under S deficiency in *sir1-1*, *cad2-1,* and *s1c2* suggested that the expression of *FRO2* was also directly or indirectly dependent on *GSH1* and/or *SIR*. Under sole Fe and combined Fe and S deficiency, the expression of *FIT* and one of its activating partners called basic helix–loop–helix protein *bHLH38* was induced in all lines (**Figures 2C,D**). However, unlike *IRT1* and *FRO2*, the expression of *FIT* and *bHLH38* did not change under S deficiency in Col-0. Under the dual deficiency of Fe and S, the expression levels of *IRT1*, *FRO2*, *FIT*, and *bHLH38* were statistically similar to those observed under Fe deficiency.

As a major chelator of ferrous ions, nicotianamine (NA) plays a critical role in long-distance transport of Fe and transfer within the cell. The induction of two *nicotianamine synthetase* genes, *NAS1*, and *NAS2*, under Fe-starved conditions in *Arabidopsis* has already been reported (Kim et al., 2005; Klatte et al., 2009). In addition to Fe deficiency, we analyzed the expression of *NAS1* and *NAS2* in response to S deficiency and dual Fe and S deficiency. The expression of *NAS1* was induced by Fe deficiency in wild type and all mutants (**Figure 2E**). In response to S deficiency, the expression of *NAS1* was 1.9-fold higher in Col-0

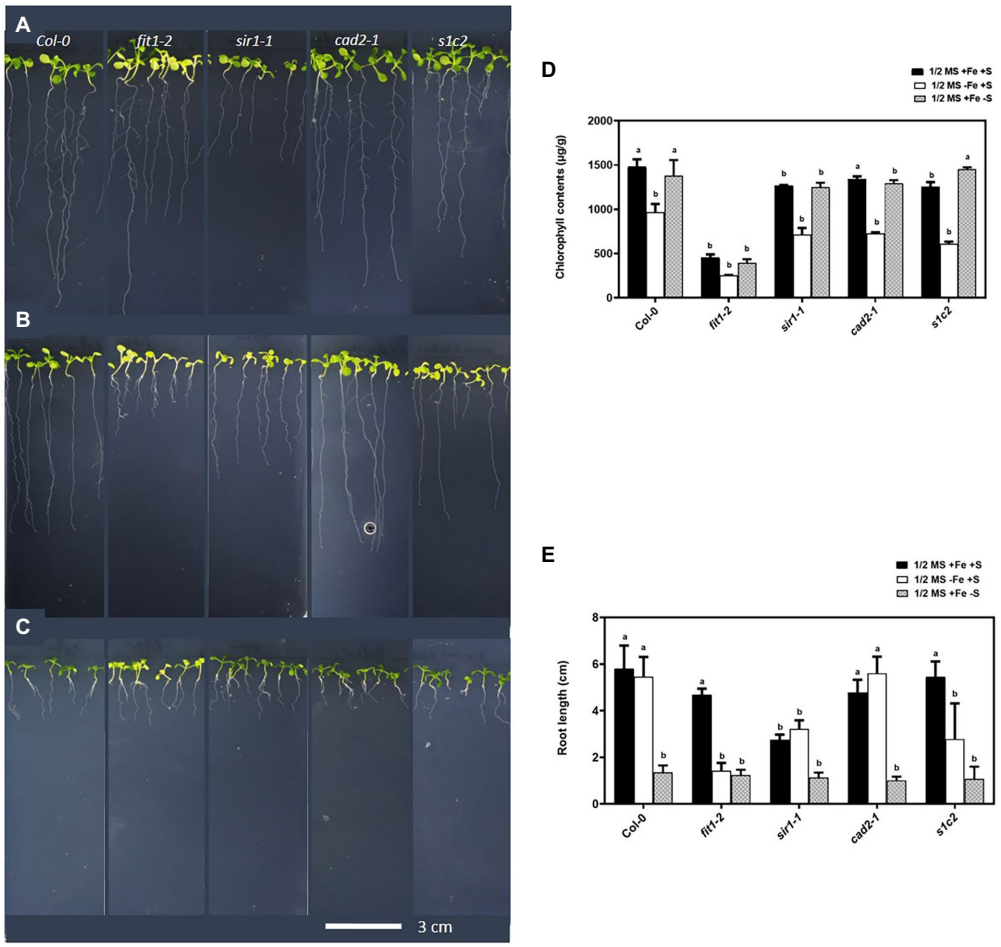

FIGURE 1 | Phenotype of *Arabidopsis* seedlings exposed to Fe and S starvation. Top view of the 1-week old seedlings transferred to: **(A)** half-strength MS medium (1/2 MS), **(B)** 1/2 MS − Fe, **(C)** 1/2 MS − S for 4 days under long-day conditions. **(D)** Chlorophyll contents, **(E)** root length. Letters indicate the statistically significant differences between the wild type (Col-0) on ½ MS + Fe + S with the other treatments in Col-0 and mutants, determined with the two-way ANOVA test followed by Dunnett's test ($p < 0.05$, $n = 3$).

compared to control conditions. However, in the mutant backgrounds, S deficiency did not cause any differential regulations of *NAS1* except *cad2-1*. Moreover, compared to individual Fe deficiency, dual starvation of Fe and S did not have any overriding effect on the expression of *NAS1* gene in the roots. Under normal growth conditions, the expression of *NAS2* gene was 2.1-fold, 1.9-fold, and 3.3-fold higher in *fit1-2*, *sir1-1*, and *cad2-1* mutant than that of Col-0, respectively (**Figure 2F**). In response to Fe deficiency, *NAS2* was highly upregulated in Col-0 and all mutants except *fit1-2*. Interestingly, in response to Fe starvation, the upregulation was 2.1-fold and 3.4-fold higher in *sir1-1* and *cad2-1* mutant, respectively, compared with Col-0. S starvation did not have any effect on the expression of *NAS2* gene in all the tested lines. Moreover, in the case of dual nutrient starvation, the expression pattern of *NAS2* for all the lines was not significantly different compared to those observed under Fe starvation alone.

Fe homeostasis is tightly regulated to maintain the optimal Fe level in plants. *Arabidopsis* FERRIC REDUCTASE DEFECTIVE 3 (FRD3) is an important component of the iron homeostasis (Rogers and Guerinot, 2002; Green and Rogers, 2004). Although the transcript level of *FRD3* is only slightly regulated in response to Fe status (Rogers and Guerinot, 2002), we observed a significant accumulation of *FRD3* transcripts in the roots of all mutants compared to Col-0, under the conditions of Fe deficiency (**Figure 2G**). Remarkably, the lack of sulfite reduction in *sir1-1* and mutation in *GSH1* allele in *cad2-1* mutant constantly upregulated the expression of *FRD3* under nonstress conditions. In response to S starvation, a tendency of downregulation was observed in the transcript levels of *FRD3* in wild type and all mutant lines, compared to their respective normal growth conditions. Moreover, under dual Fe and S starvation, the expression of *FRD3* was significantly low in *fit1-2* and *sir1-1* mutants compared to their respective Fe starved conditions.

Expression Analysis of Sulfate Transporter Genes

Expression patterns of the sulfate transporter genes from group 1 and group 2 were evaluated (**Figure 3**). The high-affinity sulfate transporter (*AtSULTR1;2*) is expressed predominately in roots

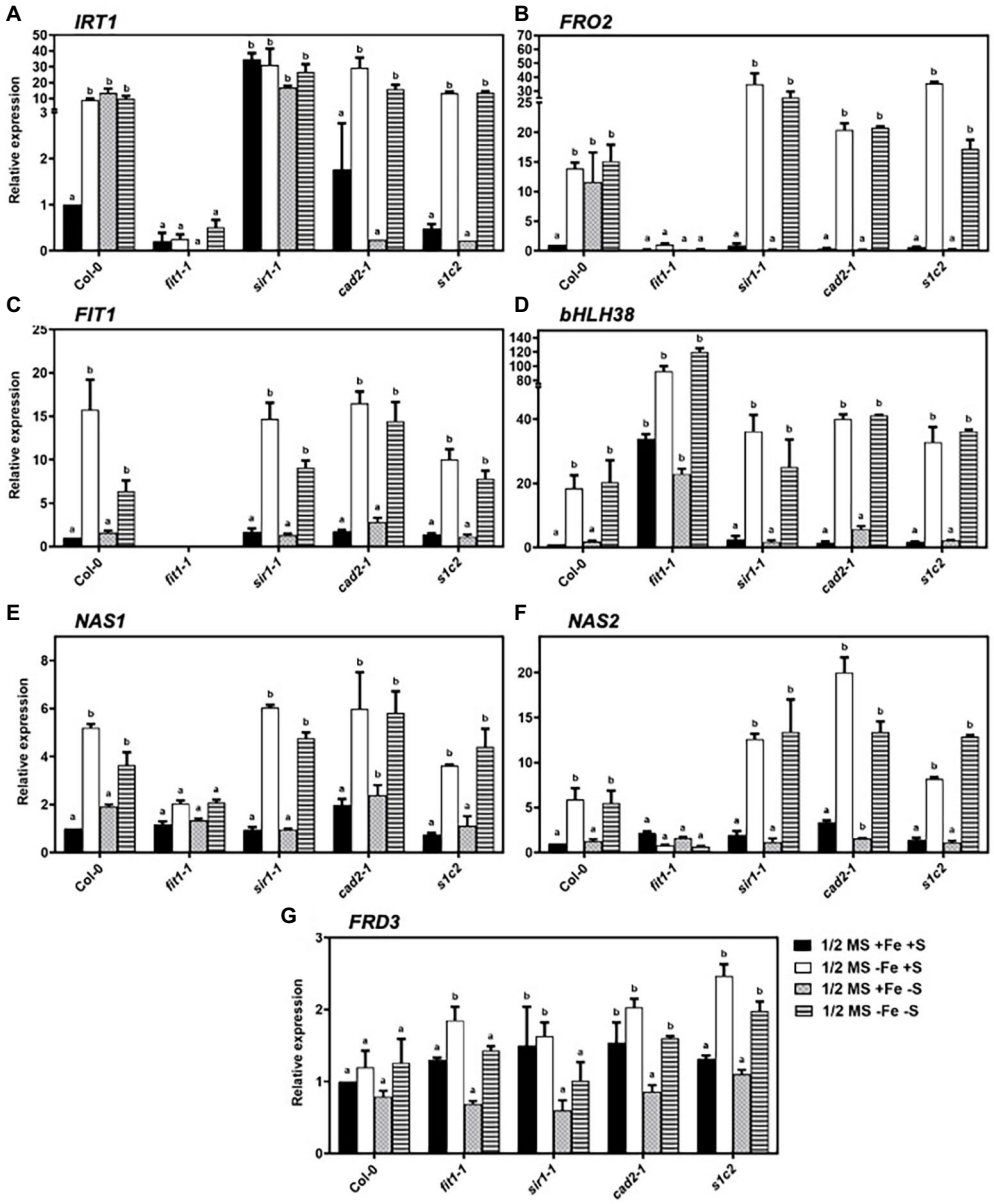

FIGURE 2 | Expression profiles of the genes related to iron-homeostasis in *Arabidopsis* roots. Relative expression by quantitative RT-PCR of *IRT1* **(A)**, *FRO2* **(B)**, *FIT* **(C)**, *bHLH38* **(D)**, *NAS1* **(E)**, *NAS2* **(F)**, and *FRD3* **(G)** in the roots of *Arabidopsis* wild type (Col-0), *fit1-2*, *sir1-1*, *cad2-1*, and *s1c2* lines of 1-week old seedlings exposed to half-strength MS medium (1/2 MS + Fe + S), Fe-deficient (1/2 MS − Fe + S), S-deficient (1/2 MS + Fe − S), and Fe and S-deficient (1/2 MS − Fe − S) media for 4 days under long-day conditions. The *y*-axis shows RNA levels normalized to that of *GADPH*. **(A–G)** Letters indicate the statistically significant differences between the wild type (Col-0) on ½ MS + Fe + S with the other treatments in Col-0 and mutants, determined with the two-way ANOVA test followed by Dunnett's test ($p < 0.05$, $n = 3$). Bars represent means ± SD.

and is responsible for the uptake of sulfate from soil solution into the root cells (Shibagaki et al., 2002; Yoshimoto et al., 2002). In response to Fe and S deficiency, the transcript of *sultr1;2* was 4.6-fold and 3-fold higher than that of Col-0 under the normal growth conditions, respectively (**Figure 3A**). In the *fit1-2* mutant, the expression of *AtSULTR1;2* tended to be higher than that of Col-0 under normal growth conditions. Interestingly, the upregulated expression of *AtSULTR1;2* under Fe deficiency was directly or indirectly dependent on *FIT* and *GSH1* because the upregulated expression of *AtSULTR1;2* disappeared in *fit1-2* and *cad2-1*. In the *cad2-1* mutant, *AtSULTR1;2* was significantly upregulated in response to dual nutrient starvation, but remained unchanged under the imposition of sole Fe or S starvation. The low-affinity sulfate transporters of group 2 are responsible for the translocation of sulfate within the plant. *AtSULTR1;2* and *AtSULTR2;2* are expressed throughout the plant in vascular tissues (Buchner et al., 2004). The expression of *AtSULTR1;2* was significantly downregulated under the sole

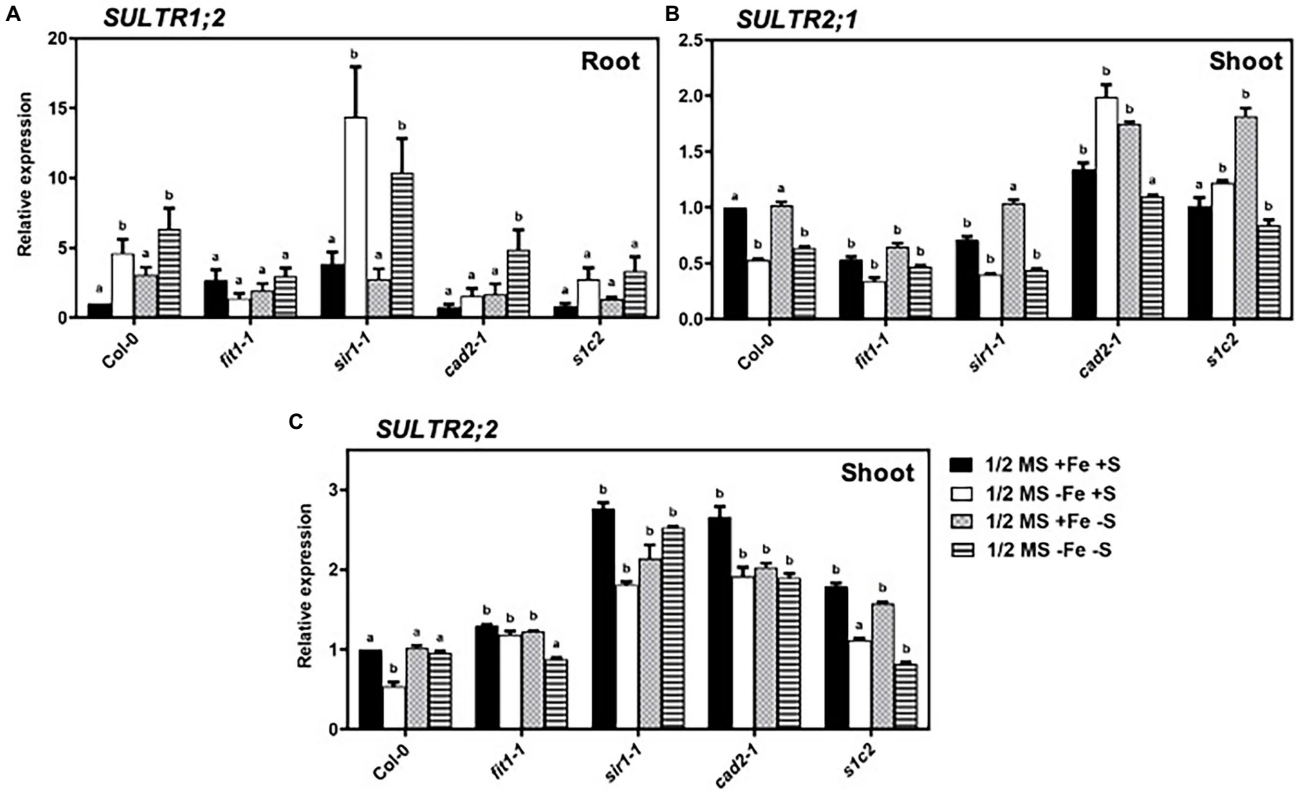

FIGURE 3 | Expression profiles of sulfate transporter genes in *Arabidopsis*. Relative expression by Quantitative RT-PCR of the genes: **(A)** *SULTR1;2* in roots, **(B)** *SULTR2;1* in shoots, **(C)** *SULTR2;2* for *Arabidopsis* wild type (Col-0), *fit1-2*, *sir1-1*, *cad2-1*, and *s1c2* lines of 1-week old seedlings exposed to half-strength MS medium (1/2 MS + Fe + S), Fe-deficient (1/2 MS − Fe + S), S-deficient (1/2 MS + Fe − S), and Fe and S-deficient (1/2 MS − Fe − S) media for 4 days under long-day conditions. The *y*-axis shows RNA levels normalized to that of *GADPH*. **(A–C)** Letters indicate the statistically significant differences between the wild type (Col-0) on ½ MS + Fe + S with the other treatments in Col-0 and mutants determined with the two-way ANOVA test followed by Dunnett's test ($p < 0.05$, $n = 3$). Bars represent means ± SD.

Fe deficiency in the shoots of Col-0, and *sir1-1* (**Figure 3B**). However, contrary to the downregulated expression of *AtSULTR2;1* under Fe deficiency in Col-0, and *sir1-1*, the expression of *AtSULTR2;1* was rather significantly upregulated under Fe deficiency in the GSH-deficient *cad2-1*and *s1c2* mutants. It is noteworthy to mention that the lack of *FIT* in the *fit1-2* mutant, constantly downregulated the expression of *AtSULTR2;1*, irrespective of the nutrient status. Moreover, the expression of *AtSULTR2;1* remained unchanged in response to 4 days of S starvation in Col-0. Dual nutrient limitations triggered quite distinct and opposite responses compared to those observed under sole Fe or S deficiency in GSH-deficient mutants. The expression of *AtSULTR2;2* was significantly downregulated only in response to sole Fe deficiency but remained unchanged in response to 4 days of S or dual nutrient starvation in the shoots of Col-0. Strikingly, contrary to the expression of *AtSULTR2;1*, the lack of *FIT* in the *fit1-2* mutant constantly activated the expression of *AtSULTR2;2* under all experimental conditions except dual nutrient limitations (**Figure 3C**). Similarly, bottleneck in assimilatory sulfate reduction and GSH biosynthesis constantly activated the expression of *AtSULTR2;2* in the *sir1-1* and *cad2-1*mutant. The expression of *AtSULTR2;2* was maintained at a significantly higher level in *s1c2* mutant irrespective of the S status. However, its expression was downregulated under dual nutrient limitation, compared to Col-0.

Expression Profiles of the Genes Related to Fe–S Cluster Biosynthesis in *Arabidopsis*

CyaY/frataxin (annotated as *AtFH* in *Arabidopsis*) is an essential component for Fe–S cluster biosynthesis (Lill and Mühlenhoff, 2008; Stemmler et al., 2010), and plays a central role in regulating Fe homeostasis in mitochondria (Radisky et al., 1999; Bulteau et al., 2004). CyaY functions as Fe donor in the assembly of Fe–S (Klinge et al., 2007; Jain et al., 2014). The expression of *CyaY/AtFH* was induced by Fe and dual Fe and S deficiency in the roots of all lines (**Figure 4A**). However, the upregulated expression of *CyaY/AtFH* under Fe and dual Fe and S deficiency was directly or indirectly dependent on *FIT* because the upregulated expression of *CyaY/AtFH* disappeared in the *fit1-2* mutant. To further check the role of *FIT* in the regulation of *CyaY/AtFH* expression, we analyzed the expression profiles of *CyaY/AtFH* in the double overexpressor of *FIT* and its activating

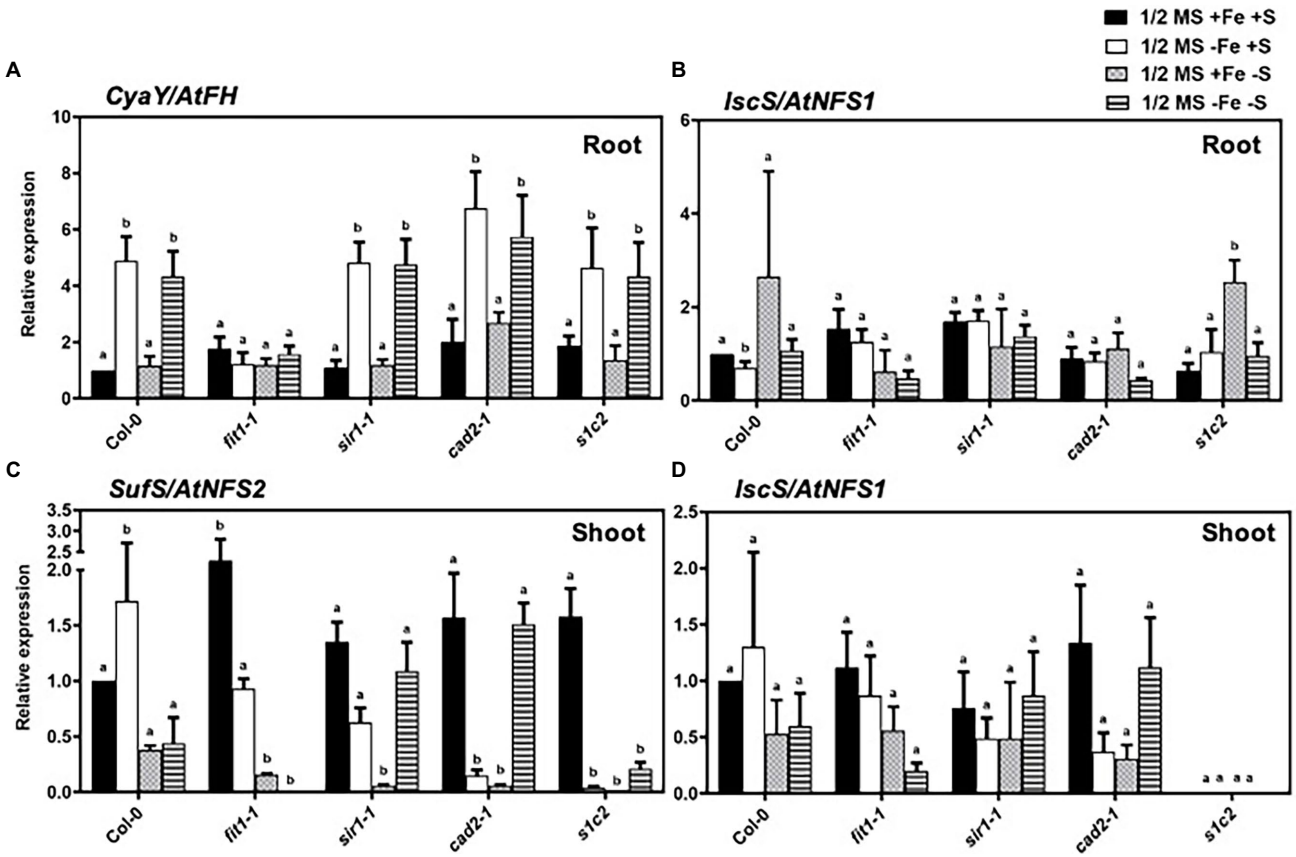

FIGURE 4 | Expression profiles of the genes related to Fe–S cluster biosynthesis in *Arabidopsis*. Relative expression by Quantitative RT-PCR of the genes: **(A)** CyaY/*frataxin* in roots, **(B)** *IscS/NFS1* in roots, **(C)** *SufS/NFS2* in shoots and **(D)** *IscS/NFS1* in shoots, for *Arabidopsis* the wild type (Col-0), *fit1-2*, *sir1-1*, *cad2-1*, and *s1c2* lines of 1-week old seedlings exposed onto half-strength MS medium (1/2 MS + Fe + S), Fe-deficient (1/2 MS − Fe + S), S-deficient (1/2 MS + Fe − S) and Fe and S-deficient (1/2 MS − Fe − S) media for 4 days under long-day conditions. The *y*-axis shows RNA levels normalized to that of *GADPH*. **(A–D)** Letters indicate the statistically significant differences between the wild type (Col-0) on ½ MS + Fe + S with the other treatments in Col-0 and mutants determined with the two-way ANOVA test followed by Dunnett's test ($p < 0.05$, $n = 3$). Bars represent means ± SD.

partner *bHLH38* (i.e., *OxFITXOXbHLH38*). *CyaY/AtFH* was constitutively overexpressed in the *OxFITXOXbHLH38* under nonstress conditions (**Supplementary Figure S2**). These experiments indicated that FIT might initiate *AtFH* expression through directly binding its promoter. We then performed ChIP-qPCR experiments to determine whether FIT directly interacts with the promoters of *AtFH*. Our ChIP-qPCR results support the *in vivo* binding of FIT to the promoters of *AtFH* (**Figure 5**). The deficiency of S alone did not cause any significant change in the expression *CyaY* in all the lines. In *Escherichia coli,* ISC and SUF are the two [Fe–S] biosynthesis systems. The group I cysteine desulfurase IscS (annotated as AtNFS1 in *Arabidopsis*) mobilizes S from cysteine in mitochondria for the biosynthesis of Fe–S clusters. The expression of *AtNFS1* did not change in response to sole Fe or S and dual deficiency of Fe and S in the shoots of all lines (**Figure 4D**). However, in the roots S deficiency did cause a significant upregulation of *AtNFS1* expression in *s1c2* mutant (**Figure 4B**). SufS (also annotated as AtNFS2 in *Arabidopsis*) is a group II cysteine desulfurase and is homologous to IscS/AtNFS1 in the plastids. The expression of *AtNFS2* was upregulated in the shoots of Col-0 under Fe deficiency (**Figure 4C**). The imposition of sole S starvation downregulated its expression in the shoots of all tested mutants compared to Col-0. It is noteworthy that in the GSH-deficient mutants (i.e., *cad2-1* and *s1c2*), sole Fe deficiency also significantly reduced its expression. Strikingly, in the *fit1-2* mutant, the expression of *AtNFS2* was upregulated under nonstress conditions.

DISCUSSION

The crosstalk between Fe and S at the physiological and molecular level has been documented in some early studies in different members of strategy I (Zuchi et al., 2009, 2015; Forieri et al., 2013, 2017; Muneer et al., 2014; Paolacci et al., 2014; Vigani et al., 2018) and strategy II plants (Astolfi et al., 2010; Ciaffi et al., 2013; Zamboni et al., 2017). The biogenesis of the Fe–S clusters is the best example of the interaction between Fe and S. The provision of reactive and potentially

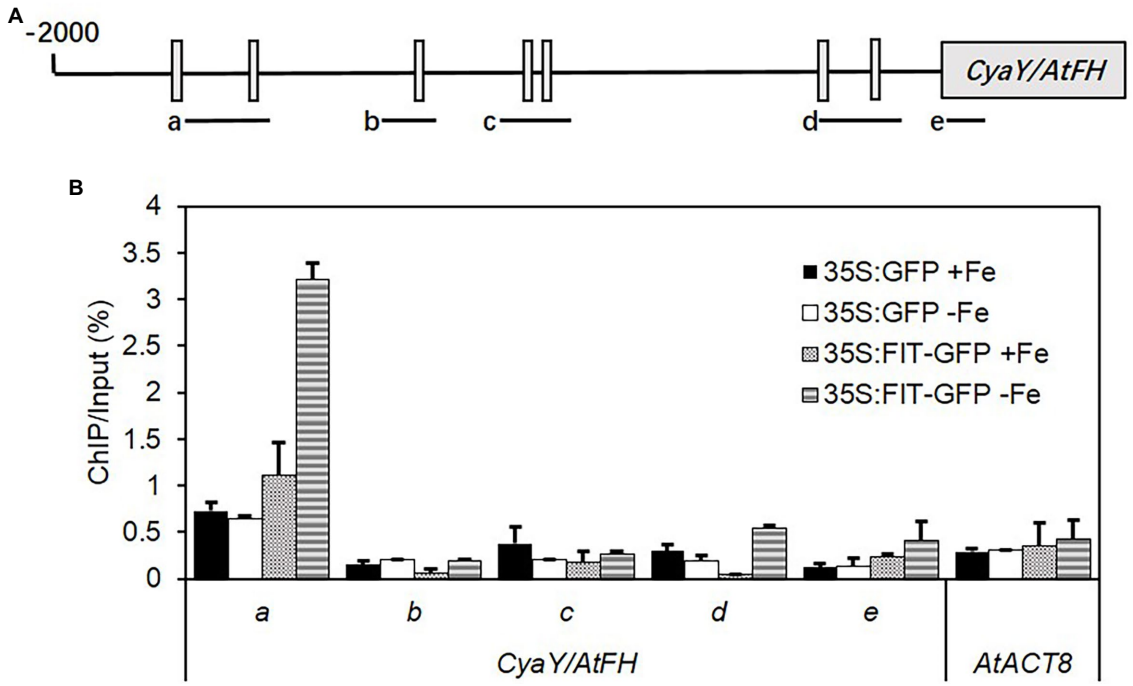

FIGURE 5 | ChIP-qPCR analysis of the binding of FIT to the promoter of *AtFH*. Chromatin was extracted from 35S:FIT-GFP and 35S:GFP seedlings after administration of low iron stress for 7 days, and then precipitated using anti-GFP antibody. Precipitated DNA was amplified with primers corresponding to the different sequence regions of the *AtFH* promoters. **(A)** The ChIP signal obtained from multiple-quantitative ChIP-PCR was quantified as the percentage of total input DNA. **(B)** Three biological replicates were performed. Standard deviations were calculated from three technical repeats. Letters a–d indicate the amplified fragments from the promoter region of *AtFH*, respectively. ACTIN8 was used as a negative control.

toxic components (Fe^{2+} and S^{2-}) in defined stoichiometric ratios for the Fe–S clusters biogenesis requires a strict and multi-level control for their balanced acquisition and distribution within the plant to prevent toxicity. Growing evidence in recent years suggests dynamic crosstalk between Fe and S networks. To understand plant responses to the individual (Fe or S) and combined (Fe and S) nutrients limitations at the physiological and molecular level, we exposed *Arabidopsis thaliana* in wild type and different mutant backgrounds for 4 days to Fe, S, or combined Fe and S deficiencies. We observed that the GSH-deficient double mutant (*s1c2*) was highly sensitive to Fe deficiency compared to Col-0, *cad2-1,* and *sir1-1* mutants (**Figure 1**). The association of the endogenous GSH with tolerance to Fe deficiency has been suggested recently (Shanmugam et al., 2015). The GSH-deficient mutant *zir1,* which has about 15% of the wild-type GSH levels, was more sensitive to Fe deficiency compared to *pad2* (21% of the wild-type GSH levels), *cad2* (39% of the wild-type GSH levels), and Col-0 (Shanmugam et al., 2015). Since the GSH steady-state level of *s1c2* is indistinguishable from that of *cad2-1* (Speiser et al., 2018), the higher sensitivity of *s1c2*, compared to *cad2-1*, under Fe deficiency suggests that the Fe sensitive phenotype is not solely dependent on lower GSH contents as assumed earlier (Shanmugam et al., 2015). This is further supported by the observation, that despite the significantly higher GSH levels (Speiser et al., 2018), the *sir1-1* mutant was even slightly more sensitive than *cad2-1* (**Figure 1**; **Supplementary Figure S1**). The sensitivity of the GSH-deficient mutant under Fe limitation is therefore intriguing and is not solely dependent on the endogenous level of total GSH or the amount of soluble protein-bound S, as the amount of soluble protein-bound S in the *s1c2* was significantly higher than *sir1-1* but lower than *cad2-1* under normal growth conditions (Speiser et al., 2018). Although other possibilities could not be ruled out, the sensitivity of *s1c2* could partially be linked to the more oxidized state of GSH in the plastids of *s1c2* compared to *cad2-1*, *sir1-1,* and Col-0 as demonstrated in the same study. Alternatively, all these factors (i.e., redox state of GSH in plastids, amount of soluble protein-bound S, and endogenous level of total GSH) may have an overall additive effect in modulating plant responses under Fe limited conditions.

We also observed that irrespective of the mutant background, the growth of seedlings was negatively affected under S deprivation, but they all looked greener compared to the seedlings grown under Fe deficiency. The latter observation is not in agreement with the previous studies reporting that S deficiency induces chlorosis in strategy II plant species (Ciaffi et al., 2013; Zamboni et al., 2017). The Fe deficiency symptoms (chlorosis) induced under S deficiency can be attributed to the inability of the strategy II plants to synthesize the S-derived phytosiderophores that are required for Fe uptake (Mori and Nishizawa, 1987). In addition to the basic differences between strategy I (reduction-based Fe uptake) and strategy II

(chelation-based Fe uptake) plants, additional levels of regulation may exist to fine-tune plant's response to Fe or S deprivation (Mendoza-Cózatl et al., 2019). The less pronounced chlorosis in *Arabidopsis* plants exposed to dual deficiency of Fe and S compared to plants exposed to sole Fe starvation has been recently reported (Robe et al., 2020). These authors have suggested that experimental conditions and species- or developmental stage-specific (i.e., seedlings vs. mature plants, young vs. mature leaves) mechanisms may be modulating plant response to the individual (S or Fe) and combined (Fe and S) nutrient starvation.

While the upregulation of *IRT1* in response to Fe deficiency (Forieri et al., 2013; Muneer et al., 2014; Zuchi et al., 2015) and S deficiency (Muneer et al., 2014; Zuchi et al., 2015) has been previously reported, here we demonstrated that the *cad2-1* allelic mutation of *GSH1* (γ-glutamylcysteine synthetase) gene overrode the typical signal of *IRT1* upregulation in the *cad2-1* and *s1c2* mutants under S deficiency. Moreover, the bottleneck in sulfate assimilation (Khan et al., 2010) due to *SIR* knockdown mutation constitutively upregulated *IRT1* expression in the *sir1-1* mutant under all experimental conditions.

The induction of *FRO2* in response to Fe deficiency is well documented (Muneer et al., 2014; Zuchi et al., 2015; Forieri et al., 2017). However, in addition to sole Fe starvation, S deficiency also upregulated the expression of *FRO2* in Col-0 seedlings compared to control conditions. These findings are consistent with the previous reports (Muneer et al., 2014; Zuchi et al., 2015). However, the upregulated *FRO2* expression under S deficiency disappeared in the *sir1-1*, *cad2-1,* and *s1c2,* suggesting that the expression of *FRO2* may be directly or indirectly dependent on *GSH1* and/or *SIR*. Moreover, given the fact that the *sir1-1*, *cad2-1*, and *s1c2* seedlings are already suffering from S deficiency even under normal growth conditions (Speiser et al., 2018), the reduced expression of *FRO2* in the *sir1-1*, *cad2-1*, and *s1c2* seedlings compared to Col-0 suggest that under severe/prolonged S starvation, the expression of *FRO2* is downregulated as a consequence of secondary adaptations. It is noteworthy that contrary to the expression pattern of *IRT1*, the expression of *FRO2* was not constitutively upregulated in the *sir1-1* mutant. The differential expression of *IRT1* and expression of *FRO2* under S deficiency in the *sir1-1* mutant suggests that some other unknown signals in the *sir1-1* mutant might be triggering the expression of *IRT1*.

The induction of *FIT* in response to Fe deficiency is well known (Colangelo and Guerinot, 2004). FIT-dependent protein complexes through hetero-dimerization with clade Ib bHLHs (e.g., bHLH38) are required for the activation of the expression of genes involved in the maintenance of Fe homeostasis such as *IRT1* and *FRO2*. We observed similar expression patterns (induction in response to sole Fe or combined S and Fe starvation) for *FIT* and *bHLH38* in our study. The upregulation of *FIT* and *bHLH38* upon Fe starvation is consistent with the previous reports (Colangelo and Guerinot, 2004; Ivanov et al., 2012). Moreover, the upregulation of *bHLH38* in the *fit1-2* mutant corroborates the previous findings that the expression of the clade Ib bHLH genes (i.e., *bHLH38*, *bHLH39*, *bHLH100*, and *bHLH101*) is not dependent on *FIT* and that the expression of *FIT* and *bHLH38* is controlled by different pathways, presumably by different signals upon Fe starvation (Wang et al., 2007). Unlike the expression pattern of *IRT1* and *FRO2*, the expression of *FIT* and *bHLH38* did not change under S deficiency in Col-0 and the *sir1-1*, *cad2-1*, and *s1c2*. It is also worth mentioning that although these expression profiles are consistent with many of the previous reports, however, under different experimental sets up opposite expression patterns, i.e., repression of *IRT1* (Forieri et al., 2013), *FRO2*, and *FIT* (Forieri et al., 2017) under S starvation have also been reported. Different growth conditions, durations of the nutrient starvations (4 days starvation in this study vs. 5 weeks starvation) and developmental/stage-specific (i.e., seedlings vs. mature plants) mechanisms may account for these differences. Moreover, contrary to (Forieri et al., 2013, 2017), the presence of sucrose; the end product of photosynthesis, in growth medium in our experiments can expected to alter plant's responses to Fe or S deprivation.

Mounting evidence suggests critical roles for GSH in cell signaling (Zhang and Forman, 2012) and its cross-communication with other established signaling molecules (Ghanta and Chattopadhyay, 2011). A variety of signaling pathways are involved in the regulation of *GSH1* (reviewed in Zhang and Forman, 2012). Therefore, it remains to be elucidated whether the differential regulation of *IRT1* and *FRO2* under S deficiency is due to mutations in the *GSH1* gene in the *cad2-1* mutant or GSH itself acts as a major player in regulating their expression. The ROS dependent regulation of Fe homeostasis related genes has been recently reported in several studies (Astolfi et al., 2021; von der Mark et al., 2021; McInturf et al., 2022). Although other possibilities could not be ruled out, the non-canonical responses of some of the known marker genes of Fe homeostasis in GSH deficient mutants suggest that presumably, the elevated ROS levels in these mutants might be responsible for the differential regulation of these genes.

NAS1, *NAS2*, and *FRD3* are key genes involved in the transport of Fe through the phloem and xylem conducting tissues, respectively. In line with the previous reports, the expression of *NAS1* and *NAS2* was upregulated under Fe-starved conditions to enhance the translocation of Fe (Kim et al., 2005; Klatte et al., 2009). S deficiency did not cause any significant changes in the expression of these two genes, which is contrary to the previous report showing S deficiency completely blocked the expression of the NA synthase gene (Zuchi et al., 2009) and NA accumulation (Zuchi et al., 2015) in tomato independently from the availability of Fe. The observed discrepancy might be linked to the different threshold levels of S deficiency perceived by plants or different mechanisms operating in the *Arabidopsis* model system and tomato as described previously. The expression of *NAS1* and *NAS2* in our study was rather upregulated under S starvation in the GSH-deficient *cad2-1* but not in *s1c2* mutant. Irrespective of the availability of S, the deficiency of Fe caused slight to moderate induction in the expression of *FRD3* in all lines which corroborates previous findings (Rogers and Guerinot, 2002). Interestingly, in wild type and all mutant lines the transcripts of *FRD3* tended to be low (although non-significantly) under S starvation, which

may be an adaptation to the lowered need of the partner nutrient Fe for Fe–S clusters biosynthesis. Under nonstress conditions, the lack of sulfite reduction in *sir1-1* and *cad2-1* allelic mutation in *GSH1* gene constantly upregulated the expression of *FRD3*.

The uptake and subsequent assimilation of sulfate are dependent both on plant S demand for growth and external S supply (Hawkesford and De Kok, 2006). The expression of the high-affinity group 1 sulfate transporter (*AtSULTR1;2*), that is responsible for the primary uptake of sulfate by the root (Buchner et al., 2010), was upregulated in response to S deficiency in agreement with previous reports (Lewandowska and Sirko, 2008; Takahashi et al., 2011; Zuchi et al., 2015; Forieri et al., 2017). Remarkably, there was a significant increase in the *AtSULTR1;2* transcript abundance after imposition of sole Fe deficiency. This is consistent to the expression pattern of *AtSULTR1;2* in tomato (Zuchi et al., 2015), and increased total S concentration in tomato (Paolacci et al., 2014) and wheat (Ciaffi et al., 2013) plants exposed to short term Fe starvation like our experimental conditions, but opposite to what has been reported in *Arabidopsis* in response to long term (4–11 days vs. 5 weeks) Fe starvation (Forieri et al., 2017). The upregulated expression of *AtSULTR1;2* disappeared in the mutant *fit1-2*, which suggest that under Fe deficiency, the expression of *AtSULTR1;2* may be directly or indirectly dependent on *FIT*. Alternatively, these observations also suggest that perception of Fe starvation signals beyond certain threshold level leads to secondary adaptations to adjust plants demands to changing requirement of the partner nutrient S. This is supported by the fact that in the *fit1-2* mutant, which is already suffering from Fe starvation even under normal Fe supply, the expression pattern of *AtSULTR1;2* exhibited an opposite but comparable trend to what has reported in *Arabidopsis* in response to long-term Fe starvation (Forieri et al., 2017).

In contrast to the expression pattern of the high-affinity group 1 sulfate transporter (*AtSULTR1;2*) in the root, the low-affinity sulfate transporters (*AtSULTR2;1* and *AtSULTR2;2*) that are responsible for translocation of sulfate within the plant (Takahashi et al., 2000) showed a different expression pattern in the shoots (**Figures 3B,C**). First, short-term exposure (4 days) to S starvation did not change the expression of these two low-affinity sulfate transporters in Col-0, which is not consistent with the previous reports showing their upregulation in response to medium term (10 days) S starvation (Zuchi et al., 2015). Secondly, in contrast to the significant upregulation of the high affinity sulfate transporter, sole Fe starvation significantly lowered the expression of *AtSULTR2;1* and *AtSULTR2;2* in Col-0. These observations suggest that Fe deficiency signals are perceived and integrated earlier in plant's responses compared to S. However, contrary to the downregulated expression of *AtSULTR2;1* under Fe deficiency in Col-0, the expression of *AtSULTR2;1* was significantly upregulated in the GSH-deficient *cad2-1* and *s1c2* mutants, which suggest that GSH might act as a signaling molecule to modulate the expression of *AtSULTR2;1*. It is noteworthy to mention that the lack of *FIT* in the *fit1-2* mutant, constantly downregulated the expression of *AtSULTR2;1*, irrespective of the nutrient status. It is noteworthy that in the *sir1-1* and *fit1-2* mutants, which are already sufferings from S and Fe starvation, respectively, even under natural conditions, the expression of *AtSULTR2;1* was kept at a significantly lower level compared to Col-0. However, the expression of *AtSULTR2;2* in the *sir1-1* and *fit1-2* mutants under unstress conditions was significantly high compared to Col-0 (**Figure 3C**). Such contrasting differences in the expression of *AtSULTR2;1* and *AtSULTR2;2* suggest different functions for these two transporters in plants exposed to long term S or Fe deficiency. Similarly, like *sir1-1* mutant, bottleneck in GSH biosynthesis also constantly upregulated the expression of *AtSULTR2;2* in the *cad2-1* mutant under all experimental conditions. *AtSULTR2;1* and *AtSULTR2;2* tend to express in vascular tissues throughout the plant (Buchner et al., 2004). *AtSULTR2;1* is believed to be responsible for uptake of S from the apoplasm within the vascular bundle and involved in root to shoot transport (Takahashi et al., 2000). Our data suggest that the reduced uptake of sulfate from the apoplast is one of the adaptation mechanisms to adjust S requirements under Fe deficiency. The adjustment of S uptake and assimilation as a Fe deficiency adaptation has been previously demonstrated (Astolfi et al., 2006; Ciaffi et al., 2013; Paolacci et al., 2014). Our work indicates that dual limitation of Fe and S can trigger quite distinct responses compared to sole Fe or S limitations, especially in the background of *cad2-1* mutant. For example, *AtSULTR1;2* was significantly upregulated in response to dual nutrient starvation, but remained unchanged under the imposition of sole Fe or S starvation in the *cad2-1* mutant. Similarly, the expression of *AtSULTR2;1* (in *cad2-1* and *s1c2*) and *AtSULTR2;2* (in *s1c2*) under dual nutrient limitations showed an opposite trend compared to sole Fe or S starved conditions. These observations underlined the significance of understanding the underlying mechanisms that govern plant responses under dual nutrient limitation to figure out strategies for sustainable plant growth in nutrient-limited environments.

The reciprocal influence between Fe and S in terms of uptake, transport, and assimilation has been demonstrated in many studies (Astolfi et al., 2006; Zuchi et al., 2009, 2015; Ciaffi et al., 2013; Forieri et al., 2013, 2017; Paolacci et al., 2014). However, the crosstalk between Fe and S in terms of regulation of genes involved in the biosynthesis of Fe–S clusters has been rarely investigated, despite the fact that the major portion of the metabolically active Fe is bound to S in the form of Fe–S clusters. Fe and S interact for the building of Fe–S assembly, and three types of machinery for Fe–S cluster assembly have been identified and are distributed in the cytosol (CIA for cytosolic Fe–S protein assembly), the mitochondria (ISC for Fe–S cluster) and the chloroplasts (SUF for S mobilization) in plants (Lill and Mühlenhoff, 2008). Since mitochondria are one of the cellular compartments where the Fe–S cluster assembly takes place. Therefore, mitochondria might be expected to play a central role in the regulation of Fe and S for the Fe–S cluster assembly. In mitochondria, frataxin (FH) plays a pivotal role in regulating Fe homeostasis (Radisky et al., 1999; Bulteau et al., 2004) and Fe–S clusters biosynthesis (Lill and Mühlenhoff, 2008; Stemmler et al., 2010). The significant upregulation of *FH* in the roots of Col-0 and all mutants only in response to sole Fe or dual Fe and S

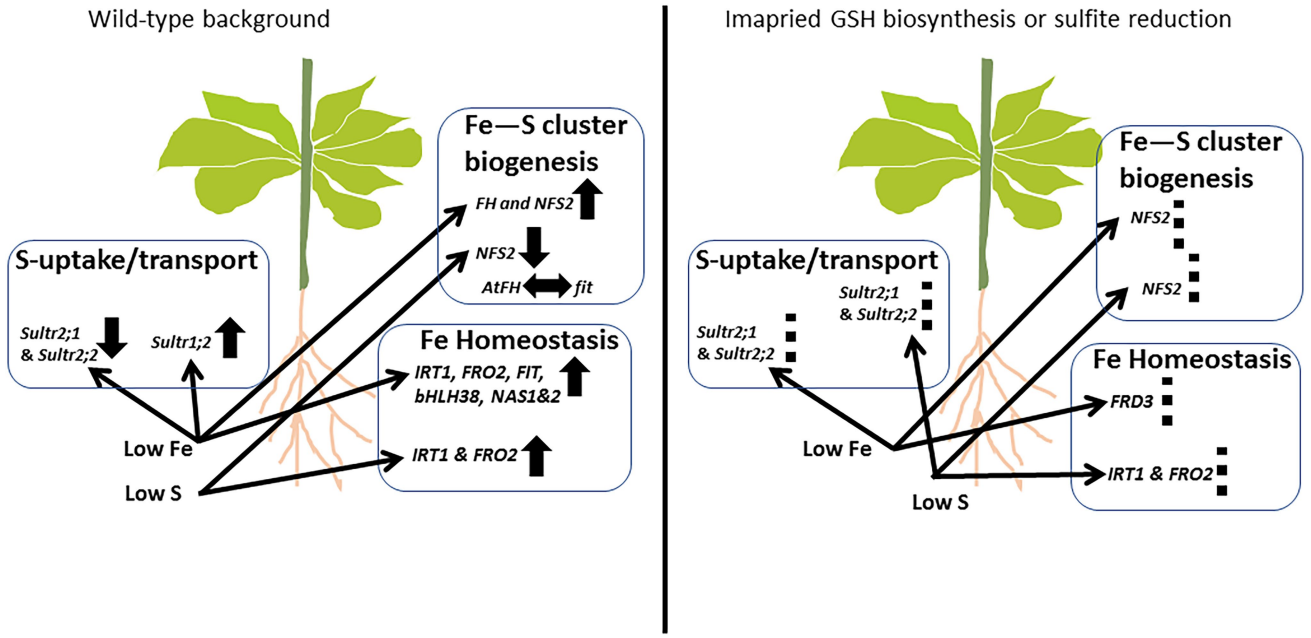

FIGURE 6 | Schematic representation of the interplay between iron and sulfur networks in *Arabidopsis*. The availability of Fe and S affect the expression of S and Fe homeostasis related gene in plants. The response pattern might depend on the severity/degree of nutrient deficiency. Bottlenecks in sulfite reduction and/or GSH biosynthesis (**right panel**) can futher modulate the cannonical responses *via* still unknown signals like ROS (Astolfi et al., 2021; von der Mark et al., 2021; McInturf et al., 2022) and others. UP arrows: Upregulation; down arrows: downregulation; left–right arrow: probable interaction; and dashed-lines: differential regulation compared to wild-type background.

deficiency suggests that the S status of the plant has apparently no role in modulating the expression of *FH*. Quite interestingly, the up-regulated expression of *FH* under Fe deficiency is directly or indirectly dependent on *FIT* because the upregulated expression of *FH* disappeared in the *fit1-2* mutant. The constitutive upregulation of *FH* expression in the double overexpresser of *FIT* and its activating partner *bHLH38* (i.e., *OxFITXOxbHLH38*) under nonstress conditions and our ChIP-qPCR experiments supports *in vivo* binding of FIT to the promoters of *AtFH*. This is an exciting new prospect for future research and additional evidence is required to validate this hypothesis. In mitochondria and plastids, the required S atoms for the assembly of Fe–S are extracted from cysteine by pyridoxal phosphate-dependent cysteine desulfurases, IscS/NFS1, and SufS/NFS2, respectively (Couturier et al., 2013). *NFS2* is specifically adapted to oxidative stress and Fe starvation (Stemmler et al., 2010). Interestingly, the expression of *NFS2* was significantly upregulated in response to Fe deficiency in the shoots of Col-0 seedlings but dramatically reduced in response to S starvation in all the mutants and to a lesser extent in Col-0. Moreover, in the *fit1-2* and the rest of the mutants, which are already suffering from Fe and S starvation, respectively, the deficiency of Fe either down-regulated (*cad2-1* and *s1c2*) or did not change (*fit1-2* and *sir1-1*) the expression of *NFS2*. Overall, these findings suggest that in terms of Fe–S clusters biogenesis, major adaptations in response to Fe deficiency occur in mitochondria (*via* regulation of *FH*), whereas adaptations to S deficiency are mainly taking place in plastids (*via* regulation of *NFS2*), to rebalance overall requirements of the plants for the two partner nutrients.

Our findings related to Fe sensitivity of the GSH-deficient mutants add significant new insights to the existing knowledge, linking the endogenous level of total GSH to Fe sensitivity under Fe limitation. The relative sensitivity of *sir1-1*, *cad2-1*, *s1c2* under Fe starvation suggests that Fe sensitivity is not solely dependent on the endogenous level of total GSH as hypothesized earlier (Shanmugam et al., 2015). We demonstrated that the known reciprocal signals between iron and sulfur networks are differentially regulated by bottlenecks in sulfite reduction and/or GSH biosynthesis (**Figure 6**). We also demonstrated that bottlenecks in sulfite reduction and/or GSH biosynthesis differentially regulate the expression of some of the known marker genes of Fe homeostasis, S uptake/transport, and Fe–S clusters biogenesis. We also elucidated the crosstalk between Fe and S in terms of expression of some of the key players involved in the assembly of Fe–S clusters biogenesis machinery in the plastids and mitochondria. We observed major adaptations in the mitochondria in response to Fe deficiency and the plastids in response to S deficiency. Our data suggest that *FH* is a potential target of FIT. While the dual limitation of Fe and S mostly generated overruling and/or synergistic signals, quite distinct responses, as opposed to sole Fe or S limitations, were also observed. These observations underscored the significance of elucidating plant responses under dual nutrient limitations for sustainable plant growth in nutrient-limited environments.

DATA AVAILABILITY STATEMENT

The original contributions presented in the study are included in the article/**Supplementary Material**, further inquiries can be directed to the corresponding authors.

AUTHOR CONTRIBUTIONS

H-QL, TC, and HW planned and designed the research. MSK, QL, MC, and HR performed experiments and analyzed data. MSK and H-QL wrote the manuscript. All authors contributed to the article and approved the submitted version.

FUNDING

This work was financially supported by the Chinese Academy of Sciences and the National Key R&D Program of China (2019YFA0903901).

SUPPLEMENTARY MATERIAL

The Supplementary Material for this article can be found online at: https://www.frontiersin.org/articles/10.3389/fpls.2022.878418/full#supplementary-material

Supplementary Figure S1 | Phenotypes of 14-days old seedlings under Fe-deficient conditions. Top view of the seedlings directly germinated on Fe-deficient half-strength MS medium for 14 days.

Supplementary Figure S2 | Expression analysis of *AtFH* in the double overexpressor *OxFIT X OxbHLH38*. Relative expression by Quantitative RT-PCR of the genes*CyaY/frataxin* in roots,for *Arabidopsis* the wildtype (Col-0) and the double overexpressor line *OxFITXOxbHLH38* of one-week old seedlings exposed to half-strength MS medium (1/2 MS +Fe +S), Fe deficient (1/2 MS -Fe +S), S deficient (1/2 MS +Fe -S) and Fe & S deficient (1/2 MS –Fe -S) media for four days under long-day conditions. The y-axis shows RNA levels normalized to that of GADPH. Letters indicate the statistically significant differences among all treatments in Col-0 and doubleoverxpresser line determined with the two-way ANOVA test followed by Tukey's test ($P < 0.05$, $n = 3$). Bars represent means ± SD.

REFERENCES

Astolfi, S., Celletti, S., Vigani, G., Mimmo, T., and Cesco, S. (2021). Interaction between sulfur and iron in plants. *Front. Plant Sci.* 12:670308. doi: 10.3389/fpls.2021.670308

Astolfi, S., Cesco, S., Zuchi, S., Neumann, G., and Roemheld, V. (2006). Sulfur starvation reduces phytosiderophores release by iron-deficient barley plants. *Soil Sci. Plant Nutr.* 52, 43–48. doi: 10.1111/j.1747-0765.2006.00010.x

Astolfi, S., Zuchi, S., Hubberten, H.-M., Pinton, R., and Hoefgen, R. (2010). Supply of Sulphur to S-deficient young barley seedlings restores their capability to cope with iron shortage. *J. Exp. Bot.* 61, 799–806. doi: 10.1093/jxb/erp346

Bauer, P., Ling, H.-Q., and Guerinot, M. L. (2007). *FIT*, the *FER*-like iron deficiency induced transcription factor in *Arabidopsis*. *Plant Physiol. Biochem.* 45, 260–261. doi: 10.1016/j.plaphy.2007.03.006

Bowler, C., Benvenuto, G., Laflamme, P., Molino, D., Probst, A. V., Tariq, M., et al. (2004). Chromatin techniques for plant cells. *Plant J.* 39, 776–789. doi: 10.1111/j.1365-313X.2004.02169.x

Buchner, P., Parmar, S., Kriegel, A., Carpentier, M., and Hawkesford, M. J. (2010). The sulfate transporter family in wheat: tissue-specific gene expression in relation to nutrition. *Mol. Plant* 3, 374–389. doi: 10.1093/mp/ssp119

Buchner, P., Stuiver, C. E. E., Westerman, S., Wirtz, M., Hell, R., Hawkesford, M. J., et al. (2004). Regulation of sulfate uptake and expression of sulfate transporter genes in *Brassica oleracea* as affected by atmospheric H2S and pedospheric sulfate nutrition. *Plant Physiol.* 136, 3396–3408. doi: 10.1104/pp.104.046441

Bulteau, A.-L., O'Neill, H. A., Kennedy, M. C., Ikeda-Saito, M., Isaya, G., and Szweda, L. I. (2004). Frataxin acts as an iron chaperone protein to modulate mitochondrial aconitase activity. *Science* 305, 242–245. doi: 10.1126/science.1098991

Ciaffi, M., Paolacci, A. R., Celletti, S., Catarcione, G., Kopriva, S., and Astolfi, S. (2013). Transcriptional and physiological changes in the S assimilation pathway due to single or combined S and Fe deprivation in durum wheat (*Triticum durum* L.) seedlings. *J. Exp. Bot.* 64, 1663–1675. doi: 10.1093/jxb/ert027

Cobbett, C. S., May, M. J., Howden, R., and Rolls, B. (1998). The glutathione-deficient, cadmium-sensitive mutant, cad2–1, of *Arabidopsis thaliana* is deficient in γ-glutamylcysteine synthetase. *Plant J.* 16, 73–78. doi: 10.1046/j.1365-313x.1998.00262.x

Colangelo, E. P., and Guerinot, M. L. (2004). The essential basic helix-loop-helix protein FIT1 is required for the iron deficiency response. *Plant Cell* 16, 3400–3412. doi: 10.1105/tpc.104.024315

Connolly, E. L., Campbell, N. H., Grotz, N., Prichard, C. L., and Guerinot, M. L. (2003). Overexpression of the FRO2 ferric chelate reductase confers tolerance to growth on low iron and uncovers posttranscriptional control. *Plant Physiol.* 133, 1102–1110. doi: 10.1104/pp.103.025122

Connolly, E. L., and Guerinot, M. L. (2002). Iron stress in plants. *Genome Biol.* 3, 1021–1024. doi: 10.1186/gb-2002-3-8-reviews1024

Couturier, J., Touraine, B., Briat, J.-F., Gaymard, F., and Rouhier, N. (2013). The iron-sulfur cluster assembly machineries in plants: current knowledge and open questions. *Front. Plant Sci.* 4:259. doi: 10.3389/fpls.2013.00259

Fan, H., Zhang, Z., Wang, N., Cui, Y., Sun, H., Liu, Y., et al. (2014). SKB1/PRMT 5-mediated histone H 4 R 3 dimethylation of I b subgroup bHLH genes negatively regulates iron homeostasis in *Arabidopsis thaliana*. *Plant J.* 77, 209–221. doi: 10.1111/tpj.12380

Forieri, I., Sticht, C., Reichelt, M., Gretz, N., Hawkesford, M. J., Malagoli, M., et al. (2017). System analysis of metabolism and the transcriptome in *Arabidopsis thaliana* roots reveals differential co-regulation upon iron, sulfur and potassium deficiency. *Plant Cell Environ.* 40, 95–107. doi: 10.1111/pce.12842

Forieri, I., Wirtz, M., and Hell, R. (2013). Toward new perspectives on the interaction of iron and sulfur metabolism in plants. *Front. Plant Sci.* 4:357. doi: 10.3389/fpls.2013.00357

Ghanta, S., and Chattopadhyay, S. (2011). Glutathione as a signaling molecule-another challenge to pathogens: another challenge to pathogens. *Plant Signal. Behav.* 6, 783–788. doi: 10.4161/psb.6.6.15147

Green, L. S., and Rogers, E. E. (2004). FRD3 controls iron localization in *Arabidopsis*. *Plant Physiol.* 136, 2523–2531. doi: 10.1104/pp.104.045633

Hawkesford, M. J., and De Kok, L. J. (2006). Managing sulphur metabolism in plants. *Plant Cell Environ.* 29, 382–395. doi: 10.1111/j.1365-3040.2005.01470.x

Hirai, M. Y., Fujiwara, T., Awazuhara, M., Kimura, T., Noji, M., and Saito, K. (2003). Global expression profiling of sulfur-starved *Arabidopsis* by DNA macroarray reveals the role of O-acetyl-l-serine as a general regulator of gene expression in response to sulfur nutrition. *Plant J.* 33, 651–663. doi: 10.1046/j.1365-313X.2003.01658.x

Ivanov, R., Brumbarova, T., and Bauer, P. (2012). Fitting into the harsh reality: regulation of iron-deficiency responses in dicotyledonous plants. *Mol. Plant* 5, 27–42. doi: 10.1093/mp/ssr065

Jain, A., Wilson, G. T., and Connolly, E. L. (2014). The diverse roles of FRO family metalloreductases in iron and copper homeostasis. *Front. Plant Sci.* 5:100. doi: 10.3389/fpls.2014.00100

Jeffrey, S. W., and Humphrey, G. F. (1975). New spectrophotometric equations for determining chlorophylls a, b, c1 and c2 in higher-plants, algae and natural phytoplankton. *Biochem. Physiol. Pflanz.* 167, 191–194. doi: 10.1016/S0015-3796(17)30778-3

Khan, M. S., Haas, F. H., Samami, A. A., Gholami, A. M., Bauer, A., Fellenberg, K., et al. (2010). Sulfite reductase defines a newly discovered bottleneck for assimilatory sulfate reduction and is essential for growth and development in *Arabidopsis thaliana*. *Plant Cell* 22, 1216–1231. doi: 10.1105/tpc.110.074088

Kim, S., Takahashi, M., Higuchi, K., Tsunoda, K., Nakanishi, H., Yoshimura, E., et al. (2005). Increased nicotianamine biosynthesis confers enhanced tolerance

of high levels of metals, in particular nickel, to plants. *Plant Cell Physiol.* 46, 1809–1818. doi: 10.1093/pcp/pci196

Klatte, M., Schuler, M., Wirtz, M., Fink-Straube, C., Hell, R., and Bauer, P. (2009). The analysis of *Arabidopsis* nicotianamine synthase mutants reveals functions for nicotianamine in seed iron loading and iron deficiency responses. *Plant Physiol.* 150, 257–271. doi: 10.1104/pp.109.136374

Klinge, S., Hirst, J., Maman, J. D., Krude, T., and Pellegrini, L. (2007). An iron-sulfur domain of the eukaryotic primase is essential for RNA primer synthesis. *Nat. Struct. Mol. Biol.* 14, 875–877. doi: 10.1038/nsmb1288

Lewandowska, M., and Sirko, A. (2008). Recent advances in understanding plant response to sulfur-deficiency stress. *Acta Biochim. Pol.* 55, 457–471. doi: 10.18388/abp.2008_3051

Lill, R., and Mühlenhoff, U. (2008). Maturation of iron-sulfur proteins in eukaryotes: mechanisms, connected processes, and diseases. *Annu. Rev. Biochem.* 77, 669–700. doi: 10.1146/annurev.biochem.76.052705.162653

McGrath, S. P., Zhao, F., and Blake-Kalff, M. (2003). History and outlook for sulphur fertilizers in Europe. *Ferti. Fertilization* 2, 5–27.

McInturf, S. A., Khan, M. A., Gokul, A., Castro-Guerrero, N. A., Höhner, R., Li, J., et al. (2022). Cadmium interference with iron sensing reveals transcriptional programs sensitive and insensitive to reactive oxygen species. *J. Exp. Bot.* 73, 324–338. doi: 10.1093/jxb/erab393

Mendoza-Cózatl, D. G., Gokul, A., Carelse, M. F., Jobe, T. O., Long, T. A., and Keyster, M. (2019). Keep talking: crosstalk between iron and sulfur networks fine-tunes growth and development to promote survival under iron limitation. *J. Exp. Bot.* 70, 4197–4210. doi: 10.1093/jxb/erz290

Mori, S., and Nishizawa, N. (1987). Methionine as a dominant precursor of phytosiderophores in Graminaceae plants. *Plant Cell Physiol.* 28, 1081–1092.

Muneer, S., Lee, B.-R., Kim, K.-Y., Park, S.-H., Zhang, Q., and Kim, T.-H. (2014). Involvement of Sulphur nutrition in modulating iron deficiency responses in photosynthetic organelles of oilseed rape (*Brassica napus* L.). *Photosynth. Res.* 119, 319–329. doi: 10.1007/s11120-013-9953-8

Nikiforova, V. J., Kopka, J., Tolstikov, V., Fiehn, O., Hopkins, L., Hawkesford, M. J., et al. (2005). Systems rebalancing of metabolism in response to sulfur deprivation, as revealed by metabolome analysis of *Arabidopsis* plants. *Plant Physiol.* 138, 304–318. doi: 10.1104/pp.104.053793

Paolacci, A. R., Celletti, S., Catarcione, G., Hawkesford, M. J., Astolfi, S., and Ciaffi, M. (2014). Iron deprivation results in a rapid but not sustained increase of the expression of genes involved in iron metabolism and sulfate uptake in tomato (*Solanum lycopersicum* L.) seedlings. *J. Integr. Plant Biol.* 56, 88–100. doi: 10.1111/jipb.12110

Pii, Y., Cesco, S., and Mimmo, T. (2015). Shoot ionome to predict the synergism and antagonism between nutrients as affected by substrate and physiological status. *Plant Physiol. Biochem.* 94, 48–56. doi: 10.1016/j.plaphy.2015.05.002

Radisky, D. C., Babcock, M. C., and Kaplan, J. (1999). The yeast frataxin homologue mediates mitochondrial iron efflux evidence for a mitochondrial iron cycle. *J. Biol. Chem.* 274, 4497–4499. doi: 10.1074/jbc.274.8.4497

Rajab, H., Khan, M. S., Wirtz, M., Malagoli, M., Qahar, F., and Hell, R. (2020). Sulfur metabolic engineering enhances cadmium stress tolerance and root to shoot iron translocation in *Brassica napus* L. *Plant Physiol. Biochem.* 152, 32–43. doi: 10.1016/j.plaphy.2020.04.017

Robe, K., Gao, F., Bonillo, P., Tissot, N., Gaymard, F., Fourcroy, P., et al. (2020). Sulphur availability modulates Arabidopsis thaliana responses to iron deficiency. *PLoS One* 15:e0237998. doi: 10.1371/journal.pone.0237998

Rogers, E. E., and Guerinot, M. L. (2002). FRD3, a member of the multidrug and toxin efflux family, controls iron deficiency responses in Arabidopsis. *Plant Cell* 14, 1787–1799. doi: 10.1105/tpc.001495

Schmidt, W. (2003). Iron solutions: acquisition strategies and signaling pathways in plants. *Trends Plant Sci.* 8, 188–193. doi: 10.1016/S1360-1385(03)00048-7

Shanmugam, V., Wang, Y. W., Tsednee, M., Karunakaran, K., and Yeh, K. C. (2015). Glutathione plays an essential role in nitric oxide-mediated iron-deficiency signaling and iron-deficiency tolerance in *Arabidopsis*. *Plant J.* 84, 464–477. doi: 10.1111/tpj.13011

Shibagaki, N., Rose, A., McDermott, J. P., Fujiwara, T., Hayashi, H., Yoneyama, T., et al. (2002). Selenate-resistant mutants of *Arabidopsis thaliana* identify Sultr1; 2, a sulfate transporter required for efficient transport of sulfate into roots. *Plant J.* 29, 475–486. doi: 10.1046/j.0960-7412.2001.01232.x

Speiser, A., Silbermann, M., Dong, Y., Haberland, S., Uslu, V. V., Wang, S., et al. (2018). Sulfur partitioning between glutathione and protein synthesis determines plant growth. *Plant Physiol.* 177, 927–937. doi: 10.1104/pp.18.00421

Stemmler, T. L., Lesuisse, E., Pain, D., and Dancis, A. (2010). Frataxin and mitochondrial FeS cluster biogenesis. *J. Biol. Chem.* 285, 26737–26743. doi: 10.1074/jbc.R110.118679

Takahashi, H., Kopriva, S., Giordano, M., Saito, K., and Hell, R. (2011). Sulfur assimilation in photosynthetic organisms: molecular functions and regulations of transporters and assimilatory enzymes. *Annu. Rev. Plant Biol.* 62, 157–184. doi: 10.1146/annurev-arplant-042110-103921

Takahashi, H., Watanabe-Takahashi, A., Smith, F. W., Blake-Kalff, M., Hawkesford, M. J., and Saito, K. (2000). The roles of three functional sulphate transporters involved in uptake and translocation of sulphate in *Arabidopsis thaliana*. *Plant J.* 23, 171–182. doi: 10.1046/j.1365-313x.2000.00768.x

Vigani, G., Pii, Y., Celletti, S., Maver, M., Mimmo, T., Cesco, S., et al. (2018). Mitochondria dysfunctions under Fe and S deficiency: is citric acid involved in the regulation of adaptive responses? *Plant Physiol. Biochem.* 126, 86–96. doi: 10.1016/j.plaphy.2018.02.022

von der Mark, C., Ivanov, R., Eutebach, M., Maurino, V. G., Bauer, P., and Brumbarova, T. (2021). Reactive oxygen species coordinate the transcriptional responses to iron availability in *Arabidopsis*. *J. Exp. Bot.* 72, 2181–2195. doi: 10.1093/jxb/eraa522

Wang, H.-Y., Klatte, M., Jakoby, M., Bäumlein, H., Weisshaar, B., and Bauer, P. (2007). Iron deficiency-mediated stress regulation of four subgroup Ib BHLH genes in *Arabidopsis thaliana*. *Planta* 226, 897–908. doi: 10.1007/s00425-007-0535-x

Watanabe, M., Hubberten, H.-M., Saito, K., and Hoefgen, R. (2010). General regulatory patterns of plant mineral nutrient depletion as revealed by serat quadruple mutants disturbed in cysteine synthesis. *Mol. Plant* 3, 438–466. doi: 10.1093/mp/ssq009

Yoshimoto, N., Takahashi, H., Smith, F. W., Yamaya, T., and Saito, K. (2002). Two distinct high-affinity sulfate transporters with different inducibilities mediate uptake of sulfate in *Arabidopsis* roots. *Plant J.* 29, 465–473. doi: 10.1046/j.0960-7412.2001.01231.x

Yuan, Y. X., Zhang, J., Wang, D. W., and Ling, H. Q. (2005). AtbHLH29 of Arabidopsis thaliana is a functional ortholog of tomato FER involved in controlling iron acquisition in strategy I plants. *Cell Res.* 15, 613–621. doi: 10.1038/sj.cr.7290331

Zamboni, A., Celletti, S., Zenoni, S., Astolfi, S., and Varanini, Z. (2017). Root physiological and transcriptional response to single and combined S and Fe deficiency in durum wheat. *Environ. Exp. Bot.* 143, 172–184. doi: 10.1016/j.envexpbot.2017.09.002

Zhang, H., and Forman, H. J. (2012). Glutathione synthesis and its role in redox signaling. *Semin. Cell Dev. Biol.* 23, 722–728. doi: 10.1016/j.semcdb.2012.03.017

Zuchi, S., Cesco, S., Varanini, Z., Pinton, R., and Astolfi, S. (2009). Sulphur deprivation limits Fe-deficiency responses in tomato plants. *Planta* 230, 85–94. doi: 10.1007/s00425-009-0919-1

Zuchi, S., Watanabe, M., Hubberten, H.-M., Bromke, M., Osorio, S., Fernie, A. R., et al. (2015). The interplay between sulfur and iron nutrition in tomato. *Plant Physiol.* 169, 2624–2639. doi: 10.1104/pp.15.00995

Conflict of Interest: The authors declare that the research was conducted in the absence of any commercial or financial relationships that could be construed as a potential conflict of interest.

Publisher's Note: All claims expressed in this article are solely those of the authors and do not necessarily represent those of their affiliated organizations, or those of the publisher, the editors and the reviewers. Any product that may be evaluated in this article, or claim that may be made by its manufacturer, is not guaranteed or endorsed by the publisher.

frontiers | Frontiers in Plant Science

ORIGINAL RESEARCH
published: 16 June 2022
doi: 10.3389/fpls.2022.930484

Optimizing Wheat Yield, Water, and Nitrogen Use Efficiency With Water and Nitrogen Inputs in China: A Synthesis and Life Cycle Assessment

Zhou Li[1], Song Cui[2], Qingping Zhang[3], Gang Xu[4], Qisheng Feng[4], Chao Chen[1] and Yuan Li[4]**

[1] Key Laboratory of Animal Genetics, Breeding and Reproduction in the Plateau Mountainous Region, Ministry of Education, College of Animal Science, Guizhou University, Guiyang, China, [2] School of Agriculture, Middle Tennessee State University, Murfreesboro, TN, United States, [3] College of Agriculture and Forestry Science, Linyi University, Linyi, China, [4] The State Key Laboratory of Grassland Agro-Ecosystems, College of Pastoral Agriculture Science and Technology, Lanzhou University, Lanzhou, China

OPEN ACCESS

Edited by:
Anoop Kumar Srivastava, Central Citrus Research Institute (ICAR), India

Reviewed by:
Luz Asio, Visayas State University, Philippines
Enkelejda Kucaj, Polytechnic University of Tirana, Albania

***Correspondence:**
Qingping Zhang
zhangqp2008@lzu.edu.cn
Yuan Li
yuan.li@lzu.edu.cn

Specialty section:
This article was submitted to Plant Nutrition, a section of the journal Frontiers in Plant Science

Received: *28 April 2022*
Accepted: *23 May 2022*
Published: *16 June 2022*

Citation:
Li Z, Cui S, Zhang Q, Xu G, Feng Q, Chen C and Li Y (2022) Optimizing Wheat Yield, Water, and Nitrogen Use Efficiency With Water and Nitrogen Inputs in China: A Synthesis and Life Cycle Assessment. Front. Plant Sci. 13:930484. doi: 10.3389/fpls.2022.930484

To meet the demand of the fast increasing population, enhancing the wheat (*Triticum aestivum* L.) yield and resource use efficiency by optimizing water and nitrogen (N) management can greatly improve agricultural sustainability and enhance regenerative farming in developing countries such as China. Based on 126 studies conducted in China between 1996 and 2018, using meta-analysis in combination with decision regression tree modeling and life cycle assessment (LCA), this study aimed to (1) quantify the effect of water and N input on wheat yield, water productivity (WP_C), and N use efficiency (NUE_f), and evaluate the subsequent environmental impact in different regions using LCA; and (2) evaluate, model, and rank the roles of environmental (e.g., soil nutrient status and climatic factors) and agronomic factors (e.g., water and N management practices) affecting wheat yield, WP_C, and NUE_f. The results showed that irrigation and N addition increased the average yield and WP_C by 40 and 15%, respectively, relative to control treatments with no irrigation or fertilizer application. The mean water saving potential (WSP) and N saving potential (NSP) in China were estimated at 11 and 10%, respectively. Soil nutrient status [e.g., initial soil phosphorus (P) and potassium (K)] and soil organic carbon content affected the wheat yield, WP_C, and NUE_f more significantly than climatic factors [mean annual temperature (MAT)] or water and N management practices. The structural equation-based modeling indicated that initial soil nutrient condition impacted productivity and resource use efficiency more at the below optimal water and N levels than above. The risk-factor-based feature ranking indicated that site-specific environmental and soil condition was highly informative toward model construction but split input of N or water had less impact on yield and input use efficiency. LCA demonstrated that to further mitigate greenhouse gas emissions, water- or N-saving management should be promoted in China. Collectively, our research implies that long-term soil health and nutrient enhancement should be more beneficial for increasing yield and resource use efficiency in wheat production.

Keywords: decision tree, irrigation, life cycle assessment, meta-regression, structural equation modeling (LISREL)

INTRODUCTION

Wheat (*Triticum aestivum* L.) is a cool-season C_3 cereal crop commonly produced worldwide. It is considered the second most important crop in developing countries followed by rice (*Oryza sativa* L.) (Narayanan, 2018). Comparable with other C_3 cereal crops, the productivity and agronomic input use efficiency of wheat is largely affected by many environmental and managerial factors, such as growing season temperature, irrigation methods, and N fertilization rate (Fan et al., 2018). In addition, a lot of fossil fuel energy is used for producing agronomic inputs, such as chemical fertilizers, leading to severe environmental pollution, particularly, in those developing countries (Taki et al., 2018). Information abounds with individual field studies investigating the impacts of one or two factors on wheat productivity and physiology at a single site (Zwart and Bastiaanssen, 2004; Qin et al., 2015). However, round evaluation of numerous factors at the same time requires systematic data synthesis and modeling effort using data at a much larger spatial and temporal scale.

China has been the leading wheat-producing country in the world since 1991. According to FAOSTAT (2017), the total wheat production area in China ranked third globally in 2014 [24 million hectares (ha)], closely following the European Union (27 million ha) and India (31 million ha). The wheat yield in China averagely increased five times from 1949 ($<$1 t ha^{-1}) to 2013 (5 t ha^{-1}) (Huang et al., 2015). Despite the advancement of modern breeding efforts and technological advancement (e.g., irrigation technology and synthetic fertilizers), the production capacity of wheat in China struggles to meet the skyrocketing demand caused by fast population increase, urbanization, and diminishing land and natural resources (Du et al., 2020). In addition, intensive monoculture-based wheat cropping systems largely rely on agronomic inputs [e.g., water and nitrogen (N)], which have significantly challenged the overall ecological and economic sustainability while maintaining productivity on a system level (Conway and Toenniessen, 1999; Lollato et al., 2019; Sidhu et al., 2019). Thus, there is a growing demand for identifying key managerial and environmental drivers affecting wheat yield, water productivity (WP_c), and N use efficiency (NUE_f) with data collected across large spatial and temporal scales to enhance agronomic and environmental sustainability (Tilman et al., 2011; Li et al., 2019). The decision tree-based regression has been involved in agricultural research to identify key factors affecting agriculture production and could be of great use in future field experiments; e.g., decision tree analyses were used to find the key predictors for characterizing soybean seed yield from commonly collected precision agriculture across Wisconsin, United States (Smidt et al., 2016).

Small grain crops, such as wheat, are highly dependent on N fertilization, which consequentially resulted in greater crude protein concentration and nutritive value compared with C_4 crops (Raun and Johnson, 1999; Gonzalez-Dugo et al., 2010). However, over-fertilization could result in low NUE_f and groundwater contamination under unfavorable environmental conditions (Tilman et al., 2011; Lollato et al., 2019; Sidhu et al., 2019). Ladha et al. (2016) reported that, on average, wheat production consumes 18% of global N fertilizer, with a 50-year average of 52 kg ha^{-1} year^{-1}. Meanwhile, the average NUE_f across major cereals is lower than 33% (Raun and Johnson, 1999). The global average of wheat WP_c was 1.09 kg m^{-3}, ranging from 0.6 to 1.7 kg m^{-3} (Zwart and Bastiaanssen, 2004). High yield variability suggests that wheat is mostly affected by genetic, environmental, or management differences. Thus, there exists enormous potential for improving WP_c and NUE_f through breeding and better management. Several studies have endorsed that the underlying interactive mechanisms impacting the WP_c and NUE_f of wheat would be complex (Zwart and Bastiaanssen, 2004; Qin et al., 2015) and thus require further systematic investigation. However, only a few meta-analysis studies on the magnitude and variability of wheat yield and resource use efficiency (i.e., WP_c and NUE_f) have been reported in China.

China has an incredibly diverse topography and highly variable soil and climatic conditions. Thus, wheat production in different regions varies significantly. Wheat is cultivated broadly in China, although the importance of wheat to the local economy differs by region (Huang et al., 2015). Thus, we hypothesized that the water saving potential (WSP) and N saving potential (NSP) varies with regions since environmental and agronomic factors play critical roles in the yield and resource use efficiency of wheat. In contrast, the complex interplay among these factors could substantially impact the trends in yield, WP_c, and NUE_f (Lollato et al., 2019; Sidhu et al., 2019; Li et al., 2020). In addition, life cycle assessment (LCA) can examine the environmental impacts, including raw material extraction and transportation, agrochemical production and transportation, and arable farming in the field (Rebitzer et al., 2004), which can well assess subsequent environmental impact caused by various inputs of water and fertilizer in different regions of China. Thus, this study aimed to (1) investigate the effects of water and N inputs on yield, WP_c, and NUE_f of wheat; (2) evaluate the extent of WSP and NSP based on the identified optimal input level and the environmental impact caused by various inputs of water and fertilizer in different regions using LCA; (3) evaluate, model, and rank the impacts of many environmental and agronomic factors on wheat yield, WP_c, and NUE_f using structural models and decision tree-based importance ranking.

Abbreviations: ADP, abiotic depletion potential; AP, available phosphorus; AK, available potassium; CI, confidence interval; CLCD, Chinese life cycle database; EP, eutrophication potential; ET, total evapotranspiration; ETx, ecotoxicity; GWP, global warming potential; SOC, initial soil organic carbon; LCA, life cycle assessment; MAT, mean annual temperature; MAP, mean annual precipitation; N, nitrogen; NSPs, N saving potentials; NSV, nitrogen saving value; Nopt, optimal N input level; NUE_f, N use efficiency; N^+, above-optimal N inputs; N^-, below-optimal N inputs; PED, primary energy demand; POFP, photochemical oxidative formation; RI, respiratory organics; *RR*, natural logarithm of the treatment over the control; RR_{NUEf}, response ratio of NUE_f; RR_{WPc}, response ratio of WP_c; RR_Y, response ratio of yield; SEM, structural equation model; WP_c, water productivity; WSPs, water saving potentials; WSV, water saving value; Wopt, optimal water input level.

MATERIALS AND METHODS

Literature Selection and Data Extraction

Literature and data selection criteria were similar to those used by Li et al. (2020; Supplementary Material). Ultimately, 126 studies, including 1,020 yield, 437 WP_c, and 82 NUE_f paired observations were included in this study. In addition, information on study location, climatic conditions [mean annual temperature (MAT) and mean annual precipitation (MAP)], and soil properties [initial soil nutrient concentrations, potassium (K), and phosphorus (P)] were collected.

In addition, four regions, namely, Northwest (Gansu, Ningxia, Qinghai, Shaanxi, and Xinjiang provinces), North (Beijing, Jilin, Hebei, Heilongjiang, Inner Mongolia, Liaoning, Shanxi, and Tianjin provinces), Center (Guangdong, Guangxi, Henan, Hubei, and Hunan provinces), and East (Anhui, Fujian, Jiangsu, Jiangxi, Shandong, Zhejiang, and Shanghai provinces), were assigned as Zhang et al. (2017; **Figure 1**), while this classification excluded regions that have no studies.

Data Process

Definitions

Water productivity (kg m^{-3}) was calculated by the following equation:

$$\mathrm{WPc}=\frac{Y}{ET} \tag{1}$$

where Y is yield (kg ha^{-1}) and ET is the total evapotranspiration (mm) (Ibragimov et al., 2007).

Fertilizer nitrogen use efficiency (kg kg^{-1}) was calculated to compute Y over the total amount of nitrogen fertilizer applied in each hectare (N, kg ha^{-1}) as follows:

$$\mathrm{NUEf}=\frac{Y}{N} \tag{2}$$

Water saving potential and NSP (Qin et al., 2016; Li et al., 2019) were calculated to the magnitude of the total water (the amount of water input, including precipitation and irrigation, in mm) and N savings, and WSP (mm, absolute value) was determined as follows:

$$\mathrm{WSP}=W^{+}-W_{opt} \tag{3}$$

where W^{+} represents the above-optimal water input, while W_{opt} indicates the optimal water input level producing the highest yield in a specific region.

The relative WSP (%) was calculated as follows:

$$\mathrm{WSP}=\left(\frac{W^{+}-W_{opt}}{W_{max}}\right)\times 100\% \tag{4}$$

where W_{max} represents the greatest W^{+}. Similarly, NSP (kg ha^{-1}, absolute value) was defined as follows:

$$\mathrm{NSP}=N^{+}+-N_{opt} \tag{5}$$

where N^{+} is the above-optimal N input, and N_{opt} is the optimal N input level producing the most significant yield in a specific region.

The relative NSP (%) was computed by the following equation:

$$\mathrm{NSP}=\left(\frac{N^{+}-N_{opt}}{N_{max}}\right)\times 100\% \tag{6}$$

where N_{max} stands for the greatest N^{+}.

In addition, water saving value (WSV) and nitrogen saving value (NSV) were calculated based on the WSP and NSP in each region and, consequently, economic benefits were computed based on the price of water and fertilizer inputs in each region (**Supplementary Table 1**).

Effects of Independent Variables

The yield (RR_Y), WP_c (RR_{WPc}), and NUE_f (RR_{NUEf}), the natural logarithm of the treatment over the control, were computed (Osenberg et al., 1999).

$$RR_{\mathrm{Y}}=\ln\left(\frac{Y_{\mathrm{t}}}{Y_{\mathrm{c}}}\right)=\ln\left(Y_{\mathrm{t}}\right)-\ln\left(Y_{\mathrm{c}}\right) \tag{7}$$

Similarly, RR_{WPc} and RR_{NUEf} were computed as follows:

$$RR_{\mathrm{WPc}}=\ln\left(\frac{WP_{\mathrm{t}}}{WP_0}\right)=\ln\left(WP_{\mathrm{t}}\right)-\ln(WP_0) \tag{8}$$

$$RR_{\mathrm{NUEf}}=\ln\left(\frac{NUE_{\mathrm{t}}}{NUE_0}\right)=\ln\left(NUE_{\mathrm{t}}\right)-\ln\left(NUE_0\right) \tag{9}$$

where Y_t, WP_t, and NUE_t represent the observed yield, WP_c, and NUE_f with irrigation and/or N fertilization in a specific year of a study, respectively, while Y_c, WP_0, and NUE_0 represent the yield, WP_c, and NUE_f without irrigation and/or N fertilization, respectively. Subsequently, the weighted response ratio (effect size) and 95% confidence interval (CI) were calculated as described by Li et al. (2019). To facilitate the explanation, percentage change was calculated as $[\exp(RR_{++})-1)\times 100\%$.

Meta-analyses for each subgroup were processed based on the region and the water and N input level (refer to section "Definitions"). This was performed with the "metafor" package, using the restricted maximum likelihood estimator (RMLE) in the rma.uni model (Viechtbauer, 2010). Study ID was set as a random effect. The mean effect size and its 95% CI were calculated with bias correction generated by bootstrapping (4,999 iterations, **Supplementary Tables 1-6**).

The structural equation model (SEM) was also used to disentangle indirect and direct effects of climate (MAT), soil properties [initial soil organic carbon (SOC), available potassium (AK), and available phosphorus (AP)], and management practices (water and N inputs) on RR_Y, RR_{WPc}, and RR_{NUEf} using the "lavaan" package (Rosseel, 2012). *A priori* regression analyses were established based on the known effects and relationships among the variables (Grace, 2006).

Decision Tree-Based Modeling

A systematic decision tree-based modeling task was also implemented in MATLAB Programing Language (The MathWorks Inc., 2017, Natick, MA, United States) to evaluate the accuracy and feasibility of constructing data analytic models for predicting target variables: RR_Y, RR_{WPc}, and RR_{NUEf}

using different ecophysiological variables observed across all included studies. Particularly, the values of 39 explanatory variables and features were manually extracted from each study (**Supplementary Table 7**). Following that, a 10-fold cross-validation (10-fold CV) training and testing paradigm was used to test modeling accuracy. The 10-fold CV routine randomly divided the entire dataset into 10 subsets of similar size. Each time, a decision tree-based prediction model was constructed based on nine subsets to test the remaining ones, and this process was repeated 10 times until all subsets of data were tested. All 39 features were also ranked according to the estimated predictor importance values calculated by summing changes in the risk due to the corresponding splits imposed on each predictor divided by the number of branch nodes.

Life Cycle Assessment

Life cycle assessment was used to evaluate the environmental impact caused by various inputs of water and fertilizer in different regions (Rebitzer et al., 2004). The evaluation scope of the LCA included the production, transportation, as well as emission and leaching due to fertilizer application in the field, while it did not involve the production and use of irrigation facilities, machinery, and equipment.

Eight environmental impact categories' characterization was used in the study, namely, global warming potential (GWP), primary energy demand (PED), acidification potential (AP), abiotic depletion potential (ADP), eutrophication potential (EP), respiratory organics (RI), photochemical oxidative formation (POFP), and ecotoxicity (ETx). The characteristic factors of ADP, AP, and EP indicators were from the CML2002 model, and GWP and RI referred to the IPCC 2007 report, the IMPACT2002+ model, and the ReCiPe model (Goedkoop et al., 2009). The lists of water and fertilizer input in each region and the field emission coefficient of pollutants with fertilizer supply stemmed from the literature review. The background data of fertilizer production come from the Chinese life cycle database (CLCD).

Economic Analysis

Given the calculated WSP, NSP, and subsequent C emissions per hectare, and the prices of irrigation, N fertilizer, carbon price, and area of irrigated wheatland in different regions, the economic benefits of water and N saving per hectare and the total saving benefits of wheat production in a specific irrigated region were calculated. The irrigation price cannot accurately reflect its real value due to various subsidies in each region, and the value of N fertilizer was calculated according to the market price in different regions in 2019. The carbon price was the average price of the main carbon trading markets in different regions in 2019 (Center: Guangzhou, East: Shanghai, North: Beijing, North: Chongqing).

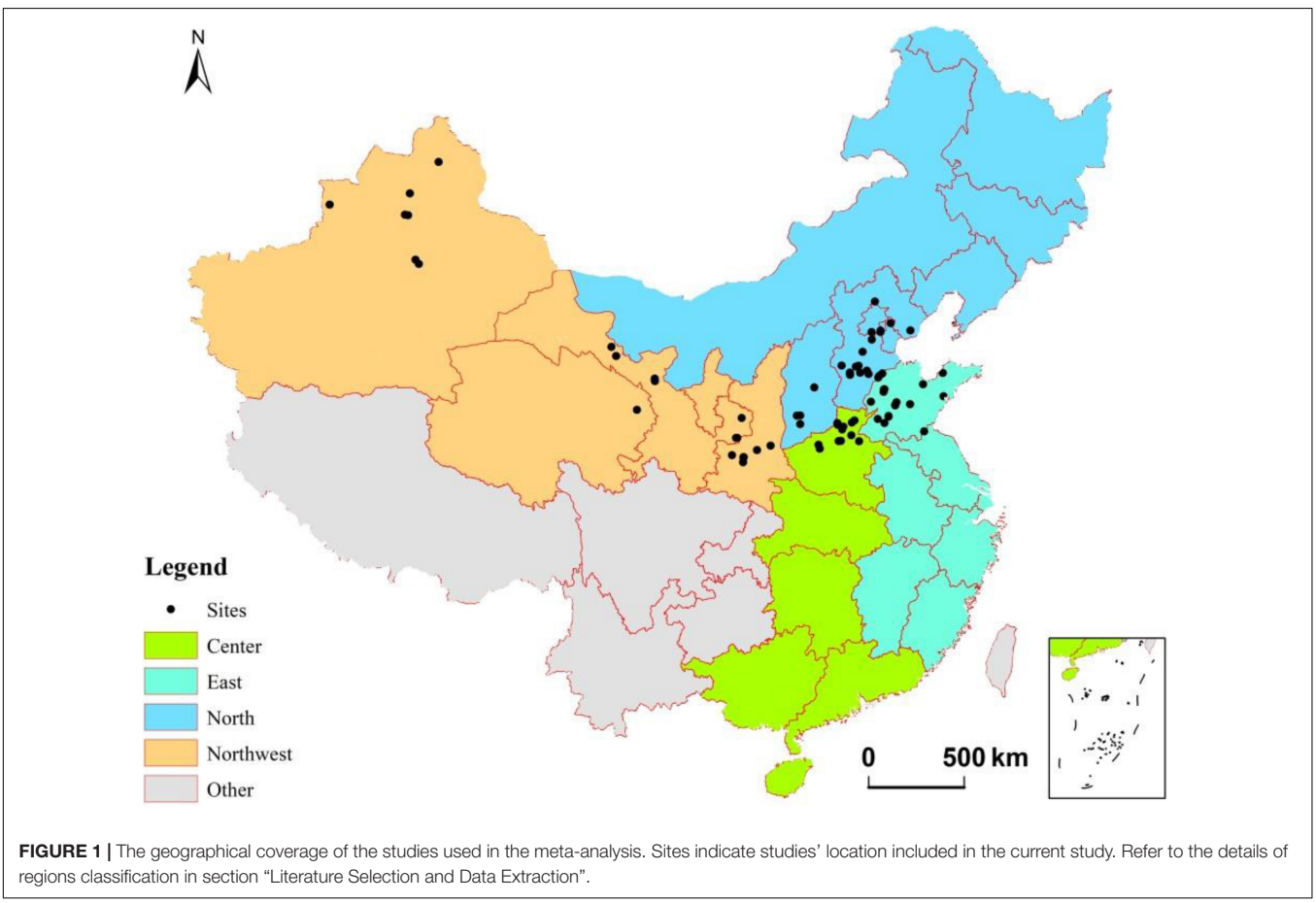

FIGURE 1 | The geographical coverage of the studies used in the meta-analysis. Sites indicate studies' location included in the current study. Refer to the details of regions classification in section "Literature Selection and Data Extraction".

RESULTS

Yields, Water Productivity, and Fertilizer Nitrogen Use Efficiency With Water and Nitrogen Addition

Overall, RR_Y and RR_{WPc} were calculated as 40 and 15% with the input of water and N, respectively ($P < 0.05$, **Figure 2**). Regardless of regions, the input level of water or N, water, and N input enhanced RR_Y. The RR_Y in the northwest of China was higher than that in the north, east, and center by 141, 211, and 53%, respectively ($P < 0.05$). The RR_Y in the center of China was significantly higher than that in the north and east of China by 57 and 103%, respectively. N^+ reduced RR_Y by 53% compared with N^- ($P < 0.05$).

Water and N input significantly increased RR_{WPc} in the northwest, north, and center of China by 55, 8, and 11%, respectively (**Figure 2**). The RR_{WPc} in northwest of China was higher than that in the north and center of China by 444 and 327%, respectively ($P < 0.05$). Water and N input increased RR_{WPc} regardless of the N input levels. N^+ reduced RR_{WPc} more than N^- by 328% ($P < 0.05$). W^- increased RR_{WPc} by 20% relative to control ($P < 0.05$).

Compared with control, water and N input significantly increased the effect size of RR_{NUEf} in the north of China by 26% (**Figure 2**), while N^+ and W^- reduced RR_{NUEf} by 9 and 18%, respectively ($P < 0.05$).

Water Saving Potential and Nitrogen Saving Potential With Water and Nitrogen Addition

The WSP had an overall mean of 11% (**Table 1**) and ranged from 0 to 57%, indicating that water input could be saved by up to 57% without significantly reducing wheat yield. However, a large variation was observed in the WSP values of different regions. For example, the WSP of center of China ranged between 0 and 31% (mean = 11%), and between 0 and 26% (mean = 10%) in the northwest of China. In the east and north of China, however, the WSP values ranged between 0–50 and 0–57%, respectively. Subsequently, water input enhanced yield when water input was lower than that of optimal level in the east ($R^2 = 0.08$) and north of China ($R^2 = 0.08$, $P < 0.001$, **Table 2**). However, an increase in water input significantly decreased yield when the water input was higher than that of optimal level in the east ($R^2 = 0.13$) and north of China ($R^2 = 0.03$, $P < 0.01$).

The NSP of all regions ranged from 0 to 62% (mean = 10%, **Table 3**), suggesting that N input could be reduced by up to 62% without largely reducing wheat yield. Large variations in the NSP of different regions were also observed. For instance, NSP ranged

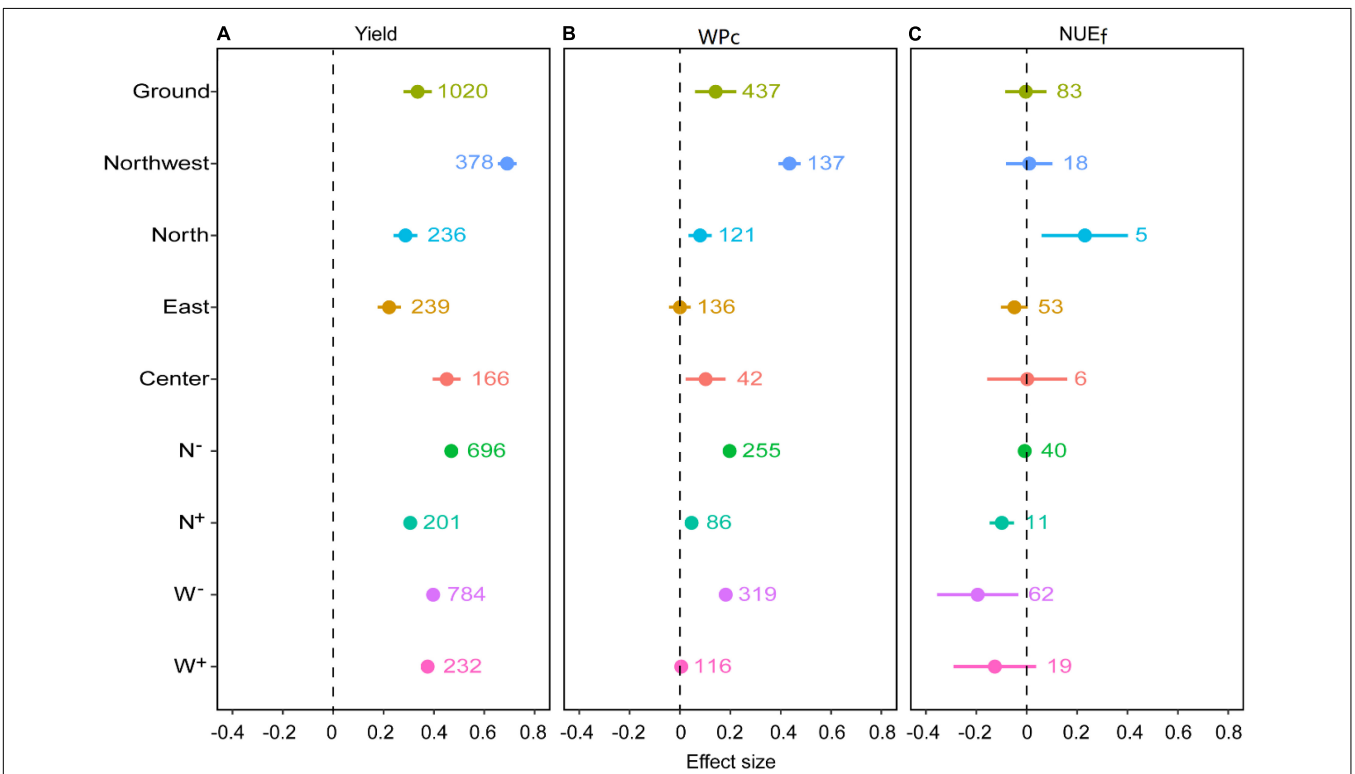

FIGURE 2 | The effect size of the total water and nitrogen inputs on **(A)** grain yield, **(B)** water productivity (WP_c), and **(C)** fertilizer nitrogen use efficiency (NUE_f) of wheat. Effect size indicates the weighted response ratio of the treatment relative to the control and CI indicates the 95% CIs. The sample size of each variable was displayed adjacent to each bar. Particularly, the total effect size (ground) was classified by regions (check the detail of classification in **Figure 1**), and levels of water and nitrogen input. The water levels that were above or below optimal water input were defined as above-optimal (N^+) and below-optimal N inputs (N^-); and above-optimal (W^+) and below-optimal water inputs (W^-). Subcategories were indicated by colors.

TABLE 1 | Estimated mean water saving potentials (WSPs) of a specific region (for details, see **Figure 1**).

Region	*n*	OPTW (mm)	N input (kg ha^{-1})	Yield (t ha^{-1})	WP_c (kg m^{-3})	NUE_f (kg kg^{-1})	WSP (mm)			WSP (%)		
							Mean	Min	Max	Mean	Min	Max
Center	201	316	205	7.4	2.1	27.1	49	0	141	11	0	31
East	292	359	197	7.6	1.9	31.6	95	0	352	13	0	50
North	404	289	191	6.5	1.7	33.2	73	0	385	11	0	57
Northwest	424	557	322	5.1	1.5	26.3	76	0	192	10	0	26
Average	330	380	229	6.7	1.8	30.0	73	0	268	11	0	41

Optimal total water input (OPTW) represents the minimal water input that produced maximum yields of a corresponding region. N input, grain yield, water productivity (WP_c), and fertilizer nitrogen use efficiency (NUE_f) represent the values associated with the optimal water input, respectively.

TABLE 2 | Linear regression model of the effects of the input level of water and nitrogen (N) on yield, water productivity (WP_c), and N use efficiency (NUE_f).

Dependent variable	Input level	Region	Equation	R^2	*P*
Yield (t ha^{-1})	W$^-$	Total	$y = 3.99x + 3.39$	0.19	<0.001
		East	$y = 2.14x + 5.63$	0.08	<0.001
		North	$y = 3.07x + 3.78$	0.13	<0.001
		Northwest	$y = 3.10x + 3.22$	0.10	<0.001
	W$^+$	Total	$y = -1.07x + 8.28$	0.03	0.004
		East	$y = -3.07x + 11.5$	0.18	<0.001
		North	$y = -0.75x + 7.65$	0.03	0.02
WP_c (kg m^{-3})	W$^-$	Total	$y = 0.16x + 1.30$	0.05	<0.001
		East	$y = -1.04x + 2.64$	0.20	0.002
		Northwest	$y = 0.94x + 0.99$	0.10	<0.001
	W$^+$	Total	$y = -0.70x + 2.58$	0.09	<0.001
		East	$y = -0.39x + 2.13$	0.14	0.04
		North	$y = -0.91x + 2.81$	0.19	<0.001
NUE_f (kg kg^{-1})	W$^-$	Total	$y = 15.81x + 18.20$	0.05	0.005
		North	$y = 30.78x + 6.67$	0.12	0.008
		Northwest	$y = 35.30x-0.20$	0.21	<0.001
Yield (t ha^{-1})	N$^-$	Total	$y = 3.22x + 4.02$	0.15	<0.001
		East	$y = 1.62x + 6.01$	0.05	0.002
		North	$y = 1.81x + 4.98$	0.07	<0.001
		Northwest	$y = 3.00x + 3.27$	0.12	<0.001
WP_c (kg m^{-3})	N$^-$	Center	$y = -1.78x + 2.97$	0.30	<0.001
		Northwest	$y = 0.98x + 1.02$	0.15	<0.001
NUE_f (kg kg^{-1})	N$^-$	Total	$y = -13.17x + 41.72$	0.04	0.01
		East	$y = -19.59x + 46.58$	0.23	0.004
		North	$y = -26.28x + 55.89$	0.14	0.007

*Levels of water and N input were classified based on optimal input level of water and N and data visualization (see **Figure 3**). See details of regions classification in section "Literature Selection and Data Extraction".*

TABLE 3 | Estimated mean nitrogen saving potentials (NSPs) of a specific region (for details, see **Figure 1**).

Region	*n*	OPTN (kg ha^{-1})	Water input (mm)	Yield (t ha^{-1})	WP_c (kg m^{-3})	NUE_f (kg kg^{-1})	NSP (kg ha^{-1})			NSP (%)		
							Mean	Min	Max	Mean	Min	Max
Center	201	240	257	7.4	2.1	27.1	44	0	120	12	0	33
East	292	240	308	7.6	1.9	31.6	10	0	60	3	0	20
North	404	195	293	6.5	1.7	33.2	68	0	314	13	0	62
Northwest	424	270	322	5.1	1.5	26.3	60	0	255	11	0	49
Average	330	236	295	6.7	1.8	30	46	0	187	10	0	41

Optimal total nitrogen input (OPTN) represents the minimal water input that produced maximum yields of a corresponding region. Water input, grain yield, water productivity (WP_c), and fertilizer nitrogen use efficiency (NUE_f) represent the values associated with the optimal N input, respectively.

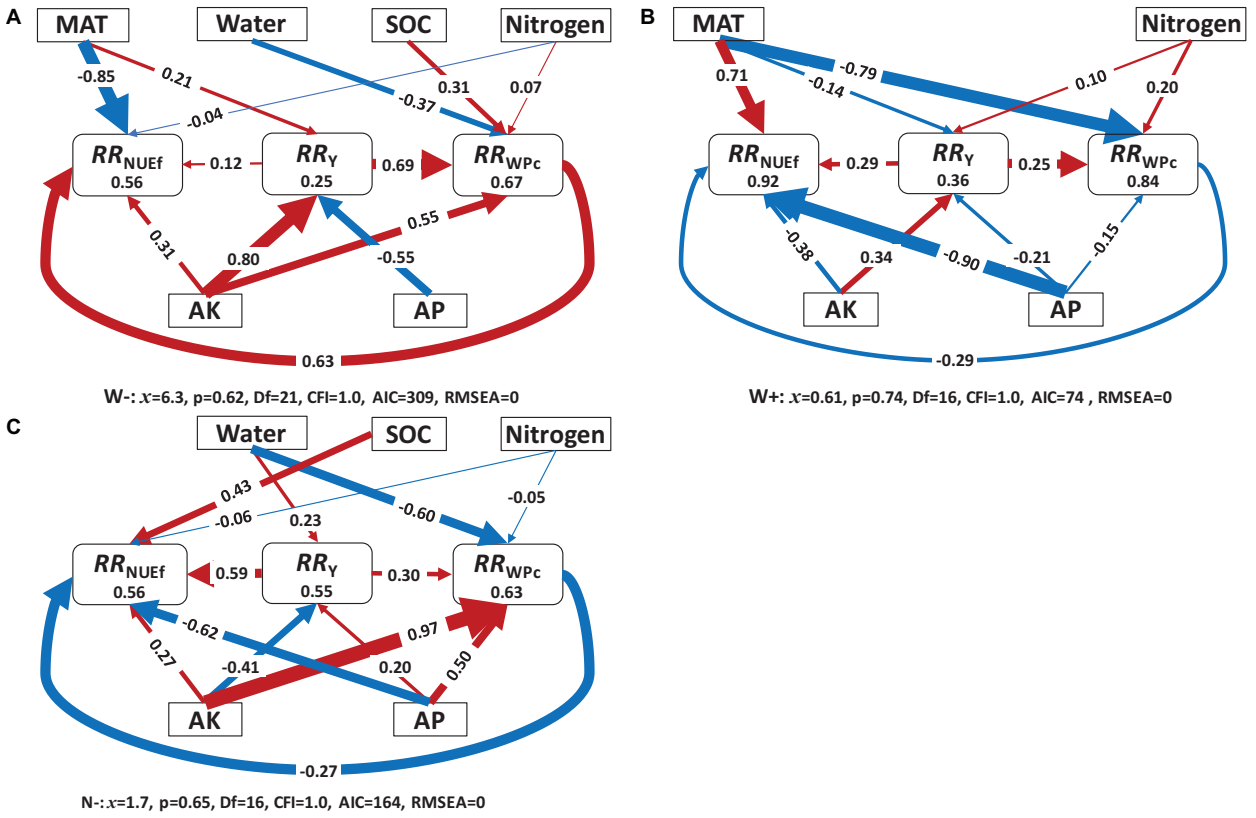

FIGURE 3 | Structural equation model showing the direct and indirect effects of environmental and management conditions on the response ratio of yield (RR_Y), water productivity (RR_{WPc}), and fertilizer nitrogen use efficiency (RR_{NUEf}) under **(A)** below-optimal water inputs (W^-), **(B)** above-optimal water inputs (W^+), and **(C)** below-optimal N inputs (N^-). Results under the above-optimal N inputs (N^+) were not shown due to data paucity. Numbers in the box indicate the variance explained by the model (R^2). Numbers at arrows are standardized path coefficients. The width of the line indicates relative statistical significance (the thicker the more significant). MAT, mean annual temperature; Water, total water input; Nitrogen, total nitrogen inputs; SOC, initial soil organic carbon concentration; AK, initial soil available potassium; AP, initial soil available phosphorus.

from 0 to 33% with means of 12 and 0–3% in the center and east of China, respectively. The NSP for the north and northwest of China ranged from 0 to 62% with means of 13 and 0–11%, respectively. Thus, an increase in N input enhanced yield when water input was lower than that of the optimal level in the north ($R^2 = 0.07$) and northwest of China ($R^2 = 0.12$, $P < 0.01$, **Table 2**).

Effect of Levels of Water and Nitrogen Input

The water input enhanced yield ($R^2 = 0.19$) and WP_c ($R^2 = 0.05$, $P < 0.05$, **Table 2**) when water input was lower than that of optimal level (**Supplementary Figures 1A,B**). Overuse of water decreased wheat yield ($R^2 = 0.03$) and WP_c ($R^2 = 0.09$, $P < 0.05$). In addition, the increase in water input enhanced NUE_f ($R^2 = 0.05$) when water input was lower than that of optimal level (**Supplementary Figure 1C**, $P < 0.05$).

The N input increased yield ($R^2 = 0.15$) and NUE_f ($R^2 = 0.04$, $P < 0.05$, **Table 2**) when N input was lower than that of optimal level (**Supplementary Figures 1D,F**). However, there were no clear patterns for the effect of the input level of N on yield, WP_c, or NUE (**Supplementary Figures 1D-F**).

Factors Affecting Response Ratio of Yield, Response Ratio of WP_c, and Response Ratio of NUE_f Identified by Structural Equation Model

For relationships among RR_Y, RR_{WPc}, and RR_{NUEf} and various environmental and agronomic factors (**Figure 3**), no correct converging model was identified for N^+. For W^-, there was a positive correlation among RR_Y, RR_{WPc}, and RR_{NUEf}. Meanwhile, AK (positive) and AP (negative) affected RR_Y substantially ($P < 0.01$), and 25% of the variation in RR_Y was explained ($P < 0.05$, **Figure 3A**). RR_{WPc} was positively impacted by AK (0.55), followed by SOC (0.31), and water input (−0.37), with 67% of the variation in RR_{WPc} explained ($P < 0.001$). However, RR_{NUEf} was negatively affected by MAT (−0.85), followed by RR_{WPc} (0.63), and AK (0.31), with 56% of the variation in RR_{NUEf} explained ($P < 0.05$).

For W^+, 36% of RR_Y variation was explained by AK, while N input, AP, and MAT, none of them, were significant ($P > 0.4$, **Figure 3B**). RR_{WPc} was positively impacted by RR_Y (0.25) and N input (0.20), but negatively affected by MAT (−0.79) and water input (−0.37), with 84% of the variation in RR_{WPc} explained

($P < 0.05$). However, RR_{NUEf} was negatively affected by AP (−0.90), followed by AK (−0.38) and RR_{WPc} (−0.29), and positively affected by MAT (0.71) and RR_Y (0.29), with 92% of the variation in RR_{NUEf} explained ($P < 0.001$).

For N^-, RR_Y was positively affected by water input (0.23), with 55% of the variation in RR_Y explained ($P < 0.001$, **Figure 3C**). RR_{WPc} was positively impacted by RR_Y (0.30), AK (0.97), and AP (0.50), but negatively affected by water input (−0.60), with 63% of the variation explained ($P < 0.001$). Meanwhile, RR_{NUEf} was negatively affected by AP (−0.62), followed by RR_{WPc} (−0.27), but positively affected by RR_Y (0.59), and SOC (0.43), with 92% of the variation explained ($P < 0.001$).

Life Cycle Assessment of Water and Nitrogen Input

Given the scaled wheatland, for a hectare of wheatland, LCA indicators resulting from water and N input in northern China were higher than that in the rest of the regions (**Table 4**), followed by the central and eastern China, and the lowest was in the northwest. Particularly, the GWP in central, eastern, and northwestern China was 92, 91, and 87% of that in northern China.

Based on the scaled wheat yield, for a one-tone yield (**Table 4**), LCA indicators resulting from water and N input in northwest China were higher than that in other regions. The GWP of the north, central, and eastern China was 90, 73, and 70% of that in northern China.

Economic Analysis of Water and Nitrogen Input

The irrigation cost varied greatly in regions of China (**Table 5**). The irrigation cost was higher in northwest and northern China, and the lowest one was in eastern China. The carbon price in the north was the highest, about 10 times higher than that in the northwest. The reduction of greenhouse gas emissions due to saved water consumption was highest in eastern China and lowest in central China (**Table 5**). For the mitigation of greenhouse gas emissions by reducing N fertilizer application, the north was more prominent and the east was the lowest (**Table 6**). Thus, the saved benefit per hectare of wheatland was mainly caused by enhanced values of water saving and reduction of carbon emission. Specifically, the northwest with higher irrigation prices had the highest water saving benefit, followed by northern and eastern China. The northwest and north could have up to 0.51 and 0.45 billion yuan WSVs, respectively. Northern China had the highest carbon reduction value because of its high carbon price.

Factors Affecting Response Ratio of Yield, Response Ratio of WP_c, and Response Ratio of NUE_f Identified by Decision Tree-Based Regression

Based on risk change per branch node of each explanatory variable and feature, the regression models ranked all features, indicating their importance in affecting the response variable (*RR*), and the top-15 and bottom-5 features were identified

TABLE 4 | Effect of nitrogen and water input on environmental indexes in a specific region (for details, see **Figure 1**).

Area	GWP	GWP per T	PED	PED per T	AP	AP per T	ADP	ADP per T	EP	EP per T	RI	RI per T	POFP	POFP per T	ETx	Etx per T
Center	1634.37	220.86	17087.05	2309.06	9.69	1.31	0.04	0.0054	3.66	0.49	1.73	0.23	2.04	0.28	383.99	51.89
East	1620.24	213.19	17030.01	2240.79	9.53	1.25	0.04	0.0053	3.50	0.46	1.75	0.23	1.94	0.26	360.04	47.37
North	1772.94	272.76	19386.30	2982.51	10.53	1.62	0.04	0.0062	3.66	0.56	1.99	0.31	2.21	0.34	407.90	62.75
Northwest	1541.81	302.32	16839.85	3301.93	9.14	1.79	0.04	0.0078	3.16	0.62	1.73	0.34	1.90	0.37	349.76	68.58

Indexes include global warming potential (GWP; kg CO_2 eq), primary energy demand (PED; MJ), acidification potential (AP; kg SO_2 eq), abiotic depletion potential (ADP; kg antimony eq), eutrophication potential (EP; kg P_3O_4 eq), respiratory inorganics (RI; kg PM2.5 eq), photochemical oxidant formation (POFP; kg NMVOC eq), and ecotoxicity (ETx; CTUe).

TABLE 5 | Estimated mean water saving (WS) or water saving value (WSV) and corresponding economic benefits in a specific region (for details, see **Figure 1**).

	Irrigation (Yuan)	WS (mm)	C price (Yuan t^{-1})	GWP save (kg CO_2 ha^{-1})	WSV (Yuan)	GWP SV (Yuan)	Total WS (Yuan ha^{-1})	GWPSV/WS (%)	Irrigation area (ha)	Region WSV (Yuan)
Center	0.30	49	20.51	93.34	147.00	1.91	148.91	1.30	2,102,596	313,097,570
East	0.15	95	29.80	180.97	142.50	5.39	147.89	3.78	2,227,713	329,456,476
North	0.42	73	61.98	139.06	306.60	8.62	315.22	2.81	1,422,983	448,552,701
Northwest	0.46	76	6.11	144.78	349.60	0.88	350.48	0.25	1,464,135	513,150,035

*See details of water saving in **Table 1**.*

TABLE 6 | Estimated mean nitrogen saving (NS) or nitrogen saving value (NSV) and corresponding economic benefits in a specific region (refer to **Figure 1**).

	N (Yuan ha^{-1})	NS (kg)	C price (Yuan t^{-1})	GWP save (kg CO_2 ha^{-1})	NSV (Yuan)	GWP SV (Yuan)	Total NS (Yuan)	GWPSV/NS (%)	Wheat area (ha)	Region NSV (Yuan)
Center	4.48	44	20.51	131.86	197.12	2.70	199.82	1.37	5,673,670	1,133,712,739
East	4.13	10	29.80	29.97	41.30	0.89	42.19	2.15	3,934,430	165,993,601
North	4.30	68	61.98	179.81	292.40	11.14	303.54	3.81	2,764,270	839,066,516
Northwest	4.31	60	6.11	137.85	258.60	0.84	259.44	0.32	2,929,640	760,065,802

*Refer to the details of nitrogen saving in **Table 3**.*

(**Figure 4**). As indicated, the site-specific information, such as study identification, climatic conditions, initial soil nutrient, and physical condition, tend to have a greater impact on modeling accuracy. Interestingly, split N application at different growth stages appeared to be the least informative feature affecting yield, WP_c, and NUE_f.

DISCUSSION

Water and Nitrogen Input Significantly Increased Wheat Yield and Water Productivity

The present national-scale meta-analysis revealed that water and N input significantly increased wheat yield and WP_c, by averages of 40 and 15%, respectively. We found that the overall mean WSP and NSP of China are 11 and 10%, respectively. This study indicated that the water and N input levels affect wheat yield and resource use efficiency, both of which varied considerably among regions. This finding partially agreed with what was reported by Liu et al. (2020) based on a meta-analysis focusing on the North China Plain but also emphasized that similar trends can also be found in other wheat production regions in China. Soil nutrient status (e.g., AP, AK, and AN) and SOC concentration were found more crucial than water and N management practices or climate (MAT) in determining yield, WP_c, and NUE_f; besides, their effects broadly interact with the water and N input levels. Overall, the effect size of water and N on the yield of northwest China was greater than in any other regions. This observation might be explained by the fact that the majority of the northwest China region is dominated by a semiarid and arid environment with salty soils and great dependency on irrigation water input (Zhang et al., 2014). Thus, the combined effects of salinity reduction and enhanced N use efficiency contributed by irrigation water could result in greater effect sizes compared with other temperate or humid areas included in this study.

Regardless of region and input level, the input of water and N during wheat production increased the yield potential. In addition, northwest and central China had greater yields than north and eastern China. This yield disparity could be attributed to differences in climatic conditions or irrigation methods (**Supplementary Figure 2**). For example, center of China features a humid climate, small fields, and furrow irrigation, which are not common in arid and semiarid environments such as northwest China. Similarly, increases in WP_c due to water and N input were highest in northwest China. This result is likely due to the practice of soil mulching with plastics (Ma et al., 2018) or straws (Qin et al., 2015), which is prevalent in the region. For example, using 1,278 observations in northwestern China, Ma et al. (2018) found that mulching with plastic files increased wheat yield and WP_c by about 20 and 22%, respectively. Due to data scarcity, however, this study did not explore soil mulching to depth and could, thus, not make a further conclusion on this study. N^- resulted in more yield increase and higher WP_c than N^+, which is in line with NSP results. This finding has important implications for optimizing N fertilization during wheat production in China, considering the current high utilization of N fertilizer. Similarly, water and N input increased WP_c, except in the east of China, where high levels of water input are typical due to the relatively greater abundance of irrigation water and precipitation. While the input of both water and N increased NUE_f in the north of China, a high level of water input only could consistently decrease NUE_f.

Water Saving Potential and Nitrogen Saving Potential With Water and Nitrogen Addition

Water and N inputs did not continuously increase yield, WP_c, or NUE_f (**Supplementary Figure 3**). According to Rathore et al. (2017), the positive effect of N input on NUE_f is primarily due to increased N availability and better crop growth (Rathore et al., 2017). In contrast, water or N overuse might induce excessive vegetative growth, limiting the partitioning of photosynthates toward the growth of reproductive tissues (Bennett et al., 1989). In addition, higher levels of N input could decrease NUE_f because of more significant losses (e.g., leaching and volatilization, among others) (Rathore et al., 2017). Soil water content can significantly affect wheat NUE_f by affecting soil N availability and plant N uptake (Ashraf et al., 2016). The addition of N also enhances wheat growth and thus increases WP_c. Moreover, previous studies have shown that N addition in N-limited soils increases WP_c (Amir et al., 1991; Qiu et al., 2008; Cossani and Sadras, 2018). Moreover, the LCA indicated that the environmental impact caused by water and N inputs varied with regions (**Table 4**), particularly N input, which implies that appropriate water and N input should be further encouraged to alleviate environmental burns in the process of wheat production. The north region yielded higher environmental indexes that might attribute to N application rate, irrigation times, and seasonal precipitation (Qiu et al., 2008; Liu et al., 2020). Our LCA results also indicated that irrigation and fertilization have a significant impact on environmental damages, such as GWP, emphasizing the need to decrease the intensity of input energy for sustainable wheat production (Taki et al., 2018).

The east and north of China had a relatively higher WSP and NSP, respectively. Given the overall high amount of water and N inputs in China, these WSP and NSP values indicate that sustainable water and N management practices could be achieved without impeding wheat grain yield in these areas. Optimizing water and N inputs should consider crop development, water, and nutrient demand holistically (Qin et al., 2016; Li et al., 2019), rather than water and N input alone, or even combined (**Supplementary Figure 3**). Regressions between the water and N input and yield, WP_c, and NUE_f revealed a series of significant linear relations ($P < 0.05$). However, some of the R^2 values were poor (between 0.04 and 0.23, **Table 2**). This finding indicates that both N and water have significant impacts on those response variables. Thus, improving sustainability on a cropping system level needs the comprehensive implementation of practices that consider a lot more than just N and water inputs alone (e.g., environmental and managerial interactions, and site-specific conditions and resources). According to our

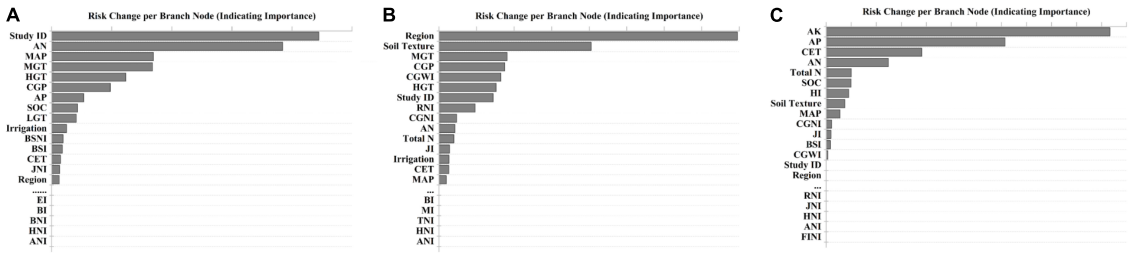

FIGURE 4 | Feature ranking (top-15 and bottom-5) based on risk change per branch node in modeling response ratios of **(A)** yield (RR_Y), **(B)** water productivity (RR_{WPc}), and **(C)** fertilizer nitrogen use efficiency (RR_{NUEf}) using decision tree-based algorithms. Refer to **Table 1** for detailed information on each variable's abbreviation.

study, to further mitigate greenhouse gas emissions and reduce energy consumption from wheat production, focuses should be placed on promoting water-saving management in eastern and northwest China (less water and adequate N), and N-saving management in central and northern China (less N and adequate water input). While for cost-saving purposes, the benefits of water saving in eastern China should be considered, and N saving in central and northern China should be highlighted. The temperate and subtropical monsoon climate zones of wheat production areas in China (all areas except for Xinjiang, Inner Mongolia, and Gansu) are deemed more suitable for planting wheat in other areas in terms of energy efficiency and resource utilization because of the ample precipitation, sunlight, and superior soil conditions (Zhao et al., 2019). Combining the results from this study, more efficient irrigation systems and N fertilizers and application methods should be focused in the future to further boost the energy output from the center, east, and the bottom parts of the north and northwest regions in China. The high GWP and PED particularly in the north portion of the northern wheat production region might require more suitable crops from an energy and resource use efficiency perspective.

Factors Affecting Response Ratio of Yield, Response Ratio of WP_c, and Response Ratio of NUE_f

As discussed earlier, this study demonstrated further investigation that soil nutrients (e.g., SOC, AP, AK, and AN) were more important than climate (MAT) or water and N management practices in determining wheat yield, WP_c, and NUE_f (**Figure 4** and **Supplementary Table 8**). The highlighted significance of improving soil property-related indices to improve productivity was consistent with prior findings. For instance, initial soil nutrients, such as AP and AK concentrations, were vital for increasing the actual yield, WP_c, and NUE_f, which could partly shadow the contributions of water and/N management practices (Lollato et al., 2019). This is because the production of grain crops, such as wheat, typically requires higher amounts of K and comparable levels of N, relative to biomass crops, as indicated in previous research (Lu et al., 2017). A recent study, synthesizing 155 long-term experiments, demonstrated that the application of P and K enhances wheat yield and NUE_f (Lollato et al., 2019). P deficiency reduces the number of spikes by limiting tiller formation, root biomass, and exploration of the soil profile (Fageria and Baligar, 1999), and thus reduce the wheat yields. A study in the Yangtze plains reported that the depletion of soil K could significantly reduce crop yield and nutrient use efficiency (Lu et al., 2017). However, as discussed earlier, overuse of water or N affects plant physiology and nutrient demand considerably, thus causing significant variation in SEM at various water or N input levels. Furthermore, although all presented overall SEM models are significant (indicated by non-significant Chi-square test statistics), results obtained from an individual path should not be over-interpreted because they might be insignificant (e.g., effects of AK, N input, AP, and MAT on RR_Y). Focuses should only be placed on those with large R^2 values and great significance levels while evaluated individually. Below- and above-optimal water input levels demonstrated very different responses between response and explanatory variables (**Figure 3**). Particularly, when water input was below the optimal range, the total water input level was critical in affecting the overall RR_{WPc}, which indirectly affects RR_Y and RR_{NUEf}. The negative coefficient could be caused by the fact there might exist additional limiting factors that hinder a positive response toward additional water input even at the suboptimal levels. When total water input was above the optimal level, the entire water input variable became insignificant and was, therefore, eliminated from the SEM model. Initial soil nutrient status (AK and AP) appeared to have a greater impact on RR_Y and RR_{WPc} when water input was below the optimal level than above. Finally, at the suboptimal N input level, total water input and SOC indicated a significant impact on RR_{WPc} and RR_{NUEf}, respectively, greatly outweighing the effects contributed by N input itself. This indicates that long-term soil C building and alternation of soil hydrological property could potentially improve wheat yield and resource use efficiency more effectively than adding exogenous N inputs. Similarly, AK and AP indicated a great significance as cereal grain crops depend greatly on K and P for seed production in addition to N. This overall observation under the suboptimal N condition hints that rather than focusing on N inputs, greater consideration should be given to the overall soil physicochemical condition, particularly for improving productivity and sustainability of wheat systems.

Climatic conditions were shown to have a great impact on wheat yield and resource use efficiency (**Supplementary Figure 2**). For example, negative correlations between MAT and RR_Y or RR_{NUEf} were identified in this study (**Figure 3**), which agreed qualitatively with a previous study based on boundary-function analysis, indicating that the maximum yields for wheat are typically obtained at moderate MAT (Andrade and Satorre, 2015). Although high-temperature stress affecting crop physiology and productivity was well documented in previous research (Peng et al., 2004), few studies dissect the impacts of temperature responses according to growing season average, low, or peak values vs. the annual values. Particularly for wheat, its main growing season typically spans the cooler time of the year, thus, including summer temperatures (where extreme annual temperatures usually occur) might be unreasonable. Therefore, within-growing season variables (e.g., temperature and precipitation) should serve as better predictors (Mubeen et al., 2016) for conducting advanced data analytic modeling as they directly affect crop heat unit accumulation and development.

The adoption of decision tree-based regression in agricultural research is not new (Smidt et al., 2016). The reason for conducting decision tree-based modeling on *RR* is that the dataset collected for this particular meta-analysis had a great level of completeness (covering a large temporal and spatial scale) and resolution (e.g., inclusion of whole-year precipitation and temperature, initial soil nutrient condition, as well as key agronomic inputs, i.e., water and N, broke down by growth stages), thus, offering an excellent opportunity for applying more sophisticated data analytic algorithms rather than standard meta-analysis methods and ANOVA. The feature ranking results (**Figure 4**) provided findings that no individual study could thoroughly investigate alone. For example, study identification remained important, indicating that site-specific environmental and managerial factors (in addition to those already included in the modeling process) were very informative in determining RR_Y and RR_{WPc} (first and seventh ranking, respectively). Initial soil nutrient conditions, such as AN, AP, and AK, had a great impact on yield and NUE_f but not much on WP_c. This finding agreed qualitatively with some other data synthesis type studies, indicating yield increases with more available soil nutrient contents (Hossard et al., 2016; Lollato et al., 2019); however, information relating to the effects of initial soil nutrients on WP_c or NUE_f alone is almost non-existent. For example, in another meta-analysis study, Liu et al. (2020) evaluated the effects of initial soil total N, pH, and bulk density on NUE_f and WP_c. However, other key nutrients (e.g., P and K) were completely ignored, and this limitation was also acknowledged by the authors. This is largely caused by the fact that the initial soil nutrient condition is an intrinsic factor correlated with each experimental site, which cannot be randomly assigned and evaluated as a treatment factor (thus, treated as blocking factors). It is worth noticing that parameters, such as AN, AP, and AK, are completely different from pre-sowing nutrient inputs. This finding suggested that maintaining long-term soil health, which leads to enhanced intrinsic soil nutrient condition, is more important than instant nutrient inputs at the pre-planting stage or in the growing season. Similarly, Mustafa et al. (2021) reported that soil conservation practices are generally more effective in improving wheat yield than other strategies (e.g., variety selection, planting date, etc.); however, no systematic analysis was used to identify the key soil conservation factors for wheat production. The initial SOC indicated a greater impact on NUE_f and yield than WP_c. Both average and peak growing-season temperatures (MGT and HGT) seemed to be very important in affecting both yield and WP_c, shadowing the effects of MAT, which indicated the importance of adopting growing-season specific climatic information rather than focusing on just annual values (Addy et al., 2020).

We are aware of the importance of the precipitation and temperature during important phases of wheat growth; however, our study is badly limited owing to a paucity of such data. Thus, broader interpretations should be made with caution. In addition, we acknowledge that different wheat types (spring vs. winter) might have different response patterns toward variation in temperatures and frequency of frost events. While based on results from this study, wheat type indicated less impact on modeling accuracy. It is also worth noting that although the current dataset contains 89% of studies (112) using winter wheat and only 11% using spring wheat (14), significant impacts caused by wheat type should still be identified using robust mathematical models such as decision trees. Finally, we acknowledge that successful production of wheat requires other inputs such as herbicides, pesticides, P, and K. However, for this meta-analysis, we chose to focus on two of the most limiting inputs dominating wheat production in China (and globally), i.e., water and N. According to Deng et al. (2021), about 76 and 82% of greenhouse gas emission reduction and NUE enhancement could be achieved in the production phase of wheat out of the entire supply chain, respectively. Water and N are the most crucial inputs during the production phase of wheat farming.

CONCLUSION

Meta-analysis indicated that irrigation and N addition increased the average yield and WP_c by 40 and 15%, respectively, relative to control treatments with no irrigation or fertilizer application. The mean WSP and NSP in China were estimated at 11 and 10%, respectively. In conjunction with modeling and LCA, this study indicated that soil nutrients and initial concentrations of P, K, and SOC affect yield, WP_c, and NUE_f more significantly than climate (MAT) or water and N management practices. These effects are more pronounced at the below-optimal water and N levels than above. Maintaining long-term soil health, which leads to enhanced intrinsic soil nutrient condition at planting, is more important than N inputs during the production phase; to further mitigate greenhouse gas emissions, water- or N-saving management should be promoted, which will vary in different regions of China. These results could guide and inform the design and implementation of large-scale modeling studies on sustainable water and N management strategies for sustainable cropping system design and reduction in energy consumption for wheat production.

DATA AVAILABILITY STATEMENT

The original contributions presented in the study are included in the article/**Supplementary Material**, further inquiries can be directed to the corresponding authors.

AUTHOR CONTRIBUTIONS

ZL: conceptualization, investigation, formal analysis, visualization, and writing – original draft. SC, QZ, and YL: conceptualization, supervision, funding acquisition, and writing – review and editing. GX: software, writing – review and editing, and validation. QF and CC: writing – review and editing. All authors contributed to the article and approved the submitted version.

FUNDING

This research was financed by the National Natural Science Foundation of China (31802133, 32101431, and 32160337), Guizhou Provincial Support Fund of Science and Technology (Qian Ke He Zhi Cheng [2022] Yi Ban 106), the Special Natural Science Foundation of Guizhou University (Gui Da Zhuan Ji He Zi [2020] 08), and the Guizhou Talent Base of Grassland Ecological Animal Husbandry (RCJD2018-13).

ACKNOWLEDGMENTS

We thank all authors who provided data for this study. We are very grateful for the critical reading of the manuscript by Narasinha J. Shurpali [Natural Resources Institute Finland (Luke)].

SUPPLEMENTARY MATERIAL

The Supplementary Material for this article can be found online at: https://www.frontiersin.org/articles/10.3389/fpls.2022.930484/full#supplementary-material

REFERENCES

Addy, J. W. G., Ellis, R. H., Macdonald, A. J., Semenov, M. A., and Mead, A. (2020). Investigating the effects of inter-annual weather variation (1968–2016) on the functional response of cereal grain yield to applied nitrogen, using data from the Rothamsted long-term experiments. *Agric. For. Meteorol.* 284:107898. doi: 10.1016/j.agrformet.2019.107898

Amir, J., Krikun, J., Orion, D., Putter, J., and Klitman, S. (1991). Wheat production in an arid environment. 1. Water-use efficiency, as affected by management practices. *Field Crops Res.* 27, 351–364.

Andrade, J. F., and Satorre, E. H. (2015). Single and double crop systems in the Argentine Pampas: environmental determinants of annual grain yield. *Field Crops Res.* 177, 137–147.

Ashraf, U., Salim, M. N., Sher, A., Sabir, S. U. R., Khan, A., Pan, S. G., et al. (2016). Maize growth, yield formation and water-nitrogen usage in response to varied irrigation and nitrogen supply under semi-arid climate. *Turk. J. Field Crops* 21, 88–96.

Bennett, J. M., Mutti, L. S. M., Rao, P. S. C., and Jones, J. W. (1989). Interactive effects of nitrogen and water stresses on biomass accumulation, nitrogen uptake, and seed yield of maize. *Field Crops Res.* 19, 297–311.

Conway, G., and Toenniessen, G. (1999). Feeding the world in the twenty-first century. *Nature* 402, C55–C58. doi: 10.1038/35011545

Cossani, C. M., and Sadras, V. O. (2018). Water-nitrogen colimitation in grain crops. *Adv. Agron.* 150, 231–274.

Deng, L., Zhang, H., Wang, C., Ma, W., Zhu, A., Zhang, F., et al. (2021). Improving the sustainability of the wheat supply chain through multi-stakeholder engagement. *J. Clean. Prod.* 321:128837. doi: 10.1016/j.jclepro.2021.128837

Du, Y., Cui, B., Zhang, Q., Wang, Z., Sun, J., and Niu, W. (2020). Effects of manure fertilizer on crop yield and soil properties in China: a meta-analysis. *CATENA* 193:104617.

Fageria, N. K., and Baligar, V. C. (1999). Phosphorus-use efficiency in wheat genotypes. *J. Plant Nutr.* 22, 331–340.

Fan, Y., Wang, C., and Nan, Z. (2018). Determining water use efficiency of wheat and cotton: a meta-regression analysis. *Agric. Water Manag.* 199, 48–60.

FAOSTAT (2017). *Production Quantities of Wheat*. Rome: FAOSTAT.

Goedkoop, M., Heijungs, R., Huijbregts, M., De Schryver, A., Struijs, J., and Van Zelm, R. (2009). *ReCiPe 2008. A Life Cycle Impact Assessment Method Which Comprises Harmonised Category Indicators at the Midpoint and the Endpoint level 1*. The Hague: Ministry of Housing, Spatial Planning and Environment, 1–126.

Gonzalez-Dugo, V., Durand, J.-L., and Gastal, F. (2010). Water deficit and nitrogen nutrition of crops. A review. *Agron. Sustain. Dev.* 30, 529–544. doi: 10.2527/1999.77suppl_284x

Grace, J. B. (2006). "Example analyses," in *Structural Equation Modeling and Natural Systems*, ed. J. B. Grace (Cambridge: Cambridge University Press), 324–349.

Hossard, L., Archer, D. W., Bertrand, M., Colnenne-David, C., Debaeke, P., Ernfors, M., et al. (2016). A meta-analysis of maize and wheat yields in low-input vs. conventional and organic systems. *Agron. J.* 108, 1155–1167.

Huang, J., Xiang, C., and Wang, Y. (2015). *The Impact of CIMMYT Wheat Germplasm on Wheat Productivity in China*. Beijing: Center for Chinese Agricultural Policy (CCAP).

Ibragimov, N., Evett, S. R., Esanbekov, Y., Kamilov, B. S., Mirzaev, L., and Lamers, J. P. A. (2007). Water use efficiency of irrigated cotton in Uzbekistan under drip and furrow irrigation. *Agric. Water Manag.* 90, 112–120.

Ladha, J. K., Tirol-Padre, A., Reddy, C. K., Cassman, K. G., Verma, S., Powlson, D. S., et al. (2016). Global nitrogen budgets in cereals: a 50-year assessment for maize, rice, and wheat production systems. *Sci. Rep.* 6:19355. doi: 10.1038/srep19355

Li, Y., Li, Z., Cui, S., Chang, S. X., Jia, C., and Zhang, Q. (2019). A global synthesis of the effect of water and nitrogen input on maize (*Zea mays*) yield, water productivity and nitrogen use efficiency. *Agric. For. Meteorol.* 268, 136–145. doi: 10.1038/s41598-020-66613-6

Li, Z., Zhang, Q., Wei, W., Cui, S., Tang, W., and Li, Y. (2020). Determining effects of water and nitrogen inputs on wheat yield and water productivity and nitrogen use efficiency in China: a quantitative synthesis. *Agric. Water Manag.* 242:106397.

Liu, B.-Y., Zhao, X., Li, S.-S., Zhang, X.-Z., Virk, A. L., Qi, J.-Y., et al. (2020). Meta-analysis of management-induced changes in nitrogen use efficiency of winter wheat in the North China Plain. *J. Clean. Prod.* 251:119632.

Lollato, R. P., Figueiredo, B. M., Dhillon, J. S., Arnall, D. B., and Raun, W. R. (2019). Wheat grain yield and grain-nitrogen relationships as affected by N, P, and K fertilization: a synthesis of long-term experiments. *Field Crops Res.* 236, 42–57.

Lu, D., Li, C., Sokolwski, E., Magen, H., Chen, X., Wang, H., et al. (2017). Crop yield and soil available potassium changes as affected by potassium rate in rice–wheat systems. *Field Crops Res.* 214, 38–44. doi: 10.1038/s41598-020-78729-w

Ma, D., Chen, L., Qu, H., Wang, Y., Misselbrook, T., and Jiang, R. (2018). Impacts of plastic film mulching on crop yields, soil water, nitrate, and organic carbon in Northwestern China: a meta-analysis. *Agric. Water Manag.* 202, 166–173. doi: 10.1016/j.agwat.2018.02.001

Mubeen, M., Ahmad, A., Wajid, A., Khaliq, T., Hammad, H. M., Sultana, S. R., et al. (2016). Application of CSM-CERES-Maize model in optimizing irrigated conditions. *Outlook Agric.* 45, 173–184.

Mustafa, G., Mahmood, H., and Iqbal, A. (2021). Environmentally friendly farming and yield of wheat crop: a case of developing country. *J. Clean. Prod.* 314:127978.

Narayanan, S. (2018). Effects of high temperature stress and traits associated with tolerance in wheat. *Open Access J. Sci.* 2, 177–186.

Osenberg, C. W., Sarnelle, O., Cooper, S. D., and Holt, R. D. (1999). Resolving ecological questions through meta-analysis: goals, metrics, and models. *Ecology* 80, 1105–1117.

Peng, S., Huang, J., Sheehy, J. E., Laza, R. C., Visperas, R. M., Zhong, X., et al. (2004). Rice yields decline with higher night temperature from global warming. *Proc. Natl. Acad. Sci. U.S.A.* 101, 9971–9975. doi: 10.1073/pnas.0403720101

Qin, W., Assinck, F. B. T., Heinen, M., and Oenema, O. (2016). Water and nitrogen use efficiencies in citrus production: a meta-analysis. *Agric. Ecosyst. Environ.* 222, 103–111.

Qin, W., Hu, C., and Oenema, O. (2015). Soil mulching significantly enhances yields and water and nitrogen use efficiencies of maize and wheat: a meta-analysis. *Sci. Rep.* 5:16210. doi: 10.1038/srep16210

Qiu, G. Y., Wang, L., He, X., Zhang, X., Chen, S., Chen, J., et al. (2008). Water use efficiency and evapotranspiration of winter wheat and its response to irrigation regime in the north China plain. *Agric. For. Meteorol.* 148, 1848–1859.

Rathore, V. S., Nathawat, N. S., Bhardwaj, S., Sasidharan, R. P., Yadav, B. M., Kumar, M., et al. (2017). Yield, water and nitrogen use efficiencies of sprinkler irrigated wheat grown under different irrigation and nitrogen levels in an arid region. *Agric. Water Manag.* 187, 232–245.

Raun, W. R., and Johnson, G. V. (1999). Improving nitrogen use efficiency for cereal production. *Agron. J.* 91, 357–363.

Rebitzer, G., Ekvall, T., Frischknecht, R., Hunkeler, D., Norris, G., Rydberg, T., et al. (2004). Life cycle assessment: part 1: framework, goal and scope definition, inventory analysis, and applications. *Environ. Int.* 30, 701–720. doi: 10.1016/j.envint.2003.11.005

Rosseel, Y. (2012). Lavaan: an R package for structural equation modeling. *J. Stat. Softw.* 48, 1–36. doi: 10.3389/fpsyg.2014.01521

Sidhu, H. S., Jat, M. L., Singh, Y., Sidhu, R. K., Gupta, N., Singh, P., et al. (2019). Sub-surface drip fertigation with conservation agriculture in a rice-wheat system: a breakthrough for addressing water and nitrogen use efficiency. *Agric. Water Manag.* 216, 273–283.

Smidt, E. R., Conley, S. P., Zhu, J., and Arriaga, F. J. (2016). Identifying field attributes that predict soybean yield using random forest analysis. *Agron. J.* 108, 637–646.

Taki, M., Soheili-Fard, F., Rohani, A., Chen, G., and Yildizhan, H. (2018). Life cycle assessment to compare the environmental impacts of different wheat production systems. *J. Clean. Prod.* 197, 195–207. doi: 10.1021/acs.est.5b04279

Tilman, D., Balzer, C., Hill, J., and Befort, B. L. (2011). Global food demand and the sustainable intensification of agriculture. *Proc. Natl. Acad. Sci. U.S.A.* 108, 20260–20264. doi: 10.1073/pnas.1116437108

Viechtbauer, W. (2010). Conducting meta-analyses in R with the metafor package. *J. Stat. Softw.* 36, 1–48.

Zhang, Q., Miao, F., Wang, Z., Shen, Y., and Wang, G. (2017). Effects of long-term fertilization management practices on soil microbial biomass in China's cropland: a meta-analysis. *Agron. J.* 109, 1183–1195.

Zhang, W.-T., Wu, H.-Q., Gu, H.-B., Feng, G.-L., Wang, Z., and Sheng, J.-D. (2014). Variability of soil salinity at multiple spatio-temporal scales and the related driving factors in the Oasis areas of Xinjiang, China. *Pedosphere* 24, 753–762.

Zhao, H., Zhai, X., Guo, L., Liu, K., Huang, D., Yang, Y., et al. (2019). Assessing the efficiency and sustainability of wheat production systems in different climate zones in China using emergy analysis. *J. Clean. Prod.* 235, 724–732.

Zwart, S. J., and Bastiaanssen, W. G. M. (2004). Review of measured crop water productivity values for irrigated wheat, rice, cotton and maize. *Agric. Water Manag.* 69, 115–133.

Conflict of Interest: The authors declare that the research was conducted in the absence of any commercial or financial relationships that could be construed as a potential conflict of interest.

Publisher's Note: All claims expressed in this article are solely those of the authors and do not necessarily represent those of their affiliated organizations, or those of the publisher, the editors and the reviewers. Any product that may be evaluated in this article, or claim that may be made by its manufacturer, is not guaranteed or endorsed by the publisher.

frontiers | Frontiers in Plant Science

ORIGINAL RESEARCH
published: 24 June 2022
doi: 10.3389/fpls.2022.927435

Belowground Carbon Efficiency for Nitrogen and Phosphorus Acquisition Varies Between *Lolium perenne* and *Trifolium repens* and Depends on Phosphorus Fertilization

Jiayu Lu[1,2], Jinfeng Yang[3], Claudia Keitel[2], Liming Yin[1], Peng Wang[1], Weixin Cheng[4] and Feike A. Dijkstra[2]*

[1] CAS Key Laboratory of Forest Ecology and Management, Institute of Applied Ecology, Chinese Academy of Sciences, Shenyang, China, [2] School of Life and Environmental Sciences, Sydney Institute of Agriculture, The University of Sydney, Sydney, NSW, Australia, [3] National Engineering Laboratory for Efficient Utilization of Soil and Fertilizer Resources, College of Land and Environment, Shenyang Agricultural University, Shenyang, China, [4] Environmental Studies Department, University of California, Santa Cruz, Santa Cruz, CA, United States

OPEN ACCESS

Edited by:
Shaojun Qiu, Institute of Agricultural Resources and Regional Planning (CAAS), China

Reviewed by:
Honghui Wu, Institute of Agricultural Resources and Regional Planning (CAAS), China
Juanjuan Fu, Northwest A&F University, China

***Correspondence:**
Peng Wang
wangpeng@iae.ac.cn

Specialty section:
This article was submitted to Plant Nutrition, a section of the journal Frontiers in Plant Science

Received: *24 April 2022*
Accepted: *03 June 2022*
Published: *24 June 2022*

Citation:
Lu J, Yang J, Keitel C, Yin L, Wang P, Cheng W and Dijkstra FA (2022) Belowground Carbon Efficiency for Nitrogen and Phosphorus Acquisition Varies Between Lolium perenne and Trifolium repens and Depends on Phosphorus Fertilization. Front. Plant Sci. 13:927435. doi: 10.3389/fpls.2022.927435

Photosynthetically derived carbon (C) is allocated belowground, allowing plants to obtain nutrients. However, less is known about the amount of nutrients acquired relative to the C allocated belowground, which is referred to as C efficiency for nutrient acquisition (CENA). Here, we examined how C efficiency for nitrogen (N) and phosphorus (P) acquisition varied between ryegrass (*Lolium perenne*) and clover (*Trifolium repens*) with and without P fertilization. A continuous ^{13}C-labeling method was applied to track belowground C allocation. Both species allocated nearly half of belowground C to rhizosphere respiration (49%), followed by root biomass (37%), and rhizodeposition (14%). With regard to N and P, CENA was higher for clover than for ryegrass, which remained higher after accounting for relatively low C costs associated with biological N_2 fixation. Phosphorus fertilization increased the C efficiency for P acquisition but decreased the C efficiency for N acquisition. A higher CENA for N and P in clover may be attributed to the greater rhizosphere priming on soil organic matter decomposition. Increased P availability with P fertilization could induce lower C allocation for P uptake but exacerbate soil N limitation, thereby making N uptake less C efficient. Overall, our study revealed that species-specific belowground C allocation and nutrient uptake efficiency depend on which nutrient is limited.

Keywords: belowground carbon allocation, biological nitrogen fixation, carbon allocation for nutrient uptake, ^{13}C-labeling, rhizosphere priming effect

INTRODUCTION

Belowground carbon (C) allocation by plants is an important driver for plant nutrient acquisition. In a global synthesis, Pausch and Kuzyakov (2018) reported that grassland species allocated on an average of 33% of gross primary productivity belowground to root biomass, rhizosphere respiration, and rhizodeposition. This belowground C is tightly associated with plant nutrient acquisition through various strategies, such as generating fine roots or root hairs, forming

symbiotic associations with nitrogen (N)-fixing bacteria or mycorrhizal fungi, or stimulating microbial activity to mobilize nutrients from soil organic matter using root exudates (Lambers et al., 2008; Richardson et al., 2009; Zhu et al., 2014). Modeling studies have indicated that variation in C allocation for nutrient acquisition between N-fixing and non-fixing plants, or between arbuscular and ectomycorrhizal plants, is helpful for understanding their competitive advantages and how this relates to their abundance and productivity (Fisher et al., 2010; Brzostek et al., 2014). However, empirical research on how much total C plants allocate belowground to obtain nutrients is rare.

To assess the C efficiency associated with nutrient acquisition, we introduce a new parameter, i.e., C efficiency for nutrient acquisition (CENA), which we define as the amount of nutrients acquired relative to C allocated belowground (Wang et al., 2022). In most studies, belowground C allocation is primarily based on measures of root production, thus ignoring other C pathways such as allocation to root respiration, root exudates, and symbiotic relationships, which are extremely difficult to quantify (Vicca et al., 2012; Pausch and Kuzyakov, 2018; Keller et al., 2021). This assessment, without considering other C pathways, may underestimate total belowground C allocation, hindering an accurate understanding of CENA. ^{13}C-labeling methods provide us with the opportunity to quantify root respiration, root exudates, and symbiotic microbial respiration, which have been successfully applied in previous studies (Schmitt et al., 2013; Ven et al., 2019). Compared to traditional methods, the isotope tracer method permits us to consider all these belowground C allocation pathways. As rhizosphere respiration and rhizodeposition may account for a large proportion of the total C allocated belowground (Pausch and Kuzyakov, 2018), accounting for all belowground C allocation pathways will be required to accurately estimate CENA.

Belowground C allocation and CENA can vary greatly among plant species due to differences in root architecture and morphological traits, root exudates, mycorrhizal association, and the capacity of biological N_2 fixation (de Neergaard and Gorissen, 2004; Schmitt et al., 2013; Keller and Phillips, 2019). For example, legumes allocated more C to rhizosphere respiration compared to grasses, because of the extra energy and C demand for biological N_2 fixation by symbiotic rhizobia (Warembourg et al., 2003), while grasses may spend more C on dense fine roots or high rates of rhizodeposition for enhancing nutrient mobilization and uptake from the soil (Schmitt et al., 2013). The interspecific difference in belowground C allocation patterns will trigger different responses in nutrient acquisition, thereby influencing CENA between legumes and grasses.

Soil nutrient availability may also be an important factor influencing belowground C allocation and CENA. Using economic principles, it can be expected that nutrients become more C expensive for plants when their availability is low (Bloom et al., 1985). Most plants are limited by N, phosphorus (P), or both (Harpole et al., 2011; Du et al., 2020), and the amount of C that plants allocate belowground may strongly depend on which nutrient is limiting their growth. Although plant demand for P is lower than for N, belowground C allocation for P uptake may be higher than for N given that soil P availability is usually much lower and less mobile compared to N (Vitousek et al., 2010). Plants secrete carboxylates to liberate inorganic P from mineral surfaces, or produce phosphatase extracellular enzymes to increase P mobilization through hydrolysis, when P availability to plants is limited (Lambers et al., 2008; Richardson et al., 2011; Wen et al., 2019). Furthermore, plants may increase belowground C allocation to support arbuscular mycorrhizal fungi to enhance P uptake under low P conditions (Smith et al., 2011; van der Heijden et al., 2015; Ven et al., 2019). Therefore, plants may allocate more belowground C to root exudates or rhizosphere respiration when plants are limited by P. Due to their capacity to fix N_2 from the atmosphere, the growth of legumes is more likely to be P-limited (Png et al., 2017), and belowground C allocation and CENA in legumes may therefore be more sensitive to P availability in soil compared to grasses.

Here, we assessed belowground C allocation and C efficiency for N and P acquisition in ryegrass (*Lolium perenne* L., C_3 grass) and clover (*Trifolium repens* L., legume) with and without P fertilization based on the same greenhouse experiment in Lu et al. (2020). By continuously labeling plants with CO_2 depleted in ^{13}C, we were able to quantify different components of belowground C allocation (root biomass, rhizosphere respiration, and rhizodeposition). We further used a ^{15}N natural abundance method to estimate biological N_2 fixation in clover and finally assessed CENA by comparing belowground C allocation to nutrient content in plant biomass after 58 days of growth. The objectives of this study were to (1) compare the difference in C efficiency for N ($CENA_N$) and for P ($CENA_P$) between ryegrass and clover and (2) assess how P fertilization affects $CENA_N$ and $CENA_P$ in ryegrass and clover. We hypothesized that (1) clover would have a higher C efficiency for N ($CENA_N$) compared to ryegrass because plant N acquisition through biological N_2 fixation is usually more C efficient compared to uptake from the soil (Fisher et al., 2010); (2) P fertilization would increase $CENA_N$ in clover because P fertilization would increase biological N_2 fixation and reduce belowground C allocation associated with P uptake from the soil. However, P fertilization would increase N limitation in ryegrass, lowering $CENA_N$; and (3) C efficiency for P ($CENA_P$) would be lower in clover because biological N_2 fixation would cause it to be more limited by P compared to ryegrass; for the same reason, P fertilization would increase $CENA_P$ more in clover than in ryegrass.

MATERIALS AND METHODS

Experimental Design

Top soil (0–15 cm depth) was collected from a grassland at John Bruce Pye Farm in Camden, NSW, Australia (33°56′42″ S, 150°40′30″ E). The soil is a red-brown chromosol (Isbell, 2002) (or Alfisol based on USDA Soil Taxonomy), with a pH of 5.4, 34% sand, 31% silt, and 35% clay. The δ^{13}C of soil organic C was −23.06‰, and the organic C, total N, and total P concentrations were 28.8, 2.5, and 0.15 mg g^{-1}, respectively. The concentrations of soil mineral N (2 M KCl extraction) and available P (0.03 M NH_4F and 0.025 M HCl) were 58.0

and 8.7 mg kg^{-1}, respectively. Mesocosms consisted of bottom-capped polyvinyl chloride (PVC) pots (diameter 15 cm, height 20 cm) and sieved (4 mm) grassland soil (equivalent to 3.20 kg of oven-dried soil). After adjusting soil moisture content to 70% water-holding capacity (21% gravimetric soil moisture content), a modified Hoagland solution with macro- and micro-nutrients was added to all mesocosms [$(NH_4)_2SO_4$ 23.8, KNO_3 25.7, $Ca(NO_3)_2{\cdot}4H_2O$ 11.9, $MgCl_2{\cdot}6H_2O$ 16.4, H_3BO_3 0.08, $ZnSO_4{\cdot}7H_2O$ 0.2, $CuSO_4{\cdot}5H_2O$ 0.02, $FeSO_4{\cdot}7H_2O$ 0.25, and $MnCl_2{\cdot}4H_2O$ 0.3 g m^{-2}]. The P was applied to the treatment with P as a KH_2PO_4 and K_2HPO_4 solution with an adjusted ratio to obtain a similar pH to the soil (4 g of P m^{-2}), while for the treatment without P, a KCl solution was applied to eliminate the introduced K fertilization effect. These mesocosms (with and without P) were planted with either ryegrass (*Lolium perenne* L.) or clover (*Trifolium repens* L.) or were left unplanted (control). These two plant species are widely used to improve pastures in many temperate regions of the world. Besides the capacity of fixing N_2 from the atmosphere, ryegrass and clover also differ greatly in root morphological and architectural traits (**Table 1**), mycorrhizal infection (Zhu et al., 2000), and quantity and quality of root exudates (Lu et al., 2020), thereby showing different strategies of carbon allocation and nutrient acquisition. Six treatments were replicated four times. After germinating, each planted mesocosm was thinned to 20 plants.

This experiment lasted for 58 days in a controlled environmental facility at the Centre for Carbon, Water, and Food, University of Sydney, Camden (NSW). During the experimental period, the air temperature was kept at 25°C during the day and at 15°C during the night. The relative air humidity was kept at 60%, and artificial lights (Heliospectra, LX602C, 600 W, ∼1 mmol m^{-2} s^{-1}) went on for 12 h every day. The concentration of CO_2 was set at 800 ppm by injecting ^{13}C-depleted CO_2 into the chamber. This was needed to reduce the $\delta^{13}C$ value of CO_2 to a desired level and also to promote plants to grow faster, so that the labeled ^{13}C signature could be detected in different pools or fluxes of belowground C allocation during a short cultivation period. Although a high level of CO_2 concentration would affect plant photosynthesis and thereby nutrient uptake dynamics, we are not aware that it would cause significant bias when comparing the treatment effects (species and P) under the same CO_2 concentration. Moreover, our study provides novel insights into a mechanistic understanding of plant–soil interactions and is relevant given that global atmospheric CO_2 concentrations may reach 800 ppm or higher by the end of this century (Collins et al., 2013). We further note that we have used this method successfully in the past (e.g., Dijkstra and Cheng, 2007a; Canarini and Dijkstra, 2015). The $\delta^{13}C$ value of CO_2 was maintained at $-20 \pm 0.3‰$ (mean ± standard deviation) throughout the experiment (measured on a G2131-i Analyzer, Picarro, Santa Clara, CA, United States). More details about continuous ^{13}C-labeling method were reported in Lu et al. (2020). All mesocosms were randomly placed in the chamber and watered every 2 days to maintain soil moisture content at 70% water-holding capacity. The distribution of these mesocosms was randomly rotated every week to eliminate potential effects caused by spatial differences in light levels within the chamber.

Measurements

Total soil respiration was measured using a gas chamber method on 30, 44, and 58 days after planting (see full details in Lu et al., 2020). Briefly, at each gas sampling time, shoots were clipped at 1 cm above the soil surface and a non-transparent PVC chamber was sealed to each mesocosm. After removing initial CO_2 inside the mesocosm and chamber by circulating air inside the mesocosm through a soda lime column, a 12 mL gas sample was taken from the septum of the chamber at 0 h (T0), 1 h (T1), and 2 h (T2), respectively. These gas samples (T0, T1, and T2) were measured for CO_2 concentration and $\delta^{13}C$ on a Delta V advantage isotope ratio mass spectrometer (IRMS) coupled to a Gasbench (Thermo Fisher Scientific, Bremen, Germany). As plants were continuously labeled with depleted ^{13}C-CO_2 ($\delta^{13}C = -20‰$), we were able to separate root-derived CO_2 (root respiration and microbial respiration of rhizodeposits) from soil-derived CO_2. At the end of the experiment, root samples were carefully picked from the mesocosm and soil samples were homogenized. The clipped shoots at each sampling time, hand-picked roots, and homogenized soil were measured for C%, N%, $\delta^{13}C$, and $\delta^{15}N$ on a Delta V advantage IRMS coupled to a Conflo IV and Flash HT (Thermo Fisher Scientific, Bremen, Germany). The plant samples were also measured for P concentration on the UV–VIS spectrophotometer (UVmini-1240), following the protocol described by Jackson (1958).

TABLE 1 | Mean diameter (MD), specific root length (SRL), specific root surface area (SRA), root tissue density (RTD), and root length density (RLD) of ryegrass and clover with and without P addition.

Treatment	MD, mm	SRL, m g^{-1}	SRA, cm^2 g^{-1}	RTD, g cm^{-3}	RLD, m cm^{-3}
Ryegrass − P	0.23 ± 0.01b	220 ± 24a	1561 ± 119a	0.11 ± 0.01b	0.32 ± 0.04a
Ryegrass + P	0.24 ± 0.01b	208 ± 11a	1533 ± 58a	0.11 ± 0.01b	0.31 ± 0.03a
Clover − P	0.29 ± 0.01a	87 ± 7b	790 ± 42b	0.17 ± 0.01a	0.11 ± 0.01b
Clover + P	0.29 ± 0.01a	87 ± 4b	801 ± 31b	0.17 ± 0.01a	0.10 ± 0.01b
ANOVA (*p*-values)					
Species	< 0.001	< 0.001	< 0.001	< 0.001	< 0.001
P	0.601	0.676	0.906	0.61	0.76
Species × P	0.684	0.649	0.792	0.956	0.903

Values are shown as mean ± SE (n = 4). Two-way ANOVA p-values are shown.

Calculations

Belowground C allocation includes C for root growth (root biomass C), rhizosphere respiration (root-derived CO_2), and rhizodeposition (root-derived SOC). For clover, rhizosphere respiration also includes a C cost for biological N_2 fixation. We calculated rhizosphere respiration at each sampling date using a mass balance method based on $\delta^{13}C$ signatures of CO_2 in planted and unplanted mesocosms (Lu et al., 2020) as follows:

$$C_{root} = C_{total} \times (\delta^{13}C_{total} - \delta^{13}C_{soil})/(\delta^{13}C_{root} - \delta^{13}C_{soil}) \quad (1)$$

$$C_{soil} = C_{total} - C_{root} \quad (2)$$

where C_{total}, C_{soil}, and C_{root} are total belowground CO_2, soil-derived CO_2, and root-derived CO_2 in planted mesocosms, respectively. $\delta^{13}C_{total}$ is the measured $\delta^{13}C$ value of total belowground CO_2 in planted treatments. $\delta^{13}C_{soil}$ is the mean $\delta^{13}C$ value of soil respiration in the unplanted control. $\delta^{13}C_{root}$ is the $\delta^{13}C$ value of root-derived CO_2 in planted treatments, which was calculated based on the $\delta^{13}C$ value of root tissue corrected by a fractionation factor of root-derived CO_2 relative to root tissue ($-1.74‰$ for grass and $-2.67‰$ for legume; Werth and Kuzyakov, 2010). We calculated the rhizosphere priming effect as the difference in soil-derived CO_2 between planted and unplanted control treatments (Lu et al., 2020).

Rhizosphere respiration during the whole 58-day experiment was then calculated using a linear extrapolation method based on the root-derived CO_2 at three sampling dates (30, 44, and 58 days after planting). It is noted that clipping before trapping belowground CO_2 may cause a decrease in root-derived CO_2 (Shahzad et al., 2012). Root-derived CO_2 was only measured during day time in this study. Root-derived CO_2 at night in wheat was sometimes lower than during the day, but at other times, night-time root-derived CO_2 was similar to day-time rhizosphere respiration (Kuzyakov and Cheng, 2001). Furthermore, we noted that the respiration of crowns and a negligible amount of shoot biomass were included in our measured rhizosphere respiration. Therefore, the calculated cumulative rhizosphere respiration during the entire experiment may have been somewhat overestimated, but unfortunately, we were unable to quantify this.

We calculated new root-derived SOC formed during the experiment (C_{new}) based on $\delta^{13}C$ signatures of soil organic C at the start and end of the experiment in planted mesocosms (Dijkstra and Cheng, 2007b) as follows:

$$C_{new} = C_{end} \times (\delta^{13}C_{initial} - \delta^{13}C_{end})/(\delta^{13}C_{initial} - \delta^{13}C_{root}) \quad (3)$$

where $C_{initial}$ and C_{end} are the total amount of soil organic C at the beginning and end of the experiment, respectively. $\delta^{13}C_{initial}$ is the $\delta^{13}C$ value of $C_{initial}$, $\delta^{13}C_{end}$ is the $\delta^{13}C$ value of C_{end}, and $\delta^{13}C_{root}$ is the $\delta^{13}C$ value of root biomass.

Carbon efficiency for nutrient acquisition was calculated as plant nutrient content divided by belowground C allocation. Plant N and P contents were calculated by multiplying tissue biomass with tissue N and P concentration. Considering the C cost for biological N_2 fixation in clover, we calculated CENA associated with belowground C allocation for plant nutrient uptake from the soil only, by subtracting C used for biological N_2 fixation from the total belowground C allocation (both for $CENA_N$ and $CENA_P$) and subtracting biologically fixed N from the total plant N content (for $CENA_N$) in clover treatments as follows:

$$CENA_N = (N_{plant} - N_{fix})/(C_{below\ allocation} - C_{biological\ N\ fixation}) \quad (4)$$

$$CENA_P = P_{plant}/(C_{below\ allocation} - C_{biological\ N\ fixation}) \quad (5)$$

where N_{plant} and P_{plant} are the N and P contents in the total plant biomass (shoots and roots) after day 58 plus the N and P contents in shoot biomass clipped on day 30 and 44, respectively. N_{fix} is the biologically fixed N in clover, $C_{below\ allocation}$ is the total belowground C allocation, and $C_{biologicalNfixation}$ is the C used for biological N_2 fixation. Carbon costs associated with biological N_2 fixation in legumes are relatively constant, ranging between 8 and 12 g C g^{-1} fixed N, depending on soil temperature (Fisher et al., 2010). Here, we used a value of 8 g C g^{-1} fixed N as the C cost for biological N_2 fixation in clover at 20°C. Biologically fixed N in clover was calculated using the ^{15}N natural abundance method (Mia et al., 2018) as follows:

$$N_{fix} = N_{clover} \times (\delta^{15}N_{ryegrass} - \delta^{15}N_{clover})/(\delta^{15}N_{ryegrass} - \delta^{15}N_{bnf}) \quad (6)$$

where N_{clover} is the N content in clover tissues, $\delta^{15}N_{ryegrass}$ and $\delta^{15}N_{clover}$ are the $\delta^{15}N$ values of ryegrass (used as a reference plant) and clover tissues, respectively, and $\delta^{15}N_{bnf}$ is the $\delta^{15}N$ value of N-fixing plants completely relying on biological N_2 fixation (without N uptake from soil), which was estimated as $-1.527‰$ for clover (Mia et al., 2018).

Statistical Analyses

Two-way ANOVA was applied to test the main and interactive effects of plant species and P fertilization on root biomass C, rhizosphere respiration, rhizodeposition, belowground C allocation, plant tissue $\delta^{15}N$, biologically fixed N, and CENA. The *post hoc* Tukey's honest significant difference (HSD) test was used to compare variables among ryegrass, ryegrass with P fertilization, clover, and clover with P fertilization treatments. Differences at $p < 0.05$ were considered significant, while differences between $p > 0.05$ and $p < 0.1$ were considered marginally significant. All statistical analyses were performed using the SPSS 20.0 (IBM SPSS Statistics 20, Armonk, United States).

RESULTS

Belowground C Allocation

Ryegrass showed larger root biomass C than clover (**Figure 1A**); clover showed larger rhizosphere respiration than ryegrass (**Figure 1B**); and the two species did not differ in rhizodeposition (**Figure 1C**). Due to the contrasting patterns of root biomass and rhizosphere respiration, there was no significant difference in belowground C allocation between the two species (**Figure 1D**).

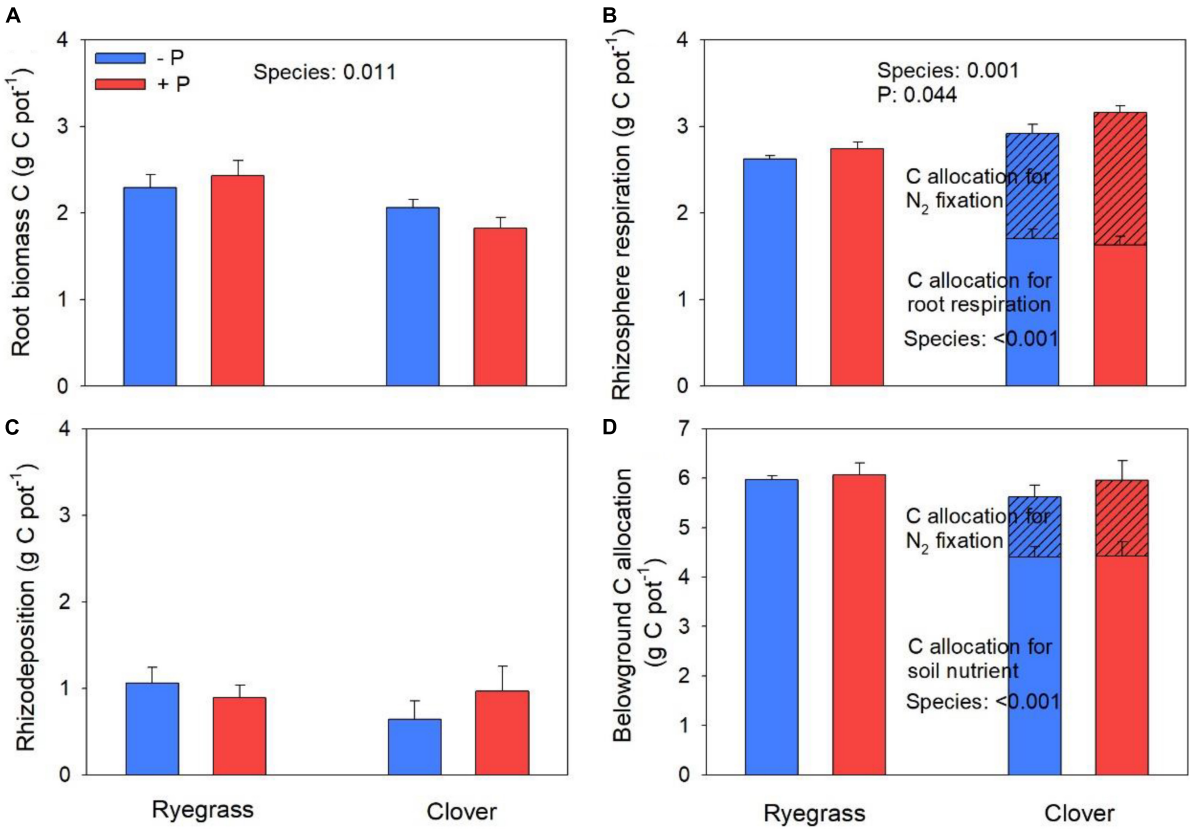

FIGURE 1 | Root biomass C **(A)**, rhizosphere respiration **(B)**, rhizodeposition **(C)**, and total belowground C allocation **(D)** of ryegrass and clover with and without P addition. For rhizosphere respiration and total belowground C allocation, allocation was separated into C allocation for biological N fixation (shaded bars) and for nutrient uptake from the soil (non-shaded bars). Sub-legend shows ANOVA *p*-values. Error bar indicates one standard error of the mean (n = 4).

Both ryegrass and clover allocated more belowground C to rhizosphere respiration (45 and 53%) and less to root biomass (40 and 34%) and rhizodeposition (15 and 13%) (**Figure 1**). For clover, the C cost for biological N fixation accounted on an average for 45% of rhizosphere respiration and 24% of total belowground C allocation, respectively. When excluding C cost for biological N_2 fixation, clover showed lower rhizosphere respiration (**Figure 1B**) and less belowground C allocation than ryegrass (**Figure 1D**). P fertilization increased rhizosphere respiration (on an average by 6%; **Figure 1B**) but did not significantly influence the total belowground C allocation of both species (**Figure 1D**).

Plant Nutrient Acquisition and Carbon Efficiency for Nutrient Acquisition

Plant N and P contents were reported in Lu et al. (2020). Briefly, clover had higher plant N and P contents than ryegrass (104 and 53% higher, respectively). On average, 37% of plant N in clover was biologically fixed by rhizobia from the atmosphere (**Table 2**). After subtracting biologically fixed N, non-fixed N in clover was still higher than in ryegrass (28%). Phosphorus fertilization significantly increased plant P content in both species (10%), marginally increased biologically fixed N in clover (27%, **Table 2**) and significantly decreased non-fixed N in both species (11%). $CENA_N$ (including C cost for biological N_2 fixation) was higher for clover than for ryegrass (**Figure 2A**). When excluding C cost for biological N_2 fixation, clover still showed a higher $CENA_N$ than ryegrass (**Figure 2B**), while $CENA_P$ was also higher for clover (**Figure 2C**), indicating that clover obtained more N and P from soil with less belowground C. Phosphorus addition increased $CENA_P$ (**Figure 2C**) but decreased $CENA_N$ in both species (**Figure 2B**), although the effects were marginally significant.

DISCUSSION

Half of the total belowground C allocation was allocated to rhizosphere respiration (including root respiration and rhizosphere microbial respiration of rhizodeposits), suggesting that autotrophic respiration plays an important role in plant belowground C allocation and the total soil CO_2 efflux (Hopkins et al., 2013). Rhizodeposition remaining in soil accounted for the lowest fraction of belowground C allocation (an average of 14%), but actual rhizodeposition rates must be higher considering that most of the rhizodeposition is lost as CO_2 *via* rapid microbial decomposition (Pausch et al., 2013;

TABLE 2 | Plant $\delta^{15}N$ values in shoot and root biomass of ryegrass and clover, and biologically fixed N in clover with and without P fertilization (T1, Day 30; T2, Day 44; T3, Day 58).

Treatments	Plant $\delta^{15}N$				Fixed N (mg pot^{-1})
	T1-shoot $\delta^{15}N$	T2-shoot $\delta^{15}N$	T3-shoot $\delta^{15}N$	Root $\delta^{15}N$	
Ryegrass − P	2.57 ± 0.06ab	2.35 ± 0.12a	1.59 ± 0.07a	1.63 ± 0.22a	0
Ryegrass + P	2.28 ± 0.08b	1.55 ± 0.13bc	1.06 ± 0.12b	1.31 ± 0.04ab	0
Clover − P	3.08 ± 0.31a	1.97 ± 0.14ab	−0.43 ± 0.06c	1.02 ± 0.17ab	151 ± 12.2
Clover + P	2.69 ± 0.1ab	1.07 ± 0.15c	−1.01 ± 0.11d	0.77 ± 0.13b	191 ± 16.4
ANOVA (*p*-values)					
Species	0.016	0.007	< 0.001	0.003	–
P	0.065	< 0.001	< 0.001	0.088	–
Species × P	0.770	0.712	0.771	0.836	–

Values are shown as mean ± SE (n = 4). Two-way ANOVA p-values are shown.

Pausch and Kuzyakov, 2018; Liu et al., 2019), which in our case was included in rhizosphere respiration. Root biomass accounted for 37% of total belowground C allocation, which was smaller than rhizosphere respiration and rhizodeposition. These results suggest that the assessment of belowground C allocation based only on root biomass is somewhat biased and that rhizosphere respiration and rhizodeposition cannot be ignored. We acknowledge that our estimates of rhizosphere respiration were based on only three flux measurements and that they were done during the day only, and as such have the greatest uncertainty that needs further investigation. Nevertheless, the distribution of belowground C among different pools or fluxes is to some degree consistent with the C allocation patterns for grassland species synthesized by Pausch and Kuzyakov (2018).

Although clover allocated less C to root biomass, it showed greater rhizosphere respiration than ryegrass, possibly because biological N_2 fixation by clover requires C. Indeed, when accounting for C allocation toward biological N_2 fixation and assuming that this C would eventually be respired as CO_2, there was a larger rhizosphere respiration in ryegrass than in clover instead (**Figure 1B**). Thus, C allocation toward biological N_2 fixation was an important component of rhizosphere respiration for clover. Previous studies also suggested that legumes had a higher demand for assimilated C as indicated by higher rhizosphere respiration than grasses (Warembourg et al., 2003; Schmitt et al., 2013). Furthermore, we estimated that the C cost for biological N_2 fixation was about 8 g C g^{-1} N (C cost at 20°C) according to Fisher et al. (2010), while the C allocation for plant N uptake from soil in clover was then 14 g C g^{-1} N (inverse of $CENA_N$, **Figure 2B**). This result suggests that biological N_2 fixation by the legume is a relatively C efficient way to acquire N as compared to plant N uptake from soil. Even if the C cost for biological N_2 fixation is higher than what we assumed (e.g., assuming 10 or 12 g C g^{-1} fixed N, respectively; Fisher et al., 2010), the C cost for biological N_2 fixation would still be cheaper than or similar to that for N uptake from soil in clover (e.g., C allocation for plant N uptake would then be 13.3 or 12.3 g C g^{-1} N, respectively). Clearly, more work is needed to compare the C cost for biological N_2 fixation vs. N uptake. Nevertheless, our results may explain why N_2-fixing plants often compete with non-fixing plants, particularly under the condition of low N availability (Vitousek and Howarth, 1991; Crews, 1999; Menge et al., 2017; Wang et al., 2022).

Consistent with our hypothesis, clover had a higher $CENA_N$ than ryegrass because, as discussed above, less C was required for biological N_2 fixation than for N uptake from soil. However, $CENA_N$ of clover was still higher than ryegrass after we accounted for the C cost associated with biological N_2 fixation. In contrast to our hypothesis, $CENA_P$ was also higher for clover than for ryegrass. Possibly, the greater rhizosphere priming effect on soil organic matter decomposition that we observed for clover by the end of the experiment in another study may contribute to the higher $CENA_N$ and $CENA_P$ (Lu et al., 2020). By the end of the experiment, available forms of N in soil were extremely low (less than 7 mg N pot^{-1} or 2 mg N kg^{-1} soil), and likely very C expensive to take up by both ryegrass and clover. Therefore, stimulation of soil organic matter decomposition by root exudates and subsequent release of N (and P) for plant uptake may be a very C-efficient way for plants to acquire nutrients from the soil (**Figure 3**; Wang et al., 2022). Previous studies also suggested that legume species could produce larger rhizosphere priming effects than non-legume species (Cheng et al., 2003; Drake et al., 2013). Alternatively, the higher $CENA_P$ in clover than in ryegrass may also be attributed to the tendency of legumes to cause greater acidification in the rhizosphere and exude carboxylates to mobilize and increase concentrations of inorganic P through dissolution or desorption (Hinsinger, 2001; Nuruzzaman et al., 2006).

In contrast to our hypothesis, P fertilization slightly decreased the $CENA_N$ in ryegrass and clover, suggesting that P fertilization caused these plants to allocate more belowground C to acquire N from soil. In this study, although biological N_2 fixation in clover marginally increased with P fertilization (**Table 2**), the increase of this relatively cheap form of N acquisition was apparently not enough to counter the increase in belowground C allocation for soil N uptake. Possibly, P fertilization may have exacerbated soil N limitation by increasing microbial N immobilization (Blanes et al., 2012; Mehnaz et al., 2019), and thus did not improve belowground C allocation. Indeed, microbial biomass N measured at the end of the experiment was significantly higher

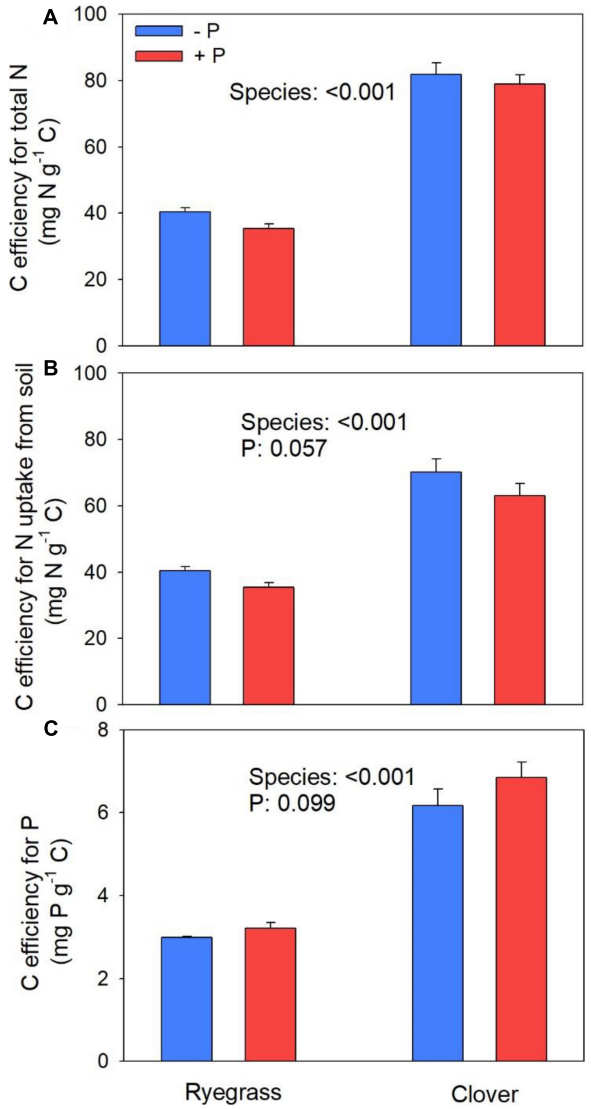

FIGURE 2 | Belowground C efficiency for N acquisition ($CENA_N$) including **(A)** and excluding **(B)** biological N_2 fixation and associated C allocation, and belowground C efficiency for P acquisition ($CENA_P$) excluding C used for biological N fixation **(C)** for ryegrass and clover with and without P addition. Sub-legend shows ANOVA *p*-values. Error bar indicates one standard error of the mean (n = 4).

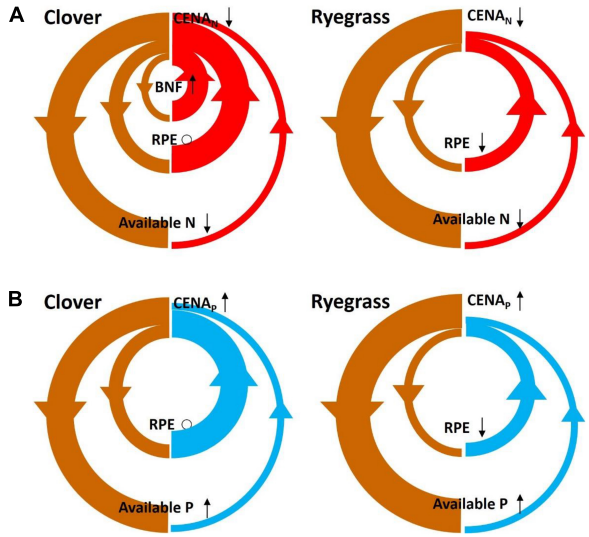

FIGURE 3 | Schematic framework showing how belowground C efficiency for N acquisition ($CENA_N$) **(A)** and for P acquisition ($CENA_P$) **(B)** vary with soil P availability for clover and ryegrass. Brown arrows, carbon flows; red arrows, nitrogen flows; and blue arrows, phosphorus flows. Thickness of arrows indicates the relative importance of C, N, and P flows, while differences in thickness between carbon and nutrient flows indicate CENA (i.e., relatively thick carbon arrows compared to nutrient arrows indicate a low CENA and vice versa). BNF, biological N_2 fixation; RPE, rhizosphere priming effect. Black arrows and circles next to $CENA_N$, $CENA_P$, BNF, RPE, available N, and available P indicate effect of P fertilization (upward arrow, positive; downward arrow, negative; circle, and no effect). For clover, $CENA_N$ decreases with P fertilization because the negative effect of P fertilization on N availability outweighs the positive effect on BNF.

with P fertilization (an average of 17%; Lu et al., 2020). In turn, increased microbial N immobilization with P fertilization may thus reduce soil available N, thereby making it more C expensive for plant uptake (**Figure 3**). It has also been suggested that C allocation could increase to maintain plant N uptake at low N conditions (Brzostek et al., 2014; Perkowski et al., 2021). Our results further imply that plant C allocation belowground for N uptake depends on P availability.

Phosphorous fertilization marginally increased the $CENA_P$ for both species, indicating that the P uptake may become somewhat less C expensive with increased soil P availability (**Figure 3**). This result is consistent with the resource optimization hypothesis that plants allocate more C to acquire limited resources (McMurtrie and Dewar, 2013). Previous studies also found that belowground C investment in P acquisition was more efficient with P fertilization (Ven et al., 2019). We expected that $CENA_P$ would increase more for clover than for ryegrass given that growth of the N-fixing clover would be more limited by P than ryegrass (Png et al., 2017). However, we found no support for this (no significant species × P interaction), but we should note that the increases in $CENA_P$ with P fertilization were relatively small and only marginally significant. Clearly, more work is needed for an in-depth understanding of the mechanisms underlying the $CENA_N$ and $CENA_P$ of grasses and legumes under different N and P availabilities.

While we did not investigate interspecific interactions on CENA, the CENA concept may have significant implications for plant community dynamics and competition for nutrients in legume-grass mixtures (Raven et al., 2018; Wang et al., 2022). When legumes have a higher CENA compared to grasses, they may temporarily outcompete grasses for soil nutrients until conditions arise that reduce CENA for legumes more than for grasses (e.g., under drought or high levels of soil N). Changes in CENA with time would also depend on how flexible plants are in switching C allocation toward different nutrient acquisition strategies (Fisher et al., 2010). Furthermore, interspecific competition for nutrients by itself, as well as the

transfer of biologically fixed N from legume to grass, could potentially influence the CENA of individual species in grassland mixtures, which could help explain the often observed temporal dynamics in legume and grass abundance in mixed pastures (Ledgard and Steele, 1992). Further research is therefore needed to investigate the role of CENA in plant community dynamics in legume-grass mixtures.

CONCLUSION

In our study, we quantified the belowground C allocation and its efficiency for N and P acquisition ($CENA_N$ and $CENA_P$, respectively). We showed that clover had higher $CENA_N$ and $CENA_P$ than ryegrass, even after accounting for the relatively low C costs associated with biological N_2 fixation, possibly because of the distinct rhizosphere priming on soil organic matter decomposition. Furthermore, P fertilization decreased $CENA_N$, possibly *via* exacerbating soil N limitation, while P fertilization increased $CENA_P$ because plant P acquisition was more efficient with increased P availability. Current modeling studies have indicated that net primary productivity and soil C storage are strongly associated with variation in the belowground C allocation for nutrient uptake (Fisher et al., 2010; Brzostek et al., 2014; Shi et al., 2016). Yet, estimates of $CENA_N$ and $CENA_P$ are lacking. To the best of our knowledge, this is one of the first studies to provide estimates for these parameters. We acknowledge that our study is based on two plant species only and in one soil type only, and that variation in CENA should be examined across a larger set of plant species, communities, and soil types during a relatively long period. Nevertheless, we believe that better understanding of $CENA_N$ and $CENA_P$ will help not only improve global C cycling model predictions but also identify management practices to increase yield and fertilizer use efficiency in agricultural systems.

DATA AVAILABILITY STATEMENT

The original contributions presented in this study are included in the article/supplementary material, further inquiries can be directed to the corresponding author.

AUTHOR CONTRIBUTIONS

JL and FD designed the experiment. JL, JY, and CK performed the experiment. JL analyzed the data. JL, LY, PW, WC, and FD wrote the manuscript. All authors contributed to the article and approved the submitted version.

FUNDING

This study was supported by the Australian Research Council (DP190102262), the National Natural Science Foundation of China (32001386), and a visiting scholarship to JL from the Joint Ph.D. Training Program by the University of Chinese Academy of Sciences.

ACKNOWLEDGMENTS

We thank Milad Bagheri Shirvan for laboratory assistance.

REFERENCES

Blanes, M. C., Emmett, B. A., Viñegla, B., and Carreira, J. A. (2012). Alleviation of P limitation makes tree roots competitive for N against microbes in a N-saturated conifer forest: a test through P fertilization and 15N labelling. *Soil Biol. Biochem.* 48, 51–59. doi: 10.1016/j.soilbio.2012.01.012

Bloom, A. J., Chapin, F. S., and Mooney, H. A. (1985). Resource limitation in plants-An economic analogy. *Annu. Rev. Ecol. Syst.* 16, 363–392. doi: 10.1146/annurev.es.16.110185.002051

Brzostek, E. R., Fisher, J. B., and Phillips, R. P. (2014). Modeling the carbon cost of plant nitrogen acquisition: mycorrhizal trade-offs and multipath resistance uptake improve predictions of retranslocation. *J. Geophys. Res. Biogeosci.* 119, 1684–1697. doi: 10.1002/2014jg002660

Canarini, A., and Dijkstra, F. A. (2015). Dry-rewetting cycles regulate wheat carbon rhizodeposition, stabilization and nitrogen cycling. *Soil Biol. Biochem.* 81, 195–203. doi: 10.1016/j.soilbio.2014.11.014

Cheng, W., Johnson, D. W., and Fu, S. (2003). Rhizosphere effects on dcomposition: control of plant species, phenology, and fertilization. *Soil Sci. Soc. Am. J.* 67, 1418–1427. doi: 10.2136/sssaj2003.1418

Collins, M., Knutti, R., Arblaster, J., Dufresne, J.-L., Fichefet, T., Friedlingstein, P., et al. (2013). "Long-term Climate Change: Projections, Commitments and Irreversibility," in *Climate Change 2013: The Physical Science Basis. Contribution of Working Group I to the Fifth Assessment Report of the Intergovernmental Panel on Climate Change*, eds T. F. Stocker, D. Qin, G.-K. Plattner, M. Tignor, S. K. Allen, J. Boschung, et al. (Cambridge: Cambridge University Press).

Crews, T. E. (1999). The presence of nitrogen fixing legumes in terrestrial communities: evolutionary vs ecological considerations. *Biogeochemistry* 46, 233–246. doi: 10.1007/BF01007581

de Neergaard, A., and Gorissen, A. (2004). Carbon allocation to roots, rhizodeposits and soil after pulse labelling: a comparison of white clover (Trifolium repens L.) and perennial ryegrass (Lolium perenne L.). *Biol. Fertil. Soils* 39, 228–234. doi: 10.1007/s00374-003-0699-x

Dijkstra, F. A., and Cheng, W. (2007a). Moisture modulates rhizosphere effects on C decomposition in two different soil types. *Soil Biol. Biochem.* 39, 2264–2274. doi: 10.1016/j.soilbio.2007.03.026

Dijkstra, F. A., and Cheng, W. (2007b). Interactions between soil and tree roots accelerate long-term soil carbon decomposition. *Ecol. Lett.* 10, 1046–1053. doi: 10.1111/j.1461-0248.2007.01095.x

Drake, J. E., Darby, B. A., Giasson, M. A., Kramer, M. A., Phillips, R. P., and Finzi, A. C. (2013). Stoichiometry constrains microbial response to root exudation-insights from a model and a field experiment in a temperate forest. *Biogeosci* 10, 821–838. doi: 10.5194/bg-10-821-2013

Du, E., Terrer, C., Pellegrini, A. F. A., Ahlstrom, A., van Lissa, C. J., Zhao, X., et al. (2020). Global patterns of terrestrial nitrogen and phosphorus limitation. *Nat. Geosci.* 13, 221–226. doi: 10.1038/s41561-019-0530-4

Fisher, J. B., Sitch, S., Malhi, Y., Fisher, R. A., Huntingford, C., and Tan, S. Y. (2010). Carbon cost of plant nitrogen acquisition: a mechanistic, globally applicable model of plant nitrogen uptake, retranslocation, and fixation. *Glob. Biogeochem. Cycles* 24:GB1014. doi: 10.1029/2009gb003621

Harpole, W. S., Ngai, J. T., Cleland, E. E., Seabloom, E. W., Borer, E. T., Bracken, M. E. S., et al. (2011). Nutrient co-limitation of primary producer communities. *Ecol. Lett.* 14, 852–862. doi: 10.1111/j.1461-0248.2011.01651.x

Hinsinger, P. (2001). Bioavailability of soil inorganic P in the rhizosphere as affected by root-induced chemical changes: a review. *Plant Soil* 237, 173–195.

Hopkins, F., Gonzalez-Meler, M. A., Flower, C. E., Lynch, D. J., Czimczik, C., Tang, J., et al. (2013). Ecosystem-level controls on root-rhizosphere respiration. *N. Phytol.* 199, 339–351. doi: 10.1111/nph.12271

Isbell, R. F. (2002). *The Australian Soil Classification*. Collingwood, Vic, Australia: CSIRO Pub.

Jackson, M. L. (1958). *Soil Chemical Analsysis*. Englewood Cliffs, NJ: Prentice-Hall, Inc.

Keller, A. B., Brzostek, E. R., Craig, M. E., Fisher, J. B., and Phillips, R. P. (2021). Root-derived inputs are major contributors to soil carbon in temperate forests, but vary by mycorrhizal type. *Ecol. Lett.* 24, 626–635. doi: 10.1111/ele.13651

Keller, A. B., and Phillips, R. P. (2019). Relationship between belowground carbon allocation and nitrogen uptake in saplings varies by plant mycorrhizal type. *Front. Forests Glob. Chang.* 2:81. doi: 10.3389/ffgc.2019.00081

Kuzyakov, Y., and Cheng, W. (2001). Photosynthesis controls of rhizosphere respiration and organic matter decomposition. *Soil Biol. Biochem.* 33, 1915–1925. doi: 10.1016/S0038-0717(01)00117-1

Lambers, H., Raven, J. A., Shaver, G. R., and Smith, S. E. (2008). Plant nutrient-acquisition strategies change with soil age. *Trends Ecol. Evol.* 23, 95–103. doi: 10.1016/j.tree.2007.10.008

Ledgard, S. F., and Steele, K. W. (1992). Biological nitrogen fixation in mixed legume/grass pastures. *Plant Soil* 141, 137–153. doi: 10.1007/BF00011314

Liu, Y., Ge, T., Zhu, Z., Liu, S., Luo, Y., Li, Y., et al. (2019). Carbon input and allocation by rice into paddy soils: a review. *Soil Biol. Biochem.* 133, 97–107. doi: 10.1016/j.soilbio.2019.02.019

Lu, J., Yang, J., Keitel, C., Yin, L., Wang, P., Cheng, W., et al. (2020). Rhizosphere priming effects of Lolium perenne and Trifolium repens depend on phosphorus fertilization and biological nitrogen fixation. *Soil Biol. Biochem.* 150:108005. doi: 10.1016/j.soilbio.2020.108005

McMurtrie, R. E., and Dewar, R. C. (2013). New insights into carbon allocation by trees from the hypothesis that annual wood production is maximized. *N. Phytol.* 199, 981–990. doi: 10.1111/nph.12344

Mehnaz, K. R., Corneo, P. E., Keitel, C., and Dijkstra, F. A. (2019). Carbon and phosphorus addition effects on microbial carbon use efficiency, soil organic matter priming, gross nitrogen mineralization and nitrous oxide emission from soil. *Soil Biol. Biochem.* 134, 175–186. doi: 10.1016/j.soilbio.2019.04.003

Menge, D. N. L., Batterman, S. A., Liao, W., Taylor, B. N., Lichstein, J. W., and Ángeles-Pérez, G. (2017). Nitrogen-fixing tree abundance in higher-latitude North America is not constrained by diversity. *Ecol. Lett.* 20, 842–851. doi: 10.1111/ele.12778

Mia, S., Dijkstra, F. A., and Singh, B. (2018). Enhanced biological nitrogen fixation and competitive advantage of legumes in mixed pastures diminish with biochar aging. *Plant Soil* 424, 639–651. doi: 10.1007/s11104-018-3562-4

Nuruzzaman, M., Lambers, H., Bolland, M. D. A., and Veneklaas, E. J. (2006). Distribution of carboxylates and acid phosphatase and depletion of different phosphorus fractions in the rhizosphere of a cereal and three grain legumes. *Plant Soil* 281, 109–120. doi: 10.1007/s11104-005-3936-2

Pausch, J., and Kuzyakov, Y. (2018). Carbon input by roots into the soil: quantification of rhizodeposition from root to ecosystem scale. *Glob. Change Biol.* 24, 1–12. doi: 10.1111/gcb.13850

Pausch, J., Tian, J., Riederer, M., and Kuzyakov, Y. (2013). Estimation of rhizodeposition at field scale: upscaling of a 14C labeling study. *Plant Soil* 364, 273–285. doi: 10.1007/s11104-012-1363-8

Perkowski, E. A., Waring, E. F., and Smith, N. G. (2021). Root mass carbon costs to acquire nitrogen are determined by nitrogen and light availability in two species with different nitrogen acquisition strategies. *J. Exp. Bot.* 72, 5766–5776. doi: 10.1093/jxb/erab253

Png, G. K., Turner, B. L., Albornoz, F. E., Hayes, P. E., Lambers, H., and Laliberte, E. (2017). Greater root phosphatase activity in nitrogen-fixing rhizobial but not actinorhizal plants with declining phosphorus availability. *J. Ecol.* 105, 1246–1255. doi: 10.1111/1365-2745.12758

Raven, J. A., Lambers, H., Smith, S. E., and Westoby, M. (2018). Costs of acquiring phosphorus by vascular land plants: patterns and implications for plant coexistence. *N. Phytol.* 217, 1420–1427. doi: 10.1111/nph.14967

Richardson, A. E., Barea, J. M., McNeill, A. M., and Prigent-Combaret, C. (2009). Acquisition of phosphorus and nitrogen in the rhizosphere and plant growth promotion by microorganisms. *Plant Soil* 321, 305–339. doi: 10.1007/s11104-009-9895-2

Richardson, A. E., Lynch, J. P., Ryan, P. R., Delhaize, E., Smith, F. A., Smith, S. E., et al. (2011). Plant and microbial strategies to improve the phosphorus efficiency of agriculture. *Plant Soil* 349, 121–156. doi: 10.1007/s11104-011-0950-4

Schmitt, A., Pausch, J., and Kuzyakov, Y. (2013). C and N allocation in soil under ryegrass and alfalfa estimated by 13C and 15N labelling. *Plant Soil* 368, 581–590. doi: 10.1007/s11104-012-1536-5

Shahzad, T., Chenu, C., Repinçay, C., Mougin, C., Ollier, J., and Fontaine, S. (2012). Plant clipping decelerates the mineralization of recalcitrant soil organic matter under multiple grassland species. *Soil Biol. Biochem.* 51, 73–80. doi: 10.1016/j.soilbio.2012.04.014

Shi, M., Fisher, J. B., Brzostek, E. R., and Phillips, R. P. (2016). Carbon cost of plant nitrogen acquisition: global carbon cycle impact from an improved plant nitrogen cycle in the Community Land Model. *Glob. Change Biol.* 22, 1299–1314. doi: 10.1111/gcb.13131

Smith, S. E., Jakobsen, I., Gronlund, M., and Smith, F. A. (2011). Roles of arbuscular mycorrhizas in plant phosphorus nutrition: interactions between pathways of phosphorus uptake in arbuscular mycorrhizal roots have important implications for understanding and manipulating plant phosphorus acquisition. *Plant Physiol.* 156, 1050–1057. doi: 10.1104/pp.111.174581

van der Heijden, M. G. A., Martin, F. M., Selosse, M. A., and Sanders, I. R. (2015). Mycorrhizal ecology and evolution: the past, the present, and the future. *N. Phytol.* 205, 1406–1423. doi: 10.1111/nph.13288

Ven, A., Verlinden, M. S., Verbruggen, E., and Vicca, S. (2019). Experimental evidence that phosphorus fertilization and arbuscular mycorrhizal symbiosis can reduce the carbon cost of phosphorus uptake. *Funct. Ecol.* 33, 2215–2225. doi: 10.1111/1365-2435.13452

Vicca, S., Luyssaert, S., Peñuelas, J., Campioli, M., Chapin, F. S., Ciais, P., et al. (2012). Fertile forests produce biomass more efficiently. *Ecol. lett.* 15, 520–526. doi: 10.1111/j.1461-0248.2012.01775.x

Vitousek, P. M., and Howarth, R. W. (1991). Nitrogen limitation on land and in the sea: how can it occur? *Biogeochemistry* 13, 87–115. doi: 10.1007/BF00002772

Vitousek, P. M., Porder, S., Houlton, B. Z., and Chadwick, O. A. (2010). Terrestrial phosphorus limitation: mechanisms, implications, and nitrogen-phosphorus interactions. *Ecol. Appl.* 20, 5–15. doi: 10.1890/08-0127.1

Wang, R., Lu, J., Jiang, Y., and Dijkstra, F. A. (2022). Carbon efficiency for nutrient acquisition (CENA) by plants: role of nutrient availability and microbial symbionts. *Plant Soil* doi: 10.1007/s11104-022-05347-y

Warembourg, F. R., Roumet, C., and Lafont, F. (2003). Differences in rhizosphere carbon-partitioning among plant species of different families. *Plant Soil* 256, 347–357. doi: 10.1023/a:1026147622800

Wen, Z., Li, H., Shen, Q., Tang, X., Xiong, C., Li, H., et al. (2019). Tradeoffs among root morphology, exudation and mycorrhizal symbioses for phosphorus-acquisition strategies of 16 crop species. *N. Phytol.* 223, 882–895. doi: 10.1111/nph.15833

Werth, M., and Kuzyakov, Y. (2010). 13C fractionation at the root-microorganisms-soil interface: a review and outlook for partitioning studies. *Soil Biol. Biochem.* 42, 1372–1384. doi: 10.1016/j.soilbio.2010.04.009

Zhu, B., Gutknecht, J. L. M., Herman, D. J., Keck, D. C., Firestone, M. K., and Cheng, W. (2014). Rhizosphere priming effects on soil carbon and nitrogen mineralization. *Soil Biol. Biochem.* 76, 183–192. doi: 10.1016/j.soilbio.2014.04033

Zhu, Y. G., Laidlaw, A. S., Christie, P., and Hammond, M. E. R. (2000). The specificity of arbuscular mycorrhizal fungi in perennial ryegrass-white clover pasture. *Agric. Ecosyst. Environ.* 77, 211–218. 87-80 doi: 10.1016/s0167-8809(99)

Conflict of Interest: The authors declare that the research was conducted in the absence of any commercial or financial relationships that could be construed as a potential conflict of interest.

Publisher's Note: All claims expressed in this article are solely those of the authors and do not necessarily represent those of their affiliated organizations, or those of the publisher, the editors and the reviewers. Any product that may be evaluated in this article, or claim that may be made by its manufacturer, is not guaranteed or endorsed by the publisher.

frontiers | Frontiers in Plant Science

ORIGINAL RESEARCH
published: 14 July 2022
doi: 10.3389/fpls.2022.853220

The Reciprocal Effect of Elevated CO_2 and Drought on Wheat-Aphid Interaction System

*Haicui Xie[1], Fengyu Shi[1], Jingshi Li[1], Miaomiao Yu[1,2], Xuetao Yang[1], Yun Li[1] and Jia Fan[2]**

[1] Hebei Key Laboratory of Crop Stress Biology, College of Agronomy and Biotechnology, Hebei Normal University of Science and Technology, Qinhuangdao, China, [2] The State Key Laboratory for Biology of Plant Diseases and Insect Pests, Institute of Plant Protection, Chinese Academy of Agricultural Sciences, Beijing, China

Due to the rising concentration of atmospheric CO_2, climate change is predicted to intensify episodes of drought. However, our understanding of how combined environmental conditions, such as elevated CO_2 and drought together, will influence crop-insect interactions is limited. In the present study, the direct effects of combined elevated CO_2 and drought stress on wheat (*Triticum aestivum*) nutritional quality and insect resistance, and the indirect effects on the grain aphid (*Sitobion miscanthi*) performance were investigated. The results showed that, in wheat, elevated CO_2 alleviated low water content caused by drought stress. Both elevated CO_2 and drought promoted soluble sugar accumulation. However, opposite effects were found on amino acid content—it was decreased by elevated CO_2 and increased by drought. Further, elevated CO_2 down-regulated the jasmonic acid (JA) -dependent defense, but up-regulated the salicylic acid (SA)-dependent defense. Meanwhile, drought enhanced abscisic acid accumulation that promoted the JA-dependent defense. For aphids, their feeding always induced phytohormone resistance in wheat under either elevated CO_2 or drought conditions. Similar aphid performance between the control and the combined two factors were observed. We concluded that the aphid damage suffered by wheat in the future under combined elevated CO_2 and drier conditions tends to maintain the status quo. We further revealed the mechanism by which it happened from the aspects of wheat water content, nutrition, and resistance to aphids.

Keywords: ***Triticum aestivum*, *Sitobion miscanthi*, elevated CO_2, drought, nutritional quality, insect resistance**

OPEN ACCESS

Edited by:
Durgesh Kumar Tripathi, Amity University, India

Reviewed by:
Van Hien La, Chonnam National University, South Korea
Renu Munjal, Chaudhary Charan Singh Haryana Agricultural University, India
Anna-Maria Botha-Oberholster, Stellenbosch University, South Africa
Yaoguo Qin, China Agricultural University, China

***Correspondence:**
Jia Fan
jfan@ippcaas.cn

Specialty section:
This article was submitted to Plant Nutrition, a section of the journal Frontiers in Plant Science

Received: *12 January 2022*
Accepted: *08 June 2022*
Published: *14 July 2022*

Citation:
Xie H, Shi F, Li J, Yu M, Yang X, Li Y and Fan J (2022) The Reciprocal Effect of Elevated CO_2 and Drought on Wheat-Aphid Interaction System. Front. Plant Sci. 13:853220. doi: 10.3389/fpls.2022.853220

INTRODUCTION

Elevated CO_2 is identified as one major driving force of global climate change, and results in higher air temperature and altered precipitation patterns, which increase the area of arid areas (IPCC, 2014; Li et al., 2014). In the agroecosystem, the co-evolution of plants and insects is influenced by distinct environmental factors, such as CO_2, soil moisture, and air temperature. Under complex climate change, to clarify the effects of multiple environmental factors—especially elevated CO_2 alongside other factors on plant-insect interactions—is crucial for better understanding the damage as well as the occurrence trends of insect pests (Murray et al., 2013; Scherber et al., 2013; Zandalinas et al., 2018; Hervé et al., 2019; Wei et al., 2022).

Elevated CO_2 changes the primary and secondary metabolism of plants by stimulating the photosynthetic rate (Zavala et al., 2017), which not only resulted in increased carbon:nitrogen ratio, but also changed the insect resistance in plants (Zavala et al., 2013; Sun et al., 2015, 2016; Guo et al., 2017; Johnson et al., 2022). Meanwhile, drought stress drives plants to develop a number of physiological responses as well, such as closing stoma, increasing carbohydrate and amino acid accumulation, and activating phytohormone signaling pathways (Mcdowell et al., 2008; Lee and Luan, 2012; Danquah et al., 2014; Ullah et al., 2018; Xie et al., 2021), which subsequently lead to the change in plant nutritional quality (water content and C/N ratio) as well as plant chemical defenses to insects (English-Loeb et al., 1997; Guo et al., 2016; Castagneyroi et al., 2018; Suarez-Vidal et al., 2019).

Combined effects of elevated CO_2 and drought on different host plants and further plant-pest interaction vary (Roth et al., 1997; Nackley et al., 2018). This host plant-species-specific pattern is not surprising and is also found in other combined effects analyses such as combined warming and elevated CO_2. Depending on the plant, warming treatment may weaken or strengthen the effect of elevated CO_2 treatment (Johns and Hughes, 2002; Murray et al., 2013; Niziolek et al., 2013). However, elevated CO_2 routinely promotes stomatal closureand root growth, and prolongs physiological activity, which is proven helpful in withstanding the negative impact of drought stress on dry biomass, water status, and water use efficiency (Wall, 2001; Roy et al., 2016; Li et al., 2017, 2019b; Miranda-Apodaca et al., 2018; Uddin et al., 2018).

Aphids are key economic pests for many crops that cause extensive feeding damage and transmit viruses (Blackman and Eastop, 2000; Züst and Agrawal, 2016). Both elevated CO_2 and drought stress indirectly affect insects in two ways, namely, the changes in plant nutritional quality and its resistance to insects (Zavala et al., 2013; Xie et al., 2021). Both ways mediated by phytohormones are important factors affecting aphid feeding, growth, and population size (Sun et al., 2016). As sap-sucking insects, the soluble sugar and free nitrogen assimilation transferred in plant phloem are the main sources of carbon and nitrogen nutrients for aphids (Oehme et al., 2013). Recent studies have revealed that aphid feeding alters the content of phytohormones (e.g. abscisic acid, ABA; Jasmonic acid, JA; salicylic acid, SA), as well as the expression of defense genes (AOC, LOX, PAL, PR-1) related to JA and SA signaling pathways in plant tissues (Guo et al., 2012; Zhang et al., 2017). Change in phytohormone content is an important index for plant resistance to aphids, and the expression is generally induced by aphid feeding. These phytohormones' signaling pathways work together to regulate plant defense response to aphids. The resulting induced resistance is common in plants. However, the specific aphid resistance effect varies between species or even genotypes (Kempel et al., 2011; Züst and Agrawal, 2016).

In the growth and development of wheat, elevated CO_2 and water stress are two constraints. This, in turn, can alter the metabolic rates, development, and aphids feeding performance. Elevated CO_2 increased wheat starch, sucrose, glucose, total non-structure carbohydrates (TNCs), TNC:nitrogen ratio, free amino acids, soluble protein and grain weight, and decreased fructose and nitrogen contents, which further enhanced the grain aphid *Sitobion avenae* Fabricius population fed on wheat (Chen and Ge, 2004), but decreased fecundity of bird cherry-oat aphid *Rhopalosiphum padi* (Navarro et al., 2020). Drought stress significantly promoted amino acid accumulation, soluble sugar, and phytohormone contents in wheat, and also increased aphid abundance and population growth rates fed on wheat (Mousa et al., 2019; Cui et al., 2020; Xie et al., 2021). Other research has shown that compared to semiarid and moist area clones, arid area clones of the aphid *Sitobion avenae* (Fabricius) tended to have longer developmental times and smaller body sizes (Ahammed et al., 2016). However, what the interaction between these two factors is and how it affects the susceptibility of wheat plants to insect attack is still completely occluded.

In the present study, we used a plant-aphid interaction system, namely wheat (*Triticum aestivum*) and its key pest aphid *Sitobion miscanthi*, which is widely misreported as *S. avenae* in China (Zhang, 1999; Jiang et al., 2019), to comprehensively and systematically investigate the combined effects of elevated CO_2 and drought stress on wheat nutritional quality and resistance to aphid, as well as how these changes in the host plants affect aphid performance. Results from this study should help to understand the occurrence trend of aphid population on wheat under elevated CO_2 and drought, which will subsequently aid in adjusting pest control strategies under the context of future climate change.

MATERIALS AND METHODS

Aphids

The grain aphid isolate *S. miscanthi* was originally collected from wheat in the Hebei province of China. This isogenic colony was started from a single parthenogenetic female and was maintained on wheat (*Triticum aestivum*) in the laboratory at 22 ± 1°C, with 75% relative humidity and 16L: 8D photoperiod. To avoid overcrowding, aphids were continuously transferred to new plants until the start of the experiment.

Plant Preparation and Treatment With Elevated CO_2 and Drought

Elevated CO_2 conditions were supplied from gas tanks. Ambient CO_2 conditions were supplied from the surrounding air entering the environmental chamber facilities. The chambers were maintained at 25 ± 1°C, 60–70% relative humidity, and 14 h light /10 h dark photoperiods with 9000 lx fluorescent lamp active radiation levels. Wheat seeds (variety Zhongmai 175) were planted in pots (7.5 cm diameter x 9.0 cm height) with a sterilized loamy field soil (organic carbon content ∼75 g kg^{-1}). Each pot was planted with several seeds, and then only one seedling kept for the coming treatments.

Closed-dynamic CO_2 chambers (CDCC) were used and the parameters set here mainly followed several classic cases which used CDCC (Chen and Ge, 2004; Guo et al., 2012; Kurepin et al., 2018; Dusenge et al., 2020). Six chambers were employed, and three of them were treated with elevated CO_2 (∼750 ± 15 ppm), the other three as their controls were maintained at ambient CO_2 (∼380 ppm). Wheat plants

were exposed to the CO_2 and drought treatments from germination to the end of the experiment. Forty pots were used for well-watered (80% of field capacity moisture) and drought (40% of field capacity moisture) treatment, respectively, in each chamber. Wheat plants (2-week-old) from half of 40 pots were collected for testing physiological indicators (one leaf each pot) after treatment, and the remaining 20 pots were further treated with aphid infestation. The testing indicators were performed in three replicates. To minimize positional effects, plants were randomly positioned within each chamber daily.

Relative Water Content Measurement

Leaf relative water content (RWC) was measured using the formula RWC (%) = (fresh weight-dry weight)*100/ (turgor weight-dry weight) (Barrs and Weatherley, 1962). Fresh weight (FW) was measured and leaves were cut off to rehydrate in distilled water for 24 h at 15°C in darkness to obtain the weight at full turgor (TW). Leaf dry weight (DW) was obtained after the samples were dried in an oven at 70°C for 48 h.

Soluble Sugar, Amino Acid, and Phytohormones Measurement

To quantify soluble sugar and amino acid concentrations in the phloem, phloem exudate from leaves was obtained using the EDTA exudation technique previously described by Tetyuk et al. (2013). For soluble sugar analysis, phloem exudate from leaves and 40% acetonitrile (40 mL) were transferred into volumetric flasks (50 ml), followed by ultrasound extraction for 30 min and dilution with 40% acetonitrile to 50 ml for use as samples. Samples of 20 μL aliquots from each treatment were injected into the HPLC-MS/MS system. Sugars were separated with a Waters BEH Amide column (4.6 mm × 250 mm, 5 μm; Waters Corporation) using 75% acetonitrile as the mobile phase with isocratic elution at a flow rate of 1.0 ml/min. The column was maintained at 30°C. For amino acid analysis, phloem exudates and pure water (60 ml) were transferred into 100 mL volumetric flasks. After ultrasonic extraction for 30 min, the volume was fixed to the scale mark with water. Then, 10 μL aliquots of each sample were injected into the HPLC-MS/MS system. Amino acids were separated using an ACQUITY HSS T3 column (100 mm × 2.1 mm, 1.8 μm; Waters Corporation) under gradient conditions with 5 mM ammonium acetate (A) and acetonitrile (B) as the mobile phases at a 0.3 ml/min flow rate. The gradient program is shown in **Supplementary Table S1**. The column was maintained at 30°C.

For the phytohormone (ABA, JA, and SA) defense response analysis, the above wheat leaves with and without aphid infection were collected. Twenty-two wingless adults were transferred to wheat leaves for 24 h at the two-leaf stage. Then, all aphids were removed. Leaves without aphid infection were used as control. Samples of leaves (0.2 g) were homogenized by liquid nitrogen. The resulting homogenate and 10 mL of ethyl acetate were transferred into a centrifuge tube, followed by ultrasound extraction for 20 min and centrifugation for 10 min at 20,000 × g. The supernatant was evaporated to dryness under a stream of nitrogen at 40°C, and the final extracts were dissolved in 1 mL of 70% methanol and used as samples for analysis. Then, 10 μL aliquots of the samples were injected into the HPLC-MS/MS system. Phytohormones were separated with an Acquity UPLC® BEH C18 column (2.1 mm. 100 mm 1.7 μm; Waters Corporation) under gradient conditions, using 0.1% formic acid (A) and methanol (B) as the mobile phases, at a flow rate of 0.3 ml min^{-1}. The gradient program for phytohormone quantification is shown in **Supplementary Table S2**. The column was maintained at 30°C.

Gene Expression Detection by RT-qPCR

Total RNA was extracted using Trizol reagent (Invitrogen, Carlsbad, CA, USA) and combined with a micro total RNA extraction kit (Tianmo, Beijing, China) following the manufacturer's instructions. The tissues were homogenized with a liquid-nitrogen-cooled mortar and ground with a pestle into a very fine dust. Homogenized tissues were covered with 1 mL of Trizol reagent. RNA degradation and contamination were monitored on 2% agarose gels. RNA purity was checked using a Nanodrop ND-1000 spectrophotometer (NanoDrop products, Wilmington, DE, USA). RNA concentration was measured using a spectrophotometer RNA Nano 6000 Assay Kit of the Agilent Bioanalyzer 2100 system (Agilent Technologies, CA, USA). Individual total RNA was isolated and corresponding type cDNA was synthesized using the TRUEscript RT kit (LanY Science & Technology, Beijing, China) following the manufacturing protocol.

When plants were at the two-leaf stage, 20 wingless *S. miscanthi* adults were transferred to the first leaf (i.e., the oldest leaf) of each plant (Zhang et al., 2017). Plants without aphid feeding were set as control. After feeding for 24 h, all aphids were removed. The relative expressions of four genes in leaves, *Lipoxygenase* (*LOX*) and *allene oxide synthase* (*AOS*) for the JA-responsive pathway (Liu et al., 2011) and the SA synthesis enzyme gene *phenylalanine ammonia lyase* (*PAL*) and the induced SA marker protein gene *pathogenesis-related protein 1* (*PR-1*) for the SA-responsive pathway (Chen et al., 2009) were determined using RT-qPCR. Actin was used as the internal control and was amplified using the primer sequences described by Liu et al. (2011). Referring to Zhang's primers (**Supplementary Table S3**, 2017), RT-qPCR was performed on an ABI 7500 Real-Time PCR System (Applied Biosystems, Foster City, CA, USA). The PCRs were performed in 20-μL reaction volumes that contained 1 μL of cDNA, 0.5 μL each of 10 μmol L^{-1} forward and reverse primers, 10 μL of 2 × SybrGreen qPCR Mastermix, and 8.0 μL of ddH_2O under the following thermal cycling conditions: 2 min at 95°C followed by 40 cycles of 10 s at 95°C and 30 s at 60°C.

Aphid Life Table Parameter Measurement

Wheat plants under the different treatments mentioned above were used to rear aphids in corresponding environmental chambers. Using a camel hair brush, a single newly emerged nymph (<6 h) was placed on the first leaf of each plant (20 aphids in total for each treatment). To prevent the aphids from escaping, the plant was confined in transparent plastic column

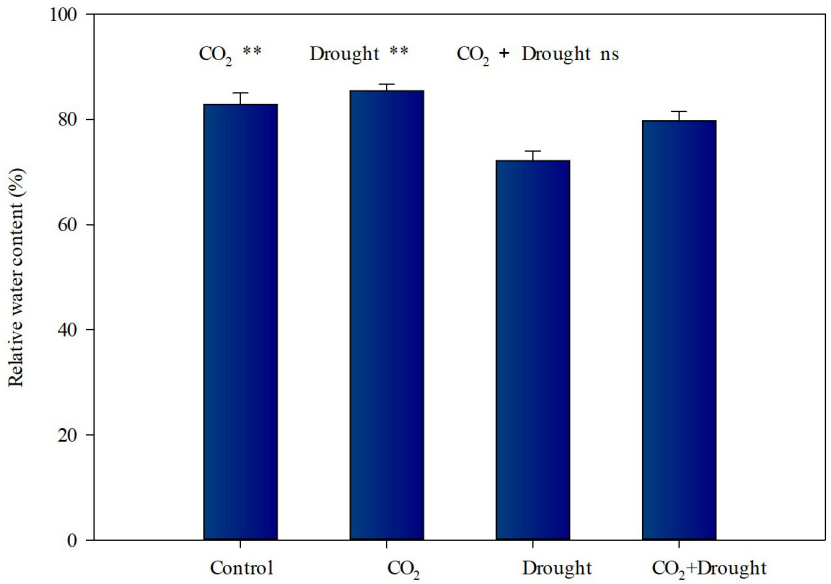

FIGURE 1 | Relative water content of *Triticum aestivum* grown under elevated CO_2 and drought conditions. Each value shown represents the mean (±SE) of three replicates. *P* values are provided for two-way ANOVA on the effects of elevated CO_2 and drought treatments on relative water content. Significant differences: $^*P < 0.05$; $^{**}P < 0.01$; ns, $P > 0.05$.

cages covered with double-deck gauze on top. All indicators were tested in triplicate. To minimize positional effects, plants were randomly positioned within each chamber daily. The above-recorded data was used to construct a life table and obtain the life table parameters (net reproductive rate R_0, intrinsic rate of increase r_m, generation time T, and finite rate of increase λ). Age-specific reproduction was used to construct a life table (Birch, 1948).

Statistical Analysis

For RT-qPCR, the fold changes in the expression of target genes were computed using the $2^{-\Delta\Delta Ct}$ normalization method (Livak and Schmittgen, 2001). For the life table parameters, r_m was computed using the Euler equation: $\sum_{x=0}^{\infty} e^{rx} l_x m_x = 1$, where l_x is survivorship of the original cohort over the age interval from day x-1 to day x (i.e., pivotal age) and m_x is the mean number of offspring produced per surviving aphid during the age interval x (Maia et al., 2000). R_0, T, and λ, were calculated as reported by Maia et al. (2000). The effects of elevated CO_2 and drought stress on relative water content, soluble sugar content, and free amino acids content as well as aphid life table parameters were tested by two-way ANOVAs (SAS Institute, Cary, NC, USA). The effects of elevated CO_2, drought, and aphid infestation on phytohormone (ABA, JA, and SA) content as well as JA- and SA-related gene expression in wheat were tested by three-way ANOVAs. Least significant different (LSD) tests were used to determine if treatment means significantly differed when ANOVAs indicated a factor was significant. For all analyses, $P < 0.05$ was considered the threshold for statistical significance.

RESULTS

Water Content in Wheat

The relative water contents of wheat under elevated CO_2 or drought stress vary in opposite ways (**Figure 1**, **Supplementary Table S4**). It increased by 6.63% under elevated CO_2 conditions (**Figure 1**), and decreased by 10.9% under drought stress conditions (**Figure 1**). The interactions between elevated CO_2 and drought stress on the relative water content of wheat were not significant (**Supplementary Table S4**).

Soluble Sugar Content in Wheat

Elevated CO_2 and drought stress significantly promoted soluble sugar accumulation in wheat (**Figure 2**, **Supplementary Table S5**). Relative to the ambient CO_2 treatment, both the glucose and total soluble sugar content increased under elevated CO_2 conditions (**Figures 2B,D**). Meanwhile, Relative to the well-watered treatment, the fructose, glucose, sucrose, and total soluble sugar content increased in wheat under drought stress (**Figures 2A–D**). The interaction effects between elevated CO_2 and drought stress on soluble sugars in wheat were not significant (**Supplementary Table S5**).

Amino Acid Content in Wheat

Nineteen amino acids in wheat were quantified (**Figure 3**, **Supplementary Table S6**). The effects of elevated CO_2 and drought stress on amino acid accumulation in wheat were different and some indicators even show opposite trends. Elevated CO_2 significantly decreased the Met, Gly, Lys, Try, Thr, Asp, His, and total amino acid content compared to ambient CO_2 treatment (**Supplementary Table S6**). Drought stress significantly increased the Phe, Glu, Tyr, Pro, Try, Asp, Asn, and total amino acid content, compared to the well-watered

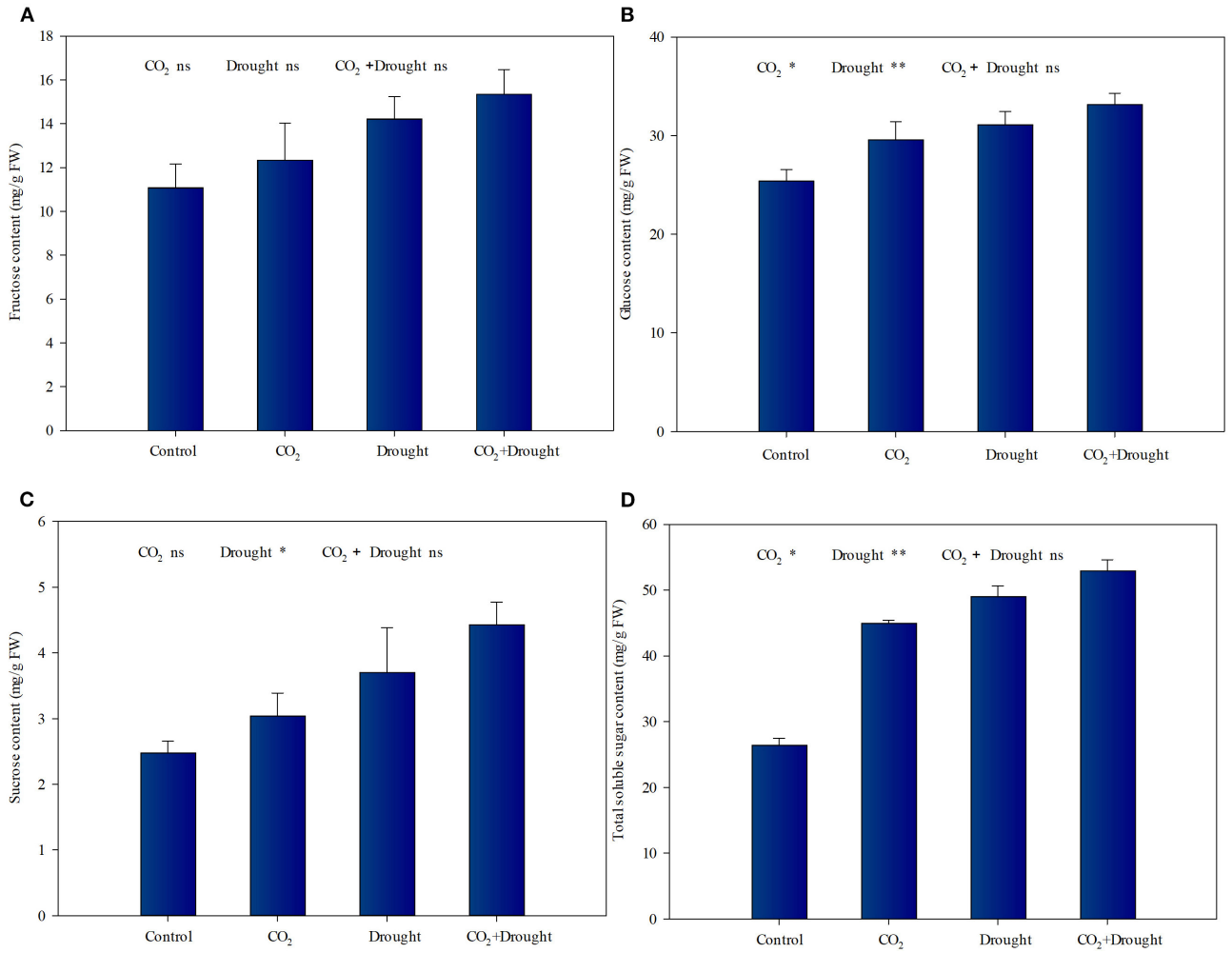

FIGURE 2 | Soluble sugars content of *Triticum aestivum* grown under elevated CO_2 and drought conditions. **(A)** fructose; **(B)** glucose; **(C)** sucrose; **(D)** total soluble sugars. Each value shown represents the mean (±SE) of three replicates. *P*-values are provided for two-way ANOVA on the effects of elevated CO_2 and drought treatments on soluble sugar content. Significant differences: $^*P < 0.05$; $^{**}P < 0.01$; ns, $P > 0.05$.

treatment (**Supplementary Table S6**). Furthermore, it showed significantly negative interaction effects between elevated CO_2 and drought stress on three amino acids including alanine and tryptophan (**Supplementary Table S6**).

Phytohormone-Dependent Defense Against Aphids

Elevated CO_2, drought stress, and aphid infestation significantly influenced the wheat phytohormone content (**Figure 4**, **Supplementary Table S7**). Relative to the ambient CO_2 treatment, elevated CO_2 decreased JA, but increased SA content (**Figures 4B,C**). Relative to the well-watered treatment, drought stress increased ABA and JA content (**Figures 4A,B**). Aphid infestation significantly increased ABA, JA, and SA content in wheat compared with control (the uninfested wheat) (**Figures 4A–C**). Moreover, the interaction effects among elevated CO_2, drought stress, and aphids infestation on wheat phytohormones were all not significant (**Supplementary Table S7**).

Furthermore, two genes from each plant hormone defense response pathway (JA and SA) in response to aphid induction in wheat were quantified by RT-qPCR. Elevated CO_2, drought stress and aphid infestation significantly influenced the relative expression of four defense-related genes (**Figure 5**, **Supplementary Table S8**). *LOX* (JA) was down-regulated, and *PR-1*, as well as PAL (SA), were up-regulated in wheat grown under elevated CO_2 (**Figures 5B–D**). Relative to the well-watered treatment, the relative expressions of *AOS* (JA) and *LOX* (JA) were up-regulated in wheat grown under drought stress (**Figures 5A,B**). Aphid infestation up-regulated the relative expression of *AOS*, *LOX* (JA), *PAL*, and *PR-1* (SA) in wheat, compared to control (the uninfested wheat) (**Figures 5A–D**). Three factors as well as any two among the three factors analyzed on four gene expressions showed no interaction effect except drought stress and aphid infestation

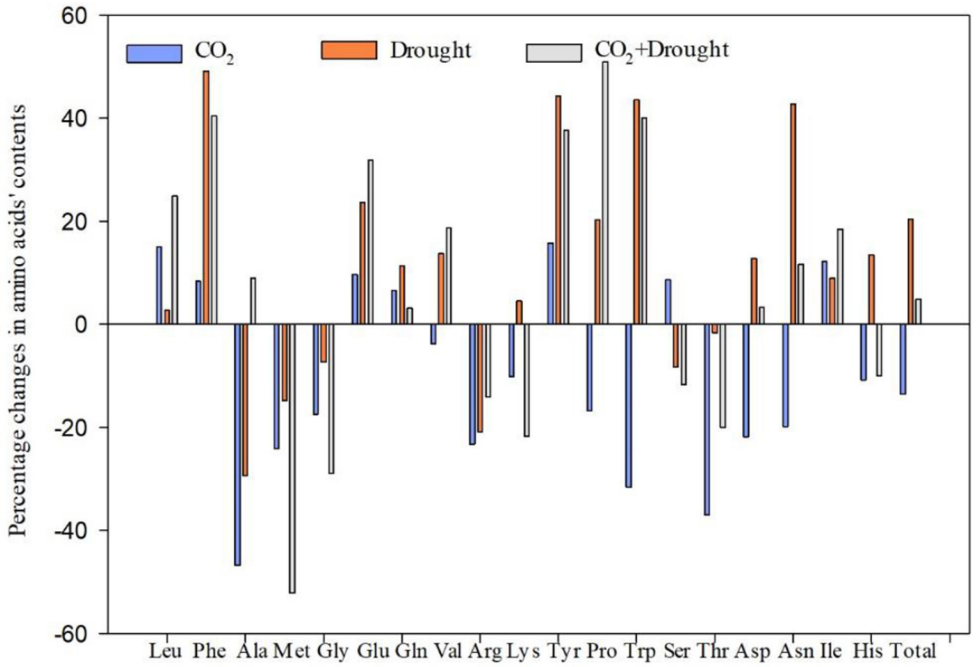

FIGURE 3 | Percentage changes in amino acid content of *Triticum aestivum* grown under elevated CO_2 and drought conditions. Percentage change value (%) = (treatment-control)*100/control.

on *LOX* which showed a significantly positive interaction effect (**Supplementary Table S8**).

Changes in Performance of Aphid Populations on Wheat

There are contrasting effects of elevated CO_2 and drought stress on the life table parameters of aphids fed on wheat (**Figure 6**, **Supplementary Table S9**). Under elevated CO_2, the R_0, r, and λ values of aphid populations increased by 10.6, 13.1, and 2.5%, respectively, compared to control (ambient CO_2) (**Figures 6A,C,D**). The R_0 values of aphid populations decreased by 12.4% under drought stress compared to the well-watered treatment (**Figure 6A**). The interaction effects between elevated CO_2 and drought stress on the aphid life table parameters were not significant (**Supplementary Table S9**).

DISCUSSION

The water content, nutritional quality (soluble sugar, amino acid, etc), and the secondary metabolic defense pathways in host plants are key limiting factors for aphids' growth and development (Douglas, 1993; Bezemer and Jones, 1998; Mewis et al., 2012; Züst and Agrawal, 2016). The effects of many single environmental factors on all the above aspects have been well-documented. It is necessary and interesting to further explore how the combined environmental factors such as elevated CO_2 and drought stress work on the aphids' limiting factors as well as further change the plant-aphid interactions.

The Combined Effects of Elevated CO_2 and Drought Treatment on Relative Water Content Tend to Balance Out.

Elevated CO_2 has been found to induce stomatal closure, which leads to lower evaporative flux density. As a result of decreases in evaporative flux density and increases in net photosynthesis, also found to occur in elevated CO_2, plants have often been shown to maintain higher water use efficiencies when grown under elevated CO_2 conditions (Barbehenn et al., 2004; Sun et al., 2015). The elevated CO_2 also can facilitate the access to sub-soil water by promoting wheat root growth (Li et al., 2017; Uddin et al., 2018). In the present study, we also found that elevated CO_2 treatment increased the water content of wheat. Meanwhile, drought stress decreased the water content as expected. Further, there was no significant interaction between these two environmental factors which indicates that their combined effects can be regarded as the simple sum of their single effects. Thus, the similar water contents between control and combined elevated CO_2 and drought treatment demonstrated that elevated CO_2 alleviates lower water content caused by drought stress.

The Combined Effects Promote Carbohydrate Accumulation

It has long been recognized that elevated CO_2 increases the photosynthetic rate of C_3 plants including wheat, and further promotes carbohydrate accumulation (Barbehenn et al., 2004; Chen et al., 2005). La et al. (2019) also indicated that plant sugar accumulation was mainly due to the increased sucrose content with the highest expression of ABA-dependent sucrose

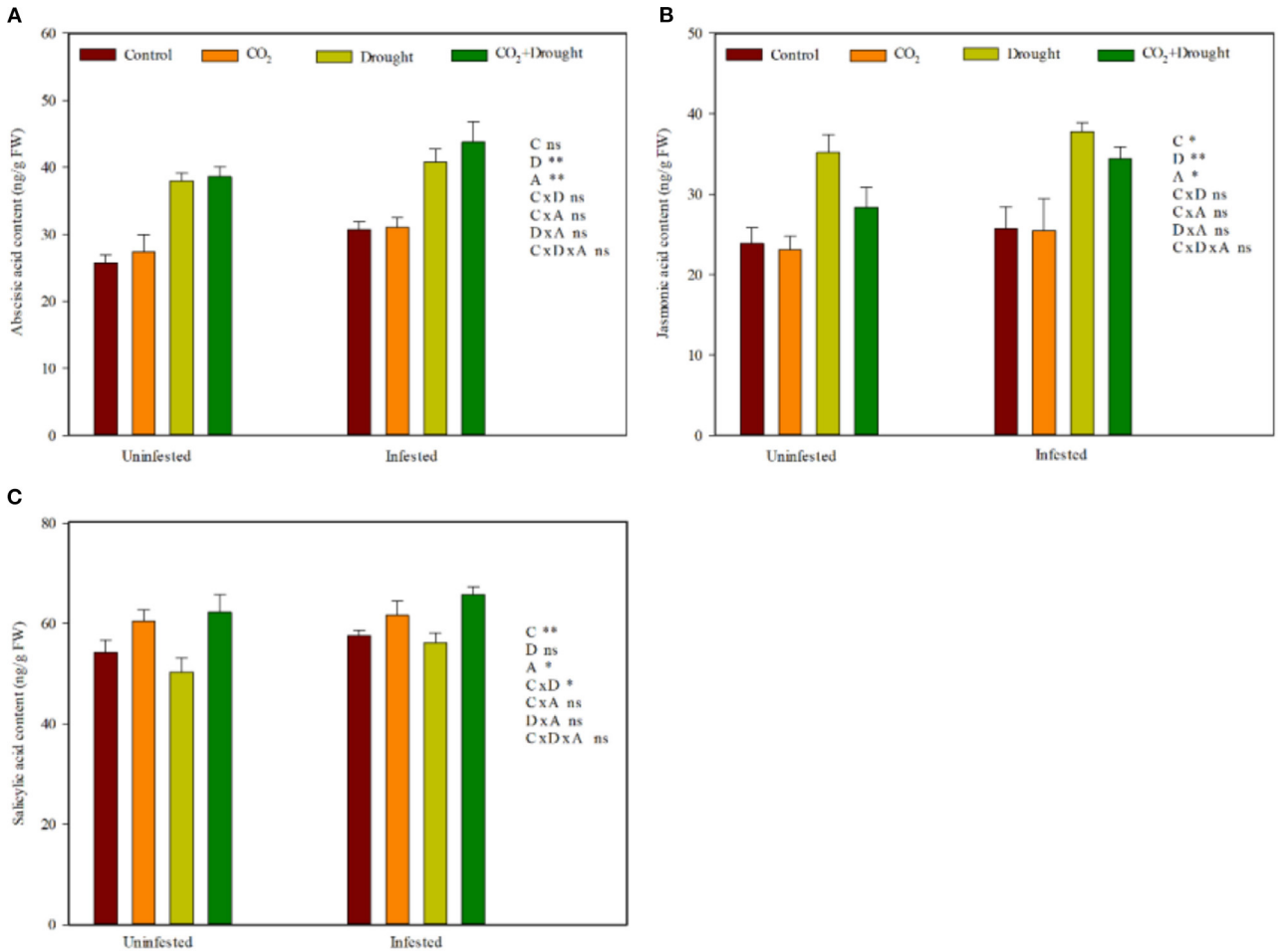

FIGURE 4 | Phytohormone content of *Triticum aestivum* grown under elevated CO_2 and drought conditions with and without aphid infestation. **(A)** abscisic acid; **(B)** jasmonic acid; **(C)** salicylic acid. Each value shown represents the mean (±SE) of three replicates. *P*-values are provided for three-way ANOVA on the effects of elevated CO_2 **(C)**, drought **(D)**, and aphid **(A)** treatments on phytohormone content. Significant differences: $^{*}P < 0.05$; $^{**}P < 0.01$; ns, $P > 0.05$.

signaling genes under drought stress. To be specific, in wheat the enhancements in carbohydrate accumulation of each single factor such as elevated CO_2 (Sun et al., 2009) and drought (Xie et al., 2021) have been verified. Also, under certain combined abiotic stresses such as drought and warming up, the increased carbohydrate accumulation had been reported (Zandalinas et al., 2018). Drought stress not only increased the energy accumulation but also coordinated with the activation of specific physiological and molecular responses in growing plants to mitigate the damaging effects of drought (Zandalinas et al., 2018). In the present study, our results supported that each factor of elevated CO_2 and drought stress significantly promoted soluble sugar accumulation in wheat.

The Combined Effect on Nitrogen Concentration Tends to Balance Out

Lower nitrogen concentration was generally found in the plants grown under elevated CO_2 (Zavala et al., 2013). Indeed, in the present study, all tested contents such as Met, Gly, Lys, Try, Thr, Asp, His, and total amino acid content of wheat were decreased under elevated CO_2. There have been several explanations for this decline phenomenon. It may be due to enhanced carbohydrates or biomass accumulation in plants grown under elevated CO_2 conditions, then the amino acid concentration was diluted (Nie et al., 1995; Smart et al., 2010; Novriyanti et al., 2012). Besides, the elevated CO_2 inhibits plant nitrogen assimilation and metabolism (Bloom et al., 2014) and further mechanism study revealed that the reduced activity of nitrate reductase finally coursed the decreased protein and amino acid contents (Dier et al., 2017; Andrews et al., 2019).

On the contrary, drought stress increased the amino acid content in this study. Previous studies have shown that the accumulation of amino acids enhances plant drought stress tolerance by regulating the activation of material metabolism in plants (Suguiyama et al., 2014). Interestingly, three up-regulated amino acids under drought stress in the present study, namely Try, Tyr, and Phe, are located in the downstream of the shikimic acid pathway, which precisely functions to adjust metabolism

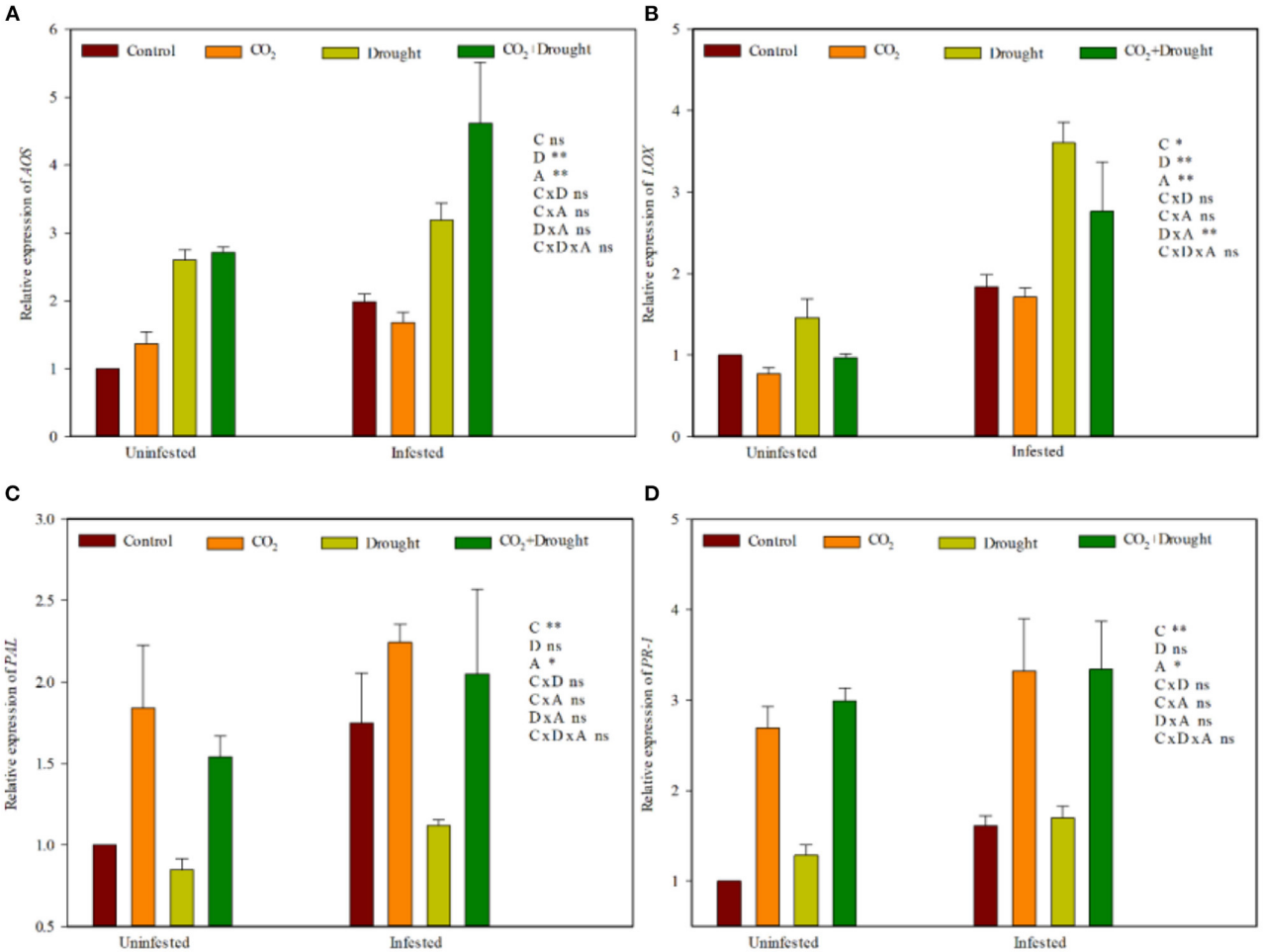

FIGURE 5 | JA- and SA-related gene expression of *Triticum aestivum* grown under elevated CO_2 and drought conditions with and without aphid infestation. **(A)** *allene oxide synthase* (*AOS*); **(B)** *Lipoxygenase* (*LOX*); **(C)** *phenylalanine ammonia lyase* (*PAL*), **(D)** *pathogenesis-related protein 1* (*PR-1*). Each value shown represents the mean (±SE) of three replicates. *P*-values are provided for three-way ANOVA on the effects of elevated CO_2 **(C)**, drought **(D)**, and aphid **(A)** treatments on JA- and SA-related gene expression. Significant differences: $^{*}P < 0.05$; $^{**}P < 0.01$; ns, $P > 0.05$.

toward secondary metabolite production and contributes to hormone metabolism in wheat (Tzin and Galili, 2010).

Their opposing effects on total amino acid contents as well as most of the other test amino acids (17 of 19) in wheat of elevated CO_2 and drought did not show interaction, except for two amino acids, Ala and Try. The interaction indicated the existence of a potential crosstalk in which they both participate and a more complicated mechanism of change patterns in certain amino acids and proteins under combined elevated CO_2 and drought treatment.

Various Phytohormone-Dependent Wheat Defenses Against Aphids

Plant response to abiotic and biotic stress commonly through ABA, JA, or SA defense signaling pathways including the accumulation of phytohormone and up-regulated related gene expression (Adie et al., 2007; Danquah et al., 2014; Zandalinas et al., 2016; Gupta et al., 2017), although the regulated process is complicated and difficult to parse. In general, the ABA signaling pathway activity up-regulated the JA signaling pathway but suppressed the SA signaling pathway when plants were grown under abiotic stress. The up-regulated JA further enhanced the effective resistance of host plants to herbivorous insects (Casteel et al., 2008; Zavala et al., 2008; Ahammed et al., 2016; Guo et al., 2016). JA and SA defense-related gene expression (*LOX*, *AOS*, *PR-1*, and *PAL*) studies showed that infiltration of *S. avenae* watery saliva in wheat leaves induced the JA and SA-dependent defense (Zhang et al., 2017).

Elevated CO_2 weakens the effective resistance of wheat to aphids by altering the phytohormone signal pathways (Guo et al., 2012, 2016; Sun et al., 2013, 2015). In the present study, elevated CO_2 down-regulated the expression levels of the JA defense-related gene *LOX* and further reduced JA accumulation. Meanwhile, it up-regulated the expression levels of the SA defense-related genes *PR-1* and *PAL* and further increased SA accumulation,

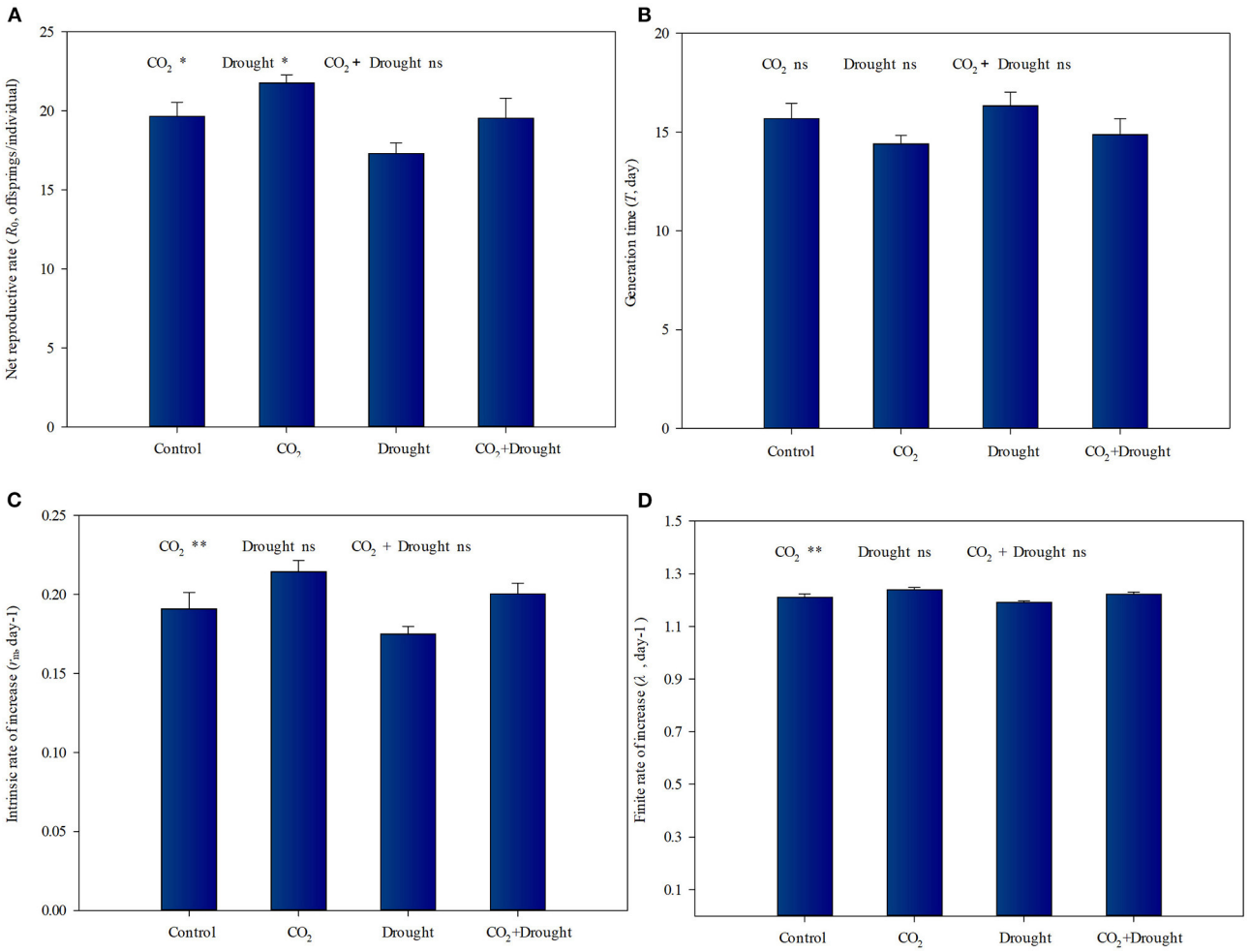

FIGURE 6 | Life table parameters of aphid reared on *Triticum aestivum* grown under elevated CO_2 and drought conditions. **(A)** net reproduction rate (R_0); **(B)** generation time (T); **(C)** intrinsic rate of increase (r_m); **(D)** finite rate of increase (λ). Each value shown represents the mean (±SE) of three replicates. *P*-values are provided for two-way ANOVA on the effects of elevated CO_2 and drought treatments on life table parameters. Significant differences: $^*P < 0.05$; $^{**}P < 0.01$; ns, $P > 0.05$.

which indicated that elevated CO_2 weakeed the resistance of wheat.

Drought stress enhanced ABA accumulation and promoted the activity of key enzymes from JA signaling pathway and therefore increased the resistance against aphids in wheat. In the present study, drought stresses up-regulated the expression of *LOX* and *AOS* from the JA pathway in wheat and increased ABA and JA accumulation, which showed that drought stress strengthens the resistance of wheat.

Moreover, aphid infestation always up-regulated the JA and SA signaling pathways by increasing JA and SA accumulation and their defense-related genes (*LOX*, *AOS*, *PR-1*, and *PAL*) regardless of the elevated CO_2 and drought conditions in the present study (**Supplementary Tables S6, 7**).

In summary, the wheat resistance to aphids produced by phytohormone under elevated CO_2, drought stresses, or aphid infestation is quite different. But the combined effects among all three factors tended to beindependent, and there was no interaction at all.

Changes in Wheat—Aphid Interaction Under Elevated CO_2 and Drought Stresses

Higher host plant water availability enhances aphid feeding efficiency (Sun et al., 2015; Guo et al., 2016). However, aphid response varied to the increasing soluble sugar in their host plants. Some reports have suggested that the increasing soluble sugar content in host plants is beneficial to aphid feeding (Li et al., 2019a). However, others showed that increased soluble sugar content is not necessarily conducive to aphid growth (Slosser et al., 2004; Alkhedir et al., 2013).

Aphids utilize a food source rich in carbohydrates but relatively low in nitrogen. Even so, they must obtain some essential amino acids such as Leu, His, Lys, etc from their host (Chen et al., 2005). Thus, the nitrogen concentration

of the host is commonly a limiting nutritional factor for aphids, as reflected in the strong correlations between this variable (nitrogen concentration of wheat) and the individual performance of aphids (Sandström and Pettersson, 1994; Hansen and Moran, 2011). Other literature further shows that the decline of amino acid content enhanced aphid ingestion efficiency which was driven by their instinct for nitrogen (Chen et al., 2005; Sun et al., 2009). Our work here supported the above ideas. Considering the increased soluble sugar accumulation and decreased total amino acid content of wheat under elevated CO_2, the improved indicators such as R_0, r, and λ values of aphid populations could benefit from the resulting increased feeding effectiveness. Besides, the increased water content also enhanced aphid feeding efficiency, which together with weakened JA-dependent defense for aphids explained why elevated CO_2 improved the occurrence of aphid populations in wheat.

However, the R_0 value of aphid populations decreased when they fed on wheat grown under drought stress. The decreased fecundity may be relative to the lower water content reducing aphid feeding efficiency and higher JA-dependent defense in wheat grown under drought stress, although drought increased the soluble sugar and amino acid accumulation in wheat. At the same time, the existing studies also showed that the increased JA and SA content enhanced the accumulation of sugars and amino acids in plants (Ilyas et al., 2017; Zhao et al., 2021). Thus, both the accumulation of phytohormone and substances may contribute to the stress resistance (drought and aphid) of wheat in this study, which could be explained through further experiment.

Although each of the two factors significantly influenced wheat water contents, nutritional quality, and phytohormone-dependent defense, further indirectly influencing the performance of aphids significantly, the combined effect on the aphid life table parameters was not significant. It showed similar aphid performance between control and combined treatment in this study, which suggested that in the case of elevated CO_2 and drought stresses, aphid damage will continue.

We concluded that the aphid damage suffered by wheat in the future under combined elevated CO_2 and drier conditions tends to maintain the status quo. We further revealed the mechanism by which it happened from aspects of wheat water content, nutrition, and resistance to aphids. It could be necessary to reveal details of the plant-insect interactions from the perspective of multiple environmental factors and species specificity and deepen our understanding of the relationship between pest occurrence and its damage to plants.

DATA AVAILABILITY STATEMENT

The original contributions presented in the study are included in the article/**Supplementary Material**, further inquiries can be directed to the corresponding author/s.

AUTHOR CONTRIBUTIONS

HX and JF conceived the idea and developed research questions. FS, YL, and HX collected and analyzed the data and prepared the original draft. MY, JL, and XY managed the experiment, collected the data, and reviewed and edited the manuscript. All authors contributed to the article and approved the submitted version.

FUNDING

This work was supported by the Science and Technology Research Project for Colleges and Universities in Hebei Province (BJ2020049) and the National Natural Science Foundation of China (31871966).

SUPPLEMENTARY MATERIAL

The Supplementary Material for this article can be found online at: https://www.frontiersin.org/articles/10.3389/fpls.2022.853220/full#supplementary-material

REFERENCES

Adie, B. A., Pérez, J., Pérez, M. M., Godoy, M., Sánchez, J. J., and Schmelz, E. A., et al. (2007). ABA is an essential signal for plant resistance to pathogens affecting JA biosynthesis and the activation of defenses in Arabidopsis. *Plant Cell* 19, 1665–1681. doi: 10.1105/tpc.106.048041

Ahammed, G. J., Li, X., Zhou, J., Zhou, Y. H., and Yu, J. Q. (2016). "Role of hormones in plant adaptation to heat stress," in *Plant Hormones Under Challenging Environmental Factors*, eds G. Ahammed and J. Q. Yu (Dordrecht: Springer) 1–21. doi: 10.1007/978-94-017-7758-2

Alkhedir, H., Karlovsky, P., and Vidal, S. (2013). Relationship between water soluble carbohydrate content, aphid endosymbionts and clonal performance of *Sitobion avenae* on cocksfoot cultivars. *PLoS One.* 8, e54327. doi: 10.1371/journal.pone.0054327

Andrews, M., Condron, L. M., Kemp, P. D., Topping, J. F., Lindsey, K., Hodge, S., et al. (2019). Elevated CO_2 effects on nitrogen assimilation and growth of C_3 vascular plants are similar regardless of N-form assimilated. *J. Exp. Bot.* 70, 683–690. doi: 10.1093/jxb/ery371

Barbehenn, R. V., Chen, Z., Karowe, D. N., and Spickard, A. (2004). C_3 grasses have higher nutritional quality than C_4 grasses under ambient and elevated atmospheric CO_2. *Glob. Change Biol.* 10, 1565–1575. doi: 10.1111/j.1365-2486.2004.00833.x

Barrs, H. D., and Weatherley, P. E. (1962). A re-examination of the relative turgidity technique for estimating water deficits in leaves. *Aust. J. Biol. Sci.* 15, 413–428. doi: 10.1071/BI9620413

Bezemer, T. M., and Jones, T. H. (1998). Plant-insect herbivore interactions in elevated atmospheric CO_2: quantitative analyses and guild effects. *Oikos* 82, 212–222. doi: 10.2307/3546961

Birch, L. C. (1948). The intrinsic rate of natural increase of an insect population. *J. Anim. Ecol.* 17, 15–26. doi: 10.2307/1605

Blackman, R. L., and Eastop, V. F. (2000). *Aphids on the World's Crops: an Identification and Information Guide*. New York, NY: John Wiley and Sons Ltd.

Bloom, A. J., Burger, M., Kimball, B. A., and Pinter, P. J. (2014). Nitrate assimilation is inhibited by elevated CO_2 in field-grown wheat. *Nat. Clim. Change.* 4, 477–480. doi: 10.1038/nclimate2183

Castagneyroi, B., Jactel, H., and Moreira, X. (2018). Anti-herbivore defences and insect herbivory: interactive effects of drought and tree neighbours. *J. Ecol.* 106, 2043–2057. doi: 10.1111/1365-2745.12956

Casteel, C. L., O'Neill, B. F., Zavala, J. A., Bilgin, D. D., Berenbaum, M. R., and Delucia, E. H. (2008). Transcriptional profiling reveals elevated CO_2 and elevated O_3 alter resistance of soybean (*Glycine max*) to Japanese beetles (*Popillia japonica*). *Plant Cell Environ.* 31, 419–434. doi: 10.1111/j.1365-3040.2008.01782.x

Chen, F. J., and Ge, F. (2004). An experimental instrument to study the effects of changes in CO_2 concentrations on the interactions between plants and insects-CDCC-1 chamber. *Entomol. Knowledge.* 41, 279–281.

Chen, F. J., Ge, F., and Parajulee, M. N. (2005). Impact of elevated CO_2 on tri-trophic interaction of *Gossypium hirsutum*, *Aphis gossypii*, and *Leis axyridis*. *Environ. Entomol.* 34, 37–46. doi: 10.1603/0046-225X-34.1.37

Chen, Z., Zheng, Z., Huang, J., Lai, Z., and Fan, B. (2009). Biosynthesis of salicylic acid in plants. *Plant Signal Behav.* 4, 493–496. doi: 10.4161/psb.4.6.8392

Cui, H., Wang, L., Reddy, G., and Zhao, Z. (2020). Mild drought facilitates the increase in wheat aphid abundance by changing host metabolism. *Ann. Entomol. Soc. Am.* 114, 79–83. doi: 10.1093/aesa/saaa038

Danquah, A., Zelicourt, D. A., Colcombet, J., and Hirt, H. (2014). The role of ABA and MAPK signaling pathways in plant abiotic stress responses. *Biotechnol Adv.* 32, 40–52. doi: 10.1016/j.biotechadv.2013.09.006

Dier, M., Meinen, R., Erbs, M., Kollhorst, L., and Manderscheid, R. (2017). Effects of free air carbon dioxide enrichment (FACE) on nitrogen assimilation and growth of winter wheat under nitrate and ammonium fertilization. *Glob Chang Biol.* 24, 40–54. doi: 10.1111/gcb.13819

Douglas, A. E. (1993). The nutritional quality of phloem sap utilized by natural aphid populations. *Ecol. Entomol.* 18, 31–38. doi: 10.1111/j.1365-2311.1993.tb01076.x

Dusenge, M. E., Madhavji, S., and Way, D. A. (2020). Contrasting acclimation responses to elevated CO_2 and warming between an evergreen and a deciduous boreal conifer. *Global Change Biol.* 26, 3639–3657. doi: 10.1111/gcb.15084

English-Loeb, G., Stout, M. J., and Duffey, S. S. (1997). Drought stress in tomatoes: changes in plant chemistry and potential nonlinear consequences for insect herbivores. *Oikos* 79, 456. doi: 10.2307/3546888

Guo, H. J., Peng, X. H., Gu, L. Y., Wu, J. Q., Ge, F., and Sun, Y. C. (2017). Up-regulation of MPK4 increases the feeding efficiency of the green peach aphid under elevated CO_2 in Nicotiana attenuata. *J. Exp. Bot.* 68, 5923–5935. doi: 10.1093/jxb/erx394

Guo, H. J., Sun, Y., Ren, Q., Zhu, S. K., Kang, L., and Wang, C. Z., et al. (2012). Elevated CO_2 reduces the resistance and tolerance of tomato plants to *Helicoverpa armigera* by suppressing the JA signaling pathway. *PLoS ONE* 7, e41426. doi: 10.1371/journal.pone.0041426

Guo, H. J., Sun, Y. C., Peng, X. H., Wang, Q. Y., Harris, M., and Ge, F. (2016). Up-regulation of abscisic acid signaling pathway facilitates aphid xylem absorption and osmoregulation under drought stress. *J. Exp. Bot.* 3, 681–693. doi: 10.1093/jxb/erv481

Gupta, A., Hisano, H., Hojo, Y., Matsuura, T., Ikeda, Y., and Mori, I. Z., et al. (2017). Global profiling of phytohormone dynamics during combined drought and pathogen stress in *Arabidopsis thaliana* reveals ABA and JA as major regulators. *Sci. Rep.* 7, 4017. doi: 10.1038/s41598-017-03907-2

Hansen, A. K., and Moran, N. A. (2011). Aphid genome expression reveals host-symbiont cooperation in the production of amino acids. *Proc. Natl. Acad. Scie. U. S. A.* 108, 2849–2854. doi: 10.1073/pnas.1013465108

Hervé, J., Koricheva, J., and Castagneyrol, B. (2019). Responses of forest insect pests to climate change: not so simple. *Curr. Opin. Insect Sci.* 35, 103–108. doi: 10.1016/j.cois.2019.07.010

Ilyas, N., Gull, R., Mazhar, R., Saeed, M., Kanwal, S., Shabir, S., et al. (2017). Influence of salicylic acid and jasmonic acid on wheat under drought stress. *Commun. Soil Sci. Plan.* 1–9. doi: 10.1080/00103624.2017.1418370

IPCC. (2014). "Impacts, adaptation and vulnerability", in *Working Group II, Contribution to the Fifth Assessment Report of the Intergovernmental Panel on climate Change, 1132*, eds. C. B. Field, V. R. Barros, D. J. Dokken, K. J. Mach, M. D. Mastrandrea, and T. E. Bilir (Cambridge: Cambridge University Press) 1–32.

Jiang, X., Zhang, Q., Qin, Y. G., Yin, H., Zhang, S. Y., and Li, Q., et al. (2019). A chromosome-level draft genome of the grain aphid *Sitobion miscanthi. GiGA Sci.* 8:1–8 doi: 10.1093/gigascience/giz101

Johns, C. V., and Hughes, L. (2002). Interactive effects of elevated CO_2 and temperature on the leaf-miner *Dialectica scalariella* Zeller (Lepidoptera: Gracillariidae) in Paterson's Curse, *Echium plantagineum* (Boraginaceae). *Glob. Change Biol.* 8, 142–152. doi: 10.1046/j.1365-2486.2002.00462.x

Johnson, S. N., Cibils-Stewart, X., Waterman, J. M., Biru, F. N., Rowe, R. C., and Hartley, S. E. (2022). Elevated atmospheric CO_2 changes defence allocation in wheat but herbivore resistance persists. *Proc. R. Soc. B Biol. Sci.* 289, 20212536. doi: 10.1098/rspb.2021.2536

Kempel, A., Schaedler, M., Chrobock, T., and Fischer, M.arkus K., M. (2011). Tradeoffs associated with constitutive and induced plant resistance against herbivory. *Proc. Natl. Acd. Sci. U. S. A.* 108, 5685–5689. doi: 10.1073/pnas.1016508108

Kurepin, L. V., Stangl, Z. R., Ivanov, A. G., Bui, V., Mema, M., and Hunter Norman, P. A., et al. (2018). Contrasting acclimation abilities of two dominant boreal conifers to elevated CO_2 and temperature. *Plant Cell Environ.* 41, 1331–1345. doi: 10.1111/pce.13158

La, V. H., Lee, B. R., Islam, M. T., Park, S. H., Lee, H., Bae, D. W., et al. (2019). Antagonistic shifting from abscisic acid- to salicylic acid-mediated sucrose accumulation contributes to drought tolerance in *Brassica napus*. *Environ. Exp. Bot.* 162:38–47. doi: 10.1016/j.envexpbot.2019.02.001

Lee, S. C., and Luan, S. (2012). ABA signal transduction at the crossroad of biotic and abiotic stress responses. *Plant Cell Environ.* 35, 53–60. doi: 10.1111/j.1365-3040.2011.02426.x

Li, L. K., Wang, M. F., Pokharel, S. S., Li, C. X., Parajulee, M. N., and Chen, F. J., et al. (2019a). Effects of elevated CO_2 on foliar soluble nutrients and functional components of tea, and population dynamics of tea aphid, *Toxoptera aurantii*. *Plant Physiol. Bioch.* 145, 84–94. doi: 10.1016/j.plaphy.2019.10.023

Li, S., Li, X., Wei, Z., and Liu, F. (2019b). ABA-mediated modulation of elevated CO_2 on stomatal response to drought. *Curr. Opin. Plant Biol.* 13, 1–7. doi: 10.1016/j.pbi.2019.12.002

Li, X., Yang, Y. Q., Sun, X. D., Lin, H. M., Chen, J. H., and Ren, J., et al. (2014). Comparative physiological and proteomic analyses of poplar (*Populus yunnanensis*) plantlets exposed to high temperature and drought. *PLoS ONE* 9, e107605. doi: 10.1371/journal.pone.0107605

Li, Y. F., Li, X., Yu, J. J., and Liu, F. L. (2017). Effect of the transgenerational exposure to elevated CO_2 on the drought response of winter wheat: stomatal control and water use efficiency. *Environ. Exp. Bot.* 136, 78–84. doi: 10.1016/j.envexpbot.2017.01.006

Liu, X., Meng, J., Starkey, S., and Smith, C. M. (2011). Wheat gene expression is differentially affected by a virulent Russian wheat aphid biotype. *J. Chem. Ecol.* 37, 472–482. doi: 10.1007/s10886-011-9949-9

Livak, K. J., and Schmittgen, T. D. (2001). Analysis of relative gene expression data using real-time quantitative PCR and the $2^{-\Delta\Delta CT}$ method. *Methods* 25, 402–408. doi: 10.1006/meth.2001.1262

Maia, A., Luiz, A. J., and Campanhola, C. (2000). Statistical inference on associated fertility life table parameters using Jackknife technique: computational aspects. *J. Econ. Entom.* 93, 511–518. doi: 10.1603/0022-0493-93.2.511

Mcdowell, N., Pockman, W. T., Allen, C. D., Breshears, D. D., Cobb, N., and Kolb, T., et al. (2008). Mechanisms of plant survival and mortality during drought: why do some plants survive while others succumb to drought? *New Phytol.* 178, 719–739. doi: 10.1111/j.1469-8137.2008.02436.x

Mewis, I., Khan, Mohammed, A. M., Glawischnig, E., Schreiner, M., and Ulrichs, C. (2012). Water stress and aphid feeding differentially influence metabolite composition in *Arabidopsis thaliana* (L.). *PLoS ONE* 7, e48661. doi: 10.1371/journal.pone.0048661

Miranda-Apodaca, J., Pérez-López, U., Lacuesta, M., Mena-Petite, A., and Muñoz-Rueda, A. (2018). The interaction between drought and elevated CO_2 in water relations in two grassland species is species-specific. *J. Plant Physiol.* 220, 193–202. doi: 10.1016/j.jplph.2017.11.006

Mousa, K. M., Gawad, A. A., Shawer, D. M., and Kamara, M. M. (2019). Drought stress and nitrogen fertilization affect cereal aphid populations in wheat fields. *J. Plant Protection Pathol.* 10, 613–619. doi: 10.21608/jppp.2019.78153

Murray, T. J., Ellsworth, D. S., Tissue, D. T., and Riegler, M. (2013). Interactive direct and plant-mediated effects of elevated atmospheric [CO_2] and temperature on a eucalypt feeding insect herbivore. *Global Change Biol.* 19, 1407–1416. doi: 10.1111/gcb.12142

Nackley, L. L., Betzelberger, A., Skowno, A., West, A. G., Ripley, B. S., and Bond, W. J., et al. (2018). CO_2 enrichment does not entirely ameliorate *Vachellia karroo* drought inhibition: a missing mechanism explaining savanna bush encroachment. *Environ. Exp. Bot.* 155, 98–106. doi: 10.1016/j.envexpbot.2018.06.018

Navarro, E. C., Lam, S. K., and Trbicki,. P. (2020). Elevated carbon dioxide and nitrogen impact wheat and its aphid pest. *Front. Plant Sci.* 11, 605337. doi: 10.3389/fpls.2020.605337

Nie, G. Y., Hendrix, D. L., Webber, A. N., Kimball, B. A., and Long, S. P. (1995). Increased accumulation of carbohydrates and decreased photosynthetic gene transcript levels in wheat grown at an elevated CO_2 concentration in the field. *Plant Physiol.* 108, 975–983. doi: 10.1104/pp.108.3.975

Niziolek, O. K., Berenbaum, M. R., and Delucai, E. H. (2013). Impact of elevated CO_2 and increased temperature on Japanese beetle herbivory. *Insect Sci.* 20, 513–523. doi: 10.1111/j.1744-7917.2012.01515.x

Novriyanti, E., Watanabe, M., Kitao, M., Utsugi, H., Uemura, A., and Koike, T. (2012). High nitrogen and elevated [CO_2] effects on the growth, defense and photosynthetic performance of two eucalypt species. *Environ. Pollut.* 170, 124–130. doi: 10.1016/j.envpol.2012.06.011

Oehme, V., Petra, H., Claus, P. W., and Zebitz, A. F. (2013). Effects of elevated atmospheric CO_2 concentrations on phloem sap composition of spring crops and aphid performance. *J. Plant Interact.* 8, 7484. doi: 10.1080/17429145.2012.736200

Roth, S., Mcdonald, E. P., and Lindroth, R. L. (1997). Atmospheric CO_2 and soil water availability: consequences for tree-insect interactions. *Can. J. Forest Res.* 27, 1281–1290. doi: 10.1139/x97-031

Roy, J., Picon-Cochard, C., Augusti, A., Benot, M.arie, L., Thiery, L., and Darosnville, O., et al. (2016). Elevated CO_2 maintains grassland net carbon uptake under a future heat and drought extreme. *Proc. Natl. Acad. Sci. U. S. A.* 113, 6224–6229. doi: 10.1073/pnas.1524527113

Sandström, J., and Pettersson, J. (1994). Amino acid composition of phloem sap and the relation to intraspecific variation in pea aphid (*Acyrthosiphon pisum*) performance. *J. Insect Physiol.* 40, 947–955. doi: 10.1016/0022-1910(94)90133-3

Scherber, C., Gladbach, D. J., Stevnbak, K., Karsten, R. J., Schmidt, I. K., and Michelsen, A., et al. (2013). Multi-factor climate change effects on insect herbivore performance. *Ecol. Evo.* 3, 1449–1460. doi: 10.1002/ece3.564

Slosser, J. E., Parajulee, M. N., Hendrix, D. L., Henneberry, T. J., and Pinchak, W. E. (2004). Cotton aphid (Homoptera: Aphididae) abundance in relation to cotton leaf sugars. *Environ. Entomol.* 33, 690–699. doi: 10.1603/0046-225X-33.3.690

Smart, D. R., Chatterton, N. J., and Bugbee, B. (2010). The influence of elevated CO_2 on non-structural carbohydrate distribution and fructan accumulation in wheat canopies. *Plant Cell Environ.* 17, 435–442. doi: 10.1111/j.1365-3040.1994.tb00312.x

Suarez-Vidal, E., Sampedro, L., Voltas, J., Serrano, L., and Zas, R. (2019). Drought stress modifies early effective resistance and induced chemical defences of Aleppo pine against a chewing insect herbivore. *Environ. Exp. Bot.* 162, 550–559. doi: 10.1016/j.envexpbot.2019.04.002

Suguiyama, V. F., Silva, E. A., Meirelles, S. T., Centeno, D. C., and Braga, M. R. (2014). Leaf metabolite profile of the Brazilian resurrection plant *Barbacenia purpurea* Hook. (Velloziaceae) shows two time-dependent responses during desiccation and recovering. *Front. Plant Sci.* 5, 96. doi: 10.3389/fpls.2014.00096

Sun, Y., Guo, H., and Ge, F. (2016). Plant-aphid interactions under elevated CO_2: some cues from aphid feeding behavior. *Front. Plant Sci.* 7, 502. doi: 10.3389/fpls.2016.00502

Sun, Y., Guo, H., Yuan, L., Wei, J. N., Zhang, W. H., and Ge, F. (2015). Plant stomatal closure improves aphid feeding under elevated CO_2. *Glob. Change Biol.* 21, 2739–2748. doi: 10.1111/gcb.12858

Sun, Y., Guo, H., Zhu-Salzman, K., and Ge, F. (2013). Elevated CO_2 increases the abundance of the peach aphid on Arabidopsis by reducing jasmonic acid defenses. *Plant Sci.* 210, 128–140. doi: 10.1016/j.plantsci.2013.05.014

Sun, Y. C., Jing, B. B., and Ge, F. (2009). Response of amino acid changes in *Aphis gossypii* (Glover) to elevated CO_2 levels. *J. Appl. Entomol.* 133, 189–197. doi: 10.1111/j.1439-0418.2008.01341.x

Tetyuk, O., Benning, U. F., and Hoffmann, B. S. (2013). Collection and analysis of Arabidopsis phloem exudates using the EDTA-facilitated method. *J. Vis. Exp.* 80, e51111. doi: 10.3791/51111

Tzin, V., and Galili, G. (2010). New insights into the shikimate and aromatic amino acids biosynthesis pathways in plants. *Mol Plant.* 3, 956–972. doi: 10.1093/mp/ssq048

Uddin, S., Löw, M., Parvin, S., Fitzgerald, G. J., Tausz-Posch, S., and Armstrong, R., et al. (2018). Elevated [CO_2] mitigates the effect of surface drought by stimulating root growth to access sub-soil water. *PLoS ONE* 13, e0198928. doi: 10.1371/journal.pone.0198928

Ullah, A., Manghwar, H., Shaban, M., Khan, A. H., Akbar, A., and Ali, U., et al. (2018). Phytohormones enhanced drought tolerance in plants: a coping strategy. *Environ. Sci. Pollut. R.* 25, 33103–33118. doi: 10.1007/s11356-018-3364-5

Wall, G. W. (2001). Elevated atmospheric CO_2 alleviates drought stress in wheat. *Agr Ecosyst. Environ.* 87, 261–271. doi: 10.1016/S0167-8809(01)00170-0

Wei, Z. H., Abdelhakim, L. O. A., Fang, L., Peng, X. Y., Liu, J., and Liu, F. L. (2022). Elevated CO_2 effect on the response of stomatal control and water use efficiency in amaranth and maize plants to progressive drought stress. *Agr. Water Manag.* 266, 107609. doi: 10.1016/j.agwat.2022.107609

Xie, H. C., Shi, J. Q., Shi, F. Y., Xu, H. Y., He, K. L., and Wang, Z. Y. (2021). Aphid fecundity and aphid defenses in wheat exposed to a combination of heat and drought stresses. *J. Exp. Bot.* 71, 2713–2722. doi: 10.1093/jxb/eraa017

Zandalinas, S. I., Balfagon, D., Arbona, V., Gomez, C. A., Inupakutika, M. A., and Mittler, R. (2016). ABA is required for the accumulation of APX1 and MBF1c during a combination of water deficit and heat stress. *J. Exp. Bot.* 67, 5381–5390. doi: 10.1093/jxb/erw299

Zandalinas, S. I., Mittler, R., Balfagón, D., Arbona, V., and Gómez-Cadenas, A. (2018). Plant adaptations to the combination of drought and high temperatures. *PhysioL. Plantarum.* 162, 2–12. doi: 10.1111/ppl.12540

Zavala, J. A., Casteel, C. L., DeLucia, E. H., and Berenbaum, M. R. (2008). Anthropogenic increase in carbon dioxide compromises plant defense against invasive insects. *Proc. Natl. Acad. Sci. U. S. A.* 105, 10631–10631. doi: 10.1073/pnas.0800568105

Zavala, J. A., Gog, L., and Giacometti, R. (2017). Anthropogenic increase in carbon dioxide modifies plant-insect interactions. *Ann. Appl. Biol.* 170, 68–77. doi: 10.1111/aab.12319

Zavala, J. A., Nabity, P. D., and DeLucia, E. H. (2013). An emerging understanding of mechanisms governing insect herbivory under elevated CO_2. *Annu. Rev. Entomol.* 58, 79–97. doi: 10.1146/annurev-ento-120811-153544

Zhang, G. (1999). *Aphids in Agriculture and Forestry of Northwest China, 1st Edn*. Beijing: China Environmental Science.

Zhang, Y., Fan, J., Francis, F., and Chen, J. L. (2017). Watery saliva secreted by the grain aphid *Sitobion avenae* stimulates aphid resistance in wheat. *J. Agr. Food Chem.* 65, 8798–8805. doi: 10.1021/acs.jafc.7b03141

Zhao, Y., Song, C. C., Brummell, D. A., Qi, S. N., Lin, Q., Duan, Y. Q., et al. (2021). Jasmonic acid treatment alleviates chilling injury in peach fruit by promoting sugar and ethylene metabolism. *Food Chem.* 338, 128005. doi: 10.1016/j.foodchem.2020.128005

Züst, T., and Agrawal, A. A. (2016). Mechanisms and evolution of plant resistance to aphids. *Nat. Plants* 2, 15206. doi: 10.1038/nplants.2015.206

Conflict of Interest: The authors declare that the research was conducted in the absence of any commercial or financial relationships that could be construed as a potential conflict of interest.

Publisher's Note: All claims expressed in this article are solely those of the authors and do not necessarily represent those of their affiliated organizations, or those of the publisher, the editors and the reviewers. Any product that may be evaluated in this article, or claim that may be made by its manufacturer, is not guaranteed or endorsed by the publisher.

frontiers | Frontiers in Plant Science

ORIGINAL RESEARCH
published: 14 July 2022
doi: 10.3389/fpls.2022.882766

Genomic Regions Associated With Seed Meal Quality Traits in *Brassica napus* Germplasm

Gurleen Bhinder, Sanjula Sharma, Harjeevan Kaur, Javed Akhatar*, Meenakshi Mittal and Surinder Sandhu*

Oilseeds Section, Department of Plant Breeding and Genetics, Punjab Agricultural University, Ludhiana, India

The defatted *Brassica napus* (rapeseed) meal can be high-protein feed for livestock as the protein value of rapeseed meal is higher than that of the majority of other vegetable proteins. Extensive work has already been carried out on developing canola rapeseed where the focus was on reducing erucic acid and glucosinolate content, with less consideration to other antinutritional factors such as tannin, phytate, sinapine, crude fiber, etc. The presence of these antinutrients limits the use and marketing of rapeseed meals and a significant amount of it goes unused and ends up as waste. We investigated the genetic architecture of crude protein, methionine, tryptophan, total phenols, β-carotene, glucosinolates (GLSs), phytate, tannins, sinapine, and crude fiber content of defatted seed meal samples by conducting a genome-wide association study (GWAS), using a diversity panel comprising 96 *B. napus* genotypes. Genotyping by sequencing was used to identify 77,889 SNPs, spread over 19 chromosomes. Genetic diversity and phenotypic variations were generally high for the studied traits. A total of eleven genotypes were identified which showed high-quality protein, high antioxidants, and lower amount of antinutrients. A significant negative correlation between protein and limiting amino acids and a significant positive correlation between GLS and phytic acid were observed. General and mixed linear models were used to estimate the association between the SNP markers and the seed quality traits and quantile-quantile (QQ) plots were generated to allow the best-fit algorithm. Annotation of genomic regions around associated SNPs helped to predict various trait-related candidates such as *ASP2* and *EMB1027* (amino acid biosynthesis); *HEMA2, GLU1,* and *PGM* (tryptophan biosynthesis); *MS3, CYSD1,* and *MTO1* (methionine biosynthesis); *LYC* (β-carotene biosynthesis); *HDR* and *ISPF* (MEP pathway); *COS1* (riboflavin synthesis); *UGT* (phenolics biosynthesis); *NAC073* (cellulose and hemicellulose biosynthesis); *CYT1* (cellulose biosynthesis); *BGLU45* and *BGLU46* (lignin biosynthesis); *SOT12* and *UGT88A1* (flavonoid pathway); and *CYP79A2, DIN2,* and *GSTT2* (GLS metabolism), etc. The functional validation of these candidate genes could confirm key seed meal quality genes for germplasm enhancement programs directed at improving protein quality and reducing the antinutritional components in *B. napus*.

Keywords: antioxidants, antinutritional traits, *Brassica napus*, cluster analysis, genome-wide association study, seed meal quality

OPEN ACCESS

Edited by:
Marta Wilton Vasconcelos, Catholic University of Portugal, Portugal

Reviewed by:
Xin-Yuan Huang, Nanjing Agricultural University, China
Vesna Dragicevic, Maize Research Institute Zemun Polje, Serbia

****Correspondence:***
Javed Akhatar
javedpbg@pau.edu
Sanjula Sharma
drsanjula@pau.edu

Specialty section:
This article was submitted to Plant Nutrition, a section of the journal Frontiers in Plant Science

Received: *24 February 2022*
Accepted: *20 April 2022*
Published: *14 July 2022*

Citation:
Bhinder G, Sharma S, Kaur H, Akhatar J, Mittal M and Sandhu S (2022) Genomic Regions Associated With Seed Meal Quality Traits in Brassica napus Germplasm. Front. Plant Sci. 13:882766. doi: 10.3389/fpls.2022.882766

INTRODUCTION

Rapeseed (*B. napus* L.) is an economically important group belonging to the family *Brassicaceae* that possesses high acreage of 36.24 million hectares and production of 73.16 million metric tons (MMT) during 2020–2021 and ranks the third largest sources of vegetable oil all over the world (Yang et al., 2019; USDA, 2021). The biggest rapeseed producing countries in 2019/2020 were Canada (19 MMT), China (13.1 MMT), and India (7.7 MMT); however, the European Union produced 16.83 MMT of rapeseed (Statista, 2021). Rapeseed is widely cultivated throughout the world as a source of oil and protein for food and feed purposes. The portion left after oil extraction from seeds of rapeseed is called as meal or cake as per the residual oil content in it. Both meal and cake are rich in protein (32–48%) (Sadeghi and Bhagya, 2009) but differ in their oil content which is 1–4% in the meal (Klein-Hessling, 2007) and 10–14% in cakes (Mahoonak and Swamylingappa, 2007). World production of rapeseed meals in 2020/2021 was 41.20 MMT, which was higher than in 2019/2020 (39.45 MMT) (USDA-FAS, 2021). Interestingly, improved oilseed production would also help in raising meal production in the forecast year by 5.2% to a total of 17 MMT (USDA, 2021).

Due to its low-volume, high-cost, high-quality protein, residual oil, and energy values, seed meal of *Brassica* is mainly streamlined into formulation of feed for dairy cattle, swine, poultry, and farmed fish (Wanasundara, 2011). The seeds of *B. napus* contain around 25–30% seed storage proteins, which are predominantly composed of cruciferin (60%), napin (20%), and other minor proteins such as oleosins and lipid transfer proteins (Gehrig et al., 1996). The richness in minerals, vitamins, well-balanced amino acid composition, high levels of sulfur containing amino acids (cysteine, methionine in napin), and efficient protein utilization in humans showed that it can be rated as a high-quality protein, compared to egg and milk proteins (Fleddermann et al., 2013). Seeds of *B. napus* also reserve carotenoids (5.34 μg/g), which possess antioxidant properties that scavenge oxygen radicals and have been accounted to decline the incidence of cardiovascular disease and cancers (Yu et al., 2008). The results of few studies have shown that quantitative trait loci (QTL) for seed oil and protein content are closely linked, and there is a negative correlation between protein and oil content (Grami et al., 1977; Gül et al., 2003). These findings are not surprising as both protein and oil compete for the same basic substrates in the biochemical pathway and therefore must be partly controlled by the same genes. Also, the presence of carotenoids protects seeds against deterioration and aging and promotes seed germination (Howitt and Pogson, 2006). Despite its high nutritional importance, rapeseed meal usage as an ingredient of food and feed is narrow due to the presence of high amount of some antinutritional compounds *viz.,* crude fiber (4.56% in yellow seeded meal and 8.86% in black seeded meal) (Jiang et al., 2015), phenolics (38.50–63.95 mg/g) (Yang et al., 2015), sinapine (7–13 mg/g) (Matthäus and Zubr, 2000), glucosinolates (GLSs) (15.49–139.09 μmol/g) (Sen et al., 2018), phytic acid (2–4% in the defatted meal, and 5–7% in the protein concentrates) (Sashidhar et al., 2020), tannins (2.71–3.91%) (Fenwick et al., 1984), etc., which cannot be quickly metabolized and have negative effect on animal health. As a consequence, a large amount of rapeseed meal remains unused and thus becomes a waste product (Aukema and Campbell, 2011).

Glucosinolates present in the Brassica seeds are hydrolyzed to pungent and biologically active isothiocyanates that have negative thyrogenic effects on animals (Walker and Booth, 2001). A modified improved quality of rapeseed developed in Canada has been named "canola" or "double low" variety, for its low content of erucic acid (<2%) in oil and glucosinolates (<30 μmol/g) in seed meal residue which have been fairly successful and considered excellent for food and feed purpose. The meal can thus be used as a protein supplement (Tripathi and Mishra, 2007). The pathways of amino acid and glucosinolate biosynthesis share common enzymes; therefore, perturbation of glucosinolate in double low varieties could affect the level of napin (Field et al., 2004; Nesi et al., 2008). The level of napin and cruciferin in seeds also affects the functionality of canola protein products, including solubility, emulsifying ability, and heat-induced gel formation. Moreover, the phenolic compounds are the major contributors to the dark color and astringent, bitter taste of the meal which is found in the seed coat and cotyledons (Hannoufa et al., 2014). The rich phenolic acid in rapeseed is sinapic acid (3, 5-dimethoxy-4-hydroxycinnamic acid). Sinapine, its choline ester, accounted for ∼80% of all phenolics, in *B. napus* seed (Wanasundara, 2011). Sinapine can complex with meal proteins and reduce their bioavailability and digestibility (Nesi et al., 2008). Hydrolysable and condensed tannins in rapeseed meal are the secondary compounds with antinutritional properties (Chung et al., 1998). *In vivo* experiments showed that hydrolysable tannins degrade into smaller compounds and injure both liver and kidney in ruminants, rodents, and poultry (Tosi et al., 2013; Bilić-Šobot et al., 2016). Phytates (myo-inositol hexaphosphoric acid) is the principal storage form of phosphorus which accumulates as insoluble crystals known as globoids in protein storage vacuoles of *Brassicaceae* seeds (Madsen and Brinch-Pedersen, 2020). Due to its ability to bind important dietary minerals (Ca, Zn, and Fe) as well as proteins and starch, it is considered as an antinutrient. Fiber fraction is linked with low digestibility and bioavailability of meal protein in feeds of animals. Total meal digestibility indicates a negative correlation with the hull and the lignin content of seed (Wanasundara, 2011). Approximately, one-third of *B. napus* meal is represented by dietary fiber with a significant amount of fiber being in the form of indigestible lignin.

Emphasis on reducing the amount of these antinutritional compounds in rapeseed meal must be given for addressing food security issue. Understanding the genetics of these traits is important for developing high-quality rapeseed meal for food and feed purpose. Genome-wide association study (GWAS) has become an effective and powerful tool for the dissection of loci associated with complex traits in the crop genomes especially for polyploids such as *B. napus*. GWAS determines the historical recombination between the trait of interest and single-nucleotide polymorphism (SNP) markers. If recombination between two loci is less frequent than expected for the unlinked regions,

then the loci are known to be in linkage disequilibrium (LD). Many studies document identification of molecular markers associated with various seed quality traits such as protein (Akhatar et al., 2020), glucosinolates (Qu et al., 2015; Tan et al., 2022), oil (Xiao et al., 2019), fatty acids (Gacek et al., 2017; Tang et al., 2019; Yao et al., 2020), and acid detergent lignin (Wang and Qin, 2017) in Brassica using GWAS approach. However, scarce information is available with Brassica breeders regarding molecular markers associated with other important seed meal quality traits mentioned above which led to the lack of understanding of the genetic systems underlying the biosynthesis of these key nutrients and antinutrients.

Keeping this in viewpoint, efforts have been made to screen the sequenced diversity set of 96 *B. napus* accessions for seed meal quality traits and to identify the genomic regions associated with these traits using GWAS.

MATERIALS AND METHODS

Seed Material, Defatting, and Phenotyping

B. napus fixed diversity set, comprising of 96 accessions, constituted the experimental materials for the present investigations. Each genotype was sown in paired rows of 2 m row length at a row-to-row and plant-to-plant spacing of 45 and 10 cm, respectively, in alpha lattice design with two replications at PAU, Ludhiana. The germplasm set was evaluated for seed meal quality traits during 2019–2020. The dry mature ground seeds of each sample were defatted using conventional Soxhlet extraction apparatus. A quantity of the dried sample (4 g) was put into the thimble, and the materials were continuously extracted for 6–7 h using petroleum ether (60–80°C) as a solvent. Further, the thimble was removed and the defatted seed meal was allowed to dry in an oven at 60°C. The drying process was repeated until a constant weight was obtained. Defatted meal was then stored in the zip lock packets at 4°C till further biochemical analysis. The concentration of ten seed quality traits *viz.,* crude protein, methionine, tryptophan, total phenols, β-carotene, glucosinolates, phytate, tannin, sinapine, and crude fiber content in seed meal were estimated using the standard procedures mentioned below.

Crude Protein Content

Crude protein was estimated using MicroKjeldahl nitrogen method (McKenzie and Wallace, 1954). Sample (0.2 g) was digested with conc. sulfuric acid (10 ml) and 2 g of catalyst mixture ($CuSO_4.5H_2O$ and K_2SO_4 in the ratio of 1: 10) to convert organic nitrogen to ammonium sulfate in solution followed by decomposition of ammonium sulfate with sodium hydroxide. The released ammonia was distilled into 2% boric acid. The nitrogen from ammonia was deduced from titration of the trapped ammonia with 0.1NHCl using dye solution (0.3 g bromocresol, 0.2 g methyl red in 400 ml of 90% ethanol). The percent nitrogen obtained was multiplied by the general factor 6.25 to give the percent crude protein.

Methionine Content

Methionine content was estimated by using method of Horn et al. (1946). About 1 g of dried seed meal sample was weighed and transferred into a 50-ml conical flask containing 2.5N HCl and autoclaved for 1 h at 121°C and 15 psi. A pinch of activated charcoal was added to the hydrolysate and heated to boil to decolorize the extract and was then filtered when hot. The volume of the filtrate was made to 25 ml with double distilled water. This filtrate (10 ml) was then transferred to a flask containing 3 ml of 5N and 0.1 ml of 10% sodium nitroprusside. After 10 min, 2 ml of 3% glycine solution was added and again after another 10 min, 4 ml of o-phosphoric acid was added and shaken vigorously. The intensity of red color was read at 520 nm. Methionine content was calculated by extrapolation on the standard graph prepared using 0.2 mg to 3 mg of methionine. Methionine content was expressed as g/100 g protein.

Tryptophan Content

Tryptophan content was determined according to Spies and Chambers (1949) method. To powdered seed meal sample (50 mg), 30 mg of p-dimethylaminobenzaldehyde (PDAB) and 10 ml of 19N H_2SO_4 were added in a flask which was then kept at room temperature in dark place for 12 h. Aliquot is centrifuged at 5,000 rpm for 30 min, and to it, 0.1 ml of 0.045% $NaNO_2$ solution was added. After an incubation of 15 min, the color developed was read at 454 nm on spectrophotometer and calculated the content of tryptophan using standard curve for tryptophan (40–200 μg). Tryptophan content was expressed as g/100 g protein.

β-carotene

Beta-carotene content was assessed according to the approved methods of AOAC (1980). About 1 g of fine defatted sample was taken in glass vials, and 10 ml of water saturated butanol (WSB) (8 butanol: 2 water v/v) was added. The vials were closed tightly and mixed vigorously for 1 min and kept overnight (18–20 h) at room temperature under dark for complete extraction of β-carotene. Next day, the vials were slightly shaken again, and the extract was filtered through Whatman No. 1 filter paper. The optical density of the filtrate was measured at 440 nm on spectrophotometer. Pure WSB was used as blank. The β-carotene content was calculated from calibration curve from known amount of β-carotene and expressed as μg/g. Standard solution of β-carotene was prepared in WSB at the concentration of 5 μg/ml.

Total Phenol Content

Total phenol content was determined by following the method of Swain and Hillis (1959). Homogenization of 0.25 g defatted dried sample was done in 10 ml of 80% methanol and refluxed on water bath for 2 h at temperature 70–75°C. The methanolic extract was pooled after refluxing, and volume was made to 10 ml by washing with 80% methanol. The methanolic extract (0.5 ml, 50 g/ml) was mixed with Folin–Ciocalteu reagent (0.5 ml) and shaken thoroughly. After 5 min, saturated solution of Na_2CO_3 (1 ml) was added. After an hour of incubation at room temperature, the absorbance of blue color was read in a spectrophotometer at

760 nm against the blank. The blank was prepared from water and reagent only. The concentration of the total phenols (mg/g GAE) was calculated from the standard curve prepared using gallic acid (10–100 μg) (Thomas Baker Chemicals Private Limited, India).

Sinapine Content

Sinapine content was determined using method by Kolodziejczyk et al. (1999). Defatted meal (1.5 g) was extracted three times with 35 ml of methanol by refluxing for 30 min. Methanol extracts were combined and evaporated transferred to a 100-ml volumetric flask, and the final volume was adjusted to 100 ml with methanol. For measurement, 100 μl of solution was diluted to 10 ml with methanol and the absorbance was recorded at 330 nm. Sinapine content in the meal was calculated from the formula:

% Sinapine = (2.184 × Absorbance × 10)/ Sample Wt. [g].

Phytic Acid

Phytic acid content in seed meal was determined by following the method of Haug and Lantzsch (1983). Seed meal (0.2g) sample was homogenized in 25 ml of 0.2N HCl and was shaken continuously for 3 h on a mechanical shaker at room temperature. The extract was filtered through Whatman paper. An aliquot of 0.5 ml of this extract was pipetted into a test tube, and total volume was made to 1.4 ml with distilled water. Further, 1 ml of ferric ammonium sulfate or ammonium ferric (III) sulfate (FAS) solution (0.2 g of FAS was dissolved in 100 ml of 2N HCl and volume made up to 1,000 ml with distilled water) was added and the contents were stirred and heated for 30 min in boiling water bath. About 1 ml of aliquot was transferred to another test tube to which 1.5 ml of 2, 2'-bipyridine solution (1 g of 2, 2'-bipyridine in 1 ml of thioglycolic acid dissolved in distilled water and volume made to 100 ml) was added. The tubes were shaken well and the color intensity was read at 519 nm against distilled water as a blank in spectrophotometer. The concentration of the phytic acid (mg/100 g) was calculated from the standard curve prepared using sodium phytate (40–200 μg).

Crude Fiber

Crude fiber content was estimated following the AOAC (1990) protocol. Moisture and fat-free meal sample (1 g) was boiled in 100 ml of 1.25% H_2SO_4 solution for 1 h under reflux. The boiled sample was washed in several portions of hot water using 2-fold cloth till it becomes acid-free. The sample was transferred to the same beaker and boiled again in 100 ml of 1.25% NaOH for another 1 h under the same condition. To make alkali-free, the residue was washed in several portions of hot water and was allowed to drain dry before being transferred quantitatively to a weighed crucible (w_o) where it is dried to constant weight (w_1) at 100°C. Constant weighed crucible (w_1) was then ignited in muffle furnace where it was burnt, only ash was left of it. The weight of the fiber was determined by difference and calculated as

$$\text{Crude fiber (\%)} = \frac{(w_1 - w_o) - (w_2 - w_o)}{\text{Weight of sample}} \times 100$$

Tannin Content

Tannin content estimation was conducted following Price et al. (1978) protocol. Defatted sample (0.2 g) was homogenized using 2 ml of reagent A (2.8% conc. HCl in methanol). Contents were vortexed for 20 min at room temperature and then centrifuged at 10,000 rpm for 10 min. The pellet was discarded and the 0.5 ml of supernatant was mixed with 2.5 ml of reagent C [1% vanillin in reagent B (22.2% of conc. HCl in methanol)] and incubated at 30°C for 20 min. Absorbance of the mixture was read at 500 nm on the spectrophotometer. Standard curve was prepared using catechin as standard in the range of 10–100 μg.

Glucosinolates

The determination of seed meal glucosinolates was performed as described by Kumar et al. (2004). About 500 mg seed was warmed at 100°C for 1 h in the oven to deactivate myrosinase. Seeds were then grounded and defatted three times using 30 ml petroleum ether each time. The residue was then dried in an oven at 100°C for 10 min. About 200 mg of fat-free sample was taken, and 0.3 ml of 60% warm methanol was added to it to deactivate the myrosinase enzyme. Tubes were then heated in water bath at 80°C for 10 min. Make sure that ethanol evaporates completely. About 4 ml of distilled water was added to it and tubes were heated further at 80°C for 15 min. The extract was centrifuged in a tube, and then, 40 μl of the supernatant was taken in other test tubes in duplicates. After addition of 4 ml of 0.2 mM Na_2PdCl_4 reagent, it was kept at room temperature for 1 h, and optical density reading (μmoles/g defatted meal) was recorded at 405 nm on the spectrophotometer. Sinigrin (16–83.0 μg) was used as standard.

Statistical Analysis

Analysis of variance (ANOVA), coefficient of variance (CV) and best linear and unbiased predictors (BLUPs) were computed using SAS 9.3 (SAS Institute Inc.) and R software version 4.1.2 (https://www.r-project.org/).

Diversity Analysis

D^2 analysis is an important multivariate distance matric method to evaluate the genetic diversity and selection of parental material for the breeding programs based on the traits measured. It is based on measuring the distance between a point and a distribution. Mahalanobis D^2 analysis was conducted using WINDOSTAT 8.0 cluster analysis tool using the Tocher's method (Rao, 1952).

Genome-Wide Association Study

Genome-wide association study was conducted to find associations between SNPs and seed meal quality traits across the 96 diversity fixed *B. napus* accessions. Genotype by sequencing-based genome assembly, SNP data, and population structure of 96 diversity fixed set of *B. napus* was available from Pal et al. (2021) which was used to identify SNPs significantly associated with seed meal quality traits. The BLUP's value for the target parameters from each accession and SNP markers (77,889) were analyzed using software Genome Association and Prediction Integrated Tool (GAPIT) version 3 (Lipka et al., 2012; Wang and Zhang, 2021). Manhattan plots were plotted using R package "CMPlot." We compared three different algorithm models for their capacity to fit the data: general linear model (GLM), mixed

linear model (MLM), and fixed and random model circulating probability unification (farm CPU). The choice of the best model was based on quantile-quantile plot (Q-Q plot), by plotting their quantiles against each other. The association between SNPs and traits was assessed based on the $-\log_{10}(p)$ value of each SNP, and the expected *p*-values were used for the selection. SNPs with an arbitrary value of $-\log_{10}(p) \geq 3$ were considered as significant, and allelic effect estimates were calculated for them.

Gene Prediction

The region of 50-kb up/downstream of the associated SNP/SNPs was scanned for identifying candidate genes using *B. napus* reference genome. The predicted gene and its orthologous sequence were then annotated by Basic Local Alignment Search Tool (BLAST) analysis against *Arabidopsis thaliana* database using Blast2GO Pro tool (Conesa and Götz, 2008). Functions of the possible candidate genes were validated from NCBI (https://www.ncbi.nlm.nih.gov/) to determine their relevance for biochemical traits in question.

Gene Pathway

GeneMANIA is a user-friendly prediction web server (https://genemania.org/) which analyze the input gene list and priorities them for their function and fit them into possible networks based on their probable interactions or co-expressions, etc. (Warde-Farley et al., 2010). It also extends the query gene list with genes that may be functionally similar or associated in the same network based on the available genomic and proteomic data. We used this tool to find the associations within significant SNPs predicted for the seed meal quality traits.

RESULTS

Phenotypic Variation in Seed Quality Traits

A total of ten seed meal quality traits *viz.,* crude protein, limiting amino acids (methionine and tryptophan), β-carotene, phenols, sinapine, phytic acid, crude fiber, tannins, and glucosinolate content were measured for three replications in *B. napus* diversity panel comprising 96 accessions. As displayed in **Table 1**, the results indicated that there were abundant phenotypic variations in 96 *B. napus* diversity panel, and all the seed meal quality traits followed a normal distribution (**Figure 1**), which benefited the dissection of the genetic architecture of the seed. Frequency distribution graph depicted that majority of genotypes had crude protein, methionine, tryptophan, β-carotene, phenols, sinapine, phytic acid, crude fiber, tannin content, and glucosinolates in the range of 38–40%, 1.0–1.5 g/100 g protein, 1.0–1.5 g/100 g protein, 3.3–3.5 μg/g, 9.3–9.7 mg/g GAE, 0.8–0.9%, 5.3–5.7%, 9.5–10.5%, 1.9–2.1%, and 75–85 μmoles/g defatted seed meal, respectively (**Figure 1**). The glucosinolate content, which varied from 12.27 to 128.31 μmoles/g defatted seed meal with an average of 72.18 μmoles/g defatted seed meal, had the maximum coefficient of variation of 40.79%, whereas crude fiber, which varied from 7.70 to 14.90% with an average of 10.94%, had the lowest coefficient of variation of 15.22%. Out of 96 *B. napus* accessions, eleven genotypes, namely, PN-45-1, FAN-628, VCN-9, OCN-106, CHARLTON, EC-609305, OCN-69, PN-47-1, BCN-16, ZY-008, and PN-87-3 showing high-quality protein, richness in the antioxidants along with less amount of antinutritional compounds were selected among all graded genotypes. Crude protein content showed a strong negative correlation with limiting amino acids *viz.,* methionine ($p = -0.734$) and tryptophan content ($p = -0.739$); however, the two limiting amino acids depicted a positive correlation ($p = 0.613$) between them. Apart from this, the glucosinolate content was positively associated ($p = 0.290$) with phytic acid (**Table 2**). Overall, the *B. napus* seed meal quality traits exhibited significant genetic variations, and it was suitable for association analysis.

Diversity Analysis

Based on D^2 analysis, all the 96 accessions were grouped into ten diverse clusters. Clusters 2 and 4 had majority of genotypes (17). From a total number of 10 traits measured, maximum contribution of 84.7% was observed for the glucosinolates followed by the contribution of 13.3% by crude protein content. The inter-cluster distance ranged from 183.0 (clusters 6 and 8) to 8,521.1 (clusters 4 and 9). The intra-cluster distances varied from 48.4 (cluster 8) to 208.6 (cluster 10). The cluster diagram based on eucledian^2 distance is shown in **Supplementary Figure S1**.

Marker Trait Associations Identifies Potential Candidate Genes Regulating Quality Traits in *B. napus* Seed Meal

To elucidate the genetic architecture of quality traits in *B. napus* seed meal, GWAS between quality traits and genotyped SNPs was performed using the panel of 96 accessions of *B. napus* diversity fixed set. A total of 789 significant SNPs out of a total of 77,889 SNPs were found to be located on 19 chromosomes of *B. napus* with distribution over the two genomes (A and C) of *B. napus*. Majority of significant SNPs were observed for the traits sinapine (101), tryptophan (100), β-carotene (99), and protein (98) whereas a limited number of significant SNPs were reported for the traits phytic acid (49) and phenol (52). Out of 789 significant SNPs, 32 loci associated with crude protein (3), methionine (3), tryptophan (3), β-carotene (1), phenols (4), sinapine (1), phytic acid (6), crude fiber (5), tannin (3), and glucosinolates (3), respectively, were identified (**Table 3**). Significantly associated SNPs per trait were displayed on Manhattan plots (**Figure 2**). The predictive Q-Q plots show that expected distribution agrees of *p*-values have a high consistency with the observations (**Supplementary Figure S2**). The SNPs for crude protein content, *ASP5 (ASPARTATE AMINOTRANSFERASE 5), ASP2 (ASPARTATE AMINOTRANSFERASE 2),* and *EMB1027 (EMBRYO DEFECTIVE 1027),* were distributed on chromosomes A03, A10, and C02, respectively. A number of two genes, such as *MS3 (METHIONINE SYNTHASE 3)* and *CYSD1 (CYSTEINE SYNTHASE D1)* annotated on A03 and *MTO1 (METHIONINE OVERACCUMULATION 1)* envisaged on chromosome C01, were found associated with methionine content. Chromosome A10 contains two genes such as *GLU1 (GLUTAMATE SYNTHASE 1)* and *PGM (COFACTOR-DEPENDENT PHOSPHOGLYCERATE MUTASE)* and chromosome A09 showed one locus-*HEMA2* (glutamyl-tRNA reductase family

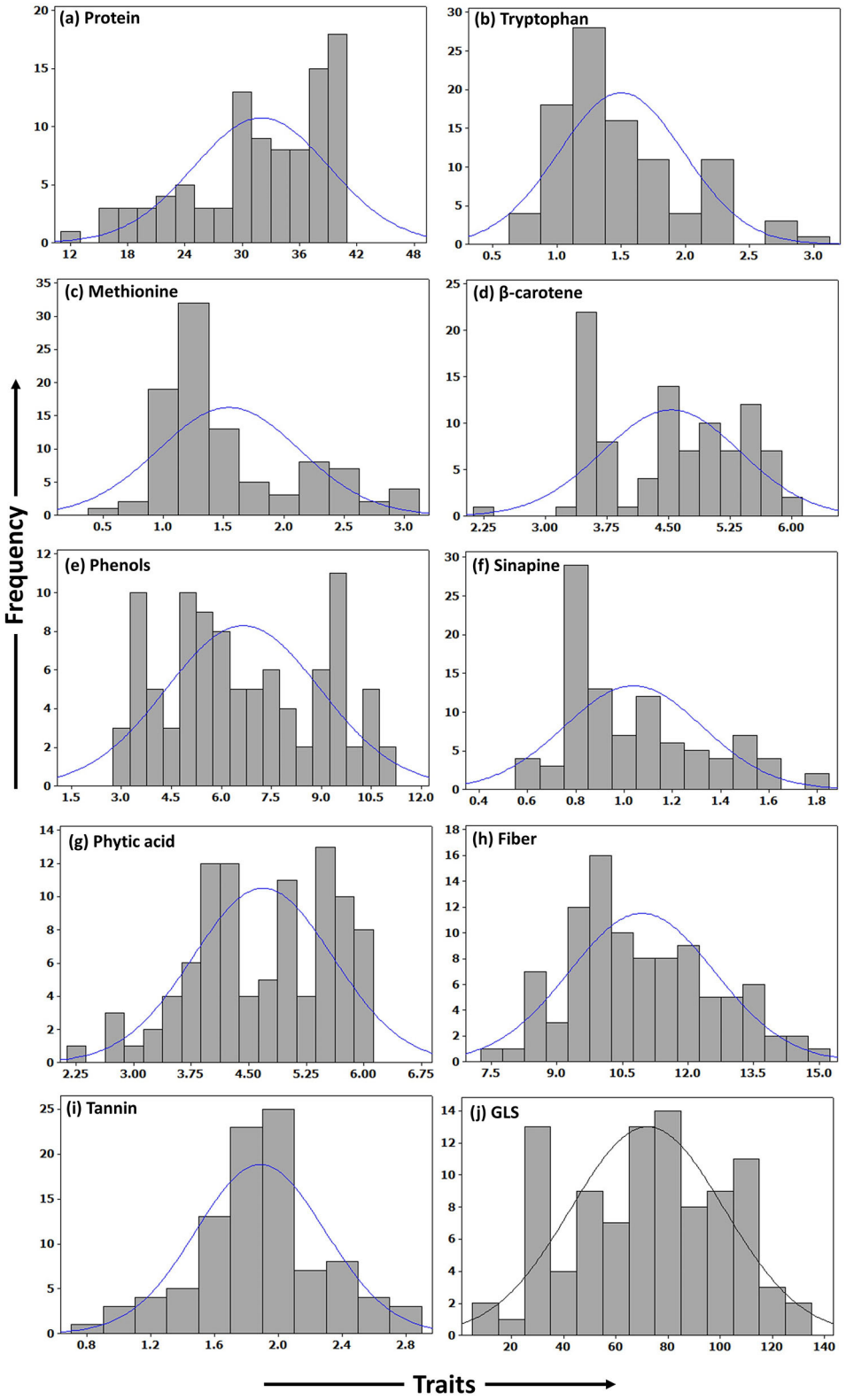

FIGURE 1 | Frequency histograms showing distribution of quality traits in seed meal of B. *napus* accessions. **(a)** Protein. **(b)** Tryptophan. **(c)** Methionine. **(d)** β-carotene. **(e)** Phenols. **(f)** Sinapine. **(g)** Phytic acid. **(h)** Fiber. **(i)** Tannin. **(j)** GLS.

protein) associated with tryptophan content. In case of β-carotene, ISPH/ *HDR (4-HYDROXY-3-METHYLBUT-2-ENYL DIPHOSPHATE REDUCTASE)* was identified on chromosome C05 at a gene distance of 32.8 kb. Significant candidate genes were predicted for antinutritional factors which include candidate *GAUT13* (*GALACTURONOSYLTRANSFERASE 13*), *UGT (UDP*-glycosyltransferase superfamily protein*), LYC (LYCOPENE CYCLASE)* and *COS1 (CORONATINE INSENSITIVE1 SUPPRESSOR 1)* on chromosomes A01, A06, A08, and C08, respectively, associated with phenols. *COS1* was envisaged at a distance of 3.59 kb from the SNP SNC_027774.2_284044517. This study also identified association of *ISPF (ISOPRENOID F)* (AT1G68970) gene on chromosome A09 with sinapine. A total of six candidate genes such as *PMT5 (POLYOL/MONOSACCHARIDE TRANSPORTER 5)* on chromosome A01, *PLDALPHA1 (PHOSPHOLIPASE D ALPHA 1)* on chromosome A05, *SAC8 (SAC DOMAIN-CONTAINING PROTEIN 8)* on chromosome A06, *PRAF1 (REGULATOR OF CHROMOSOME CONDENSATION (RCC1) FAMILY WITH FYVE ZINC FINGER DOMAIN-CONTAINING PROTEIN)* on chromosome A07, *PIP5Ks (PHOSPHATIDYLINOSITOL-4-PHOSPHATE 5-KINASE)* on chromosome A09, and *CCI1 (CLAVATA COMPLEX INTERACTOR 1)* on chromosome C02 were predicted for phytic acid. Genes involved in crude fiber synthesis pathway, i.e., *NAC073 (NAC domain-containing protein 73)* were predicted two times on chromosome C01. Functional annotation also predicted two genes *viz., BGLU45 (BETA GLUCOSIDASE 45)* and *BGLU46 (BETA GLUCOSIDASE 46)* between 2.77 and 4.75 kb on either side of the peak SNPs on chromosome C01 for lignin biosynthesis. Annotation also predicted *CYT1 (CYTOKINESIS DEFECTIVE 1)* on chromosome C03 encoding forglucose-1-phosphate adenylyltransferase family protein, an important component in cellulose biosynthesis. GWAS also allowed for recognition of three candidates such as *SOT12 (SULFOTRANSFERASE 12), SK1 (SHIKIMATE KINASE 1),* and *UGT88A1 (UDP-GLUCOSYL TRANSFERASE 88A1)* on chromosomes A02, C07, and C08, respectively, associated with tannins. Functional annotation predicted two genes such as *DIN2 (DARK INDUCIBLE 2)* and *GSTT2 (GLUTATHIONE S-TRANSFERASE THETA 2)* on chromosome C08 and one candidate *CYP79A2 (CYTOCHROME P450 79A2)* on chromosome A10 associated with glucosinolates. Out of the two genes predicted on chromosome C08, *GSTT2* was close to SNP SNC_027774.2_32661558 at a distance of 3.9 kb. The gene expression profile of these genes was studied from Brassica EDB database (https://brassica.biodb.org/) for *B. napus,* and the results are shown in **Supplementary Figure S3**.

Gene Pathway

All the identified candidate genes were queried into GeneMANIA web server to predict their interaction, and it results into a big network showing a complex genetic relationship among them (**Figure 3**). Many genes are related by their functional protein domain whereas others are expressing together and physically interacting with each other to perform a similar role in cell. For example, *BGLU45* and *BGLU46*, this pair of genes have been identified on same chromosome C01 in close vicinity of a single SNP. In the gene network, they are co-expressing and physically interacting and are predicted to be responsible for affecting the crude fiber content in Brassicas. Similarly, genes identified for glucosinolates, *DIN2,* and *CYP79A2* are also co-expressing, which further gives an idea that they may be playing a role in regulation of glucosinolate pathway in plants. No direct association between the identified genes for protein was detected by GeneMANIA, but the program extended the network by associating another family member of same family, *MS2*, with *MS3 based* on the shared protein domain. A total of two of the identified genes, *ASP5* and *ASP2*, belong to the same family. According to GeneMANIA results, they are shown to share the protein domains as well. They are not found to be interacting directly with each other, but they are observed to be interacting with a same set of genes.

DISCUSSION

The rapeseed meal constitutes an alternative source of plant protein and holds the potential to remove malnutrition problem. However, it has limited application due to the presence of

TABLE 1 | Phenotypic variation for ten seed meal quality traits in B. napus diversity panel.

Trait	Min.	Max.	Mean ± SD	CV
Protein (%)	11.67	39.38	32.00 ± 7.12	22.26
Methionine (g/100 g protein)	0.53	3.00	1.54 ±0.59	38.19
Tryptophan (g/100 g protein)	0.73	3.01	1.50 ±0.49	32.54
β-carotene (μg/g)	2.35	5.99	4.53 ±0.84	18.48
Phenols (mg/g GAE)	3.01	11.17	6.65 ±2.31	34.69
Sinapine (%)	0.56	1.81	1.04 ±0.29	27.55
Phytic acid (%)	2.35	6.00	4.68 ±0.91	19.42
Crude Fiber (%)	7.70	14.90	10.94 ±1.67	15.22
Tannin (%)	0.77	2.72	1.89 ±0.41	21.51
Glucosinolates (μmoles/g)	12.27	128.31	72.18 ±29.44	40.79

PTN, protein; AOX, antioxidants; ANU, antinutrients; Min., minimum; Max., maximum; SD, standard deviation; CV, coefficient of Variation which was estimated as the ratio of the standard deviation to the mean of all accessions.

TABLE 2 | Pearson correlation coefficients for seed meal quality traits.

	Phenols	β-carotene	Crude protein	Methionine	Tryptophan	Phytic acid	Fiber	Tannin	GLS	Sinapine
Phenols	1.000	0.160	−0.165	0.039	0.038	0.117	−0.057	−0.043	0.062	−0.010
β-carotene		1.000	0.004	−0.043	−0.024	−0.074	0.053	−0.031	−0.030	−0.067
Crude protein			1.000	**−0.734*** **	**−0.739*** **	−0.138	0.026	0.146	−0.061	−0.030
Methionine				1.000	**0.613*** **	0.135	−0.030	−0.120	0.168	−0.004
Tryptophan					1.000	0.135	0.055	−0.023	0.039	0.061
Phytic acid						1.000	−0.196	0.090	**0.290** **	−0.059
Fiber							1.000	0.101	0.004	−0.066
Tannin								1.000	0.130	0.070
GLS									1.000	0.028
Sinapine										1.000

*Trait pairs affecting quality traits in B. napus diversity panel. *** and ** Significance levels at p value 0.001 >0.337 and 0.01 >0.267 respectively.*

antinutritional compounds which results in extensive wastage of rapeseed meal. To make rapeseed meal fit for food and feed purpose, it is essential to improve the quality of its meal by decreasing the amount of antinutritional compounds. The development of strains with increased protein, limiting amino acids and β-carotene content coupled with low meal phenols, sinapine, phytic acid, crude fiber, tannins, and glucosinolates in seed meal is a major crop improvement goal in *B. napus*. Also, the work on genetics of these traits will promote the usage of high-quality rapeseed meal at large scale.

The outcomes of the present report showed phenotypic correlations among the ten seed meal quality traits in question. For instance, limiting amino acids (methionine and tryptophan) had significant negative correlation with protein content and significant positive correlation with each other. Based on this observation, it can be concluded that increase in protein content will be accompanied by a decrease in the levels of sulfur amino acid (methionine) and tryptophan in Brassicas. Research studies have also shown a negative relationship of seed protein concentration with methionine, tryptophan, cysteine, lysine, and threonine, whereas arginine and glutamic acid increase with seed protein concentration (Medic et al., 2014; Pfarr et al., 2018). However, it is possible to surpass the problem associated with the inverse relationship between protein concentration and sulfur containing amino acids. Studies have shown that the effect of coordinated application of nitrogen and sulfur increased the concentration of protein and essential amino acids in soybean (Moro Rosso et al., 2020), oilseed mustard (Mohiuddin et al., 2011), maize grains (Liu et al., 2021), chickpea (Chiaiese et al., 2004), and wheat and barley (de Ruiter and Karl, 2001), thereby significantly improving nutritional quality of these crops. In oilseed Brassica, the reason for this improvement could be due to the fact that nitrogen is an integral part of the protein and the protein of rapeseed contains relatively large quantities of S containing amino acids such as methionine and cystine (Gardner et al., 1985). The glucosinolate content had a significant positive correlation ($p = 0.290$) with phytic acid content, which is consistent with the previous studies done in *B. juncea* (Sharma et al., 2019). Diversity analysis results depicted the formation of ten clusters with variable number of genotypes in D^2 analysis, which signifies the presence of genetic diversity in the germplasm. Based on the inter-cluster distances, genotypes present in clusters 4 and 9 were most diverge for the quality traits measured whereas genotypes in clusters 6 and 8 exhibited least divergence. The best genotypes could be selected based on the mean performance of the genotypes for various quality traits and inter-cluster distances. The best performing genotypes were found in clusters 4 (EC-609305, FAN-628, OCN-106, PN-45-1, PN-87-3, ZY-008) and cluster 7 (BCN-16, CHARLTON, OCN-69, PN-47-1, VCN-9). These lines had low content of antinutritional factors, high protein content, and high amount of antioxidants which could be used as parents in crossing programs for breeding rapeseed varieties.

Genome-wide association analysis, based on millions of molecular markers, is currently widely used in the analysis of complex quality traits for crops such as wheat (Yang et al., 2021), maize (Zheng et al., 2021), pea (Gali et al., 2019), soybean (Shook et al., 2021), flaxseed (Soto-Cerda et al., 2018), and Brassica (Xiao et al., 2019). Many reports addressed use of GWAS for the identification of candidate genes associated oil content (Pal et al., 2021), fatty acids (Tang et al., 2019), glucosinolate (Qu et al., 2015), and fiber fractions (Gajardo et al., 2015; Körber et al., 2016) in *B. napus*. GWAS in combination with transcriptome analysis was also explored to predict seven functional candidate genes for the seed oil content in *B. napus* (Xiao et al., 2019). However, work on the identification of significant SNPs associated with methionine, tryptophan, β-carotene, phytic acid, sinapine, etc., by GWAS has been rarely been reported, to our knowledge, and an overview of networks involved in genetic control of these traits is lacking. It is thus desirable to identify the molecular markers and candidate genes associated with these quality traits in *B. napus* which could provide valuable information about their genetic control. Hence, we investigated the genetics of seed meal quality traits through GWAS based on *B. napus* diversity panel. In this study, a total of 789 significant candidate regions were searched, of which 32 possible candidate genes for seed quality traits were predicted. We identified several genes assigned to seed meal quality traits. These were placed both on A (A01, A02, A03, A05, A06, A07, A08, A09, A10) and C (C01, C02, C03, C05, C07, C08) genome chromosomes. We obtained three candidate genes

TABLE 3 | Summary of the significant candidate genes of seed quality traits.

Trait	Candidate gene	SNP IDs	SNP location	Gene distance (bp)	AT ID	Chr.	–log10P	Gene function
Crude Protein	*ASP5*	SNC_027759.2_44220783	44220783	23664	AT4G31990	A03	3.47	Amino acid biosynthesis
	ASP2	SNC_027766.2_13294871	13294871	43670	AT5G19550	A10	3.92	Amino acid biosynthesis
	EMB1027	SNC_027768.2_8835114	8835114	33113	AT4G26300	C02	3.48	Amino acid biosynthesis
Methionine	*MS3*	SNC_027759.2_4885674	4885674	21484	AT5G20980	A03	3.04	Methionine biosynthesis
	CYSD1	SNC_027759.2_21536878	21536878	25775	AT3G04940	A03	3.17	Methionine biosynthesis
	MTO1	SNC_027767.2_23748159	23748159	8113	AT3G01120	C01	4.47	Methionine accumulation
Tryptophan	*HEMA2*	SNC_027765.2_44309263	44309263	39699	AT1G09940	A09	3.19	Tryptophan biosynthesis
	GLU1	SNC_027766.2_21272659	21272659	34503	AT5G04140	A10	3.07	Tryptophan biosynthesis
	PGM	SNC_027766.2_21272659	21272659	31690	AT5G04120	A10	3.07	Tryptophan biosynthesis
β-carotene	*HDR*	SNC_027771.2_29995244	29995244	32802	AT4G34350	C05	3.33	MEP Pathway
Phenols	*GAUT13*	SNC_027757.2_35744643	35744643	17832	AT3G01040	A01	3.24	Lignification
	UGT	SNC_027762.2_2096323	2096323	25421	AT3G55700	A06	4.10	Polyphenol biosynthesis
	LYC	SNC_027764.2_19576124	19576124	15007	AT3G10230	A08	3.59	Beta carotene biosynthesis
	COS1	SNC_027774.2_28404517	28404517	3591	AT2G44050	C08	3.98	Riboflavin biosynthesis
Sinapine	*ISPF*	SNC_027765.2_8996403	8996403	49451	AT1G63970	A09	3.00	MEP Pathway
Phytic acid	*PMT5*	SNC_027757.2_27740015	27740015	39548	AT3G18830	A01	3.30	Myo-inositol transport
	PLDALPHA1	SNC_027761.2_26966958	26966958	28955	AT3G15730	A05	3.23	Regulator
	SAC8	SNC_027762.2_34136832	34136832	15543	AT3G51830	A06	3.35	Phosphoinositides regulator
	PRAF1	SNC_027763.2_16570114	16570114	17113	AT1G76950	A07	3.12	Phosphatidylinositol binding
	PIP5Ks	SNC_027765.2_10864712	10864712	47184	AT1G60890	A09	3.35	Phosphatidylinositol (4,5)-biphosphate biosynthesis
	CCI1	SNC_027768.2_9049336	9049336	16929	AT5G65480	C02	3.22	Phosphatidylinositide binding
Crude fiber	*NAC073*	SNC_027767.2_8367432	8367432	13635	AT4G28500	C01	3.13	Cellulose and hemicellulose biosynthesis
	NAC073	SNC_027767.2_8367432	8367432	32549	AT4G28500	C01	3.13	Cellulose and hemicellulose biosynthesis
	BGLU46	SNC_027767.2_41296329	41296329	2771	AT1G61820	C01	3.24	Lignin biosynthesis
	BGLU45	SNC_027767.2_41336199	41336199	4750	AT1G61810	C01	3.27	Lignin biosynthesis
	CYT1	SNC_027769.2_22881292	22881292	22019	AT2G39770	C03	3.23	Cellulose biosynthesis
Tannin	*SOT12*	SNC_027758.2_26548840	26548840	26643	AT2G03760	A02	3.23	Flavonoids regulator
	SK1	SNC_027773.2_58538393	58538393	15937	AT2G21940	C07	3.08	Shikimate pathway
	UGT88A1	SNC_027774.2_36266109	36266109	16233	AT3G16520	C08	3.54	Flavonoid biosynthesis
GLS	*CYP79A2*	SNC_027766.2_18835337	18835337	4307	AT5G05260	A10	3.14	Glucosinolates biosynthesis
	DIN2	SNC_027774.2_32661558	32661558	37007	AT3G60140	C08	3.33	Glucosinolate catabolism
	GSTT2	SNC_027774.2_32661558	32661558	3903	AT5G41240	C08	3.33	Isothiocyanates conjugation

viz., ASP5 (Wilkie et al., 1995), *ASP2* (Schultz et al., 1998), *and EMB1027* (Duchêne et al., 2005) on chromosomes A03, A10, and C02, respectively, which encode for aspartate aminotransferase 5, aspartate aminotransferase 2, and arginyl-tRNA synthetase, (class Ic) which was directly involved in the synthesis or regulation of various amino acids, building blocks of proteins. The results correspond with previous studies, reporting SNPs significantly associated with protein content on chromosome C02 of *B. napus* (Tang et al., 2019). Few reports have focused on the identification of QTL associated with total seed protein in canola (Schatzki et al., 2014; Chao et al., 2017; Behnke et al., 2018). Even fewer reports of QTL are associated with amino acid (Wen et al., 2016). Brassica quality breeding programs have made efforts to increase protein content and improve the composition of essential amino acids such as lysine (Falco et al., 1995; Wang et al., 2011) and methionine (Kohno-Murase et al., 1995; Galvez et al., 2008). On chromosome A03, we predicted two loci, *MS3* and *CYSD1,* encoding for methionine synthase 3 and cysteine synthase D1, respectively. The former was found to be involved in methionine biosynthesis (Ravanel et al., 2004), and the latter plays a role in cysteine synthesis, later required for methionine biosynthesis (Yamaguchi et al., 2000). Another significant candidate, *MTO1*-encoded pyridoxal phosphate (PLP)-dependent transferases superfamily protein, which was located on chromosome C01 has a function in methionine accumulation (Inaba et al., 1994). A total of two loci, *GLU1* and *PGM,* were annotated on the regions surrounding the significant SNP, SNC_027766.2_21272659 on chromosome A10 at a distance of 34.5 and 31.7 kb, respectively. *GLU1* encoding for glutamate synthase 1 plays a role in glutamate biosynthesis which is a part

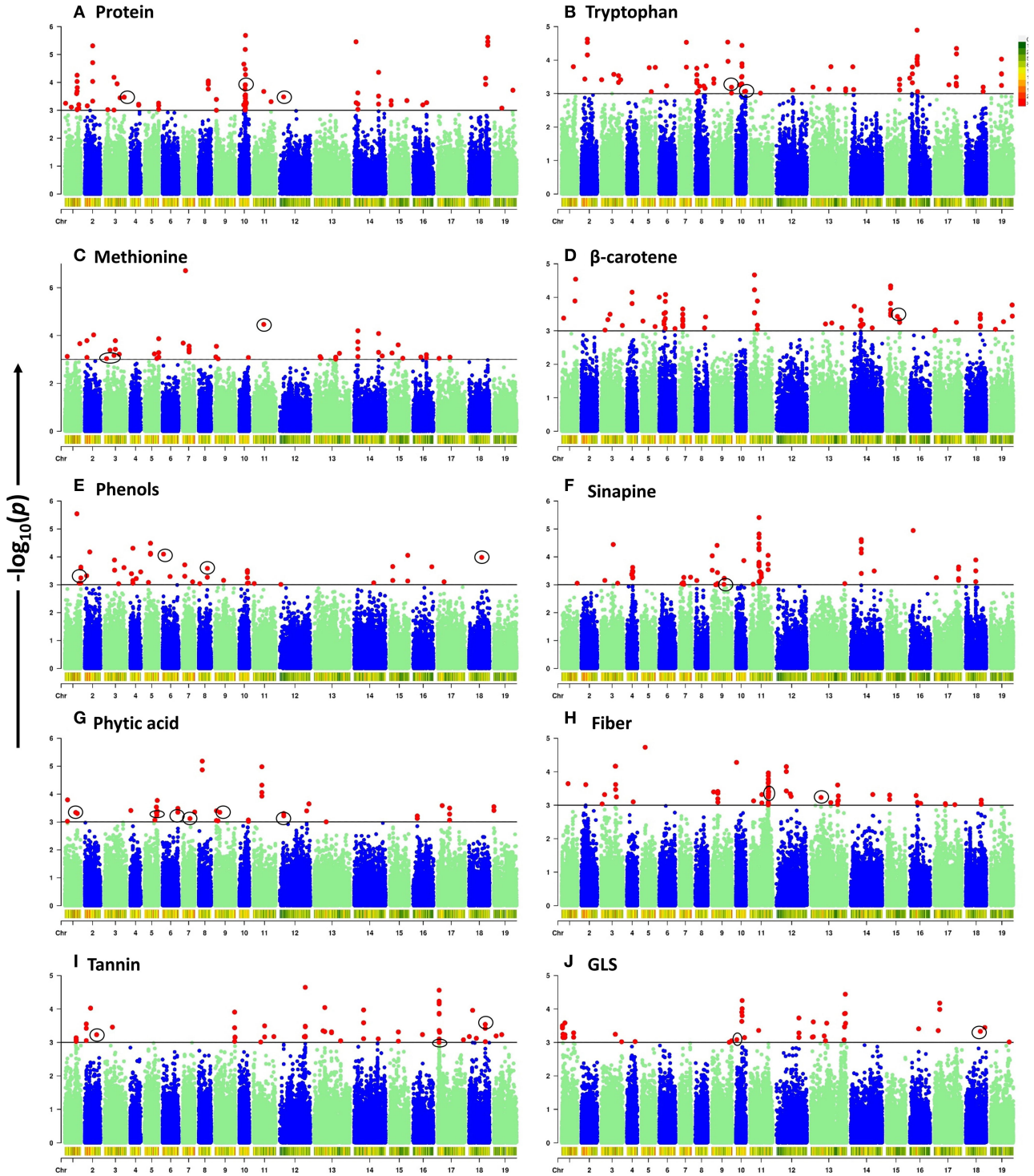

FIGURE 2 | Manhattan plots of genome-wide association analysis for ten seed meal quality traits. -$\log_{10}(p)$ values are plotted against position on each chromosome. Black lines at -$\log_{10}(p) = 3$ indicate the genome-wide significance threshold. SNPs with -$\log_{10}(p) \geq 3$ were considered as significant. Chromosomes 1–10 represent A genome mentioned as A01–A10 and chromosomes 11–19 represent C genome mentioned as C01–C09 in manuscript. **(A)** Protein. **(B)** Tryptophan. **(C)** Methionine. **(D)** β-carotene. **(E)** Phenols. **(F)** Sinapine. **(G)** Phytic acid. **(H)** Fiber. **(I)** Tannin. **(J)** GLS.

of tryptophan biosynthetic pathway (Muñoz-Nortes et al., 2017), *PGM* encoding for phosphoglycerate mutase family protein is a part of serine biosynthetic pathway, and serine is required for tryptophan biosynthesis (Chiba et al., 2012). *HEMA2* encoding for glutamyl-tRNA reductase family protein which was located on chromosome A09 also has involvement in tryptophan

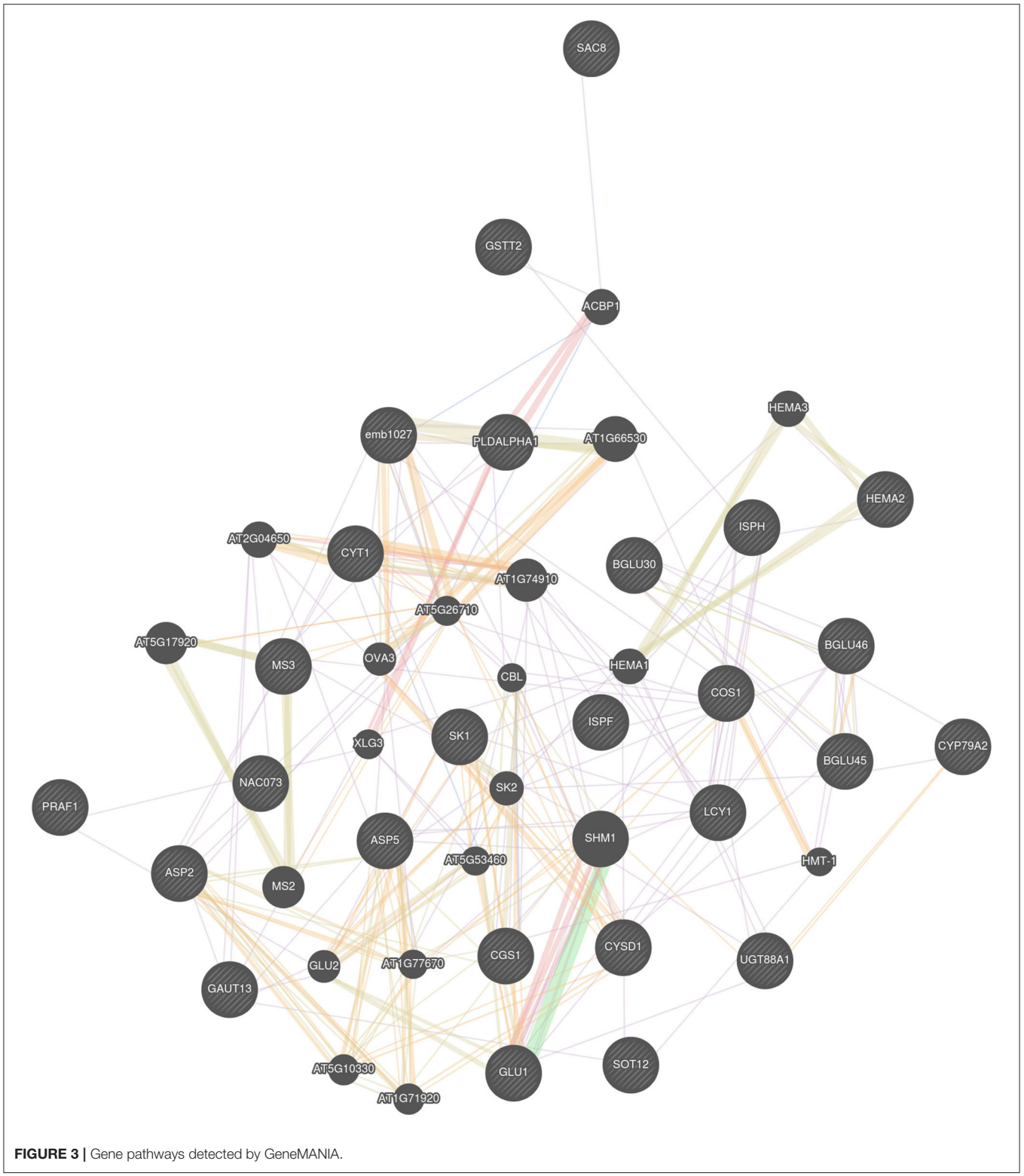

FIGURE 3 | Gene pathways detected by GeneMANIA.

biosynthesis. *HDR*, annotated for the antioxidant β-carotene, encodes for 4-hydroxy-3-methylbut-2-enyl diphosphate reductase which acts as a regulator in methyl-D-erythritol 4-phosphate (MEP) pathway (Guevara-García et al., 2005). For phenol content, *GAUT13*-encoded galacturonosyl transferase 13 that is involved in lignification (Wang et al., 2013), *UGT*-encoded UDP-Glycosyltransferase superfamily protein, part of flavonoid (polyphenolic compounds) biosynthesis (Yin et al., 2017),

LYC-encoded lycopene cyclase having a role in β-carotene biosynthesis (Cunningham et al., 1996), and *COS1*-encoded 6,7-dimethyl-8-ribityllumazine synthase involved in penultimate step of riboflavin biosynthesis (Jordan et al., 1999), were predicted using GWAS. A candidate gene *ISPF* was envisaged for sinapine on chromosome A09 and is known to be involved in non-mevalonate pathway and biosynthesized isopentenyl diphosphate and dimethylallyl diphosphate (MEP pathway) (Hsieh and Goodman, 2006). Various candidates were predicted for phytic acid and are involved in its biosynthesis pathways. *PMT5*-encoding polyol/monosaccharide transporter 5 was found involved in the transport of myo-inositol (Klepek et al., 2005). Most of the reported actions of phytic acid, including its effect on mineral absorption, have been linked to the chemical properties of the phosphate groups of myo-inositol ring (Silva and Bracarense, 2016). *PLDALPHA1* encoded for phospholipase D alpha 2 is an important regulator of phosphoinositide binding (Qin et al., 1997). Biosynthesis of phytic acid involves the myo-inositol production that involves the synthesis of compounds such as phosphoinositides, phosphatidylinositol, and so on. *SAC8* encoded SAC domain-containing protein 8, which acts as the regulators of phosphoinositides (Zhong and Ye, 2003), *PRAF1* encoding for regulator of chromosome condensation (RCC1) family with FYVE zinc finger domain-containing protein is involved in phosphatidylinositol binding (how to correlate it with phytic) (Jensen et al., 2001), *PIP5Ks* encoding for phosphatidylinositol-4-phosphate 5-kinase family protein catalyzes the synthesis of phosphatidylinositol (4, 5)-biphosphate binding (Van den Bout and Divecha, 2009) and *CCI1* encoding for CCI1; Clavata complex interactor 1 protein has a phosphatidylinositide-binding activity (Gish, 2013). A gene involved in cellulose and hemicellulose biosynthesis—*NAC073* (Hussey et al., 2011), another cellulose biosynthetic gene—*CYT1* (Lukowitz et al., 2001), lignin biosynthetic genes—*BGLU45* and *BGLU46* (Escamilla-Treviño et al., 2006; Chapelle et al., 2012) were identified on C genome for crude fiber content in our association study. Tannins are a major group of polyphenols, and various candidates were predicted for tannins in our study. *SOT12* encoding for sulfotransferase 12 is involved in regulation of flavonoids (Hashiguchi et al., 2013), *SK1*encoding for shikimate kinase 1 plays a role in shikimate pathway (Fucile et al., 2008) and *UGT88A1* encoding for UDP-glucosyl transferase 88A1 is involved in the biosynthesis of flavonoid—quercetin (Lim et al., 2004). A total of three genes were annotated for glucosinolates. *CYP79A2* encoding for phenylalanine N-monooxygenase-like protein was annotated at a gene distance of 4.3 kb and is known to be involved in biosynthesis of glucosinolates by converting L-phenylalanine to phenylacetaldoxime (Wittstock and Halkier, 2000), *DIN2* encoding for glycosyl hydrolase superfamily protein has a function in glucosinolates catabolism and are known as putative myrosinases (Morikawa-Ichinose et al., 2020), and *GSTT2* encoding for glutathione S-transferase theta 2 is involved in the conjugation of isothiocyanates which are naturally released from glucosinolates precursors (Wagner et al., 2002).

CONCLUSION

Quality improvement is the main focus of the Brassica breeding programs. Scarce information is available with Brassica breeders regarding molecular markers associated with seed meal quality traits especially for traits—β-carotene, tannin, sinapine, fiber, phytic acid, etc. The outcomes of our study helped in the identification of eleven genotypes and thirty-two candidate genes significantly associated with these seed meal quality traits of *B. napus* which would offer helpful insight to promote breeding of high-quality varieties in Brassica. Further work may involve functional validation of the identified candidate genes that will underpin the genetic systems underlying the biosynthesis of these key nutrients and antinutrients basis of seed quality in Brassica.

DATA AVAILABILITY STATEMENT

The datasets presented in this study can be found in online repositories. The names of the repository/repositories and accession number(s) can be found below: National Center for Biotechnology Information (NCBI) BioProject database under accession number PRJNA814866.

AUTHOR CONTRIBUTIONS

SSh designed and supervised the study. GB performed the phenotyping experiments. SSh and HK analyzed the phenotypic data and wrote the paper. SSa provided genotype by sequencing based genome assembly, SNP data, and population structure of diversity fixed set of B. napus. JA, HK, and MM conducted association mapping. SSh, HK, and JA reviewed the manuscript. All authors contributed to the article and approved the submitted version.

ACKNOWLEDGMENTS

The *B. napus* germplasm and advance breeding lines, used in this study, were collected/developed and maintained by ICAR National Professor Dr. S. S. Banga. The authors duly acknowledge Dr. S. S. Banga, for providing the seeds of the examined germplasm.

SUPPLEMENTARY MATERIAL

The Supplementary Material for this article can be found online at: https://www.frontiersin.org/articles/10.3389/fpls.2022.882766/full#supplementary-material

Supplementary Figure S1 | Mahalnobis euclidean^2 distance depicting inter- and intra-cluster distance among ten clusters of 96 *B. napus* accessions by Tocher's method.

Supplementary Figure S2 | Quantile-quantile (Q-Q) plots of estimated $-\log_{10}(p)$ value from association analysis of ten seed meal quality traits using MLM model.

Supplementary Figure S3 | Heatmap of candidate genes expression (RPKM value) profiling of *B. napus* germplasm on different stages.

REFERENCES

Akhatar, J., Singh, M. P., Sharma, A., Kaur, H., Kaur, N., Sharma, S., et al. (2020). Association mapping of seed quality traits under varying conditions of nitrogen application in *Brassica juncea* L. Czern & Coss. *Front. Genet*. 11, 744. doi: 10.3389/fgene.2020.00744

AOAC (1980). *Official Methods of Analysis, Association of Official Analytical Chemists*. Washington, DC: AOAC.

AOAC (1990). *Official Method of Analysis No. 93406, 960.52, 960.39, 962.09, 923.08 and 985.29*, 15th Edn. Arlington, VA: Association of Official Analytical Chemists.

Aukema, H., and Campbell, L. (2011). "Oil nutrition and utilization," in *Canola, Chemistry, Production, Processing and Utilization*, eds J. K. Daun, N. A. M. Eskin, and D. Hickland (Urbana, IL: AOCS Press), 245–280.

Behnke, N., Suprianto, E., and Möllers, C. (2018). A major QTL on chromosome C05 significantly reduces acid detergent lignin (ADL) content and increases seed oil and protein content in oilseed rape (*Brassica napus* L.). *Theor. Appl. Genet*. 131, 2477–2492. doi: 10.1007/s00122-018-3167-6

Bilić-Šobot, D., Kubale, V., Škrlep, M., Candek-Potokar, M., Prevolnik Povše, M., Fazarinc, G., et al. (2016). Effect of hydrolysable tannins on intestinal morphology, proliferation and apoptosis in entire male pigs. *Arch. Anim. Nutr*. 70, 378–388. doi: 10.1080/1745039X.2016.1206735

Chao, H., Wang, H., Wang, X., Guo, L., Gu, J., Zhao, W., et al. (2017). Genetic dissection of seed oil and protein content and identification of networks associated with oil content in *Brassica napus*. *Sci. Rep*. 7, 1–16. doi: 10.1038/srep46295

Chapelle, A., Morreel, K., Vanholme, R., Le-Bris, P., Morin, H., Lapierre, C., et al. (2012). Impact of the absence of stem-specific β-glucosidases on lignin and monolignols. *Plant Physiol*. 160, 1204–1217. doi: 10.1104/pp.112.203364

Chiaiese, P., Ohkama-Ohtsu, N., Molvig, L., Godfree, R., Dove, H., Hocart, C., et al. (2004). Sulphur and nitrogen nutrition influence the response of chickpea seeds to an added, transgenic sink for organic sulphur. *J. Exp. Bot*. 55, 1889–1901. doi: 10.1093/jxb/erh198

Chiba, Y., Oshima, K., Arai, H., Ishii, M., and Igarashi, Y. (2012). Discovery and analysis of cofactor-dependent phosphoglycerate mutase homologs as novel phosphoserine phosphatases in *Hydrogenobacter thermophilus*. *J. Biol. Chem*. 287, 11934–11941. doi: 10.1074/jbc.M111.330621

Chung, K. T., Wei, C. I., and Johnson, M. G. (1998). Are tannins a double-edged sword in biology and health? *Trends Food Sci. Technol.* 9, 168–175. doi: 10.1016/S0924-2244(98)00028-4

Conesa, A., and Götz, S. (2008). Blast2GO: a comprehensive suite for functional analysis in plant genomics. *Int. J. Plant Genomics* 2008, 619832. doi: 10.1155/2008/619832

Cunningham, F. X., Pogson, B., Sun, Z., McDonald, K. A., DellaPenna, D., and Gantt, E. (1996). Functional analysis of the beta and epsilon lycopene cyclase enzymes of Arabidopsis reveals a mechanism for control of cyclic carotenoid formation. *Plant Cell* 8, 1613–1626. doi: 10.1105/tpc.8.9.1613

de Ruiter, J. M., and Karl, D. P. (2001). The influence of nitrogen and sulfur fertilizer on amino acid composition of wheat and barley grain. *Agron. New Zeal*. 31, 87–98.

Duchêne, A. M., Giritch, A., Hoffmann, B., Cognat, V., Lancelin, D., Peeters, N. M., et al. (2005). Dual targeting is the rule for organellar aminoacyl-tRNA synthetases in *Arabidopsis thaliana*. *Proc. Natl. Acad. Sci*. 102, 16484–16489. doi: 10.1073/pnas.0504682102

Escamilla-Treviño, L. L., Chen, W., Card, M. L., Shih, M. C., Cheng, C. L., and Poulton, J. E. (2006). *Arabidopsis thaliana* β-glucosidases BGLU45 and BGLU46 hydrolyse monolignol glucosides. *Phytochemistry* 67, 1651–1660. doi: 10.1016/j.phytochem.2006.05.022

Falco, S. C., Guida, T., Locke, M., Mauvais, J., Sanders, C., Ward, R. T., et al. (1995). Transgenic canola and soybean seeds with increased lysine. *Bio/Technology* 13, 577–582. doi: 10.1038/nbt0695-577

Fenwick, G. R., Curl, C. L., Pearson, A. W., and Butler, E. J. (1984). The treatment of rapeseed meal and its effect on chemical composition and egg tainting potential. *J. Sci. Food Agric*. 35, 757–761. doi: 10.1002/jsfa.2740350711

Field, B., Cardon, G., Traka, M., Botterman, J., Vancanneyt, G., and Mithen, R. (2004).Glucosinolate and amino acid biosynthesis in arabidopsis. *Plant Physiol*. 135, 828–839. doi: 10.1104/pp.104.039347

Fleddermann, M., Fechner, A., Rößler, A., Bähr, M., Pastor, A., Liebert, F., et al. (2013). Nutritional evaluation of rapeseed protein compared to soy protein for quality, plasma amino acids, and nitrogen balance - A randomized cross-over intervention study in humans. *Clin. Nutr*. 32, 519–526. doi: 10.1016/j.clnu.2012.11.005

Fucile, G., Falconer, S., and Christendat, D. (2008). Evolutionary diversification of plant shikimate kinase gene duplicates. *PLoS Genet*. 4, e1000292. doi: 10.1371/journal.pgen.1000292

Gacek, K., Bayer, P. E., Bartkowiak-Broda, I., Szala, L., Bocianowski, J., Edwards, D., et al. (2017). Genome-wide association study of genetic control of seed fatty acid biosynthesis in *Brassica napus*. *Front. Plant Sci.* 7, 2062. doi: 10.3389/fpls.2016.02062

Gajardo, H. A., Wittkop, B., Soto-Cerda, B., Higgins, E. E., Parkin, I. A., Snowdon, R. J., et al. (2015). Association mapping of seed quality traits in *Brassica napus* L. using GWAS and candidate QTL approaches. *Mol. Breed*. 35, 1–19. doi: 10.1007/s11032-015-0340-3

Gali, K. K., Sackville, A., Tafesse, E. G., Lachagari, V. B., McPhee, K., Hybl, M., et al. (2019). Genome-wide association mapping for agronomic and seed quality traits of field pea (*Pisum sativum* L.). *Front. Plant Sci*. 10, 1538. doi: 10.3389/fpls.2019.01538

Galvez, A. F., Revilleza, M. J., de Lumen, B. O., and Krenz, D. C. (2008). "Enhancing the biosynthesis of endogenous methionine-rich proteins (MRP) to improve the protein quality of legumes via genetic engineering," in *Food for Health in the Pacific Rim: 3rd International Conference of Food Science and Technology* (Trumbull, CT: Food & Nutrition Press, Inc.), 540–552.

Gardner, F. P., Pearce, R. B., and Mitchel, R. L. (1985). *Growth and Development. Physiology of Crop Plants*. Ames, IA: Iowa State University Press.

Gehrig, P. M., Krzyzaniak, A., Barciszewski, J., and Biemann, K. (1996). Mass spectrometric amino acid sequencing of a mixture of seed storage proteins (napin) from *Brassica napus*, products of a multigene family. *Proc. Natl. Acad. Sci. U. S. A*. 93, 3647–3652. doi: 10.1073/pnas.93.8.3647

Gish, L. A. (2013). *Identification of Components Controlling Meristem Homeostasis*. Michigan: University of Michigan.

Grami, B., Stefansson, B. R., and Baker, R. J. (1977). Genetics of protein and oil content in summer rape: heritability, number of effective factors, and correlations. *Can. J. Plant Sci*. 57, 937–943. doi: 10.4141/cjps77-134

Guevara-García, A., San Román, C., Arroyo, A., Cortés, M. E., de la Luz Guti9rrez-Nava, M., and León, P. (2005). Characterization of the Arabidopsis clb6 mutant illustrates the importance of posttranscriptional regulation of the methyl-d-erythritol 4-phosphate pathway. *Plant Cell*. 17, 628–643. doi: 10.1105/tpc.104.028860

Gül, M., Becker, H. C., and Ecke, W. (2003). QTL mapping and analysis of QTL x nitrogen interactions for protein and oil contents in *Brassica napus* L. in 11th International Rapeseed Congress. *Copenhagen*. 91–99.

Hannoufa, A., Pillai, B. V. S., and Chellamma, S. (2014). Genetic enhancement of *Brassica napus* seed quality. *Trans. Res*. 23, 39–52. doi: 10.1007/s11248-013-9742-3

Hashiguchi, T., Sakakibara, Y., Hara, Y., Shimohira, T., Kurogi, K., Akashi, R., et al. (2013). Identification and characterization of a novel kaempferol sulfotransferase from *Arabidopsis thaliana*. *Biochem. Biophys. Res. Commun*. 434, 829–835. doi: 10.1016/j.bbrc.2013.04.022

Haug, W., and Lantzsch, H. J. (1983). Sensitive method for the rapid determination of phytate in cereals and cereal products. *J. Sci. Food Agric*. 34, 1423–1426. doi: 10.1002/jsfa.2740341217

Horn, M. J., Jones, D. B., and Blum, A. E. (1946). Colorimetric determination of methionine in proteins and food. *J. Biol. Chem*. 166, 313–320. doi: 10.1016/S0021-9258(17)35008-1

Howitt, C. A., and Pogson, B. J. (2006). Carotenoid accumulation and function in seeds and non-green tissues. *Plant Cell Environ*. 29, 435–445. doi: 10.1111/j.1365-3040.2005.01492.x

Hsieh, M. H., and Goodman, H. M. (2006). Functional evidence for the involvement of Arabidopsis IspF homolog in the nonmevalonate pathway of plastid isoprenoid biosynthesis. *Planta* 223, 779–784. doi: 10.1007/s00425-005-0140-9

Hussey, S. G., Mizrachi, E., Spokevicius, A. V., Bossinger, G., Berger, D. K., and Myburg, A. A. (2011). SND2, a NAC transcription factor gene, regulates genes involved in secondary cell wall development in Arabidopsis fibres

and increases fibre cell area in Eucalyptus. *BMC Plant Biol.* 11, 1–17. doi: 10.1186/1471-2229-11-173

Inaba, K., Fujiwara, T., Hayashi, H., Chino, M., Komeda, Y., and Naito, S. (1994). Isolation of an *Arabidopsis thaliana* mutant, mto1, that overaccumulates soluble methionine (temporal and spatial patterns of soluble methionine accumulation). *Plant Physiol.* 104, 881–887. doi: 10.1104/pp.104.3.881

Jensen, R. B., Lacour, T., Albrethsen, J., Nielsen, M., and Skriver, K. (2001). FYVE zinc-finger proteins in the plant model *Arabidopsis thaliana*: Identification of PtdIns3P-binding residues by comparison of classic and variant FYVE domains. *Biochem. J.* 359, 165–173. doi: 10.1042/bj3590165

Jiang, J., Wang, Y., Xie, T., Rong, H., Li, A., Fang, Y., et al. (2015). Metabolic characteristics in meal of black rapeseed and yellow-seeded progeny of *Brassica napus-Sinapis alba* hybrids. *Molecules* 20, 21204–21213. doi: 10.3390/molecules201219761

Jordan, D. B., Bacot, K. O., Carlson, T. J., Kessel, M., and Viitanen, P. V. (1999). Plant riboflavin biosynthesis: cloning, chloroplast localization, expression, purification, and partial characterization of spinach lumazine synthase. *J. Biol. Chem.* 274, 22114–22121. doi: 10.1074/jbc.274.31.22114

Klein-Hessling, H. (2007). Value canola meal before using it. *World Poult.* 23, 24–28.

Klepek, Y. S., Geiger, D., Stadler, R., Klebl, F., Landouar-Arsivaud, L., Lemoine, R., et al. (2005), Arabidopsis POLYOL TRANSPORTER5, a new member of the monosaccharide transporter-like superfamily, mediates H+-symport of numerous substrates, including myo-inositol, glycerol, and ribose. *Plant Cell.* 17, 204–218. doi: 10.1105/tpc.104.026641

Kohno-Murase, J., Murase, M., Ichikawa, H., and Imamura, J. (1995). Improvement in the quality of seed storage protein by transformation of *Brassica napus* with an antisense gene for cruciferin. *Theor. Appl.Genet.* 91, 627–631. doi: 10.1007/BF00223289

Kolodziejczyk, P. P., Wang, X., Marianchuk, M., Lu, W., and Amarowicz, R. (1999). Phenolics in rapeseed: capillary electrophoresis as a novel analytical method for detection of sinapine, sinapic acid esters and ferulates. *Quantum* 3, 1–23.

Körber, N., Bus, A., Li, J., Parkin, I. A., Wittkop, B., Snowdon, R. J., et al. (2016). Agronomic and seed quality traits dissected by genome-wide association mapping in *Brassica napus. Front Plant Sci*. 7, 386. doi: 10.3389/fpls.2016.00386

Kumar, S., Yadav, S. K., Chauhan, J. S., Singh, A. K., Khan, N. A., and Kumar, P. R. (2004). Total glucosinolate estimation by complex formation between glucosinolates and tetrachloropalladate(II) using ELISA reader. *J. Food Sci. Technol.* 41, 63–65. Available online at: https://eurekamag.com/research/004/368/004368826.php

Lim, E. K., Ashford, D. A., Hou, B., Jackson, R. G., and Bowles, D. J. (2004). Arabidopsis glycosyltransferases as biocatalysts in fermentation for regioselective synthesis of diverse quercetin glucosides. *Biotechnol. Bioeng.* 87, 623–631. doi: 10.1002/bit.20154

Lipka, A. E., Tian, F., Wang, Q., Peiffer, J., Li, M., Bradbury, P. J., et al. (2012). GAPIT: genome association and prediction integrated tool. *Bioinformatics* 28, 2397–2399. doi: 10.1093/bioinformatics/bts444

Liu, S., Cui, S., Ying, F., Nasar, J., Wang, Y., and Gao, Q. (2021). Simultaneous improvement of protein concentration and amino acid balance in maize grains by coordination application of nitrogen and sulfur. *J. Cereal Sci.* 99, 103189. doi: 10.1016/j.jcs.2021.103189

Lukowitz, W., Nickle, T. C., Meinke, D. W., Last, R. L., Conklin, P. L., and Somerville, C. R. (2001). Arabidopsis cyt1 mutants are deficient in a mannose-1-phosphate guanylyltransferase and point to a requirement of N-linked glycosylation for cellulose biosynthesis. *Proc. Natl. Acad. Sci. U. S. A.* 98, 2262–2267. doi: 10.1073/pnas.051625798

Madsen, C. K., and Brinch-Pedersen, H. (2020). Globoids and phytase: the mineral storage and release system in seeds. *Int. J. Mol. Sci.* 21, 7519. doi: 10.3390/ijms21207519

Mahoonak, A. S., and Swamylingappa, B. (2007). "A new method for preparation of non-toxic, functional protein hydrolysate from commercial mustard cake," in *Proceedings of the 12th International Rapeseed Congress, V* (Wuhan), 142–145.

Matthäus, B., and Zubr, J. (2000). Variability of specific components in *Camelina sativa* oilseed cakes. *Ind. Crops Prod.* 12, 9–18. doi: 10.1016/S0926-6690(99)00040-0

McKenzie, H. A., and Wallace, H. S. (1954). The Kjeldahl determination of nitrogen. *Aus. J. Chem.* 17, 55–59. doi: 10.1071/CH9540055

Medic, J., Atkinson, C., and Hurburgh, C. R. (2014). Current knowledge in soybean composition. *J. Am. Oil Chem. Soc.* 91, 363–384. doi: 10.1007/s11746-013-2407-9

Mohiuddin, M., Paul, A. K., Sutradhar, G. N. C., Bhuiyan, M. S. I., and Zubair, H. M. (2011). Response of nitrogen and sulphur fertilizers on yield, yield components and protein content of oilseed mustard (Brassica spp). *Int. J. Bioresour. Stress Manag.* 2, 93–99. Available online at: https://indianjournals.com/ijor.aspX?target=ijor:ijbsm&volume=2&issue=1&article=016

Morikawa-Ichinose, T., Miura, D., Zhang, L., Kim, S. J., and Maruyama-Nakashita, A. (2020). Involvement of BGLU30 in glucosinolate catabolism in the Arabidopsis leaf under dark conditions. *Plant Cell Physiol.* 61, 1095–1106. doi: 10.1093/pcp/pcaa035

Moro Rosso, L. H., Carciochi, W. D., Naeve, S. L., Kovács, P., Casteel, S. N., and Ciampitti, I. A. (2020). Nitrogen and sulfur fertilization in soybean: Impact on seed yield and quality. *Kans. Agric. Exp. Stn. Res. Rep.* 6, 18. doi: 10.4148/2378-5977.7934

Muñoz-Nortes, T., Pérez-Pérez, J. M., Sarmiento-Mañús, R., Candela, H., and Micol, J. L. (2017). Deficient glutamate biosynthesis triggers a concerted upregulation of ribosomal protein genes in Arabidopsis. *Sci Rep.* 7, 1–14. doi: 10.1038/s41598-017-06335-4

Nesi, N., Delourme, R., Brégeon, M., Falentin, C., and Renard, M. (2008). Genetic and molecular approaches to improve nutritional value of *Brassica napus* L. seed. *C. R. Biol.* 331, 763–771. doi: 10.1016/j.crvi.2008.07.018

Pal, L., Sandhu, S. K., and Bhatia, D. (2021). Genome-wide association study and identification of candidate genes for seed oil content in *Brassica napus. Euphytica* 217, 1–5. doi: 10.1007/s10681-021-02783-2

Pfarr, M. D., Kazula, M. J., Miller-Garvin, J. E., and Naeve, S. L. (2018). Amino acid balance is affected by protein concentration in soybean. *Crop Sci.* 58, 2050–2062. doi: 10.2135/cropsci2017.11.0703

Price, M. L., Butler, L. G., Featherston, W. R., and Rogler, J. C. (1978). Detoxification of high tannin sorghum grain. *Nutr. Rep. Int.* 17, 229–236.

Qin, W., Pappan, K., and Wang, X. (1997). Molecular heterogeneity of phospholipase D (PLD): cloning of PLDγ and regulation of plant PLDγ, -β, and -α by polyphosphoinositides and calcium. *J. Biol. Chem.* 272, 28267–28273. doi: 10.1074/jbc.272.45.28267

Qu, C. M., Li, S. M., Duan, X. J., Fan, J. H., Jia, L. D., Zhao, H. Y., et al. (2015). Identification of candidate genes for seed glucosinolate content using association mapping in *Brassica napus* L. *Genes* 6, 1215–1229. doi: 10.3390/genes6041215

Rao, C. R. (1952). *Advanced Statistical Methods in Biometric Research. - PsycNET*. New York, NY: Wiley.

Ravanel, S., Block, M. A., Rippert, P., Jabrin, S., Curien, G., Rébeill,é, F., et al. (2004). Methionine metabolism in plants: chloroplasts are autonomous for *de novo* methionine synthesis and can import S-adenosylmethionine from the cytosol. *J. Biol. Chem.* 279, 22548–22557. doi: 10.1074/jbc.M313250200

Sadeghi, M. A.„ S. (2009). Effect of recovery method on different property of mustard protein. *World J. Dairy Food Sci.* 4, 100–106. Available online at: https://idosi.org/wjdfs/wjdfs4(2)/3.pdf

Sashidhar, N., Harloff, H. J., and Jung, C. (2020). Identification of phytic acid mutants in oilseed rape (*Brassica napus*) by large-scale screening of mutant populations through amplicon sequencing. *New Phytol.* 225, 2022–2034. doi: 10.1111/nph.16281

Schatzki, J., Ecke, W., Becker, H. C., and Möllers, C. (2014). Mapping of QTL for the seed storage proteins cruciferin and napin in a winter oilseed rape doubled haploid population and their inheritance in relation to other seed traits. *Theor. Appl.Genet.* 127, 1213–1222. doi: 10.1007/s00122-014-2292-0

Schultz, C. J., Hsu, M., Miesak, B., and Coruzzi, G. M. (1998). Arabidopsis mutants define an in vivo role for isoenzymes of aspartate aminotransferase in plant nitrogen assimilation. *Genetics* 149, 491–499. doi: 10.1093/genetics/149.2.491

Sen, R., Sharma, S., Kaur, G., and Banga, S. S. (2018). Near-infrared reflectance spectroscopy calibrations for assessment of oil, phenols, glucosinolates and fatty acid content in the intact seeds of oilseed Brassica species. *J. Sci. Food Agric.* 98, 4050–4057. doi: 10.1002/jsfa.8919

Sharma, A., Aacharya, M., Punetha, H., Sharma, S., Kumari, N., and Rai, P. K. (2019). Biochemical characterization and their correlations in *Brassica juncea* genotypes. *Int. J. Curr. Microbiol. Appl. Sci.* 8, 2408–2417. doi: 10.20546/ijcmas.2019.801.254

Shook, J. M., Zhang, J., Jones, S. E., Singh, A., Diers, B. W., and Singh, A. K. (2021). Meta-GWAS for quantitative trait loci identification in soybean. *G3 Genes Genom. Genet.* 11, jkab117. doi: 10.1093/g3journal/jkab117

Silva, E. O., and Bracarense, A. P. F. (2016). Phytic acid: From antinutritional to multiple protection factor of organic systems. *J. Food Sci.* 81, 1357–1362. doi: 10.1111/1750-3841.13320

Soto-Cerda, B. J., Cloutier, S., Quian, R., Gajardo, H. A., Olivos, M., and You, F. M. (2018). Genome-wide association analysis of mucilage and hull content in Flax (*Linum usitatissimum* L.) seeds. *Int. J. Mol. Sci.* 19, 2870. doi: 10.3390/ijms19102870

Spies, J. R., and Chambers, D. C. (1949). Chemical determination of tryptophan in proteins. *Anal. Chem*. 21, 1249–1266. doi: 10.1021/ac60034a033

Statista. (2021). *Worldwide Production of Rapeseed by Country*. Available online at: https://www.statista.com/statistics/263930/worldwide-production-of-rapeseed-by-country (accessed August 24, 2021).

Swain, T., and Hillis, W. E. (1959). The phenolic constituents of *Prunus domestica*. The quantitative analysis of phenolic constituents. *J. Sci. Food Agric*. 10, 63–68. doi: 10.1002/jsfa.2740100110

Tan, Z., Xie, Z., Dai, L., Zhang, Y., Zhao, H., Tang, S., et al. (2022). Genome- and transcriptome-wide association studies reveal the genetic basis and the breeding history of seed glucosinolate content in *Brassica napus*. *Plant Biotechnol*. 20, 211–225. doi: 10.1111/pbi.13707

Tang, M., Zhang, Y., Liu, Y., Tong, C., Cheng, X., Zhu, W., et al. (2019). Mapping loci controlling fatty acid profiles, oil and protein content by genome-wide association study in *Brassica napus*. *Crop J.* 7, 217–226. doi: 10.1016/j.cj.2018.10.007

Tosi, G., Paola, M., Mauro, A., Arianna, B., Minieri, S., Luigi, M., et al. (2013). Efficacy test of a hydrolysable tannin extract against necrotic enteritis in challenged broiler chickens. *Ital. J. Anim. Sci*. 12, e62. doi: 10.4081/ijas.2013.e62

Tripathi, M. K., and Mishra, A. S. (2007). Glucosinolates in animal nutrition: a review. *Anim.Feed Sci. Technol.* 132, 1–27. doi: 10.1016/j.anifeedsci.2006.03.003

USDA (2021). *World Agricultural Production*. Washington, DC: USDA.

USDA-FAS (2021). *Oilseeds: World Markets and Trade*. Washington, DC: USDA-FAS.

Van den Bout, I., and Divecha, N. (2009). PIP5K-driven PtdIns(4,5)P2 synthesis: Regulation and cellular functions. *J. Cell Sci*. 122, 3837–3850. doi: 10.1242/jcs.056127

Wagner, U., Edwards, R., Dixon, D. P., and Mauch, F. (2002). Probing the diversity of the Arabidopsis glutathione S-Transferase gene family. *Plant Mol. Biol*. 49, 515–532. doi: 10.1023/A:1015557300450

Walker, K. C., and Booth, E. J. (2001). Agricultural aspects of rape and other Brassica products. *Eur. J. Lipid Sci. Technol.* 103, 441–446. doi: 10.1002/1438-9312(200107)103:7<441::AID-EJLT441>3.0.CO;2-D

Wanasundara, J. P. (2011). Proteins of brassicaceae oilseeds and their potential as a plant protein source. *Crit. Rev. Food Sci. Nutr*. 51, 635–677. doi: 10.1080/10408391003749942

Wang, H., and Qin, F. (2017). Genome-wide association study reveals natural variations contributing to drought resistance in crops. *Front. Plant Sci*. 8, 1–12. doi: 10.3389/fpls.2017.01110

Wang, J., Chen, L., Liu, Q. Q., Sun, S. S. M., Sokolov, V., and Wang, Y. P. (2011). Transformation of LRP gene into *Brassica napus* mediated by *Agrobacterium tumefaciens* to enhance lysine content in seeds. *Genetika* 47, 1433–1437. doi: 10.1134/S1022795411120167

Wang, J., and Zhang, Z. (2021). GAPIT version 3: Boosting power and accuracy for genomic association and prediction. *Genom. Proteom. Bioinform*. 19, 629–640. doi: 10.1016/j.gpb.2021.08.005 [Epub ahead of print].

Wang, X., Wang, H., Long, Y., Li, D., Yin, Y., Tian, J., et al. (2013). Identification of QTLs associated with oil content in a high-oil *Brassica napus* cultivar and construction of a high-density consensus map for QTLs comparison in *B. napus*. *PLoS ONE* 8, e80569. doi: 10.1371/journal.pone.0080569

Warde-Farley, D., Donaldson, S. L., Comes, O., Zuberi, K., Badrawi, R., Chao, P., et al. (2010). The GeneMANIA prediction server: biological network integration for gene prioritization and predicting gene function. *Nucleic Acids Res.* 38, 214–220. doi: 10.1093/nar/gkq537

Wen, J., Xu, J. F., Long, Y., Wu, J. G., Xu, H. M., Meng, J. L., et al. (2016). QTL mapping based on the embryo and maternal genetic systems for non-essential amino acids in rapeseed (*Brassica napus* L.) meal. *J. Sci. Food Agric*. 96, 465–473. doi: 10.1002/jsfa.7112

Wilkie, S. E., Roper, J. M., Smith, A. G., and Warren, M. J. (1995). Isolation, characterisation and expression of a cDNA clone encoding plastid aspartate aminotransferase from *Arabidopsis thaliana*. *Plant Mol. Biol*. 27, 1227–1233. doi: 10.1007/BF00020897

Wittstock, U., and Halkier, B. A. (2000). Cytochrome P450 CYP79A2 from *Arabidopsis thaliana* L. catalyzes the conversion of L-phenylalanine to phenylacetaldoxime in the biosynthesis of benzyl glucosinolate. *J. Biol. Chem*. 275, 14659–14666. doi: 10.1074/jbc.275.19.14659

Xiao, Z., Zhang, C., Tang, F., Yang, B., Zhang, L., Liu, J., et al. (2019). Identification of candidate genes controlling oil content by combination of genome-wide association and transcriptome analysis in the oilseed crop *Brassica napus*. *Biotechnol. Biofuels* 12, 1–16. doi: 10.1186/s13068-019-1557-x

Yamaguchi, Y., Nakamura, T., Kusano, T., and Sano, H. (2000). Three Arabidopsis genes encoding proteins with differential activities for cysteine synthase and β-cyanoalanine synthase. *Plant Cell Physiol*. 41, 465–476. doi: 10.1093/pcp/41.4.465

Yang, R., Jiang, Y., Xiu, L., and Huang, J. (2019). Effect of chitosan pre-soaking on the growth and quality of yellow soybean sprouts. *J. Sci. Food Agric*. 99, 1596–1603. doi: 10.1002/jsfa.9338

Yang, S.-C., Arasu, M. V., Chun, J. H., Jang, Y. S., Lee, Y. H., Kim, I. H., et al. (2015). Identification and determination of phenolic compounds in rapeseed meals (*Brassica napus* L.). *J. Agric. Chem. Environ.* 4, 14. doi: 10.4236/jacen.2015.41002

Yang, Y., Amo, A., Wei, D., Chai, Y., Zheng, J., Qiao, P., et al. (2021). Large-scale integration of meta-QTL and genome-wide association study discovers the genomic regions and candidate genes for yield and yield-related traits in bread wheat. *Theor. Appl. Genet*. 134, 3083–3109. doi: 10.1007/s00122-021-03881-4

Yao, M., Guan, M., Zhang, Z., Zhang, Q., Cui, Y., Chen, H., et al. (2020). GWAS and co-expression network combination uncovers multigenes with close linkage effects on the oleic acid content accumulation in *Brassica napus*. *BMC Genom*. 21, 1–12. doi: 10.1186/s12864-020-6711-0

Yin, Q., Shen, G., Di, S., Fan, C., Chang, Z., and Pang, Y. (2017). Genome-wide identification and functional characterization of UDP-glucosyltransferase genes involved in flavonoid biosynthesis in *Glycine max*. *Plant Cell Physiol.* 58, 1558–1572. doi: 10.1093/pcp/pcx081

Yu, B., Lydiate, D. J., Young, L. W., Schäfer, U. A., and Hannoufa, A. (2008). Enhancing the carotenoid content of *Brassica napus* seeds by downregulating lycopene epsilon cyclase. *Transgenic Res.* 17, 573–585. doi: 10.1007/s11248-007-9131-x

Zheng, Y., Yuan, F., Huang, Y., Zhao, Y., Jia, X., Zhu, L., et al. (2021). Genome-wide association studies of grain quality traits in maize. *Sci. Rep*. 11, 1–12. doi: 10.1038/s41598-021-89276-3

Zhong, R., and Ye, Z. H. (2003). The SAC domain-containing protein gene family in Arabidopsis. *Plant Physiol.* 132, 544–555. doi: 10.1104/pp.103.021444

Conflict of Interest: The authors declare that the research was conducted in the absence of any commercial or financial relationships that could be construed as a potential conflict of interest.

Publisher's Note: All claims expressed in this article are solely those of the authors and do not necessarily represent those of their affiliated organizations, or those of the publisher, the editors and the reviewers. Any product that may be evaluated in this article, or claim that may be made by its manufacturer, is not guaranteed or endorsed by the publisher.

Advantages of publishing in Frontiers

OPEN ACCESS
Articles are free to read for greatest visibility and readership

FAST PUBLICATION
Around 90 days from submission to decision

HIGH QUALITY PEER-REVIEW
Rigorous, collaborative, and constructive peer-review

TRANSPARENT PEER-REVIEW
Editors and reviewers acknowledged by name on published articles

Frontiers
Avenue du Tribunal-Fédéral 34
1005 Lausanne | Switzerland

Visit us: www.frontiersin.org
Contact us: frontiersin.org/about/contact

REPRODUCIBILITY OF RESEARCH
Support open data and methods to enhance research reproducibility

DIGITAL PUBLISHING
Articles designed for optimal readership across devices

FOLLOW US
@frontiersin

IMPACT METRICS
Advanced article metrics track visibility across digital media

EXTENSIVE PROMOTION
Marketing and promotion of impactful research

LOOP RESEARCH NETWORK
Our network increases your article's readership